A Selection of published/presented papers

Volume II (2)
(1986-1990)

Papers 34-70

S Lee

A Selection of published/presented papers

Volume II (2)
(1986-1990)

Papers 34-70

34 "Application of plasma neutrons for half-life measurements"
Singapore J. Phys. 4, 131 (1987)
S.P. Moo and S. Lee

35 "Measurement of nitrogen laser channel current, inductance and resistance"
IEEE J. Quantum Electronics QE-23, 283 (1987)
A.J. Smith, K.H. Kwek, T.Y. Tou, A.V. Gholap and S. Lee

36 "Recent results from Rotamak Experiments at Flinders University"
Paper read at the 8th U.S. Compact Toroid Symposium, University of Maryland, June 1987
H. Kirolous, A. Knight, D. Brotherton-Ratcliffe, Wu Cheng, S. Lee and I.R. Jones

37 "A small plasma focus device for neutron, X-ray and electron beam studies"
Paper read at the Spring College on Plasma Physics, ICTP, Trieste, June 1987, (in Procs.)
T.Y. Tou, K.H. Kwek, Y.C. Yong and S. Lee

38 "A TEA nitrogen laser for optical diagnostic for a plasma focus"
Paper read at the Spring College on Plasma Physics, ICTP, Trieste, June 1987 (in Procs.)
K.H. Kwek, T.Y. Tou, and S. Lee

39 "The design, construction and performance studies of a Linear Z-pinch for current-stepping experiments"
Paper read at the Spring College on Plasma Physics, ICTP, Trieste, June 1987 (in Procs.)
S.H. Saw, C.S. Wong and S. Lee

30 "Numerical design of the UNU/ICTP Plasma Focus"
Paper read at the Second Tropical College on Applied Physics, Malaysia, April 1986 (to appear in Procs.)
K.H. Kwek, T.Y. Tou and S. Lee

31 "Determining nitrogen laser channel parameters"
J. Fiz. Mal., 7, 125 (1986)
K.H. Kwek, A.J. Smith, T.Y. Tou, A.V. Gholap and S. Lee

32 "Design and operation of a hard-pumped ruby laser system"
Malaysian J. Sci. 8: (1986)
Harith Ahmad and S. Lee

33 "Preliminary results of the UNU/ICTP Plasma Focus"
J. Fiz. Mal. 7, 1 (1986)
S. Lee et.al.

34 "Application of plasma neutrons for half-life measurements"
Singapore J. Phys. 4, 131 (1987)
S.P. Moo and S. Lee

35 "Measurement of nitrogen laser channel current, inductance and resistance"
IEEE J. Quantum Electronics QE-23, 283 (1987)
A.J. Smith, K.H. Kwek, T.Y. Tou, A.V. Gholap and S. Lee

36 "Recent results from Rotamak Experiments at Flinders University"
Paper read at the 8th U.S. Compact Toroid Symposium, University of Maryland, June 1987
H. Kirolous, A. Knight, D. Brotherton-Ratcliffe, Wu Cheng, S. Lee and I.R. Jones

37 "A small plasma focus device for neutron, X-ray and electron beam studies"
Paper read at the Spring College on Plasma Physics, ICTP, Trieste, June 1987, (in Procs.)
T.Y. Tou, K.H. Kwek, Y.C. Yong and S. Lee

38 "A TEA nitrogen laser for optical diagnostic for a plasma focus"
Paper read at the Spring College on Plasma Physics, ICTP, Trieste, June 1987 (in Procs.)
K.H. Kwek, T.Y. Tou, and S. Lee

39 "The design, construction and performance studies of a Linear Z-pinch for current-stepping experiments"
Paper read at the Spring College on Plasma Physics, ICTP, Trieste, June 1987 (in Procs.)
S.H. Saw, C.S. Wong and S. Lee

40 "Streak laser shadowgraphy of the plasma focus"
Paper read at the Asian Physics Symposium, Kuala Lumpur, Malaysia, October 1987 (to appear in Procs.)
T.Y. Tou, E.H. Yee, B.C. Tan and S. Lee

41 "Observation of temperature variations in a plasma focus from soft X-ray measurements"
Paper read at the Asian Physics Symposium, Kuala Lumpur, Malaysia, October 1987 (to appear in Procs.)
T.Y. Tou, and S. Lee

42 "Pulsed plasma X-ray sources for applications in lithography and microscopy"
Paper read at the Asian Physics Symposium, Kuala Lumpur, Malaysia, October 1987 (to appear in Procs.)
C.S. Wong, S.P. Moo, S.H. Saw and S. Lee

43 "Sharing of fusion-related technology among developing countries"
Invited paper read at the Energy Independence Conference at Rio de Janeiro, August 1987; also to appear in revised version in Majalah Fizik
Proc. Fusion Energy and Plasma Physics, 754 (1988) World Scientific (Ed. : P.H. Sakanaka)
S. Lee

44 "Physics and perspectives of small plasma devices"
Asia-Pacific Physics News, Vol 3, June/July 1988
S. Lee

45 "A simple facility for the teaching of plasma dynamics and plasma nuclear fusion"
American J. Phys. 56, 62 (1988)
S. Lee et. al.

46. "Third World Nuclear Fusion Programmes and South-South Collaboration in Plasma Technology"
Invited paper delivered at Third Tropical College on Applied Physics, June 1988, Kuala Lumpur,
Procs. "Laser and Plasma Technology" Ed. C.S. Wong et.al., World Scientific (1990)
S. Lee and M.H.A. Hassan

47 "Half-life Measurements Using Plasma Neutrons"
1988, Proc. 3rd Tropical College on Appl. Phys. Kuala Lumpur
S.P. Moo, C.K. Chakrabarty and S. Lee

48 "High Resolution Plasma Visualisation by Subnanosecond Optical Techniques"
J. Phys. Mal., 9, 36 - 40 (1988)
K.H. Kwek, T.Y. Tou and S. Lee

49 "A Preionised Nitrogen Laser as a Diagnostic Light Source for Fast Pulse Experiments"
IEEE Trans. Instrumentation & Measurements IM-38, 1 103-107 (1989)
K.H. Kwek, T.Y. Tou and S. Lee

50 "Multi-slit streak photography for plasma dynamics studies"
Review Sci. Instru., 59, 11 2370-2374 (1989)
T.Y. Tou and S. Lee

51 "Density ratios in compressions driven by radiation pressure"
Laser and Particle Beams, 6, 597-606 (1988)
S. Lee

52 "A Numerical Study of the Effect of Y on the Shock Speed for Atomic and Molecular Hydrogen"
J. Fiz. Mal., 9, 93 (1988)
S.H. Saw, S. Lee and C.S. Wong

53 "Technology of a Small Plasma Focus"
Invited lecture at the Spring College on Plasma Physics - Trieste, Italy, May-June 1989
Proc. Small Plasma Physics Experiments II pp. 114-169 (1990)
World Scientific (Edited by S. Lee and P.H. Sakanaka)
S. Lee

54 "A Current-Stepping Technique to Enhance Pinch Compression - An Experimental Study"
Small Plasma Physics Experiments (II) pp. 289-295 (1990)
S.H. Saw, S. Lee and C.S. Wong

55 "Non-Pertubing Plasma Focus Measurements in the Run Down Phase"
IEEE Trans. Plasma Science 17, 311-315 (1989)
T.Y. Tou, S. Lee and K.H. Kwek

56 "Current sheath structures of the Plasma Focus in the Run-down Phase"
IEEE Trans. Plasma Science 18, p. 826-830 (1990)
K.H. Kwek, T.Y. Tou and S. Lee

57 "Half-life Measurements of ^{116}In Using Plasma Focus Neutrons"
J. Fiz. Mal., 10, 57 (1989)
S.P. Moo, C.K. Chakrabarty and S. Lee

58 "Sequenced Nitrogen Lasers"
J. Appl. Phys. 65, 4133-4137 (1989)
S. Lee, K.H. Kwek, Jalil Ali, M.V.H.V. Prabhakar, Y.S.Shishodia and A.G. Warmate

59 "Fusion Programmes in Malaysia"
Invited lecture at the Symposium on South-North Collaboration - June 1989 Trieste, Italy, June 1989
S. Lee

60 "Observations of Compact Torus FRC in single-phase Operation of a Transistorised Rotamak"
J. Fiz. Mal., 10, 61 (1989)
S. Lee, S.Y. Xu, G. Cotrell and I.R. Jones

61 "Pulse Technology, Laser Development and Technology Resource Network"
Invited Plenary Paper at Second Regional Symposium on Optoelectronics, 27th-28th Nov 1989, Jakarta, Indonesia (also delivered as invited paper at First National Symp. on Laser Technology, UTM, Skudai, Malaysia in Oct 1989
S. Lee

62 "Diagnostics of the Plasma Focus"
Invited Paper at the Beijing College on Plasma Physics: Diagnostics, Oct 29 - Nov 1989, Beijing, P.R. China
Proc. pg. 5-19 (Edited by S.T. Tsai and Y.A. Li) 1989
S. Lee

63 "A Compact Low Voltage Flash X-ray Tube"
Japan J. Appl. Phys. 28, 1264 (1989)
C.S. Wong, S. Lee, C.X. Ong and O.H. Chin

64 "Shadowgraphy of Laser Induced Sparks"
J. Fiz. Mal., 11, 24 (1990)
S.S. Kumar, S. Lee, H.B. Ahmad and C.Y. Jing

65 "A Simple Shadowgraphy system and some results"
Jurnal Fizik Malaysia, 11, 1, (1990)
S. Lee et. al.

66 "Plasma Focus Dynamics - Its Role in An AAAPT Training Programme"
Invited Paper-Association Plasma Studies of China Third Summer School - University of Tsingdao, Tsingdao, P.R. China 15-22 August 1990; Procs. Ed. by Tsai Shih-Tung and Li Yin-An pg. 53 (1990), also presented as invited paper at Quaid-I-Azam University, Islamabad, Pakistan during Basic Course on Plasma Physics Oct. 29th., 1990
S. Lee

67 "Training Programmes for Research Transfer-Experience and Results"
Invited Paper Int. Conf. on Physics & Physicists for Development - Univ. of Twente, Netherlands 11-12th Sept. 1990
S. Lee

68 "Effect of Targets on Plasma Focus Dynamics"
IEEE Trans Plasma Science, Dec 1990 (scheduled)
S. Lee et. al.

69 "Laser Induced Plasmas and Fusion"
Guest Lectures - Second South East Asian Laser School, Yogyakarta, Indonesia (7 - 18th, Jan. 1991)
S. Lee

70 "An Investigation of the Ion Beam of a Plasma Focus Using a Metal Obstacle and a Deuterated Target"
IEEE Trans. on Plasma Science (accepted)
S.P. Moo, C.K. Chakrabarty and S. Lee

Sing. J. Phys., Vol. 4, No. 1, 1987. 131-133 (Research Note)

APPLICATION OF PLASMA NEUTRONS FOR HALF-LIFE MEASUREMENTS

S.P. Moo and S. Lee
Physics Department, University of Malaya
59100 Kuala Lumpur, Malaysia

The application of a simple plasma focus device as a neutron source for short half life measurements is described. Preliminary measurements of the half life of ^{116}In yield a value of 13.9 ± 0.6 s.

Introduction

Neutron emission from plasma focus devices using the D-D reaction has been reported by about 20 research groups in some ten countries over the last 15 years.[1,2] The neutrons are produced in bursts, each lasting for about 100 ns. The plasma neutrons are essentially monoenergetic, the mean energy being about 2.5 MeV while the spread (FWHM) is about 300 keV. The neutron yields reported ranged from 10^6 to 10^{10} per burst and satisfy a scaling law of the form $Y \propto I^{3.3}$ where Y is the neutron yield and I the plasma current.[2] Except for three early papers,[3,4,5] two on neutron radiography and the other on pulsed activation analysis, there are no further reports on applications of plasma neutrons. This is perhaps understandable as many different types of neutron sources have been available for the last two decades.

Recently, a low cost plasma focus device based on a 3.3 kJ single capacitor and a low maintenance parallel plate spark gap has been developed and tested.[6] Using deuterium as the filling gas, the device produces with reliability about 10^8 neutrons per burst. The design of the device is so simple that six sets have been made and transferred to several countries under the auspices of the United Nations University and the International Centre for Theoretical Physics. A question that emerges from the evaluation of this simple plasma focus is whether such a device can be used as a source of neutrons for research/teaching. With this question in mind, we have attempted some half life measurements using the plasma focus as an irradiation source. Since the saturation factor $\{1 - e^{-0.693 t_i / t_{\frac{1}{2}}}\}$ increases and approaches unity as the ratio of the irradiation time (t_i) to the half life ($t_{\frac{1}{2}}$) increases, it is immediately apparent that the short duration of the plasma focus neutrons enhances the activation of short lived isotopes.

In this paper, we report some preliminary results on the measurement of the half life of ^{116}In.

Method

When ^{115}In captures a neutron, the compound nucleus formed promptly deexcites by gamma ray emissions to either the ground state of ^{116}In or an isomeric state ($^{116}In^{m}$). Both these states decay by β emission with half lives of 14 s and 54 min respectively. The equipment used in the present measurement of the half life of the ground state of ^{116}In is shown schematically in Fig. 1. The fast neutrons from the plasma focus are slowed down by 4 cm of paraffin before impinging upon an indium foil of thickness 0.2 mm. The β-particles emitted are detected by an Ne-102 plastic scintillator optically coupled to a photomultiplier. A multi-channel analyser (MCA) operating on the multiscaling mode at 3 s dwell time records the activity of the indium foil as a function of time, both before and after the neutron burst.

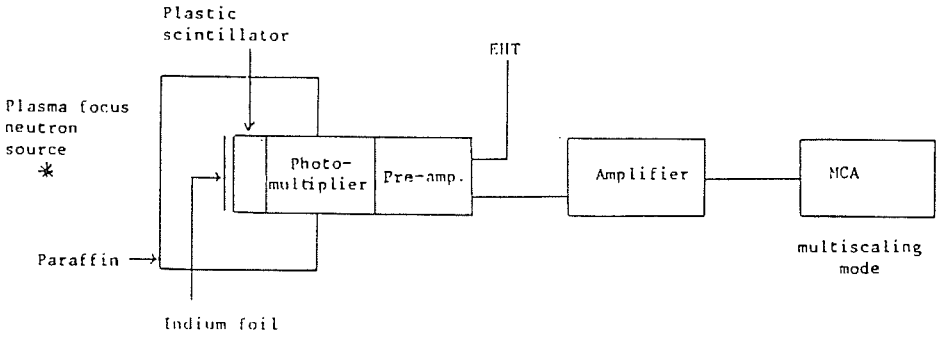

Fig. 1. Schematic diagram of equipment for half life measurements.

Results and Discussion

In this preliminary study, three independent measurements of the indium activity are made. The maximum counts in the three measurements are below 600/channel. At the low count rate encountered, dead time losses in the MCA is negligible. For the determination of the half life of ^{116}In, the counts recorded in 16 channels (48 s) of the decay curve, starting from the second channel after the neutron burst, are analysed. Over this interval the β-activity of the relatively long lived isomeric state is taken to be constant as it changes by only 1%. Furthermore, calculations indicate that the contribution from the isomeric state to the total β-activity initially is only 2%. In our data analysis, therefore, the contribution to the channel counts from the isomeric state is treated as a component of the constant background.

After background subtraction, a least squares fit is applied to the decay curve in the interval of interest. Values of the half life obtained from the three independent measurements are 14.4 ± 1.0 s, 13.3 ±0.6 s and 14.1 ± 1.3 s, giving an average of 13.9 ±0.6 s. Our value is comparable with reported values of 13.4 ±0.4 s (Domanic and Sailor),[7] 14.05 ± 0.26 s (Ducat and Thomas),[8] 14.5 ± 0.4 s (Capron and VanderStricht)[9] and 15.6 ± 0.5 s (Brzosko et. al.).[10]

Efforts are now underway to improve the error in the individual measurements by increasing the count rates and by reducing the background. As only three measurements are made the error of ±0.6 s is to be regarded as a rough estimate only. The error can be improved by increasing the number of independent measurements.

Acknowledgement

These measurements were made during experiments supported by The United Nations University, the International Centre for Theoretical Physics and the University of Malaya research grant F232/74.

REFERENCES

1. G. Decker and R. Wienecke, Physica 82C, 155 (1976).
2. H. Conrads, Neutron Physics and Nuclear Data in Science and Technology, Vol. 2, Edited by S. Cierjacks, Pergamon Press, 237 (1983).
3. D. Ruffner, Neutrographie am Plasma-Fokus, IPF 74-3, Institut fur Plasmaforschung Universitat Stuttgart (1974).
4. H. Rapp, E. Rauchle and D. Ruffner, Mater. Eval. 33, 269 (1975).
5. E. Bar Auraham and Y. Porath, Nucl. Instr. and Meth. 123, 5 (1975).
6. S. Lee, T.Y. Tou, M.A. Eissa, A.V. Gholap, K.H. Kwek, S.P. Moo, S. Mulyodrono, A.J. Smith, Suryadi, W. Usada and M. Zakaullah, J. Fiz. Mal. 7, 1 (1986); Rev. Sci. Instru. (submitted).
7. F. Domanic and V.L. Sailor, Phys. Rev. 119, 208 (1960).
8. A. Ducat and R.H. Thomas, Nucl. Phys. 15, 525 (1960).
9. P.C. Capron and A. VanderStricht, Nucl. Sci. Abstr. 13, No. 358 (1959).
10. J. Brzosko, P. Decowski, K. Siwek-Diament and Z. Wilhelmi, Nucl. Phys. 74, 438 (1965).

Measurement of Nitrogen Laser Channel Current, Inductance, and Resistance

A. J. SMITH, K. H. KWEK, T. Y. TOU, A. V. GHOLAP, AND S. LEE

Abstract—The laser channel current, inductance, and resistance of a nitrogen laser have been measured using a magnetic probe and have been found to have values of ~42 kA, 1.6 nH, and 0.1 Ω, respectively, for a laser channel gap of 1.6 cm operated at 10 kV and 60 torr. The results of the measurement confirm a double discharge mechanism for the nitrogen laser.

I. Introduction

THE nitrogen laser has been the subject of several recent parametric studies aimed at determining the optimum operating conditions of the device. In these studies, the critical quantities for determining nitrogen laser performance are the laser channel inductance and resistance (L_{g0}, r_g). These quantities determine the laser channel discharge current as well as the electrical power absorbed by the laser channel.

The quantities L_{g0} and r_g have been described [1] as "unmeasurable" so that in many studies [1]–[4], they are either taken as parameters in the circuit analysis, or computed using a gas discharge model, or deduced by matching theoretical and experimental voltage waveforms. While some of these studies have thrown light on these quantities L_{g0} and r_g, a more direct method of measuring these quantities appears desirable. In this study, the laser discharge current in a Blumlein-type nitrogen laser is measured using a magnetic probe, and from the laser-channel current waveform, the values of L_{g0} and r_g are directly measured.

The laser pulse is measured simultaneously using a fast photodiode, and thus it is ascertained that the observed channel discharge current does indeed coincide with the laser pulse. These measurements and their interpretation in terms of a laser circuit theory are described in the following sections.

II. Theory

The circuit theory of the nitrogen laser has been discussed earlier, for example, in [2]. Essentially, the laser consists of a laser channel represented by L_{g0} and r_g, and two parallel plate capacitors C_1 and C_2 with very low inductances L_1 and L_2, charged to V_0. The arrangement is as shown in the circuit of Fig. 1. L_{g1} and L_{g2} are the inductances of the plates connecting C_1 and C_2 to the laser channel. The capacitor C_2 is connected to a parallel-plate swinging cascade spark gap represented by L_e and r_e in the diagram. For these measurements, values of the parameters are $C_1 \sim 58$ nF, $C_2 \sim 28$ nF, $L_1 \sim 0.13$ nH, $L_2 \sim 0.07$ nH, $L_{g1} = L_{g2} \sim 0.8$ nH, and $L_e \sim 13$ nH. The quantities L_{g0} and r_g are to be measured.

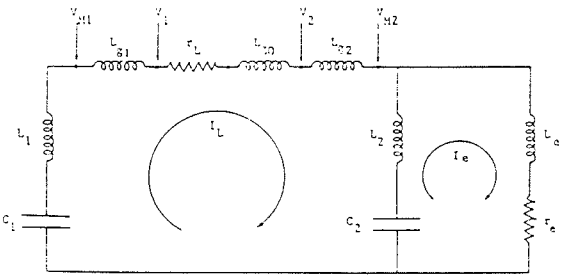

Fig. 1. Equivalent circuit for the nitrogen laser. I_L: current flowing through the laser channel. I_e: current flowing through the external spark gap. V_1-V_2: voltage across laser channel. V_{M1}-V_{M2}: voltage across laser channel measured at nearest accessible points, thus including inductances due to connecting plates.

At $t = 0$, the external spark gap switches and the voltage V_2 (on the C_2 side of the laser channel) swings from V_0 towards $-V_0$ with a time constant $\sim \sqrt{(L_e C_2)}$ since $L_e >> L_2$. The rate of rise of laser channel voltage is therefore on the order of $2V_0/\sqrt{(L_e C_2)}$, which is usually sufficient to cause a uniform breakdown all along the laser channel at a later time $t = t_s$ when the voltage across the channel attains a sufficient value. The main discharge between C_1 and C_2 then occurs with a periodic time of

$$T \sim 2\pi\sqrt{\left\{(L_1 + L_2 + L_g)\cdot\left(\frac{C_1 \cdot C_2}{C_1 + C_2}\right)\right\}} \quad (1)$$

where $L_g = L_{g1} + L_{g2} + L_{g0}$. This is modulated by a slower discharge with a time constant $\sqrt{\{L_e(C_1 + C_2)\}}$ which eventually removes the remnant stored energy through the external spark gap r_e. For the laser action, this slower discharge is of no consequence.

The effective damping parameter of the laser gap discharge is given by

$$\alpha = \frac{r_g}{Z_L} \quad (2)$$

where the surge impedance of the laser channel circuit is

Manuscript received May 9, 1986; revised October 24, 1986. This work was supported in part by a grant from ICTP and in part by the University of Malaya under Grant F232/73.

A. J. Smith is with the Department of Physics, Njala University College, PMB Freetown, Sierra Leone.

K. H. Kwek, T. Y. Tou, and S. Lee are with the United Nations University Training Programme on Plasma and Laser Technology, Department of Physics, University of Malaya, 59100 Kuala Lumpur, Malaysia.

A. V. Gholap is with the Department of Physics, Rivers State University of Science and Technology, Port Harcourt, Nigeria.

IEEE Log Number 8612378.

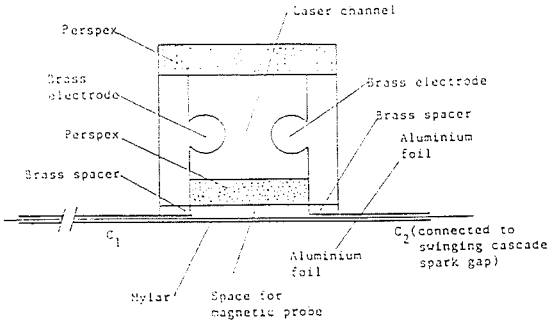

Fig. 2. Cross-sectional view of the nitrogen laser showing the locations of the laser channel and the space provided for magnetic probe insertion.

$$Z_L = \sqrt{\left\{\frac{L_1 + L_2 + L_g}{C_1 C_2/(C_1 + C_2)}\right\}}. \qquad (3)$$

III. Experimental

A. The Laser

The laser channel (Fig. 2) consists of two $\frac{5}{8}$ in horizontally placed brass rods (as electrodes), 46 cm long, soft-soldered onto two $\frac{1}{2}$ in thick brass strips (50 × 5 cm) which provide external contact for the electrodes. These pieces are insulated from each other by top and bottom $\frac{1}{2}$ in thick perspex separators which ensure that the electrodes are held at a constant separation of 1.6 cm along their entire length. The laser light is brought out through two holes in the perspex end pieces ($\frac{1}{2}$ in thick, $6\frac{1}{4} \times 6\frac{1}{4}$ cm). The 2 cm diameter holes are covered by 1 mm thick quartz pieces. The various brass and perspex parts of the channel are screwed together through a thin layer of silicone rubber which provides vacuum seal for the chamber.

The parallel plate capacitors C_1 and C_2 consist of a common earth plate, which is a 45 × 80 cm strip of aluminum kitchen foil laid on top of a flat aluminum plate (for electrical contact and support). On top of the aluminum foil are laid four sheets of 1 mil mylar which extends at least 10 cm beyond the edges of the conductors all around. The high-voltage plates of C_1 and C_2 are 45 × 45 cm and 45 × 23 cm strips of aluminum foil laid on top of the mylar sheets. These high-voltage capacitor plates are separated by a 4.6 cm gap over which the laser channel is placed so that each side of the laser channel (see Fig. 2) makes pressure contact with one of the capacitors. The capacitor C_2 is connected to the swinging cascade spark gap.

For these experiments, the laser peak power is maintained above 200 kW.

B. The Magnetic Probe

The magnetic probe consists of a ten-turn coil of SWG 40 wire on a former of 1 mm diameter enclosed in a 3 mm glass tube. The coil leads are twisted around each other and soldered to a BNC jack connector outside the glass tube. In order to insert the probe underneath the laser channel, it was necessary to raise the channel by inserting a 6 mm strip of brass between the channel electrode contacts and the high-voltage aluminum capacitor plates. This creates a space for the magnetic probe (Fig. 2). The probe is inserted with its axis parallel to the channel axis. In this position, the probe lies directly underneath the channel discharge current and over that portion of the earth plate which connects C_1 and C_2 and carries the return discharge current. The probe signal is passively integrated with a 12 μs RC time constant. The laser pulse is measured using a fast photodiode FND-100. The observations are made with a 100 MHz storage oscilloscope inside a screened cage.

The magnetic probe was calibrated by using the field at the center of two-turn Helmholtz coil, energized by a 0.62 μF capacitor charged to 10 kV. The current I in the Helmholtz coil was measured by a Rogowski coil to be 4.056 kA. The field at the center of the coil was found to be

$$B_z = \left(\mu_0 \frac{nI}{a}\right)\left(\frac{8}{5^{3/2}}\right) = 0.158 \text{ tesla}$$

for a coil of radius a = 4.6 cm. The measured probe signal of 0.165 V then gives a calibration factor of

$$K_B = \frac{0.165}{0.158} = 1.044 \text{ V/tesla}.$$

IV. Results and Discussion

A. General Features of the Oscillograms

The results of the measurements are summarized by the set of oscillograms shown in Fig. 3. Fig. 3(a) shows the magnetic probe signal with the channel at atmospheric pressure and the value of V_0 = 10 kV so that only the spark gap breaks down. The high-frequency oscillations in the signal are identified as electrostatic pickup resulting from reflections in the transmission line C_2 as this capacitor discharges through the spark gap inductance.

Fig. 3(b) shows the typical probe signal with the laser channel at 60 torr nitrogen so that after the spark gap is triggered, the laser channel discharges. The new feature of the probe signal, i.e., the lower frequency damped oscillations which commences ~ 100 ns after the spark gap breakdown, is due to the laser gap current. In order to ascertain that this is indeed the laser current signal, we have superimposed it with a photodiode signal of the laser pulse by using the add mode of the dual trace oscilloscope. The added signal is shown in Fig. 3(d). Fig. 3(c) shows the photodiode signal alone. The magnetic probe and photodiode signals are taken with matched cables for which the signal transit times do not differ by more than 0.5 ns.

B. Measurement of Circuit Parameters

From the current signal of Fig. 3(b), we measure the periodic time of the damped oscillations of the channel current as T = 50 ns. We apply (1) with C_1 = 58 nF and C_2 = 28 nF and obtain $L_1 + L_2 + L_g$ = 3.4 nH. Subtracting away L_1 = 0.13 nH, L_2 = 0.07 nH, and L_{g1} =

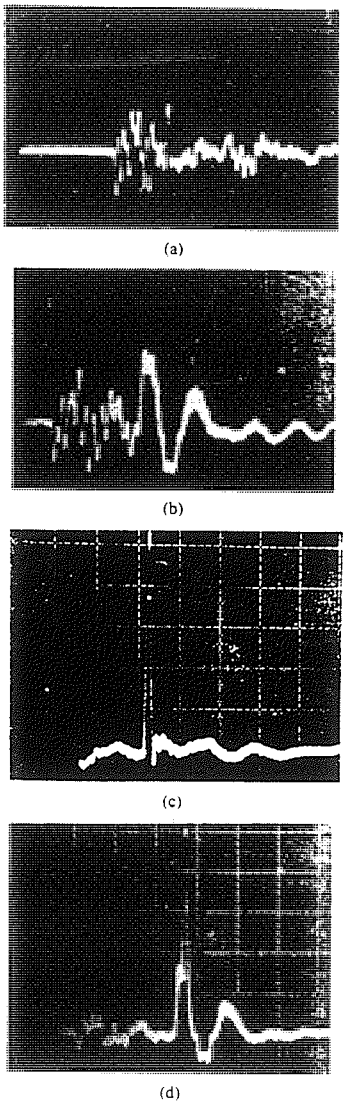

Fig. 3. Oscillograms of magnetic and photodiode signals. Time base is 50 ns/div. (a) Magnetic probe signal. Laser at atmospheric pressure. No laser channel discharge. (b) Magnetic probe signal. Laser at 60 torr nitrogen. Discharge with lasing action (0.1 V/div). (c) Photodiode signal of laser pulse. Laser operated under same condition as in (b). (d) Photodiode signal superimposed onto magnetic probe signal. Laser operated under same condition as in (b).

L_{g2} = 0.8 nH, as calculated from geometry, gives the laser channel inductance as

$$L_{g0} = 1.6 \text{ nH}.$$

The surge impedance of the laser channel circuit Z_L may now be computed from (3) as

$$Z_L = \sqrt{\left(\frac{3.4 \text{ nH}}{18.9 \text{ nF}}\right)} = 0.42\ \Omega.$$

We next calculate the channel resistance from the measured damping parameter of the laser channel current. From Fig. 3(b), the average reversal ratio (peak amplitude of $(n+1)$th half cycle/peak amplitude of nth half cycle) measured from the first three half cycles in f = 0.69. By taking a damped sinusoidal approximation, it may easily be shown that f is given by

$$f = \frac{\exp\left(\frac{-R}{2L}\left\{\frac{nT}{2} + \frac{T}{2}\right\}\right)}{\exp\left(\frac{-R}{2L}\left\{\frac{nT}{2}\right\}\right)} = \exp\left(-\alpha\frac{\pi}{2}\right). \quad (4)$$

Here R is the total circuit resistance, L is the total circuit inductance, and α, the effective damping factor of the circuit, is the ratio of R to the surge impedance. For this laser discharge circuit, α is given by (2). From the measured value of f, (4) gives α = 0.24. Thus, from (2), we have

$$r_g = \alpha Z_L = 0.1\ \Omega$$

which is the measured time-averaged laser channel resistance for this laser operated at 10 kV, 60 torr pressure.

C. Measurement of Laser Current and Laser Channel Voltage

The magnetic probe placed in its position below the laser channel measures a magnetic field B which is related to the laser loop current I_L by the equation

$$B = \frac{\mu_0 I_L}{l} \quad (5)$$

where l = 0.46 m is the length of the last channel. From the oscillogram of Fig. 3(b), the peak voltage measured from the magnetic probe is 0.12 V, which from the magnetic probe calibration factor gives a peak magnetic field of 0.115 T corresponding to a peak channel current of

$$\hat{I}_L = 42.1 \text{ kA}.$$

From this measured peak current and the surge impedance of the laser channel circuit may also be obtained the voltage across the laser channel V_g when the laser channel breaks down. The following approximate equation is used:

$$\hat{I}_L = \frac{V_g}{Z_L}. \quad (6)$$

This gives

$$V_g = 17.7 \text{ kV}.$$

This means that in the operation of this nitrogen laser at 10 kV and 60 torr nitrogen, the laser channel begins to break down when its C_2 side electrode has swung down to −7.7 kV from its original +10 kV.

Finally, the peak electrical power input into the laser channel may be estimated using the measured value of r_g = 0.1 Ω as

$$\text{peak resistive power input} = r_g \hat{I}_L^2 = 177 \text{ MW}.$$

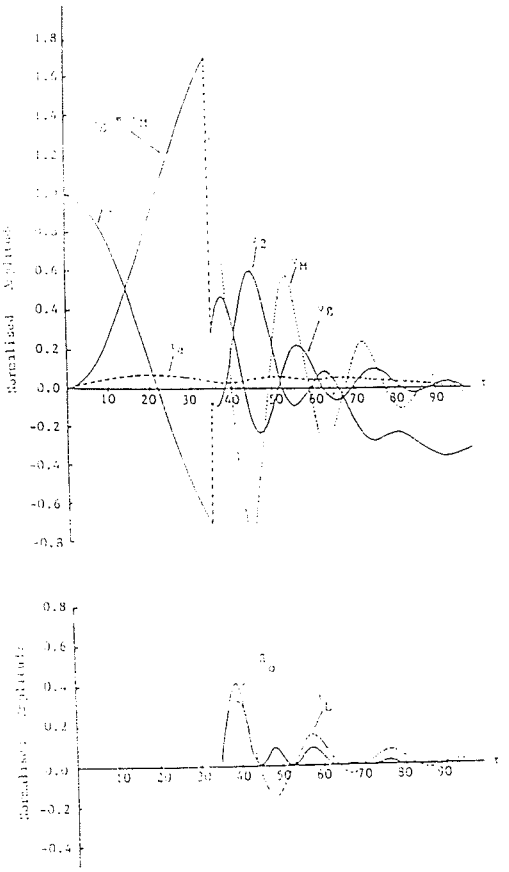

Fig. 4. Computed [2] results of currents, voltages, and laser gap power for $\alpha = 0.3$. All solutions are normalized. i_L: laser channel current. i_s: external gap switch current. v_2: voltage on one side of the laser channel. v_L: voltage drop across laser channel. v_M: voltage drop across accessible points of measurements. v_M is equal to v_g before the laser channel discharges. π_0: power absorbed by laser channel. τ: normalized time.

In Fig. 4 is shown a theoretical plot [2] of the laser channel current I_L (normalized) for $\alpha = 0.3$. Also shown are other computed quantities of the circuit. For example, v_g is the voltage (normalized) across the laser gap. As can be seen from Fig. 4, after the laser gap has broken down, the voltage v_M that may be measured across accessible points V_{M1} and V_{M2} (see Fig. 1) differs considerably from v_g because of the additional unavoidable inductances of L_{g1} and L_{g2}. This illustrates the difficulty in interpreting voltage measurements for the purpose of, for example, ascertaining the resistive power of the laser gap. This difficulty does not arise with the measurement of the laser channel current I_L which is the same quantity whether measured at the laser channel or at the earth return plate.

A comparison between the measured laser channel current or magnetic field waveform of Fig. 3(b) for measured $\alpha = 0.24$ and the computed laser channel current waveform of Fig. 4 for $\alpha = 0.3$ shows good agreement between the two waveforms, except that the measured current waveform shows a squaring-out effect in the first two half cycles, probably due to transmission line effect of the strip-line capacitors C_1 and C_2.

V. Conclusion

The agreement between these observations and the theory for the transversely excited nitrogen laser [2] lends confidence to that theory. In essence, the double discharge process proposed in that theory, in which C_2 discharges relatively slowly through the large spark gap inductance followed by the faster discharge of C_1 into C_2, is confirmed by these observations.

Operating this nitrogen laser at 10 kV, 60 torr, a simple measurement with a magnetic probe fixes the following laser channel parameters: channel inductance of 1.6 nH, channel resistance of 0.1 Ω, and a peak channel current of 42.1 kA. With the use of this simple technique, the channel parameters of nitrogen lasers may be determined under different operating conditions. This could assist in optimization efforts.

Acknowledgment

A. J. Smith and A. V. Gholap gratefully acknowledge UNU Fellowships without which this work could not have been possible.

References

[1] C. Iwasaki and T. Jitsuno, "An investigation of the effects of the discharge parameters on the performance of a TEA N_2 laser," *IEEE J. Quantum Electron.*, vol. QE-18, pp. 423–427, Mar. 1982.

[2] S. Lee, A. V. Gholap, A. J. Smith, K. H. Kwek, A. C. Chew, T. Y. Tou, and S. Sapru, "Parametric study of the nitrogen laser," *J. Fiz. Mal.*, vol. 6, pp. 165–174, 1985.

[3] T. Mitani, "Parametric study of the 357.7-nm oscillation in a TE (transversely excited) N_2 laser," *J. Appl. Phys.*, vol. 52, pp. 3159–3166, May 1981.

[4] W. A. Fitzsimmons, L. W. Anderson, C. E. Riedhauser, and J. M. Vrtilek, "Experimental and theoretical investigation of the nitrogen laser," *IEEE J. Quantum Electron.*, vol. QE-12, pp. 624–633, Oct. 1976.

Recent Results from Rotamak Experiments at Flinders University

H. Kirolous A. Knight D. Brotherton-Ratcliffe Wu Cheng* S. Lee†
I.R. Jones

School of Physical Sciences,
The Flinders University of South Australia,
Bedford Park, S.A. 5042, Australia.

1 Introduction

In a Rotamak [1] the plasma current is driven by entrainment of the electron fluid in an applied rotating magnetic field (Figure 1). To date Rotamak experiments have been undertaken in devices having the orthogonal coil systems used to generate the rotating magnetic field located on the outside surfaces of spherical pyrex discharge vessels. Stable and long-lived compact torus configurations have been generated in these vessels.

In this poster results from two Rotamak experiments at Flinders University will be presented. Firstly, detailed results will be described from a metal-walled experiment which has similar input power to the previous pyrex-walled devices. The motivation for this experiment is the need for future high power experiments to have metallic vacuum vessels. Secondly, an experiment will be described in which a rotating magnetic field is used to drive current in a cylindrical pyrex-walled device creating a highly prolate field-reversed configuration (F.R.C.).

2 A Metal-Walled Rotamak

Figure 2 shows a diagram of the Rotamak. Table 1 summarises various experimental parameters and details.

2.1 Magnetic Probe Measurements

The array of Hall magnetic probes shown in Figure 2 was used to collect a time-series database for B_r and B_z comprising an 80×33 $r-z$ grid (refer to coordinate system of Figure 1). The reproducibility of discharges enabled each point on the grid to be measured using separate discharges. The frequency response of the Hall probes was such that each point in the time series represented an average of the magnetic configuration over about 40 cycles of the rotating field. To analyse collected data, at various times throughout the discharge, two-dimensional vector polynomials with the property $\nabla \cdot B = 0$ were fitted to the signals. The order of these polynomials was chosen to be high enough to fit all statistically relevant trends but not too high as to start introducing spurious oscillations due to the finite spatial separation of the data.

Contour diagrams of the poloidal flux, $\psi = 2\pi \int_0^r r' B_z(r', z, t) dr'$ and the current density, $J_\phi = (1/\mu_0)(\nabla \times B)_\phi$ calculated from the polynomial fits are shown in Figures 3 and 4 respectively for t=20 ms.

Figure 3 shows two distinct magnetic configurations. The inner configuration is a compact torus with a separatrix well inside the radius of the rotating field coils. Figure 4 shows the direction of current in this configuration to be such that the electrons are being convected in the direction of the applied rotating magnetic field. The magnitude of this current is around 300 Amps. The outer configuration, which has not previously been observed in Rotamaks because of the absence of an interspace between the discharge wall and the rotating field coils, consists of three toroidal current loops, one of which has current in the opposite

*On leave from The Institute of Physics, Chinese Academy of Sciences, Beijing.
†On leave from The Department of Physics, University of Malaya, Kuala Lumpur.

8th U.S. Compact Toroid Symposium, University of Maryland
June 1987.

direction to the inner configuration current. One explanation of this peculiar and unexpected outer feature may come from a sustained plasma flow [2].

2.2 Grad-Shafranov Modelling

In the Rotamak, ponderomotive and plasma-flow forces can be non-negligible in the time averaged MHD equilibrium equation. In this section we ignore these forces and try to model the complicated outer configuration with ROTA [3] a modified Grad-Shafranov equilibrium code. The rationale for this process is the elucidation of whether or not the above two forces are necessary for the explanation of the form of the outer configuration.

Using the polynomial fits we plot in Figure 5 a diagram of J_ϕ/r vs ψ. Grad-Shafranov theory predicts that J_ϕ/r should be a single-valued function of ψ. Taking as a fit to this data the smooth curve of Figure 6, and using this as input to ROTA (together with the measured total current and the exact form of the applied equilibrium field) we plot in Figures 7 and 8 the predicted magnetic flux and current surfaces. Clearly some of the experimental features are present, but others such as the two magnetic axes are not. By choosing different forms for the fit in Figure 6, consistent with the errors intrinsic to Figure 5, it is possible to create a configuration with ROTA that has two magnetic axes but *always* with the loss of the required structure of the three outer current loops. In fact by looking at Figures 3 and 4, the outer configuration can be seen to violate the condition that J_ϕ/r be a single-valued function of ψ. Thus either plasma flow or ponderomotive force appear necessary for the reconciliation of theory and experiment. Nevertheless, it is interesting that the Grad-Shafranov equation can model configurations of approximately the same type as observed, perhaps indicating that the plasma gas pressure is held in balance predominantly by the $J \times B$ force and only adjusted slightly by RF pressure and flow.

3 A Field-Reversed Rotamak Experiment

Figure 9 shows a schematic diagram of the field-reversed Rotamak. Table 1 shows various experimental parameters.

3.1 Magnetic Probe Measurements

A similar array of Hall magnetic probes to that used in the metal-walled Rotamak was employed to collect a database of B_z time histories comprising a 29×14 $r-z$ grid (refer to Figure 9 for coordinate system). The excellent reproducibility of discharges enabled each point of the above grid to be taken using a separate shot. The collected data were analysed by fitting two-dimensional polynomials to the signals $B_z(r,z)$ at various times and then calculating the poloidal flux, ψ and current density, J_ϕ (defined above) via the polynomial coefficients. In this poster we only present results from a single time, $t = 19$ ms. Figure 10 shows raw B_z data at $z = 0$ with a cut of the fitted surface in the $(B_z - r)$ plane. The reversal of the applied field is evident. Figures 11 and 12 show respectively contours of the poloidal flux and current density. Clearly the time-averaged configuration is a well-defined highly prolate compact torus. The total current driven is 2600 Amps.

3.2 Langmuir Probe Measurements

A similar database to the above magnetic measurements was collected using a double Langmuir probe. Characteristic curves were measured for 1024 time points on an $r-z$ grid of 11×14. Once again, in this poster only measurements pertaining to $t = 19$ ms will be presented. The characteristic curves have been used to obtain the electron temperature (T_e) and density (n_e) on the above grid assuming that the effective probe collecting area is the physical area of the probe. Two dimensional polynomials have been fitted to the data enabling contour plots of n_e (Figure 13), T_e (Figure 14) and $P_e \equiv kn_eT_e$ (Figure 15) to be generated. Comparing Figure 15 with Figure 11 it is apparent that the electron pressure contours are very similar to the poloidal flux contours.

Following the rationale of section 2.2 we plot in Figure 16 the experimental data of P_e vs ψ. Grad-Shafranov theory states that $P \equiv P_i + P_e$ should be a single-valued function of ψ. Clearly, given the experimental error, particularly in the derivation of n_e, and the fact that T_i is expected to be significantly less than T_e, it would appear that in this experiment ponderomotive and flow forces may play a somewhat negligible role.

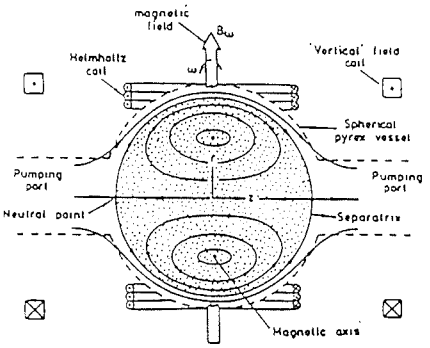

Fig. 1 – A typical Rotamak.

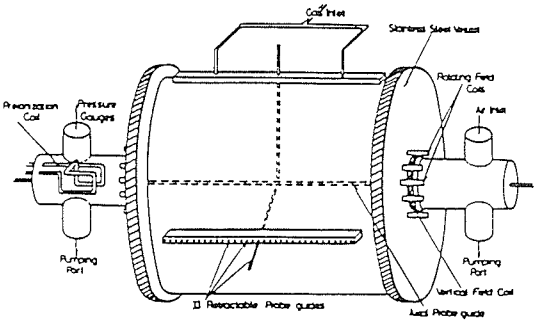

Fig. 2 – The metal-walled Rotamak.

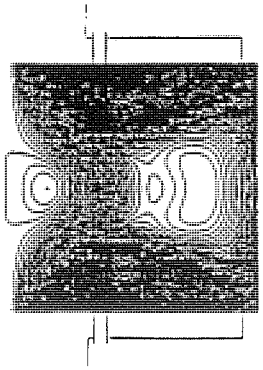

Fig. 3 – Contour plot of poloidal flux in the $r-z$ plane Lines represent the metal wall and the RF coils.

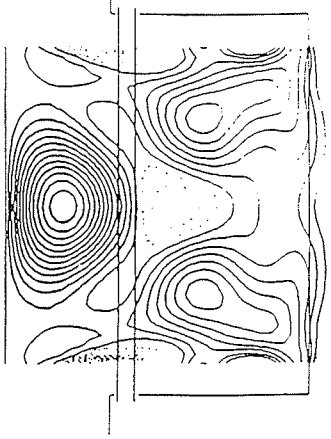

Fig. 4 – Contour plot of the current density in the $r-z$ plane.

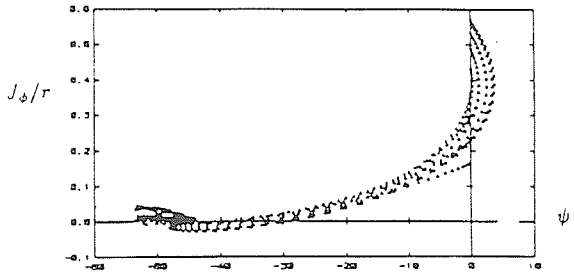

Fig. 5 – Experimental J_ϕ/r vs ψ (arb. units).

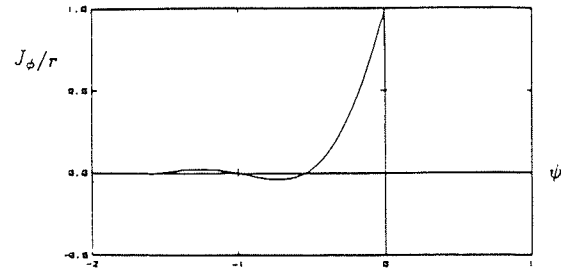

Fig. 6 – Trial function fit to Figure 5 used as input to ROTA.

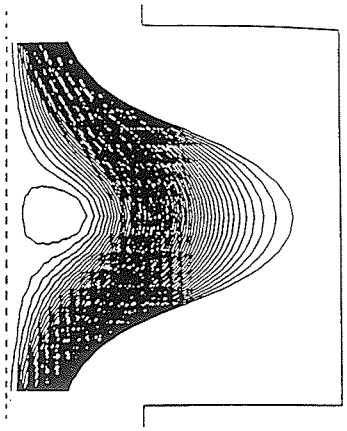

Fig. 7 – ROTA poloidal flux in the $r-z$ plane.

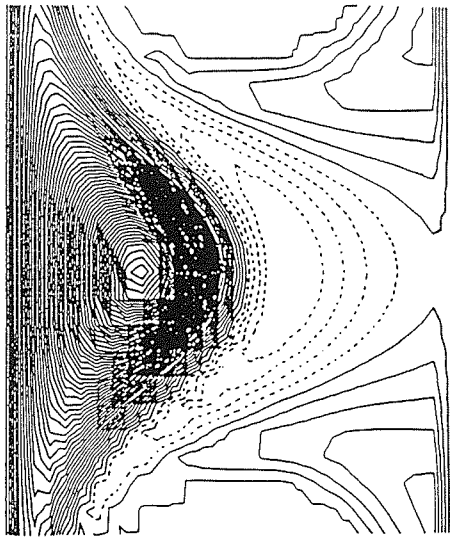

Fig. 8 – ROTA current density in the $r-z$ plane.

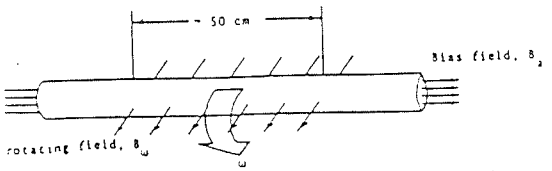

Fig. 9 – Schematic diagram of the FRC Rotamak.

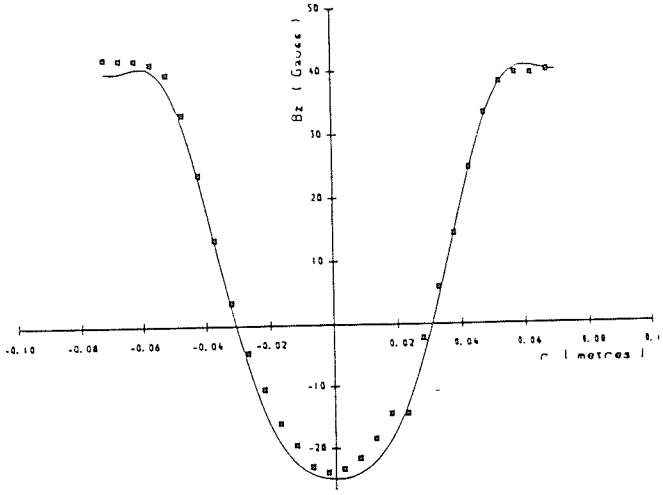

Fig. 10 – Experimental $B_z(r)$ points at $z = 0$ with cut through the polynomial surface fit to B_z.

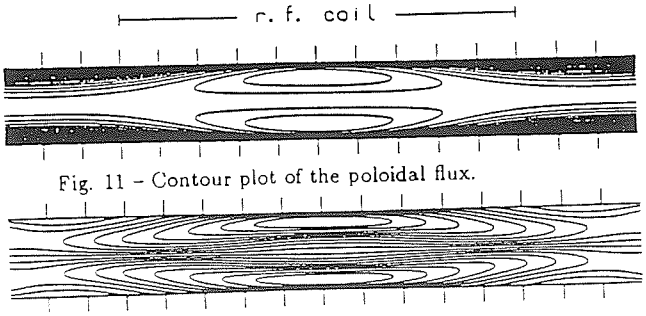

Fig. 11 – Contour plot of the poloidal flux.

Fig. 12 – Contour plot of the current density. Total current is 2600 Amps.

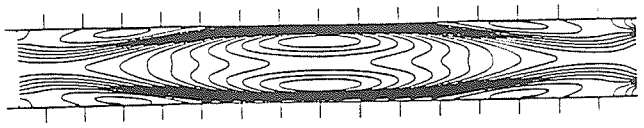

Fig. 13 – Contour plot of n_e. Peak n_e is 3.5×10^{13} cm^{-3} Contour spacing is 0.16×10^{13} cm^{-3}.

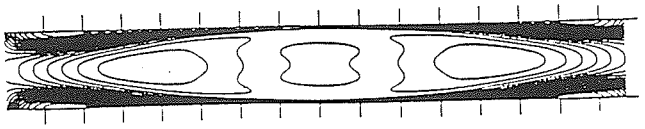

Fig. 14 – Contour plot of T_e. Peak T_e is 7.6 eV. Contour spacing is 0.36 eV.

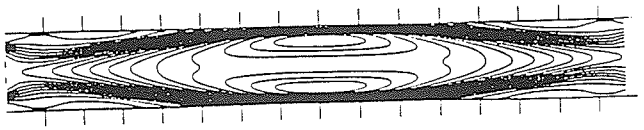

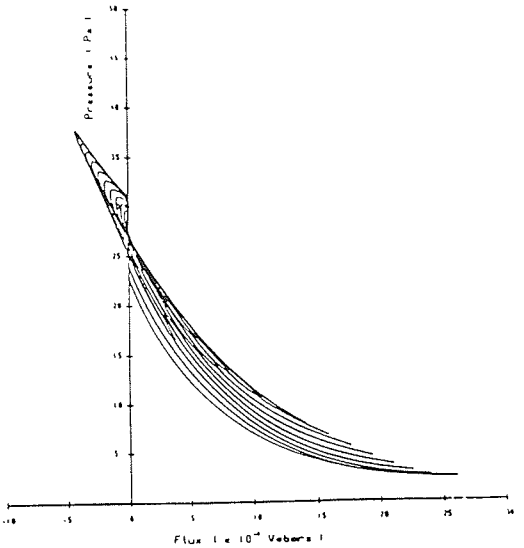

Fig. 16 – P_e (Pa) vs ψ (10^{-6} Wb)

	Metal Rotamak	FRC Rotamak
Frequency of Rotating Field	1 MHz	1 MHz
Gas	H_2	Ar
Pressure	1 mTorr	8 mTorr
Equilibrium Field	16 Gauss	40 Gauss
PLasma Current	600 Amps	2600 Amps
Pulse Duration	40 ms	40 ms

Table 1 – Experimental parameters. J_ϕ/r

REFERENCES

[1] e.g. Hugrass, W.N. *et. al.* (1980) *Phys. Rev. Lett.* 44, 1676.

[2] Kirolous, H. (1986) Ph.D. Thesis, Flinders University.

[3] Storer, R.G. (1982) *Plasma Physics* 24, 543.

ACKNOWLEDGEMENT

We gratefully acknowledge the financial support from the Australian Research Grants Scheme, The Australian Institute of Nuclear Sciences and Engineering and Flinders University Research Budget.

Fig. 15 – Contour plot of electron pressure P_e. Peak is 38 Pa. Contour spacing is 1.92 Pa.

A SMALL PLASMA FOCUS DEVICE FOR NEUTRON, X-RAY AND ELECTRON BEAM STUDIES

T.Y. Tou, K.H. Kwek, Y.C. Yong* and S. Lee
Department of Physics
University of Malaya
59100 Kuala Lumpur
MALAYSIA

ABSTRACT

A 2 kJ plasma focus is designed to operate at 10 kV for the purpose of studying electron beam and X-ray emissions in argon discharge. Preliminary testings in deuterium filling produce, over an average of 10 shots, $(1.0 - 4.5)\times10^{6}$ neutrons per shot over the pressure range of (2.5 - 5.0) mbar.

I Introduction

Recently, six sets of compact, cost-effective 3.3 kJ plasma focus have been successfully tested and delivered to various developing countries under the "United Nation University Training Programme on Plasma and Laser Technology" which was conducted at the University of Malaya, Kuala Lumpur, Malaysia in 1985. This compact plasma focus, called UNU/ICTP Plasma Focus Facility[14], was carefully designed, based on a dynamic model[1,2] to produce plasma in the plasma fusion regime for postgraduate teaching.

* Mathematics and Science Centre, Ngee Ann Polytechnic, Singapore.

Small Plasma Physics Experiments - Ed. S. Lee & P.H. Sakanaka, World Scientidic Publishing Co. (1988)

In response to that programme, a small plasma focus which is to be used primarily for X-ray and electron beam studies is immediately under consideration so that it may be added to the list of educational devices.

The reasons for designing yet another plasma focus are (1) argon gas is to be used because it is cheaper than deuterium, (2) lower operating voltage and (3) argon focus was found to produce more intense x-rays because of its smaller final pinch radius ratio[3,4] and high atomic number.

II The plasma focus device

The design parameters of this small plasma focus are very much borrowed from the 12 kJ Universiti Malaya Dense Plasma Focus 1 (UMDPF1)[5,6] which have been optimized geometrically for high neutron yield. With argon filling, the UMDPF1 has been found to produce strong and consistent focussing action at (9 - 14) kV and (1.0 - 3.0) mbar. Higher voltages and pressures than the above mentioned ranges were found to be undesirable. Electron temperatures as high as 5.0 keV were measured[3] using foil absorption technique[7,8]. X-ray pin-hole photographs[3] revealed the formation of an array of intense spots along the plasma column which may suggest strong local heating due to the m = 0 instabilities. Such adverse focussing action may produce more energetic electron beams than that of deuterium focus. The existence of a collimated beam of electrons having energies $\geq$ 100 keV and currents $\sim 10^2$ A in deuterium focus has been demonstrated by Harries et al[9] and Herziger et al[10] using X-ray techniques.

A 10 kV, 40 μF capacitor bank is chosen to power the focus tube. The design parameters , which closely resemble those of the UMDPF1, are summarised below:

Inner Electrode	Radius	: 0.95 cm
	Length	: 15.5 cm
	Effective length	: 12.3 cm
Outer Electrode	Radius	: 4.0 cm
	Length	: 16.0 cm
Glass Insulator	Radius	: 1.35cm
	Length	: 3.2 cm

III Experimental method

Figure 1 shows the detailed diagram of the small plasma focus tube and the vacuum chamber. A hollow inner electrode is chosen to allow electron beams, produced after the radial pinch phase , to propagate down the tube(see no.13) to be detected by various techniques. The inner electrode is designed such that its length is adjustable (see no.14) to facilitate any goemetrical optimization that may be necessary. The glass insulator(see no.6), coaxial to the inner electrode, is held by a rubber gasket(see no.15) which was designed and manufactured locally for the UNU/ICTP PFF and also for this device. A knife-edge (see no.14) is machined to promote uniform discharge during the initial high voltage breakdown at the glass insulator. The vacuum chamber is designed with diagnostic ports for X-ray measurements, streak photography, laser diagnostics and magnetic field measurements.

The whole experimental set-up is shown schematically in Figure 2. A single ignitron is used to switch the 10 kV, 40 μF capacitor bank during the preliminary operations. It will be replaced by a swinging-cascade-spark-gap.

IV Preliminary results

Since this system is designed with close reference to UMDPF1, the operating characteristics are expected to be like those of the UMDPF1 and it would be interesting to find out. Initial tests are thus carried out with deuterium filling with the expectation that this system should produce neutron at the higher pressure range of (1.0 - 7.0) mbar.

Foil activation technique[11,12,13] was used to monitor the neutron output. Over the pressure range (2.5 - 5.0)mbar , yields of $(1.0 - 4.5)\times10^{6}$ neutrons per shot were detected. This system is thus successfully tested to operate at a high pressure regime, avoiding the problem of restriking at the glass insulator, which normally would have happened in systems operating in the low pressure regime. Figure 3 shows the neutron yield variations with deuterium gas filling pressure. Each experimental data for the neutron yield is an average of 10 consecutive shots. It can be seen that the operating pressure range is rather narrow in contrast to the much wider range that is obtained from the UMDPF1.

V Future Work

It should be pointed out, from the analysis of the measured current waveform, that the 40 μF capacitor bank is delivering about 130 kA of current into the focus tube. The ignitron used is

of the type GL7703 which is specified to deliver peak current of 100 kA. Thus, the ignitron has been overloaded during the preliminary testings. It shall be replaced with a cost-effective, home-made swinging-cascade-spark-gap. This would improve the rise time of the discharge current and the neutron yield is expected to improve.

Measurements that are being planned for this device are:

(1) Electron beam measurements by current probe and Faraday cup

(2) Soft X-ray measurements by foil absorption technique and pin-hole photography.

VI Conclusion

A 10 kV, 2 kJ plasma focus has been sucessfully tested to produce strong focussing actions and neutron flux of $(1.0 - 4.5)\times10^{6}$ are measured over a pressure range of (2.5 - 5.0) mbar. The yield is comparatively low for a device of such energy range with peak current of 130 kA. It is believed that with some geometrical optimizations an improved yield can be expected. The device is also expected to produce consistent strong focussing actions with argon gas filling so that it can be operated as a cheap and efficient source of electron beams and X-rays.

References

1. S. Lee, in "Laser and Plasma Technology" edited by S.Lee, B.C. Tan, C.S.Wong and A.C. Chew, World Scientific, Singapore, p.37, 64 and 387 (1985)

2. S. Lee, in "Radiation in Plasma Physics" edited by B. Namara, World Scientific, Singapore 1984, Vol. II, p.78.

3 T.Y. Tou, Ph.D. thesis (Universiti Malaya), Malaysia (1987)

4. T.Y. Tou and S. Lee, Procs. First Tropical College on Applied Physics, Paper XIV, p.672 (1983).

5. Y.H. Chen, Ph.D. thesis (Universiti Malaya), Malaysia (1978).

6. S. Lee and Y.H. Chen, Spring College on Plasma Physics, ICTP, Trieste, Italy (1981). Published in Fusion Energy, IAEA-SMR-82, p.296-303(1981).

7. C.S. Wong, Ph.D. thesis (Universiti Malaya), Malaysia (1983)

8. F.C. Jahoda, E.M. Little, W.E. Quinn, G.A. Sawyer and T.F. Stratton, Phys. Rev. 119, 843 (1960).

9. W.L. Harries, J.H. Lee and D.R. McFarland, Plasma Phys., 20, 95 (1978)

10. G. Herziger, H. Krompholz, L. Michel, D. Schlieferbock and K. Schonbach, Phys. Lett. 69a, 37 (1978)

11. C.S. Wong, S.Lee and S.P. Moo , Mal. J. Sci., 6(B), p.167(1980).

12. Ch. Maisonnier, C. Gourlan, G. Luzzi, L. Papagno, F. Pecorella, J.P. Rager, B.V. Robouch, M. Samuelli, Plasma Phys. and Controlled Nuclear Fusion Research, (1971)

13. J.H. Lee, L.P. Shomo and K.H. Kim, Phys. Fluids, 15, 2433 (1972).

14. S. Lee, T.Y. Tou, S.P. Moo, M.A. Eissa, A.V. Gholap, K.H. Kwek, S. Mulyodrano, A.J. Smith, Suryadi, W. Usada and M. Zakaullah. American J. Phys. 56, 62 (1988); also J.Fiz.Malaysia 7, 1 (1986)

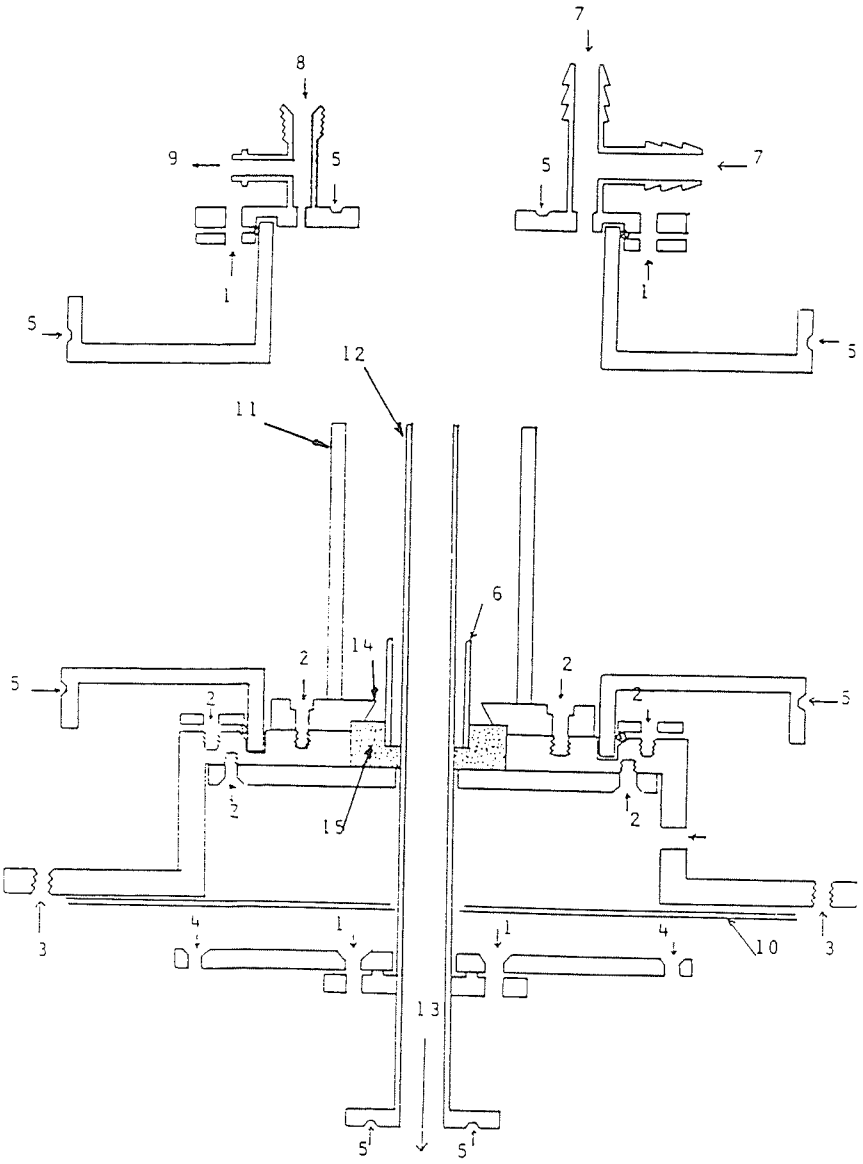

Figure 1 Detailed diagram of the plasma focus device.
1: to be tightened with screw and nut
2: to be tightened with screw only
3: tightened to the return of the coaxial cables
4: tightened to the centre-core of the coaxial cables
5: 'O'-ring groove; 6: glass insulator; 7: gas inlet
8: to pressure gauge; 9: to rotary pump; 10: mylar sheets
11: outer electrode rod; 12: inner electrode
13: direction of electron beam propagation
14: knife-edge; 15: rubber gasket

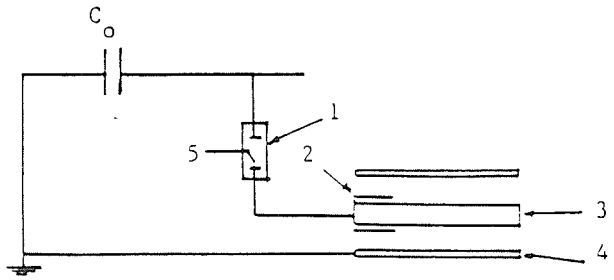

Figure 2 Schematic of the experimental set-up of the 10 kV, 2 kJ plasma focus

C_o : 40 μF capacitor bank
1 : Ignitron
2 : glass insulator
3 : Inner electrode
4 : Outer electrode
5 : Trigger pulse to ignitron

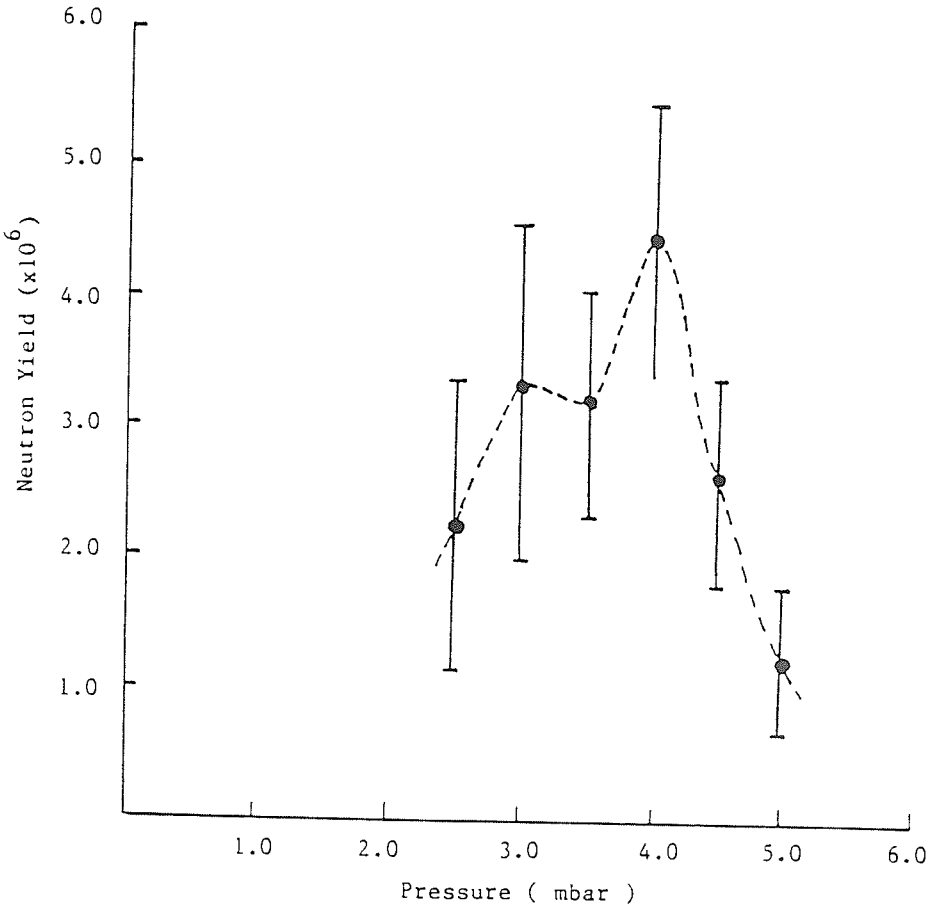

Figure 3 Neutron yield as a function of deuterium pressure

A TEA nitrogen laser for optical diagnostics of the plasma focus

K.H. Kwek, T.Y. Tou and S. Lee
Department of Physics
University of Malaya
59100 Kuala Lumpur
Malaysia

Abstract

A simple and compact TEA nitrogen laser suitable for interferometric measurements on the plasma focus has been realised. Homogeneous beam quality having output energy of about 300 μJ and 1 ns pulse duration is easily obtained. This laser can also be used for Schlieren and shadow photography.

I Introduction

Optical probing of the nanosecond time scale of the dynamic processes in the dense plasma focus requires light sources of short duration and high intensity. Towards this end, the nitrogen laser remains the best light source from the point of view of the pulse duration, intensity and wavelength. With the nitrogen laser, probing of electron density in the plasma up to a critical value of about $n_e \simeq 10^{28}$ m^{-3} ($n_e = 1.115 \times 10^{15} / \lambda^2$ m^{-3}, where λ = 337.1 nm) can be achieved. In nitrogen lasers, excitation at atmospheric pressures yield short duration light pulses down to picosecond range[1,2].

This paper describes a simple and compact transversely excited atmospheric (TEA) nitrogen laser with pulse duration and energy of the order of 1 ns and 100 μJ suitable for optical diagnostics such as shadow and schlieren photography. A method of preionisation introduced into such design ensures the production of good quality laser beam that renders the laser useful for

Small Plasma Physics Experiments - Ed. S. Lee & P.H. Sakanaka
World Scientific Publishing Co. (1988)

interferometry work. These lasers can be constructed at modest expense.

II The nitrogen laser

The construction of the TEA nitrogen laser shown in Fig. 1 is similar to that discussed in our earlier papers[3,4] except for the design of the laser channel. The circuit theory of the parallel plate transmission line type of laser has been discussed in previous papers[3,4,5]. The two energy storage capacitors C_1 and C_2 of the Blumlein circuit consist of a common earth plate, which is a 22 x 60 cm strip of aluminium kitchen foil laid on top of a flat brass plate (for electrical contact and support). On top of the foil are laid 3 sheets of 2 mil mylar which extends at least 10 cm beyond the edges of the conductors all around. The high voltage plates of C_1 and C_2 are 22 x 17 cm and 22 x 40 cm strips of aluminium foil laid on top of the mylar sheets. These high voltage capacitor plates are separated by a gap of 1.5 cm over which the laser channel is placed so that each side of the channel (Fig. 1a) makes pressure contact with one of the capacitors. On top of the foils are placed glass plates (6 mm thick) of appropriate dimensions to prevent mechanical flexing of the foils during charging and discharging of the capacitors. The measured values of C_1 and C_2 are 15 and 6 nF respectively. The capacitor C_2 is mounted to a swinging cascade trigger spark gap.

The two electrodes of the laser channel of 20 cm long are made of $\frac{1}{2}$ inch brass rods soft soldered on to brass strips with cross-sectional dimensions of $\frac{1}{4}$ x 1 inch and 20 cm long. All strips and rods are carefully polished with the edges well

rounded to prevent corona. The laser channel is enclosed in a perspex chamber. Admission and evacuation of the nitrogen gas at atmospheric pressure is made through the middle and the ends of the tube respectively. The interelectrode separation can be adjusted to give optimum laser pulse energy.

III Measurements and performance

An interelectrode distance of 3 mm gives optimum laser energy output of about 100 μJ at a charging voltage of 15 kV. The laser pulse duration was measured with a fast FND-100 photodiode and a storage oscilloscope (Tektronix 7834) giving a pulse width of 2 ns. However, we believe that the duration is ~1ns , taking into account of the time resolution of the measuring system.

The laser was used to observe the macroscopic behaviour of plasma focus discharges using the techniques of shadowgraphy, schlieren photography and interferometry. Details of the Mather type plasma focus devices used have been reported elsewhere[6,7]. Fig. 2 shows a sequence of shadowgrams depicting the temporal development of a plasma focus discharge of the 12 kJ UMDPF1 device from the collapse phase to the disruption of the plasma column and the formation of the ionising wavefront. Time reference is taken with respect to the peak of the characteristic voltage spike of the voltage signal. Fig. 3 shows a schlieren photograph of a plasma focus column being disrupted by m=0 instability. The photograph was taken on another optical set-up on the 2 kJ small plasma focus device but using the same laser.

When the laser was used with the Mach-Zehnder interferometer the interferograms (fringe pattern obtained by tilting one of the

mirrors to produce background fringes) obtained were of poor quality as shown in Fig. 4. The fringes are barely discernable due to the presence of vertical striations. These poor quality interferograms resulted from the use of poor quality laser beams which are inhomogeneous and not uniform in intensity. Such inhomogeneity and non-uniformity in the beam can be seen more clearly by expanding the beam several times its original size. Examination of the discharge across the laser channel revealed the presence of streamer-like filaments along the discharge channel. At several locations, formation of electrical arcs were observed. These streamers and arcs disturbed the homogeneity of the laser beam. Thus, whilst the laser has been succesfully employed in shadowgraphy and schlieren photography, its beam quality needs improvement to enable it to be utilised in interferometry work where the requirment is more stringent.

IV Preionisation and modifications

Experiments[8,9] revealed that for the production of uniform high pressure glow discharges some kind of preionisation is indispensable. One such method, introduced by Hasson and Bergmann[10] is the use of corona blades where the sharp edges are leading to high electric fields strengths thus providing the extraction of free carriers. These blades act as auxilliary corona electrodes which serve to provide an initial distributed corona discharge to photoionise and prepare the main gap for glow formation.

The laser channel electrodes are replaced by another set

designed to include the use of corona blades. The new electrodes are made from 20 cm long brass strips with cross-sectional dimensions of ½ x 1 in and shaped as shown in Fig. 5. In the arrangement shown, the capacitors C_1 and C_2 are similar to the ones used earlier except that the edges of the high voltage capacitor plates (aluminium foils) are allowed to protrude beyond the edges of the laser electrodes to act as corona blades. These form the set of blades on the lower side of the laser channel. Similar set of corona blades are placed on the upper side of the laser channel. The laser channel gap is set to 3 mm while the blade separation, while not very critical, is typically set to about 40% greater than that of the main gap. The strips of mylar sheets serve to help the formation of corona discharges. A perspex plate is screwed onto the laser electrodes on the upper side. A hole in the middle of the plate allows the introduction of nitrogen gas into the channel.

With the presence of the preioniser, the discharge along the channel is observed to be a uniform glow discharge without the presence of arcs or filaments. Whilst the pulse duration remained unchanged, the energy output has improved to about 300 μJ. More importantly, the beam quality has improved giving a very uniform and homogeneous laser output. This can be seen from the interferograms shown in Fig. 6.

V Conclusion

The TEA nitrogen laser described is a powerful light source for optical diagnostics of transient and dense plasmas. It has the advantage of being simple to construct and inexpensive. With

suitable electrode designs and the use of supplementary preionisation corona blades, the laser can be used for set-ups like the Mach-Zehnder interferometer where the requirements on the optics are stringent.

References

1. H. Strohwald and H. Salzmann, Appl. Phys. Lett. 28, 272 (1976)
2. J.T. Lue, IEEE Trans. Instrum. Meas. IM-34, 436 (1985)
3. K.H. Kwek, A.J. Smith, T.Y. Tou, A.V. Gholap and S. Lee, J. Fiz. Mal. 7, 125 (1986)
4. A.J. Smith, K.H. Kwek, T.Y. Tou, A.V. Gholap and S. Lee, IEEE J. Quantum Electronics, QE-23, 283 (1987)
5. S. Lee, A.V. Gholap, A.J. Smith, K.H. Kwek, A.C. Chew, T.Y. Tou and S. Sapru, J. Fiz. Mal. 6, 165 (1985)
6. S. Lee and Y.H. Chen, Spring College on Plasma Physics, ICTP, Trieste, Italy (1981). Published in Fusion Energy, IAEA-SMR-82, p.296-303 (1981)
7. T.Y. Tou, S. Lee, K.H. Kwek and Y.C. Yong, "A small plasma focus device for neutron, X-ray and electron beam studies", (this proceeding)
8. V. Hasson, D. Preussler, J. Klimek and H.M. von Bergmann, Appl. Phys. Lett. 25, 1 (1974)
9. N.A. Kurnik, S.J. Tubbs, K. Bidhichand, L.W. Ryan Jr. and A. Javan, IEEE J. Quantum Electronics, QE-11, 174 (1975)
10. V. Hasson and H.M. von Bergmann, J. Phys. E. Sci. Instrum., 9, 73 (1976)

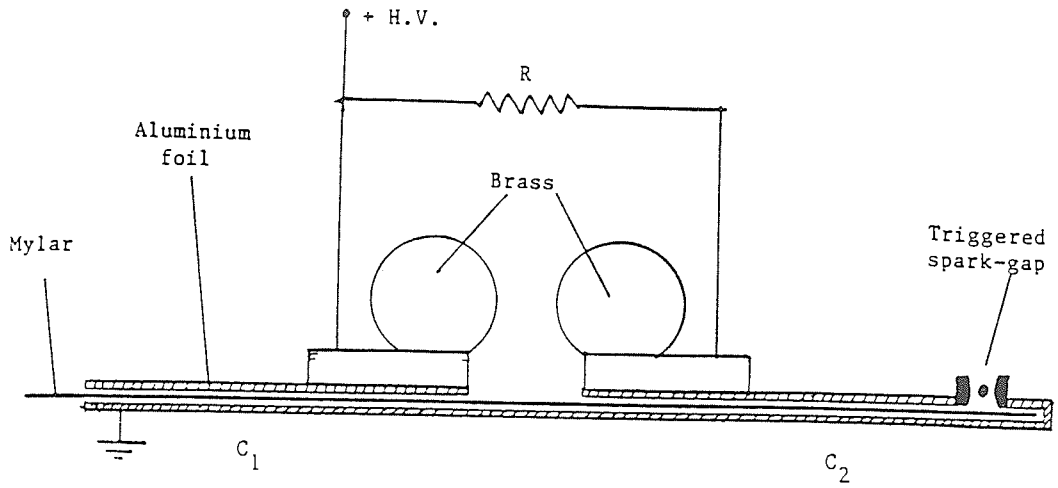

Figure 1a Cross-sectional view of the TEA nitrogen laser (The perspex chamber is not shown)

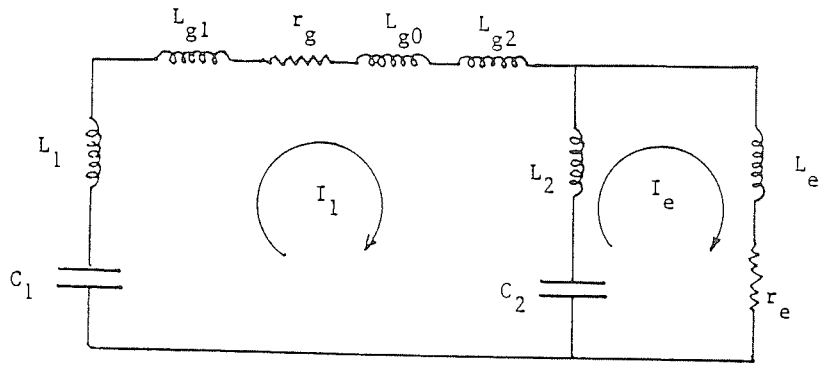

Figure 1b The equivalent circuit of the nitrogen laser.

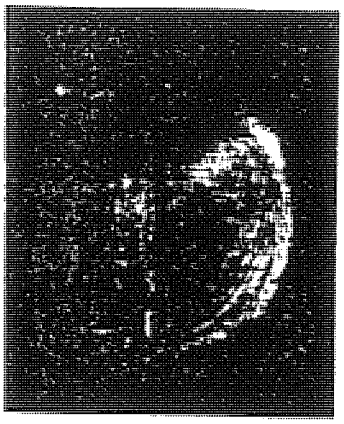

t = -60 ns

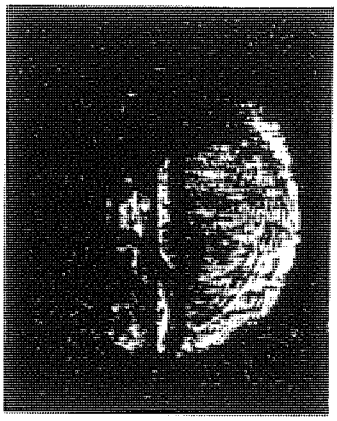

t = -30 ns

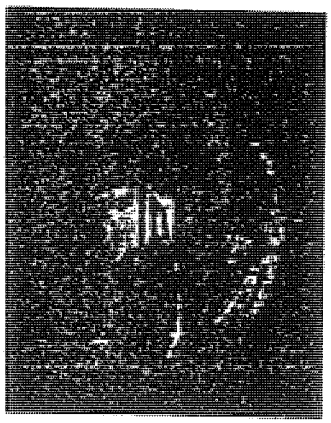

t = + 10 ns

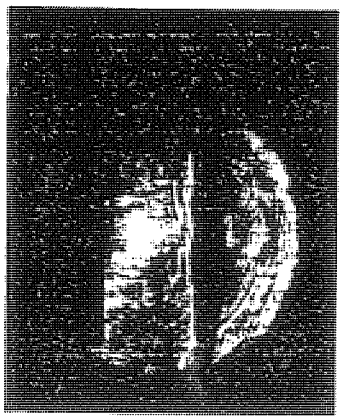

t = + 20 ns

Figure 2 Example of four shadowgrams obtained on plasma focus discharges of the UMDPF1 device operated in deuterium (8 mbar) at 15 kV.

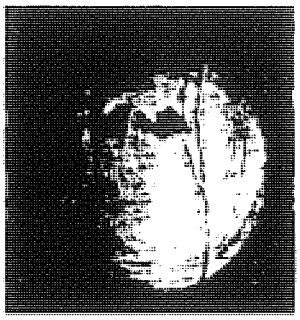

Figure 3 Example of a schlieren photograph taken on a plasma focus discharge of the small focus.

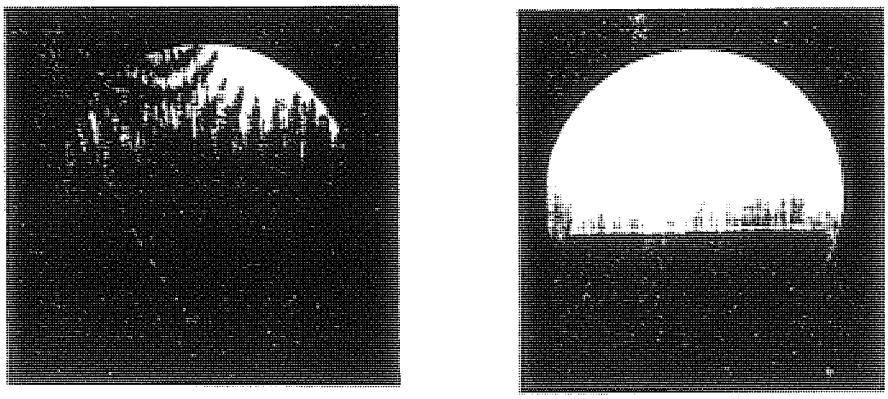

(a) (b)

Figure 4 Examples of the poor quality interferograms obtained.
(a) interferogram with coarse fringe pattern
(b) interferogram with fine fringe pattern.
In both interferograms the fringes are barely discernable.

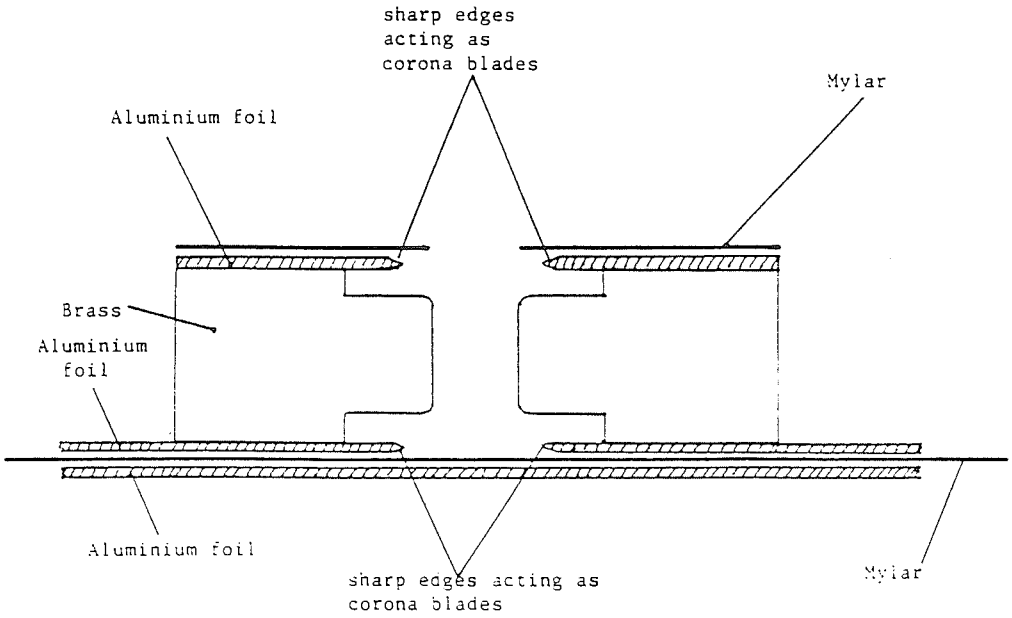

Figure 5 Cross-sectional view of the modified laser channel showing the inclusion of corona blades using aluminium foils. (The perspex cover plate is not shown)

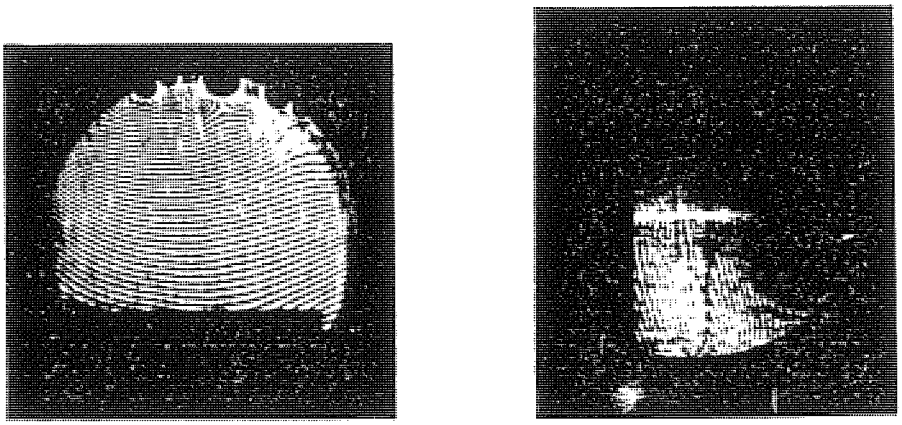

(a) (b)

Figure 6 Examples of the interferograms obtained with the improved laser. Interferogram (a) is a background fringe pattern. The fringes are clearly seen. Interferogram (b) is taken on a plasma focus discharge of the UMDPF1 showing the fringe shifts due to the presence of the plasma.

The Design, Construction and Performance Studies of a Linear Z-Pinch for Current-Stepping Experiments.

S.H.Saw, C.S.Wong, S.Lee
Plasma Research Laboratory
Physics Department
University of Malaya
59100 Kuala Lumpur
Malaysia

Abstract

The Slug Model and the Energy Balance Theory are used in the designing of a 2.4 kJ linear Z-pinch machine. The machine has a discharge radius of 7.5 cm and an axial length of 15 cm. It is powered by a 60 μF capacitor bank operated at 9 kV. The rate of rise of current is 8.1×10^{10} A/s. Preliminary observations on Hydrogen discharges at 0.8 mbar indicate consistent pinching at an average shock speed of 3.8 cm/μs giving a final plasma column of radius 2 cm when the shock front hits the axis at 2 μs after the start of the discharge. The low shock speed is deliberately designed to facilitate the implementation of current-stepping to study compression enhancement.

Small Plasma Physics Experiments - Ed. S. Lee & P.H. Sakanaka
World Scientific Publishing Co. (1988)

Introduction

The Z-pinch has recently received rekindled interest due to the proposed possibility of obtaining a final column of enhanced compression which fulfils the Lawson criterion and at the same time has enhanced stability due to the finite Larmor radius effect[1]. There have been several proposals for pinch compression enhancement. Among them, Lee[2] has proposed the technique of current-stepping as a prelude to radiation collapse. This technique relies on the fact that when an equilibrium pinch radius ratio is approached as defined by the energy balance condition, it is possible to shift the equilibrium pinch radius ratio to a reduced value by rapidly increasing or stepping up the driving current since the equilibrium pinch radius ratio depends only on the time-form function of the current shape. Numerical computation based on the slug model indicates a reduction factor of 2 for the final pinch radius ratio which corresponds to a density compression factor of 4 with the superposition of a second fast rising current profile at an appropriate instant. A Z-pinch machine is designed for the study of the current-stepping technique. It is driven by a slow bank and has a relatively large radius for such a low energy system. The resulting compression and final radius of the plasma column will be relatively slow and large respectively. This is to facilitate the implementation of current-stepping via the introduction of a second faster bank (as compared to the first); and any reduction in the radius of the final plasma column as a result of current-stepping can be also observed and measured easily.

I. The design and construction of the linear Z-pinch machine.

The generalised slug model[3,4,5] is used in the design of the Z-pinch machine. According to this model, a slug of plasma implodes inward between a shock front and a driving magnetic piston. The imploding pinch dynamics can be divided into 2 consecutive phases; namely the strong shock compression phase and the slow dynamics phase. The characteristic pinch time, t_p is given by

$$t_p = \left[\frac{\rho_o}{\mu_o(\gamma+1)}\right]^{\frac{1}{2}} \frac{4\pi r_o^2}{I_o} \qquad (1)$$

where ρ_o is the ambient gas density, r_o is the radius of the pinch tube, I_o the constant discharge current, γ the specific heat ratio and μ_o the permeability of free space.

The first design consideration is to match the expected pinch time to the current rise-time, t_r. For a L-C discharge, the current rises sinusoidally to about $0.7I_o$ where $I_o=V_o/(\sqrt{L_o/C_o})$ and V_o, L_o and C_o are respectively the initial discharge voltage, the total external inductance of the system and the capacitance of the bank. Therefore the equilvalent constant current is about $0.45\ I_o$. From equation (1), the expected pinch time, $t_{p'}$ becomes

$$t_{p'} = 2.2\ t_p \qquad (2)$$

Also, the current rise-time is given by

$$t_r = \frac{2\pi}{4}\sqrt{L_o C_o} \qquad (3)$$

Thus for proper time matching,

$$t_r = t_{p'} = 2.2\ t_p \qquad (4)$$

The second design consideration in designing a pinch machine is to provide a good energy coupling between the capacitor bank and the pinch machine. This has been shown to be governed by the parameter

$$\beta = \frac{\mu_o\, l}{2\pi L_o} \qquad (5)$$

where $\mu_o\, l/2\pi$ is the characteristic inductance of the pinch tube of length l cm and L_o is the total external inductance of the system. Computation using the generalised slug model[5] shows that for good energy coupling, a value of $\beta > 0.1$ is necessary.

The availability of a capacitor bank provides the starting point for the design work carried out here. In the present case, a 60 μF, 10kV capacitor bank consisting of 3 units of 20 μF, 10 kV capacitors with an equilvalent series inductance of 40 nH each connected in parallel is used. The total external inductance is estimated to be 73 nH. Having fixed C_o and L_o, using equation (3), the current rise-time is found to be 3.2 μs. From equation (4), t_p is fixed at 1.5 μs. This gives $a = t_o/t_p$ as 1.4 where $t_o = \sqrt{L_o C_o}$. For a pinch of average pinching speed of 3 cm/μs (maximum speed of 10 cm/μs) a pinch tube of initial radius of 9 cm is appropriate. However, due to practical constraints, the radius of our pinch tube has been fixed at 7.5 cm. The average pinching speed is then 2.5 cm/μs. From equation (1), the suitable operating pressure for the pinch can be calculated. For a 9 kV discharge in Hydrogen, the suitable pressure is 1.3 mbar.

Having fixed r_o, we must now fix the length of the axial pinch. A length of 15 cm is chosen giving a value of $\beta = 0.4$.

From the above considerations, the following parameters are arrived at for the pinch tube;

C_o = 60 μF

L_o = 73 nH

V_o = 9 kV

r_o = 7.5 cm

l = 15 cm

ρ_o = 1.0×10^{-4} kgm^{-3} (P=1.3 mbar H_2)

which give the following parameters;

I_o = 258 kA

t_o = 2.1 μs

t_r = 3.2 μs

$(dI_o/dt)_{t=o}$ = 8.1×10^{10} A/s

t_p = 1.5 μs

$t_{p'}$ = 3.2 μs

α = 1.4

β = 0.4

The construction of the Z-pinch machine is as shown in Fig. 1. The chamber is a glass cylinder of length 21 cm and diameter 15 cm with thickness of 6 mm. The discharge length is 15 cm. The anode and cathode are in the form of annular rings (with ten 6mm diameter rods, length 5 cm extending radially inwards) made from brass. The current return is via a squirrel-cage to another brass ring adjacent to the anode and insulated by a perspex cap.

The discharge circuitry is as shown in Fig. 2. Three units of 20 μF, 10 kV capacitors each with equilvalent series inductance of 40 nH

are connected using parallel plates in series to a swinging cascade spark gap[6] to the anode of the Z-pinch machine. The parallel plate configuration is used for capacitors connection to reduce inductance. The schematic of the capacitor and the swinging cascade is shown in Fig. 3. The swinging cascade spark gap is set to hold 9 kV and break down when the triggering pin is supplied with a negative pulse of 10.6 kV(rise-time 3 μs). The negative pulse is supplied by a high voltage SCR (HVSCR) of output approximately 700 V stepped up to the required 10.6 kV by a television transformer.

II. Testing with Numerical Model.

The dyanamics of the Z-pinch designed above can be visualised by performing the computation using the slug model with $\alpha=1.4$ and $\beta=0.4$. The results obtained are shown in Fig. 4. The current waveform and the corresponding voltage spike which are observed at the time of minimum compression are typical features of a Z-pinch discharge.

III. Preliminary Observations.

The discharge tube is evacuated to a base pressure of 10^{-3} mbar. It is then flushed with Hydrogen gas for a number of times before filling to the required pressure. The current and voltage signals and streak photography of the discharge are recorded simultaneously(Fig.5). Voltage measurement is by means of a capacitive probe incorporated to the system while the Rogowski coil is used to

record the current signal. Fig. 6 shows a typical set of results obtained for a 9 kV H_2 discharge at a filling pressure of 0.8 mbar H_2. The shock front is observed to consistently hit the axis at about 2.0 μs from the start of the discharge with an average shock speed of 3.8 cm/μs. From the streak photograph, it is observed that when the shock front hits the axis, the plasma collapse to a column of radius 2 cm which further compresses to a radius of 1.0 cm at about 0.2 μs later. On comparison with numerical computation with $\gamma=5/3$, it is found that the radial trajectory decreases faster experimentally. From estimation of magnetic Reynold number, it is found that the compression is rather diffusive at the early stage of the pinch, which accounts for the faster compression and smaller final radius achieved. Numerical computation using the slug model with the correction for the specific heat ratio, γ and with the mass loss factor incorporated supports this conclusion. The γ-correction is necessary because for most part of the compression the shock speed is slow and corresponds to $\gamma=1.2$. At the final compression γ increases to about 1.4.

As a more complete sweeping of the gas particles by the magnetic piston during the first compression is an important prelude to current-stepping, the Z-pinch machine needs to be optimised first to improve the electromagnetohydrodynamic coupling between the piston and the gas.

IV. Conclusion.

The Z-pinch machine for current-stepping is designed based on the slug model. Preliminary observations indicate that consistent pinching of the plasma column is achieved. For a 9 kV discharge at

0.8 mbar H_2, it is observed that at the pinch time of 2.0 μs the average shock speed is 3.8 cm/μs and a plasma column of radius 2 cm is obtained. Once optimised, this machine is suitable for the study of the effect of current-stepping on the enhancement of pinch compression. Its relatively slow compression and large final plasma column would facilitate the observation of the reduction in the radius of the plasma column due to the effect of current-stepping.

References.

1. Haines MG, Phys. Scr., T2/2, 380-390 (1982)
2. S.Lee, J. Phys.D:Appl. Phys., 17, 733-741 (1984)
3. J.Ali, S.Lee,T.Y.Tou & Y.C.Yong, J.Fiz.Mal., 5, 153-162 (1984)
4. D.E.Potter, Nuclear Fusion, 18, 813 (1978)
5. S.Lee, J.Phys.D:Appl. Phys., 16, 2463 (1983)
6. A.J.Smith,Suryadi,Jasbir Singh & S.Lee, Procs.2nd Trop. Coll. on Appl.Sc., Laser & Plasma Tech.,K.Lumpur,M'sia (1986) - To be published.

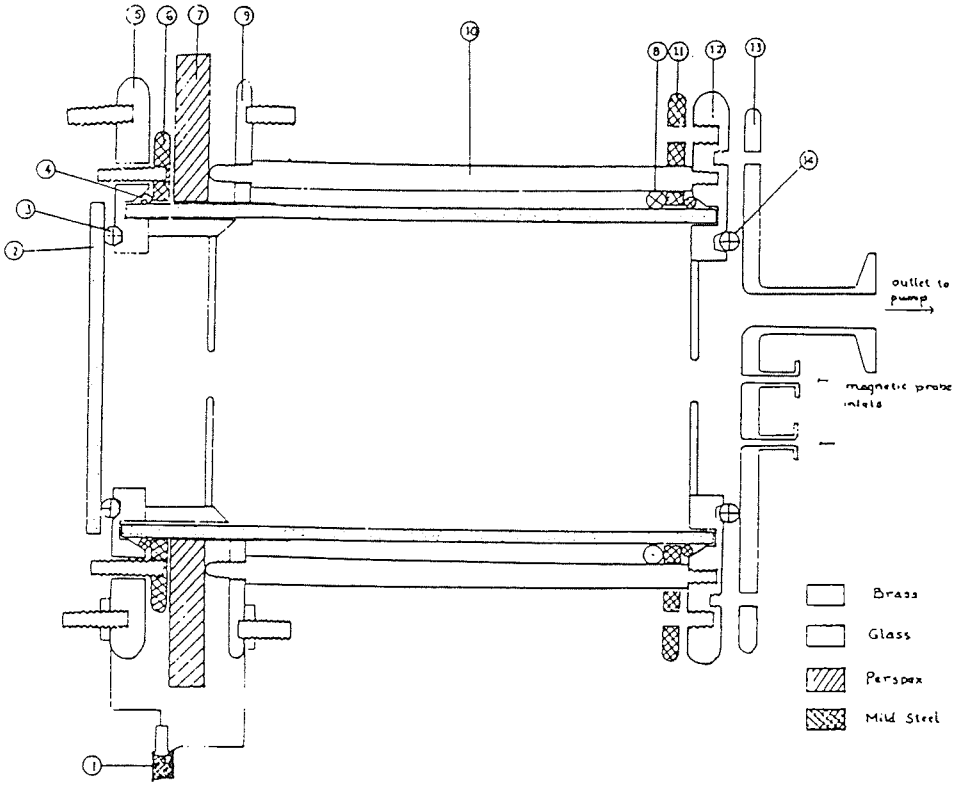

Fig. 1 Design of the linear Z-pinch.

1. Input coaxial cables
2 Glass plate
3. O-ring seal
4. O-ring seal
5. Anode collector plate
6. Mild steel flange
7. Perspex insulating cap
8. Rogowski coil
9. Cathode return plate
10. Cathode return bars
11. Mild steel flange
12. Cathode collector plate
13. Back flange
14. O-ring seal

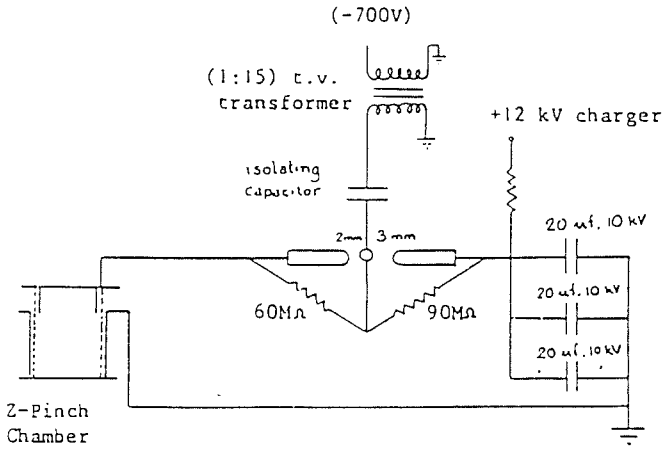

Fig. 2 Discharge circuitry of the linear Z-pinch.

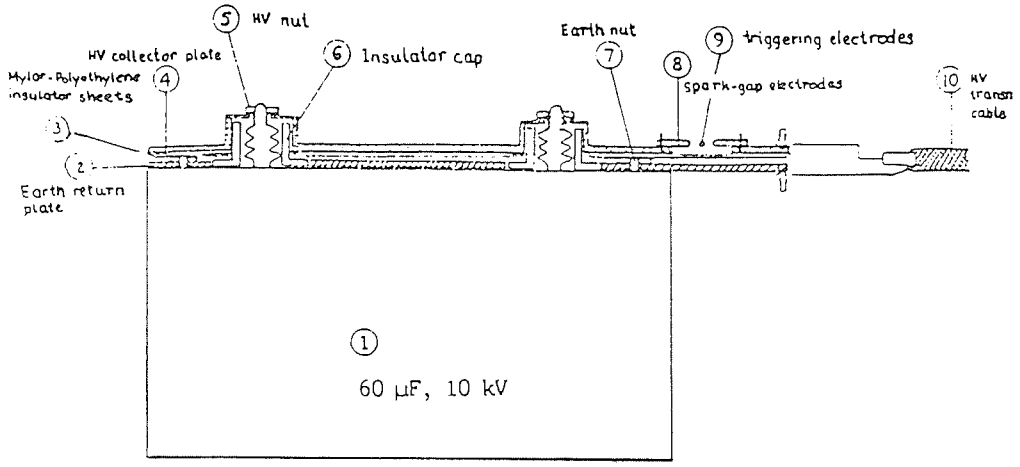

Fig. 3 The capacitor and spark-gap connections.

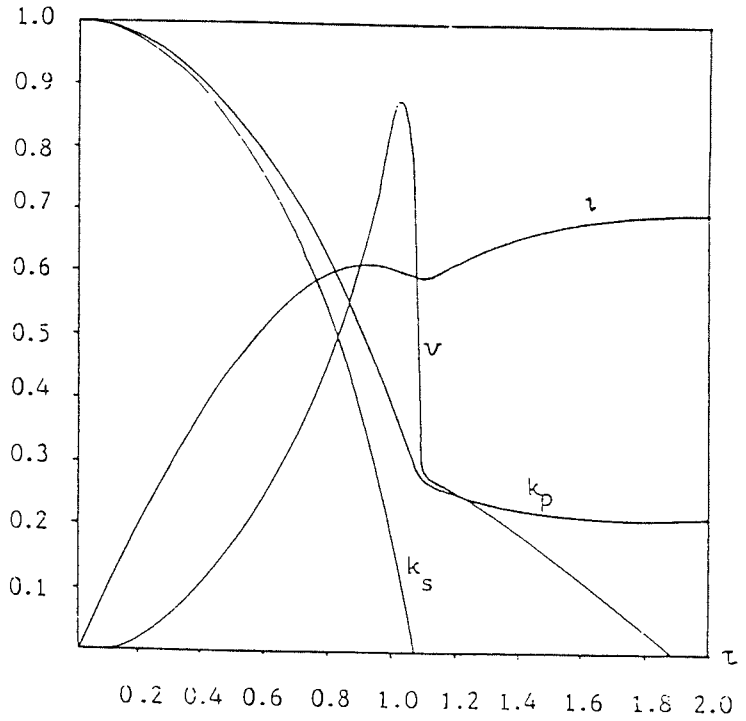

Fig. 4 Computed dynamics of the designed Z-pinch machine with $\alpha = 1.4$ and $\beta = 0.4$.
(k_p = normalised piston trajectory, k_s = normalised shock trajectory, ι = normalised current, υ = normalised voltage, τ = normalised time.)

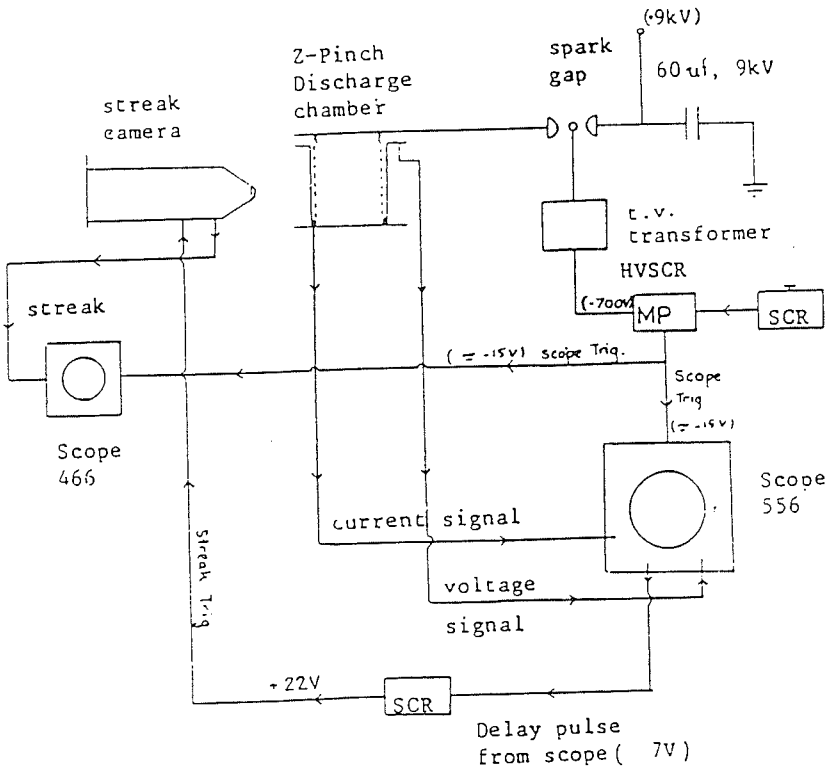

Fig. 5 A schematic of the linear Z-pinch experimental set-up.

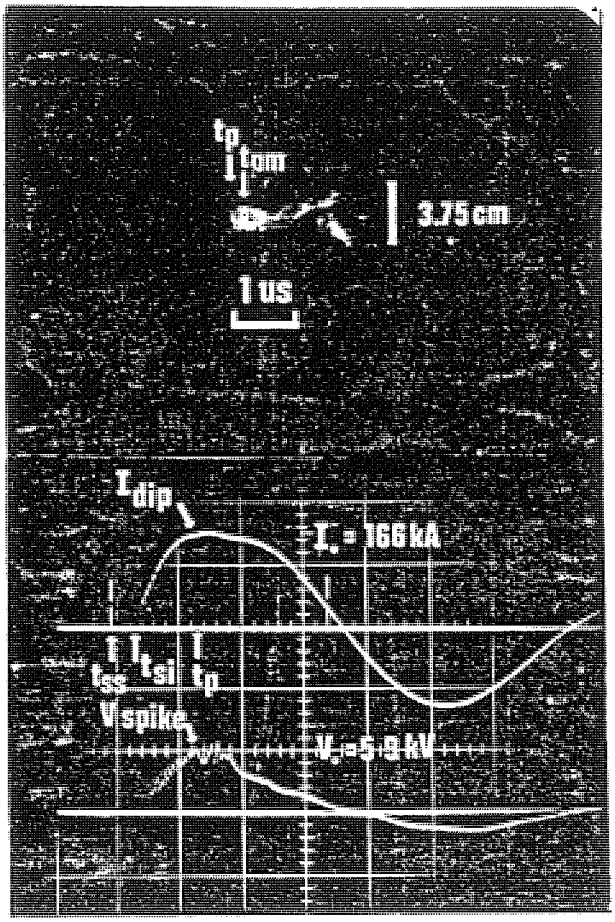

Scale:
108 kA/cm,
2 μs/cm

Scale:
5.625 kV/cm
2 μs/cm

Fig. 6. Top : Streak picture of Hydrogen discharge at 0.8 mbar.
Bottom : Corresponding current and voltage pulses.
(t_{ss} is the start of the streak pulse,
t_{si} is the start of the current pulse,
t_p is the pinch time.)

STREAK LASER SHADOWGRAPHY OF THE PLASMA FOCUS

T.Y. Tou*, E.H. Yee**, B.C. Tan and S. Lee

Plasma Research Laboratory
Physics Department, Universiti Malaya
59100 Kuala Lumpur, Malaysia

Abstract

A home-made dye laser with lasing wavelength centering at $\lambda \sim 4850$ Å is used as a light source for the streak mode of shadowgraphy. This optical diagnostic system finds a useful application in the study of the radial pinch dynamics in the plasma focus discharge, particularly in noble gases such as argon.

Introduction

Pulsed dye-lasers can now be generated at any wavelength from the near-UV to the near-infrared using both flashlamp and laser pumping. Most applications of dye lasers reported so far depend on their unique capability to be tuned continuously over a wide range of wavelength. Some of the applications are Raman Scattering[1], Resonance Fluorescence[2,3,4], atmospheric pollution detection[5,6] and LIDAR[7,8,9].

For optical disgnostics in transient plasma discharges, the technique of mode-locking has been employed in dye-laser systems to generate a train of sub-nanosecond pulses for stroboscopic schlieren photography of the radial pinch dynamics in the plasma focus[10,11].

The streak mode of interferometry in plasma focus have also been demonstrated using He-Ne[12] and ruby[13] lasers. In this paper, we demonstrate the feasibility of using a home-made dye laser[21] for the streak mode of shadowgraphy in plasma focus experiment.

Present address:

*Plasma Research Laboratory, R S Phys. Sc. I.A.S.,
Australian National University, ACT 2601, Australia.

**Intel, Penang, Malaysia.

The information thus obtained on plasma dynamics is of great importance in the study of compression dynamics[22] in general and specificially for the plasma focus in which it has been recently suggested[23] that the neutron yield could be much more sensitive to the compression velocity than indicated by accepted scaling laws.

Shadow Method

Basically the shadow method[14,15] depends upon the second derivative of the refractive index μ of the medium to be investigated. When a probing beam of parallel light rays tranverses a medium along the x-direction, as shown in Fig. 1a, the distribution of the refracted light intensity will be uniform if $\partial\mu/\partial y$ is a constant. There will, however, be a non-uniform distribution of refracted light intensity of $\partial^2\mu/\partial y^2 \neq 0$, as shown in Fig. 1b, and the total fractional change ΔI in the light intensity I is given by

$$\sum\frac{\Delta I}{I} = \ell\int_o^L \frac{1}{\mu}\left(\frac{\partial^2\mu}{\partial y^2} + \frac{\partial^2\mu}{\partial z^2}\right) dx \qquad (1)$$

considering also that contributed by $\partial^2\mu/\partial z^2$ in the z-direction. The term L is the thickness of the medium and ℓ is the distance of the screen, on which the shadow effect is captured, from the medium.

This equation is rewritten as

$$\sum\frac{\Delta I}{I} \simeq -1.05 \times 10^{-22}\ \ell\int_o^L \left(\frac{\partial^2 Ne}{\partial y^2} + \frac{\partial^2 Ne}{\partial z^2}\right) dx \qquad (2)$$

by substituting into it

$$\mu = 1.0 - 1.05 \times 10^{-22}\ Ne\ . \qquad (3)$$

where Ne is the electron density.

The numerical co-efficient of Ne is calculated with known parameters in our plasma focus[15] and with the dye laser wavelength centering at $\lambda \sim 4850$ Å. The fractional change in the refracted light intensity is, therefore, dependent on the second derivative of the electron density.

Experimental Set-up

Figure 2 shows schematically the experimental set-up of the streak mode of laser shadowgraphy in the plasma focus facility-UMDPF[16,17]. The

dye-laser system[18] employs a coaxial flashlamp for optical pumping which, in turn, is powered by a 25 kV, 3 μF capacitor bank. For this experiment, the capacitor bank is charged to 14-16 kV. The lasing medium is a solution of Coumarin-480 dissolved in methanol at 7.5×10^{-4} mole of concentration. The lasing wavelength spreads from 4750 Å to 4950 Å with a pulse width (FWHM) ≈ 0.6 μs, as shown in Fig. 3.

A uniform laser beam of 5 cm diameter is obtained by means of a small diaphragm, beam expander and collimator. This beam is guided to capture the radially collapsing plasma sheath off the end of the inner electrode. In order to see the shadow effect on the translucent screen which stops the laser beam, a narrow band pass filter with its greatest transmission at or near λ is used to exclude the visible plasma light.

A streak camera is used to record the temporal changes of the shadow on the translucent screen and for this technique, one has to limit its observation to a small cross-section Δz of the Z-pinch like plasma column. This is done by placing a narrow slit, externally, on appropriate position between the translucent screen. Neglecting, if any, the changes in the electron density profile in this small section Δz in the z-direction, the temporal fractional changes in the refracted light intensity along the slit is then written as

$$\left[\frac{\Delta I(t)}{I(t)}\right] = -1.05 \times 10^{-22} \, \ell \int_0^L \frac{\delta^2 Ne(t)}{\delta y^2} \, dx \qquad (4)$$

for a time-dependent electron profile Ne(t) during the radial pinch phase.

The streak camera is properly timed to record the shadow changes within its streak span.

Results

The above mentioned time-resolved shadowgraphy has found an useful application in studying the radial pinch dynamics in the argon focus. Figure 4a shows a streak image of the radial pinch (of collapsing plasma sheath) in the argon focus, operating at 15 kV and about 2 mbar. When the plasma sheath collapses onto the axis, a comparatively enomorous amount of visible luminosity is recorded and this often over-exposes the polariod film (Type 667) used. The non-uniform emission of visible

plasma light at different times in argon focus poses a problem in setting an appropriate aperture[19].

Figure 4b shows a laser shadowgram in the streak mode for the argon focus. As long as the laser beam is uniform during the radial pinch phase of the argon focus, the shadow effect is distinctly recorded. The problem of appropriate aperture setting for admitting non-uniform plasma light reduces to that for sufficient illumination by laser beam. The spatial resolution of the shadow of the plasma sheath depends also on the width of the narrow slit behind the transluscent screen. The narrow slit in this experiment has a width $\lesssim$ 0.3 mm set by a spacer of known dimension and provides sufficient spatial resolution for the temporal changes of the shadow of the plasma sheath.

Conclusion

The home-made dye laser employing Coumarin-480 at 7.5×10^{-4} molar concentration as laser medium has found an application in the streak mode of the laser shadowgraphic study of the plasma focus dynamics in its radial pinch phase. This optical diagnostic method is particularly useful in recording the shadow effects of the radially collapsing plasma sheath in argon focus and for studying the specific heat ratio effect[20] on compression. A uniform laser beam is easily obtainable by means of a diaphragm with which uniform illumination on the camera film is ensured. In contrast, the normal streak photography depending on the plasma luminosity is found to be difficult in the setting of an appropriate aperture when there is a great temporal change in the plasma light intensity.

It is possible that the streak mode of Schlieren photography could also be done using the above mentioned set-up.

References

1. G.T. Nice, Appl. Opt. 11, 699 (1972).
2. H. Walter, J.L. Hall, Appl. Phys. Lett. 17, 239 (1970).
3. M.B. Denton, H.V. Malmstadt, Appl. Phys. Lett. 18, 485 (1971).
4. C.F. Burrell, H.J. Kunze, Phys. Rev. Lett. 28, 1 (1972a); Phys. Rev. Lett. 29, 1445 (1972b).
5. I. Melngailis, IEEE Transact. GE-10, 7 (1972).

6. E.D. Hinkley, P.L. Kelley, Science 171, 635 (1971).

7. A.J. Gibson, J. Sc. Instr. 2, 802 (1969).

8. C.J. Schuler, C.T. Pike, H.A. Miranda, Appl. Opt. 10, 1689 (1971).

9. S.H. Melfi, Appl. Opt. 11, 1605 (1972).

10. C.R. Haas, R. Noll, R.F. Ruhl, G. Herziger, Nucl. Fusion 24, 1216 (1984).

11. G. Decker, R. Deutsch, W. Kies, J. Rybach, Plasma Physics and Controlled Nucl. Fusion 27, 609 (1985).

12. I.M. Zolototrubov, I.P. Skoblik, A.G. Tolstolutski, V.I. Privezentsev, Sov. Phys. Tech. Phys. 19, 1061 (1975).

13 Fumio Hamada, Katsuji Shimoda, Katsumi Hirano, Phys. Fluids 22, 1217 (1979).

14. H.W. Liepmann, A. Roshko, "Elements of Gasdynamics" (John Wiley & Sons, Inc., New York and London, 1975), p.162 .

15. S. Lee, Y.H. Chin, Bull. Mal. Inst. Phys. 2, 105 (1981).

16. Y.H. Chen, Ph.D. Thesis, UM, Malaysia (1978).

17. S. Lee, Y.H. Chen, "Spring College on Plasma Physics", ICTP, Trieste, Italy (1981). Published in Fusion Energy - IAEA-SMR-82, p.296-303 (1981).

18. E.H. Yee, M.Sc. Thesis, UM, Malaysia (1983).

19. T.Y. Tou, Ph.D. Thesis, UM, Malaysia (1986).

20. S. Lee, Plasma Phys. 25, 571 (1983); Australia J. Phys. 36, 891 (1983); J. Applied Phys. 54, 3603 (1983).

21. E.H. Yee, B.C. Tan, Bull. Phys. M'sia 3, 139 (1982).

22. S. Lee, "Density ratios in compressions driven by radiation pressure" - accepted for publication by Laser and Particle Beams.

23. S. Lee, "The Sharing of Fusion Related Technology among Developing Countries" - Invited Review Paper at the International Energy Independence Conference, Rio de Janeiro, August 1987, to appear in Procs.

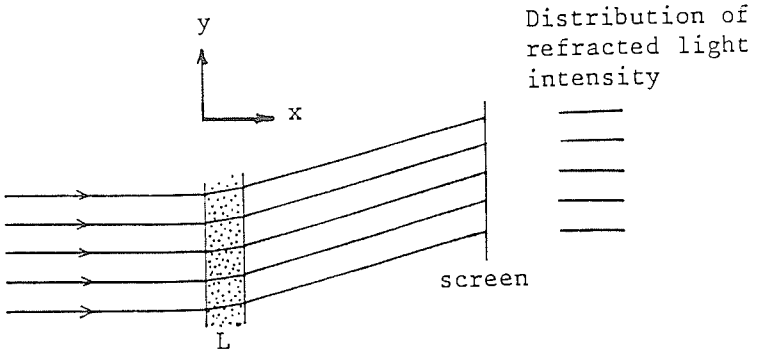

Figure 1a Parallel rays passing through a medium with constant gradient $\partial\mu/\partial y$ (μ=refractive index).

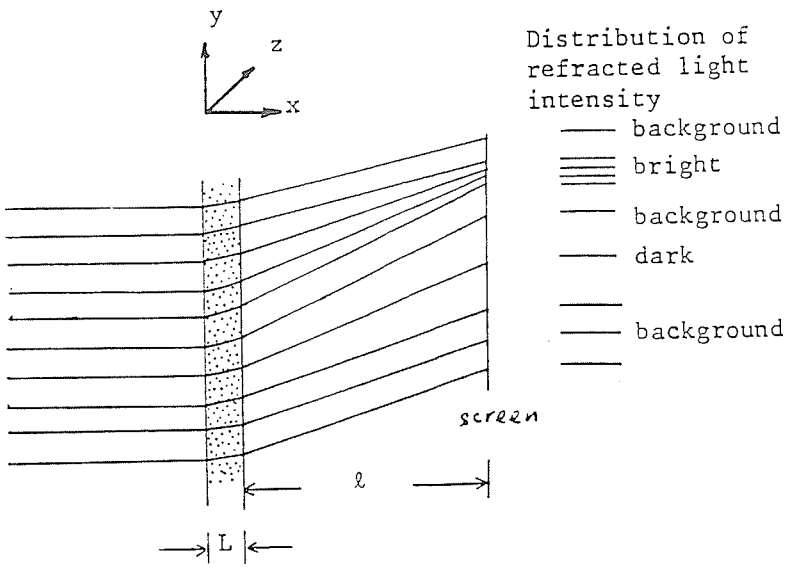

Figure 1b Non-uniform distribution of light intensity when $\partial^2\mu/\partial y^2 \neq 0$.

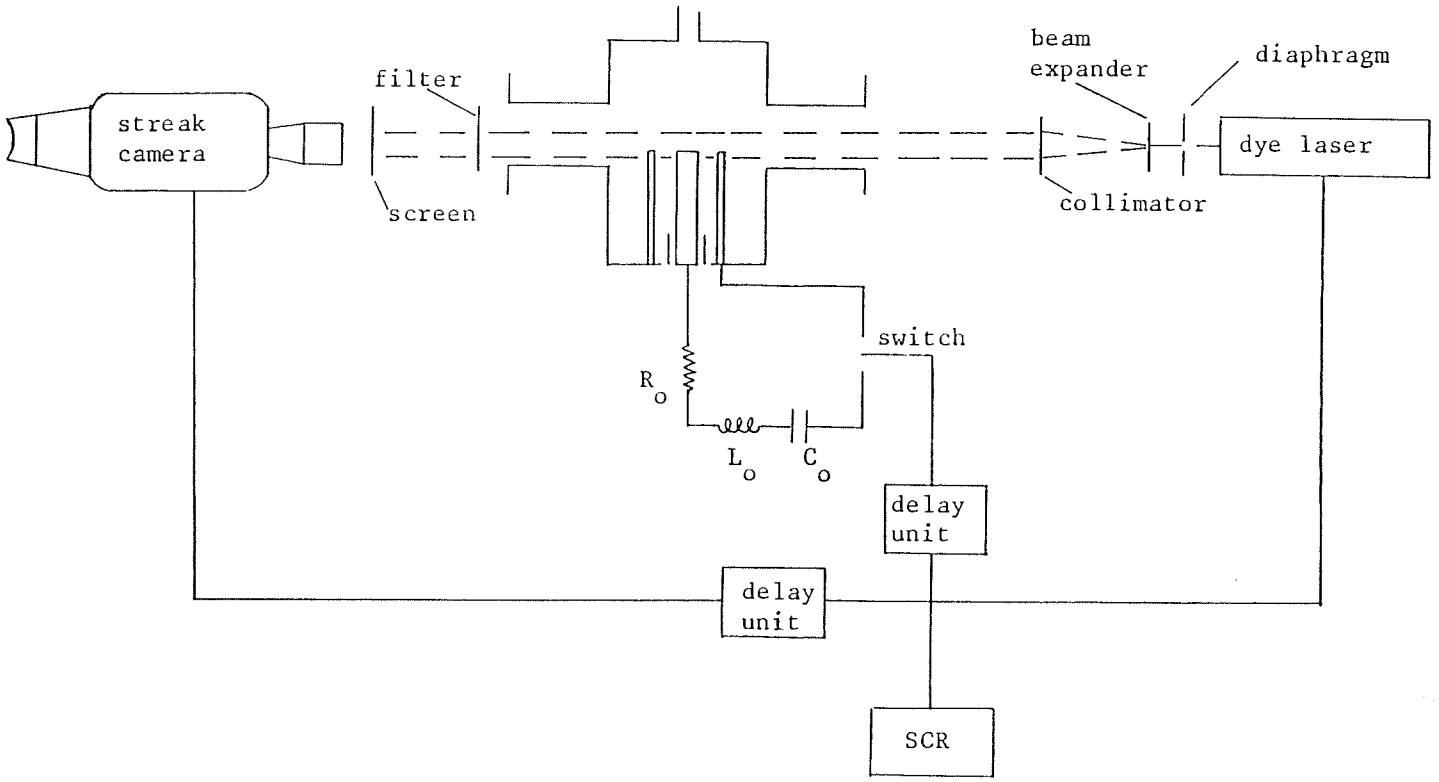

Figure 2 Schematic of the experimental set-up of the streak mode of laser shadowgraphy in plasma focus.

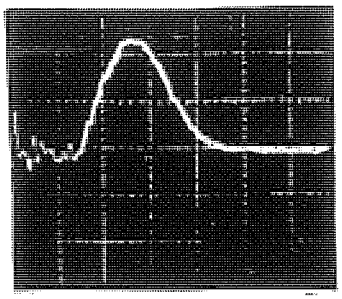

Figure 3 Photodiode signal of the dye laser output.

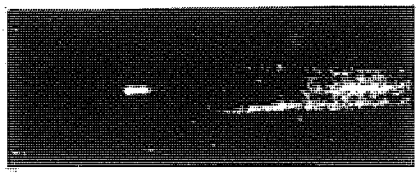

Figure 4a Normal streak photograph of the radial pinch phase in argon focus.

Figure 4b Streak laser shadowgraph of the radial pinch phase in argon focus.

OBSERVATION OF TEMPERATURE VARIATIONS IN A PLASMA FOCUS FROM SOFT X-RAY MEASUREMENTS

T.Y. Tou* and S. Lee

Plasma Research Laboratory
Physics Department, Universiti Malaya
59100 Kuala Lumpur, Malaysia

Abstract

A range of electron temperatures is obtained for the deuterium focus with the foil-absorption technique. This is correlated to the observed formations of hot spots on the time-integrated X-ray pinhole photographs. Together with other reported information, the correlation shows that the temporal evolution of the focus plasma could have contributed strongly to the range of electron temperatures.

Introduction

At least two sources of X-rays are distinctly present in the plasma focus development. The first is the result of the electron bombardment of the anode by the current-conducting electrons in the focus plasma. Some of these electrons are accelerated to high energies exceeding 100 keV by the pinch effect. The characteristics of this source are similar to those produced in the high voltage X-ray tube. The second source is in the pinched plasma. This source is derived from the presence of the electrons in the ion fields and produces a soft X-ray spectrum which varies with the location Z of the plasma and time t, indicating its temporal development.

*Present Address: Plasma Research Laboratory, R S Phys Sc. I.A.S., Australian National University, ACT 2601, Australia.

One common method to study the structures of the X-ray emitting plasma is by means of a X-ray pinhole camera[1-10]. The time-integrated X-ray pinhole photo revealed interesting fine structures[1-7] and m=0 instabilities, as suggested by several authors[1,3]. This technique was upgraded to become a nano-second time-resolved pinhole camera[8-10] with which temporal evolution of the focus pinch and fine structures of filamentation[10] were recorded.

Another plasma parameter that can be deduced from the measurements of the soft X-ray spectrum is the electron temperature. The short-lived pinched plasma was reported to have a range of electron temperatures[1,11,21]. It thus appears, from the electron-temperature measurements, that the pinched plasma may have regions of differing electron temperatures.

In this paper, the observations from the X-ray pinhole photo are correlated to the measured electron temperatures.

Experimental I X-ray pinhole photography

The schematic of the experimental set-up for the X-ray pinhole photography is shown in Fig. 1. The size of the pinhole is about 300 μm. It is covered by a 25-μm Beryllium foil to exclude the visible plasma light. Another layer of 25-μm mylar sheet is used to seal the pinhole so as to prevent air-leak into the plasma focus chamber. The pinhole camera is maintained at equal pressure to the plasma focus chamber except when it is opened for film release.

Figure 2 shows a time-integrated X-ray pinhole photo of the deuterium focus plasma. There are at least four observable features. The first is the cone-shaped plasma structure adjacent to the anode surface. The formation of this structure is attributed to a pinching action at this region which, in turn, leads to the accumulation of mass during the pinching process. Such an accumulation of mass at this region has been confirmed in a focus with solid anode by nanosecond TEA-N_2 shadowgraphy[12].

The second feature is a properly pinched plasma column adjacent to the cone-shape plasma structure, in the down-stream direction. A further feature concerns some spots observed to be present within this more diffused pinch column. The existence of such spots has also been

reported[1-7,18]. Finally, strong illuminations come from behind the cone-shaped plasma structure. The source is very likely associated with the copious copper plasma which is produced by the electrons bombarding the anode.

The formation of hot spots are more clearly seen in argon focus in greater number, as shown in Fig. 3. The size of the pinhole is just enough to spatially resolve these spots. Such an array of highly illuminated spots may indicate regions of higher temperature and high density plasma. Some authors relate these spots to the on set of the m=0 instabilities[1,3,18].

Experimental II Measurement of electron temperature Te

The electron temperature of the focus plasma has been measured with the foil-absorption technique[13,14,15]. Figure 4 shows schematically the present experimental set-up. A pair of X-ray detectors (Quantrad Model 100-PIN-250) are carefully mounted so as to receive X-rays from the same volume of focus plasma. Same combinations of foils are first mounted in front of each detector for excluding the possible plasma light and to prevent signal saturation. The amplitudes of the signals are compared in order to normalize the sensitivity of one detector to the other. Subsequently, additional foils are placed in front of one detector so that the signal-amplitudes are increasingly attenuated. The ratio (or transmission ratio) of the signals, taking into account the normalization factor, is always less than 1.0 and gets smaller with respect to additional foils.

To estimate the electron temperature of the focus plasma, the experimental transmission ratios are plotted onto a graph containing the calculated transmission ratios so that the electron temperatures may be inferred. Theoretically, the transmission ratio of the X-ray intensities from two detectors is given by

$$R_t(Te,\chi_b) = \frac{\int E(\lambda,Te)\ \exp(-\sum_a \mu_a \chi_a - \sum_b \mu_b \chi_b)\,d\lambda}{\int E(\lambda,Te)\ \exp(-\sum_a \mu_a \chi_a)\,d\lambda}$$

where Te is the electron temperature (eV), λ the wavelength of the X-rays ($\mathring{A}$), χ_a the thickness of each foil that constitutes the initial

combination and χ_b represents that of each additional foil. The mass absorption coefficients μ_a and μ_b are obtained from published literature. The subscripts a and b indicate the type of material for the initial foils and the subsequent additional foils.

For a fully ionized deuterium focus plasma, only the Bremsstrahlung emission need be considered so that we have

$$E(\lambda,Te) = 1.9x10^{-28} \frac{N_e N_i Z_i^2}{\lambda^2 Te} \exp(-12395/\lambda Te) \text{ per unit wavelength } (\text{Å}).$$

Here N_e is the electron density, N_i the ion density and Z_i the charge number of the ion.

Figure 5 contains the theoretical curves for the transmission ratio $R_t(\chi_b)$ as a function of the additional foil thickness χ_b. The figure also shows the experimental points of the transmission ratio and these points show that 1.5 keV < Te < 2.0 keV. It should be noted that for this range of electron temperatures, the initial foil combination contains a 5-μm Al-foil. As the thickness of this Al-foil is increased to 40 μm, a higher range of electron temperatures 2.0 keV < Te < 3.5 keV is measured, as shown in Fig. 6, at the same operating conditions, namely the discharge voltage and gas pressure.

It appears that there are regions of differing electron temperatures in the focus plasma. The measurement of electron temperatures by foil absorption technique is thus able to detect these differing electron temperatures corresponding to different plasma regions by changing the thickness of the initial foils; that of the Al foil in this case. One may thus suggest that, from the above measurements, a range of electron temperature 1.5 keV < Te < 3.5 keV exists in the focus plasma which agrees well with the reported values[1].

Correlation

In each discharge several spikes are always observed from the X-ray diodes and in order to identify the particular pulse or pulses that correspond to the X-ray from the focus plasma, time-correlation between these X-ray spikes and the voltage signal is necessary. Figure 7 shows a single X-ray pulse which coincides with the characteristic voltage

signal. The other pulses that occur (usually 150-200 ns) later are due to the X-ray emission from the sputtered copper plasma moving away from the surface of the anode[20].

The X-ray pulse which occurs at a time corresponding to the voltage spike has a FWHM $\sim$ (20 - 30) ns that agrees with those reported[3]. This value of FWHM may be taken as the life-time of the X-ray emitting focus plasma. The life-times of the hot spots inside the more diffused column are shorter and expected to be 5-10 ns[3]. These spots were reported to emit X-rays of higher energies[2,3] and may be taken to have higher electron temperatures. If one accepts the commonly suggested m=0 instabilities[1,3,18] as the mechanism that causes the formation of these hot spots, then this takes place at a later moment of the dense focus phase.

Thus it would appear that the observed differing regions of differing temperatures also may occur at different times in the evolution of the focus plasma.

Discussion and Conclusion

The formation of hot spots in the deuterium focus, is also and more distinctly observed in the argon focus. The array of highly localised spots on the Z-axis (Fig. 3) supports the suggestions of m=0 instabilities[1,3,18]. There were, however, other reports[2,5] that these spots could form considerably off the Z-axis and had thus led to the suggestion of the non-symmetrical force-free structures[19] or of m=1 instabilities. It appears that more effort, both experimental and theoretical, is required to achieve better understanding of the formation of the X-ray structures.

It should be noted that the X-ray pinhole photo is time-integrated. Differing degrees of illumination on these photo by the X-rays may be taken to indicate regions of plasmas of differing electron temperatures. This may be evident in the different ranges of electron temperatures measured by the foil-absorption technique. Furthermore, the shift of the experimental points (the transmission ratio), with respect to foil-thickness, toward higher energy curves in Fig. 6 clearly indicates the existence of a range of electron temperature. One may think of differing regions of plasma with their electron temperatures overlapping each

other. However, X-rays of higher energies are associated with the hot spots which are formed towards the later moments of the dense focus plasma. The upper limit of the measured range of electron temperatures may then be referred to the hot spots and the lower limit to the more diffused plasma column formed after the radial pinch phase[21]. It appears that the temporal evolution of parts of the focus plasma into hot spots could have contributed strongly to the measured range of electron temperatures.

References

1. J.W. Mather, Phys. Fluids 8, 366 (1965).
2. W.H. Bostick, V. Nardi and W. Prior, J. Plasma Phys. 8, 7 (1970).
3. K.H. Schonbach, L. Michel and H. Fische, Appl. Phys. Lett. 25, 547 (1974).
4. G.R. Neil and R.S. Post, Plasma Phys. 23, 425 (1980).
5. M. Sadowski, H. Herold, H. Schmidt and M. Shakhatre, Phys. Lett. 105A, 117 (1984).
6. S. Lee and H. Conrads, Phys. Lett. 57, 233 (1976).
7. Y.H. Chen and S. Lee, Int. J. Electronics 35, 341 (1973).
8. L. Bettinali, F. Pecorella and J.P. Roger, Rev. Sci. Instrum. 42, 1834 (1971).
9. M.J. Bernstein and F. Hai, Rev. Sci. Instrum. 41, 1843 (1970).
10. B. Nahrath, M. Shakhatre and G. Decker, Rev. Sci. Instrum. 47, 88 (1976).
11. P.J. Bottoms, J.P. Carpenter, J.W. Mather, K.D. Wave and A.H. Williams, Bull. Am. Phys. Soc. 13, 1543 (1968).
12. K.H. Kwek, T.Y. Tou and S. Lee, presented in the "Spring College on Plasma Physics", ICTP, Trieste, Italy, 1987.
13. F.C. Jahoda, E.M. Little, W.E. Quinn, G.A. Sawyer and T.F. Stratton, Phys. Rev. 119, 843 (1960).

14. V.F. Aleksin, V.A. Suprunenko, E.A. Sukhomlin and N.I. Reva, Soviet Phys. Tech. Phys. 11, 465 (1966).

15. T.P. Donaldson, Plasma Phys. 20, 1279 (1978).

16. J.A. Victoreen, J. Appl. Phys. 14, 95 (1943).

17. B.A. Henke, R. White and B. Lundberg, J. Appl. Phys. 28, 98 (1957).

18. R. Hass, H. Krompholz, L. Michel, F. Ruhl, K. Schonbach and G. Herziger, Phys. Lett. 88A, 403 (19..).

19. A Sestero, B.V. Robouch and S. Podda, Plasma Phys. 22, 1039 (1980).

20. S. Lee, Harith Ahmad, T.Y. Tou, K.H. Kwek and C.S. Wong, J. Fiz. Mal. 6, 23 (1985).

21. T.Y. Tou, Ph.D. Thesis, UM, Malaysia (1987).

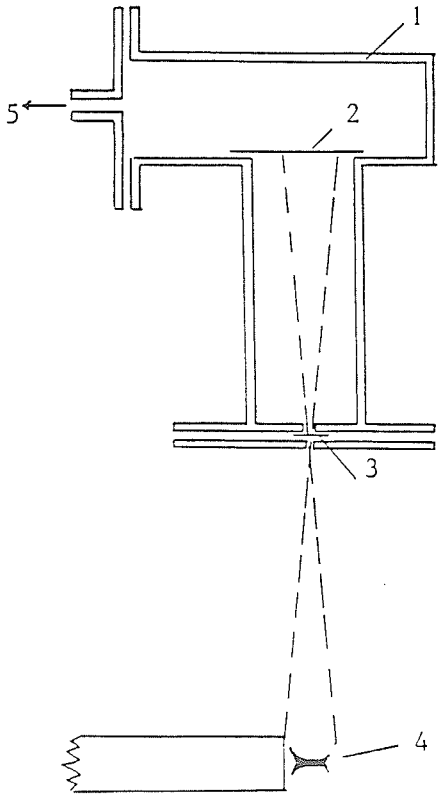

Figure 1 Experimental set-up for the X-ray pinhole photography.

1 - pinhole camera
2 - film
3 - mylar and Al (or Be) foil
4 - plasma
5 - to rotary pump

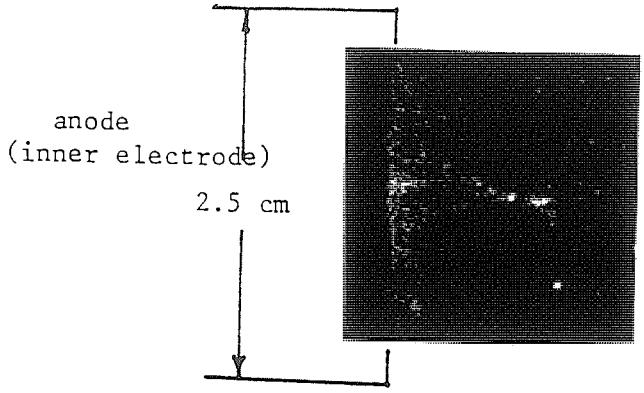

Figure 2 X-ray pinhole photograph of deuterium focus.

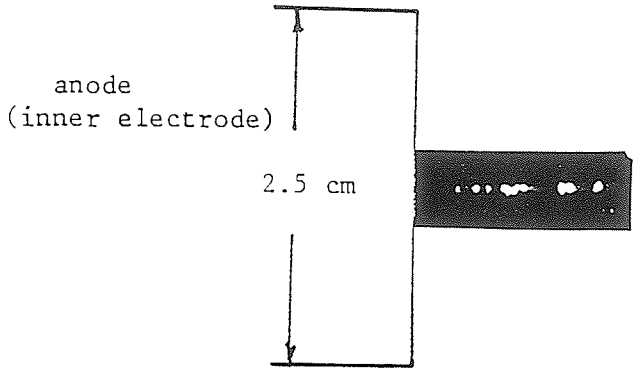

Figure 3 X-ray pinhole photograph of argon focus.

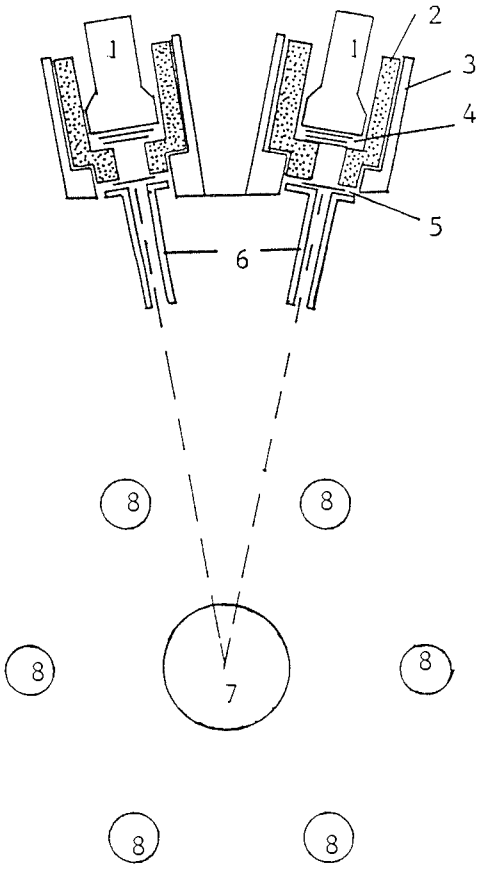

Figure 4 Foil-absorption technique using two PIN diode detectors.

1 - PIN diodes
2 - perspex holder
3 - copper
4 - foils (Al, Be or mylar)
5 - mylar (for vacuum seal)
6 - collimator
7 - inner electrode or anode of the plasma focus
8 - outer electrodes

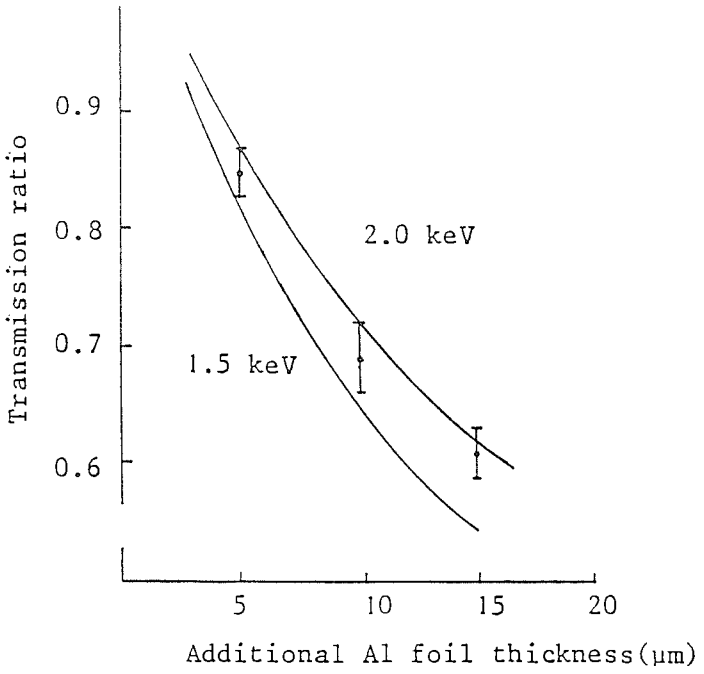

Figure 5 Transmission ratio as a function of additional Al foil thickness.
(— calculated; experimental)

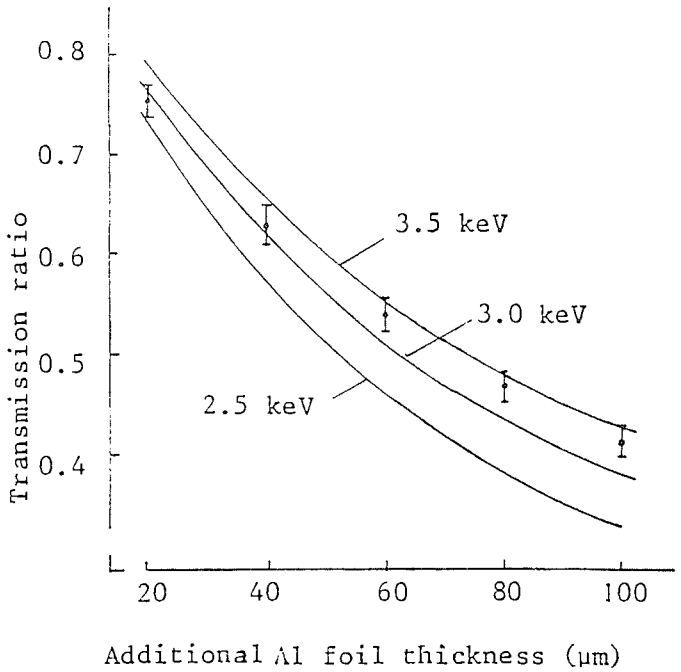

Figure 6 Transmission ratio as a function of additional Al foil thickness.

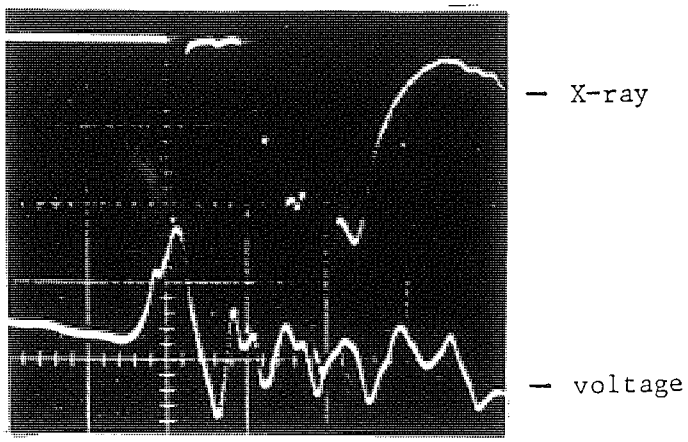

Figure 7 Time-correlation between X-ray signal and voltage signal. Time-base is 100ns/div.

PULSED PLASMA X-RAY SOURCES FOR APPLICATIONS IN LITHOGRAPHY AND MICROSCOPY

C.S.Wong, S.P.Moo, S.Lee and S.H. Saw
Plasma Research Laboratory
Physics Department
University of Malaya
59100 Kuala Lumpur
MALAYSIA

Abstract

Recently, there has been much interest in developing pulsed plasma devices as x-ray sources for applications in lithography and microscopy. In this paper, we survey the x-ray emission properties of two plasma devices, namely the plasma focus and the vacuum spark and consider their potential as pulsed soft x-ray sources.

1. Introduction

The use of x-ray lithography for the fabrication of submicron devices has already been shown[1] to be well justified as compared to conventional optical lithography, both from the point of view of cost effectiveness as well as quality. Three main categories of x-ray sources are being considered currently for applications in x-ray lithography and microscopy. These are: (1) the conventional electron beam-target systems; (2) the storage ring systems (Synchrotron); and (3) the pulsed plasma systems. Of these, the first two categories of devices have already been successfully employed in the production of working integrated circuits[2] and also in contact microscopy of biological specimen[3]. On the other hand, the pulsed plasma x-ray sources, although still in the development stage, offer several advantages over the other two categories of x-ray sources. These include compactness; low cost; simple operation and high x-ray flux. In fact, the feasibility in using the gas-puff z-pinch[4] and the plasma focus[5] for x-ray lithography has been demonstrated recently.

In this paper, we give a survey of the x-ray emission characteristics of two plasma focus devices - the UMDPF1[6] at University of Malaya; and the DPF78 at the Institut für Plasmaforschung (FRG)[7]. For the reason of compactness, the cost effective UNU/ICTP Plasma Fusion Facility[8] is proposed to be modified for operation as a pulsed x-ray source for x-ray lithography and microscopy studies in this laboratory.

Recently, it has been demonstrated that the laser initiated

vacuum spark device can be optimised as a reproducible x-ray source[9]. In view of the extremely high x-ray flux produced in this device, the possibility of developing it as an alternative pulsed x-ray source for application in x-ray lithography and microscopy will also be considered here.

2. The plasma focus

Conventionally, the plasma focus is operated with deuterium as the working gas for fusion neutron production. X-ray emission from such a plasma is contributed mainly by the free-free (Bremsstrahlung) continuum. For a deuterium plasma at a nominal electron temperature of 1 keV, the Bremsstrahlung emission spectrum peaks at $\lambda = 6.2$ Å . Such an x-ray source is found not suitable for application in x-ray lithography and microscopy due to its low flux and broad emission spectrum.

For the purpose of producing characteristic line radiations in the x-ray region, the plasma focus must be operated with high Z gases such as argon, krypton and neon. The focussed plasmas produced in these gases are found to emit strongly the hydrogen-like and helium-like line radiations. For example, the emission spectrum of an argon plasma focus is expected to consist of strong line radiatons at wavelengths of around 4 Å superimposed onto a relatively low background of free-free and free-bound continuum. Similarly, a krypton plasma focus is expected to emit characteristic line radiations in the wavelength range of 6 to 8 Å.

The x-ray emission from the UMDPF1 plasma focus operated at

12 kV, 4.3 kJ with pure argon as the working gas has been investigated recently in this laboratory[6]. The electron temperature of the plasma is determined by the x-ray foil-absorption technique to be in the range of 4 to 5 keV. Thus the expected continuum x-ray emission spectrum has its maximum at wavelength of 1.2 to 1.5 A, with prominent lines at around 4 A. The structure of the x-ray emission regions has been observed using an x-ray pinhole camera, showing the existence of highly localised regions of intense x-ray emission.

In a similar experiment performed on the DPF78 plasma focus device (60 kV, 28 kJ) operated with an admixture of H_2-Ar as the working gas[7], intense x-ray spots are also observed. The x-ray emitted from these hotspots have been measured[10] to consist predominantly of the argon K-shell emissions. Although the x-ray spots are frequently observed along the axis of the focus tube, their axial positions may vary from shot-to-shot over a distance of more than 3 cm.

It should be pointed out that both the UMDPF1 and the DPF78 are not optimised with respect to their x-ray emission. Their physical designs are also by no means compact. In comparison, the cost effective UNU/ICTP Plasma Fusion Facility[8] which is a small plasma focus powered by a single 15 kV, 30 μF Maxwell capacitor, is ideal to be developed into a pulse x-ray source. It has been shown in a plasma focus device of similar size that[5] x-ray conversion efficiency of as high as 3.7% can be achieved with appropriate optimization procedures. A program to develop the UNU/ICTP PFF plasma focus into a pulsed x-ray source for

applications in lithography and microscopy is now underway.

3. The vacuum spark

The vacuum spark is an extremely simple pulsed plasma device which is capable of producing intense bursts of soft and hard x-rays. With reference to Fig. 1, its operation can be described as follows: A pair of electrodes, embedded in a low pressure chamber ($P < 10^{-5}$), is connected in parallel to a capacitor bank which is charged to a high voltage, say 20 kV. Breakdown is initially prohibited by the low pressure. Discharge can be triggered either by a sliding spark between the cathode and a third electrode[11] (Fig.1a); or by using a high power ruby laser[12] (Fig.1b). In both cases, a puff of weakly ionized vapour of the anode material is injected into the interelectrode space either by electron beam bombardment or laser vaporisation of the anode tip. The plasma thus produced consists of the high Z anode material such as Mo, Fe, Ni etc., and it may be heated to an electron temperature of 4 to 10 keV[12]. The x-ray emitted from a vacuum spark plasma then consists of predominantly the hard components, with the peak of the continuum occuring at wavelength in the range of 1 to 3 Å. For a molybdenum vacuum spark plasma, line radiation of wavelength as short as 0.7 Å (Mo-Kα) may be detected, although the softer Mo L-shell emission at λ = 5.4 Å is also present. The presence of the hard x-ray component may impose some difficulties in using the vacuum spark as an x-ray source for application in lithography and microscopy.

In order to produce x-ray line radiation at longer

wavelengths, lower Z materials such as carbon and silicon may be used for the anode material. Plasmas produced with these anode materials are expected to emit line radiations at wavelengths of 45 Å for carbon and 7 Å for silicon.

Alternatively, the vacuum spark can be operated at a higher pressure of 10^{-3} or 10^{-2} torr. In this case, an external switch is necessary, and gases such as argon, krypton and neon can be used as the working gas instead of air. This arrangement also enables the wavelength range of the x-ray emission to be extended to the softer region. In this mode of operation, the discharge may be more appropriately called a low pressure spark discharge. Its discharge mechanism is expected to differ from that of a conventional vacuum spark.

X-ray pinhole imaging of the vacuum spark plasma exhibits similar hot spot features[11,12] as in the plasma focus. An estimate of the x-ray energy from the PIN diode measurements of the x-ray spots shows that each of these spots may emit up to 250 mJ into 4π. Some typical x-ray pinhole images of a laser-initiated, 20 kV, 4.4 kJ vacuum spark device with stainless steel anode[12] are shown in Fig. 2. For this particular vacuum spark system, its system parameters such as the discharge voltage and the inter-electrode spacing have been optimised so that the x-ray spots are observed consistently. It can be seen from Fig.2 that the x-ray spots are formed within the space between the electrodes, but both its axial and radial positions are found to vary from shot-to-shot This may severely affect the performance of the vacuum spark as a x-ray source.

4. Conclusion

We have given a brief survey on some of the x-ray emission properties of two pulsed plasma devices, namely the plasma focus and the vacuum spark. In general, in view of their ability to produce intense x-ray pulses of specific wavelength consistently, and the possibility of building compact systems, these devices have great potential to be developed as pulsed x-ray sources for applications in lithography and microscopy. However, there are several obstacles to be overcome before they become commercially viable pulsed x-ray sources. One of the most serious shortcomings is the spatial uncertainty of the x-ray emitting regions in these devices. Much work is still needed in this direction.

References

1. Alan D. Wilson, Solid State Technology, May 1986, p249.
2. J. Kirz and D. Sayre, "Soft X-ray Microscopy of Biological Specimen" in 'Synchrotron Radiation Research' eds. S. Doniach and H. Winick, Plenum Press, N.Y.(1980).
3. B.B. Triplett and S. Jone, SPIE Proceedings, p333(1982).
4. J. Bailey, Y. Ettinger, A. Fisher and R. Feder, Appl. Phys. Lett. 40, 33(1982).
5. Y. Kato and S.H. Be, Appl. Phys. Lett. 48, 686(1986).
6. T.Y. Tou, Ph.D. Thesis, University of Malaya(1987).
7. C.S. Wong, H. Herold, P. Choi and C. Deeney, this proceedings.
8. S. Lee et al, Am. J. Phys., in press.
9. C.S. Wong and S. Lee, Rev. Sci, Instrum. 55, 1125(1984).

10. P. Choi, C. Deeney, C.S. Wong, H. Herold and A. Wieder, paper presented at the Plasma Focus and Z-pinch Workshop held in Toledo, Spain (1987). To be published in proceedings.
11. S. Lee and H. Conrads, Phys. Lett. 57A, 233(1976).
12. C.S. Wong, Ph.D. Thesis, University of Malaya(1983).

Figure captions

Fig. 1. Schematics of the vacuum spark device. (a)Sliding spark triggered; and (b) Laser triggered.

Fig. 2. X-ray pinhole images of some typical vacuum spark discharges.

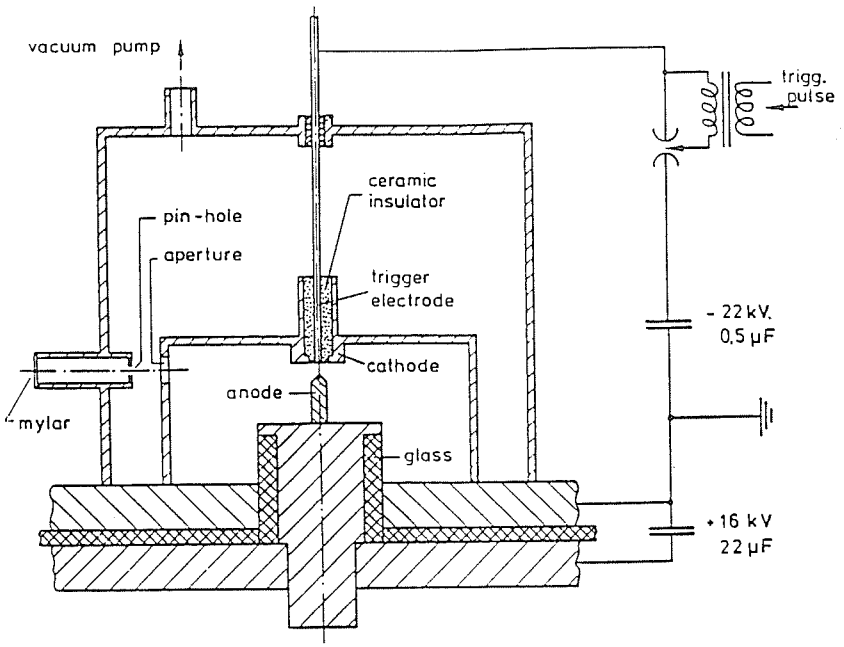
vacuum pump
trigg. pulse
ceramic insulator
pin-hole
aperture
trigger electrode
- 22 kV. 0,5 µF
cathode
anode
mylar
glass
+16 kV 22 µF

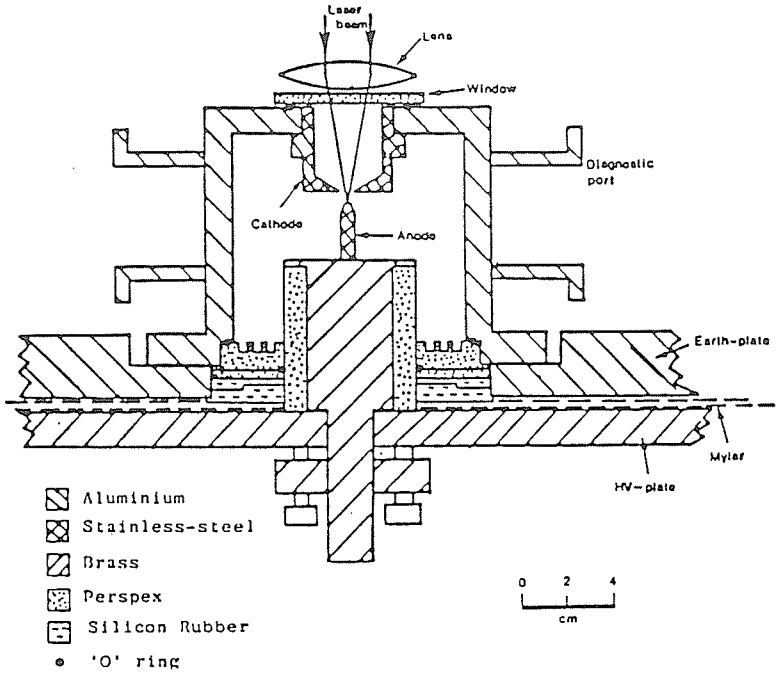
Laser beam
Lens
Window
Diagnostic port
Cathode
Anode
Earth-plate
Mylar
HV-plate
Aluminium
Stainless-steel
Brass
Perspex
Silicon Rubber
'O' ring
0 2 4
cm

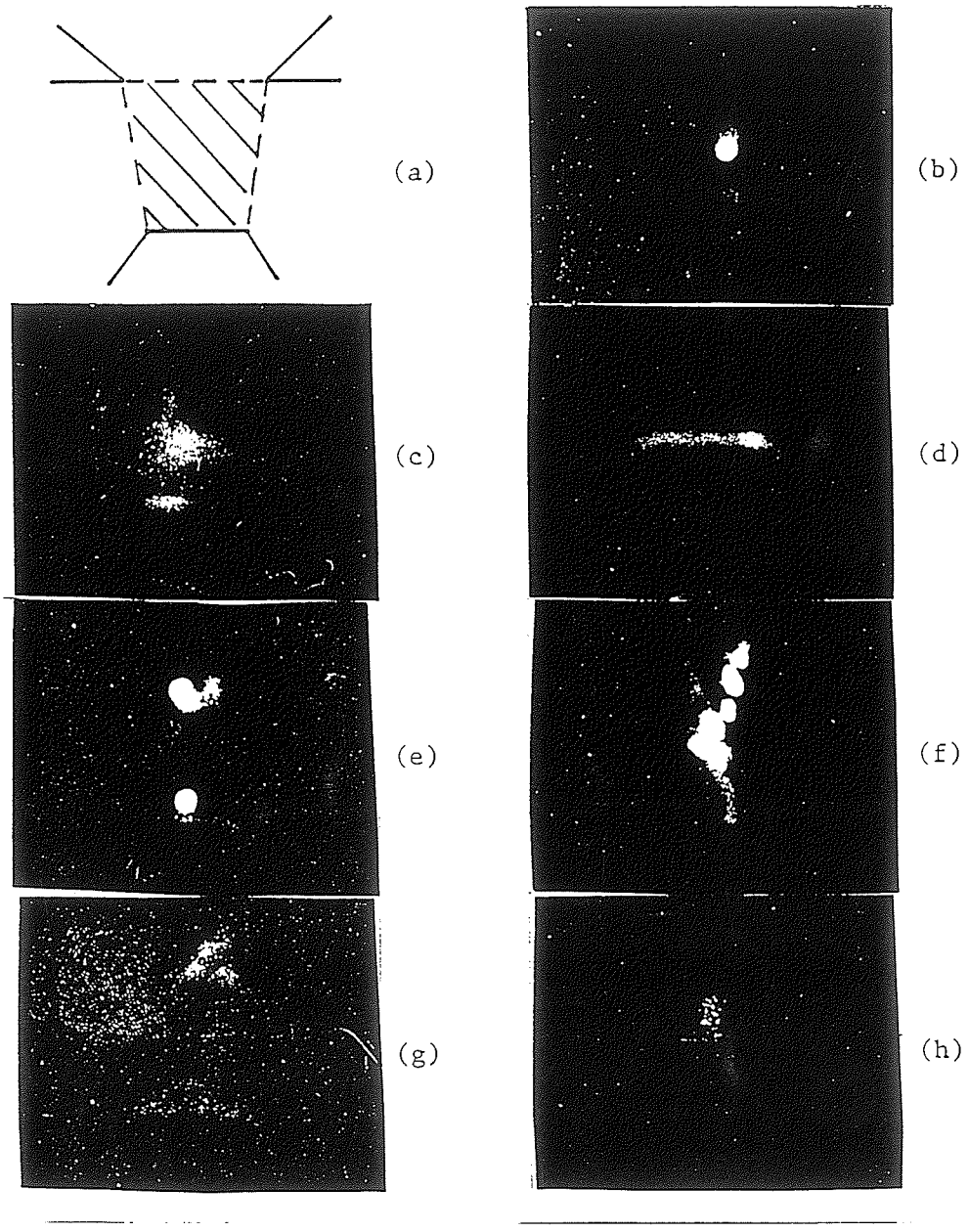
(a)
(b)
(c)
(d)
(e)
(f)
(g)
(h)

SHARING OF FUSION RELATED TECHNOLOGY AMONG DEVELOPING COUNTRIES

S. Lee
Physics Department
University of Malaya
59100 Kuala Lumpur
Malaysia

ABSTRACT

A program to initiate experimental plasma physics in developing countries has been started as a definite step for technology sharing. Cost effectiveness of several devices has been carefully considered from the viewpoint of physical mechanisms and existing technology. From this consideration emerges the plasma focus which whilst requiring no extraordinary technology yet could be packaged into a comprehensive facility for training in plasma production, plasma dynamics, plasma diagnostics and measurement of plasma x-rays, REB and fusion neutrons, with a very wide scope for the establishment of indigeneous training and research. It is shown that the simplicity of the approach is no barrier to the richness of plasma phenomena. Indeed the simplicity allows a clear comparison of pinch devices and, for example, enables two crucial limitations of existing plasma focus devices to be singled out, the overcoming of which could result in a many-fold jump in neutron yield. Hence the need for basic studies of these limitations. These and other studies could just as well be made on small devices. The UNU Training Programme resulted from the above consideration and evolved around the UNU/ICTP PFF, a small plasma focus with interesting physics and cost-effective technology. The extension of future training programmes to cover other important devices, for example, of the FRC type such as the Rotamak could widen the scope of this sharing of plasma and fusion technology.

Invited review paper prepared for presentation at the Energy Independence Conference Fusion Energy and Plasma Physics, 17-21 August 1987 at Rio de Janeiro, Brazil.

"Fusion Energy and Plasma Physics" Ed. P.H. Sakanaka
World Scientific Publishing Co. (1988)

INTRODUCTION

Plasma physics has attained considerable importance in its present applications and also with its potential application associated with fusion energy. Considerable effort, for example the Plasma Physics Colleges organised by the ICTP Trieste, has been expended to provide plasma physics education at an international level aimed towards stimulating the study of plasma physics even in developing countries[1,2]. This worthwhile educational effort encounters considerable difficulties at the experimental level particularly from the equipment point of view. Many scientists from smaller developing countries have been trained in postgraduate plasma physics programmes in developed countries or have carried out periods of research in such experimental facilities. On their return to their home institutions they face the daunting challenge of building up some simple, yet effective research facilities to provide continuity in their experimental research experience and also to train their students.

There is not even a clear idea as to which experiment could be usefully developed although low cost, cost effectiveness, simplicity and good educational value combined with a large variety of plasma phenomena amenable to study by simple diagnostics should be among the factors to be considered in relation to devices for developing countries. Thus the glow discharge has often been suggested as a suitable plasma for study in a developing country. The glow discharge has several applications, for example deposition and sputtering of thin films, and can also be used as a medium for the experimental study of plasma waves. It serves as a good starting point to develop plasma jets and arcs which may be used as plasma torches or heaters for industrial and metallurgical applications or for applications in MHD power generation.

To move upwards in temperature so that one may aspire to study the fusion aspects of plasma physics one may consider building an electromagnetic shock tube to study shock heating or a linear z-pinch for the study of imploding shocks and magnetic compressions. These are 'classical' devices with well-known technology and the z-pinch even in the low cost scaled-down form necessary for this educational exercise could produce a plasma of sufficient density and temperature to be of interest even though no measurable nuclear fusion may be expected. The plasma focus goes one stage better. It is an excellent device for teaching plasma dynamics and thermodynamics besides being a rich source for a variety of plasma phenomena including soft x-rays and plasma nuclear fusion. The plasma focus is superior to both the electromagnetic shock tube and the linear z-pinch in its range of plasma parameters, combining as it does the essential mechanisms of the devices in such a properly sequenced manner that all the features of both devices, and many more, are

produced in one single simple low cost device, when properly designed.

As a result of informal discussions among participants from developing countries at the 1983 Plasma Physics College at the ICTP it was decided to develop the plasma focus as one of the educational devices for the initiation of experimental plasma and fusion research in the smaller developing countries as an effort to develop and share fusion related technology among ourselves[3]. This project received support from the United Nations University whose Rector Dr. Soedjatmoko added a further dimension when he stated in a communication:

> "We at the (UNU) have strong reasons to believe that plasma physics will be one of the major technologies of the future in developing as well as industrialised countries. We find great merit in ... argument that developing countries should begin now to experiment with and develop modest plasma systems in order to acquire practical knowledge and skills to better employ technologies based on plasma physics once major breakthroughs permit the utilization ... for the production of energy as well as for other applications."

COST EFFECTIVE PHYSICS

In order to implement a project whereby a developing country may produce a suitable package for sharing technology with other developing countries with the aim of initiating experimental plasma research it is necessary to consider the cost effectiveness of the device to be chosen. Does it produce a rich variety of plasma phenomena? Does it require an expensive vacuum system? Can its power supplies, control electronics and basic diagnostics be packaged at reasonable cost? What physical mechanisms operate to make the chosen device perform better at lower packaging cost than other devices? Can we understand and model the design and performance of the device so that we may effectively do research on it? What are the areas of research and potential applications of the device?

From the point of view of the production of a plasma with conditions of density and temperature sufficient for plasma fusion studies at an affordable cost there is little doubt that the class of fast magnetic compression devices known generally as the pinch, including the linear z-pinch, the superfast pinch, the gas-puff pinch and the plasma focus offers the best potential. We have considered this class of device and found that the plasma focus is most cost effective having the same power supply, control electronics and basic diagnostic requirements as the simple z-pinch and a much cheaper vacuum system with only rotary pump requirement, yet producing more intense plasma phenomena including copious x-rays, relativistic electron beam (REB) and fusion neutrons, all in one small easily packaged facility. What is the physics behind this cost effectiveness?

COST EFFECTIVENESS OF VARIOUS TYPES OF PINCHES

We first recall that the neutron yield Y from a plasma fusion source is:

$$Y = \frac{1}{2} n^2 \langle \sigma v \rangle \text{ (volume) (time)} \qquad (1)$$

We note that Y is proportional to the square of n, the number density of the fusion fuel. We also note that starting from temperatures below 1 keV as one struggles to heat a plasma up towards a few keV, the effective cross section $\langle \sigma v \rangle$ for a thermalised deuterium plasma rises very rapidly with fuel temperature T. For example between 1 to 2 keV $\langle \sigma v \rangle$ for the D-D fusion reaction goes up by a factor of 25! - and between 2 to 5 keV, another factor of 30!. Thus the neutron yield is very sensitive to temperature. It is also proportional to the square of density.

In the pinch a large electric current is discharged from a capacitor bank through a gas between two electrodes (see Fig. 1). The current rises rapidly and due to the skin effect and wall conditions, electric breakdown first occurs across the glass wall of the container, forming a sheath of current along the glass wall. The electromagnetic $\underset{\sim}{J} \times \underset{\sim}{B}$ force in such a geometry acts radially inwards at every point of the current sheath so that, if the current is large enough, the current sheath and the heated gas (plasma) it entrains implode supersonically to form a hot dense column around the axis of the device.

The condition of balance between the hydrostatic pressure of the hot plasma and the constricting magnetic pressure gives the equation for the plasma temperature as:

$$T = \frac{\mu_o I^2}{8\pi N} \qquad (2)$$

where $N = \pi n r^2$ is the line density (particles m^{-1}) of the pinch. From this equation it would appear that since the temperature T depends on I^2 any temperature can be reached simply by increasing I to a sufficient value. However a pinch is essentially a dynamic device. The formation of the column has to occur in a time matched to the risetime of the current pulse, otherwise essentially the column is no longer there to obey the pressure balance equation when the current has risen to its peak value. Because of the dynamic nature of the problem the final temperature reached depends also on the implosion speed of the front of the plasma layer, which takes the form of a strong shock front. For deuterium the temperature dependence has the form:

$$T = 2.3 \times 10^{-5} \text{ (shock speed)}^2 \qquad (3)$$

Because of the dynamic nature of the problem it is essential for optimum use of the capacitor energy for the imploding shock wave to reach the axis at about the time of peak current. Now a typical well-designed capacitor bank

for a pinch (say 20 kV, 60 μF, low inductance) has a current risetime of about 3 μs. In general it is difficult (and expensive) to design a capacitor bank of this conventional type for a much shorter risetime, and the bigger the bank capacity the longer tends to be the risetime.

So we consider a typical current risetime of 3 μs. A typical implosion speed cannot be much less than 10 cm/μs. At this speed the shock temperature in deuterium is 2×10^5 K; any slower and it is doubtful whether the magnetic 'piston' would be clearly formed. Even at this slow speed a radius of 30 cm for the pinch tube is required in order to match the current risetime. Now the imploding magnetic pressure is

$$p_m = \frac{\mu_o I^2}{8\pi^2 r^2} \tag{4}$$

and with such a large pinch tube radius it is difficult to get enough magnetic pressure in the early stages of the implosion to start a clean compression unless the gas pressure is low. Thus a conventional pinch is limited by a (slow) current risetime of 3 μs, so that the pinch has to be operated with a large radius and hence low initial density. Moreover the speed (and hence temperature) becomes limited because of time-matching consideration.

What about the compressed density? We may apply a lossless energy balance theory[4] and allowing for a reflected shock overpressure show that the radius ratio κ_m (final radius r_m/initial radius r_o) is defined in a cylindrical supersonic pinch by the equation:

$$\iota_m^2 = \frac{2(\gamma_m - 1)}{f_m \ell_m} \int_1^{\kappa_m} \frac{\iota^2 \ell \, d\kappa}{\kappa} \tag{5}$$

where κ, ι and ℓ are the normalised, generally time dependent radius, current and length of the pinch, the subscript m refers to the quantity at the moment of peak compression, γ is the specific heat ratio and f_m is the reflected shock overpressure factor at the moment the shock reflected from the axis hits the pinching current sheath, ending the pinch compression. This equation gives us the following useful information:

(a) κ_m (and hence the compressed density ratio $\Gamma = \kappa_m^{-2}$) does not depend on the absolute magnitude of the current or the absolute length of the pinch.

(b) κ_m (hence Γ) depends on the time function of the current[5] and length.

(c) κ_m (hence Γ) depends on γ_m[6] and f_m. The smaller is γ_m, the smaller is κ_m and the larger is Γ. As γ_m approaches the lower limiting value of 1, κ_m approaches zero and Γ tends to infinity. The large is f_m, the smaller is κ_m and the larger is Γ. The value of f for a reflected shock on-axis, i.e. just after reflection is $f \simeq 4$ for cylindrical geometry[7]. As the

reflected shock travels out from the axis we may expect f to decrease towards a limiting value of 1.

For example for a constant current pinch with constant length, with $\gamma = {}^{5}/_{3}$ and $f_m = 1.6$, eqn. (5) gives $\kappa_m = 0.301$ and hence a density compression ratio of $\Gamma = 11$. The corresponding figures for the deuterium plasma focus are estimated to be $\kappa_m = 0.14$ and $\Gamma = 50$. These values are independent of the magnitude of the plasma current. This limitation of the ability to compress is a serious one and implies that the performance of the pinch as a radiation source depends on its initial density.

There are several concepts to overcome this limitation. The gas-embedded axis-initiated z-pinch uses a laser to start a pinch discharge on-axis thus obviating the problem of matching the electrical risetime to the pinch collapse time and allowing the formation of a very small radius pinch (sub mm radius) in a very dense plasma (initial density up to several atmospheres). The device is however plagued with problems of instability[8]. The hollow pinch uses a controlled gas jet[9,22] to form a thin plasma sheath which is then pinched into a vacuum. Using argon, krypton or xenon, the sheath does not thicken very much during the implosion because these gases are in the 'freely ionizing' regime[6] with a γ value having a small value of the order of 1.1. Because of the short distance between the imploding shock front and the magnetic piston the reflected shock from the axis hits the piston after a much shorter distance than that compared with a conventional pinch. The value of f_m is hence closer to 4 than in a conventional pinch with its thicker plasma sheath. Thus the hollow-pinch has a reduced κ_m and has been operated successfully in the heavier gases, particularly krypton and xenon, for the production of x-rays for x-ray lithography and microscopy. However from the technical point of view the hollow pinch requires the additional development of a rather precise gas valve system. It is also not known to operate well in deuterium, probably because the collapsing deuterium sheath thickens as its γ goes to ${}^{5}/_{3}$ once the sheath reaches a speed of the order of 10 cm/μs.

Ultra high power pinches have also been operated with pulse forming lines to reduce current risetimes so that the pinch may be operated at smaller radius, hence higher density[15]. This high power approach adds more complex and expensive technology.

On the other hand the plasma focus uses a very simple principle to overcome the time mismatch. Essentially it allows a conventional (slow risetime of 3 μs or more) capacitor bank to drive a very fast pinch (typically 1 cm radius in 50 ns) at a sufficiently high density and a large current during the time of pinch. Thus at low cost plasma conditions may be achieved which are more intense than that produced even in high-cost pinches.

The plasma focus uses a conventional capacitor bank to drive a device which has two sections:- the first section is a coaxial electromagnetic shock tube whose length is matched to the capacitor risetime. The rising capacitor current drives a shock wave axially down the shock tube at a suitable speed until the shock wave reaches the end of the tube at peak current. Then by the geometry of the device (see Fig. 2) the axial drive phase is simply converted to a radial compression or pinch phase.

The pinch phase is very intense (see Eqns. 2 and 4) because it starts at a very large current (typically 500 kA) and at a relatively small radius (typically 1 cm). Thus the operating pressure may be relatively high (10 torr in D_2 for a plasma focus against 0.1 torr or less for a pinch). The increased density and temperature more than compensates for the reduced volume in terms of the neutron yield Y as given in Eqn. (1).

Having seen from the basic physics mechanism that the plasma focus is capable of high levels of performance without special technological development the next step in the development of an educational package is to consider the modelling and design of a practical device.

COST EFFECTIVE DESIGN OF A PLASMA FOCUS

Design of the plasma focus may be based on a dynamic model[10] (see Fig. 3) which considers the focus dynamics in two separate phases - the axial run-down (shock tube) phase which crucially delays the radial focus, or pinch phase until the plasma current has reached its peak value. The first design point is therefore to have:

$$t_r = t_{a\ exp} \tag{6}$$

where

$$t_r = \frac{2\pi}{4} t_o \tag{7}$$

with

$$t_o = \sqrt{L_o C_o} \tag{8}$$

and

$$t_{a\ exp} \sim 2t_a \tag{9}$$

where

$$t_a = 2\pi \left[\frac{(c^2-1)}{\mu \ell n c}\right]^{\frac{1}{2}} \frac{z_o\ \rho_o^{\frac{1}{2}}}{(I_o/a)} \tag{10}$$

Equation (10) comes from the equation of motion of the axial phase and equation (9) from an analysis of the trajectory.

Here t_r is the current rise time and $t_{a\ exp}$ is the transit time of the plasma layer for the axial phase. The quantities t_o and t_a are characteristic times of the axial phase according to the model[10]. Here L_o is the inductance

of the capacitor C_o together with all connections up to the plasma section of the focus tube, c = b/a, 'a' and 'b' are respectively the inner and outer radii of the focus tube, z_o its length, ρ_o the ambient gas density, μ the permeability of the plasma (same as the permeability of free space) and

$$I_o = V_o/(L_o/C_o)^{\frac{1}{2}} \tag{11}$$

where V_o is the initial voltage on the capacitor.

The second design point involves the characteristic 'pinching' time of the plasma focus phase. This may be shown from the equations of motion of the radial phase to be

$$t_p = \frac{4\pi}{\mu^{\frac{1}{2}}(\gamma+1)^{\frac{1}{2}}} a \frac{\rho_o^{\frac{1}{2}}}{(I_o/a)} \tag{12}$$

where γ is the specific heat ratio of the plasma. From this expression of t_p it is noted that the ratio of the characteristic axial transit time to characteristic focus time is

$$\frac{t_a}{t_p} = \frac{(\gamma+1)^{\frac{1}{2}}}{2} \frac{(c^2-1)^{\frac{1}{2}}}{(\ell nc)^{\frac{1}{2}}} F \tag{13}$$

where $F = z_o/a$.

A crucial factor in the operation of the Mathers plasma focus is that the axial phase occurs over a relatively long period $t_{a\ exp}$ enabling the build up of capacitor current. The pinch phase then occurs over a relatively short period t_p. During this time t_p approximately 10 - 20% of the intially stored energy is transferred to the pinch plasma in approximately 2% of the current rise time. This results in a power enhancement factor during the pinching phase which is crucial to the proper operation of the plasma focus. It is important then that the ratio t_a/t_p be of the order of 30 - 50 for the Mathers focus.

The third point to be considered in the design is that there are limits[10] of speed and pressure in the operation of the plasma focus. In deuterium for good focussing and consistent neutron yield, the axial speed just before focussing should be between the limits 6 - 10 cm/μs; the lower limit being the minimum speed required for a good snow-plowing action in the axial phase and the higher limit being imposed by restriking[10,11] of the discharge at the back-wall or in the shock tube section. The limits of test gas pressure appears to be between 0.5 torr to 20 torr for deuterium; the lower limit apparently governed by re-striking; the upper limit by current filamentation[12].

The design of a plasma focus may take as a starting point the availability, or choice, of a capacitor bank. For the present exercise from the point of view

of economy and cost-effectiveness a single Maxwell capacitor rated at C_o = 30 μF, V_o = 15 kV with an equivalent series inductance, ESL, of less than 40 nH was selected. A parallel-plate geometry was selected for the capacitor connections and the switch, with coaxial cables being used to connect to the plasma focus input flanges. The value of L_o was estimated at 110 nH. Having fixed C_o and L_o Eqs. (8) and (7) give a value of t_r of 2.9 μs. Eq. (11) yields I_o = 248 kA. The time matching condition of Eq. (6) fixes $t_{a\ exp}$ at 2.9 μs. The value of z_o was then chosen at 16 cm to give an average axial speed of 5.5 cm/μs or a peak axial speed[10] of ~ 9 cm/μs just before the focus phase. This axial speed is expected to be suitable for a good focussing action in deuterium.

The value of I_o is considerably smaller than most operational plasma focus machines which typically have I_o of the order of 500 kA or more. Observing from Eq. (10) that the axial speed is ~ $I_o/(a(c^2-1)^{\frac{1}{2}}\rho_o^{\frac{1}{2}})$ and from Eq. (12) that the radial speed is ~ $I_o/(a\ \rho_o^{\frac{1}{2}})$ it is noted that a reduction in I_o may be compensated in the first instance by a reduction in 'a' in order to maintain the axial speed within the speed limit indicated earlier. Thus we design for a = 9.5 mm and b = 32 mm which are smaller than typical values of most operational plasma focus devices. Moreover the value of $\frac{b}{a}$ ~ 3.4, in this case, is near optimum. It is also noted that the value $t_a/t_p \simeq 40$ for this design.

Having fixed the values of I_o, z_o, b and a and t_r it remains to fix the value of ρ_o from Eq. (10). This gives $\rho_o = 0.21 \times 10^{-3}$ kgm^{-3}. This is the density of deuterium at 0.9 torr, which is within the pressure limits for deuterium focus operation as mentioned earlier.

The above design parameters have been subjected to a computation using a dynamic model[10] in which the axial trajectory is computed using a snow-plow model and the radial dynamics is traced using a generalized slug-model which considers a pinching plasma of increasing length with the plasma layer lying between a shock front at position r_s and magnetic piston at position r_p (see Fig. 3). This model has the advantage of giving a realistic final pinch radius ratio. Using the design parameters for the present device, the scaling parameters for the generalised slug model are:

$$\alpha = \frac{t_o}{t_a} = 1.26, \qquad \text{and} \quad \beta = \frac{L_a}{L_o} = 0.36,$$

where L_a = maximum inductance of axial phase = $z_o(\mu/2\pi)\ell nc$. Also

$$\alpha_1 = \frac{t_a}{t_p} = 40.4, \qquad \text{and} \quad \beta_1 = \frac{\beta}{\ell nc} = 0.294$$

The other parameters used for the model are c = 3.37, F = 16.84 and $\gamma = \frac{5}{3}$ (for fully ionised deuterium).

The computation indicates a strong focus with a large focussing voltage spike. The parameter α was varied between 0.7 to 1.5 (corresponding to pressure range of 0.5 torr to 2 torr) and the computation repeated at each α. Good focussing was indicated over this range of pressure. These computation results add confidence to the design of the plasma focus. However it has been found that machine effects such as current and mass shedding[10], reduced channel size due to boundary effects and current re-strike[11] which are not included in the dynamic model may alter the actual performance of the plasma focus. It is therefore to be expected that in actual operation the focus may need to be tuned by a variation of the five parameters V_o, ρ_o, z_o, a and b. If the design is not too far from optimum, operation over a range of ρ_o may be sufficient to establish a regime of good focus.

THE EXPERIMENTAL FACILITY

The experimental facility designed from the above physical model is shown in Figs. 4, 5 and 6. Fig. 4 shows the plasma focus circuit using a swinging-cascade spark gap switch triggered via a TV transformer. Fig. 5 shows the parallel-plate spark gap arranged in a low-inductance configuration on top of the capacitor with 16 output coaxial cables (No. 18 in Figs. 5 and 6) which connect the spark gap output to the plasma focus input flange as shown in Fig. 6. The plasma chamber (No. 32) consists of a 30 cm length of $6\frac{1}{2}$ inch mild steel tubing and the required vacuum is provided by a small single stage rotary pump with ultimate base pressure of 0.01 torr. The design of the focus tube electrodes has several important features[13] particularly regarding the mounting of the backwall glass insulator (No. 30). Diagnostics are also indicated in Fig. 6.

RESULTS

The system was tested between 13-15 kV in various gases including air, argon, hydrogen and deuterium. The strength of the focussing action is gauged from the current dip and voltage spike. (Current is measured using a Rogowski coil and voltage using a voltage divider.) Figure 7a shows an oscillogram of the current and voltage waveforms of the plasma focus in 0.5 torr of air, with focussing action about 1 μs after peak current. Figure 7b shows a deuterium focus, at 13 kV, 2.5 torr with focussing action occurring at peak current. The deuterium focus shows signs of a secondary focus occurring some 0.4 μs after the first voltage spike. The occurrence of definite clean dynamics in the axial region preceding the focus region is confirmed by magnetic probe measurements. Figure 7c shows the output of magnetic probe (lower trace) placed at z = 10.2 cm (i.e. in the axial drive region 10.2 cm from the backwall) in a discharge of 15 kV, 3.5 torr of deuterium.

From this oscillogram and in comparison with the current oscillogram (upper trace) it is found that the current sheath arrives at z = 10.2 cm 0.6 μs before focussing occurs off the end of the anode at z = 16 cm giving a speed of 9.7 cm/μs (corresponding, from shock theory, to a temperature ~ 2×10^5 K) over this section (z = 10.2 cm to z = 16 cm) of the axial drive region. From the rise time (10% to 90%) of the magnetic signal and the speed this gives a current sheath thickness of 2cm. The thickness and speed of this current sheath in the axial phase is typical of that in a good plasma focus system.

In dueterium when operated at 15 kV and optimum pressure conditions of 3 torr consistent counts of 1000-2000 are obtained using the PM-scintillator counter. This corresponds to 0.5 - 1 $\times 10^8$ neutrons per shot.

The system shows remarkably consistent and reproducible operation. For the purpose of a training programme sponsored by the UNU, six systems were assembled one after the other and tested over a period of two months. Each system (designated as the UNU/ICTP PFF) was assembled and tested over a period of one week averaging between 100-200 shots in the various gases. Once a system has been established to be operating normally, that is without undue leakage and after an initial period of out-gassing involving some three to five discharges, proper focussing is achieved for better than 95% of the discharges, apart from those discharges deliberately operated outside the established suitable pressure range for the gas used.

THE UNU TRAINING PROGRAMME ON PLASMA AND LASER TECHNOLOGY

Based on the above detailed consideration of the plasma focus the UNU Training Programme (also sponsored by the ICTP) was conducted in Kuala Lumpur by the Plasma Physics Research Group and the Laser Physics Research Group of the University of Malaya (UM) from October 1985 to April 1986. The following summarises the Training Programme:

Aim:

To initiate experimental plasma/laser research in several developing countries.

Method:

By transfer of a comprehensive integrated package of expertise plus basic components and equipment - sufficient to enable the UNU Fellow to build and operate, and do measurements on, a basic plasma/laser facility back at his home institution.

Package for transfer:

electrodes
vacuum chamber
pulsed control switching electronics

power supplies
high power discharge systems
diagnostic systems
design, testing and research procedures
computational packages for microcomputer
modelling of circuit and plasma dynamics

Programme:

October to December 1985 - Lectures and experiments on existing devices in the UM laboratories including pulsed electronic modules, power supplies, glow discharge, electromagnetic shock tubes (EMST), plasma focus, computation packages on circuit and plasma dynamics; and various lasers; system planning, design, construction and development of all sub-systems for each facility chosen by the individual Fellow.

December 1985 - February 1986 - development, assembly and testing of each set of facility; research work on the various devices.

March 1986 - reports and further planning;
preparation for shipment of equipment;
writing of research papers[13,14]
presentation of some research results to the Second Tropical College on Applied Physics[14].

Fellows:

Eight UNU Fellows from Egypt (1), India (1), Indonesia (3), Pakistan (1), Nigeria (1), and Sierra Leone (1).

Sponsorship:

UNU for Fellowships and institutional support
ICTP for equipment grant for UNU Fellows
University of Malaya for facilities
Malaysian Institute of Physics for organisation.

Research Transfer for 1985/86 Programme

	UNU/ICTP Plasma Fusion Facility	EMST High Speed Flow Simulator	N_2 Laser System	Glow Discharge
Egypt	1		1	
India			1	
Indonesia	1	1		1
Pakistan	1			
Nigeria	1		1	
Sierra Leone	1		1	

Progress on return home

A year after the equipment were received by the UNU Fellows back at their respective home institutions their progress may be summarised as follows. The plasma focus facility is now operational at Al-Azhar University, Cairo (Dr. M.A.A. Eissa). It has been redesigned and modified and a facility each is operational at the Yogyakarta Nuclear Research Centre (PPNY) (Suryadi and W. Usada) and at Qaid-I-Azam University, Islamabad (M. Zakaullah). Resulting from the UNU training, Qaid-I-Azam University is also planning several other plasma devices including a 16 kJ plasma focus. Dr. A.V. Gholap (River State University of Science and Technology, Port Harcourt) and Dr. A.J. Smith (Njala University College, Sierra Leone) have each one M.Sc. student completing thesis work on the nitrogen laser and planning to proceed to Ph.D. research on the UNU/ICTP PFF which is marginally operational at each of these two institutions because of very difficult technical conditions. A nitrogen laser is also operational at Sri Pratap College, Srinagar (Dr. S. Sapru). S. Mulyodrono (National Space and Aeronautics Agency, Jakarta) has started on a Ph.D. programme on hypersonic flow simulation and em propulsion using the EMST as the basic facility. M. Zakaullah is also using the UNU/ICTP PFF as the basic facility in pursuing the first experimental plasma physics Ph.D. programme in Pakistan. Four Fellows have been awarded TWAS research grants.

SECOND UNU/ICTP TRAINING PROGRAMME

This is scheduled for a period of six months to start at the end of 1987.

WHAT CAN BE DONE WITH THIS FUSION FACILITY

For the plasma focus, the concept of technology sharing has already been demonstrated by the UNU Training Programme. It may be pertinent to try to advance the ideas by asking what can be done with the UNU/ICTP PFF.

CHARACTERISTICS

To discuss this we first summarise the characteristics of the UNU/ICTP PLASMA FUSION FACILITY:

Capacitor voltage	V_o	15 kV
Capacitance	C_o	30 μF
Stored energy	E	3.3 kJ
Inductance	L_o	110 nH
Inner radius	a	0.95 cm
Outer radius	b	3.2 cm
Length	z_o	16 cm

Characteristic current I_o	250 kA
Peak current	160 kA
Current risetime	3 μs
Average axial shock speed	6 cm/μs
Peak axial shock speed	10 cm/μs
Average radial shock speed	12 cm/μs
Peak radial shock speed	≃ 25 cm/μs
Neutron yield (at 3 torr D_2) Y	10^8 per discharge

Types of plasmas (strongly focussed):

Deuterium	1 - 5 torr
Hydrogen	1.1 - 6 torr
Helium	0.7 - 3.5 torr
Argon	0.3 - 2 torr
Air	0.5 - 1.1 torr
Carbon dioxide	range undetermined, but below 1 torr

Copious x-rays are also emitted from these plasmas.

Diagnostics

The simple diagnostics that have been designed for the UNU/ICTP PFF are now summarised here:

Current measurement	Rogowskii coil
Voltage measurement	Resistive probe, capacitive probe
Magnetic field	Magnetic coil
Speed measurement	Current probe, voltage probe, magnetic probe, photodiode
Measurement of dynamics and electrodynamics	Current probe, voltage probe and magnetic probe used in conjunction with circuit and snow-plow analysis and computation
Neutron measurement	Activation counter using Geiger-Mueller tubes; also time-of-flight method
X-ray measurement	Pin-hole camera; PIN diodes*
Density distribution and dynamics	Laser (e.g. Nitrogen laser),* shadowgraphy and holography

Computer packages

Computation models specifically developed (mainly) for microcomputers include:

Modified snow-plow model for the axial phase

Generalised slug-model for the radial phase

Energy balance model for estimating the minimum compression radius (gross)

Thermodynamic computations for the specific heat ratios and ionisation fractions for argon, and the effects of these on the dynamics.*

* During the 1985/86 Training Programme practical training in these sections were not carried out because of shortage of time.

The UNU/ICTP PFF BROKEN DOWN INTO SUB-SYSTEMS

To give a better picture of the fusion facility the sub-systems making up the facility are listed here and shown in Fig. 8:

Focus electrodes and vacuum chamber
rotary pump and gas system
capacitor bank
spark gap and triggering electronics
control and synchronising electronics
high power charger for the capacitor bank
interfacing systems and connections
diagnostics such as current, voltage and magnetic probes,
neutron counter, photo diode, shadowgraphic systems

Training and Research Topics

Having listed the characteristics of the plasma focus, types of plasmas produced, performance, diagnostics and computation packages and also the sub-systems making up the fusion facility we shall now summarise the training and research topics that may be carried out on such a device almost immediately it is set up by trained staff.

System technology and construction
System characterisation and optimisation
Development of diagnostics
Development of computation-modelling, parametric variation and optimisation
Plasma dynamics
Neutron measurements[23] and neutron scaling, fusion physics
Neutron enhancement by dynamic, thermodynamic and target methods[23]
Application as pulsed neutron source e.g. for half-life measurements[20]
X-ray measurement and production
X-ray enhancement and application as source for lithography and microscopy[19]
Relativistic electron beam (REB) measurement[24] and applications
Plasma focus for inertial confinement studies[18]
Sputtering and deposition of anode materials and special anode inserts[21,16]
Study of particle accelerating mechanism and application[16]
Compression enhancement and generation of megaGauss magnetic fields[22].

Several of the topics in this list have hardly been researched upon and may form extended research programmes. As an example we consider the following research project.

Example of applications : Enhancement of neutron production from dynamical consideration

Such a project may be simply posed, yet could have far reaching consequences. We consider the effect on fusion yield of operational speed and density of the

plasma focus assuming a uniform compressional model. First we record two experimental observations:

1. Plasma focus machines, through the whole range of sizes and energies operate in deuterium with a peak axial speed of 10 cm/μs. This speed is uniform for all devices and apparently cannot be exceeded.
2. Plasma focus machines are operated at as high a pressure as will give a consistent good neutron yield. For all but the smallest machines, the initial filling pressure is 10 - 20 torr, and apparently cannot be exceeded.

We consider these two limitations on speed and initial density, the consequential scaling law and the possibility of dramatically improving the scaling law if these two limitations may be removed. Thus we seek to show that basic research may be done even on small machines such as the UNU/ICTP PFF to look into the physical mechanisms causing these limitations with a view to finding out how to overcome them.

Speed limitation

By considering the theoretical axial and radial trajectories and experimental observations on current and mass shedding it may be shown that for all machines the peak axial speed $\hat{v}_z \sim {}^{z_o}/_{t_a}$ and the peak radial speed $\hat{v}_p \sim 1.1\ {}^{a}/_{t_p}$.

Thus
$$\frac{\hat{v}_p}{\hat{v}_z} = 1.1\ \frac{t_a}{t_p} \quad \frac{1}{F} = \frac{1.1\ (\gamma+1)^{\frac{1}{2}}(c^2-1)^{\frac{1}{2}}}{2\ell n\ c} \tag{14}$$

For $\gamma = {}^{5}/_{3}$ (fully ionized deuterium) and with c = 2.5 to 3.5 for most machines, the ratio $\hat{v}_p/\hat{v}_z$ has a nearly constant value of 2.4. Thus remarkably for all machines, from 1 kJ to 1 MJ the peak radial collapse speed is the same, 25 cm/μs. This fixes the forward shock temperature on-axis at (from Eq. (3)) 1.4×10^6 K and the on-axis reflected shock temperature at 2.5 times i.e. 3.6×10^6 K. Further compression brings the temperature of the gross plamsa column to just under 1 keV. This appears to apply to the whole range of plasma focus machines.

Density limitation

For the plasma focus, equation (5) gives the radius ratio for $\gamma_m = {}^{5}/_{3}$ and $f_m = 1.6$ to be $\kappa_m = 0.14$. Thus operating at 10 torr, the gross compressed density is $5 \times 10^{17} \times \left(\frac{1}{0.14}\right) = 3 \times 10^{19}$ deuterons/c.c. This again applies to all but the most underpowered machines.

These two observed speed and filling density limitations give the remarkable fact that all attempts to scale up the plasma focus in energy, for greater neutron yield, is subject to compressional limits on temperature and density of respectively about 1 keV and several times 10^{19}/c.c. . How do these limitations dictate the neutron scaling law?

Neutron Scaling Law

From Eq. (10) we may show

$$v_{axial} \sim (I_o/a)\rho_o^{-\frac{1}{2}} \tag{15}$$

Now since v_{axial} is fixed and ρ_o is fixed for all machines the ratio (I_o/a) is fixed.

Hence $a \sim I_o$

But $r_m \sim a$ since $\kappa_m = r_m/a$ is fixed

Therefore $r_m^2 \sim I_o^2$ (16)

It is further observed and agrees with modelling that the length ℓ_f of the focus at maximum compression scales linearly with 'a'.

Thus $\ell_f \sim a \sim I_o$ (17)

It is also a reasonable assumption, if one may consider the focus as a uniform column, that the lifetime of the plasma column τ_f scales linearly with r_m, hence with a and I_o .

Thus $\tau_f \sim I_o$, (18)

Combining equations (16) - (18) we have

$$(r_m^2 \ell_f)\, \tau_f \sim I_o^4 \tag{19}$$

But the plasma current I_f may be considered to scale linearly with I_o, so we may write

$$(r_m^2 \ell_f)\, \tau_f \sim I_f^4 \quad . \tag{20}$$

Imposing the temperature and density uniformity for all machines equation (1) then gives us the neutron yield scaling law as:

$$Y \sim I_f^4 \quad . \tag{21}$$

Noting that the stored capacitor energy $E = \frac{1}{2} L I_o^2$, we have, for machines with minimised inductance L, the other form of the scaling law:

$$Y \sim E^2 \tag{22}$$

Improving the scaling

Equations (21) and (22) are indeed the scaling laws observed for plasma focus machines[16,17]. The way with which we have derived these laws enables us to see immediately how we may improve the scaling if we could remove the speed (temperature) and density limitations. Suppose we could operate the plasma focus at a doubled axial speed. Eq. (14) would then ensure a doubled radial speed and eq. (3) then suggests a quadrupled plasma temperature to several keV because of the dependence of $\langle\sigma v\rangle$ on temperature as discussed earlier. The value of $\langle\sigma v\rangle$ and hence Y may then go up by a factor of at least

several tens giving a quantum leap to the yield Y. At present it is observed that at axial speeds above 10 cm/μs, the focussing action is erratic and inconsistent. Effort should be made to discover the physical mechanism behind this. For example if it were caused by secondary breakdown along the backwall insulator, the geometry or material may be improved. The required current density (I_o/a) would be 1.4 MA/cm of radius (for 10 torr operation) compared to the present 700 KA/cm.

Secondly it would be important to operate at higher number density n. An increase of n by a factor of 10 will require an operating pressure of 100 torr. The increased figure of 1.4 MA/cm will then be increased further to 4 MA/cm. Besides the effect on Y, the increase in n is also required to increase the Lawson product $n\tau$. It is hence of importance to find out the physical mechanism limiting the operational pressure to 20 torr.

Once the 2 limitations may be removed, a reactor scale plasma focus may be considered, operating at an axial speed of 20 cm/μs in 100 torr D-T with focus current of 20 MA and inner radius of 10 cm. The energy requirement could be only tens of MJ.

Before such speculations are seriously made however it is important to study the feasibility of the removal of the speed and density limitations. This study may be made even in small machines such as the UNU/ICTP PFF.

Widening the sharing

The devices discussed so far - the glow discharge, the e.m. shock tube, the z-pinch and the plasma focus - cover a range of plasma conditions from a weakly ionized steady state relatively low temperature plasma to a highly ionized pulsed plasma undergoing copious nuclear fusion reactions. The packaging of these devices has proven to be useful. The next step would be to extend the exercise to the important study of magnetic and plasma configuration of the compact torus and the FRC type. It has been shown that the spheromak may be generated starting from a configuration very similar to the plasma focus and that a RFP may be generated from a theta pinch geometry. It would be useful for a cost analysis to be performed on these devices with a view to identify which device if any could be cost-effectively packaged for the purpose of research initiation.

One FRC device appears particularly suitable for such a package. Besides its potential as a current-drive candidate for fusion reactor schemes the Rotamak[25,26] may be scaled down and assembled as a very cost effective package for the experimental study of field reversed configurations lasting for a very reproducible and steady period of tens of millisecond with plasma temperatures and density of respectively a few eV and 10^{13}/c.c.

In a small Rotamak a steady bias field B_z typically 10G may be set up by

external coils in a spherical glass vessel, typically 10 cm in radius, defining a direction 'z'. A rotating field B_ω, typically 5G is set up pointing in a direction normal to the z-axis and rotating around the z-axis in the θ-direction with frequency ω. This B_ω field may be set up by two pairs of coils, the axis of each pair being normal to the z-axis and also normal to each other. Two RF generators are required typically operating at 1 MHz and each connected to a pair of coils mentioned above. The outputs of the RF generators, of the same amplitude, are arranged to be out of phase by 90°. The resulting field is a constant amplitude field rotating about the z-axis. Provided the Rotamak frequency condition and the penetration condition are fulfilled the steadily rotating B_ω very effectively drives a steady azimuthal current I_θ which will in turn produce a magnetic field in the -z direction if the rotating direction is appropriately chosen.

Based on previous Rotamak work at Flinders University of South Australia it appears that several hundred amperes may be driven causing field reversal for an input RF power of several kilowatt. Whilst engaged in research programmes to scale-up his Rotamak devices, Professor I.R. Jones of Flinders University has also taken steps to develop low cost variable frequency MOSFET-switched RF modules with each module driving several kW at 1 MHz. This development may well prove to be very important for the eventual packaging of an FRC device for educational purposes for the developing countries, resulting in the further sharing of plasma technology. (As this paper was being typed the author in collaboration with Prof. Jones successfully demonstrated at the Flinders Rotamak Laboratory the operation of a 'transistorised' Rotamak FRC, driving a field-reversing steady plasma current of 250A for 40 ms with RF output of 2 kW at only 170 V. FRC compact tori were produced with single phase drive (1 pair of RF coils only) and also with conventional Rotamak two phase drive.)

CONCLUSION

The concept of sharing of fusion related technology among developing countries has been proposed and demonstrated comprehensively in one case of the plasma focus. A cost effectiveness analysis based on phasics and existing relatively simple technology has resulted in the design of an integrated package, the UNU/ICTP PFF which has been instrumental in the initiation and strengthening of experimental plasma research in several developing countries. The relatively low-technology approach of the package does not appear to detract from the performance of the research facility and is no barrier to the many possible applications of the plasma focus. Indeed the simplicity of the approach allows the singling out of two limitations, the speed and density limitations, which if removed could cause the focus neutron yield, for a given storage energy or available current, to multiply possibly a hundred-fold. It is hoped that the sharing of technology may extend to include packages for FRC devices such as the Rotamak.

ACKNOWLEDGEMENT

The sponsorship of the United Nations University, the International Centre for Theoretical Physics and the University of Malaya for the programmes leading to this paper is gratefully acknowledged. This paper was prepared while the author was Visiting Professor at The Flinders University of South Australia.

REFERENCES

1. B. McNamara, "Twenty Years of Plasma Physics at the International Centre for Theoretical Physics" in 'Twenty Years of Plasma Physics' Edited by B. McNamara, World Scientific, Philadelphia and Singapore, p. XIII (1985).

2. International Fusion Research Council "Status Report on Controlled Thermonuclear Fusion", Nuclear Fusion 18-1, 137 (1978).

3. Regional Centres for Research Transfer Within South-East Asian Countries - S. Lee; Invited paper presented at the International Conference on Physics for Development at the International Centre for Theoretical Physics, Trieste, Italy, 8-12 October 1984.

4. S. Lee, Plasma Phys. 25, 571 (1983).

5. S. Lee, J.Phys.D : Applied Phys. 17, 733 (1984).

6. S. Lee, Australian J. Phys. 36, 891 (1983).

7. G. von Guderley, Luftfahrtforschung 19, 302 (1942).

8. A.E. Dangor et al., Phys.Rev.A 27, 2751 (1983).

9. J. Weinberg, A. Fisher, Applied Phys. Lett. 47, 1116 (1985).

10. S. Lee in 'Radiation in Plasma' edited by B. McNamara, World Scientific, Singapore, Vo. II, 978 (1984). Also S. Lee in 'Laser and Plasma Technology' edited by S. Lee et al., World Scientific, Singapore, 387 (1985).

11. J.W. Mather, P.J. Bottoms, J.P. Carpenter, K.D. Ware and A.H. Williams, Report No. IAEA-CN-28/D5, 561 (1972).

12. J.P. Rager, L.E. Bilbao, H.A. Bruzzone, V. Gourlan, U. Guidoni, H. Kroeglar, S. Podda, B.V. Robouch, K. Steinmetz, 'Experiments on the neutron production phase of the Frascati 1 MJ Plasma Focus', Eighth Int. Conf. on Plasma Physics and Controlled Nuclear Fusion Research, Brussels, June 1980.

13. S. Lee et al., Amer.J.Phys., accepted for publication Oct-Dec. issue 1987.

14. A.J. Smith, K.H. Kwek, T.Y. Tou, A.V. Gholap and S. Lee
IEEE J. Quantum Electronics QE-23,283 (1987).
S. Lee, T.Y. Tou, M. Eissa, A.V. Gholap, K.H. Kwek, S.P. Moo, S. Mulyodrono, A.J. Smith, Suryada, W. Usada and M. Zakaullah
J. Fiz. Mal. 7, 1 (1986)
also Singapore J. Phys. 3, 75 (1986)
also J. Fiz. Mal. 6, 165 (1985)
C.S. Wong, O.H. Chin, M. Eissa, A.V. Gholap, S. Mulyodrono, C.X. Ong, S. Sapru, S.H. Saw, A.J. Smith, Suryadi and W. Usada - J.Fiz.Mal. 7, (1986)
Also 11 research papers and reports read at the Second Tropical College on Applied Physics.

15. M.G. Haines, Physica Scripta T2/2, 380 (1982).

16. G. Decker, R. Wienecke, Physica C 82, 155 (1976).

17. W. Kies, "Plasma focus - Physics and technology" review paper presented at Second Tropical College on Applied Physics, Kuala Lumpur, March 1986, to appear in Procs.

18. R. Gratton, A.R. Piriz, J.O. Pouzo, Nuclear Fus. 26, 483 (1986).

19. Y. Kato, S.H. Be, Appl. Phys. Lett. 48, 686 (1986).

20. S.P. Moo, S. Lee, Singapore J. Phys. 4, 131 (1987).

21. S. Lee, Harith Ahmad, T.Y. Tou, K.H. Kwek, C.S. Wong, J. Fiz. Mal. 6, 23 (1985).

22. F.J. Wessel, Hafiz Rahman, "Applications of z-pinches" paper presented at Spring College on Plasma Physics June 1987 ICTP Trieste, to appear in Procs.

23. P. Cloth, H. Conrads, Nucl. Sci. and Eng. 62, 591 (1977).

24. W. Neff, H. Krompholz, F. Ruchl, K. Schoenbach and G. Herziger, Phys. Lett. 79A, 165 (1980).

25. W.N. Hugrass, I.R. Jones, K.F. McKenna, M.G.R. Phillips, R.G. Storer and H. Tuczek, Phys. Rev. Lett. 44, 1676 (1980).

26. I.R. Jones et al., Aust. J. Phys. 40, 157 (1987).

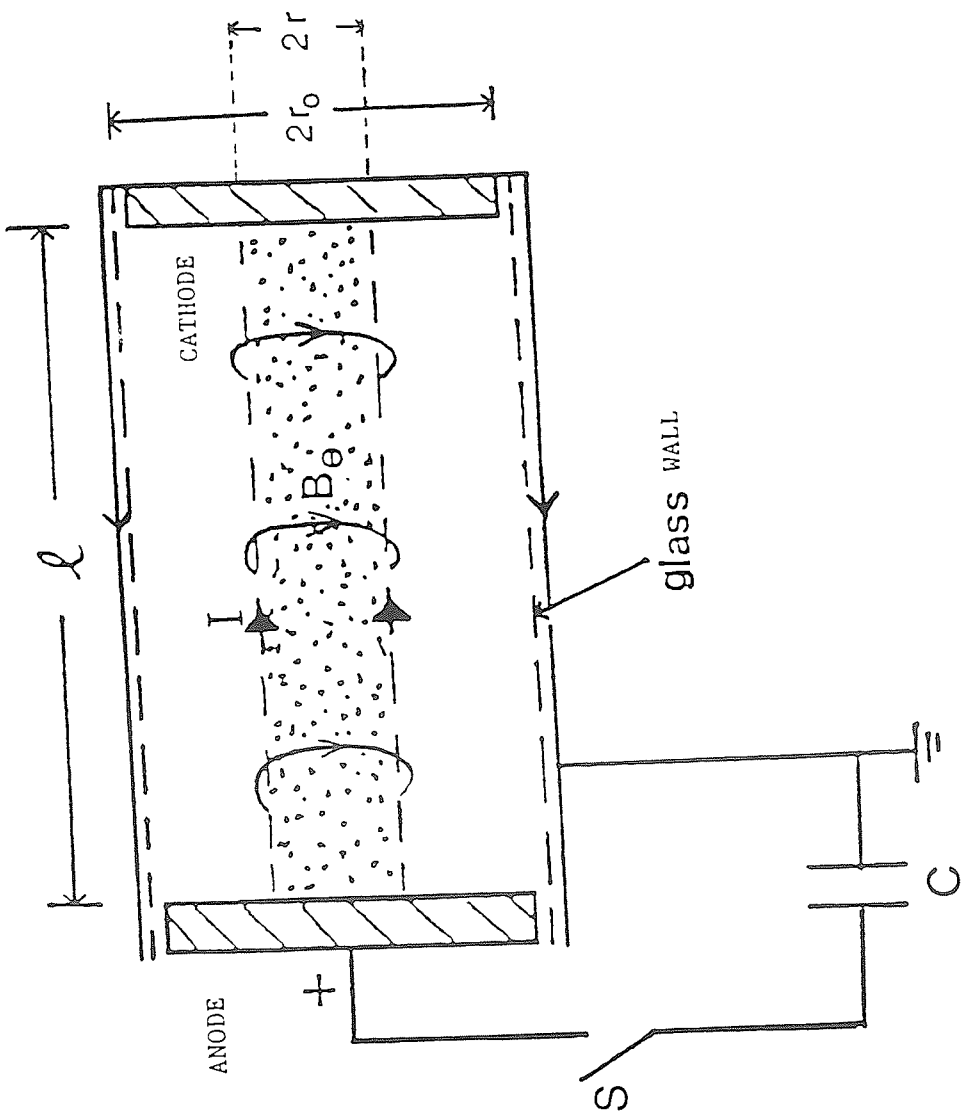

Fig.1 Illustrating the principle of the plasma pinch

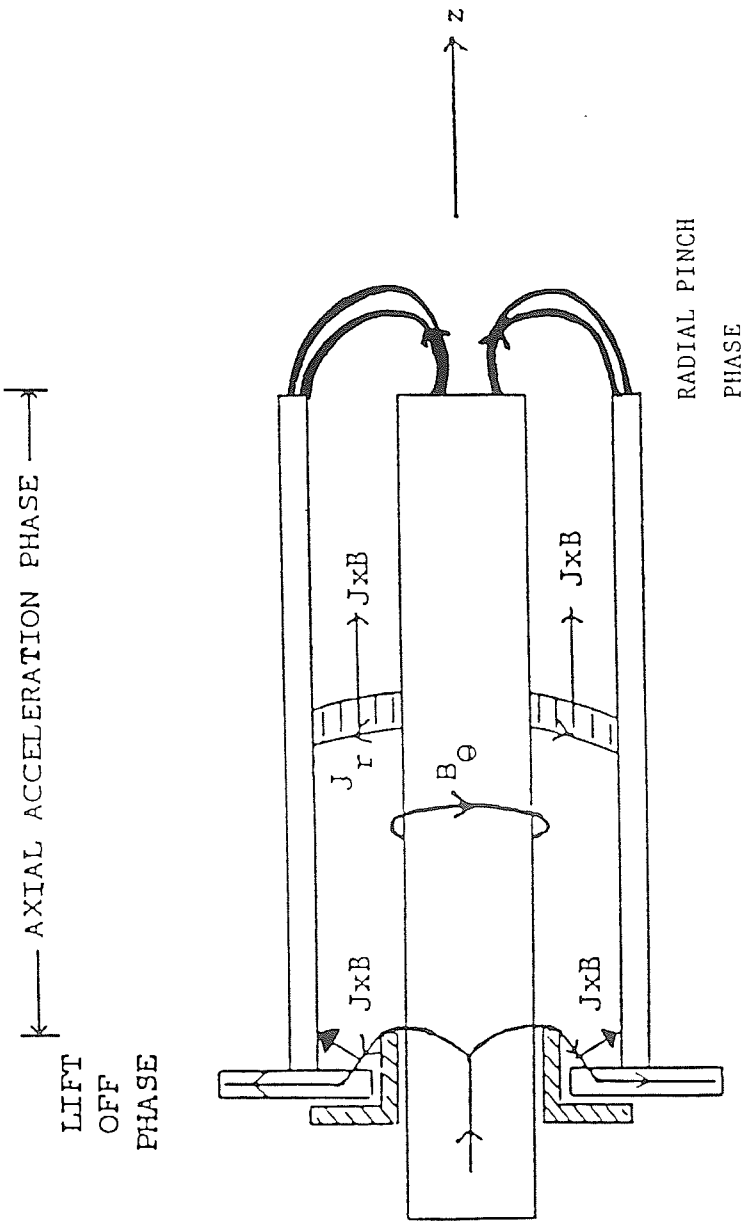

Fig. 2 Illustrating the two phases of the Plasma Focus

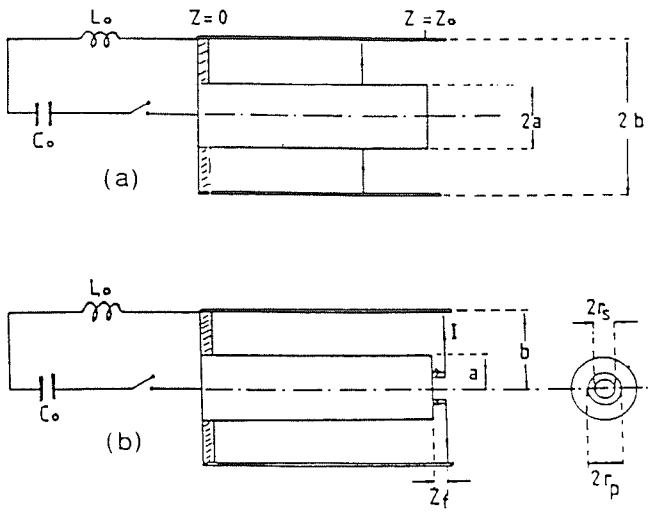

Fig. 3 (a) The axial run-down (shock tube) phase of the plasma focus.
(b) The radial focus (pinch) phase of the plasma focus.

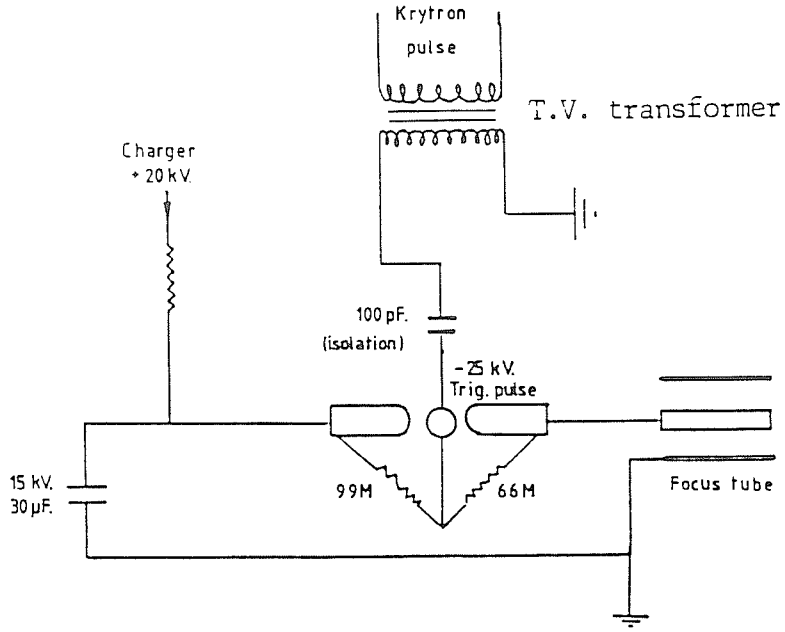

Fig. 4 Circuit for the swinging-cascade spark gap and focus tube.

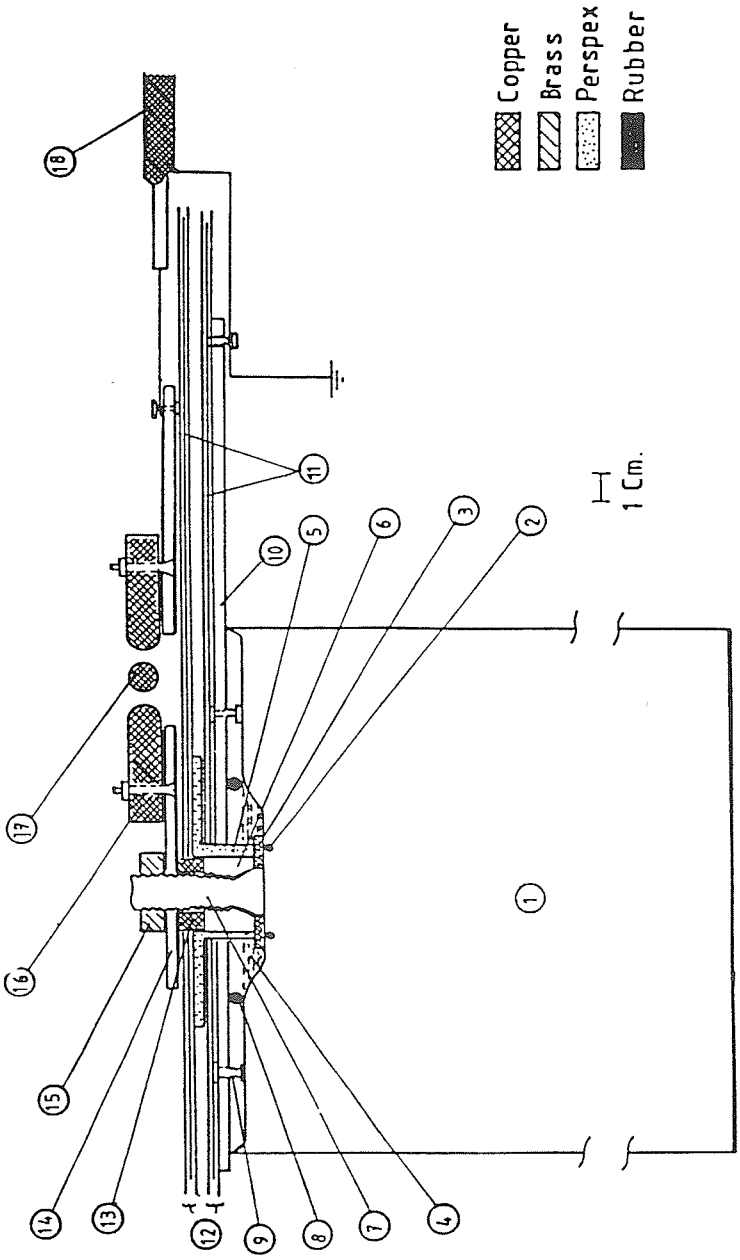

Fig. 5 The capacitor connecting plates, the spark gap and output coaxial cables. 1 = 15 kV, 30 μF capacitor; 2 = capacitor O-ring seal; 3 = washer; 4 = oil; 5 = nylon cap; 6 = steel nut; 7 = capacitor output seal; 8 = O-ring seal; 9 = earth stud; 10 = earth plate; 11 = 5-mil mylar film; 12 = polyethelene film; 13 = copper ring HV connector; 14 = capacitor high voltage (HV) output plates; 15 = lock nut for HV plate; 16 = HV electrode for swinging cascade spark gap; 17 = trigger electrode; and 18 = output coaxial cables (16 in parallel).

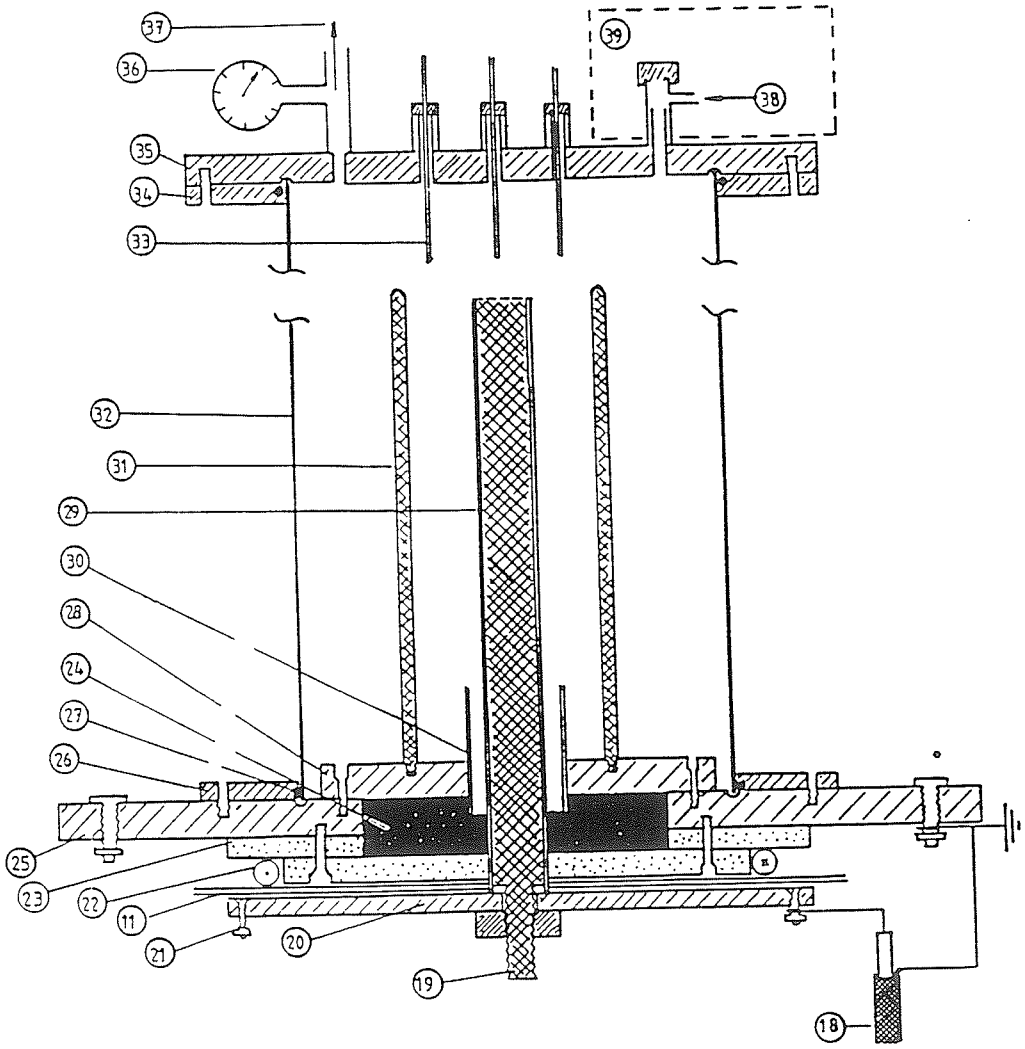

Fig. 6 The plasma focus tube
18 = input coaxial cables (16 in parallel); 19 = stud of anode; 20 = anode collector plate; 21 = connecting points for coaxial cable HV lead; 22 = Rogowski coil; 23 = perspex spacer; 24 = rubber holder; 25 = cathode collector plate; 26 = mild steel flange; 27 = O-ring seal; 28 = focus cathode support plates; 29 = focus anode; 30 = glass insulator; 31 = focus cathode (6 rods); 32 = mild steel focus chamber; 33 = movable magnetic probe in glass jacket; 34 = flange; 35 = back flange; 36 = diaphragm gauge; 37 = outlet to vacuum pump; 38 = inlet for test gas; 39 = wax container with indium foil and PM-scintillator activation counter.

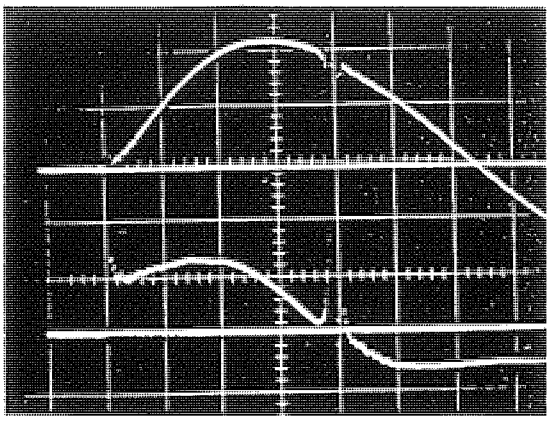

Fig. 7a Current (upper trace) and voltage (lower trace) of plasma focus in air.

13 kV, 0.5 torr
Top trace: 73 kA/cm
Bottom trace: 2kV/cm
Time scale (horizontal); 1 μs/cm

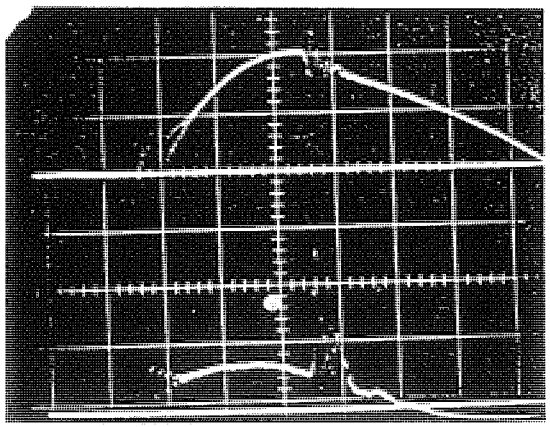

Fig. 7b Current and voltage trace of plasma focus in deuterium.

13 kV, 2.5 torr
Top trace: 75 kA/cm
Bottom trace: 4 kV/cm
Time scale (horizontal): 1 μs/cm

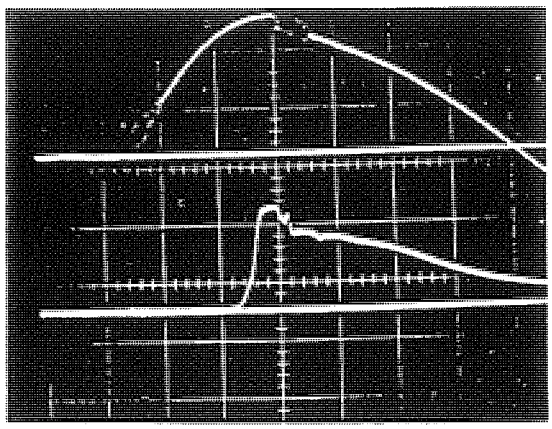

Fig. 7c Current and magnetic trace of plasma focus in deuterium

15 kV, 3.5 torr
Magnetic probe placed at z = 10.2 cm
Top trace: 73 kA/cm
Bottom trace: 0.6 T/cm

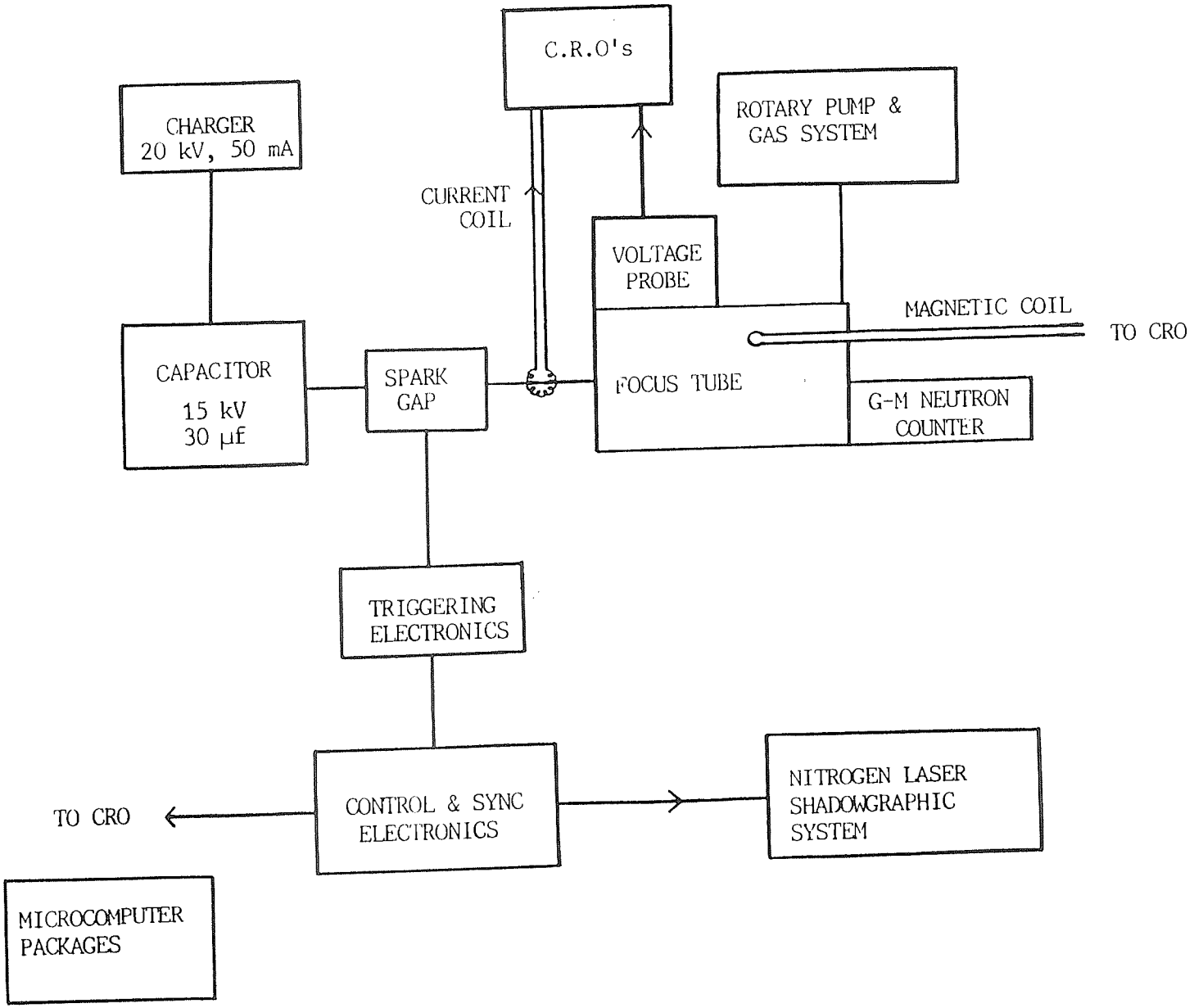

FIG. 8 SUB-SYSTEMS FOR THE UNU/ICTP PLASMA FUSION FACILITY

Physics and Perspectives of Small Plasma Devices

A programme to initiate experimental plasma physics in developing countries has been started as a definite step for technology sharing. Cost effectiveness of several devices has been carefully considered from the viewpoint of physical mechanisms and existing technology. The resulting programme has been tested using a plasma focus package which has been successfully transferred to several countries.

S. Lee

Introduction

Plasma physics has attained considerable importance in its present applications and also with its potential associated with fusion energy. Considerable effort, for example the Plasma Physics Colleges organised by the International Centre for Theoretical Physics (ICTP) Trieste, has been expended to provide plasma physics education at an international level aimed towards stimulating the study of plasma physics even in developing countries[1,2]. This worthwhile educational effort encounters considerable difficulties at the experimental level particularly from the equipment point of view. Many scientists from smaller developing countries have been trained in postgraduate plasma physics programmes in developed countries or have carried out periods of research in such experimental facilities. On their return to their home institutions they face the daunting challenge of building up some simple, yet effective research facilities to provide continuity in their experimental research experience and also to train their students.

At present there is not even a clear idea as to which experiment could be usefully developed although low cost, cost effectiveness, simplicity and good educational value combined with a large variety of plasma phenomena amenable to study by simple diagnostics should be among the factors to be considered in relation to devices for developing countries. Thus, glow discharge has often been suggested as a suitable plasma for study in a developing country. The glow discharge has several applications, for example deposition and sputtering of thin films, and can also be used as a medium for the experimental study of plasma waves. It serves as a good starting point to develop plasma jets and arcs which may be used as plasma torches or heaters for industrial and metallurgical applications or for applications in MHD power generation.

To move upwards in temperature so that one may aspire to study the fusion aspects of plasma physics one may consider building an electromagnetic shock tube to study shock heating or a linear z-pinch for the study of imploding shocks and magnetic compressions. These are 'classical' devices with well-known technology. The z-pinch even in the low cost scaled-down form necessary for this educational exercise could produce a plasma of sufficient density and temperature to be of interest even though no measurable nuclear fusion may be expected. The plasma focus goes one stage better. It is an excellent device for teaching plasma dynamics and thermodynamics besides being a rich source for a variety of plasma phenomena including soft x-rays and plasma nuclear fusion. The plasma focus is superior to both the electromagnetic shock tube and the linear z-pinch in its range of plasma parameters, combining as it does the essential mechanisms of the devices in such a properly sequenced manner that all the features of both devices, and many more, are produced in one single simple low cost device, when properly designed.

As a result of informal discussions among participants from developing countries at the 1983 Plasma Physics College at the ICTP it was decided to include the plasma focus as one of the educational devices for the initiation of experimental plasma and fusion research in the smaller developing countries as an effort to develop and share fusion related technology among ourselves[3]. This project received support from the United Nations University (UNU) whose Rector Dr. Soedjatmoko added a further dimension when he stated in a communication: "We at the (UNU) have strong reasons to believe that plasma physics will be one of the major technologies of the future in developing as well as industrialised countries. We find great merit in ... argument that developing countries should begin now to experiment with and develop modest plasma systems in order to acquire practical knowledge and skills to better employ technologies based on plasma physics once major breakthroughs permit the utilization ... for the production of energy as well as for other applications."

Cost Effective Physics

In order to implement a project whereby a developing country may produce a suitable package for sharing technology with other developing countries with the aim of initiating experimental plasma research it is necessary to consider the cost effectiveness of the device to be chosen. Does it produce a rich variety of plasma phenomena? Does it require an expensive vacuum system? Can its power supplies, control electronics and basic diagnostics be packaged at reasonable cost? What physical mechanisms operate to make the chosen device perform better at lower packaging cost than other de-

S. Lee is professor at the Department of Physics, University of Malaya, Kuala Lumpur, Malaysia.

vices? Can we understand and model the design and performance of the device so that we may effectively do research on it? What are the areas of research and potential applications of the device?

From the point of view of the production of a plasma with conditions of density and temperature sufficient for plasma fusion studies at an affordable cost there is little doubt that the class of fast magnetic compression devices known generally as the pinch, including the linear z-pinch, the superfast pinch, the gass-puff pinch and the plasma focus offers the best potential. We have considered this class of device and found that the plasma focus is most cost effective having the same power supply, control electronics and basic diagnostic requirements as the simple z-pinch and a much cheaper vacuum system with only rotary pump requirement, yet producing more intense plasma phenomena including copious x-rays, relativistic electron beam (REB) and fusion neutrons, all in one small easily packaged facility. What is the physics behind this cost effectiveness?

Cost Effectiveness of Various Types of Pinches

We first recall that the neutron yield Y from a plasma fusion source is:

$$Y = \frac{1}{2} n^2 \langle \sigma v \rangle \text{ (volume) (time)} \qquad (1)$$

We note that Y is proportional to the square of n, the number density of the fusion fuel. We also note that starting from temperatures below 1 keV as one struggles to heat a plasma up towards a few keV, the effective cross section $\langle \sigma v \rangle$ for a thermalised deuterium plasma rises very rapidly with fuel temperature T. For example between 1 to 2 keV $\langle \sigma v \rangle$ for the D-D fusion reaction goes up by a factor of 25! – and between 2 to 5 keV, another factor of 30!. Thus the neutron yield is very sensitive to temperature. It is also proportional to the square of density.

In the pinch a large electric current is discharged from a capacitor bank through a gas between two electrodes (see Fig. 1). The current rises rapidly and due to the skin effect and wall conditions, electric breakdown first occurs across the glass wall of the container, forming a sheath of current along the glass wall. The electromagnetic **J** x **B** force in such a geometry acts radially inwards at every point of the current sheath so that, if the current is large enough, the current sheath and the heated gas (plasma) it entrains implode supersonically to form a hot dense column around the axis of the device.

The condition of balance between the hydrostatic pressure of the hot plasma and the constricting magnetic pressure gives the equation for the plasma temperature as:

$$T = \frac{\mu_0 I^2}{8\pi N} \qquad (2)$$

where $N = \pi n r^2$ is the line density (particles m^{-1}) of the pinch. From this equation it would appear that since the temperature T depends on I^2 any temperature can be reached simply by increasing I to a sufficient value. However a pinch is essentially a dynamic device. The formation of the column has to occur in a time matched to the risetime of the current pulse, otherwise essentially the column is no longer there to obey the pressure balance equation when the current has risen to its peak value. Because of the dynamic nature of the problem the final temperature reached depends also on the implosion speed of the front of the plasma layer, which takes the form of a strong shock front. For deuterium the temperature dependence has the form:

$$T = 2.3 \times 10^{-5} \text{ (shock speed)}^2 \qquad (3)$$

Because of the dynamic nature of the problem it is essential for optimum use of the capacitor energy for the imploding shock wave to reach the axis at about the time of peak current. Now a typical well-designed capacitor bank for a pinch (say 20 kV, 60 μF, low inductance) has a current risetime of about 3 μs. In general it is difficult (and expensive) to design a capacitor bank of this conventional type for a much shorter risetime, and the bigger the bank capacity the longer tends to be the risetime.

So we consider a typical current risetime of 3 μs. A typical implosion speed cannot be much less than 10 cm/μs. At this speed the shock temperature in deuterium is 2×10^5 K. At any speed slower than that it is doubtful whether the magnetic 'piston' would be clearly formed. Even at this slow speed a radius of 30 cm for the pinch tube is required in order to match the current risetime. Now the imploding magnetic pressure is

$$P_m = \frac{\mu_0 I^2}{8\pi^2 r^2} \qquad (4)$$

and with such a large pinch tube radius it is difficult to get enough magnetic pressure in the early stages of the implosion to start a clean compression unless the gas pressure is low. Thus a conventional pinch is limited by a (slow) current risetime of 3 μs, so that the pinch has to be operated with a large radius and hence low initial density. Moreover the speed (and hence temperature) becomes limited because of time-matching consideration.

What about the compressed density? We may apply a lossless energy balance theory[4] and allowing for a reflected shock overpressure to show that the radius ratio κ_m (final radius r_m / initial radius r_0) is defined in a cylindrical supersonic pinch by the equation:

$$\iota_m^2 = \frac{2(\gamma_m - 1)}{f_m l_m} \int_1^{\kappa_m} \frac{\iota^2 l d\kappa}{\kappa} \qquad (5)$$

where κ, ι and l are the normalised, generally time dependent radius, current and length of the pinch, the subscript m refers to the quantity at the moment of peak compression, γ is the specific heat ratio and f_m is the reflected shock overpressure factor at the moment the shock reflected from the axis hits the pinching current sheath, ending the pinch compression. This equation gives us the following useful information:

(a) κ_m (and hence the compressed density ratio $= \kappa_m^{-2}$) does not depend on the absolute magnitude of the current or the absolute length of the pinch.

(b) κ_m (hence Γ) depends on the time function of the current[5] and length.

(c) κ_m (hence Γ) depends on γ_m[6] and f_m. The smaller is γ_m, the smaller is κ_m and the larger is Γ. As γ_m approaches the lower limiting value of 1, κ_m approaches zero and Γ tends to infinity. The larger is f_m, the smaller is κ_m and the larger is Γ. The value of f for a reflected shock on-axis, i.e. just after reflection is $f \approx 4$ for cylindrical geometry[7]. As the reflected shock travels out from the axis we may expect f to decrease towards a limiting value of 1.

For example for a constant current pinch with constant length, with $\gamma = 5/3$ and $f_m = 1.6$, eq. (5) gives $\kappa_m = 0.301$ and hence a density compres-

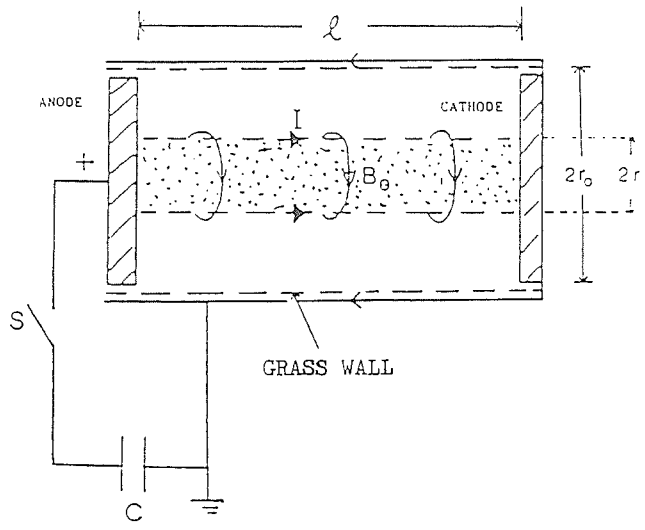

Figure 1
Illustrating the principle of the plasma pinch

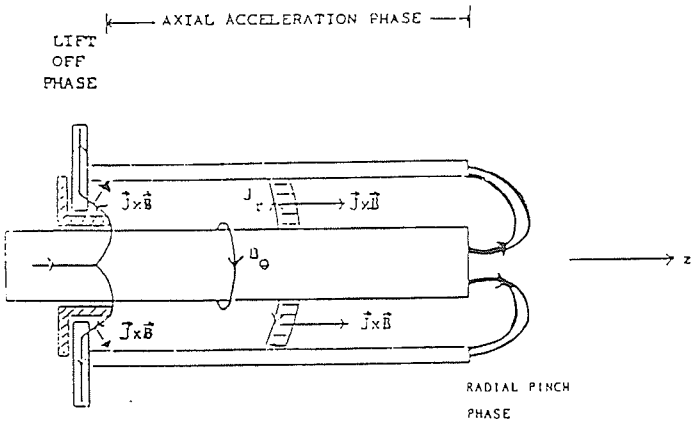

Figure 2
Illustrating the two phases of the Plasma Focus

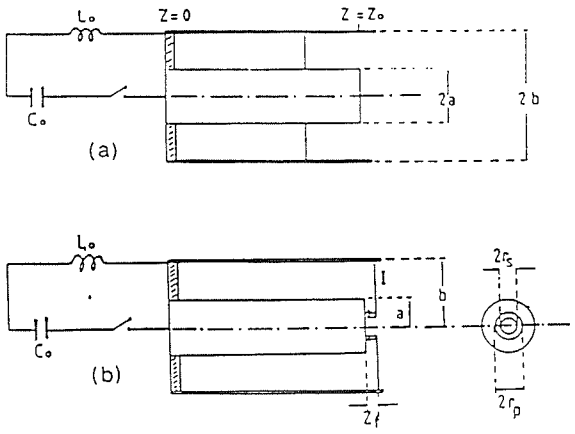

Figure 3
(a) The axial run-down (shock tube) phase of the plasma focus.
(b) The radial focus (pinch) phase of the plasma focus.

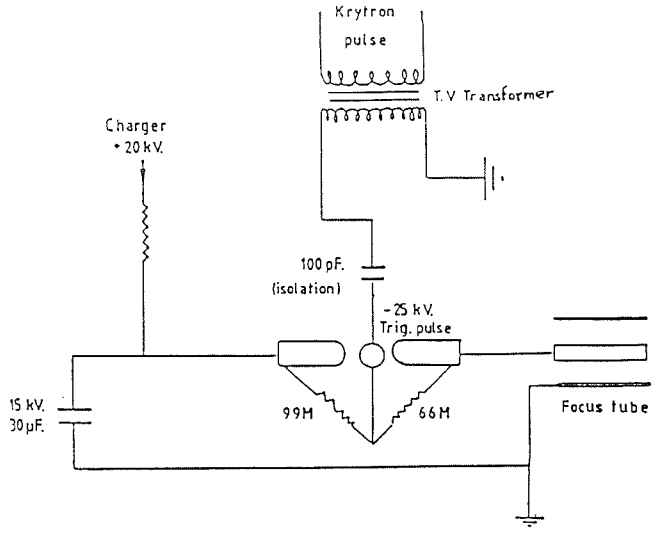

Figure 4
Circuit for the swinging-cascade spark gap and focus tube.

sion ratio of $\gamma=11$. The corresponding figures for the deuterium plasma focus are estimated to be $\kappa_m=0.14$ and $\gamma=50$. These values are independent of the magnitude of the plasma current. This limitation of the ability to compress is a serious one and implies that the performance of the pinch as a radiation source depends on its initial density.

There are several concepts to overcome this limitation. The gas-embedded axis-initiated z-pinch uses a laser to start a pinch discharge on-axis thus obviating the problem of matching the electrical risetime to the pinch collapse time and allowing the formation of a very small radius pinch (sub mm radius) in a very dense plasma (initial density up to several atmospheres). The device is however plagued with problems of instability [8]. The hollow pinch uses a controlled gas jet [9,22] to form a thin plasma sheath which is then pinched into a vacuum. Using argon, krypton or xenon, the sheath does not thicken very much during the implosion because these gases are in the 'freely ionizing' regime [6] with a value having a small value of the order of 1.1. Because of the short distance between the imploding shock front and the magnetic piston the reflected shock from the axis hits the piston after a much shorter distance than that compared with a conventional pinch. The value of f_m is hence closer to 4 than in a conventional pinch with its thicker plasma sheath. Thus the hollow-pinch has a reduced κ_m and has been operated successfully in the heavier gases, particularly krypton and xenon, for the production of x-rays for x-ray lithography and microscopy. However, from the technical point of view the hollow pinch requires the additional development of a rather precise gas valve system. It is also not known to operate well in deuterium, probably because the collapsing deuterium sheath thickens as its γ goes to 5/3 once the sheath reaches a speed of the order of 10 cm/μs.

Ultra high power pinches have also been operated with pulse forming lines to reduce current risetimes so that the pinch may be operated at smaller radius, hence higher density[15]. This high power approach requires the use of more complex and expensive technology.

On the other hand the plasma focus uses a very simple principle to overcome the time mismatch. Essentially it allows a conventional (slow risetime of 3μs or more) capacitor bank to derive a very fast pinch (typically 1 cm radius in 50 ns) at a sufficiently high density and a large current during the time of pinch. Thus at low cost plasma conditions may be achieved which are more intense than that produced even in high-cost pinches.

The plasma focus uses a conventional capacitor bank to drive a device which has two sections:- the first section is a coaxial electromagnetic shock tube whose length is matched to the capacitor risetime. The rising capacitor current drives a shock wave axially down the shock tube at a suitable speed until the shock wave reaches the end of the tube at peak current. Then by the geometry of the device (see Fig. 2) the axial drive phase is simply converted to a radial compression or pinch phase.

The pinch phase is very intense (see Eqs. 2

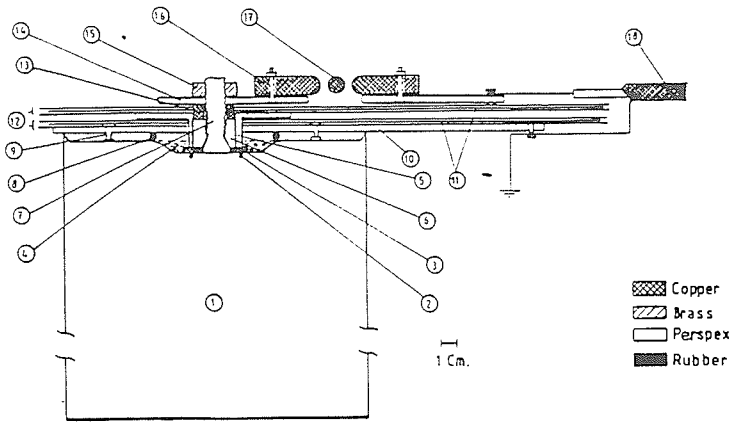

Figure 5
The capacitor connecting plates, the spark gap and output coaxial cables.
1= 15kV, 30μF capacitor; 2 = capacitor O-ring seal; 3 = washer; 4 = oil; 5 = nylon cap; 6 = steel nut; 7 = capacitor output seal; 8 = O-ring seal; 9 = earth stud; 10 = earth plate; 11 = 5-mil mylar film; 12 = polyethelene film; 13 = copper ring HV connector; 14 = capacitor high voltage (HV) output plates; 15 = lock nut for HV plate; 16 = HV electrode for swinging cascade spark gap; 17 = trigger electrode; and 18 = output coaxial cables (16 in parallel).

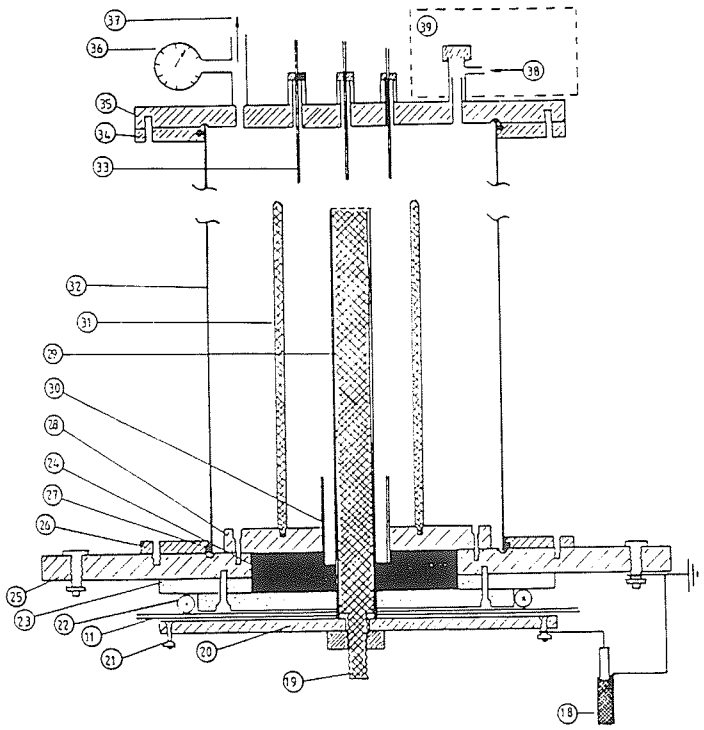

Figure 6
The plasma focus tube
18 = input coaxial cables (16 in parallel); 19 = stud of anode; 20 = anode collector plate; 21 = connecting points for coaxial cable HV lead; 22 = Rogowski coil; 23 = perspex spacer; 24 = rubber holder; 25 = cathode collector plate; 26 = mild steel flange; 27 = O-ring seal; 28 = focus cathode support plates; 29 = focus anode; 30 = glass insulator; 31 = focus cathode (6 rods); 32 = mild steel focus chamber; 33 = movable magnetic probe in glass jacket; 34 = flanges; 35 = back flange; 36 = diaphragm gauge; 37 = outlet to vacuum pump; 38 = inlet for test gas; 39 = wax container with indium foil and PM-scintillator activation counter.

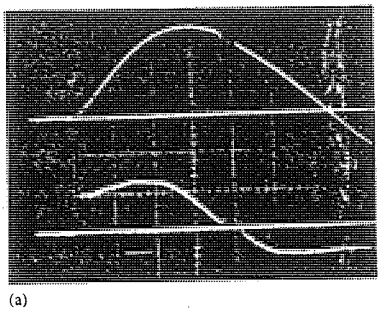

(a)

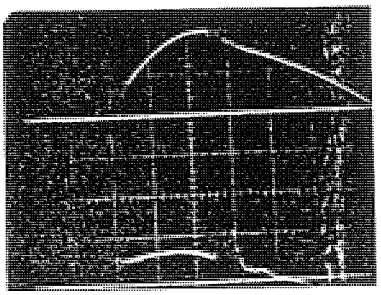

(b)

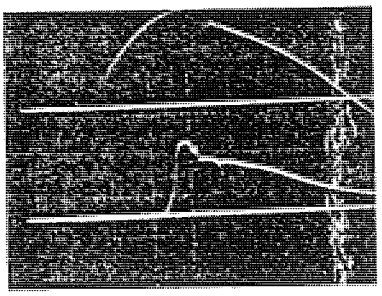

(c)

Figure 7
(a) Current (upper trace) and voltage (lower trace) of plasma focus in air: 13kV, 0.5 torr; Top trace: 73 kA/cm; Bottom trace: 2kV/cm; Time scale (horizontal): 1 μs/cm (b) Current and voltage trace of plasma focus in deuterium: 13kV, 2.5 torr; Top trace: 75 kA/cm; Bottom trace: 4 kV/cm; Time scale (horizontal): 1 μs/cm. (c) Current and magnetic trace of plasma focus in deuterium: 15kV, 3.5 torr; Magnetic probe placed at z = 10.2 cm; Top trace: 73 kA/cm; Bottom trace: 0.6 *T*/cm

and 4) because it starts at a very large current (typically 500 kA) and at a relatively small radius (typically 1 cm). Thus the operating pressure may be relatively high (10 torr in D_2 for a plasma focus against 0.1 torr or less for a pinch). The increased density and temperature more than compensates for the reduced volume in terms of the neutron yield *Y* as given in Eq. (1).

Having seen from the basic physics mechanism that the plasma focus is capable of high levels of performance without special technological development the next step in the development of an educational package is to consider the modelling and design of a practical device.

Cost Effecitve Design of a Plasma Focus

Using these simple ideas a dynamic model[10] (see Fig. 3) is developed. This considers the focus dynamics in two separate phases — the axial run-down (shock tube) phase which crucially delays the radial focus, or pinch phase until the plasma current has reached its peak value. The model couples the electric circuit to the plasma dynamics and is written to facilitate the design, on any micro-computer, of an optimum plasma focus in terms of a parameter which enables the matching of the electrical risetime to the axial run-down time, a second parameter α_1 which adjusts the ratio of the axial run-down time to the radial pinch time so that this factor may be thought of as a power enhancement factor, and a third parameter which adjusts the ratio of the device inductance to the external circuit inductance. Other parameters in the model include the ratio of external to internal radii, the aspect ratio and the specific heat ratio. This latter ratio is a thermodynamic function of temperature and affects the radial pinch structure and dynamics.

The Experimental Facility and Results

The design of a plasma focus may take as a starting point the availability, or choice of a capacitor bank. For the present exercise from the point of view of economy and cost-effectiveness a single Maxwell capacitor rated at C_0=30 μF, V_0=15 kV of inductance less than 40 nH was selected.

The experimental facility designed from the above physical model is shown in Figs. 4, 5 and 6. Fig. 4 shows the plasma focus circuit using a swinging-cascade spark gap switch triggered via a TV transformer. Fig. 5 shows the parallel-plate spark gap arranged in a low-inductance configuration on top of the capacitor with 16 output coaxial cables (No. 18 in Figs. 5 and 6) which connect the spark gap output to the plasma focus input flange as shown in Fig. 6. The plasma chamber (No. 32) consists of a 30 cm length of 6½ inch mild steel tubing and the required vacuum is provided by a small single stage rotary pump with ultimate base pressure of 0.01 torr. The design of the focus tube electrodes has several important features[13] particularly regarding the mounting of the backwall glass insulator (No. 30). Diagnostics are also indicated in Fig. 6.

Results

The system was tested between 13-15 kV in various gases including air, argon, hydrogen and deuterium. The strength of the focussing action is gauged from the current dip and voltage spike. (Current is measured using a Rogowski coil and voltage using a voltage divider.) Figure 7a shows an oscillogram of the current and voltage waveforms of the plasma focus in 0.5 torr of air, with focussing action about 1 s after peak current. Figure 7b shows a deuterium focus, at 13 kV, 2.5 torr with focussing action occurring at peak current.

These oscillograms show a terminal axial speed of 10 cm/μs corresponding from Eq. 3 to a deuterium plasma temperature of 2 x 10^5 K. The observed current sheath is well-formed with a thickness of 2 cm at the end of the axial phase as estimated from the oscillogram. The current dip and voltage spike are indicative of a good pinching action during the radial phase, in agreement with the model.

In deuterium when operated at 15 kV and optimum pressure conditions of 3 torr consistent counts of 1000-2000 are obtained using the PM-scintillator counter. This corresponds to 0.5-1 x 10^8 neutrons per shot.

The system shows remarkably consistent and reproducible operation. For the purpose of a training programme sponsored by the UNU, six systems were assembled one after the other and tested over a period of two months. Each system (designated as the UNU/ICTP PFF) was assembled and tested over a period of one week averaging between 100-200 shots in the various gases. Once a system has been established to be operating normally, that is without undue leakage and after an initial period of out-gassing involving some three to five discharges, proper focussing is achieved for better than 95% of the discharges, apart from those discharges deliberately operated outside the established suitable pressure range for the gas used.

Table 1
Research Transfer for 1985/86 Programme

	UNU/ICTP Plasma Fusion Facility	EMST High Speed Flow Simulator	N_2 Laser System	Glow Discharge
Egypt	1		1	
India			1	
Indonesia	1	1		1
Pakistan	1			
Nigeria	1		1	
Sierra Leone	1		1	

The UNU Training Programme on Plasma and Laser Technology

Based on the above detailed consideration of the plasma focus the UNU Training Programme (also sponsored by the ICTP) was conducted in Kuala Lumpur by the Plasma Physics Research Group and the Laser Physics Research Group of the University of Malaya (UM) from October 1985 to April 1986. The following summarises the Training Programme:

Aim:

To initiate experimental plasma/laser research in several developing countries.

Method:

By transfer of a comprehensive integrated package of expertise plus basic components and equipment — sufficient to enable the UNU Fellow to build and operate, and do measurements on, a basic plasma/laser facility back at his home institution.

Package for transfer:

electrodes
vacuum chamber
pulsed control switching electronics
power supplies
high power discharge systems
diagnostic systems
design, testing and research procedures
computational packages for microcomputer modelling of circuit and plasma dynamics

Programme:

October to December 1985 — Lectures and experiments on existing devices in the UM laboratories including pulsed electronic modules, power supplies glow discharge, electromagnetic shock tubes (EMST), plasma focus, computation packages on circuit and plasma dynamics; and various lasers; system planning, design, construction and development of all sub-systems for each facility chosen by the individual Fellow. (see Table I).

December 1985 – February 1986 – development, assembly and testing of each set of facility; research work on the various devices.

March 1986 – reports and further planning; preparation for shipment of equipment; writing of research papers[13,14] presentation of some research results to the Second Tropical College on Applied Physics[14].

Sponsorship:

UNU for Fellowships and institutional support
ICTP for equipment grant for UNU Fellows
University of Malaya for facilities
Malaysian Institute of Physics for organisation.

Progress on return home

A year after the equipment were received by the UNU Fellows back at their respective home institutions their progress may be summarised as follows. The plasma focus facility is now operational at Al-Azhar University, Cairo (Dr. M.A.A. Elissa). It has been redesigned and modified and a facility each is operational at the Yogyakarta Nuclear Research Centre (PPNY) (Suryadi and W. Usada) and at Qaid-I-Azam Islamabad (M. Zakaullah). Resulting from the

UNU training, Qaid-I-Azam University is also planning several other plasma devices including a 16 kJ plasma focus. Dr. A.V. Gholap* (River State University of Science and Technology, Port Harcourt) and Dr. A.J. Smith (Njala University College, Sierra Leone) have each one M.Sc. student completing thesis work on the nitrogen laser and planning to proceed to Ph.D. research on the UNU/ICTP PFF which is marginally operational at each of these two institutions because of very difficult technical conditions. A nitrogen laser is also operational at Sri Pratap College, Srinagar (Dr. S. Sapru). S. Mulyodrono (National Space and Aeronautics Agency, Jakarta) has started on a Ph.D. programme on hypersonic flow simulation and em propulsion using the EMST as the basic facility. M. Zakaullah is also using the UNU/ICTP PFF as the basic facility in pursuing the first experimental plasma physics Ph.D. programme in Pakistan. Four Fellows have been awarded TWAS (Third World Academy of Sciences) research grants.

What can be done with this fusion facility

For the plasma focus, the concept of technology sharing has already been demonstrated by the UNU Training Programme. It may be pertinent to try to advance the ideas by asking what can be down with the UNU/ICTP PFF.

Characteristics

To discuss this we first summarise the characteristics of the UNU/ICTP PLASMA FUSION FACILITY:

Capacitor voltage	V_0	15 kV
Capacitance	C_0	30 F
Stored energy	E	3.3 kJ
Inductance	L_0	110 nH
Inner radius	a	0.95 cm
Outer radius	b	3.2 cm
Length	z_0	16 cm
Characteristic current	I_0	250 kA
Peak current		160 kA
Current risetime		3 s
Average axial shock speed		6 cm/ s
Peak axial shock speed		10 cm/ s
Average radial shock speed		12 cm/ s
Peak radial shock speed ≈ 25 cm/s		
Neutron yield (at 3 torr D_2) Y		10^8 per discharge

Types of plasmas (strongly focussed):

Deuterium	1 - 5 torr
Hydrogen	1.1 - 6 torr
Helium	0.7 - 3.5 torr
Argon	0.3 - 2 torr
Air	0.5 - 1.1 torr
Carbon dioxide	range undetermined, but below 1 torr

Copious x-rays are also emitted from these plasmas.

Diagnostics

The simple diagnostics that have been designed for the UNU/ICTP PFF are now summarised here:

Current measurement	Rogowskii coil
Voltage measurement	Resistive probe, capacitive probe
Magnetic field	Magnetic coil
Speed measurement	Current probe, voltage probe, magnetic probe, photodiode
Measurement of dynamics and electrodynamics	Current probe, voltage probe and magnetic probe used in conjunction with circuit and snow-plow analysis and computation
Neutron measurement	Activation counter using Geiger-Mueller tubes; also time-of-flight method
X-ray measurement	Pin-hole camera; PIN diodes
Density distribution and dynamics	Laser (e.g. Nitrogen laser), shadowgraphy and holography

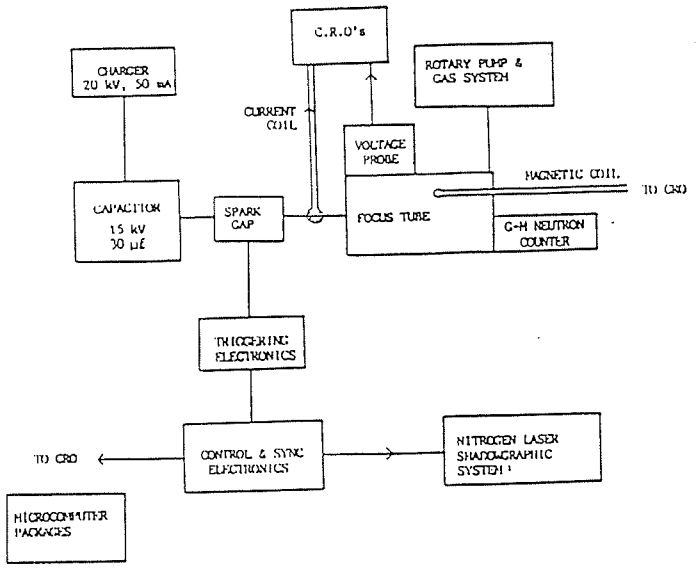

Figure 8
Sub-systems for the UNU/ICIP plasma fusion facility.

Computer packages

Computation models specifically developed (mainly) for microcomputers include:

Modified snow-plow model for the axial phase
Generalised slug-model for the radial phase
Energy balance model for estimating the minimum compression radius (gross)
Thermodynamic computations for the specific heat ratios and ionisation fractions for argon, and the effects of these on the dynamics.

The UNU/ICTP PFF broken down into sub-systems

To give a better picture of the fusion facility the sub-systems making up the facility are shown in Fig. 8.

Training and Research Topics

Having listed the characteristics of the plasma focus, types of plasmas produced, performance, diagnostics and computation packages and also the sub-systems making up the fusion facility we shall now summarise the training and research topics that may be carried out on such a device almost immediately it is set up by trained staff.

System technology and construction
System characterisation and optimisation
Development of diagnostics
Development of computation-modelling, parametric variation and optimisation
Plasma dynamics
Neutron measurements[23] and neutron scaling, fusion physics

*(Dr. A.V. Gholap's student has successfully completed his M.Sc.)

Neutron enhancement by dynamic, thermodynamic and target methods[23]
Application as pulsed neutron source e.g. for half-life measurements[20]
X-ray measurement and production
X-ray enhancement and application as source for lithography and microscopy[19]
Relativistic electron beam (REB) measurement[24] and applications
Plasma focus for inertial confinement studies[18]
Sputtering and deposition of anode materials and special anode inserts[21,16]
Study of particle accelerating mechanism and application[16]
Compression enhancement and generation of megaGauss magnetic fields[22]

Several of the topics in this list have hardly been researched upon and may form extended research programmes.

As an example we look at the plasma focus neutron scaling law. The generally accepted scaling law states that the neutron yield Y is proportional to the plasma electric current to the power of four. Using the simple model described above for the UNU/ICTP PFF we can show that this scaling law is a consequence of a speed limitation observed for all plasma focus machines. Present design techniques limit all plasma focus machines to an axial speed of 10 cm/μs and the radial collapse speed to 25 cm/μs, resulting in a temperature limit of 1 keV in the compressed column. This is a very severe limitation since the fusion cross section $\langle\sigma v\rangle$ of Eq. 1 is extremely sensitive to temperature scaling as $T^{4.2}$ in the temperature range of 1-5 keV. If this speed limitation were removed it may be shown that the neutron scaling would improve to Y proportional to the plasma electric current to the power of eight. Such a scaling law would revolutionise the focus as a serious fusion reactor concept in the same class as the deuterium fibre pinch [27]!

To establish this new regime of plasma focus operation the physical mechanisms imposing this speed limitation should be systematically studied. This could best be done on a small plasma focus such as the UNU/ICTP PFF. Being a simple machine it could be easily modified according to the dictates of the experiment.

Widening the sharing

The devices discussed so far — the glow discharge, the e.m. shock tube, the z-pinch and the plasma focus — cover a range of plasma conditions from a weakly ionized steady state relatively low temperature plasma to a highly ionized pulsed plasma undergoing copious nuclear fusion reactions. The packaging of these devices has proven to be useful. The next step would be to extend the exercise to the important study of magnetic and plasma configuration of the compact torus and the FRC type. It has been shown that the spheromak may be generated starting from a configuration very similar to the plasma focus and that a RFP may be generated from a theta pinch geometry. It would be useful for a cost analysis to be performed on these devices with a view to identify which device if any could be cost-effectively packaged for the purpose of research initiation.

One FRC device appears particularly suitably for such a package. Besides its potential as a current-drive candidate for fusion reactor schemes the Rotamak[25,26] may be scaled down and assembled as a very cost effective package for the experimental study of field reversed configurations lasting for a very reproducible and steady period of tens of millisecond with plasma temperatures and density of respectively a few eV and 10^{13}/c.c.

In 1986 the author visited the Flinders University of South Australia and in collaboration with Prof. I.R. Jones demonstrated at the Flinders Plasma Research Laboratory the operation of a 'transistorised' Rotamak FRC, driving a field-reversing steady plasma current of 250A for 40 ms in a single-phase Rotamak mode using a 1 MHz RF of 2 kW at only 170V. This device has great potential for development as a very cost-effective research-initiation package.

Conclusion

The concept of the sharing of fusion related technology among developing countries has been proposed and demonstrated comprehensively in one case using the plasma focus. A cost effectiveness analysis based on the physics and existing relatively simple technology has resulted in the design of an integrated package, the UNU/ICTP PFF which has been instrumental in the initiation and strengthening of experimental plasma research in several developing countries thus giving new perspectives to the development of small plasma experiments. The relatively low-technology approach of the package does not appear to detract from the performance of the research facility and is no barrier to the many possible applications of the plasma focus. Indeed the simplicity of the approach allows the singling out of the speed limitation of present generation plasma focus machines, which limitation if removed could result in a large multifold increase in focus neutron yield with an improved scaling proportional to plasma current to the power of eight!

It may not be untimely to propose a coordinated training programme based on specially designed packages such as the UNU/ICTP PFF or a similar Rotamak package as a means to increase the experimental research capability of physicists in developing countries.

References

[1] B. McNamara, "Twenty Years of Plasma Physics at the International Centre for Theoretical Physics" in 'Twenty Years of Plasma Physics' Edited by B. McNamara, World Scientific, and Singapore, p. XIII (1985).

[2] International Fusion Research Council "Status Report on Controlled Thermonuclear Fusion ", Nuclear Fusion 18-1, 137 (1978).

[3] Regional Centres for Research Transfer Within South-East Asian Countries—S. Lee; Invited paper presented at the International Conference on Physics for Development at the International Centre for Theoretical Physics, Trieste, Italy, 8-12 October 1984.

[4] S. Lee, Plasma Phys. 25, 571 (1983).

[5] S. Lee, J. Phys. D.: Applied Phys. 17, 733 (1984).

[6] S. Lee, Australian J. Phys. 36, 891 (1983).

[7] G. von Guderley, Luftfahrtforschung 19, 302 (1942).

[8] A.E. Dangor et al., Phys. Rev. A 27, 2751 (1983).

[9] J. Weinberg, A. Fisher, Applied Phys. Lett. 47, 1116 (1985).

[10] S. Lee in 'Radiation in Plasma' edited by B. McNamara, World Scientific, Singapore, Vol. II, 978 (1984). Also S. Lee in 'Laser and Plasma Technology' edited by S. Lee et al., World Scientific, Singapore, 387 (1985).

[11] J.W. Mather, P.J. Bottoms, J.P. Carpenter, K.D. Ware and A.H. Williams, Report No. IAEA-CN-28/D5, 561 (1972).

[12] J.P. Rager, L.E. Bilbao, H.A. Bruzzone, V. Gourlan, U. Guidoni, H. Kroeglar, S. Podda, B.V. Robouch, K. Steinmetz, 'Experiments on the neutron production phase of the Frascati 1 MJ Plasma Focus', Eighth Int. Conf. on Plasma Physics and Controlled Nuclear Fusion Research, Brussels, June 1980.

[13] S. Lee et al., Amer. J. Phys., 56, 62 (1988).

[14] A.J. Smith et al., IEEE J. Quantum Electronics QE-23,283 (1987); S. Lee et al., J. Fiz. Mal. 7, 1 (1986); Singapore J. Phys. 3, 75 (1986); J. Fiz. Mal. 6, 165 (1985). C.S. Wong et al., J. Fiz. Mal. 7, (1986). Also 11 research papers and reports read at the Second Tropical College on applied Physics.

[15] M.G. Haines, Physica Scripta T2/2, 380 (1982).

[16] G. Decker, R. Wienecke, Physica C. 82, 155 (1976).

[17] W. Kies, "Plasma focus — Physics and technology" review paper presented at Second Tropical College on Applied Physics, Kuala Lumpur, March 1986, to appear in Procs.

[18] R. Gratton, A.R. Piriz, J.O. Pouzo, Nuclear Fus. 26 483 (1986).

[19] Y. Kato, S.H. Be. Appl. Phys. Lett. 48, 686 (1986)

[20] S.P. Moo and S. Lee, Singapore J. Phys. 4, 131 (1987).

[21] S. Lee et al., J. Fiz. Mal. 6, 23 (1985).

[22] F.J. Wessel, Hafiz Rahman, "Applications of z-pinches" paper presented at Spring College on Plasma Physics June 1987 ICTP Trieste, to appear in Proceedings.

[23] P. Cloth, H. Conrads, Nucl. Sci. and Eng. 62, 591 (1977).

[24] W. Neff, H. Krompholz, F. Ruchl, K. Schoenbach and G. Herziger, Phys. Lett. 79A, 165 (1980).

[25] W.N. Hugrass, et al., Phys. Rev. Lett. 44, 167 (1980).

[26] I.R. Jones et al., Aust. J. Phys. 40, 157 (1987).

[27] J.D. Sethian et al., Phys. Rev. Lett. 59, 892 (1987)

A simple facility for the teaching of plasma dynamics and plasma nuclear fusion

S. Lee, T. Y. Tou, S. P. Moo, M. A. Eissa,[a] A. V. Gholap,[b] K. H. Kwek, S. Mulyodrono,[c] A. J. Smith,[d] Suryadi,[e] W. Usada,[e] and M. Zakaullah[f]
United Nations University Training Programme on Plasma and Laser Technology, Physics Department, University of Malaya, 59100 Kuala Lumpur, Malaysia

(Received 11 July 1986; accepted for publication 23 February 1987)

A small plasma focus (3.3 kJ) is designed from the viewpoint of simplicity, reliability, and cost effectiveness to act as a source of pulsed high-density plasmas. The simplicity of the device and associated diagnostics coupled with its rich variety of plasma phenomena makes this device ideal for the teaching of plasma nuclear fusion particularly for developing countries where such facilities are at present rarely available. Six sets of the device have been constructed and tested in various gases with better than 95% reliability and reproducibility in various plasma phenomena including neutron production of $0.5–1.0\times10^8$ per discharge when operated in 3-Torr deuterium. The design principles, procedures, and parameters are discussed and test results shown.

I. INTRODUCTION

Plasma physics has attained sufficient importance in its present applications and also in its potential application associated with plasma fusion energy that there have been considerable recent efforts (e.g., the Plasma Physics Colleges organized by the International Centre for Theoretical Physics, Trieste) to provide plasma physics education at an international level aimed towards stimulating the study of plasma physics even in developing countries.[1,2] Published literature has also played a role in these efforts.[3–13] This worthwhile educational effort encounters considerable difficulties at the experimental level particularly from the equipment point of view. There is not even a clear idea as to which experiment to develop, although low-cost, cost effectiveness, simplicity, and educational value combined with a large variety of plasma phenomena amenable to study by simple diagnostics should be among the factors to be considered in relation to devices for developing countries. Thus the glow discharge, the electromagnetic shock tube, and the linear Z pinch may be considered as the most likely candidates for this exercise, particularly since these are "classical" devices with well-known technology. However, these three devices, even the linear Z pinch in the low-cost scaled-down form necessary for this educational exercise, do not produce plasma conditions anywhere near necessary for measurable nuclear fusion. We have therefore considered the plasma focus as another educational device for this purpose.

The plasma focus is an excellent device for teaching plasma dynamics and thermodynamics besides being a rich source for a variety of plasma phenomena including soft x rays and plasma nuclear fusion. It is certainly superior to both the electromagnetic shock tube and the linear Z pinch in its range of plasma parameters, combining as it does the essential features of both devices in such a properly sequenced manner that the features of the electromagnetic shock tube and the pinch, and many more, may be produced in one single simple low-cost device, if properly designed.

However, plasma focus facilities are not commonly available and there has not been any systematic investigation on the design of such a facility in terms of simplicity, cost effectiveness, and ease of duplication. In the course of the United Nations University Training Programme on Plasma and Laser Technology it became necessary to design and operate such a facility so that several sets could be easily duplicated for transfer to various countries for teaching and educational purposes. What evolved from the programme is the UNU/ICTP PFF (United Nations University/International Centre for Theoretical Physics Plasma Fusion Facility) which is a 3.3-kJ plasma focus system powered by a single 15-kV, 30-μF Maxwell capacitor switched by a simple parallel-plate swinging cascade air gap. Low-cost features include the use of a step-up transformer from a standard television set to trigger the spark gap. Thus the only item that needs to be purchased (apart from metal sheets, miscellaneous materials, and components) to build the device is the Maxwell capacitor. A small rotary pump is sufficient for the vacuum and a 50-MHz oscilloscope is sufficient for the diagnostics.

The system produces remarkably consistent focusing action in several gases including air, argon, hydrogen, helium, carbon dioxide, and deuterium. A consistent neutron yield of $0.5–1.0\times10^8$ neutrons per discharge is obtained at 3 Torr of deuterium operating the focus at 15 kV and 180 kA current.

In this article we discuss the design principles and procedures and the design parameters and performance when subjected to computation. The experimental arrangements are then described together with simple diagnostics measuring plasma current, voltage, and magnetic field which give information on plasma dynamics. A simple arrangement for measuring neutron yield is also presented. The results of test measurements are discussed.

II. THEORY AND DESIGN

The focus design is based on a dynamic model[14,15] (see Fig. 1) that considers the focus dynamics in two separate phases—the axial rundown (shock tube) phase that crucially delays the radial focus, or pinch phase, until the plasma current has reached its peak value. The design point is therefore to have

$$t_r = t_{a\,\mathrm{exp}}, \tag{1}$$

where

$$t_r = (2\pi/4)t_0, \tag{2}$$

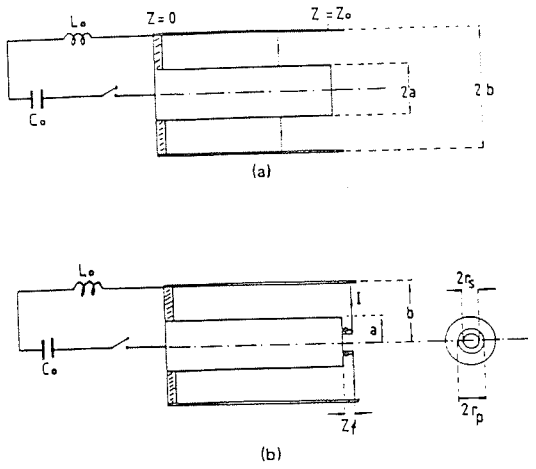

Fig. 1. (a) The axial run-down (shock tube) phase of the plasma focus. (b) The radial focus (pinch) phase of the plasma focus.

with

$$t_0 = \sqrt{L_0 C_0}, \tag{3}$$

and

$$t_{a\,\mathrm{exp}} \sim 2t_a, \tag{4}$$

where

$$t_a = \left(\frac{4\pi^2(b^2 - a^2)}{\mu \ln(b/a)}\right)^{1/2} \frac{z_0 \rho_0^{1/2}}{I_0}. \tag{5}$$

Here t_r is the current rise time and $t_{a\,\mathrm{exp}}$ is the transit time of the plasma layer for the axial phase. The quantities t_0 and t_a are characteristic times of the axial phase according to the model.[15] Here L_0 is the inductance of the capacitor C_0 together with all connections up to the plasma section of the focus tube, "a" and "b" are, respectively, the inner and outer radii of the focus tube, z_0 its length, ρ_0 the ambient gas density, μ the permeability of the plasma (same as the permeability of free space), and $I_0 = V_0/(L_0/C_0)^{1/2}$, where V_0 is the initial charge on the capacitor.

The second design point involves the characteristic "pinching" time of the plasma focus phase. This may be shown to be[14]

$$t_p = \frac{4\pi}{\mu^{1/2}(\gamma + 1)^{1/2}} a^2 \frac{\rho_0^{1/2}}{I_0}, \tag{6}$$

where γ is the specific heat ratio of the plasma. From this expression of t_p it may be shown that the ratio of the characteristic axial transit time to characteristic focus time is

$$t_a/t_p = cF,$$

where F is the aspect ratio z_0/a, and $c = b/a$.

A crucial factor in the operation of the Mathers plasma focus is that the axial phase occurs over a relatively long period $t_{a\,\mathrm{exp}}$ enabling the build up of capacitor current. The pinch phase then occurs over a relatively short period t_p. During this time t_p, approximately 10%–20% of the initially stored energy is transferred to the pinch plasma in approximately 2% of the current rise time. This results in a power enhancement factor during the pinching phase that is crucial to the proper operation of the plasma focus. It is important then that the ratio t_a/t_p be of the order of 30–50 for the Mathers focus.

The third point to be considered in the design is that there are limits[14] of speed and pressure in the operation of the plasma focus. In deuterium, for good focusing and consistent neutron yield, the axial speed just before focusing should be between the limits 6 and 10 cm/μs; the lower limit being the minimum speed required for a good snow-plowing action in the axial phase and the higher limit being imposed by restriking[14,16] of the discharge at the backwall or in the shock tube section. The limits of test gas pressure appear to be between 0.5 and 20 Torr for deuterium; the lower limit apparently governed by restriking; the upper limit by current filamentation.[17]

The design of a plasma focus may take as a starting point the availability, or choice, of a capacitor bank. For the present exercise from the point of view of economy and cost effectiveness, a single Maxwell capacitor rated at $C_0 = 30$ μF, $V_0 = 15$ kV with an equivalent series inductance, ESL, of less than 40 nH was selected. A parallel-plate geometry was selected for the capacitor connections and the switch, with coaxial cables being used to connect to the plasma focus input flanges. The value of L_0 was estimated at 110 nH. Having fixed C_0 and L_0, Eqs. (3) and (2) give a value of t_r of 2.9 μs and $I_0 = 248$ kA. The time-matching condition of Eq. (1) fixes $t_{a\,\mathrm{exp}}$ at 2.9 μs. The value of z_0 was then chosen at 16 cm to give an average axial speed of 5.5 cm/μs or a peak axial speed of $\sim$9 cm/μs just before the focus phase. This axial speed is expected to be suitable for a good focusing action in deuterium.

The value of I_0 is considerably smaller than most operational plasma focus machines that typically have I_0 of the order of 500 kA or more. Observing from Eq. (5) that the axial speed is $\sim I_0/[(b^2 - a^2)\rho_0]^{1/2}$ and from Eq. (6) that the radial speed is $\sim I_0/(a\rho_0^{1/2})$, it is noted that a reduction in I_0 may be compensated in the first instance by a reduction in a and $(b^2 - a^2)^{1/2}$ in order to maintain the axial speed within the speed limit indicated earlier. Thus we design for $a = 9.5$ mm and $b = 32$ mm which are smaller than typical values of most operational plasma focus devices. Moreover, the value of $b/a \sim 3.4$, in this case, is near optimum.[18] It is also noted that the value $t_a/t_p \sim 40$ for this design.

Having fixed the values of I_0, z_0, b and a, and t_r it remains to fix the value of ρ_0 from Eq. (5). This gives $\rho_0 = 0.21 \times 10^{-3}$ kg^{-3}. This is the density of deuterium at 0.9 Torr, which is within the pressure limits for deuterium focus operation as mentioned earlier.

Summarizing the design parameters we have $C_0 = 30 \times 10^{-6}$ F, $L_0 = 110 \times 10^{-9}$ H, $V_0 = 15 \times 10^3$ V, $a = 0.95 \times 10^{-2}$ m, $b = 3.2 \times 10^{-2}$ m, $z_0 = 0.16$ m, and $\rho_0 = 0.21 \times 10^{-3}$ kg^{-3} (0.9 Torr D_2), giving $I_0 = 2.48 \times 10^5$ A, $c = 3.37$, $F = 16.84$, $t_0 = 1.82 \times 10^{-6}$ s, $t_r = 2.86 \times 10^{-6}$ s, $t_a = 1.45 \times 10^{-6}$ s, $t_{a\,\mathrm{exp}} = 2.9 \times 10^{-6}$ s, $t_p = 35.8 \times 10^{-9}$ s, and $t_a/t_p = 40.4$.

The above design parameters have been subjected to a computation using a dynamic model[14,15] in which the axial trajectory is computed using a snow-plow model and the radial dynamics is traced using a generalized slug model that considers a pinching plasma of increasing length with the plasma layer lying between a shock front at position r_s and magnetic piston at position r_p (see Fig. 1). This model has the advantage of giving a realistic final pinch radius

ratio. Using the design parameters for the present device, the scaling parameters for the generalized slug model are

$$\alpha = t_0/t_a = 1.26, \quad \text{and} \beta = L_a/L_0 = 0.36,$$

where L_a = maximum inductance of axial phase $= z_0(\mu/2\pi)\ln c$. Also

$$\alpha_1 = t_a/t_p = 40.4, \quad \beta_1 = \beta/\ln\ c = 0.294.$$

The other parameters used for the model are $c = 3.37$, $F = 16.84$, and $\gamma = \frac{5}{3}$ (for fully ionized deuterium).

The computation indicates a strong focus with a large focusing voltage spike. The parameter α was varied between 0.7 and 1.5 (corresponding to pressure range of 0.5–2 Torr) and the computation repeated at each α. Good focusing was indicated over this range of pressure. These computation results add confidence to the design of the plasma focus. However, it has been found that machine effects such as current and mass shedding, reduced channel size due to boundary effects, and current restrike that are not included in the dynamic model may alter the actual performance of the plasma focus. It is therefore to be expected that in actual operation the focus may need to be tuned[18] by a variation of the five parameters V_0, ρ_0, z_0, a, and b. If the design is not too far from optimum, operation over a range of ρ_0 may be sufficient to establish a regime of good focus. This is the procedure adopted in the present experiment.

III. EXPERIMENTAL ARRANGEMENT

A simple parallel-plate spark gap with a swinging cascade configuration (see Fig. 2) was developed giving a low inductance at minimum cost. The ratio of the gap is 3:2 ($4\frac{1}{2}$–3 mm). The gap is triggered via an isolating capacitor from an 800-V SCR unit via a TV transformer that was found to have a step-up ratio of 17 times and a rise time of 1 μs. The isolating capacitor is a 1-m length of UR67 coaxial cable. The parallel-plate spark gap is made from $\frac{1}{4}$-in.-thick copper plates and proved maintenance free for 200 discharges between 13–15 kV before it was cleaned. The triggering jitter was found to be within $\pm$ 50 ns. The circuit is shown in Fig. 2.

The arrangement for the capacitor, the connecting plates, the spark gap, and the output coaxial cables is shown in Fig. 3(a). To keep the inductance low, the Earth plate of the capacitor (labeled no. 10) is extended nearly up to the anode and insulation is provided by a nylon cap (no. 5) around the anode stud. The cap dips into a pool of oil (no. 4) that is prevented from splashing out by means of an O-ring (no. 8). Mylar sheets (no. 11), 2 in. wider all around than the conducting plates, sandwiched by polyethylene sheets (no. 12) complete the insulation between the HV plate (no. 14) and the Earth plate as shown in Fig. 3(a). The Earth plate (no. 10) runs unbroken to the output position where the Earths of the coaxial cables connect. On top of the insulating sheets the HV plate is connected to the spark gap. Between the spark gap electrodes and all along it is placed a $\frac{1}{4}$-in.-diam copper tubing (no. 17) that acts as the trigger electrode. The output plate of the spark gap is connected to the focus tube by means of 16 coaxial cables (no. 18) used in parallel.

Essential to the structure of the focus tube is the backwall [see Fig. 3(b)] insulator. The glass insulator (no. 30) plays an important role in the symmetrical formation of the current sheet and has to be properly mounted to avoid being broken by vibrations. In the present design this glass insulator is mounted in a rubber holder (no. 24) which when compressed tightly and symmetrically by the brass flange (no. 28) grips the glass insulator. The rubber holder also acts as a vacuum and high-voltage seal. Figure 3(b) also shows the anode collector plate (no. 20) and the cathode collector plates (no. 25) onto which the coaxial cables connect.

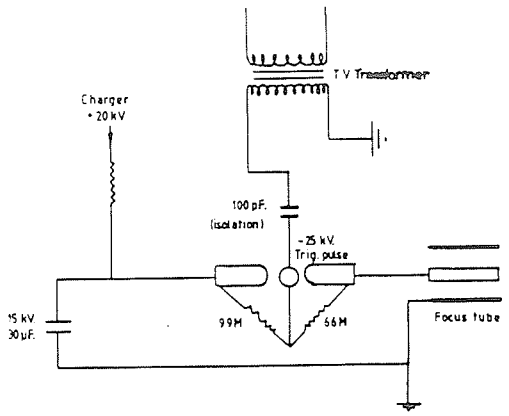

Fig. 2. Circuit for the swinging-cascade spark gap and focus tube.

The plasma chamber (no. 32) consists of a 30-cm length of $6\frac{1}{4}$-in.-diam mild steel tubing that is chromed. Vacuum is provided by a single-stage rotary pump reaching an ultimate base pressure $\sim$0.01 Torr. The system was adjusted for a leakage rate of less than 2 μ/min and pressure is read with a mechanical diaphragm gauge. Operating at a test pressure of 1 Torr and with a delay of less than 5 min between gas filling and focus operation, the air impurity in the system is about 2%. This level of vacuum proved to be sufficient for operating with good focus in various gases and good neutron yield when operated in deuterium.

To measure the relative strength of the plasma focus action, a Rogowski coil (no. 22) with an integration time constant of 200 μs displayed on a 50-MHz CRO is used to measure the current flowing into the anode. A resistive voltage divider (not shown in figure) with 15-ns response time is strapped across the anode collector plate (no. 20) and the cathode collector plate (no. 25) to measure the voltage across the focus tube. In a plasma focus device, the axial drive phase is characterized by a smooth near-sinusoidal rising current and a corresponding smooth waveform with a voltage value[14] that is proportional to the axial drive speed as the rate of change of current reduces to zero at peak current. As the focus occurs, the strong electromechanical action draws energy from the magnetic field pumping the energy into the compressing plasma. This mechanism is indicated in the distinctive current dip and voltage spike displayed by the current and voltage waveforms. In general, the stronger the focus, the more severely the plasma is compressed and the bigger the current and voltage spike.

To measure the magnetic field a 10-turn 1-mm coil jacketed in a 3-mm glass tubing (no. 33) is inserted into the focus tube and orientated to measure the azimuthal magnetic field. The passage of the current sheath driving the

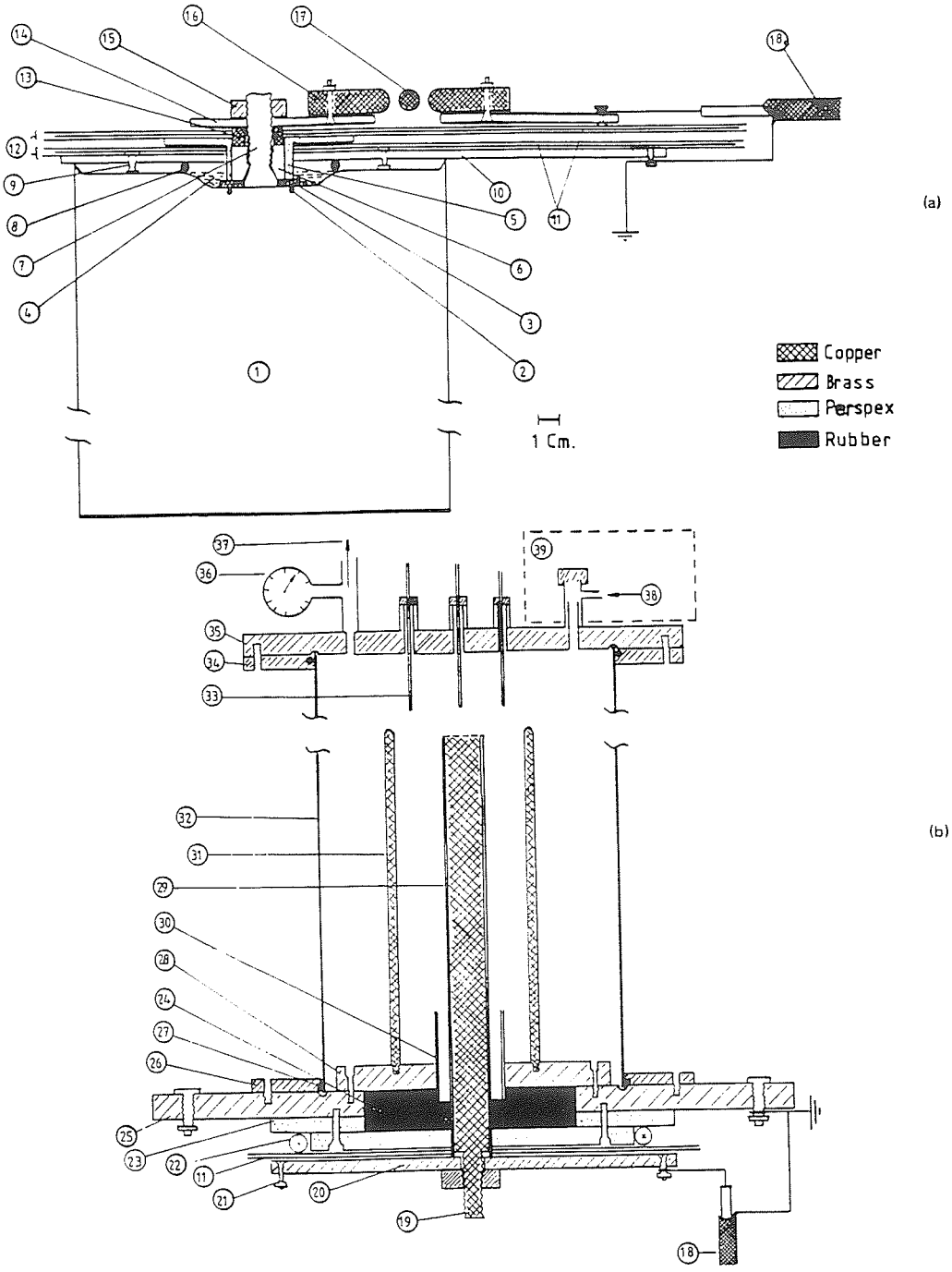

Fig. 3. (a) The capacitor connecting plates, the spark gap, and output coaxial cables. 1 = 15-kV, 30-μF capacitor; 2 = capacitor O-ring seal; 3 = washer; 4 = oil; 5 = nylon cap; 6 = steel nut; 7 = capacitor output seal; 8 = O-ring seal; 9 = Earth stud; 10 = Earth plate; 11 = 5-mil Mylar film; 12 = polyethelene film; 13 = copper ring HV connector; 14 = capacitor high-voltage (HV) output plates; 15 = lock nut for HV plate; 16 = HV electrode for swinging cascade spark gap; 17 = trigger electrode; and 18 = output coaxial cables (16 in parallel). (b) The plasma focus tube. 18 = input coaxial cables (16 in parallel); 19 = stud of anode; 20 = anode collector plate; 21 = connecting points for coaxial cable HV lead; 22 = Rogowski coil; 23 = perspex spacer; 24 = rubber holder; 25 = cathode collector plate; 26 = mild steel flange; 27 = O-ring seal; 28 = focus cathode support plates; 29 = focus anode; 30 = glass insulator; 31 = focus cathode (6 rods); 32 = mild steel focus chamber; 33 = movable magnetic probe in glass jacket; 34 = flange; 35 = brass flange; 36 = diaphragm gauge; 37 = outlet to vacuum pump; 38 = inlet for test gas; 39 = wax container with indium foil and PM-scintillator activation counter.

plasma layer may be measured as a sharp rise in magnetic field as the sheath sweeps past the probe. This measurement may be used to confirm the dynamics required to ensure a good focus.

An indium foil activation system is used to count fusion neutrons from the plasma. This system consists of an indium foil covering an NE 102 scintillator sitting on the photocathode of a 2-in. photomultiplier tube. The assembly is placed in a paraffin wax enclosure so as to thermalize the fusion neutrons. The detector is placed on the end flange of the plasma focus tube (no. 39). The PM tube is connected to a counter via a discriminator and a preamplifier and has a calibration constant of 5×10^4 neutrons per count, the counts being taken for a 30-s period immediately after the focus is fired.

IV. RESULTS

The system was tested between 13 and 15 kV in various gases including air, argon, hydrogen, and deuterium. The strength of the focusing action is gauged from the current dip and voltage spike. Figure 4(a) shows an oscillogram of the current and voltage waveforms of the plasma focus in 0.5 Torr of air, with focusing action about 1 μs after peak current. Figure 4(b) shows a deuterium focus, at 13 kV, 2.5 Torr with focusing action occurring at peak current. The deuterium focus shows signs of a secondary focus occurring some 0.4 μs after the first voltage spike. The occurrence of definite clean dynamics in the axial region preceding the focus region is confirmed by magnetic probe measurements. Figure 4(c) shows the output of a magnetic probe (lower trace) placed at $z = 10.2$ cm (i.e., in the axial drive region 10.2 cm from the backwall) in a discharge of 15 kV, 3.5 Torr of deuterium. From this oscillogram and in comparison with the current oscillogram (upper trace) it is found that the current sheath arrives 0.6 μs before focusing occurs off the end of the anode at $z = 16$ cm giving a speed of 9.7 cm/μs (corresponding, from shock theory, to a temperature $\sim 2 \times 10^5$ K) over this section ($z = 10.2$–16 cm) of the axial drive region. From the rise time (10%–90%) of the magnetic signal and the speed this gives a current sheath thickness of 2 cm. The thickness and speed of this current sheath is typical of that in a good plasma focus system. The current dip during focusing is also seen as a dip in the magnetic probe output that shows two other current dips occurring at 0.2 and 0.6 μs after the first dip. These confirm the occurrence of multiple focusing in deuterium in the device.

In air good focus was obtained at 13 and 15 kV in a narrow pressure range of 0.5–1.1 Torr. In argon the pressure range for good focusing is greater at 0.3–3 Torr. At 15 kV very strong focusing action was obtained at 0.8 Torr. In helium the range of focusing is from 0.7 to 3.5 Torr while in carbon dioxide focusing is observed below 1 Torr. In hydrogen the pressure range for focusing is 1.1–6 Torr. However, it is noticed that the focusing action, although definite, is not as intense, in terms of a focusing voltage spike, as in argon. The strongest focus in hydrogen occurs at 3.3–4.3 Torr. In deuterium strong focus is observed at 1–5 Torr with best focusing at 2.5–3 Torr.

In deuterium when operated at 15 kV and optimum pressure conditions of 3 Torr consistent counts of 1000–2000 are obtained using the PM-scintillator counter. This corresponds to 0.5–1×10^8 neutrons per shot.

The system shows remarkably consistent and reproducible operation. Six systems were assembled one after the other and tested over a period of 2 months. Each system was assembled and tested over a period of 1 week averaging between 100–200 shots in the various gases. Once a system

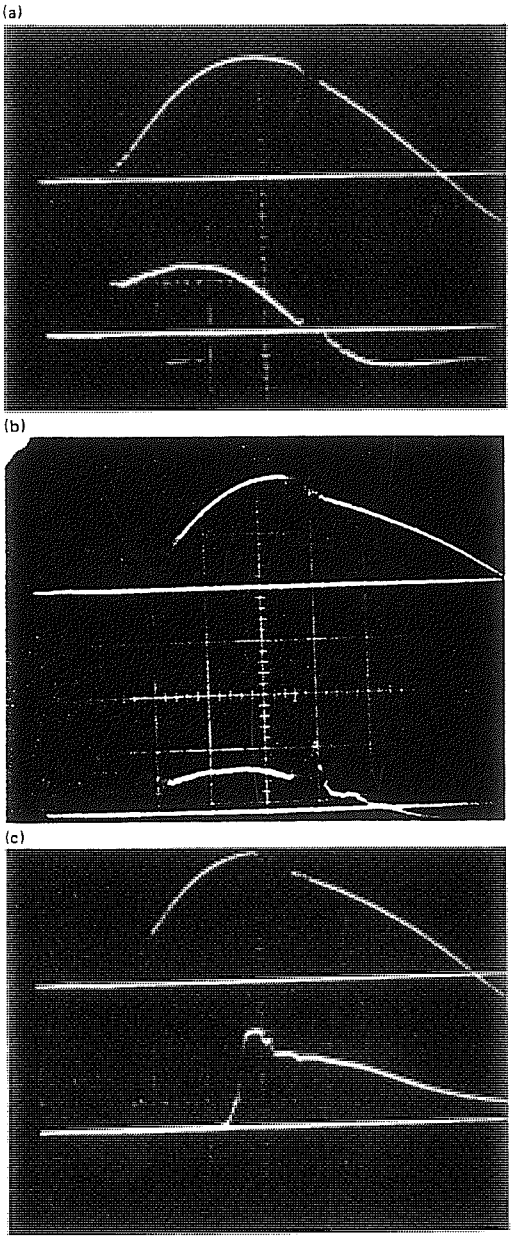

Fig. 4. (a) Current (upper trace) and voltage (lower trace) of plasma focus in air: 13 kV, 0.5 Torr; Top trace: 73 kA/cm; Bottom trace: 2 kV/cm; Time scale (horizontal): 1 μs/cm. (b) Current and voltage trace of plasma focus in deuterium: 13 kV, 2.5 Torr; Top trace: 75 kA/cm; Bottom trace: 4 kV/cm; Time scale (horizontal): 1 μs/cm. (c) Current and magnetic trace of plasma focus in deuterium: 15 kV, 3.5 Torr; Magnetic probe placed at $z = 10.2$ cm; Top trace: 73 kA/cm; Bottom trace: 0.6 T/cm.

has been established to be operating normally, that is, without undue leakage and after an initial period of out-gasing involving some three to five discharges, proper focusing is achieved for better than 95% of the discharges, apart from those discharges deliberately operated outside the established suitable pressure range for the gas used.

V. DISCUSSION

It is of interest to estimate the range of temperatures and densities available in this device. This is best discussed separately for each of the two phases of operation, namely, the axial drive phase and the radial collapse phase. In deuterium in typical operating conditions in the axial drive phase between $Z = 8$ and $Z = 16$ cm a steady plasma temperature of 2×10^5 K may be estimated (as shown above from the measured shock speed) in a slug length of 4 cm. For operating at an ambient density of 3 Torr of deuterium, complete ionization is achieved at this temperature giving an ion density and an electron density each of about 10^{18} per cm^3 since a shock mass density ratio of 4 may be expected for a strong fully ionized deuterium shock. In the radial focus phase, soft x-ray techniques[19,20] have been used to estimate temperatures in a similar small plasma focus to be 0.7–3 keV while interferometric techniques[21] have been used to measure peak electron densities in the maximum compressed pinch column of $1–5 \times 10^{19}$ per cm^3. These experimental results agree with computations based on the dynamic theory[15] already discussed in Sec. II.

When heavier gases such as argon are used as the test gas the dynamic theory predicts enhanced compression due to the specific heat ratio[22] being reduced below 5/3. In the case of argon, higher temperature (about 4 keV) and electron densities (10^{20} per cm^3), may then be predicted by the dynamic theory applied to the pinch phase. There is also experimental evidence[23] to back up these predictions.

At such high temperatures, thermodynamic computations show that even argon becomes almost fully ionized[22] and experimental work shows that worthwhile spectroscopic studies may be made of the focus using, e.g., argon as a test gas. Peacock[23] *et al.* have used a 2-m Rowland circle grating spectrograph and a de Broglie spectrometer to obtain spectrograms of argon and neon focus discharges. The results are sufficiently reproducible for identification of transitions in H-like and He-like Ne and Ar ions. If line profile scans are to be made then it is usual to obtain a profile over a number of discharges. The question of reproducibility then becomes important. In the present setup the reproducibility has been studied by using two simultaneous monitoring criteria. First, the neutron yield of each discharge is monitored and those that are beyond 10% of the average may be rejected. Second, the voltage spike is monitored for its time position and its shape (rate of rise, single spike, or multiple spikes). The time position of its peak (single peak spike) may be used as a reference point to fix the time position of the photomultiplier output. A discharge with a voltage spike shape that does not conform with the average shape may also be rejected. A close study of the data shows that when the system is properly set up and adjusted, at least 80% of the discharges are sufficiently reproducible for scanning applications.

It may also be of interest to inquire about the types of experiments that may be done on a plasma focus machine. First, as already mentioned in detail earlier, the axial drive phase may be used to study plasma dynamics and energetics.[19] The use of simple voltage, current, and magnetic probes, together with a coupled circuit-dynamic analysis enables one to obtain the dynamics and energetics of the system and also shock plasma temperature and densities. These may be confirmed with spectroscopic and interferometric measurements to check the validity of the dynamic model used.

In the radial pinch phase, the pinching action is more severe than the Z or theta pinch for two reasons. The first is that the use of the axial drive phase delays the focus pinch so that it occurs at peak current and enables a smaller radius pinch to occur at higher ambient density. Second, the smaller radius pinch is an elongating pinch that also contributes to an enhancement of pinch compression due to the smaller resulting pinch radius ratio.[24] Thus even a small plasma focus achieves sufficiently intense plasma conditions to produce consistent nuclear fusion and may be used as the lowest-cost device for demonstrating nuclear fusion from a plasma. Even a simple 3-kJ device such as the one presently discussed here may be used as a starting point for studying neutronics.[25] For example, measurement of the half-life of ^{116}In has been carried out[26] using the UNU/ICTP PFF as the neutron source. It is known that the deuterium focus produces a deuteron beam[21] of several hundred keV. The effect of this beam on targets may also be studied for the enhancement of neutron yield.[25] The corresponding electron beam, accelerated in the opposite direction into the anode, has relativistic speed[27] and may be taken out of the system by using a hollow electrode. Thus the focus may also be used as a REB source. These two effects, i.e., consistent neutron and REB production, are not available in the Z pinch and theta pinch[23] because of insufficient densities (10^{17} per cm^3) and temperatures (several hundred eV). This demonstrates the enhanced intensity of the plasma focus device.

The REB may also be used to sputter anode material downstream of the focus.[21,28] By using different materials as inserts in the anode face, different materials may be sputtered.

Other experiments and applications may be listed.[21] In the experience of the UNU Training Programme[29] the study of plasma dynamics particularly in the axial drive phase and the demonstration and study of plasma nuclear fusion are in themselves sufficiently interesting and of sufficient scope for a good beginning to be made in the field of experimental plasma physics.

VI. CONCLUSION

A simple cost-effective plasma focus device based on a 3.3-kJ single capacitor and a maintenance-free parallel-plate spark gap has been designed and operated as a reproducible and reliable neutron source (10^8 neutrons per discharge in deuterium), as well as a reliable source of focused plasmas of air, argon, hydrogen, helium, and carbon dioxide. In a period of 3 months six sets of the equipment were constructed and tested in the course of a UNU Training Program. These sets are now being reassembled in various countries as postgraduate teaching facilities. The remarkably reproducible results suggest that this device may be readily built as a very cost-effective facility for the teaching of plasma dynamics, plasma phenomena, and plasma nuclear fusion. This could be a valuable contribution, particularly to the developing countries where dense plasma facilities are hardly available.

ACKNOWLEDGMENTS

We (MAE, AVG, AJS, S, MS, WU, MZ) acknowledge UNU Fellowships without which this work could not have been completed. A grant from the I.C.T.P. and a research grant F232/74 from the University of Malaya are also acknowledged, likewise the technical help of Jasbir Singh and T. S. Toh.

[a] Present address: Physics Department, Al-Azhar University, Cairo, Egypt.
[b] Present address: Physics Department, Rivers State University of Science and Technology, Port Harcourt, Nigeria.
[c] Present address: Indonesian National Institute of Aeronautics and Space (LAPAN), Jakarta, Indonesia.
[d] Present address: Physics Department, Njala University College, Sierra Leone.
[e] Present address: PPBMI, BATAN, National Atomic Energy Agency, Yogyakarta, Indonesia.
[f] Present address: Physics Department, Quaid-I-Azam University, Islamabad, Pakistan.

[1] B. McNamara, in *Twenty Years of Plasma Physics*, edited by B. McNamara (World Scientific, Philadephia and Singapore, 1985), p. XIII.
[2] International Fusion Research Council, Nucl. Fusion **18-1**, 137 (1978).
[3] P. A. Sturrock *et al.*, Am. J. Phys. **34**, 104 (1966).
[4] S. C. Brown *et al.*, Am. J. Phys. **31**, 637 (1963).
[5] F. W. Crawford and D. B. Ilic, Am. J. Phys. **44**, 319 (1976).
[6] C. S. Malcatchy, Am. J. Phys. **45**, 910 (1977).
[7] I. Alexeff, Am. J. Phys. **45**, 860 (1977).
[8] O. K. Mawards, Am. J. Phys. **34**, 112 (1966).
[9] R. Jones, Am. J. Phys. **47**, 198 (1979).
[10] K. Arnett, R. Anderson, and R. Alexander, Am. J. Phys. **49**, 767 (1981).
[11] R. G. Gibson, Am. J. Phys. **51**, 1028 (1983).
[12] P. Beiersdorfer and E. J. Clothiaux, Am. J. Phys. **51**, 1031 (1983).
[13] P. D. Scholz and T. P. Anderson, Am. J. Phys. **38**, 279 (1970).
[14] S. Lee, in *Laser and Plasma Technology*, edited by S. Lee, B. C. Tan, C. S. Wong, and A. C. Chew (World Scientific, Singapore, 1985), pp. 37, 64, and 387.
[15] S. Lee, in *Radiation in Plasma*, edited by B. Namara (World Scientific, Singapore, 1984), Vol. II, p. 978.
[16] J. W. Mather, P. J. Bottoms, J. P. Carpenter, K. D. Ware, and A. H. Williams, Report No. IAEA-CN-28/D-5, 561 (1972).
[17] J. P. Rager, L. E. Bilbao, H. A. Bruzzone, V. Gourlan, U. Guidoni, H. Kroeglar, S. Podda, B. V. Robouch, and K. Steinmetz, in Eighth Int. Conf. on Plasma Physics and Controlled Nuclear Fusion Research, Brussels, June 1980.
[18] S. Lee and Y. H. Chen, Fusion Energy-1981 (ICTP, Trieste) IAEA-SMR-82, Vienna, p. 297.
[19] J. W. Mather, Phys. Fluids **8**, 366 (1965).
[20] Y. H. Chen and S. Lee, Int. J. Electron. **35**, 341 (1973).
[21] G. Decker and R. Wienecke, Proc. Twelfth Int. Conf. on Phenomena in Ionized Gases, Eindhoven, 1975; Physica **82C**, 155 (1976).
[22] S. Lee, Austr. J. Phys. **36**, 891 (1983).
[23] N. J. Peacock, R. J. Speer, and M. G. Hobby, J. Phys. B **2**, 798 (1969).
[24] S. Lee, J. Appl. Phys. **54**, 3603 (1983); Plasma Phys. **25**, 571 (1983).
[25] P. Cloth and H. Conrads, Nucl. Sci. Eng. **62**, 591 (1977).
[26] S. P. Moo and S. Lee, Singapore J. Phys. 4, 131 (1987)
[27] W. Neff, H. Krompholz, F. Ruehl, K. Schoenbach, and G. Herziger, Phys. Lett. **79A**, 165 (1980).
[28] S. Lee, Harith Ahmad, T. Y. Tou, K. H. Kwek, and C. S. Wong, J. Fiz. Mal. **6**, 23 (1985).
[29] S. Lee, T. Y. Tou, M. A. Eissa, A. V. Gholap, K. H. Kwek, S. P. Moo, S. Mulyodrono, A. J. Smith, Suryadi, W. Usada, and M. Zakaullah, J. Fiz. Mal. **7**, 1 (1986).

Proc. 3rd Tropical College on Appl. Phys., 1988
Review Paper

THIRD WORLD NUCLEAR FUSION PROGRAMMES AND SOUTH-SOUTH COLLABORATION IN PLASMA TECHNOLOGY

S. Lee* and M.H.A. Hassan

International Centre for Theoretical Physics
and
Third World Academy of Sciences
Trieste, Italy

Permanent address: Physics Department, University of Malaya
59100 Kuala Lumpur, MALAYSIA

INTRODUCTION

It has often been argued that certain areas of research should be avoided by developing countries because of cost consideration. One such area is Plasma Physics and Nuclear Fusion. Witness the gigantic fusion installations of the top national and international fusion centres and the sophisticated equipment of even small plasma physics laboratories in developed countries.

Despite such arguments there exists more than 50 institutions in 28 countries in the Third World with plasma and fusion programmes. Some of these programmes like the Brazilian or Indian fusion programmes have attained the status of national programmes with multi-million dollar funding which although miniscule compared with e.g.JET, is still orders of magnitude better funded than the typical plasma projects of other developing countries. What then of these typical underfunded plasma laboratories? Is there anything significant that they can do?

There had appeared in the past few years an effort which has demonstrated that good experiments, indeed working fusion facilities, may be built at very low cost using the figure of $5000.00 (the maximum value of a TWAS research grant) as a limiting budget. A working fusion facility the UNU/ICTP PFF has been developed during a 1986 training programme in Kuala Lumpur and sets, constructed by the trainees themselves, have been transported back home by the trainees, reassembled and are now being used as postgraduate training facilities.

At this point of time when the developing countries are taking important steps to improve their facilities in plasma research on the one

hand through national programme and on the other hand through low-cost creation and sharing of technology it seems desirable to review the extent of Third World fusion programmes and put into this context the exciting work in the innovative development of low-cost facilities to enable more developing countries to share in plasma and fusion research.

For this purpose this paper is divided into two parts. The First Part, a review of Third World Fusion Programmes consists mainly of material in tabular form which has already been presented by M.H.A. Hassan to the International Fusion Research Council (IFRC) in Vienna on the 20-22 January 1988. The Second Part extends the review to examine a pioneering effort in south-south collaboration which promises an impact on the development of plasma technology in many developing countries.

PART I

I. Figure 1 shows the locations of Third World Institutions with Fusion Programmes.

II. A list of Institutions with Fusion Programmes is given in Table 1.

Table 1: NUCLEAR FUSION PROGRAMMES IN THE THIRD WORLD
List of Institutions with Fusion Programmes

Country	Name and Address of Institution	City
1 ARGENTINA	Comision Nacional de Energia Atomica (CNEA) Avenida del Libertador 8250, 1429	Buenos Aires
2 ARGENTINA	PRIFIP, Consejo Nacional de Investigaciones Cientificas y Tecnicas Universidad de Buenos Aires, Pabellon 1 Ciudad Universitaria, 1428	Buenos Aires
3 ARGENTINA	PROFET, Universidad Nacional de Centro de la Provincia de Buenos Aires Pinto 399,7000	Tandil
4 BANGLADESH	Department of Physics Jahangirnagar University Savar	Dhaka

Fig. 1. NUCLEAR FUSION PROGRAMMES IN THE THIRD WORLD
Location of Institutions with Fusion Programmes

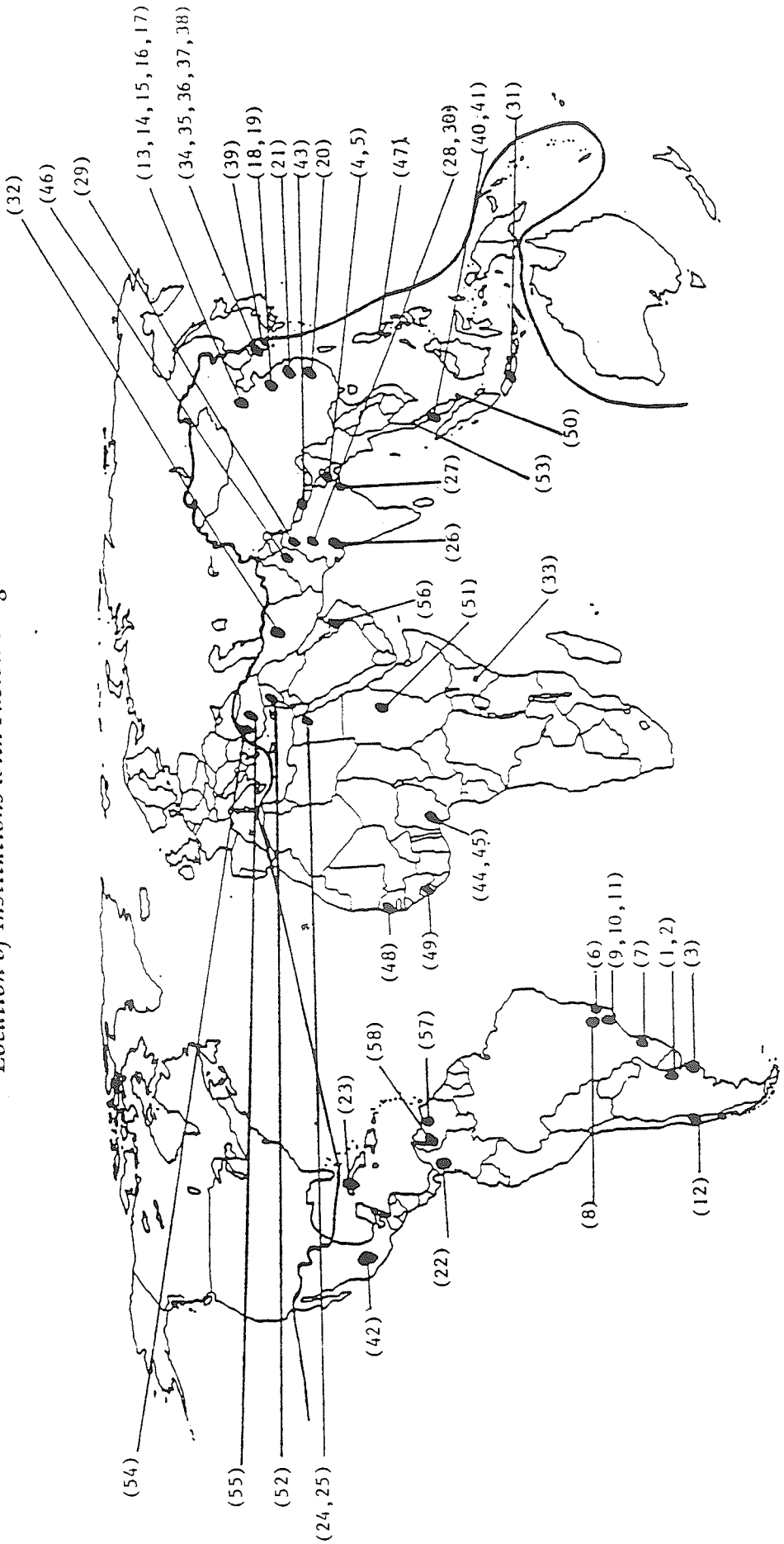

Country	Name and Address of Institution	City
5 BANGLADESH	Institute of Nuclear Science and Technology Atomic Energy Research Establishment Ganak Bari, Savar P. O. Box 3787	Dhaka
6 BRAZIL	Instituto de Fiscia Universidade Federal Fluminense Outeiro de Sao Joae Batista Niteroi 24 210	Rio de Janeiro
7 BRAZIL	Instituto de Fisica Universidad Federal do Rio Grande do Sul Av. Prof. Luiz Englert s/n. 90000 Porto Alegre	Rio Grande do Sul
8 BRAZIL	Instituto de Estudos Avancados Centro Tecnico Aerospacial Rodovia dos Tamoios KM 5.5 CEP 12200	Sao Jose dos Campos
9 BRAZIL	Instituto de Fisica, Universidade de Sao Paulo Cidade Universitaria Caixa Postal 20516, 01498	Sao Paulo
10 BRAZIL	Instituto de Pesquisas Espaciais Caixa Postal 515 Av. dos Astronautas No. 1758 12200 Sao Jose dos Campos	Sao Paulo
11 BRAZIL	Universidade Estadual de Campinas Caixa Postal 1170 13 100 Campinas	Sao Paulo
12 CHILE	Pontificia Universidad Catolica de Chile Casilla 6177	Santiago
13 CHINA	Department of Electrical Engineering Tsinghua (Quinghua) University	Beijing
14 CHINA	Institute of Atomic Energy P. O. Box 275	Beijing
15 CHINA	Institute of Mechanics, Academia Sinica	Beijing

Country	Name and Address of Institution	City
16 CHINA	Institute of Physics, Academia Sinica	Beijing
17 CHINA	Peking University Institute of Theoretical Physics	Beijing
18 CHINA	Institute of Plasma Physics Academia Sinica P. O. Box 26, Anhui Province	Hefei
19 CHINA	University of Science and Technology 24 Jinzhai Road, Anhui	Hefei
20 CHINA	Southwestern Institute of Physics P. O. Box 15	Leshan, Sichuan
21 CHINA	Department of Physics and Institue of Modern Physics, Fudan University	Shanghai
22 COLOMBIA	Universidad de Antioquia Apdo Aereo 1226 Ciudad Universitaria, Antioquia	Medellin
23 CUBA	Instituto de Investigacion Tecnica Fundamental Calle O No. 8	La Habana, 4
24 EGYPT	Nuclear Research Centre Atomic Energy Authority P. O. Box 13759	Cairo
25 EGYPT	Physics Department, Al Azhar University	Cairo
26 INDIA	Institute of Plasma Research Navarangpura, 380 009	Ahmedabad
27 INDIA	Saha Institute of Nuclear Physics 92 Acharya Prafulla Chandra Road 700 009	Calcutta
28 INDIA	Indian Institute of Technology Delhi 110 016	New Delhi
29 INDIA	Mathematics Department University of Roorkee	Roorkee, Uttar Pradesh
30 INDIA	Department of Physics/University Science Instrumentation Centre University of Rajasthan	Jaipur
31 INDONESIA	Yogyakarta Nuclear Research Centre National Atomic Energy Agency	Yogyakarta

Country	Name and Address of Institution	City
32 IRAN	Nuclear Research Centre Atomic Energy Organization of Iran P. O. Box 11365-8486	Tehran
33 KENYA	Physics Department University of Nairobi	Nairobi
34 KOREA, REP	Department of Nuclear Engineering Seoul National University Shinrim-dong, Kwanak-gu, 151	Seoul
35 KOREA, REP	Hanyang University 17 Haengdang-dong Sungdong-gu 133	Seoul
36 KOREA, REP	Korea Advanced Energy Research Institute (KAERI), P. O. Box 7, Chongryang 131	Seoul
37 KOREA, REP	Korea Advanced Institute of Science and Technology (KAIST) P. O. Box 131, Chongryang	Seoul
38 KOREA, REP	Korea Institute of Technology	Seoul
39 KOREA, REP	Kyungpook National University 1370 Sanyuk-dong, Bauk-gu 635	Taegu
40 MALAYSIA	Physics Department, University of Malaya	Kuala Lumpur
41 MALAYSIA	Physics Department Technology University of Malaysia	Kuala Lumpur
42 MEXICO	Instituto Nacional de Investigaciones Nucleares, Agriculture 21 11800	Mexico City
43 NEPAL	Department of Physics Tribhuvan University P. O. Box 3757, Tripureswar	Kathmandu
44 NIGERIA	Department of Physics University of Ilorin, P.M.B. 1515	Ilorin
45 NIGERIA	Physics Department Rivers State University of Science and Technology	Port Harcourt
46 PAKISTAN	Physics Department Quaid-I-Azam University P. O. Box 1090	Islamabad
47 PHILIPPINES	National Institute of Physics University of the Philippines Quezon City	Manila

Country	Name and Address of Institution	City
48 SENEGAL	Laboratoire de Physique Fondamentale et d'Etudes Energetiques University of Dakar, Dakar-Fann	Dakar
49 SIERRA LEONE	Department of Physics Njala University College Private Mail Bag	Freetown
50 SINGAPORE	Mathematics and Science Centre Ngee Ann Polytechnic	Singapore
51 SUDAN	University of Khartoum P. O. Box 321	Khartoum
52 SYRIA	Department of Physics University of Damascus	Damascus
53 THAILAND	Physics Department Prince of Songkla University	Hatyai
54 TURKEY	Ankara Research and Training Centre Besevlar	Ankara
55 TURKEY	Cekmece Nuclear Research and Training Centre P. K. 1 Havaalani	Istanbul
56 UNITED ARAB EMIRATES	Physics Department United Arab Emirates University P. O. Box 15551	Al'Ayn
57 VENEZUELA	Universidad Simon Bolivar Apdo 80659 Prados del Este 1080	Caracas
58 VENEZUELA	Universidad de los Andes Avda 3, Independencia Edif. Rectorado 5101	Merida

III In Table 2 is compiled some information of Third World Institutions with experimental facilities in fusion.

Table 2: NUCLEAR FUSION PROGRAMMES IN THE THIRD WORLD
LABORATORIES WITH EXPERIMENTAL FACILITIES

A) LATIN AMERICA

1) ARGENTINA

Institution	Field Reversed Pinch	Plasma Focus	Topics	Key Person
a) CNEA Buenos Aires	‡Fast Linear Field Reversed θ-Pinch (1982) R = 8 cm, L = 30-60 cm, B = 0.3 T		‡Formation and stability of RC of FRC	8
b) PRIFIP Buenos Aires		‡PFI Mather (1973) 0.95, 2.7, 20 cm 20 kV, 1.4 kJ ‡PFII Mather (1980) 1.9, 3.5, 50 cm 35 kV, 20 kJ	‡Breakdown phase and current sheath structure in Plasma Focus	19
c) PROFET Buenos Aires		‡PACO Mather (1984) 2, 5, 5 cm 31 kV, 1.8 kJ	‡Heating & Radiation ‡Plasma-solid interaction ‡Laser-plasma interaction	12

2) BRAZIL

Institution	Tokamak	Pinches	Others	Topics	Key Person
a) UNICAMP Campinas		‡TUPA linear θ-pinch (82) a=15 cm, L=100 cm, B=1 T ‡Field reversed θ-pinch (85) R=16 cm, L=80 cm, B=0.7 T		‡FRC Equilibrium ‡Stability ‡Transport ‡ICH	8
b) IFUSP Sao Paulo	‡TBR-1 Tokamak (1980) R = 30 cm a = 11 cm B_T = 0.5 T			‡Torodial stability	12
c) UFF Niteroi			‡Linear Magnetic Mirror (1983) a=8.5 cm, L=255 cm, B_0 =0.1 T	‡Instabilites ‡Waves	13
d) INPE Sao Jose dos Campos			‡Gyrotron high power microwave generation ‡Multimagnetic dipole discharge (1980) ‡Plasma centrifuge (1984) ‡Vacuum chambre test facility	‡Microwave power for ECH ‡Electrostatic propulsion ‡IA waves and solitons ‡Double layers	24
e) IEAV Sao Jose dos Campos			‡Carbon Dioxide Laser 10J, 20ns	‡Laser-plasma interaction	9

OTHER LATIN AMERICAN COUNTRIES

Country	Institution	Facilities	Research Topics	Key person
3) CHILE	PUC Santiago	‡Pseudo-spark discharge (1985) ‡Gas-embedded Z-pinch (1987)	‡Electron and Ion beam generation in discharge ‡Stability of gas-embedded Z-pinch	4
4) MEXICO	ININ Mexico City	‡Tokamak (1986) R = 23 cm, a = 8 cm, B_τ = 0.47T		8
5) VENEZUELA	USB Caracas	‡Duo-plasma device (1983) D = 50 cm, L = 100 cm	‡Basic plasma parameters ‡Waves	5

B) ASIA

1) CHINA

Institution	Tokamak	Field Reversed Pinch	Mirrors	Others	Topics	Key Person
a) Institute of Physics (AS) Beijing	‡CT-6B (1974) R = 45 cm a = 10 cm B_τ = 1.3 T	‡FRPI (1984) R = 6.5 cm L = 55.5 cm B = 0.8 T	‡OEX simple Mirror (1987) a = 15 cm L = 50 cm B_0 = 0.8 T Ratio: 4 - 6		‡Stability ‡Transport ‡ECRH ‡FRC formation and heating	50
b) Institute of Plasma Physics (AS) Hefei	‡HT-6B (1982) R = 45 cm a = 12.5 cm B_τ = 1.2 T ‡HT-6M (1984 R = 65 cm) a = 20 cm B_τ = 1.5 T ‡HPT-I R = 40 cm a = 8 cm B_τ = 1 T ‡HT-U (under construction) R = 125 cm a = 35 cm B_τ = 3 T		‡HER simple Mirror (1983) a = 12.5 cm L = 38 cm B_0 = 0.45 T Ratio: 2 - 2		‡Tokamak reactor design ‡Equilibrium and transport ‡MHD instabilities ‡Wall conditioning ‡Impurity transport	76

CHINA (Cont.)

Institution	Tokamak	Field Reversed Pinch	Mirrors	Others	Topics	Key Person
c) Institute of Physics Leshan	‡HL-1 (1985) R = 102 cm a = 20 cm B_T = 5 T	‡CF-II R = 10 cm L = 185 cm B = 0.5 T	‡MM-1 simple Mirror (1975) a = 11 cm L = 48 cm B_0 = 2.1 T Ratio: 1-75 ‡MM-2 Minimum B Mirror (1972) a = 11 cm L = 56 cm B_0 = 0.6 T Ratio: 2		‡Equilibrium and transport ‡Wave heating	22
d) University of Science and Technology Hefei	‡KT-5B R = 30 cm a = 6 cm B_T = 0.5 T					
e) Tsinghue University Beijing				‡DPF-100 (1977) Plasma Focus 3.5, 6. 22 cm 30 kV, 36 kJ ‡DPF-200 (1984) 11, 13, 29 cm 45 kV, 207 kJ		11
f) Institute of Atomic Energy Beijing				‡Particle Beam		19

2) INDIA

Institution	Tokamak	Compact Torus	Others	Topics	Key person
a) IPR Ahmedabad	‡ADITYA (1987) R = 75 cm a = 25 cm B_T = 1.5 T B_p = 0.2 T	‡CT formed by REB (1984) R = 20 cm L = 150 cm B = 0.05 T	‡BETA-TORUS R = 45 cm a = 15 cm B_0 = 0.5 T ‡Double plasma machine (1976) D = 50 cm L = 150 cm	‡Waves and instabilities ‡Relativistic electron Beam ‡Scrape off layer ‡RF plasma interaction	10
b) IITD Delhi			‡Uniformly magnetized linear device (1985) D = 15 cm L = 250 cm B_0 = 0.1 T ‡Beam-plasma system (under construction) D = 10 cm L = 150 cm	‡Microwave interaction ‡ECH ‡Non-linear interaction	12
c) SINP Calcutta	‡Tokamak (from Japan) R = 30 cm a = 8.4 cm B_T = 2 T		‡Linear Z-pinch (under construction)	‡Low density discharge ‡Transport ‡RF current drive	

OTHER ASIAN COUNTRIES

Country	Institution	Tokamak	Plasma Focus	Others	Topics	Key Person
3) Iran	Nuclear Research Centre Tehran	‡ALVANDIIC R = 45.5 cm a = 12.6 cm B_T = 1.2 T			‡Diagnostics ‡Transport	5
4) Indonesia	Yogyakarta Nuclear Research Centre		‡Mathers type 1, 3, 16 cm 20 kV, 6 kJ	‡Glow discharge		5

OTHER ASIAN COUNTRIES (Cont.)

Country	Institution	Tokamak	Plasma Focus	Others	Topics	Key Person
5) Korea Repulic	a) Seoul National University	‡SNUT-79 (1985) R = 65 cm a = 15 cm B_T = 3 T	‡PF-1 Mather 2.1, 4.6, 14 cm 20 kV, 50 kJ		‡OH Experiments	8
	b) KAERI Seoul	‡KAERIT Tokamak R = 27 cm a = 5 cm B_T = 4.2 T			‡OH Discharge	4
	c) Kyungpook University			‡KUTAM Tandem Mirror	‡Basic experiments	2
6) Malaysia	University of Malaya Kuala Lumpur	‡Tokamak (1984) R = 25 cm a = 5 cm B_T = 0.5 T	‡UMDPF1 Mather (1973) 1.3,4.3,15.5 cm 40 kV, 50 kJ ‡UNU/ICTP PFF Device 15 kV, 3 kJ	‡Electromagnetic Shock tube ‡Vacuum Spark ‡Glow discharge ‡Rotamak ‡Pinch ‡Laser systems	‡Plasma Focus diagnostics and fusion neutrons ‡Torodial pinch - discharge and probe measurements ‡Current stepping in pinch	15
7) Pakistan	Quaid-I-Azam University Islamabad		‡PF (1987)	‡Theta Pinch (1988) (from Germany)		12
8) Turkey	a) Turkish Atomic Energy Authority Ankara		‡DPF-2 Mather (1984) 2.5, 5, 18 cm 10-20 kV, 10 kJ ‡DPF-MD/1 Mather 1987 (as above, but multiple poloidal B)	‡SK/ITT-1 (1984) Compact Torus Magnetized -Tube R_f = 10 cm H = 8 cm B = 0.075 T ‡SK/CG-1 (under construction) Four C-Guns R_f = 25 cm H = 22 cm B = 1.5 T		5
	b) Cekmece Nuclear Research and Training Centre Istanbul			‡Magneto-plasma I (1975) D = 6 cm L = 50 cm B = 0.1 T ‡Magneto-Plasma II (1980) D = 4 cm L = 100 cm B = 0.3 T	‡Ion acoustic wave study ‡Plasma-wave interaction	3

C) AFRICAN COUNTRIES

Country	Institution	Plasma Focus	Others	Key Person
1) Egypt	a) Atomic Energy Authority Cairo	Plasma Focus - Mather a = 1.6 cm, b = 3.3 cm L = 31.5 cm 18 kV, 10 kJ	* Linear θ - pinch (1983) L = 80 cm, a = 8 cm, B = 1.8 T * Linear θ - pinch (1984) L = 350 cm, a = 8 cm, B = 2.5 T	17
	b) Al Azhar University Cairo	UNU/ICTP Plasma Fusion Device a = 1.0 cm, b = 3.2 cm L = 16 cm 15 kV, 3.3 kJ	* Pinch * Shock Tube * Lasers	6
2) Nigeria	Rivers State University of Science and Technology Port Harcourt	UNU/ICTP Plasma Fusion Device a = 1.0 cm, b = 3.2 cm L = 16 cm 15 kV, 3.3 kJ		3
3) Sierra Leone	Njala University College	UNU/ICTP Plasma Fusion Device a = 1.0 cm, b = 3.2 cm L = 16 cm 15 kV, 3.3 kJ		2

IV Some statistical data is presented in the following Tables:

Table 3: Countries and Institutes with Fusion Programmes and Facilities

Table 4: Distribution of Countries by Region

Table 5: Tokamaks in the Third World

Table 6: Division of Countries according to Strength of Fusion Programmes

Table 7: Brazilian National Plasma Programme

Table 3: COUNTRIES AND INSTITUTES WITH FUSION PROGRAMMES AND FACILTIES

Country	No. of Insitutes with Fusion Programmes	No of Institutes with Experimental Facilities	Key Researchers (estimates)
Argentina	3	3	39
Bangladesh	2		6
Brazil	6	5	66
Chile	1	1	4
China	9	6	~200
Colombia	1		3
Cuba	1		3
Egypt	2	2	23
India	5	3	>30
Indonesia	1	1	4
Iran	1	1	5
Kenya	1		3
Korea Rep	6	3	22
Malaysia	2	1	18
Mexico	1	1	8
Nepal	1		4
Nigeria	2	1	6
Pakistan	1	1	12
Philippines	1		2
Senegal	1		3
Sierra Leone	1	1	2
Singapore	1		2
Sudan	1		2
Syria	1		2
Thailand	1	1	2
Turkey	2	2	8
United Arab. E	1		2
Venezuela	2	1	5
Totals: 28	58	34	> 486

Table 4: THIRD WORLD COUNTRIES WITH FUSION PROGRAMMES
Distribution of Countries by Region

ASIA	LATIN AMERICA	AFRICA
Bangladesh China India Indonesia Iran Korea, Rep. Malaysia Nepal Pakistan Philippines Singapore Syria Thailand Turkey United Arab E.	Argentina Brazil Chile Colombia Cuba Mexico Venezuela	Egypt Kenya Nigeria Senegal Sierra Leone Sudan
Totals: 15	7	6

Table 5: TOKAMAKS IN THE THIRD WORLD

Country	Device	a (cm)	R (cm)	B_τ (T)	I_p (KA)	τ_E (ms)	Ne (10^{19} m^{-3})	Te (kV)	Ti (kV)	β_τ (%)
Brazil	TBR-1	11	30	0.5	12	1	1.5	0.12		0.1
China	CT-6B	10	45	1.3	30	1-2	1-4	0.3	0.1	0.5
	HT-6B	12.5	45	1.2	40	1-3	3	0.25	0.08	1
	HT-6M	20	65	1.5	120	10	7	0.6	0.2	1
	MPT-X	8	40	1						
	HT-U	35	125	3						
	HL-I	20	102	3-4	225	16-18	7.2	1.8	0.87	
	KT-5B	6	30	0.5	15	2		0.1	0.03	
India	ADITYA	25	75	1.5	250	6	1	0.5	0.3	
Iran	ALVAND	12.6	45.5	0.8	6		2	0.1	0.05	0.2
Korea	SNUT-79	15	65	3	120	50	10	0.5		0.4
	KAERIT	5	27	4.2						
Malaysia	Tokamak	5	25	0.5	40	0.1	1	0.1	0.1	0.2
Mexico	NOVILLO	8	23	0.47	120	0.15	2	0.15	0.05	0.1

Table 6: DIVISION OF COUNTRIES
ACCORDING TO STRENGTH OF FUSION PROGRAMMES

A	B	C
Argentina	Chile	Bangladesh
Brazil	Egypt	Colombia
China	Iran	Cuba
India	Mexico	Indonesia
Korea, Rep.	Pakistan	Kenya
Malaysia	Turkey	Nepal
		Nigeria
		Philippines
		Senegal
		Singapore
		Sierra Leone
		Sudan
		Syria
		Thailand
		United Arab E.

A: Countries with strong Fusion Programmes
B: Countries with reasonable Fusion Programmes
(critical mass achieved)
C: Countries with weak Fusion Programmes
(mainly theoretical, subcritical mass)

Table 7: BRAZILIAN NATIONAL PLASMA PROGRAMME

* MCT approves US$ 64 M over next four years in support of

- Basic research
- Plasma technology: Development of devices and instruments for research and industry
- Fusion

* Grants to be used for

- setting up a National Plasma Laboratory (51 M)
(main experiment: RF-Driven Compact Tokamak
R = 30 cm, a = 20 cm)
- strengthening experimental facilities at existing Laboratories (13 M)
[USP, UNICAMP, ITA-IEAV, UFF, UFRGS]

V The next 3 tables 8-10 summarises the Plasma Physics Programmes of the ICTP.

ICTP PLASMA PHYSICS PROGRAMMES

Table 8: ACTIVITIES AT ICTP

* 1964: International Seminar on Plasma Physics
* 1965: One year programme (directed by M Rosenbluth)
* 1970:
  - 4 months Research Group on Plasma Physics (directed by B.B. Kadomtsev)
  - IAEA planned discussion on International Cooperation in Controlled Fusion Research (report published in Nuclear Fusion Vol. 10, p. 113)
* 1977 - 1987: 6 Colleges on Plasma Physics
  - Colleges run for 4 weeks divided between Fusion, Laser and Space Plasmas
  - Participants from Developing Countries (40%); Europe, Japan, USA and USSR (60%)
  - On average 70 participants from Developing Countries attended each College
* 1980: Workshop on Drift Waves
* 1984: Twenty years of Plasma Physics at ICTP (Workshop organised by B. McNamara)

Table 9: OUTSIDE ACTIVITIES SUPPORTED BY ICTP

* 1982: First Latin American Workshop on Plasma Physics (Brazil)
* 1984: First Tropical College on Laser and Plasma Technology (Malaysia)
* 1985/86: First UNU/ICTP Training Programme on Plasma and Laser Technology (Malaysia)
  - Establishment of UNU/ICTP Research and Training Plasma Fusion Facility (plasma focus, electromagnetic shock tube, nitrogen laser system, glow discharge system)
  - Development of Plasma Focus Facility in Egypt, Indonesia, Pakistan, Nigeria and Sierra Leone
* 1986: Second Tropical College (Malaysia)
* 1987: Energy Independence Conference (Brazil) (Fusion Energy and Plasma Physics)
* 1988: Third Tropical College (Malaysia)
* 1988: (UNU)ICTP Training Programme on Plasma and Laser Technology (Malaysia)
* 1988: Formation of Asian African Association for Plasma Training - AAAPT (Malaysia)

Table 10: ICTP ASSOCIATESHIP SCHEME

* 17 Associates in Plasma Physics from 13 Developing Countries

VI The conclusions to this review are summarised in the next 3 tables (Tables 11-13).

Table 11: BENEFITS OF PLASMA PHYSICS RESEARCH IN THE THIRD WORLD

A) Long-Term

: Enable Third World Countries to monitor the perspectives of Fusion and its potential for their own future energy needs.

: Contribute to and influence the International Fusion Research Programmes

B) Short-Term

: Develop new Technologies with wide Non-Fusion applications:

Examples:
- Plasma Torches
- Radiation Generators
- Plasma Centrifuge
- Particle beams
- Vacuum techniques
- Pulsed power technology

Table 12: PRIORITIES AND FUTURE OUTLOOK

* Shortage of Funds implies:

Selectivity of Appropriate and most effective types of experiments.

* Group A

Develops medium-size Tokamaks with specific objectives

* Group A and B

Develop alternative (Non-Tokamak) concepts (e.g. Field Reversed Pinch, Plasma Focus and Rotamak)

* Group C

Intensive training to reach critical mass

Table 13: ENHANCING FUSION RESEARCH IN THE THIRD WORLD

A) Improvement of Research Facilities:

: Research Grants for equipments and supplies (TWAS)
: Donation of Books and Journals (ICTP/TWAS)
: Donation of Equipment (Fusion Labs in Advanced Countries)
: Grants for indigeneous design of equipment and facilities

B) South-South Collaboration

: TWAS South-South Fellowship Programme
: UNU/ICTP Programme
: Latin American Plasma Programme
: Asian African Association for Plasma Training

C) North-South Collaboration

: Bilateral agreements and exchange of visits
: Long term visits to BIG Fusion Projects in the North (e.g. JET, TFTR, JT-60, T-IS)
: Participation in International Fusion Programmes such as INTOR and ITER
: Participation in International Conferences (ICTP, IAEA)

PART II

In part II we discuss the subject of South-South Collaboration by examining a specific example namely the United Nations University/International Centre for Theoretical Physics (UNU/ICTP) Training Programme in Plasma and Laser Technology in Kuala Lumpur 1985/86.

VII This programme resulted from efforts to initiate research in experimental plasma physics in some developing countries. Specific discussions were held in 1983 during the ICTP Trieste Spring College on Plasma Physics. A proposal was made to IAEA to have regional training programmes on specific devices in Egypt, Argentina and Malaysia. In 1984, UNU agreed to fund a Malaysian training programme. This was duly held in 1985/86 with ICTP funding for the vital aspect of follow-up equipment. Following this a second training programme is scheduled to be run in 1988.

THE UNU/ICTP TRAINING PROGRAMME (1985/86)

Aim: To initiate/strengthen experimental plasma/laser research in several developing countries.

Method: By transfer of
* an integrated package of expertise
* basic components and equipment.

Chosen devices:
* Multipurpose dense plasma facility
  : UNU/ICTP Plasma Fusion Facility/High Mach Number Simulator
  : Electromagnetic Shock Tube
* Nitrogen Laser System
* Glow Discharge System

Progress:

October-December 1985:

Lectures and experiments. Writing a research paper from one of the experiments, planning, compute modelling and design. Construction and development of equipment taking into accopunt individual aims and resources.

December 1985-February 1986:

Development of the UNU/ICTP Plasma Fusion Facility. Development, assembly and testing of each facility until each is fully operational. Research work carried out.

March 1986:

Preparation of reports and research papers. Participation at Second Tropical College. Preparation of equipment for air shipment.

List of Research Papers:

1. American J. Phys. 56, 62 (1988) - S. Lee, T.Y. Tou, S.P. Moo, M.A. Eissa, A.V. Gholap, K.H. Kwek, S. Mulyodrono, A.J. Smith, Suryadi, W. Usada and M. Zakaullah.
2. IEEE J. Quan. Elec. QE23, 283 (1987) - A.J. Smith, K.H. Kwek, T.Y. Tou, A.V. Gholap and S. Lee.
3. Singapore J. Phys. 3, 75 (1986) - S. Lee et. al.
4. J. Fiz. Malaysia 6, 165 (1985) - S. Lee et. al.
5. J. Fiz. Malaysia 7, 45 (1986) - C.S. Wong et. al.
6. J. Fiz. Malaysia 7, 1 (1986) - S. Lee et. al.
7. J. Fiz. Malaysia - K.H. Kwek et. al.
8. Singapore J. Phys. 4, 131 (1987) - S.P. Moo et. al.

and 15 papers at Second Tropical College 1986 and ICTP Spring College 1987, presented by UNU Fellows, to appear in the Proceedings of the two Colleges.

Progress achieved by UNU Fellows on returning home:

April 1986 Nitrogen laser operational at Port Harcourt

End 1986 UNU/ICTP PFF operational at Yogyakarta, Cairo, Islamabad. Nitrogen Laser operational at Srinaga.

1987 UNU/ICTP PFF operational at Port Harcourt and Sierra Leone.

Dec 1987 Nuclear fusion neutrons measured from UNU/ICTP PFF at Islamabad.
M.Sc. Programme reported at Sierra Leone.
First M.Sc. awarded at Port Harcourt.
Ph.D. programmes reported from Quaid-I-Azam, Port Harcourt and Bandung.
Quaid-I-Azam planning 16 kJ focus and pinch experiments.

1988 First Ph.D. thesis on experimental plasma fusion physics reported from Quaid-I-Azam.

VIII KEY POINTS OF TRAINING PROGRAMME

i) Device to be developed and transferred must be carefully chosen to have
   a) special cost effective features
   b) large variety of phenomena for research and postgraduate studies

ii) Device must be carefully packaged from consideration of technical, pedogogical and economic aspects.

iii) Concept of sub systems has great advantage.

Choice of Devices:

A variety of small plasma devices were considered carefully. From the fusion point of view the plasma fcous was selected to be superior, requiring less technical resources than other pulse plasma devices and yet producing more intense plasma phenomena including copies x-ray, relativistic electron beam and fusion neutrons. The physics behind this cost-effectiveness has been identified as the pulse power enhancement inherent in the two-phase mechanism of the focus which allows for time matching of the electrical rise time to the time of pinch; so that a conven tional capacitor is sufficient to produce nuclear fusion in the focussed plasma of even a small machine like the UNU/ICTP PFF.

Concept of sub-systems

The training programme centres on the adaptive design, construction and experiments of a complete research facility made up from sub-systems including power supplies, control and switching electronics, discharge electrode system and low inductance connections, vacuum chamber, diagnostics, modelling microcomputer packages and design, construction, assembly, testing and research procedures.

The sub-systems as designed for the UNU/ICTP PFF are shown schematically in Fig. 2. The detailed design of the machine as shown in Figs 3a and 3b and the electrical circuit in Fig. 4. The resulting low-cost machine has produced research results already reported in various research papers mentioned earlier.

IX CURRENT TRAINING AND RESEARCH TOPCIS

The UNU/ICTP PFF open up a large number of research areas and application topics. These may be summarised as follows:

System technology, design and construction
System characterisation and optimisation
Development of diagnostics
Development of computation - modelling, parametric variation and optimisation
Plasma dynamics
Neutron measurements and neutron scaling
Fusion physics and technology
Neutron enhancement by dynamic, thermodynamic and target methods
Application as pulsed neutron source e.g. for half-life measurements
X-ray production and measurements

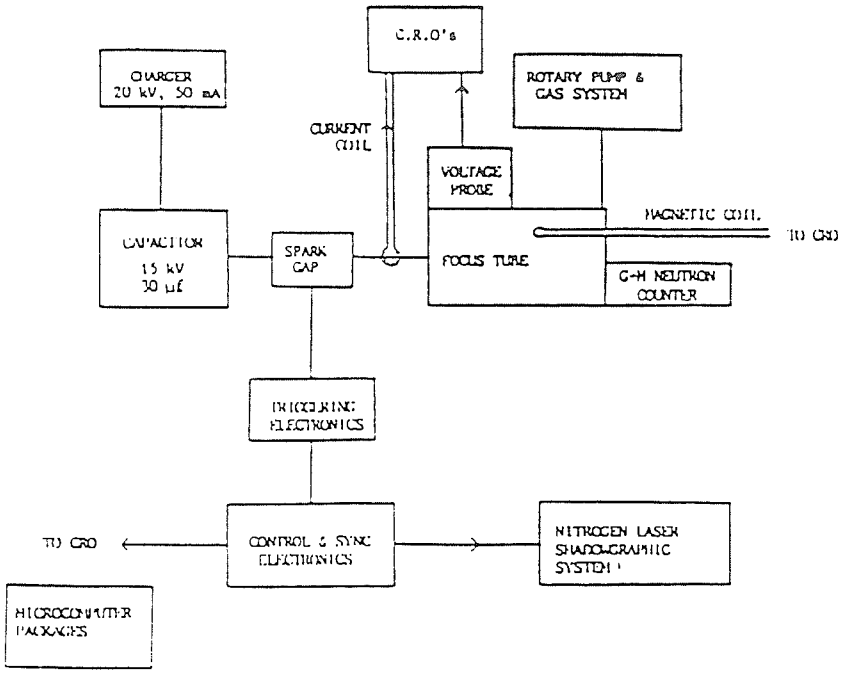

Fig. 2. Sub-systems for the UNU/ICTP plasma fusion facility

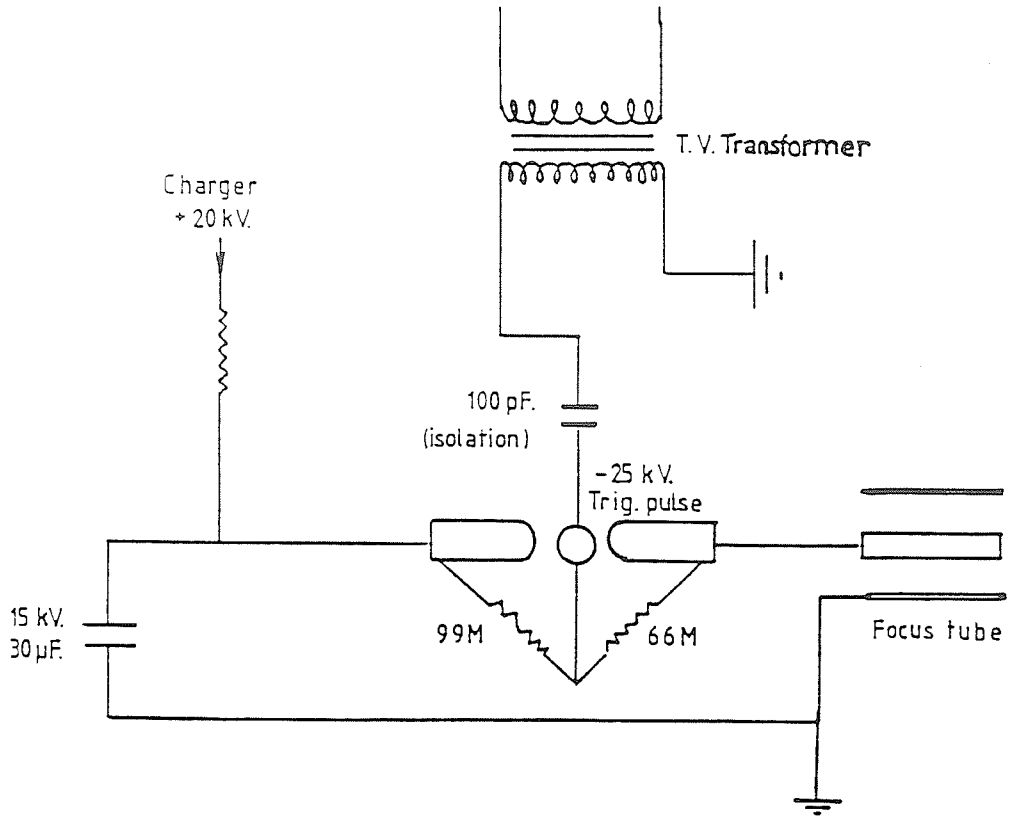

Fig. 4. Circuit for the swinging cascade spark gap and focus tube.

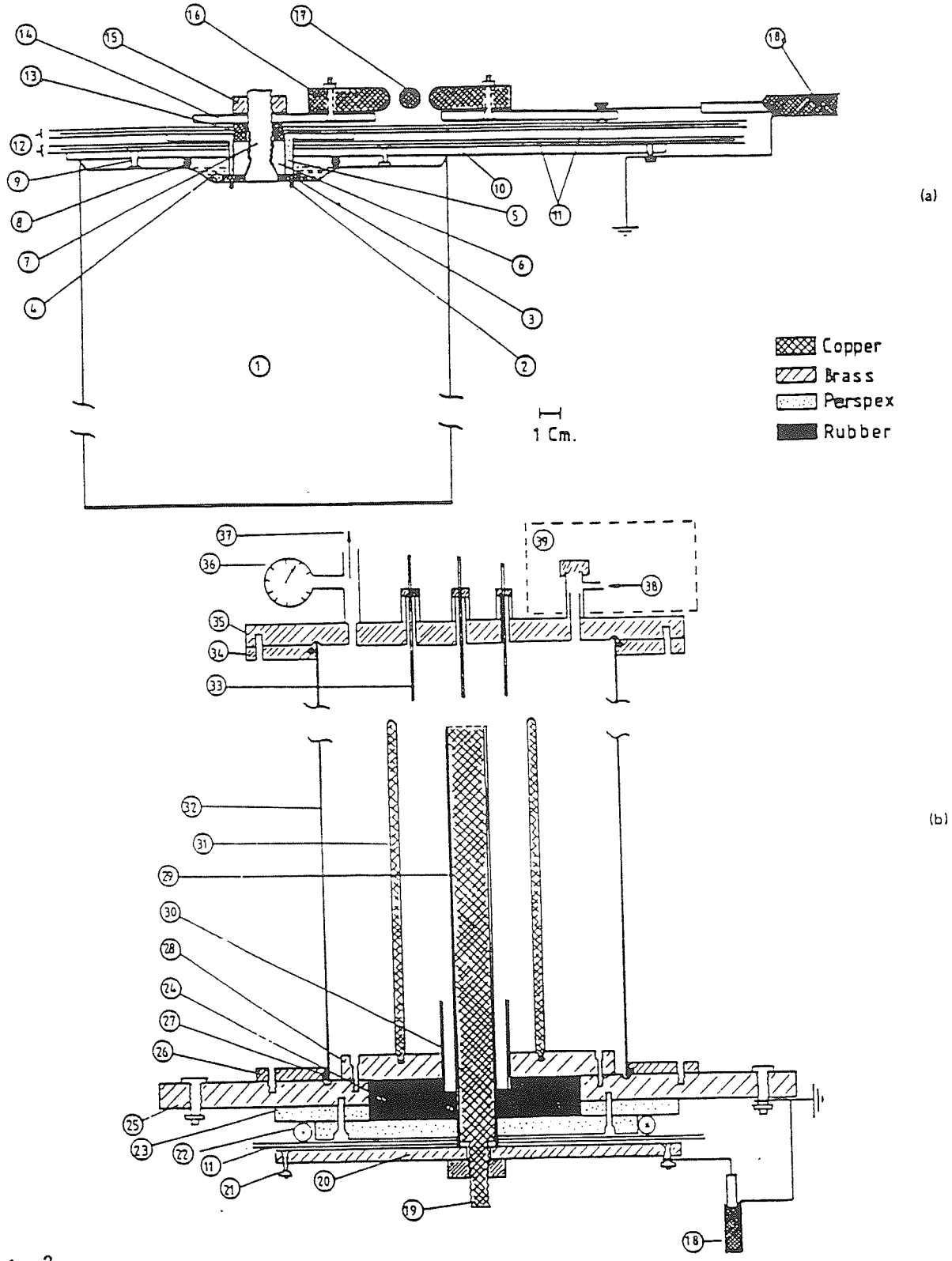

Fig. 3

(a) The capacitor connecting plates, the spark gap, and output coaxial cables. 1 = 15-kV, 30-μF capacitor; 2 = capacitor O-ring seal; 3 = washer; 4 = oil; 5 = nylon cap; 6 = steel nut; 7 = capacitor output seal; 8 = O-ring seal; 9 = Earth stud; 10 = Earth plate; 11 = 5-mil Mylar film; 12 = polyethelene film; 13 = copper ring HV connector; 14 = capacitor high-voltage (HV) output plates; 15 = lock nut for HV plate; 16 = HV electrode for swinging cascade spark gap; 17 = trigger electrode; and 18 = output coaxial cables (16 in parallel). (b) The plasma focus tube. 18 = input coaxial cables (16 in parallel); 19 = stud of anode; 20 = anode collector plate; 21 = connecting points for coaxial cable HV lead; 22 = Rogowski coil; 23 = perspex spacer; 24 = rubber holder; 25 = cathode collector plate; 26 = mild steel flange; 27 = O-ring seal; 28 = focus cathode support plates; 29 = focus anode; 30 = glass insulator; 31 = focus cathode (6 rods); 32 = mild steel focus chamber; 33 = movable magnetic probe in glass jacket; 34 = flange; 35 = back flange; 36 = diaphragm gauge; 37 = outlet to vacuum pump; 38 = inlet for test gas; 39 = wax container with indium foil and PM-scintillator activation counter.

X-ray enhancement and application as sources for
lithography and microscopy
Relativistic electron beam (REB) measurement and applications
Sputtering and deposition of anode materials
using special anode inserts
Study of particle accelerating mechanisms and applications

The level of most of these topics may be at the M.Sc., Ph.D. or for postdoctoral research. For developing countries, the UNU/ICTP PFF is particular suitable for training of postgraduates and for technology training programmes.

X NEUTRON SCALING WITH THE UNU/ICTP PFF

As an example of a research topic that may be investigated with the UNU/ICTP PFF, we may consider the neutron scaling of the plasma focus. Experimental scaling for existing plasma focus machines from 1 kJ to 1 MJ gives a scaling of $Y \sim I_f^x$, I_f = focus current and with x in the range of 3.3 - 4.8. We may ask two questions. What Physics underline this scaling? Can this scaling be improved?

Physics underlying conventional scaling:

Thermonuclear component of the deuterium focus:

$$Y_{th} = \tfrac{1}{2} n_f^2 \langle \sigma v \rangle \pi (r_f^2 \ell_f) \tau_f \qquad (1)$$

where we may take the focus radius r_f as

$$r_f = a\, k_f \qquad (2)$$

where a = radius of anode

k_f = radius ratio = a constant value of 0.12 for deuterium focus, and the length of the plasma is

$$\ell_f = a(1 - k_f) \qquad (3)$$

The focus lifetime may be taken as r_f divided by the small disturbance speed, with a lifetime enhancement factor f_{en}. Therefore

$$\tau_f = \frac{r_f\, f_{en}}{C_1 \left[\frac{I_o}{a}\right] / \rho_o^{\frac{1}{2}}} \qquad (4)$$

where $C_1 = \frac{I_f}{I_o} \frac{\sqrt{\mu}}{2\pi} \left\{ \left(\frac{1}{\ell_f}\right)^2 + \frac{\gamma f_{rs}}{2} \right\}^{\frac{1}{2}}$

where I_f = focus current

I_o = characteristic current

μ = permeability

γ = specific heat ratio

and f_{rs} = reflected shock overpressure

The on-axis shock speed is

$$V_f = C_2 \left[\frac{I_o}{a}\right] / \rho_o^{\frac{1}{2}} \tag{5}$$

where

$$C_2 = \frac{1.1\mu^2 \ (1+\gamma)^{\frac{1}{2}}}{4\pi}$$

From Eqn. (5) we may write for the radius of the anode

$$a = C_2 \frac{I_o}{V_f \ \rho_o^{\frac{1}{2}}} \tag{6}$$

The focus temperature may be written from pressure consideration as

$$T_f = C_3 \ \left(\frac{I_o}{a}\right)^2 / \rho_o \tag{7}$$

where $C_3 = \frac{\mu}{4\pi^2} \frac{M}{R_o \chi} f_{rs} \left(\frac{I_f}{I_o}\right)^2$

M = molecular weight

R_o = universal gas constant

χ = departure coefficient

Hence from Eqns. (5) and (7) we may write the focus temperature

$$T_f = C_4 \ V_f^2 \tag{8}$$

where $C_4 = C_3 / C_2^2$

noting that C_1, C_2, C_3, C_4 may be taken as constants.

Next put Eqns. (2), (3), (4) and (6) into Eqn. (1) and obtain

$$Y_{th} = C_5 \frac{I_o^4}{V_f^5} \langle\sigma v\rangle \tag{9}$$

where $C_5 = \frac{1-k_f}{2k_f\, m_D^2} f_{en} \frac{C_2^5}{C_1}$

with m_D = mass of deuteron.

From nuclear data we may fit in the range of T from 1-5 keV

$$\langle\sigma v\rangle_{D-D} = C_N\, T^{5.5} \tag{10}$$

where C_N = a constant

Put Eqns. (10) and (8) and then Eqn. (7) into Eqn. (9) and

$$Y_{th} = C\, I_f^4 \{(\frac{I_f}{a})/\rho_o^{\frac{1}{2}}\}^4 \tag{11}$$

where $C = C_5 C_4^{5/2} C_3^2 C_N (I_o/I_f)^8$.

Put Eqn. (5) into Eqn. (11) and we have

$$Y_{th} = C_c\, I_f^4 \tag{12}$$

where $C = C(V_f^4/C_2^4)(I_f/I_o)^4$

The quantity I_f/I_o is approximately a constant.

For present day focus devices

V_f = 25 cm/μs

giving T_f = 1 keV

It may be seen that this limit of focussing speed is what limits the thermonuclear part of the neutron yield to $Y_{th} \sim I_f^4$.

We may also consider the beam-gas component of neutron yield. Present generation plasma focus produces predominantly beam-gas neutron to an extent of 90% resulting from deuteron beams with energy from 50 keV to 1 MeV. Increasing the focus temperature may increase the deuteron beam energy but does not dramatically increase beam-gas neutron yield. Using a

simple model such as an inductive model may yield for the beam-gas neutrons

$$Y_{b-g} \sim \frac{I_f^{4.5} \rho_o^{\frac{1}{2}}}{V_f^{3/2}} \qquad (13)$$

where D-D cross section σ and its function with beam-energy has been approximately accounted for.

Thus for a constant speed focus

$$Y_{b-g} \sim I_f^{4.5}$$

with a further relatively minor dependence on density.

SUMMARY

The observed scaling law

$$Y \sim I_f^4$$

is due to constant speed operation with the same speed V_f = 25 cm/μs in all devices resulting in a fixed temperature operation $T_f \leq 1$ keV so that the advantage of vastly increased fusion cross section with temperature is not made use of. There are two advantages in arranging for focus speed to significally exceed 25 cm/μs pushing temperature well significally above 1 keV. These are:

1. The neutron yield will become predominatly thermonuclear.
2. The thermonuclear yield will scale as

$$Y_R \sim I_f^8$$

for fixed a and ρ_o.

SPEED LIMIT

Experimentally there is an observed upper limit for the focussing speed of 25 cm/μs corresponding to an axial speed limit of 10 cm/μs.

The physics of this speed limit should be studied so that it may be overcome and the advantage of increased speed leading to vastly increased yield may be used.

Some recent shadowgraphic studies supported by a TWAS grant have shown indications that as the axial speed increases above 10 cm/μs, separation between the magnetic piston and shock front due to a γ (specific heats ratio) effect becomes too great leading to a radial collapse in which the

radial shock wave may become decoupled from the radially compressing piston.

SUGGESTED REMEDIES

From these studies the following remedies are suggested to prevent the decoupling effect:

1. seeding with noble gas to keep at a reduced value even at axial speeds above 10 cm/ s.
2. keeping the axial phase physically short. This will lead to requirement of fast current rise time and Marx technology.
3. development of a gas puff focus - to prevent mass accretion and layer thickening during axial traversal.
4. electrode profiling

These techniques may be best developed and tested in simple, flexible machines like the UNU/ICTP PFF.

XI EXTENDING THE SHARING

(i) Packaging other devices
- (a) Field reversed pinch
- (b) Micro-Tokamak
- (c) Transistorised Rotamak
  (Compact torus FRC driven by rotating B field.
  Steady current drive of 0.1 A/W)
  - Ref. Flinders University of South Australia.
- (d) Application devices
  Radiation sources, beam source
  X-ray laser punmp source
  Plasma torch
  Plasma sputtering and spraying

(ii) Other countries as training centres
- (a) China
- (b) Egypt
- (c) India

(iii) Asian African Association for Plasma Training
- (a) News bulletin
- (b) Coordinated series of training programmes
- (c) Equipment design and acquisition
- (d) Fellowship exchange scheme

XII CONCLUSION FOR PART II

(i) South-South Collaboration may be based on technology sharing.

(ii) Concept of packaging has proven to be successful.

(iii) A well chosen device provides many research possibilities e.g. UNU/ICTP PFF

(iv) Collaboration will be extended by packaging more devices involving more training centres using the consultative framework of the AAAPT.

Proc. 3rd Tropical College on Appl. Phys., 1988.
Contributed Paper

HALF-LIFE MEASUREMENTS USING PLASMA NEUTRONS

S.P. Moo, C.K. Charkrabarty and S. Lee

Plasma Research Laboratory, Physics Department,
University of Malaya, 59100 Kuala Lumpur, MALAYSIA

Abstract

A small dense plasma focus device producing neutrons of intensity 10^8 n per pulse and of duration 50-100 ns has been successfully used as a pulsed neutron source for half-life measurements. As examples, half-life measurements of the ground state of ^{116}In and of the isomeric state $^{24}Na^m$ are described.

Introduction

Many laboratories[1,2] have reported neutron emission from the dense plasma focus using the D-D reaction. However, only two applications of the plasma focus neutrons have been demonstrated; one on neutron radiography[3] and the other one on pulsed neutron activation of sodium[4] followed by half-life measurement of $^{24}Na^m$. In both applications neutron intensities of $\approx 10^{10}$ neutrons per discharge were used.

Recently, a low cost plasma fusion facility has been developed and tested (the UNU/ICTP PFF[5]). The system is sufficiently simple in design and reliable in operation that six sets have been made and transferred to several countries under the auspices of the United Nations University and the International Centre for Theoretical Physics. The system consists of a 3.3 kJ plasma focus powered by a single, 30 μF Maxwell capacitor and switched by a simple parallel-plate swinging cascade air gap. Operating at 15 kV and 180 kA current it produces a consistent yield of $0.5\text{-}1.0 \times 10^8$ neutrons per discharge at 3 torr deuterium.

Is such a small focus useful as a neutron source for research/teaching? To answer this question we have looked at a simple application of the plasma focus as a pulsed neutron source for half-life measurements. For a given neutron flux impinging on a sample, the activity produced is proportional to the factor $\{1 - \exp(-0.693 t_i / t_{1/2})\}$. Since

this factor increases and approaches unity as the ratio of the irradiation time (t_i) to the half-life ($t_{1/2}$) increases, it is immediately apparent that the short duration (50-100 ns) of the plasma focus neutrons enhances the activation of short lived isotopes. In this paper, we report half -life measurements of the ground state of ^{116}In and of the isomeric state $^{24}Na^m$.

Method

Natural indium consists of ^{115}In (95.8 % abundance) and ^{113}In (4.2 % abundance). When ^{115}In captures a neutron, the compound nucleus formed promptly deexcites by gamma ray emission to either the ground state of ^{116}In or an isomeric state ($^{116}In^m$). Both these states decay by β emission with half-lives of 14 s and 54 min respectively. The isotope ^{113}In also becomes β active on capturing neutrons. However, because of its low abundance and small cross section, its contribution to the total β activity is less than 0.2 %.

The equipment used in the irradiation and measurement of the half-life of the ground state of ^{116}In is shown schematically in Fig.1. The D-D neutrons from the plasma focus are slowed down by 40 mm of paraffin before impinging upon an indium foil of diameter 50 mm and thickness 0.2 mm. The β particles emitted are detected by an NE-102 plastic scintillator optically coupled to a photomultiplier. A multi-channel analyser (MCA) operating on the multiscaling mode at 3 s dwell time records the activity of the indium foil as a function of time, both before and after the neutron burst.

For the activation of sodium, the metal foil- plastic scintillator system of Fig. 1 is replaced by a 75 mm diameter, 75 mm long NaI scintillator. When the NaI crystal is exposed to slow neutrons of short duration, the dominant state formed is the isomeric state $^{24}Na^m$ which emits 472 keV γ radiation. The large size of the NaI crystal compensates for the small neutron cross section for ^{23}Na to $^{24}Na^m$ (0.4 b) and improves the efficiency for the detection of the γ radiation. A dwell time of 10 ms is used in this case.

Results and discussion

In this investigation, fifteen independent measurements of the indium activity are made. Fig.2 shows a typical decay curve. The maximum counts

in the measurements ranged between 300/channel and 1100/channel. At these low count rates, dead time losses are negligible. For the determination of the half-life of ^{116}In, the counts recorded in 30 channels (90 s) of the decay curve, starting from the second channel after the neutron burst, are considered. Over this interval the β activity of the relatively long lived isomeric state is taken to be constant since it changes by only 2 %. Furthermore, calculation indicates that the initial contribution from the isomeric state to the total β activity is less than 2 %. In our data analysis, therefore, the contribution to the channel counts from the isomeric state is treated as a component of the constant background.

After background subtraction, a weighted least squares fit[6,7] is applied to each of the decay curves in the region where the net counts exceed three times the background counts. Our results show that even with the present low count rates, the fitting routine yields a consistent value for the half-life when the fitted interval exceeds about 10 channels (2 $t_{1/2}$).

The half-life calculated from 15 independent measurements are listed in Table 1. It ranges from 13.11 s to 14.90 s while the individual errors ranged from 0.27 s to 0.92 s. The weighted average is 14.20 s while the statistical error is ± 0.11 s. Uncertainity arising from background subtraction and from dead time losses is expected to contribute a systematic error of less than ± 0.1 s. Adding the two errors in quadrature yields a total error of ± 0.15 s. Our value of 14.20 ± 0.15 s is very close to the value of 14.05 ± 0.26 reported by Ducat and Thomas[8]. Other values reported are; 13.4 ± 0.4 s (Domanic and Sailor[9]), 14.5 ± 0.4 s (Capron and VanderStricht[10]) and 15.6 ± 0.5 s (Brzosko et al.[11]).

For sodium, a total of fourteen independent measurements are made. The maximum counts ranged from 300/channel to 1000/channel. Fig. 3 shows a typical decay curve. It is consistent with a single decay component, the contribution to the count rates from the long lived isotope ^{24}Na (15 h) is negligible. In the analysis of the data each of the decay curves is corrected for dead-time losses using the method of Shanks and Junod[12], the measured dead-time for the NaI scintillator-photomultiplier system being 5 μs. A weighted least squares fit is again applied to each of the decay curves after background subtraction as in the case of In. The calculated values of the half-life is listed in Table 1. The weighted average is 19.78 ± 0.34 ms. A possible systematic error of 0.2 ms is included in the

error quoted. Our value of the half-life of $^{24}Na^{m}$ compares well with reported values of 19.6 ± 0.5 ms (Salaita[13]), 20 ± 0.7 ms (Meyers and Schats[14]), 19.9 ± 0.3 ms (Schardt[15]), 18.3 ± 0.6 ms (Glagolev and Yampolskii[16]), 20 ± 2 ms (Campbell and Fettweis[17]) and 20 ± 1 ms (Glagolev et al.[18]).

Acknowledgement

This work was supported by The Government of Malaysia and the University of Malaya under IRPA Program 4-07-04-40.

References

1. G. Decker and R. Wienecke, Physica 82C, 155 (1976).
2. H.Conrads, Neutron Physics and Nuclear Data in Science and Technology, Vol. 2, Edited by S Cierjacks, Pergamon Press, 237 (1983).
3. D. Ruffner, Neutrographie am Plasma-Fokus, IPF 74-3, Institut fur Plasmaforschung, Universitat Stuttgart (1974) and H. Rapp, E. Rauchle and D. Ruffner, Mater. Eval. 33, 269 (1975).
4. E. Bar Auraham and Y. Porath, Nucl. Instr. and Meth. 123, 5 (1975).
5. S. Lee, T.Y. Tou, S.P. Moo, M.A. Eissa, A.V. Gholap, K.H. Kwek, S. Mulyodrono, A.J. Smith, Suryadi, W. Usada and M. Zakaullah, Am. J. Phys. 56,62 (1988).
6. S.L. Meyer, Data Analysis for Scientists and Enginners, Wiley, New York (1975).
7. K.S. Krane and L. Schecter, Am. J. Phys. 50, 82 (1982).
8. A. Ducat and R.H. Thomas, Nucl. Phys. 15, 525 (1960).
9. F. Domanic and V.L. Sailor, Phys. Rev. 119, 208 (1960).
10. P.C. Capron and A. VanderStricht. Nucl. Sci. Abstr. 13, No.358 (1959).
11. J. Brzosko, P. Decowski, K. Siwek-Diament and Z. Wilhelmi, Nucl. Phys. 74, 438 (1965).
12. J. Shanks, TEES-2671-2 (1962) p. 5/15; E. Junod, Etudes d'analyse par activation, Le comptage des radionucleides de periodes courtes, Vol. 1, CEA-R-2980 (1966); both as reported in M. Wiernik, Nucl. Instr. and Meth. 95, 13 (1971).
13. G.N. Salaita, Nucl. Phys. A170, 193 (1971).
14. P. Meyers and J.J.C. Schats, Physica 32, 179 (1966).

15. A.W. Schardt, Phys. Rev. 122, 1871 (1961).
16. V.L. Glagolev and P.A. Yampolskii, JEPT (Sov. Phys.) 13, 520 (1961).
17. E.C. Campbell and P.F. Fettweis, Nucl. Phys. 13, 92 (1959).
18. V.L. Glagolev, O.M. Kovrizhnylch, Y.V. Makorov and P.A. Yampolskii, JEPT (Sov. Phys.) 9,742 (1959).

Table 1. The half-lives of ^{116}In and $^{24}Na^{m}$.

Run no.	^{116}In (s)	$^{24}Na^{m}$ (ms)
1	14.90 ± 0.74	20.50 ± 2.09
2	13.94 ± 0.92	19.58 ± 1.18
3	13.97 ± 0.41	21.12 ± 0.92
4	14.28 ± 0.58	20.07 ± 2.90
5	14.34 ± 0.28	21.03 ± 0.88
6	14.25 ± 0.39	19.73 ± 0.76
7	14.04 ± 0.46	18.66 ± 2.35
8	13.12 ± 0.79	19.86 ± 1.42
9	13.11 ± 0.73	20.42 ± 1.53
10	14.49 ± 0.62	18.71 ± 1.42
11	14.30 ± 0.55	19.27 ± 0.85
12	14.55 ± 0.46	20.16 ± 1.10
13	14.60 ± 0.27	19.13 ± 0.53
14	13.80 ± 0.44	19.75 ± 1.45
15	13.87 ± 0.30	
Weighted mean value	14.20 ± 0.15	19.78 ± 0.34

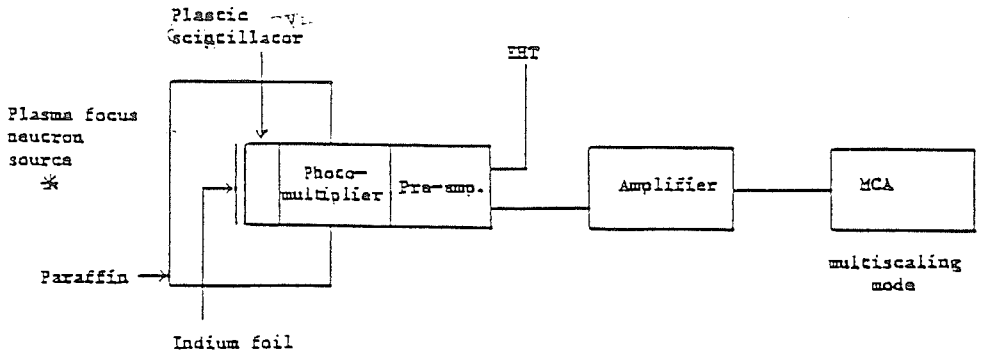

Fig. 1. Schematic diagram of equipment for half-life measurements.

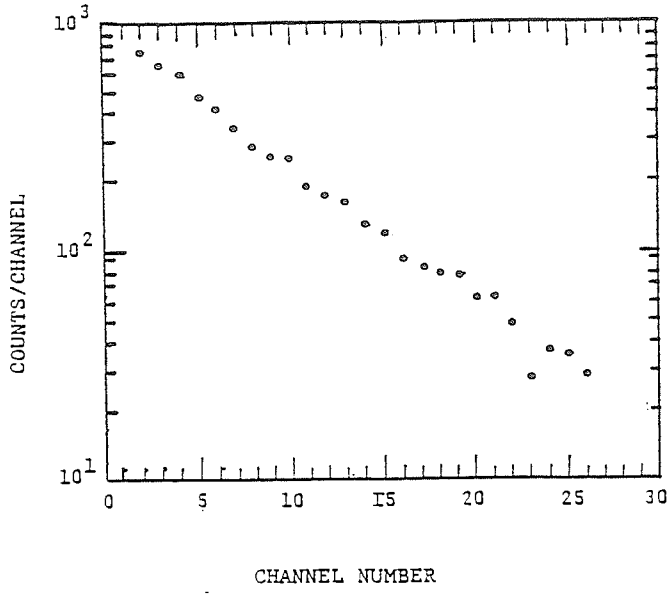

Fig. 2 Beta decay curve of ^{116}In.

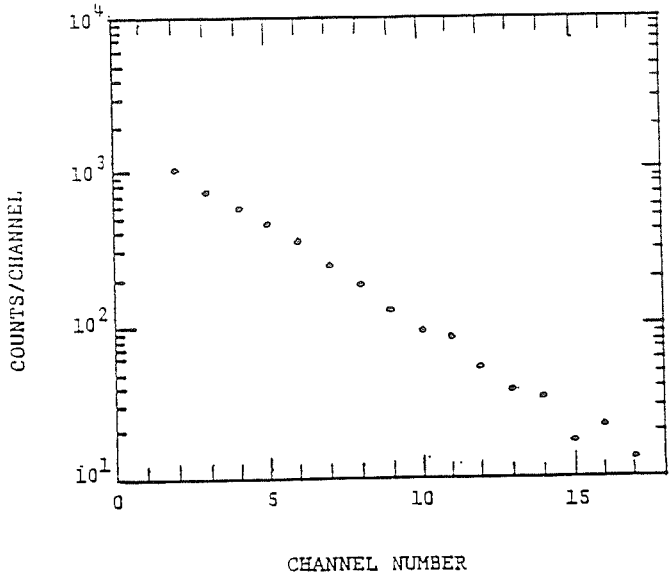

Fig. 3. Decay curve of $^{24}Na^{m}$.

J. Fiz. Mal. 9, 36 (1988)

HIGH RESOLUTION PLASMA VISUALIZATION BY SUBNANOSECOND OPTICAL TECHNIQUES

K.H. KWEK, T.Y. TOU* and S. LEE
Department of Physics, University of Malaya
59100 Kuala Lumpur, Malaysia

Received 28 April 1988

Abstract

The design of an aluminium foil-mylar preionized TEA nitrogen laser is described. The laser produces a high quality homogeneous beam that meets the stringent requirement of a Mach-Zehnder interferometer. Its subnanosecond pulse width makes it suitable for the study of fast pulsed experiments. The applicability of the optical diagnostic system is demonstrated for a rapidly changing plasma in the plasma focus discharge.

Introduction

There is an ever growing interest in producing short nitrogen laser pulses due to the application of this kind of laser to time resolved studies not only in pulsed plasma experiments but also in biological, chemical and quantum systems. In nitrogen lasers, transverse excitation at and above atmospheric pressures yield short duration light pulses from one nanosecond down to some tens of picoseconds[1]. Utilisation of such pulses would thus provide short enough exposure times to 'freeze' the motion of the current carrying plasma sheath of the plasma focus, for example, where the velocities are of the order of 10 cm/μs. Good spatial resolution can thus be achieved.

However, in the development of transversely excited atmospheric (TEA) nitrogen lasers one is often faced with the problem of obtaining a homogeneous discharge across the laser gap to achieve high efficiency and good quality laser beam. In transverse discharge geometries, where the electrode separation is small compared to the length, increasing values of E/p and pd (where E is the applied field strength, p is the gas pressure and d is the electrode separation) lead to the development of an inhomogeneous discharge mode. The discharge in such instances breaks up into individual spark channels. The method of producing discharge by way of the sudden application of a strong electric field considerably in excess of the breakdown threshold across the laser gap requires a high voltage electrical pulse having a very fast rise time in order to avoid the formation of filamentary arcs within the discharge volume.

Various methods[2,3,4,5,6] have been used to provide the initial distribution of free electrons, or preionization, necessary for the production of homogeneous gas discharge. Amongst these techniques, the use of an electron beam is perhaps the most efficient method but the technical difficulties involved do not place established electron beam facilities at the disposal of all laboratories. This paper deals with a compact and easily constructed TEA nitrogen laser with preionization provided through low-energy surface corona discharges from a simple combination of aluminium foils and mylar sheets. It is then used as a light source for optical studies in a plasma.

Laser System

The laser is powered by the conventional Blumlein circuit schematically described in Fig. 1. The circuit theory of the parallel plate transmission line type of laser has been discussed in previous papers[7,8,9]. The two energy storage capacitors C_1, and C_2 of the circuit were constructed using aluminium foils and mylar sheets in a similar manner as described in our earlier papers[8,9]. Figure 2 shows the design of

*Present address: Plasma Research Laboratory, R.S. Phys. S., The Australian National University, A.C.T. 2601, Australia.

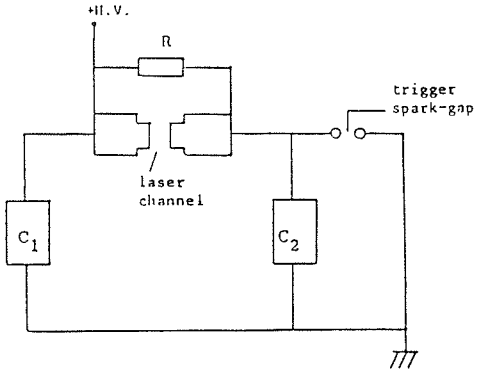

Fig. 1 Equivalent circuit of the nitrogen laser.

the laser. The measured values of C_1 and C_2 are 15 nF and 6 nF respectively. On top of the foils are placed glass plates of appropriate dimensions to prevent mechanical flexing of the foils during charging and discharging of the capacitors. The laser is triggered through a swinging cascade triggered spark gap. The electrodes of the laser channel are made of 20 cm long brass strips with cross-sectional dimensions of 0.5 in. X 1 in. and shaped as shown in Fig. 2b. A perspex cover

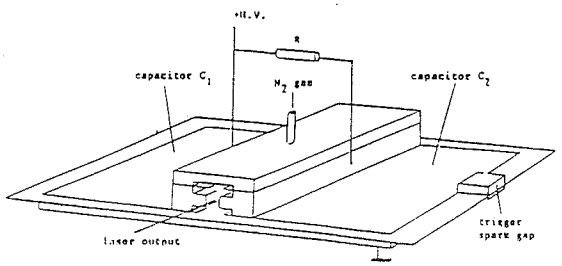

Fig. 2a Sketch of the TEA nitrogen laser.

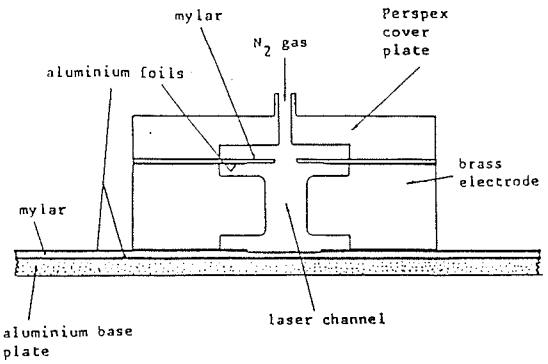

Fig. 2b Cross-sectional view of the laser channel showing the inclusion of the preionizer system using aluminium foil-mylar combination. The mylar strips improve the preionization effect.

plate is screwed onto the laser electrodes on the upper side over the top. Admission and evacuation of the nitrogen gas at atmospheric pressure is made through the middle and the ends of the channel respectively.

In the arrangement shown, the edges of the high voltage capacitor plates (aluminium foils) are allowed to protrude beyong the edges of the laser electrodes into the laser cavity to act as corona blades for preionization. These form the set of blades on the lower side of the laser channel. Similar set of corona blades are placed on the upper side of the laser channel. The laser channel gap is set to 3 mm while the blades separation is typically set to about 40% greater than that of the main gap. The edges of the foils function as auxiliary corona electrodes which provide an initial distributed corona discharge to photoionize and prepare the laser channel for glow formation. The low-energy surface discharges acting as preionizing uv radiation sources are formed early during the rise of the voltage pulse across the laser gap and are distributed by corona charging of the mylar surfaces that extend beyond the edges of the foils. Preionization from the surface discharges is not as effective in the absence of the mylar sheets.

Measurements and Performance

In the absence of the preionizers, the appearance of the discharge along the main laser gap is that of a glow discharge with the presence of strong streamer-like filaments. These streamers prevail with increasing laser gap and are randomly placed, from pulse to pulse, along the channel. Electrical arcs may be formed due to the surface defects created during electrical discharge. The presence of the streamers and arcs can be attributed to the insufficiently fast voltage ramp created across the laser electrodes at such high pressure. The presence of electrical arcs reduces the laser output energy. An inter-electrode distance of 3 mm gives optimum laser energy output of about 100 μJ at a charging voltage of 15 kV. A pulse width of 2 ns at half-maximum was measured using a fast FND photodiode. However, we believe that the duration is $\lesssim$ 1 ns (as shown later), taking into account of the time

resolution of the measuring system. The presence of the streamers and arcs disturbs the homogeneity of the laser beam. The non-uniformity of the laser beam becomes apparent when the laser is used in optical setups where the requirements are stringent.

With the presence of the preionizers, the discharge takes the appearance of a bluish glow. The streamers and arcs are absent. Optimum energy is still obtained at a gap separation of 3 mm but with an improved value of 300 μJ at 15 kV. The measured laser pulse duration remains the same. However, the laser beam quality is greatly improved.

Application

In order to demonstrate the utility of the laser it is coupled to an optical setup to observe the macroscopic behaviour of the high density plasma which is formed in a dense plasma focus. The device is of the Mather type with filling pressures of 1 – 10 torr deuterium, energized by a 7 – 12 kJ capacitor bank charged to 15 – 20 kV[10]. The velocities of the current sheath ranges from 10 cm/μs to 30 cm/μs. The characteristic dimension of the plasma is of the order of 1 mm, and the electron density is of the order of 10^{19} cm $^{-3}$.

The optical setup as shown in Fig. 3 is

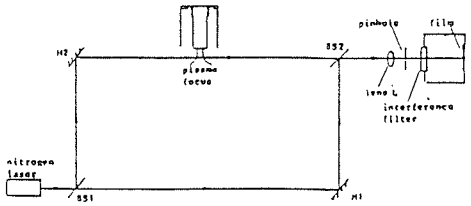

Fig. 3 Schematic of the Mach-Zehnder interferometer. Schlieren and shadowgraphic setup can be obtained by covering the reference beam and setting up the appropriate focussing optics.

basically a Mach-Zehnder interferometer and is sufficiently flexible to be used for schlieren and shadow photograph techniques. BS1 and BS2 are beam splitters while M1 and M2 are full mirrors. The fringes are localised in the plasma position and are imaged onto the film plane by Lens L. The pinhole, located at the focal plane of L, together with a narrow bandwidth interference filter suppresses the intense plasma radiation. Schlieren and shadow photography can be employed by covering the reference beam and setting up the appropriate locations of the focussing lenses.

Using a time delay generator, the laser is synchronized with the discharge so that, by changing the delay in successive shots, the temporal behaviour of the plasma electron density profile can be studied. The synchronization is checked by superimposing the output of a photodiode which picked up part of the laser light, on the voltage trace. Time is referenced to the peak of the voltage signal.

Figure 4a is an example of a shadowgram showing the radial collapse of the current sheath of plasma focus discharge while Fig. 4b shows a

Fig 4 (a)

schlieren photograph of a plasma focus column being disrupted by m = 0 instabilities.

Fig 4 (b)

Fig. 4 Examples of the shadow and schlieren images obtained using the laser without preionizers. (a) Shadowgram (b) Schlieren image.

The above shadow and schlieren photographs were taken using the laser without the preionizers. When the laser was used with the Mach-Zehnder interferometer setup, the interferogram obtained were of poor quality as is

shown by the vacuum interferogram in Fig. 5a. The fringes are barely discernible due to the presence of vertical striations. These poor quality interferograms resulted from the use of poor quality laser beams which are inhomogeneous and not uniform in intensity. Such inhomogeneity and non-uniformity in the beam becomes conspicuous upon expanding the beam several times its original size. Thus, while the laser can be employed in schlieren and shadow photography to provide useful information of the plasma, albeit the quality is not very good, it was rendered useless in interferometry work by poor beam quality. With the presence of the preionizers, the uniform glow discharge along the laser channel produced uniform and homogeneous beam that enabled the interferogram shown in Fig. 5b to be obtained.

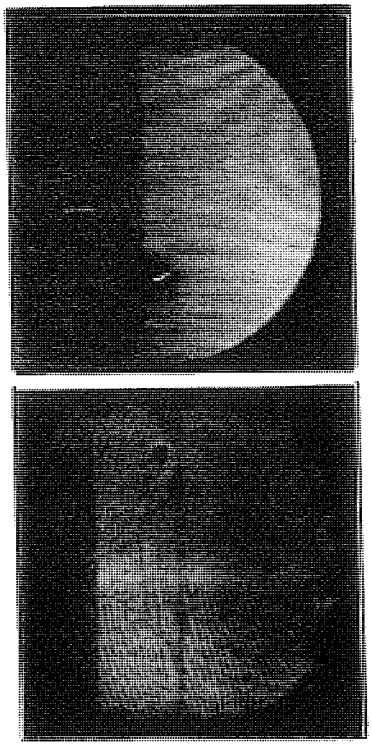

(a)

(b)

Fig. 5 Examples of the interferograms obtained.
(a) Vacuum interferogram obtained using laser without preionizers. Poor quality.
(b) Interferogram of a plasma focus discharge obtained using laser with preionizers.

The improved laser was used to take schlieren photographs of the plasma focus. The results shown in Fig. 6 clearly indicate improved

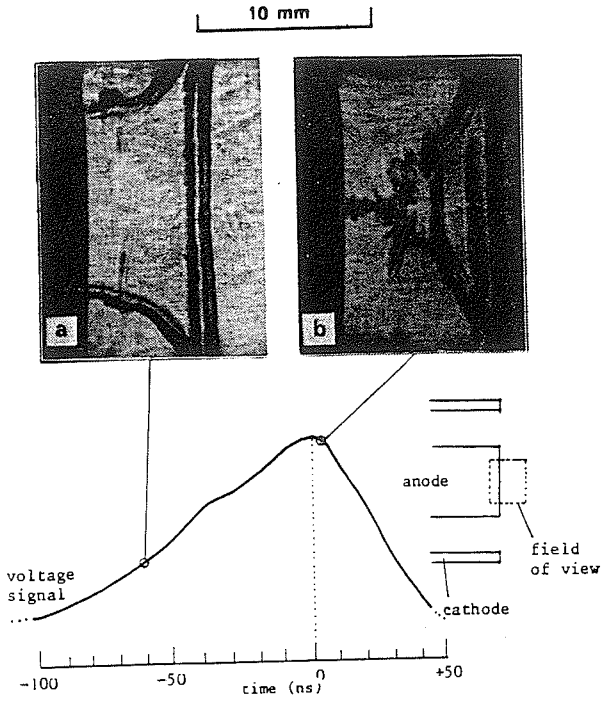

Fig. 6 Improved schlieren photographs of the plasma focus discharge showing (a) the radial collapse of the current sheath, and (b) the plasma column being disrupted by m=0 type instabilities. Time is referenced with respect to the peak of the voltage signal.

schlieren photographs of the radial collapse phase. Density structures of the collapsing plasma layer can be seen more clearly. In fact, the quality of the schlieren pictures are sufficiently good to enable quantitative information such as the electron density and density gradient to be estimated when supplemented with the use of computer simulation as was done by Decker et al[11].

For radial velocities of the order of 20 – 30 cm/μs and an exposure time of 1 ns the motional displacement is about 200 to 300 μm. From the schlieren picture of the radial collapse (Fig. 6a), structures finer than the above limit can be differentiated. This indicates that the exposure time and hence the laser pulse width is in the subnanosecond range. The improved laser beam together with the very short pulse width make the laser schlieren photography setup especially suitable for the study of the axial rundown phase of the plasma focus discharge where the axial velocities are in the range of 5 to 10 cm/μs. The

motional displacement would then be less than 100 um. This fine spatial resolution would enable the observation of plasma sheath structures in the micrometre range. Figure 7 shows schlieren

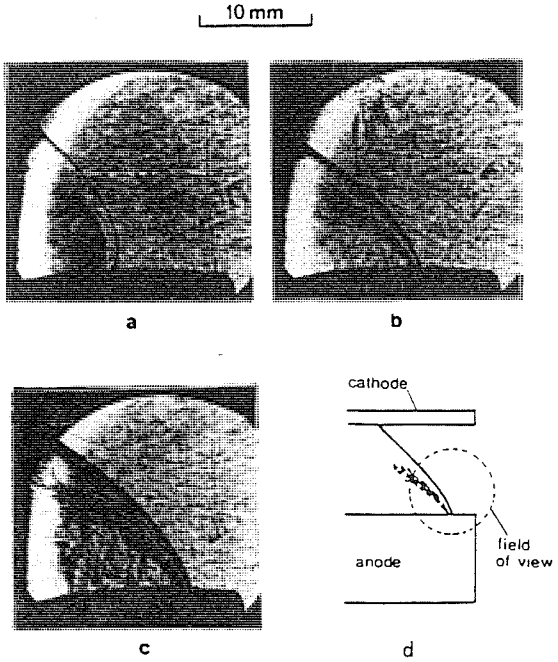

Fig. 7 Schlieren images of the plasma focus discharge in the axial rundown phase. The plasma focus device was operated by 15 kV and deuterium gas at (a) 1mbar, (b) 9mbar, and (c) 14 mbar.

images recorded in the axial rundown phase of the plasma focus discharge. The study of the behaviour the current sheath propagating at various speeds in the rundown phase can provide insight into the scaling characteristics of neutron production in the plasma focus. This is the subject matter of another investigation the results of which would be reported in another paper[12]

Conclusions

The TEA nitrogen laser with the use of preionizers as described provides a powerful laser light source with good beam quality for optical diagnostics of transient and dense plasmas. The combination of the thin aluminium foils and mylar sheets provides an extremely simple but effective preionization scheme. This combined with properly shaped electrodes leads to the production of short duration, high energy and good quality laser pulses from transverse discharges at atmospheric pressure. The preionizers, by providing the enough initial electron density to produce a good main discharge, relaxes the constraint on the fast voltage rise that is needed. The scheme should also prove useful for discharges at above atmospheric pressures. It should be mentioned that we have not needed to replace the preionizers in our laser although they have been in regular use for several months. In any case, replacement of the preionizers would be a relatively simple procedure. An important consideration is that the laser and the preionizers can be constructed at modest expense and yet be a useful tool for optical diagnostics of transient and dense plasmas.

Acknowledgement

This work was supported in part by a grant from the Third World Academy of Sciences (TWAS RG 87-84) and in part by the University of Malaya under the Grant F95/77.

References

1. H. Strohwald and H. Salzmann, Appl. Phys. Lett. 28, 272 (1972).
2. J.I. Levatter and S.C. Lin, J. Appl. Phys. 51, 210 (1980).
3. G. Herziger, R. Wollermann-Windgasse and K.H. Banse, Appl. Phys. 24, 267 (1981).
4. N.A. Kurnik, S.J. Tubbs, K. Bidhichand, L.W. Ryan Jr. and A. Javan, IEEE J. Quantum Electron QE-11, 174 (1975).
5. E.E. Bergmann, Appl. Phys. Lett. 28, 84 (1976).
6. V. Hasson and H.M. von Bergmann, J. Phys. E: Sci. Instrum. 13, 632 (1980).
7. S. Lee, A.V. Gholap, A.J. Smith, K.H. Kwek, A.C. Chew, T.Y. Tou and S. Sapru, J. Fiz. Mal. 6, 165 (1985).
8. K.H. Kwek, A.J. Smith, T.Y. Tou, A.V. Gholap and S. Lee, J. Fiz. Mal. 7, 125 (1986).
9. A.J. Smith, K.H. Kwek, T.Y. Tou, A.V. Gholap and S. Lee, IEEE J. Quantum Electron QE-23, 283 (1987).
10. S. Lee and Y.H. Chen, Spring College on Plasma Physics, ICTP, TRieste, Italy (1981). Published in Fusion Energy, IAEA-SMR-82, 296 (1981).
11. G. Decker, R. Deutsch, W. Kies and J. Rybach, Appl. Opt. 24, 823 (1985).
12. K.H. Kwek, S. Lee and T.Y. Tou, "Paper under preparation".

A Preionized Nitrogen Laser as a Diagnostic Light Source for Fast Pulsed Experiments

K. H. KWEK, T. Y. TOU, AND S. LEE

Abstract—**The design of an aluminum foil–Mylar preionized TEA nitrogen laser is described. The laser produces a high quality homogeneous beam that meets the stringent requirement of a Mach–Zehnder interferometer. The applicability of the optical diagnostic system is demonstrated for a rapidly changing plasma in the plasma focus discharge.**

I. Introduction

THE UNDERSTANDING of the processes involved in the production of high density plasmas, such as laser produced plasmas, pinch, and plasma focus experiments requires information on the concentration and space–time evolution of the electron density. Optical diagnostic techniques based on plasma refractivity are usually preferred in the determination of such quantities because the plasma conditions are not perturbed by the measurement itself. Such probing of the nanosecond time scale of the dynamic processes requires light sources of sufficiently short duration and high intensity. Towards this end, the nitrogen laser remains the best light source from the point of view of pulse duration, intensity, and wavelength. With the nitrogen laser, probing of the plasma with electron density up to a critical value of $\sim 10^{28}$ m^{-3} ($n_{\text{critical}} = 1.12 \times 10^{15}/\lambda^2$ m^{-3}) can be achieved.

The mechanism of the laser is such that the lifetime of the upper $C^3\pi_u$ level at about 40 ns is much shorter than that of the lower $B^3\pi_g$ level which is about 6 μs. An important consideration is that the pumping rate should be faster than the lifetime of the upper level, so that an inversion of the population can be attained before spontaneous emission decay. At higher pressure, the lifetime of the upper level becomes even shorter, and consequently it becomes harder to establish the inversion threshold. In nitrogen lasers, excitation at and above atmospheric pressures yield short duration light pulses from one nanosecond down to some tens of picoseconds [1]. Utilization of such pulses would thus provide short enough exposure times to "freeze" the motion of the current carrying plasma sheath of the plasma focus, for example, where the velocities are of the order of 10^7 cm/s. Good spatial resolution can thus be achieved.

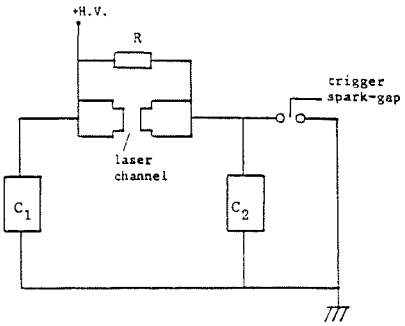

Fig. 1. Equivalent circuit of the nitrogen laser.

However, in the development of transversely excited atmospheric (TEA) nitrogen lasers one is often faced with the problem of obtaining a homogeneous discharge across the laser gap to achieve a high efficiency and good quality laser beam. Electrical breakdown of gases is usually characterized by the generalized parameters E/p and pd, where E is the applied field strength, p is the gas pressure, and d is the electrode separation. In transverse discharge geometrics, where the electrode separation is small compared to the length, increasing values of E/p and pd lead to the development of inhomogeneous discharge mode. The discharge in such instances breaks up into individual spark channels. Also, the method of producing the discharge by the sudden application of a strong electric field considerably in excess of the breakdown threshold across the laser gap requires a high voltage electrical pulse having a very fast rise time in order to avoid the formation of filamentary arcs within the discharge volume.

Efficient laser pumping in the presence of severe arcing is impossible due to the inadequate excitation rates in the regions of low current density and the too rapid thermal equilibrium rate in the regions of very high current density [2]. In addition, the resultant nonuniform distributions of refractive index within the inhomogeneously excited medium make the formation of high quality optical laser beams difficult.

In high pressure transverse gas discharges, to attain the required homogeneous glow discharge it is necessary to have an initial distribution of free electrons within the dis-

Manuscript received May 4, 1988. This paper was supported in part by the Third World Academy of Sciences under Grant TWAS-RG-87-84 and by the University of Malaya under Grant F95/77.

K. H. Kwek and S. Lee are with the Department of Physics, University of Malaya, Kuala Lumpur, Malaysia.

T. Y. Tou was with the University of Malaya, Kuala Lumpur, Malaysia. He is now with the Plasma Research Laboratory, Research School of Physical Sciences, the Australian National University, Canberra, Australia.

IEEE Log Number 8824671.

0018-9456/89/0200-0103$01.00 © 1989 IEEE

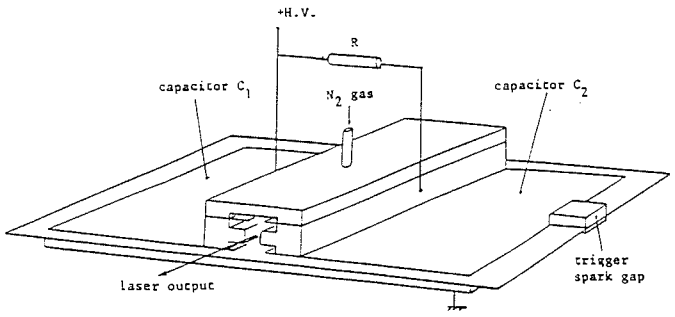

(a)

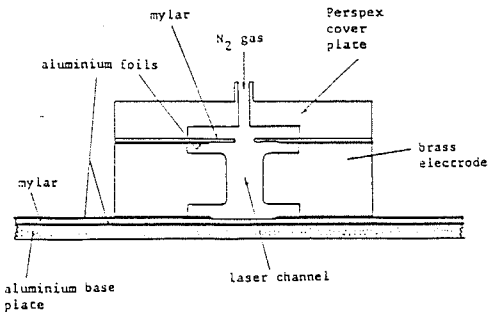

(b)

Fig. 2. (a) Sketch of a basic TEA nitrogen laser with Blumlein circuit. (b) Cross-sectional view of the laser channel showing the inclusion of the preionizer system using aluminium foil–Mylar combination. The mylar strips improve the preionization effect.

charge volume at the onset of the breakdown process. This initial distribution of free electrons, or preionization, can be provided by any suitable volume ionization source such as ultraviolet light, X-rays, γ rays, electron beams, corona discharge, etc. [3], [4].

This paper deals with a compact and easily constructed TEA nitrogen laser with preionization provided through low-energy surface corona discharges from a simple combination of aluminum foils and mylar sheets. It is then used as a light source for optical studies in a plasma.

II. The Nitrogen Laser

The laser is excited by the conventional Blumlein circuit schematically described in Fig. 1. The circuit theory of the parallel plate transmission line type of laser has been discussed in previous papers [5]–[7]. The two energy storage capacitors C_1 and C_2 of the circuit consist of a common earth plate, which is a 22 cm × 60 cm strip of aluminum kitchen foil laid on top of a flat aluminum plate (for electrical contact and mechanical support). Fig. 2 shows the constructional details of the laser. On top of the foil are laid 3 sheets of 2 mil Mylar which extends at least 10 cm beyond the edges of the conductors all round. The high voltage plates of C_1 and C_2 are 22 cm × 40 cm and 22 × 17 cm strips of aluminum foil laid on top of the mylar sheets. The measured values of C_1 and C_2 are 15 and 6 nF, respectively. On top of the foils are placed glass plates (6-mm thick) of appropriate dimensions to prevent mechanical flexing of the foils during charging and discharging of the capacitors. The capacitor C_2 is mounted to a swinging cascade triggered spark gap. These high voltage capacitor plates are separated by a gap over which the laser channel is placed so that each side of the channel makes pressure contract with one of the capacitors. The electrodes of the laser channel are made of 20-cm long brass strips with cross-sectional dimensions of 0.5 in × 1 in and shaped as shown in Fig. 2(b). The perspex plate is screwed onto the laser electrodes on the upper side over the top. Admission and evacuation of the nitrogen gas at atmospheric pressure is made through the middle and the ends of the channel, respectively.

In the arrangement shown, the edges of the high voltage capacitor plates (aluminum foils) are allowed to protrude beyond the edges of the laser electrodes into the laser cavity to act as corona blades for preionization. These form the set of blades on the lower side of the laser channel. A similar set of corona blades is placed on the upper side of the laser channel. The laser channel gap is set to 3 mm

while the blades separation is typically set to about 40 percent greater than that of the main gap. The edges of the foils function as auxiliary corona electrodes which provide an initial distributed corona discharge to photoionize and prepare the laser channel for glow formation. The low-energy surface discharges acting as preionizing UV radiation sources are formed early during the rise of the voltage pulse across the laser gap and are distributed by corona charging of the Mylar surfaces that extend beyond the edges of the foils. Preionization from the surface discharges is not as effective in the absence of the Mylar sheets.

III. Measurements and Performance

In the absence of the preionizers, the appearance of the discharge along the main laser gap is that of a glow discharge with the presence of strong streamer-like filaments. These streamers prevail with increasing laser gap and are randomly placed, from pulse to pulse, along the channel. Electrical arcs may be formed due to surface defects created during electrical discharge. The presence of the streamers and arcs can be attributed to the insufficiently fast voltage ramp created across the laser electrodes at such high pressure. The presence of electrical arcs reduces the laser output energy. An interelectrode distance of 3 mm gives optimum laser energy output of about 100 μJ at a charging voltage of 15 kV. The laser pulse duration was measured with a fast FND-100 photodiode and a storage oscilloscope (Tektronix 7834) giving a pulsewidth of 2 ns at half-maximum. However, we believe that the duration is ~ 1 ns, taking into account of the time resolution of the measuring system. The presence of the streamers and arcs disturbs the homogeneity of the laser beam. The nonuniformity of the laser beam becomes apparent when the laser is used in optical setups where the requirements are stringent.

With the presence of the preionizers, the discharge takes the appearance of a bluish glow. The streamers and arcs are absent. Optimum energy is still obtained at a gap separation of 3 mm but with an improved value of 300 μJ at 15 kV. The laser pulse duration remains the same. The laser beam quality is greatly improved.

IV. Application to a Plasma Experiment

In order to demonstrate the utility of the laser it is coupled to an optical set up to observe the macroscopic behavior of the high density plasma which is formed in a dense plasma focus. The device is of the Mather type with filling pressures of 1–10 torr deuterium, energized by a 7–12 kJ capacitor bank charged to 15–20 kV [8]. The velocities of the current sheath ranges from 10^7 cm/s to 3×10^7 cm/s. The characteristic dimension of the plasma is of the order of 1 mm, and the electron density is of the order of 10^{25} m^{-3}.

The optical set up as shown in Fig. 3 is basically a Mach–Zehnder interferometer and is sufficiently flexible to be used for Schlieren and shadow photograph techniques. $BS1$ and $BS2$ are beam splitters while $M1$ and $M2$ are full mirrors. The fringes are localized in the plasma position and are imaged onto the film plane by lens L. The pinhole, located at the focal plane of L, together with a narrow bandwidth interference filter suppresses the intense plasma radiation. Polaroid type 667 film was used. Schlieren and shadow photography can be employed by covering the reference beam and setting up the appropriate locations of the focusing lenses.

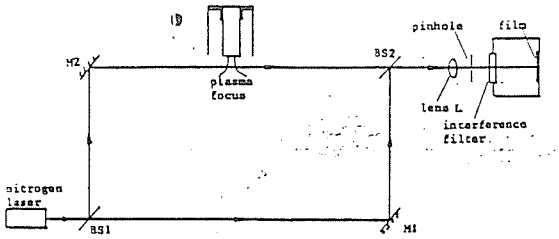

Fig. 3. Schematic set up of the Mach–Zehnder interferometry. Schlieren and shadowgraphic setup can be obtained by covering the reference beam and setting up the appropriate focusing optics.

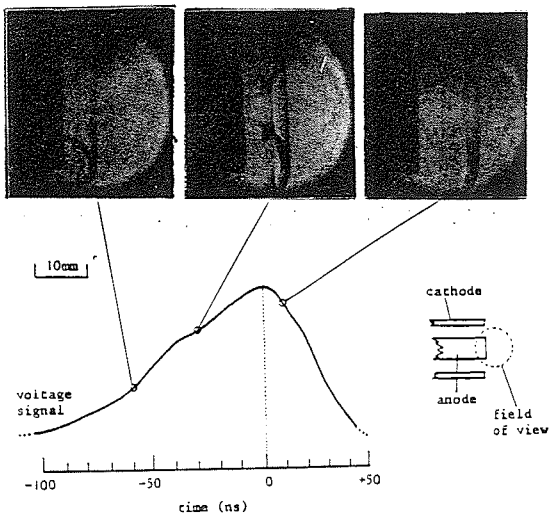

Fig. 4. Examples of shadowgrams obtained on plasma focus discharges with discharge voltage of 15 kV and working gas at 8-mbar deuterium. Time zero is based on the characteristic peak of the voltage signal.

Using a time delay generator, the laser is synchronized with the discharge so that, by changing the delay in successive shots, the temporal behavior of the plasma electron density profile can be studied. The synchronization is checked by superimposing the output of a photodiode which picked up part of the laser light, on the voltage trace. Time is referenced to the peak of the voltage signal.

Fig. 4 shows a sequence of shadowgrams depicting the temporal development of the plasma focus discharge from the collapse phase to the disruption of the plasma column and the formation of the ionizing wavefront. Fig. 5 shows a Schlieren photograph of a plasma focus column being disrupted by $m = 0$ instabilities.

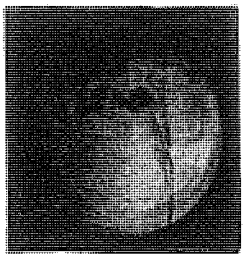

Fig. 5. Example of a Schlieren photograph taken on a plasma focus discharge showing the plasma column being disrupted by instabilities.

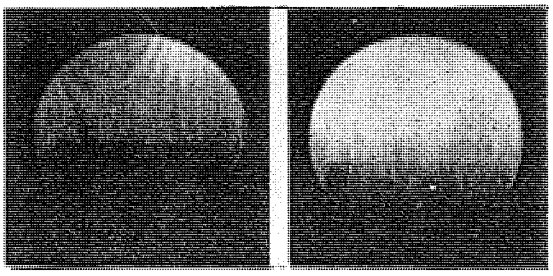

(a) (b)

Fig. 6. Examples of the poor quality interferogram obtained. (a) Interferogram with coarse fringe pattern. (b) Interferogram with fringe pattern. In both interferograms the fringes are barely discernible.

The above shadow and Schlieren photographs were taken using the laser without the preionizers. When the laser was used with the Mach–Zehnder interferometer setup, the interferograms (vacuum interferograms with fringe pattern obtained by tilting one of the mirrors) obtained were of poor quality as is shown in Fig. 6. The fringes are barely discernible due to the presence of vertical striations. These poor quality interferograms resulted from the use of poor quality laser beams which are inhomogeneous and not uniform in intensity. Such inhomogeneity and nonuniformity in the beam becomes conspicuous upon expanding the beam several times its original size. Thus while the laser can be employed in Schlieren and shadow photography to provide useful information of the plasma, albeit the quality is not very good, it was rendered useless in interferometry work by poor beam quality.

With the presence of the preionizers, the uniform glow discharge along the laser channel produced a uniform and homogeneous beam that enabled interferograms (shown in Fig. 7) to be obtained. In another experiment, the improved laser was used to take Schlieren photographs of the plasma focus. The results shown in Fig. 8 clearly indicate improved Schlieren photographs. The quality of the Schlieren pictures are sufficiently good to enable quantitative information such as the electron density and density gradient to be extracted when supplemented with the use of computer simulation as was done by Decker *et al.* [9].

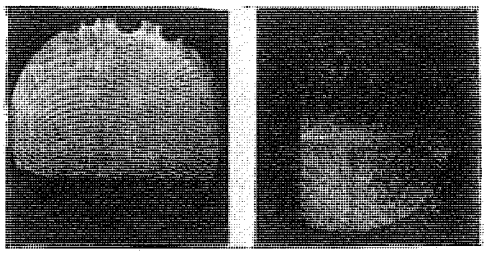

(a) (b)

Fig. 7. Examples of the interferograms obtained with improved laser using preionizers. Interferogram (a) is a background fringe pattern. The fringes are clearly seen. Interferogram (b) is taken on a plasma focus discharge showing the fringe shifts due to the presence of the plasma.

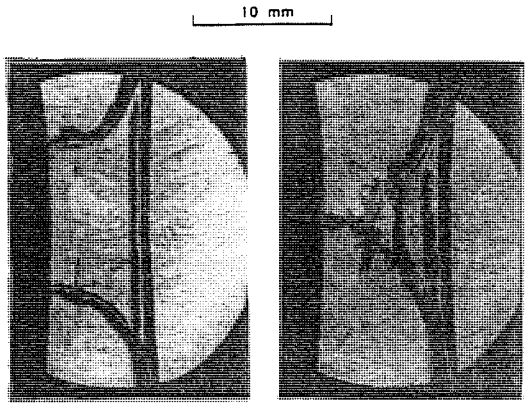

Fig. 8. Examples of Schlieren photographs obtained using the improved laser using preionizers.

V. Conclusions and Discussions

The TEA nitrogen laser with the use of preionizers as described provides a powerful laser light source with good beam quality for optical diagnostics of transient and dense plasmas. The combination of the thin aluminum foils and mylar sheets provides an extremely simple but effective preionization scheme. This combined with properly shaped electrodes leads to the production of short duration, high energy and good quality laser pulses from transverse discharges at atmospheric pressure. The preionizers, by providing enough initial electron density to produce a good main discharge, relaxes the constraint on the fast voltage rise that is needed. The scheme should also prove useful for discharges at above atmospheric pressures. It should be mentioned that we have not needed to replace the preionizers in our laser although they have been in regular use for several months. In any case, replacement of the preionizers would be a relatively simple procedure. An important consideration is that the laser and the preionizers can be constructed at modest expense and yet be a useful tool for optical diagnostics of transient and dense plasmas.

REFERENCES

[1] H. Strohwald and H. Salzmann, "Picosecond uv laser pulses from gas discharges in pure nitrogen at pressures up to 6 atm.," *Appl. Phys. Lett.*, vol. 28, pp. 272–274, 1972.

[2] J. I. Levatter and S. C. Lin, "Necessary conditions for the homogeneous formation of pulsed avalanche discharges at high gas pressures," *J. Appl. Phys.*, vol. 51, pp. 210–222, 1980.

[3] G. Herziger, R. Wollermann-Windgasse, and K. H. Banse, "On the homogeneization of transverse gas discharges by preionization," *Appl. Phys.*, vol. 24, pp. 267–272, 1981.

[4] V. Hasson and H. M. von Bergmann, "Spatial control of pulsed high pressure preionization stabilized glow discharges," *J. Phys. E: Sci. Instrum.*, vol. 13, pp. 632–638, 1980.

[5] S. Lee, A. V. Gholap, A. J. Smith, K. H. Kwek, A. C. Chew, T. Y. Tou, and S. Sapru, "Parametric study of the nitrogen laser circuit," *J. Fiz. Mal.*, vol. 6, pp. 165–174, 1985.

[6] K. H. Kwek, A. J. Smith, T. Y. Tou, A. V. Gholap, and S. Lee, "Determining nitrogen laser channel parameters," *J. Fiz. Mal.*, vol. 7, pp. 125–127, 1986.

[7] A. J. Smith, K. H. Kwek, T. Y. Tou, A. V. Gholap, and S. Lee, "Measurement of the nitrogen laser channel current, inductance and resistance," *IEEE J. Quantum Electron.*, vol. QE-23, pp. 283–286, 1987.

[8] S. Lee and Y. H. Chen, "Geometric optimization of the dense plasma focus," in *Fusion Energy-1981*, ICTP, Trieste, pp. 297–303, 1981.

[9] G. Decker, R. Deutsch, W. Kies, and J. Rybach, "Computer simulated schlieren Optics," *Appl. Opt.*, vol. 24, pp. 823–828, 1985.

Multislit streak photography for plasma dynamics studies

T. Y. Tou[a] and S. Lee

Physics Department, University of Malaya, 59100 Kuala Lumpur, Malaysia

(Received 21 September 1987; accepted for publication 24 July 1988)

A microscope slide with several transparent slits installed in a streak camera is used to record time-resolved two-dimensional information when a curved luminous plasma sheath traverses these slits. Applying this method to the plasma focus experiment, the axial run-down trajectory and the shapes of the plasma sheath at various moments can be obtained from a single streak photograph.

INTRODUCTION

Streak cameras have been widely used to study pinch dynamics in plasma focus and various types of classical pinch devices. These were done by placing a narrow slit perpendicular to the pinch axis so that the radial collapse of the luminous plasma sheath was recorded as a function of time. When the slit was placed parallel to the z axis of such devices as the shock tube,[1-8] coaxial plasma accelerator,[9] and the plasma focus,[10] the transit of the luminous shock wave[1-8] and the plasma sheath[9,10] in the axial run-down region was correspondingly recorded as a function of time. A distance–time diagram was thus obtained whose slope often could only be related to an average run-down velocity in the annuli of these devices.

Another common technique[6,11,12] for obtaining a distance–time diagram in shock tube was to position an array of light detectors along the tube, and the output pulses from these light detectors were recorded on oscilloscope for timing purposes.

It is well known that the run-down velocities in these devices are nonconstant particularly during the early axial run-down phase. Furthermore, the shock wave and plasma sheath are known to exhibit nonplanar radial structures. We note that with these two techniques, the details of both the run-down velocities and the radial structures could not easily be revealed. In this article, we report a technique where multiple slits are used to obtain the axial run-down trajectory or the distance–time diagram of the plasma sheath in the annulus of a plasma focus. This effectively allows a run-down velocity profile of the plasma sheath to be obtained from a single streak photograph. By introducing a slight variation to the experimental setup, we are able to obtain qualitatively the curvature of the plasma sheath at different moments of the axial run-down phase.

Streak speed of the camera requires frequent adjustment depending on the operating conditions of the plasma focus. We have devised an *in situ* calibration method. This required minimum variation to the experimental setup for the multislit technique.

In Sec. I, we describe the experimental setup for the multislit technique in a plasma focus. The experimental observations, analysis, and results obtained on the run-down velocities of the plasma sheath will be presented in Sec. II A, and the shapes of the plasma sheath at three different times will be presented in Sec. II B. Finally, the *in situ* calibration method for the streak camera will be presented in Sec. III.

I. EXPERIMENT

The experimental setup is shown schematically in Fig. 1. A streak camera (John Hadland Co.) with type S-11 photocathode tube is focused through an array of five slits (which are housed at the primary real image plane of the streak camera) at the vertical object plane along the z axis of a Mather-type[13] plasma focus. The array of slits is constructed with strips of aluminized Mylar sheet glued with adjustable gaps in between, onto a microscope slide. The gap or slit between any two strips of aluminized Mylar sheets is controlled by placing between them a metallic foil or a wire of known thickness. The average slit width is about 0.1 mm, but since the object image shows five times demagnification, the effective slit width is taken as 0.5 mm. For plasma sheath thicknesses of 5–10 mm, this effective slit width could still provide sufficient spatial resolution.

The experiment begins with the determination of the slit positions at the z axis of the plasma focus tube in the laboratory reference frame. For this, a diffused light source is used to illuminate the plasma focus tube from the far side and a snapshot, with the streak camera in focus mode, is taken of the annulus of the plasma focus tube. This is followed by another snapshot with the microscope slide containing the slits installed at the primary real image plane inside the streak camera. Images from the two snapshots are then superimposed on the same film (Polaroid, ASA3000). Fig-

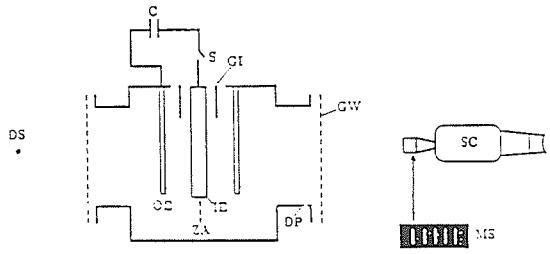

FIG. 1. Schematic of the experimental setup. SC: streak camera, MS: microscope slide containing an array of five slits, ZA: z axis of the plasma focus tube, IE: inner electrode, OE: outer electrode, GI: glass insulator, DP: diagnostic port, GW: glass window, DS: diffused light source, C: capacitor bank and S: switch. Note that the microscope slide is housed inside the streak camera.

 0034-6748/88/112370-05$01.30

ure 2(a) shows the photograph which contains the images of the inner electrode of the plasma focus and the slits, shown here as the luminous vertical lines. This photo is enlarged to facilitate the determination of the slit positions, found to be $z_n \simeq 5.1, 7.9, 10.1, 12.6, 15.3$ cm where the subscript n indicates the nth slit. The point $z = 0$ is fixed at the back wall of the plasma focus tube [see Fig. 2(a)]. Measurement errors incurred in the z values are mainly due to the uncertainties in the image-enlargement factor, the measurement of the slit distance from the end of the inner electrode and, least important, the finite slit width. An average value of $\Delta z \lesssim \pm 0.1$ cm is estimated for each of the slits.

Figure 2(b) illustrates the propagation of the plasma sheath in the annulus of the plasma focus tube and the imaging system. Owing to its parabolic curvature, the part of the plasma sheath adjacent to the inner electrode arrives first at the slit positions. As the plasma sheath traverses the slit position(s) it illuminates the slit(s) on the microscope slide like two simultaneous point sources moving radially away from either side of the inner electrode. The approximate size of these light sources is about 0.1 mm (the slit width) by 1–2 mm corresponding to the width of plasma sheath demagnified five times. The temporal changes in the r positions of these two light sources are imaged on the film; this results in two simultaneous lines of luminosity originating from either side of the inner electrode.

The streak camera is delay-triggered with respect to the plasma focus discharge so that the timing between these two events can be correlated. The oscillogram in Fig. 3(b) shows

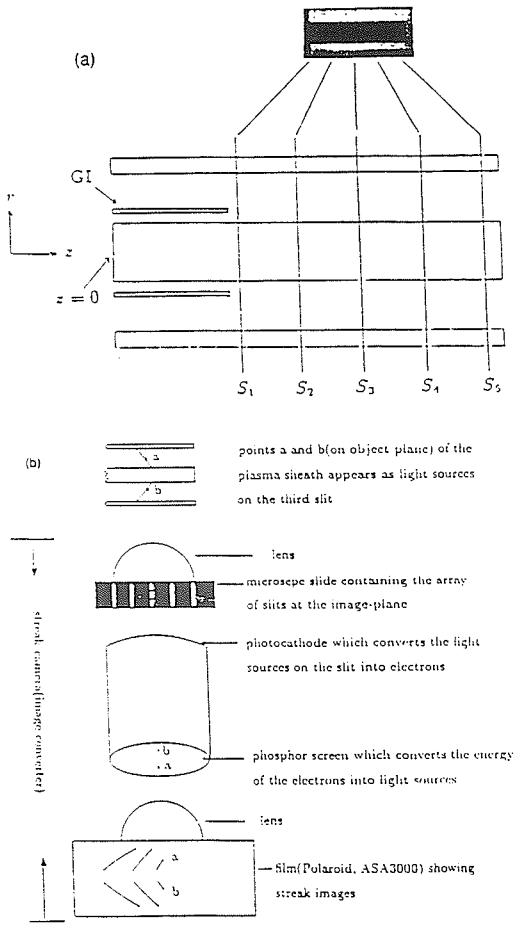

FIG. 2. (a) Photograph showing the superimposed images of the inner electrode (dark) and the slits (luminous vertical lines). GI: glass insulator. (b) Schematic of the multislit imaging system employing a streak camera.

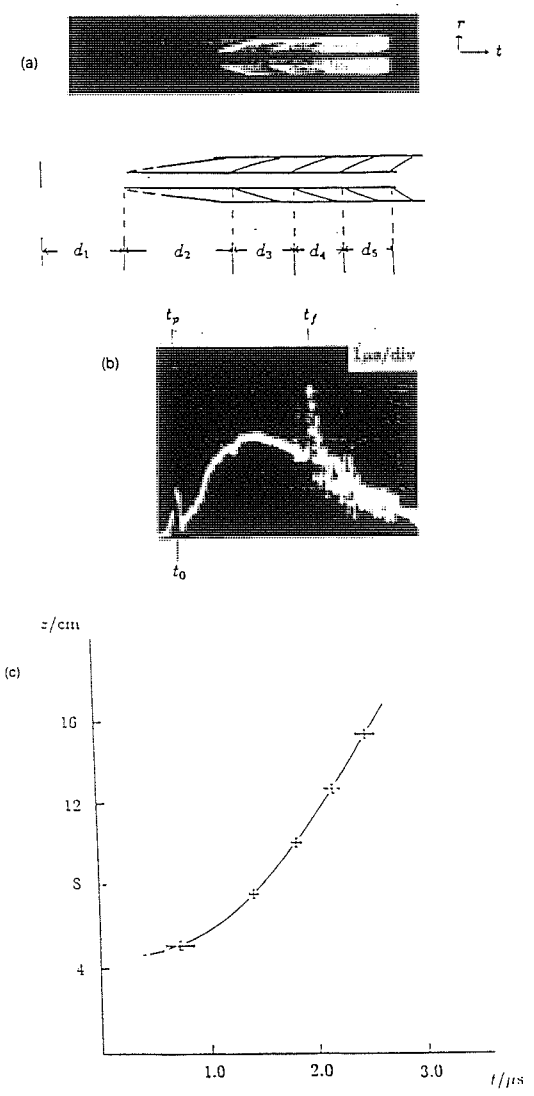

FIG. 3. (a) Multiple streak images for a deuterium plasma focus discharge at 10 mbar and 14 kV. (b) A sharp pulse at time t_p indicates the start of the imaging process in the streak camera. The microsecond voltage signal shows the commencing of the plasma focus discharge at the t_0 and the maximum radial compression at time t_f. (c) The axial run-down trajectory (z–t plot) of that part of the plasma sheath adjacent to the inner electrode.

two electrical signals, a sharp output pulse from the streak camera at time t_p indicates the start of the imaging process; and the microsecond pulse is the voltage signal of a plasma focus discharge. At time t_0, a negative slope in the plasma-focus voltage signal suggests the initial high-voltage breakdown at the glass insulator (see Fig. 1). The plasma focus was operated at 10 mbar of D_2 filling pressure and 14 kV of capacitor-charging voltage.

A characteristic pinch-voltage spike is always observed at time t_f, in the plasma-focus voltage signal, which is generated primarily because of the large inductance change of the current-carrying plasma sheath during the radial collapse phase [see Fig. 4(a), the radially converging streak image rc]. Thus, the peak of this pinch-voltage spike may be taken to correspond to the maximum compression of the plasma column [indicated by point *mc* in Fig. 4(a)]. This assumption allows us to utilize the time t_f as a time reference in Sec. II B.

II. ANALYSIS AND RESULTS

A. Axial run-down trajectory

Any point along the line of luminosity in Fig. 3(a) is given by a coordinate $P_n(r,z)$ where r and z define its radial and axial positions, respectively, and the subscript n indicates that image recorded by the nth slit. In order to simplify the analysis, we shall describe only the axial run-down of that part of the plasma sheath that is adjacent to the inner electrode. For this, the value of r is always 1.25 cm, the radius of the inner electrode. The value of z is fixed by the position of each of the slits which are presented in the previous section. The arrival time t_n of the plasma sheath at slit S_n is given by

$$t_n = t_d + \sum_{i=1}^{n} d_i/u_s, \quad n \leqslant 5, \tag{1}$$

where t_d is the temporal delay between the streak-camera operation and the initial high voltage breakdown in the plasma focus tube. The term u_s is the streak speed and d_i is the streak span between $(i-1)$th and ith streak images, as are shown in Fig. 3(a).

The value of t_d is determined using the add mode for oscilloscope display of the streak-triggering pulse and the voltage waveform of the plasma focus discharge, as shown in Fig. 3(b). For this case, $t_d = 0$ and from Eq. (1) the arrival times $t_n \simeq 0.70, 1.42, 1.80, 2.16, 2.48\,\mu s$ are calculated for the plasma sheath arriving at $z_n \simeq 5.1, 7.7, 10.1, 12.7, 15.3$ cm, respectively.

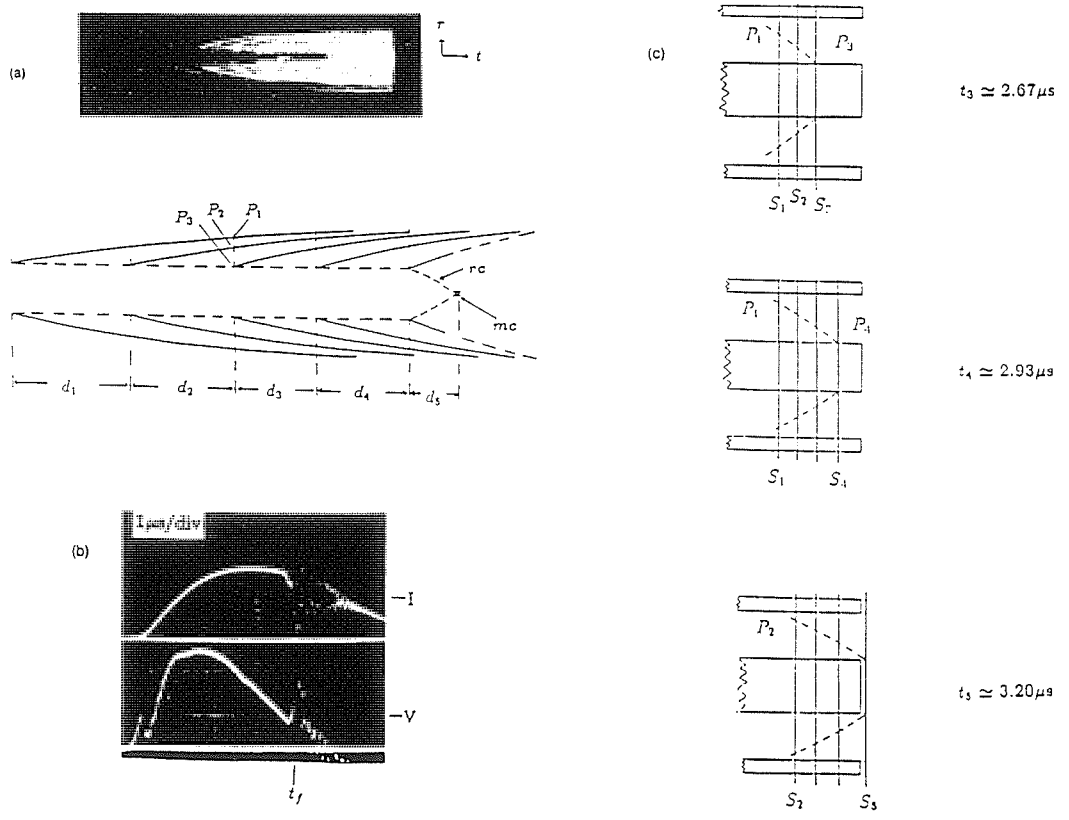

FIG. 4. (a) Multiple streak images of the argon plasma sheath which are obtained at a nearer distance from the plasma focus tube. The sketched streak images are about 2.58 times larger. (b) Current (I) and voltage (V) signals of the argon plasma focus discharge. The time t_f is used as a time reference [(Eq. (2)]. (c) Shapes of the argon plasma sheath at times t_3, t_4, and t_5, respectively (data from Table I).

Figure 3(c) shows the axial run-down trajectory of that part of the plasma sheath that is adjacent to the inner electrode. The horizontal error bars represent the uncertainties in the calculated arrival times t_n. From this figure, instantaneous plasma sheath velocities can be measured. Approaching the end of the inner electrode, the velocity is maintained at about 10 cm/μs. This observation substantiates other reports[14,15] of an upper limit for the plasma sheath velocity. Since the plasma sheath velocity attains a constant value, the rate of change of inductance becomes constant and, therefore, a steady-state plasma sheath may be defined for this part of the run-down phase.

B. Shape of the plasma sheath

In this experiment, the streak camera is moved nearer to the plasma focus tube in order to obtain a better magnification. A different array of five slits are used and they appear at $z_n \simeq 12.0$, 12.8, 13.6, 14.6, 16.3 cm. The fifth slit is about 3 mm off the end of the inner electrode; this slit images both the axial run-down and the radial collapse of the plasma sheath. Figure 4(a) shows such a photograph for argon discharge at 3 mbar and 14 kV.

The arrival time t_n at the nth slit is calculated with a different equation:

$$t_n = t_f - \sum_{i=n}^{5} d_i/u_i, \quad n \leq 5, \tag{2}$$

where t_f is the time when the peak of the characteristic pinch-voltage spike [see Fig. 4(b)] occurs. Since the time t_f is used as the time reference, the streak-triggering pulse need not be displayed. This would, however, be necessary if the fifth or last slit is placed before the end of the inner electrode, and for this, Eq. (1) would have to be used. From Eq. (2), times of arrival are, respectively,

$$t_n \simeq (1.94, 2.33, 2.67, 2.93, 3.20)\,\mu\text{s}.$$

Figure 4(a) also shows a careful sketch of the streak images from which we obtain some coordinates for various streak images, recorded simultaneously by different slits at the following times $t_3 \simeq 2.67\,\mu$s, $t_4 \simeq 2.93\,\mu$s, and $t_5 \simeq 3.20\,\mu$s (see Table I). When the above sets of points are plotted onto a cylindrical coordinate system, the shapes of the plasma sheath are obtained at various moments of the run-down, as shown in Fig. 4(c). The shapes of the plasma sheath in these three figures are in close resemblance to each other, while the velocity attains an upper-limit value. These observations may further strengthen the suggestion, in the previous section, of a steady-state plasma sheath approaching the end of the plasma-focus annulus.

III. *IN SITU* CALIBRATION

For the above types of experiments, the streak speed is often adjusted such that the five images are recorded within the entire streak span. Following each adjustment of the streak speed, calibration is necessary. This is done by using a slit to record the radial collapse of the plasma sheath and simultaneously displaying, on the add mode of the oscilloscope, the streak-triggering pulse, and the voltage waveform of the plasma focus discharge. Figure 5(a) shows the length

TABLE I. Coordinates representing the r and z positions of the plasma sheath, recorded simultaneously by different slits at times t_3, t_4, and t_5, respectively.

Time	$P_n(r,z)$	Recorded by
	$P_1(2.90,12.0)$	S_1
$t_3 \simeq 3.20\,\mu$s	$P_2(2.70,12.8)$	S_2
	$P_3(1.25,13.6)$	S_3
	$P_1(3.05,12.0)$	S_1
$t_4 \simeq 2.93\,\mu$s	$P_2(2.80,12.8)$	S_2
	$P_3(2.15,13.6)$	S_3
	$P_4(1.25,14.6)$	S_4
	$P_2(3.15,12.8)$	S_2
$t_5 \simeq 2.67\,\mu$s	$P_3(2.80,13.6)$	S_3
	$P_4(2.40,14.6)$	S_4
	$P_5(1.25,15.3)$	S_5

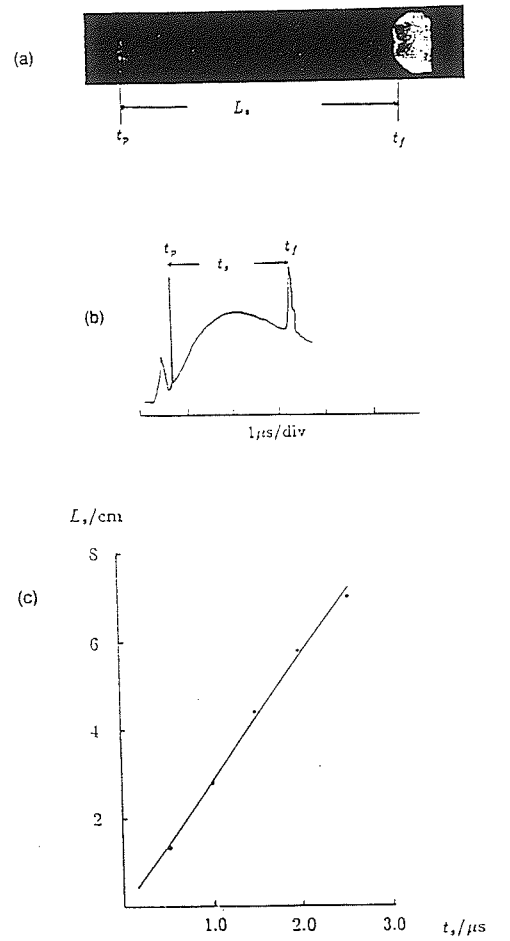

FIG. 5. (a) L_s is the null streak span between the start of the imaging process and the recording of the maximum radial compression of the plasma column. (b) The time t_s between the streak-camera pulse and the peak of the characteristic pinch-voltage spike corresponds to the null streak span L_s [Fig. 5(a)]. (c) The gradient of the plot of L_s vs t_s is the calibrated streak speed.

of a null streak span L_s before the maximum compression of the plasma column is recorded. This value L_s corresponds to the time t_s between the streak-triggering pulse, and the peak of the characteristic voltage spike, as shown in Fig. 5(b). With different time delays to the streak camera, different values of L_s and their corresponding t_s 's are obtained. A plot of L_s vs t_s, as shown in Fig. 5(c), gives the gradient, which is the streak speed $u_s \simeq 2.7$ cm/μs for the above-mentioned experiments.

[a] Present address: Plasma Research Laboratory, R. S. Phys. S., A.N.U., Canberra, Australia.

[1]E. A. McLean, C. E. Faneuff, A. C. Kolb, and H. R. Griem, Phys. Fluids 3, 843 (1960).
[2]R. G. Fowler, Phys. Fluids 4, 544 (1961).
[3]C. T. Chang, Phys. Fluids 4, 1085 (1961).
[4]Philip J. Hart, Phys. Fluids 5, 38 (1962).
[5]M. Cloupeau, Phys. Fluids 6, 679 (1963).
[6]L. S. Levine, Phys. Fluids 11, 1479 (1968).
[7]S. P. Gill, Phys. Fluids Suppl., I88 (1969).
[8]S. Ludvik and H. K. Messerle, in Proceedings of the Seventh International Shock Tube Symposium, edited by I. I. Glass, Toronto, Canada, 1969, p. 207.
[9]Y. H. Chen, M.Sc. thesis, University of Malaya, Malaysia, 1972.
[10]A. C. Chew, M.Sc. thesis, University of Malaya, Malaysia, 1974.
[11]J. Keck, Phys. Fluids 5, 631 (1962).
[12]L. S. Levine, Phys. Fluids 11, 208 (1970).
[13]J. W. Mather, in *Methods of Experimental Physics* (Academic, New York, 1971), Vol. 9, Pt. B, p. 187.
[14]J. Keck, Phys. Fluids 7, S16 (1964).
[15]D. E. Potter, Phys. Fluids 14, 1911 (1971).

Laser and Particle Beams (1988), *vol.* 6, *part* 3, *pp.* 597–606
Printed in Northern Ireland

Density ratios in compressions driven by radiation pressure

By S. LEE†
The Flinders University of South Australia, School of Physical Sciences, Bedford Park, S.A. 5042, Australia

(Received 18 May 1987 and in revised form 31 September 1987)

It has been recently suggested (Hora & Miley 1984) that in the cannonball scheme of laser compression the pellet may be considered to be compressed by the 'brute force' of the radiation pressure. For such a radiation-driven compression, this paper applies an energy balance method to give an equation fixing the radius compression ratio κ which is a key parameter for such intense compressions. A shock model is used to yield specific results. For a square-pulse driving power compressing a spherical pellet with a specific heat ratio of 5/3, a density compression ratio Γ of 27 is computed. Double (stepped) pulsing with linearly rising power enhances Γ to 1750. The value of Γ is not dependent on the absolute magnitude of the piston power, as long as this is large enough. Further enhancement of compression by multiple (stepped) pulsing becomes obvious. The enhanced compression increases the energy gain factor G for a 100 μm DT pellet driven by radiation power of 10^{16} W from 6 for a square pulse power with 0·5 MJ absorbed energy to 90 for a double (stepped) linearly rising pulse with absorbed energy of 0·4 MJ assuming perfect coupling efficiency.

1. Introduction

Some basic concepts of laser target compression have recently been reviewed by H. Hora and G. H. Miley (1984). Amongst these are the adiabatic self-similarity compression, ablative compression with central ignition, nonlinear force pushing and the cannonball concepts. In the review it is stressed that the cannonball target concept proposed by Yabe *et al.* (1975) is one of the most promising approaches to overcome the difficulties faced by the other concepts. The adiabatic self-similarity compression using carefully shaped laser pulses (Kidder 1974; Brueckner & Jorna 1974) is a theoretical reference case unlikely to be realized experimentally. The ablative compression with central ignition is very sensitive to interaction problems, preheat and asymmetries whilst the nonlinear force pushing concept requires ultrahigh intensities. The cannonball scheme overcomes these difficulties and though facing its own technical difficulty of expensive and complicated target construction, has already undergone initial experiments with good success using medium-power lasers (Miyanaga *et al.* 1983; Yamanaka 1985).

In the cannonball concept the empty space or hohlraum between a spherical hollow high-Z mantle and a smaller concentric spherical inner fuel core target pellet is filled with a uniform distribution of laser radiation. According to Hora and Miley (1984) this monochromatic hohlraum radiation compresses the pellet by the 'brute force' of the radiation pressure so that if the radiation pressure is sufficiently large for the compressional velocity to be supersonic then the pellet will be compressed through a snowplow process.

† Permanent address: Physics Department, University of Malaya, 59100 Kuala Lumpur, Malaysia.

0263-0364/88/0003–0597$05.00

For this type of piston-like drive, the application of energy and pressure principles is alone sufficient to determine the gross compression ratio which is one of the key parameters characterizing the end-state of any intense compressional process. This follows from earlier work in which S. Lee (1983) applies energy and pressure balance to a fast magnetic pinch-type compression to compute the pinch radius ratio and shows that the compressed radius ratio does not depend on the absolute magnitude of the compressing magnetic field. It was shown that in practical cases the large density compression ratios required to satisfy the concept of a fast pinch reactor (Haines 1982) cannot be achieved in a single magnetic compression. To enhance the density ratio a current-stepping technique which essentially uses a two-step compression has been suggested (Lee 1984) as a possible prelude to further enhancement due to radiation cooling.

In laser-driven compressions for fusion purposes, the energy gain G for a 50:50 DT plasma at an optimized temperature of 10·3 keV may be expressed (Hora & Miley 1984) as

$$G = \left(\frac{E}{E_{BE}}\right)^{\frac{1}{3}} \Gamma^{\frac{2}{3}} \tag{1}$$

where $\Gamma = \rho_m/\rho_0$ is the ratio of compressed density to the initial solid state DT density ρ_0 and $E_{BE} = 1{\cdot}6$ MJ with E being the energy absorbed by the pellet from the laser pulse. This formula may also be written as

$$G = \left(\frac{E}{E_{BE}}\right)^{\frac{1}{3}} \kappa_m^{-2} \tag{2}$$

where $\kappa_m = r_m/r_0$ is the radius ratio of the compression.

Because of the dependence of G on $\Gamma^{\frac{2}{3}}$ or equivalently on κ_m^{-2} it is important to be able to compute κ_m in a simple physical way. It is of further importance if the method suggests a reduction in κ_m equivalent to an enhancement of Γ.

In this paper the concept of limiting density ratios for radiation-driven compressions is examined in a simplified general manner. Structural considerations are not central. For example, the use of a shock model is only to obtain specific results and should not distract from the cental theme of energy balance. The application of this principle shows immediately that the compression ratio is not dependent on the absolute magnitude of the piston power but rather on the pulse shape. Limiting compression ratios are obtained for some simple piston power pulse shapes. A double pulse (or pulse-stepping) technique is then suggested and the enhanced compression ratios are computed. Using this method, the basic physics is clearly seen though the problem is obviously idealized. The required pulse shapes are readily specified and techniques for further enhancement, for example, by multiple pulsing becomes self-evident. The effect of compression enhancement on the energy gain factor G is also computed for several specific cases.

2. Theory

2.1. *Shock wave picture*

Consider a solid spherical pellet irradiated uniformly by intense radiation as illustrated in figure 1. The radiation power R (J s^{-1}) has associated with it radiation intensity $I = R/(4\pi r^2)$ (J s^{-1} m^{-2}) and radiation pressure $P_R = I/c = 3{\cdot}3 \times 10^{-9} R/(4\pi r^2)$ (N m^{-2}) where c is the speed of light.

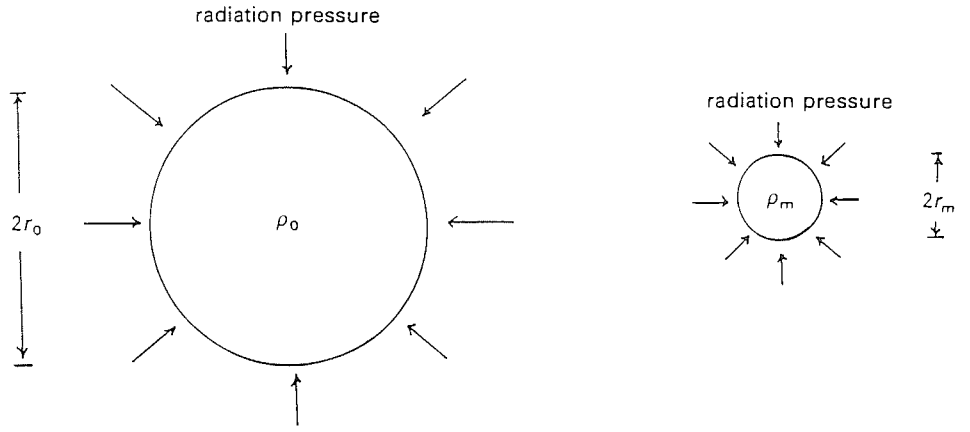

FIGURE 1. Idealized representation of spherical compression of pellet by radiation piston.

Assume that the radiation pressure is fully effective on the surface of the pellet and continues to be fully coupled for the period of the radiation pulse. The radiation pressure will then press on the surface of the pellet like a spherical piston and will maintain this piston-like behaviour as the pellet undergoes compression. This assumption is consistent with the estimation of *limiting* compression ratios as any deviation from piston behaviour of the radiation-pellet front (for example the pellet surface becoming transparent to the radiation) will result in a lesser value of the gross compression. Assume that the radiation pressure is sufficient to cause the radiation piston to implode supersonically (but non-relativistically). Then a shock front will propagate ahead of the piston; the shock front being the transition region between ambient pellet condition and piston compressed condition. The situation is shown in figure 2a where both the imploding piston and the converging (forward) shock front are moving inwards.

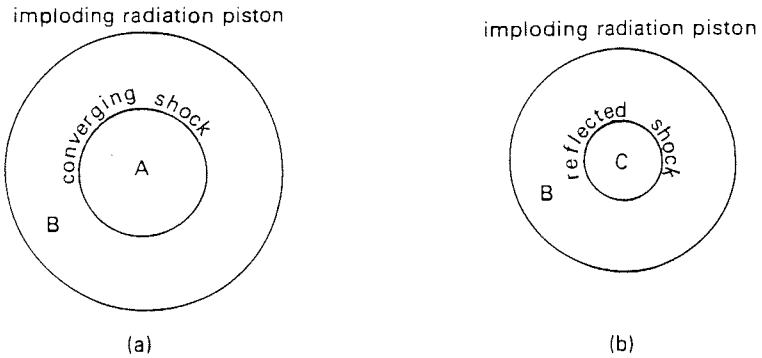

FIGURE 2. (a) Imploding radiation piston driving a converging (forward) shock, before the forward shock has hit the centre. Region A = ambient pellet condition, region B = piston compressed (singly shocked) conditon. (b) Imploding radiation piston driving a diverging (reflected) shock, after the forward shock has hit the centre. Region B = singly shocked region, region C = doubly shocked region.

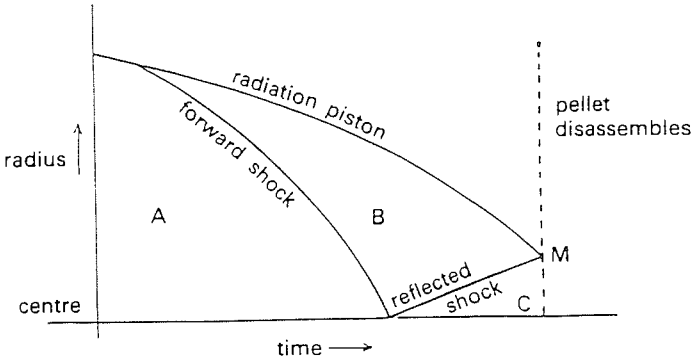

FIGURE 3. Trajectory of pellet compression showing regions A, B and C of figure 2.

For a shock front converging into the ambient material, the conservation equations across the front require that the shocked plasma behind it also be moving radially inwards. This requires that when the forward shock has converged onto the centre a reflected radially diverging shock front must propagate, behind which the doubly shocked plasma is, on the average across the central sphere stationary.

One property of the imploding piston is that it is subsonic relative to the plasma heated and compressed by the forward shock driven by the piston. Thus it is a reasonable assumption that the pressure in the region between the converging shock front and the piston (labelled region B in figure 2a) is uniform and is equal to the piston pressure. This is also true of the region between the piston and the reflected shock, also labelled region B in figure 2b. The reflected shock region (labelled region C in figure 2b) is a region of both increased density and temperature relative to region B. Hence region C has a higher pressure than region B. We assign a factor f_{rs} to denote the pressure-jump factor across the reflected shock. Thus when the reflected shock hits the radiation piston, the double-shocked inner sphere, whose particles have been constrained to be stationary due to the continuous influx of particles from region B, but are now no longer so constrained, disassembles. The situation is as shown in figure 3. In this figure the point M shows the configuration as the reflected shock hits the radiation piston. It is the point of minimum radius corresponding to maximum compression and the point when, according to this model, pellet disassembly starts.

2.2. *Energy and pressure equations*

Consider the energy in the system at the point of time represented by M. The work done (per unit mass) W by the radiation piston on the target (assuming perfect coupling) in compressing the target from initial radius r_0 to radius r_m is

$$W_m = \frac{1}{(\frac{4}{3}\pi\rho_m r_m^3)} \int_{r_m}^{r_0} \frac{3{\cdot}3\times10^{-9}}{(4\pi r^2)} R(4\pi r^2)\,dr \tag{3}$$

where ρ is the mass density, r the piston radius and the subscript m dentoes the quantity at the point of time M.

The plasma internal energy U is

$$U_m = \frac{G}{W}\chi\frac{T_m}{\gamma-1} \tag{4}$$

where G is the Universal Gas Constant, W the molecule weight, χ the departure coefficient, T the plasma temperature and γ the specific heat ratio.

At the time M, the plasma sphere has no directed kinetic energy, so that, assuming no losses, we may put $W_m = U_m$ and hence obtain the plasma temperature at time M as

$$T_m = \frac{3{\cdot}3 \times 10^{-9}}{\frac{4}{3}\pi\rho_m r_m^3} \frac{(\gamma - 1)}{\frac{G}{W}\chi} \int_{r_m}^{r_0} R\, dr. \tag{5}$$

Next we consider the pressure relationship at this time. The plasma kinetic pressure $P_m = (G/W)\chi\rho_m T_m$ exceeds the radiation pressure P_{R_m} by the reflected shock pressure jump factor f_{rs}. This gives us

$$T_m = \frac{3{\cdot}3 \times 10^{-9} R_m f_{rs}}{4\pi r_m^2 \rho_m (G/W)\chi}. \tag{6}$$

From equations (5) and (6) we obtain the combined energy and pressure balance condition as

$$R_m = \frac{3(\gamma - 1)}{f_{rs} r_m} \int_{r_m}^{r_0} R\, dr. \tag{7}$$

Equation (7) specifies the radius r_m at which the energy and pressure conditions of equations (5) and (6) are simultaneously met. This equation shows that the radius ratio r_m/r_0 is independent of the absolute magnitude of the radiation power which may be R_m or any multiple of it. The radius ratio is a function only of γ, f_{rs} and the pulse shape of R. This pulse shape of R would be a function of r and consequently also of time t since r would generally be a function of t. In order to see the significance of this balance condition we consider here several simple radiation pulse shapes.

Case 1. R = constant. Constant or square pulse radiation power.

Take $\gamma = \frac{5}{3}$, for a fully ionized plasma. With $R = R_m$ = constant, equation (7) integrates to

$$\chi_m = r_m/r_0 = 2/(2 + f_{rs}) \tag{8}$$

and we may construct a table to give us the radius ratio and density ratio $\rho_m/\rho_0 = \kappa_m^{-3}$ at maximum compression as a function of the reflected shock pressure ratio f_{rs} taken as a parameter from 1 to 10.

f_{rs}	κ_m	ρ_m/ρ_0
1	0·67	3·38
1·5	0·57	5·36
2	0·5	8
3	0·4	15·6
4	0·33	27
5	0·29	42·9
6	0·25	64
10	0·17	216

It is instructive to follow values of the LHS function F_L and RHS function F_R of equation (7) as the compression proceeds from $\kappa = 1$. This is normally computed during a trajectory computation, but in this case since this problem is being solved without a trajectory computation we indicate these function values schematically in

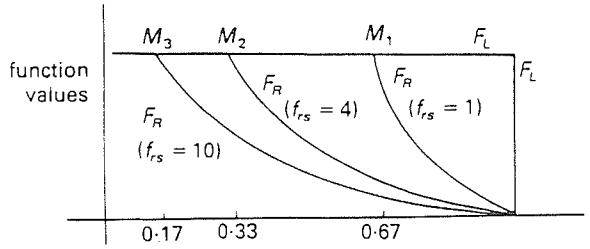

FIGURE 4. Illustrating the convergence of function values of F_L and F_R of equation (7) for a square pulse.

figure 4 for the three cases $f_{rs} = 1$, $f_{rs} = 4$ and $f_{rs} = 10$. In this figure the points M_1, M_2 and M_3 represent the intersection points of the curves F_R and F_L, respectively, for the cases of $f_{rs} = 1$, $f_{rs} = 4$ and $f_{rs} = 10$. These points represent the points of maximum compression, respectively for the three cases as expressed by equation (7).

It is seen that, for a given pulse shape of R, the compression depends strongly on the value of f_{rs}. It has been shown by von Guderley (1942) that the value of f_{rs} near the point of reflection is typically 6, 4·5 and 3·5, respectively, for planar, cylindrical and spherical shocks. We shall take the value of $f_{rs} = 4$ for our consideration. Using this value of f_{rs} for the case of square pulse radiation power, the radius ratio κ_m is 0·33 corresponding to a density ratio of 27. This compares with a density ratio of 33 (Brueckner & Jorna 1974) for a single shock compression followed by adiabatic compression.

Case 2. $R = R_m(r - r_0)/(r_m - r_0)$. *Radiation power linearly rising with decreasing r.*

For this case equation (7) integrate to

$$\kappa_m^2 - \kappa_m = \frac{3}{f_{rs}}(\gamma - 1)(\kappa_m - \kappa_m^2/2 - \tfrac{1}{2}) \tag{9}$$

which for $\gamma = \frac{5}{3}$ and $f_{rs} = 4$ gives

$$\kappa_m = 0{\cdot}2 \quad \text{and} \quad \rho_m/\rho_0 = 125.$$

Thus a rising radiation power during compression gives rise to greater compression than a constant power. This agrees with Brueckner & Jorna (1974). This is evident from an analysis of equation (7) or the schematic of figure 4. It is also evident from equation (7) that a pulse which rises faster than that of Case 2 will produce even greater compression.

Case 3. *Stepped double pulse. Both pulses of constant power; the second pulse has n times the amplitude of the first pulse.*

The advantage of using a double pulse may be seen from equation (7). Let us follow the functions F_R and F_L of equation (7) during a compression using constant power. From figure 4 we have seen that for $f_{rs} = 4$ the values of F_R and F_L converge at $\kappa = 0{\cdot}33$. If, as this point is approached, the radiation power is stepped up to n times the amplitude of the first pulse, then the convergence point of F_R and F_L is shifted to a smaller value of κ as shown in figure 5 where it is seen that a new balance point $\kappa_m < 0{\cdot}33$ is established.

In practice, because the reflected shock will have hit the piston despite the sudden rise of piston power to nR_m, it is necessary for the value of n to be greater than f_{rs}. We take the case of $n = 6$ and assume that when the piston reaches $\kappa = \kappa_1$ where $\kappa_1 \gtrsim 0{\cdot}33$

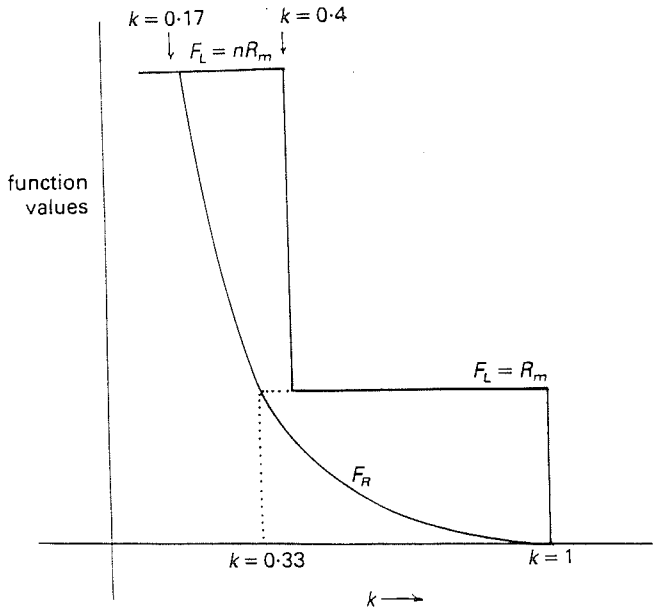

FIGURE 5. Illustrating the effect of a stepped square pulse in shifting the convergence point of functions F_L and F_R to a smaller radius.

the radiation power is stepped up to $6R_m$. Then when the reflected shock hits the piston, the reflected shock is turned back towards the axis, reflects off the axis and again moves towards the piston, hitting it with a pressure rise factor again of four times the increased piston pressure of $6R_m$. Then a re-examination of equations (1)–(4) for this situation shows that equation (7) now becomes

$$nR_m = \frac{3(\gamma - 1)}{f_{rs} r_m} \left(\int_{r_1}^{r_0} R_m \, dr + \int_{r_m}^{r_0} nR_m \, dr \right) \tag{10}$$

giving for $\gamma = \frac{5}{3}$, $f_{rs} = 4$, $n = 6$ and $\kappa_1 = 0{\cdot}4$:

$$12\kappa_m = \int_{0{\cdot}4}^{1} d\kappa + 6 \int_{\kappa}^{0{\cdot}4} d\kappa \tag{11}$$

so that we have $\kappa_m = 0{\cdot}17$ and the $\rho_m/\rho_0 = 204$. Thus this double pulse technique has increased the density compression 7-fold as compared with a single pulse.

Case 4. *Stepped double pulse. Both pulse linearly rising with decreasing r, the second pulse with a gradient n = 6 times that of the first pulse*

In this case, switching the second pulse on when the piston has reached $\kappa = 0{\cdot}3$ (noting from Case 2 that the balance point for the first pulse only is at $\kappa = 0{\cdot}2$) gives $\kappa_m = 0{\cdot}083$ with corresponding density ratio of 1750; a 14-fold increase in denstiy compression when compared to the single linear pulse.

3. Discussion

Although a shock model is used for the above computation it should be stressed here that this model is used only so that specific results may be computed. The model is not

central to the energy and pressure balance condition as expressed in equation (7). Indeed if a situation is envisaged in which no reflected shock developed or reflected shock effects are not important then we put $f_{rs} = 1$ into equation (7).

The use of $f_{rs} = 4$ is an approximation. As the reflected shock moves away from the point of reflection the value of f_{rs} should gradually decrease. The rate of reduction should also depend on the time function of the driving pressure. Since the value of r_m/r_0 depends on f_{rs} (see equation 7) it would be useful to consider the shock reflection more carefully in order to compute a more realistic f_{rs} for each case. This is, however, outside the scope of this paper.

The above cases have been chosen for simplicity of interpretation and of integration of equation (7) without the need to obtain the trajectory. In an experimental situation the power pulse would be specified as a function of time, rather than of radius, so that the computation of F_R of equation (7) would have to be done simultaneously with the computation of the trajectory $r(t)$ as a function of time. For simplicity we may use a snowplow model such as

$$\frac{d}{dt}\left((r_0^3 - r^3)\frac{dr}{dt}\right) = -\frac{3{\cdot}3 \times 10^{-9}}{\frac{4}{3}\pi\rho_0} R(t). \tag{12}$$

This equation normalizes to

$$\frac{d}{dt}\left((1 - \kappa^3)\frac{d\kappa}{d\tau}\right) = -\alpha^2 \mathbb{R} \tag{13}$$

where $\kappa = r/r_0$, $\tau = t/t_0$, $\mathbb{R} = R/R_0$, with scaling parameter $\alpha = t_0/t_p$, where t_0 would be associated with a characteristic time (for example rise time) of radiation pulse characterized by magnitude R_0 and t_p is given by

$$t_p = \left(\frac{4\pi \times 10^8 \rho_0 r_0^4}{R_0}\right)^{\frac{1}{2}}. \tag{14}$$

For example: Taking $\alpha = 1$, $r_0 = 10^{-4}\,m$, $\rho_0 = 180\ \mathrm{kg\,m^{-3}}$ then have

$$t_p = t_0 = 5 \times 10^{-3} R_0^{-\frac{1}{2}} \tag{15}$$

where t_p may be interpreted as the characteristic time of the compression. Some characteristic times and speeds are deduced from equation (15) as follows:

R_0 (Pulse peak power) (Watt)	t_p (Characteristic compression time) (p s)	r_0/t_p (Characteristic compression speed) ($m\,s^{-1}$)
10^{14}	500	2×10^5
10^{15}	160	$6{\cdot}3 \times 10^5$
10^{16}	50	2×10^6

TABLE 1. Characteristic snowplow compression times and speeds

For a given radiation pulse $R(t)$, equation (13) may be solved for selected values of α. This equation by itself gives a trajectory which goes to $r = 0$, a non-physical situation. However, with concurrent use of equation (7), the limit of the trajectory may

be determined. A more realistic model such as a slug model may, of course, also be used.

We now consider the energy gain factor G. We note that the gain equation (1) or (2) is written for an optimized kinetic temperature of 10·3 keV. So for the consideration of G it is necessary to estimate the compressed temperature T_m. From equation (6) we may write:

$$T_m = \frac{8{\cdot}8 \times 10^{-8} R_m \kappa_m}{(r_0')^2} \tag{16}$$

for a 50:50 DT pellet where r_0' = initial pellet radius in units of 100 μm. We note that T_m may be increased either by increasing R_m or reducing r_0. For a given power R_m we may use equation (16) to estimate T_m. We may use equation (14) or Table 1 to estimate the required pulse length and hence input energy E. Then we may use equation (7) to compute κ_m. The gain factor G may then be computed from equation (2).

As an example we use $R_m = 10^{16}$ W and $r_0 = 100\,\mu$m of 50:50 DT and present the results in Table 2 for gain factors computed for the four cases discussed earlier.

	Case 1 Square pulse	Case 2 Linearly rising pulse	Case 3 Stepped square pulse	Case 4 Stepped linearly rising pulse
T_m (keV)	26	16	14	7
E (MJ)	0·5	0·4	0·45	0·38
κ_m	0·33	0·2	0·17	0·083
G	6	16	23	90

TABLE 2. Energy gain factors for $r_0 = 100\,\mu$m, $R_m = 10^{16}$ W

We may also consider reducing the power to $R_m = 10^{15}$ W. Then to maintain the temperature near optimum value equation (16) shows that r_0 should be reduced to 32 μm, reducing the required pulse lengths by 3·2, from equation (14). The input energy is thus reduced by 32 times. However because of the slow dependence of G on E, the gain is reduced only by a factor of 0·31. Thus for the stepped linearly rising pulse of case 4, a radiation power peaking at 10^{15} W is required to deliver an absorbed energy of only 12 kJ for a gain factor of 28.

4. Conclusion

The limits of compression for magnetic drivers as well as radiation drivers are determined by energy and pressure considerations. The specific case of a radiation driven pellet compression is considered here. The radiation pulse is considered to interact with the pellet as a piston driving a strong shock which upon convergence at the centre reflects towards the piston with a pressure rise factor of 4. Using this model an energy-pressure balance condition is derived for the radius of maximum compression. The physics of this balance condition is then demonstrated by considering several simple cases. These are summarized in Table 3.

	Radius ratio κ_m	Density compression Γ_m
R = constant; square pulse radiation power	0·33	27
$R = R_m \frac{(r - r_0)}{(r_m - r_0)}$; power linearly rising	0·2	125
Double pulse; both constant power, $n = 6$	0·17	204
Double pulse; both with linearly rising power, $n = 6$	0·083	1750

TABLE 3. κ_m and Γ_m for 4 types of compressing pulse shapes

The method is simple and gives new insight into the limits of compression as simply a condition set by energy and pressure balance. The method also gives an indication as to how these limits may be extended by pulse shaping. It is applicable to pulse shapes of any type. Since the method assumes perfect piston coupling, any imperfection in coupling would give lower compression ratios than those indicated. The method may easily be extended to multiple pulse steps of number greater than 2, with consequent greater compressions.

The effect of the enhanced compression on the gain factor G is quite remarkable. For a 100 μm DT pellet irradiated by laser power of 10^{16} W applied as a square pulse a value of G of 6 may be attained with an absorbed energy of 0·5 MJ. Applying the power as a two-step linearly rising pulse peaking at 10^{16} W, G increased to 90 with an absorbed energy of 0·4 MJ.

The present work considers much higher radiation intensity than previous work on ablation-driven pressures applied to the compression of microballoons (Max *et al.* 1980; B. Yaakobi *et al.* 1981; T. Mochizuki *et al.* 1983; T. Yabe *et al.* 1983). This much higher radiation intensity is required to compress the solid spheres considered in this paper. The absence of ablation in pure radiation-pressure compression also increases the required radiation intensity.

Acknowledgments

The author would like to thank Professor Abdus Salam, the International Atomic Energy Agency and UNESCO for hospitality at the International Centre for Theoretical Physics, Trieste, where part of this work was completed. Financial assistance from the Flinders University of South Australia and the United Nations University are also acknowledged.

REFERENCES

BRUECKNER, K. A. & JORNA, S. 1974 *Rev. Mod. Phys.*, **46,** 325.
HAINES, M. G. 1982 *Phys. Scr.*, **T2/2,** 380.
HORA, H. & MILEY, G. H. 1984 *Laser Focus/Electro-Optics*, **20/2,** 59.
KIDDER, R. E. 1974 *Nuclear Fusion*, **14,** 797.
LEE, S. 1983 *Plasma Physics*, **25,** 571.
LEE, S. 1984 *J. Phys.*, D **17,** 733.
MAX, C. E. *et al.* 1980 *Phys. Rev. Lett.*, **45,** 28.
MIYANAGA, N. *et al.* 1983 Europhys. Conf. Abst. 7D Part II (Controlled Fus Aachen).
MOCHIZUKI, T. *et al.* 1983 *Japan J. Appl. Phys.*, **22,** L133.
VON GUDERELY, G. 1942 *Luftfahrtforschung*, **19,** 302.
YAAKOBI, B. *et al.* 1981 *Opt. Comm.*, **39,** 175.
YABE, T. *et al.* 1975 Rept IPPJ-235 (Inst. Plasma Phys., Univ. Nagoya), 6.
YABE, T. *et al.* 1983 *Japan J. Appl. Phys.*, **22,** L88.
YAMANAKA, C. 1985 *Nuclear Fusion*, **25,** 1343.

J. Fiz. Mal. 9,93 (1988)

A NUMERICAL STUDY OF THE EFFECT OF γ ON SHOCK SPEED FOR ATOMIC HYDROGEN AND MOLECULAR HYDROGEN.

S.H. SAW, S. LEE and C.S. WONG
Plasma Research Laboratery, Department of Physics,
University of Malaya, 59100 Kuala Lumpur.
Malaysia.

Received 6 September, 1988

Abstract

In this paper, the effect of the specific heat ratio, γ on the shock speed for both the atomic hydrogen model and the molecular hydrogen model are investigated. A comparison between these two models are also conducted to investigate the accuracy of approximating the molecular hydrogen with an atomic hydrogen. This is important in the study of pinch compressions as it has been shown that one of the factors governing the radius ratio of the pinch compressions is the specific heat ratio, γ.

Introduction

In the study of hydrogen pinch compressions, the hydrogen gas has usually been treated as a monatomic gas with a constant specific heat ratio, $\gamma = 1.67$. This approximation is reasonable for those H_2 pinch compressions designed to be driven by fully ionizing strong shocks with shock speed far exceeding 10 cm/μs. Under these conditions, the thermal energy becomes the most dominant mode of energy gained resulting in a situation where the thermal energy per particle greatly exceeds the ionizing energy per particle.

For slow hydrogen pinches[1] driven by weakly ionizing shocks, this is no longer true as the various modes of energy gained via rotation, vibration, dissociation, ionization and electronic excitation become significant. As a result γ deviates from the constant value of 1.67. In the molecular state γ begins to decrease with increasing temperature and ultimately increases back to 1.67 at high temperature beyond the fully ionizing shocks regime. Since one of the factors governing the radius ratio of the pinch compression is γ, it is vital especially during the earlier stages of a pinch when the compressing shocks are only weakly ionizing to include the proper variation of γ in order to compute the trajectory more accurately.

In this paper a numerical study is carried out to obtain the variation of γ with shock speed for hydrogen shocks. Two models, the monatomic and the diatomic model will be considered. In both the models the 1–D plane Shock Jump Equations[3], the Thermal Equation of state, the Saha Equation and the Caloric Equation of the State form a close system[4].

Calculation of γ

For shocks of Mach > 10 the 1–D Shock Jump Equations relating to the ambient particles and the shock particles measured in the shock fixed coordinates may be written as

$$\rho_1 q_1 = \rho_2 q_2 \qquad [1]$$

$$\rho_1 q_1^2 = \rho_2 q_2^2 + P_2 \qquad [2]$$

$$\tfrac{1}{2} q_1^2 = \tfrac{1}{2} q_2^2 + H_2 \qquad [3]$$

$$P_2 = \frac{R_0}{M} \rho_2 T_2 \chi \qquad [4]$$

$$H_2 = \frac{\gamma}{\gamma - 1} \frac{P_2}{\rho_2} \qquad [5]$$

where the subscript 1 refers to the ambient condition and subscript 2 refers to the shock condition. ρ, q, P and H are the density, particle velocity, pressure, and enthalpy respectively. R_o is the universal gas constant and M is the molecular weight of the gas. Both χ and γ are temperature

dependent. $\chi(T)$ is the departure coefficient of the gas describing the degree of dissociation and ionizing in the Thermal Equation of State. From the above shock equations, an expression relating the shock temperature and velocity is obtained as

$$T_2 = q_1^2 \frac{M}{R_0}\left[\frac{\Gamma - 1}{\Gamma}\right]\frac{1}{\chi} \qquad [6]$$

where Γ is the compression ratio and is given by

$$\Gamma = \frac{\rho_2}{\rho_1} = \frac{\gamma + 1}{\gamma - 1} \qquad [7]$$

In order to solve for γ at any temperature, T_2, χ and $\mathbb{H}_2$ must be known. $\chi(T)$ is obtained from the Thermal Equation of State together with the Saha Equation while $\mathbb{H}_2$ can be obtained from the Caloric equation of state. The Thermal Equation of State, the Saha Equation and the Caloric Equation of State for monatomic and diatomic hydrogen are described as follows.

(a) Monoatomic Hydrogen

$$H \xrightarrow{U_I} H^+ + e$$

where U_I is the ionizing potential of the hydrogen atom (13.595 eV).

The Thermal Equation of State is

$$P_2 = \frac{R_0}{M_H}\rho_2 T_2(1 + \alpha) \qquad [8a]$$

The departure coefficient χ for this situation is $\chi = (1 + \alpha)$, where α, the degree of ionization of hydrogen is the ratio of the number of electrons or hydrogen ions (N_e or N_{H+}) to the total number of neutral particles and positive ions ($N_t = N_H + N_{H+}$) and M_H is the atomic weight of the hydrogen atom. α is solved as a function of temperature from the Saha Equation[5].

$$\frac{\alpha^2}{(1-\alpha)} = 8.0 \times 10^{-6} \times \frac{M_H}{\rho_1} \times T_2^{3/2} \times \frac{Z_{eH^+}}{Z_{eH}} \times \exp(-U_I/kT_2) \qquad [9a]$$

where Z_{eH^+} and Z_{eH}[6] are the electronic partition function of hydrogen ion and hydrogen atom respectively. These values may be computed beforehand from the general expression for the partition function as given below,

$$Z = \sum_i g_i e^{-U_i/kT} \qquad [10a]$$

where U_i is the i-electronic excitation energy level and g_i is the corresponding statistical weight and the summation is taken over all available excitation energies.

The Caloric Equation of State is given by

$$\mathbb{H} = \frac{5}{2}\frac{R_0}{M} T_2 \chi + \frac{\alpha U_I}{M_H} + \frac{\alpha U_{eH^+}}{M_{H^+}} + \frac{(1-\alpha)U_{eH}}{M_H} \qquad [11a]$$

where U_{eH^+} and U_{eH} are the electronic excitation energy for the hydrogen ion and the hydrogen atom respectively. Similarly U_{eH^+} and U_{eH} are computed from the general expression for the excitation energy as given below,

$$U = \sum_i U_i g_i e^{-U_i/kT} \qquad [12a]$$

where U_i is the i-excitation energy level and g_i is the corresponding statistical weight and the summation is over all the available excitation energies.

From equation [4], [5] and equation [11a] γ is computed as a function of T_2 using

$$\left[\frac{\gamma}{\gamma - 1}\right] = \frac{5}{2} + \frac{\alpha U_I + \alpha U_{eH^+} + (1-\alpha)U_{eH}}{R_0 T_2 \chi} \qquad [13a]$$

The shock speed is then obtained from Eqn. [6] and [7].

(b) Diatomic Hydrogen

$$H_2 \xrightarrow{U_D} 2H$$

$$H \xrightarrow{U_I} H^+ + e$$

where U_D is the dissociation energy (4.476eV) of the H_2 molecule and U_I is the ionization energy of the H atom.

The Thermal Equation of State now becomes

$$P_2 = \frac{R_0}{M_{H_2}} \rho_2 T_2 (1 + \delta + 2\alpha) \qquad [8b]$$

where δ, the degree of dissociation is the ratio of the number of H_2 molecules dissociated to the total number of H_2 initially present in the system, N_t α, the degree of ionization is related to the ratio of the number of H^+ ion to N_t $\chi(T)$ now takes the value of $(1 + \delta + 2\alpha)$.

The Saha Equations involved are

(i) for dissociation,

$$\frac{4(\delta-\alpha)^2}{(1-\delta)} = 0.44 M_{H_2} \frac{T_2^{3/2}}{\rho_1} \frac{Z^2_{eH}}{(Z_r Z_v Z_H)_{H_2}} \exp(-U_D/kT_2) \qquad [9b]$$

where $(Z_r Z_v Z_H)_{H_2}$ [7,8] are the rotational, vibrational and electronic partition function of the H_2 molecule respectively. These quantities are computed in the same manner as for the monatomic H mentioned earlier. The diatomic molecule here is taken as a homonuclear rigid rotator and a harmonic oscillator. M_{H_2} is the atomic weight of the hydrogen molecule.

(ii) for ionization

$$\frac{2\alpha}{\delta-\alpha} = 8.0 \times 10^{-6} \frac{M_{H_2}}{\rho_1} T_2^{3/2} \frac{Z_{eH^+}}{Z_{eH}} \exp(-U_I/kT_2) \qquad [9c]$$

where Z_{eH^+} and Z_{eH} are the electronic partition function of the hydrogen ion and atom respectively. Similarly these quantities are computed as before. From equation [9b] and [9c], δ and α are solved and $\chi(T)$ can be determined.

The Caloric Equation of State is

$$IH = \frac{5}{2}\frac{R_0}{M_{H_2}} T_2 (1 + \delta + 2\alpha) + \frac{(1-\delta)U_{vib}}{M_{H_2}} + \frac{(1-\delta)U_{rot}}{M_{H_2}} + \frac{\delta U_D}{M_{H_2}} + \frac{\alpha U_I}{M_H} + \frac{(d-\alpha)U_{eH}}{M_H} + \frac{(1-d)U_{eH_2}}{M_{H_2}} + \frac{\alpha U_{eH^+}}{M_{H^+}} \qquad [10b]$$

where the computed quantities U_{eH}, U_{eH_2} and U_{eH^+} are the electronic excitation energy of the H atom, the H_2 molecule and the H^+ ion respectively. U_{rot} and U_{vib} are the rotational and vibrational excitation energy of the H molecule.

γ is again computed as a function of T_2 using

$$\left[\frac{\gamma}{\gamma-1}\right] = \frac{5}{2} + A + B$$

where

$$A = \frac{\left[(1-\delta)(U_{rot} + U_{vib} + U_{eH_2}) + \delta U_D\right]}{R_0 T_2 (1 + \delta + 2\alpha)}$$

$$B = \frac{\left[\frac{\alpha U_I}{M_H} + \frac{(\delta-\alpha)U_{eH}}{M_H} + \frac{U_{eH^+}}{M_H^+}\right]}{\frac{R_0 T_2 (1 + \delta + 2\alpha)}{M_{H_2}}} \qquad [11b]$$

Finally the shock speed is obtained as a function of T from Eqn [6] and [7] as before.

Solutions

The solutions obtained for γ using both the monatomic and diatomic models for ambient pressure of 0.8 mbar hydrogen is as shown in Fig. 1 to Fig. 3. It is found that excluding molecular effects the hydrogen atom starts ionizing at about 8 000 K and becomes fully ionized at about 22 000 K. During this period γ drops from 1.67 to a minimum of 1.16 with the onset of ionization and later increases to 1.2 as the hydrogen approaches complete ionization. In the case of the model including molecular effects, it is found that hydrogen starts dissociating at about 2 000 K and becomes fully dissociated at about 4 500 K follows by ionization at 8 000 K to 22 000 K. During this time γ varies from 1.67

to a minimum of 1.38 at about 85 K when the rotation degree of freedom becomes effective. With further increase of temperature γ drops to a minimum of 1.11 with the onset of the vibrational degree of freedom which later increases to 1.2 as vibrational degree of freedom becomes fully excited and the H_2 molecule becomes fully dissociated. Following this, γ decreases with the onset of ionization to a minimum of 1.14 which subsequently increases as it becomes fully ionized. The corresponding shock speed is as shown in Fig. 3. It is observed that there are 2 regions of small gradient where the increase of shock speed with temperature are larger. These first and second regions correspond to the effect of dissociation and ionization respectively. After this period γ increases slowly with increasing temperature towards 1.67 as the hydrogen atom becomes both fully ionized and fully excited. The shock speed increases slowly with the square root of temperature, T_2. This shows that it is reasonable to approximate the diatomic hydrogen with a monatomic model for very strong ionizing shocks especially if the initial potential is taken as $U_I + U_D$. However for shock velocity below 4.00 cm/μs, γ is not constant and γ-atomic and γ-molecular differs greatly.

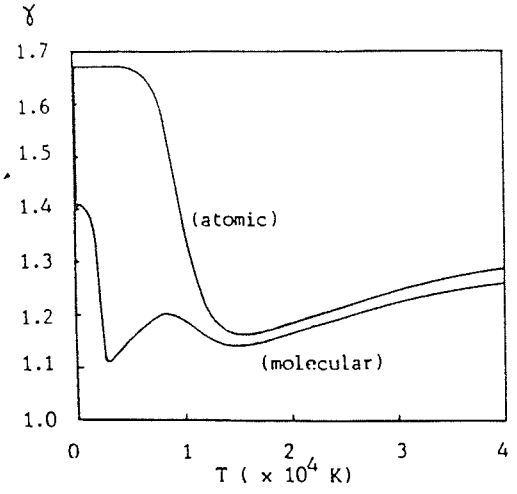

Fig. 1 Variation of Variation of γ with Temperature for Hydrogen Gas at 0.8 m bar.

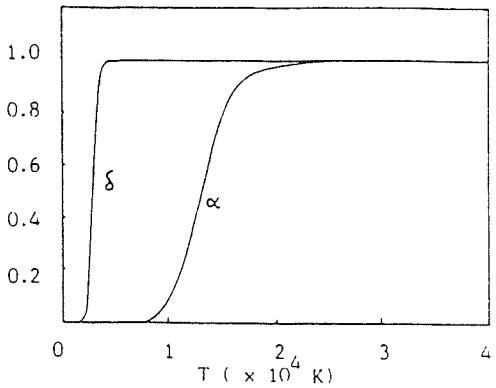

Fig. 2 Degree of Dissociation (δ) and Degree of Ionization (α) versus Temperature for Hydrogen gas at 0.8. mbar.

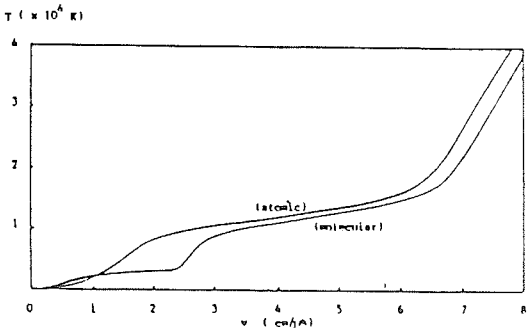

Fig. 3 Temperature versus Shock Speed for Hydrogen Gas at 0.8. mbar.

Conclusion

The numerical studies conducted here prove that for weakly ionizing shock speed below 4 cm/μs the proper variation of γ should be considered. It is also inaccurate to approximate it with an atomic model. Since gas compression is a function of γ, this variation must be incorporated into the compressional dynamics in order to obtain a more accurate representation.

References

1. S.H. Saw, C.S. Wong & S. Lee; in Procs. of the Symposium on small – scale Lab. Plasma Physics Experiments, 1987, pp116.
2. S. Lee; Aust. J. Phys., 36, 891 (1983).
3. A.G. Gaydon; The Shock Tube in High Temp. Chemical Physics, Chapman & Hall Ltd., London

(1963), Chapter 2.
4. A.B. Cambell; Plasma Physics & Magnetofluid Mechanics, McGraw-Hill (1963), Chapter 5 & 6.
5. S.Lee; Laser & Plasma Technology, Ed. S.Lee et. al World Scientific, Chapter 6.
6. A.J. Pointor; Introduction to Statistical Physics, Longman, Chapter 7.
7. G. Herberz; Spectra to Diatomic Molecules.
8. C.E. Moore; Atomic Energy Levels.

TECHNOLOGY OF A SMALL PLASMA FOCUS INCORPORATING SOME EXPERIENCES WITH THE UNU/ICTP PFF

S. LEE

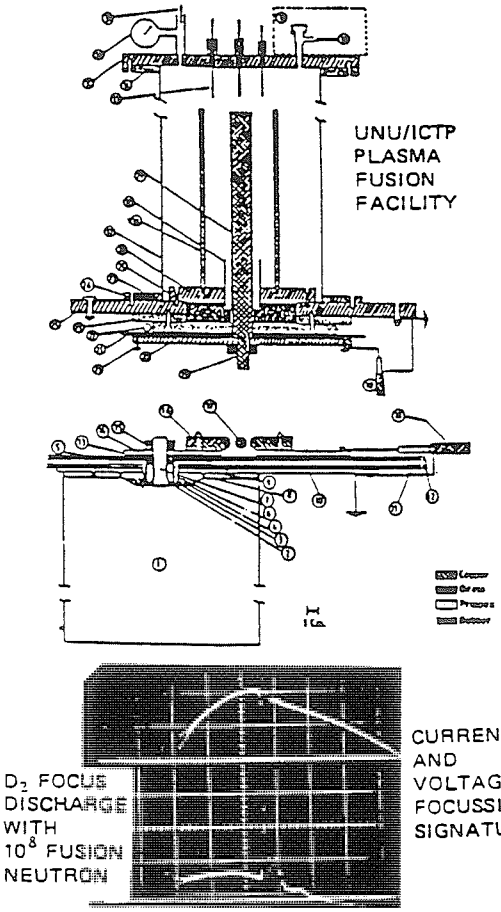

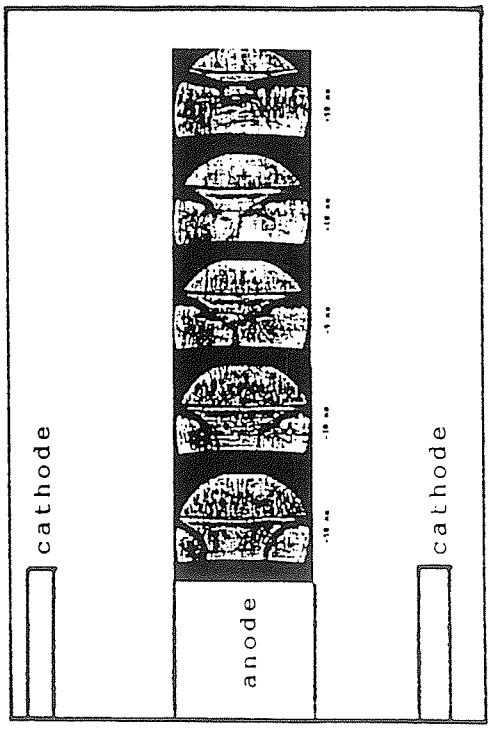

A sequence of Schlieren images showing the plasma structure and dynamics.

Presented at the
Symposium on Small Scale Laboratory Plasma Physics Experiments
(5-7th June 1989)
Spring College on Plasma Physics
(15th May - 9th June 1989)

Small Plasma Experiments II - Ed. S. Lee & P.H. Sakanaka
World Scientific Publishing Co. (1990)

TECHNOLOGY OF A SMALL PLASMA FOCUS

S. Lee

Plasma/Pulse Research Laboratories
Physics Department/IPT
University of Malaya
59100 Kuala Lumpur, Malaysia

TECHNOLOGY OF A SMALL PLASMA FOCUS

S. Lee

INTRODUCTION

1.1 General Characteristics of the Plasma Focus:

The early work of Filippov[1-3] and Mather [4-6] on the plasma focus has shown that in this device a hot ($\sim$ 1 keV) and dense ($\sim 10^{19}$ cm^{-3}) plasma is created with a lifetime $\sim$ 50 ns. Considerable interest was directed on this device because of the high $n\tau$ value of the plasma and the readily detected bursts of fusion neutrons when operated in deuterium. It has been demonstrated that a capacitor energy of E = 100 J is sufficient to produce a detectable burst of $N = 10^5$ neutrons. This compares with the 1 MJ Frascati machine on the other end of the scale producing 10^{13} neutrons. A typical machine within the means of a small laboratory may have 10 kJ storage and produces 10^9 neutrons per burst. The yield-energy relationship is simple ($N \sim E^2$) as illustrated by Fig. 1.

Besides being a ready source of hot dense plasma and fusion neutrons (Fig. 2) the focus also emits copious amounts of soft x-ray (Fig. 3). The large range of plasma phenomena readily available from this easily constructed machine has led to its study in many laboratories around the world[7 - 27].

As a simplification, the focus may be considered as a device which operates in two distinct phases (Fig. 4) an axial acceleration phase in which the characteristics of the device is very similar to an electromagnetic shock tube; and a radial compression phase in which the plasma behaviour may be approximated to a compressing plasma pinch with a length which increases as the radius decreases[28,29,35]. In these two phases the plasma may be considered from the viewpoint of the classical snow-plow model as a well defined plasma slug driven by a magnetic piston (current sheet). These two phases set the stage for the third phase, the short-lived dense plasma phase followed by a fourth phase[30] during which a process of turbulent magnetic

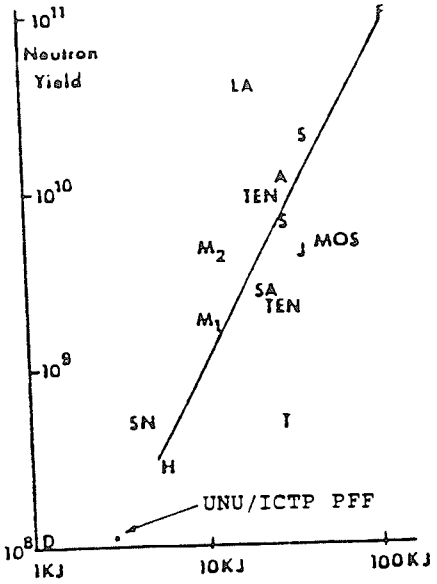

Fig.1 Neutron production as a function of energy.

F=Frascati; LA=Los Alamos; S=Stuggart; A=El Segunda Aerospace; TEN=Tennessee; MOS=Moscow; J=Julich; SA=Sandia; SN=Steven; T=Texas; M_1=UMDPF1; M_2=UMDPF2; H=Hoboken; D=Darmstadt. (Ref.26, modified)

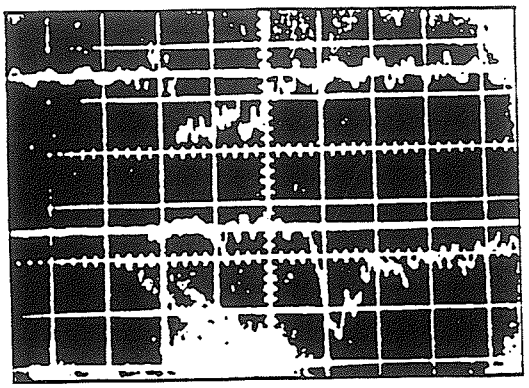

Fig.2 Time-of-flight oscillogram obtained in the measurement of neutron energy. Top trace records output from near detector. Bottom trace records output from far detector placed 10.2 m behind near detector. Horizontal scale 200 ns per cm. (Ref.21)

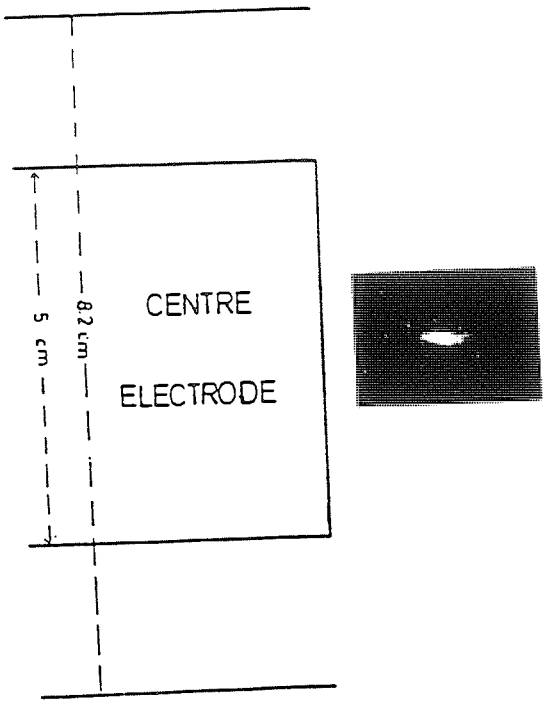

Fig.3 *Soft x-ray photograph in transverse view. The surface of the centre electrode is beyond the left side of the photograph as shown to scale. Voltage, 29.6 kV. Pressure: 1.3 torr. Condenser bank energy 13 kJ.* (REf.41)

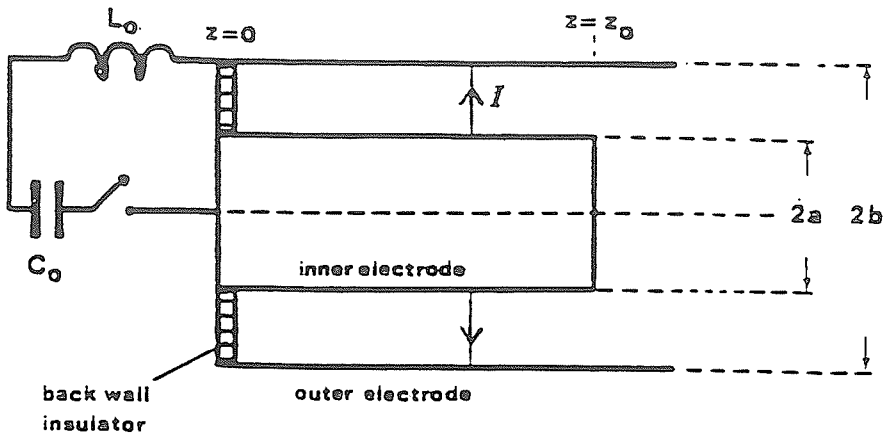

Fig. 4a Phase1: axial acceleration phase

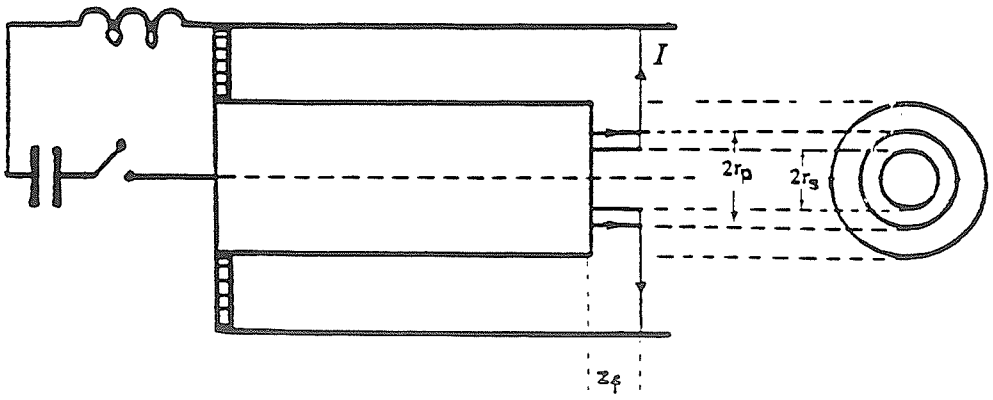

Fig. 4b Phase 2: radial compression phase

(Ref.28)

field penetration[38] results in a quiescent plasma column of relatively large diameter. There is evidence that most of the fusion neutrons are produced during the transition from the third to fourth phase.

1.2 The Device:

The general configuration of the plasm focus device is as shown in Fig. 5.

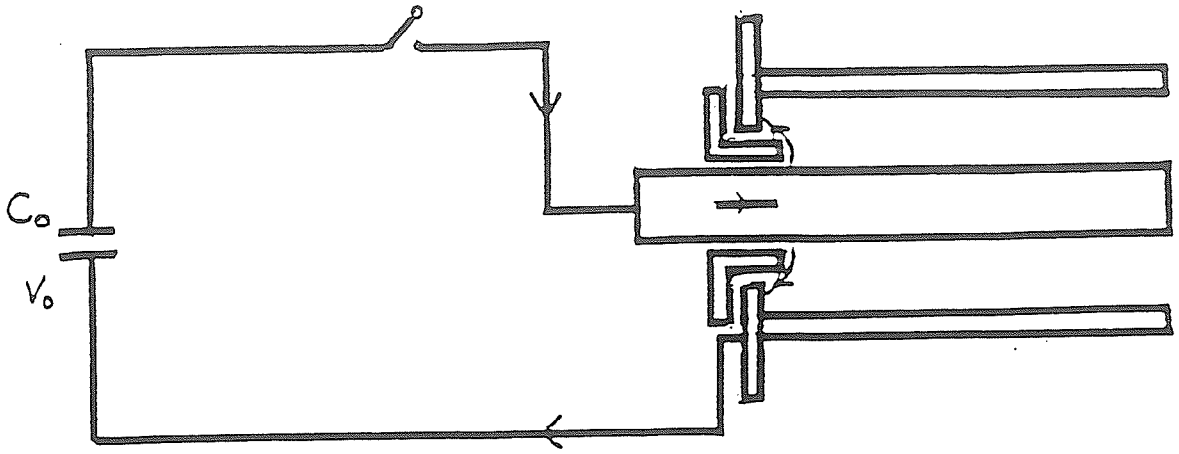

Fig. 5: Schematic of the discharge circuit

1.3 The Phases of Plasma Development:

Break-down and surface discharge:

The device consists of an inner electrode and a coaxial outer electrode separated by an insulator at the starting end. The power source is a capacitor C_o charged to voltage V_o and switched on to the inner electrode by switch S. When S is closed the voltage appears across the two electrodes and when the conditions are properly adjusted a discharge occurs across the surface of the insulator between the inner and outer electrodes. The $\vec{J} \times \vec{B}$ force on this axially symmetric surface current is radially outwards (Fig. 6a). This lifts the current off the insulator in a cylindrical sheet. One end of this sheet remains attached to the inner electrode at the circular junction where the inner electrode meets the insulator. The other end moves radially outwards across the back wall which forms part of the outer electrode.

Axial acceleration phase:

When this lift-off is completed the current flows radially outwards from the inner electrode to the outer electrode in radially symmetric sheet slightly canted in the forward direction (z) at the inner electrode. In this position the $\vec{J} \times \vec{B}$ force on the current sheet is axially down the tube (i.e. in the z direction). The current sheet, scooping up the gas

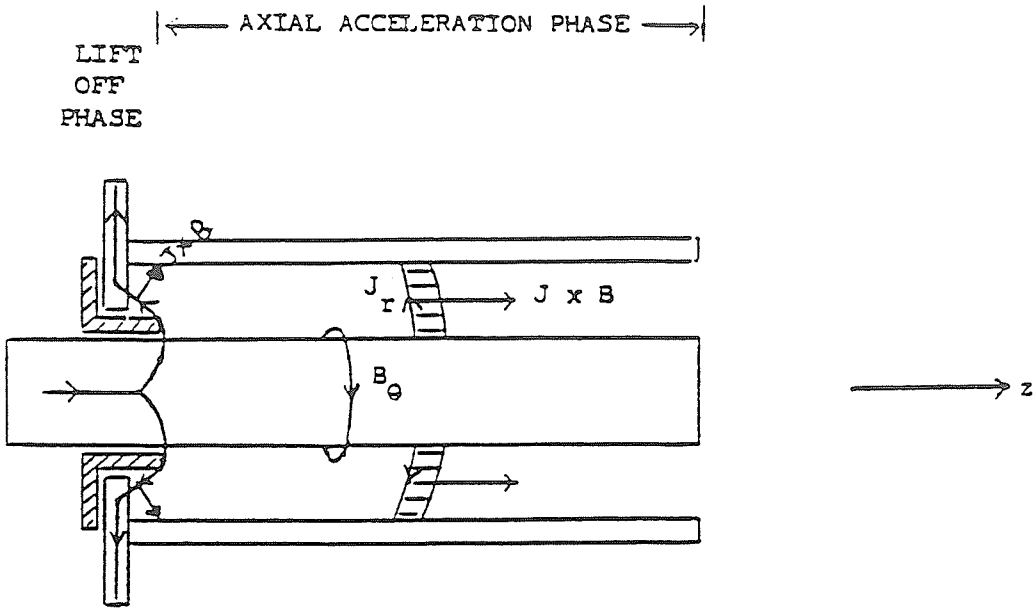

Fig. 6 The driving force in the
a) breakdown region: the JXB force just after breakdown, causing current sheath lift-off.
b) axial acceleration region: the JXB force during the axial phase.

it encounters is thus accelerated down the tube (Fig. 6b). In this phase of axial acceleration the behaviour of the current sheet and the plasma it drives is similar to the situation in an electromagnetic shock tube.

Radial collapse phase:

When the current sheet reaches the end of the centre electrode, the end of the sheet which has been sliding along the centre electrode in the axial direction begins to slide across the face of the centre electrode in the radial inward direction. The other end which has been sliding along the outer electode in the axial direction continues in its motion (Fig. 4b).

Dense plasma phase and focus phase:

In this implosion, a dense plasma column is formed on the axis of the focus tube just off the face of the centre electrode. Towards the end of this dense plasma phase m=0 instabilities set in. The column breaks up and very rapidly a large diameter phase is formed.

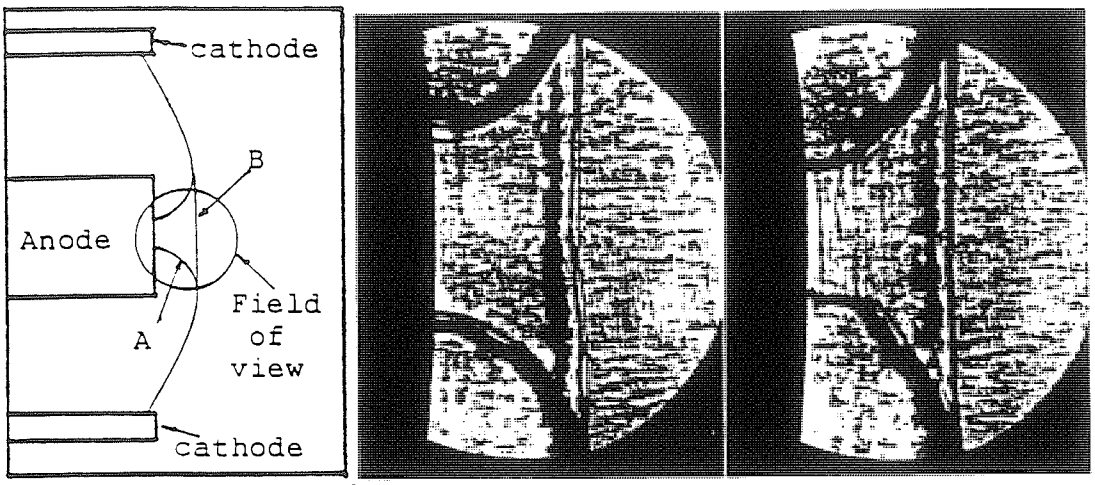

Fig. 7 A sequence of Schlieren images showing the plasma structures and dynamics. Experimental conditions: 9 mbar deuterium at 14 kV. (Ref. 50)

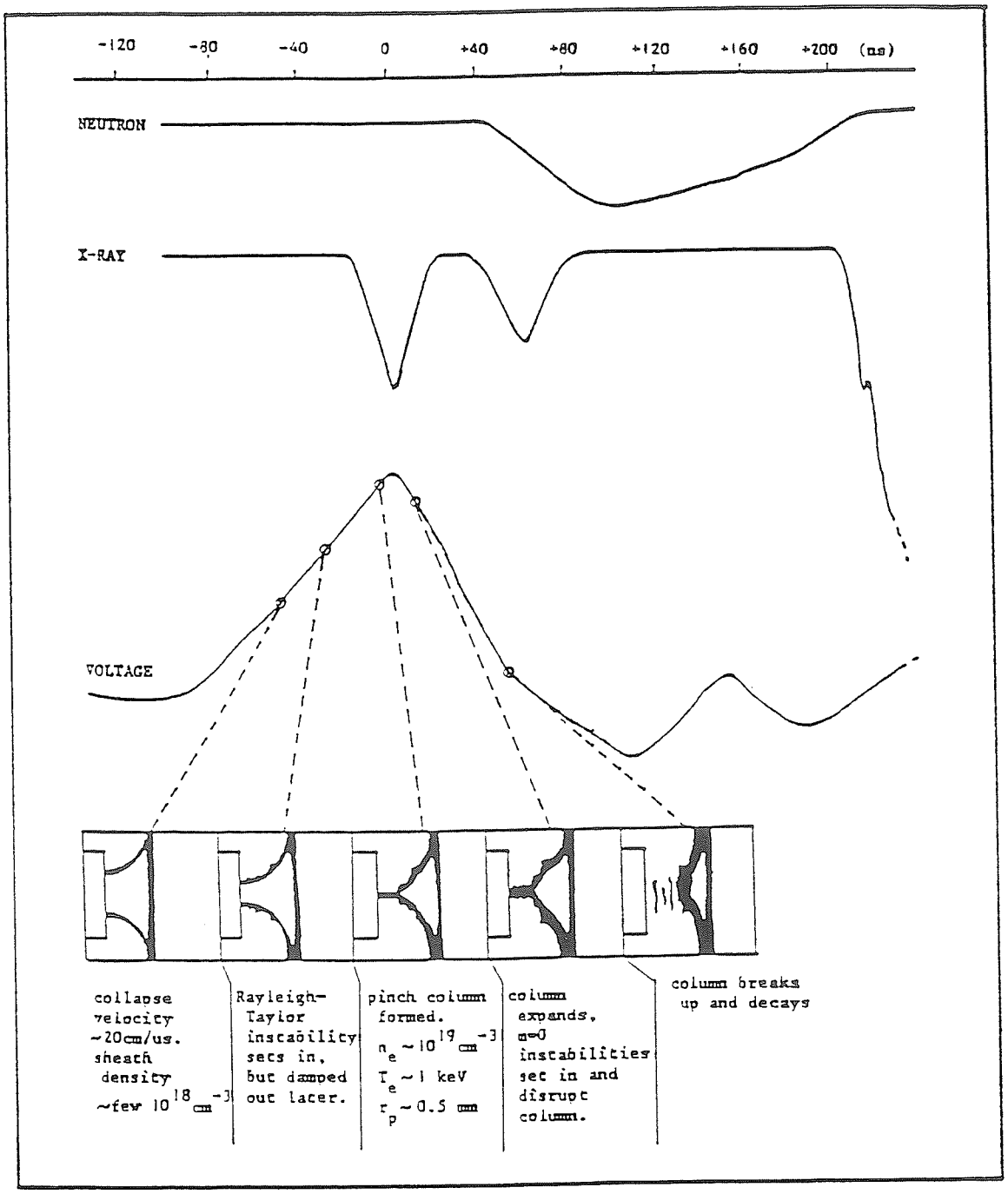

Fig.8 Summary of the temporal development of the radial implosion process (Ref. 50).

The sequence of events from the implosion to the formation of the large diameter plasma has been described in a sequence of framing photographs by Decker and Wienecke[30]. More details of plasma structure giving particularly information on electron density gradient have been obtained by Kwek[49,50] using an entirely Third World home-made Schlieren system including a home-made nitrogen laser light source. This Schlieren sequence (Fig. 7) of radial collapse and subsequent phases are correlated to the measured tube voltage, x-ray and neutron[50] (Fig. 8).

Laser shadowgraphs have also been taken which confirm the main features in the collapse phase and the dense plasma phase (Fig. 9).

Following the dense plasma phase, the column is very rapidly disrupted. This rapid disruption is consistently observed, for example, in the shadowgraphy of Fig. 9 (see the frame at t = + 50 ns). There is also consistent evidence[30] to show that whilst the soft x-ray from the plasma is associated mainly with the dense plasma phase, the hard x-ray is more to be associated with the instability phase and the neutron production peaks between the instability and the expansion phase.

The angular distribution of the neutrons from the plasma focus has been extensively studies (for example, see Fig. 10).

1.4 Classic Indication of Focus Action:

Figure 11 shows the classic indications of strong focussing action (note the severe current dip and the corresponding voltage spike near the middle of the horizontal axis), which in a deuterium focus invariably signals the production of neutrons.

1.5 A Low Cost Device:

The IAEA Consultants' Meeting in Swierk, Poland[45] in December 1978 has recommended the plasma focus as one of the two devices which might be purchased or constructed by a developing country with the intention of studying high temperature plasmas. A figure of likely cost of US$10,000 was mentioned in the Report.

For the purpose envisaged by the Consultants' Report the focus is certainly an eminently suitable machine, as within one low-cost well-behaved machine shock waves, pinch and focus phenomena may be studied: with plasma conditions extending to fusion conditions with copious emission of x-rays and fusion neutrons.

This has been demonstrated in a package designated as the UNU/ICTP PFF (United Nations University/International Centre for Theoretical Physics Plasma Fusion Facility)[51,52] developed for a series of UNU and ICTP sponsored training programmes aimed at initiating experimental plasma research in developing countries. As a result of the training programmes this device with various modifications and improvements is in varying stages of development in Pakistan, Indonesia, India, Egypt, Nigeria, Sierra Leone and Thailand. The training programmes have initiated and assisted in the production of several M.Sc. theses on experimental laser and plasma physics at the Rivers State University of Science and Technology in Nigeria and the UNU/ICTP PFF programme has produced the first Ph.D. in experimental plasma/fusion physics in Pakistan[53].

1.6 Sub-systems of the UNU/ICTP PFF:

For effective initiation of experimental research in developing country experience has shown that the technology/research transfer process is most effectively carried out by the concept of open-box (as opposed to black box) sub-systems. The package is divided into sub-systems (see Fig. 12), each sub-system specifically designed for simplicity, cost-effectiveness and transferability. Each sub-system is then designed and constructed by a trainee and tested to be operational. The sub-systems are then assembled, tested to obtain good and consistent dynamics in various gases and finally to produce a consistent and reproducible neutron yield when operated in deuterium.

The package is then disassembled, packed and airfreighted back to the trainee's home institute, and reassembled and modified for the trainee's own developmental and research purposes.

Since the purposes of this monograph is to describe the technology of a small plasma focus in a manner useful for developing countries it is elected to follow the proven pedagogical approach of the UNU/ICTP PFF. Chapter 2 will describe a simplified dynamic model which enables the focus to be simulated and designed, leading very naturally to computation packages and design criteria, discussed in Chapter 3. Chapter 4 deals with the hard-ware of the UNU/ICTP PFF in sub-system form whilst Chapter 5 describes some possible applications of the plasma focus including some ideas on improving its scaling.

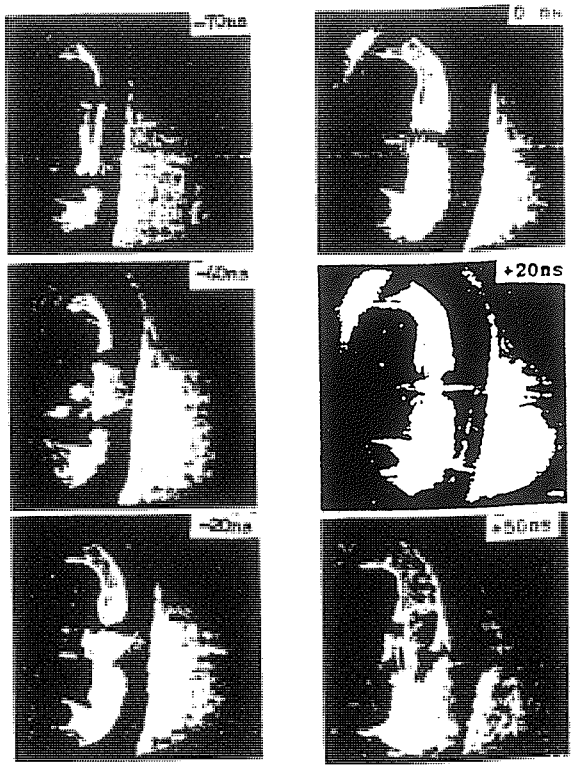

Fig.9. Side on laser shadowgraph of a 20-kV 60 μF, 4-Torr deuterium plasma focus, showing a pinch ratio $r_p/r_0 \sim 0.13$. (Ref. 35,36)

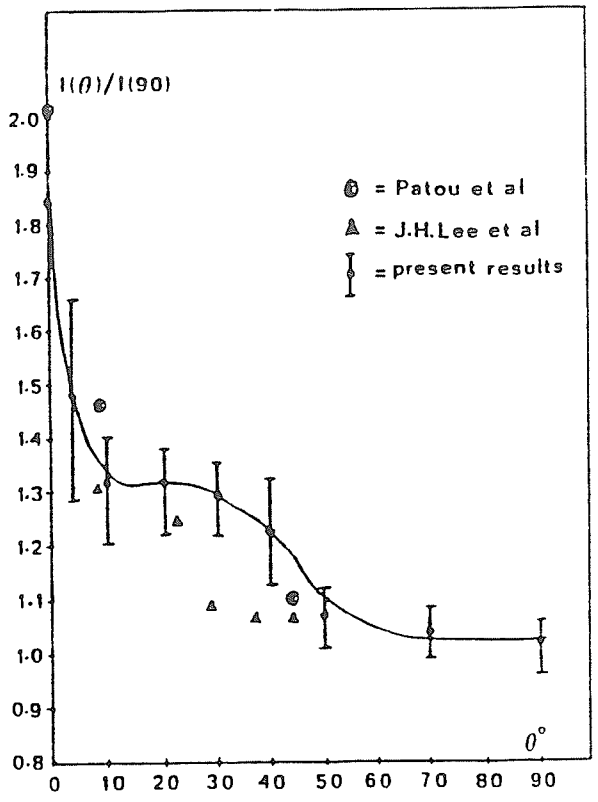

Fig. 10 Results of angular distribution of neutrons from plasma focus. (REf.42)

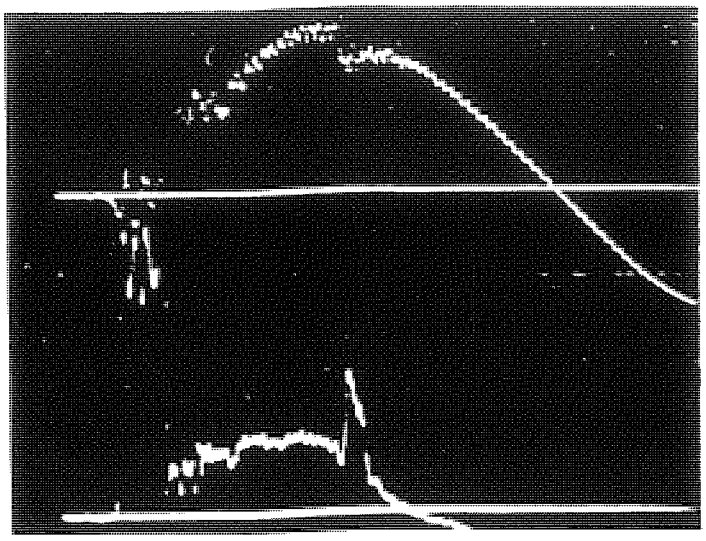

Fig. 11 *Typical current dip and voltage spike of a focusing shot. Top trace: current oscillogram: vertical scale: 200 kA per cm. Bottom trace: voltage oscillogram: vertical scale: 6 kV per cm, horizontal scale: 1 μsec per cm. The characteristic current dip and voltage spike of a good focus are evident at t = 4 μsec.*

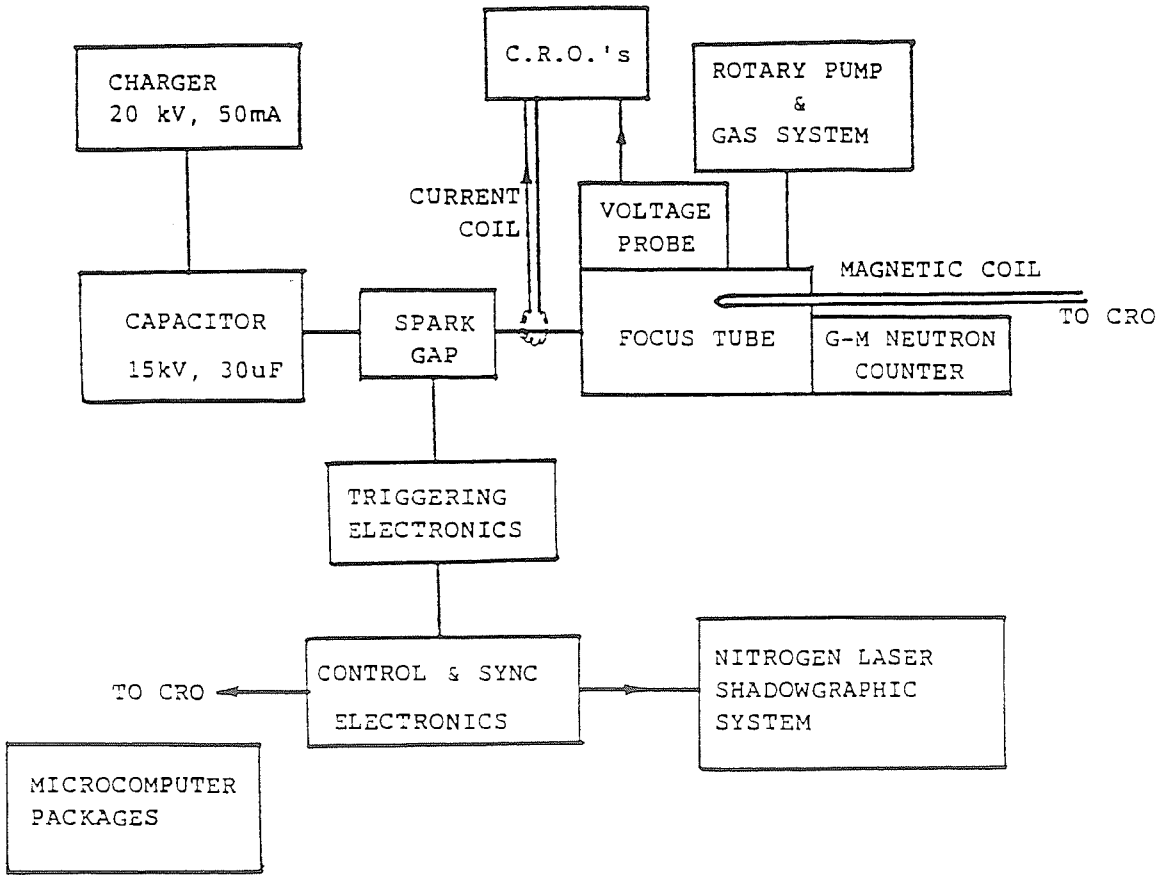

Fig. 12 Sub-systems for the UNU/ICTP PLASMA FUSION FACILITY

DYNAMIC THEORY OF THE PLASMA FOCUS

2.1 Review:

The plasma focus is now well established as a device by which a hot, dense plasma may be produced with consequent generation of fusion neutrons. The key technical and experimental features of this device are now well documented so that a simple functional device may be built without resorting to sophisticated technology. The situation concerning the theoretical treatment of the device is however quite different. The axial acceleration region poses no problem, but there has been no simple method of computing even the dynamics of the radial pinching phase. Potter[44] has set up a two-dimensional code which gives a detailed description of the axial acceleration phase as well as the radial pinching phase, However the code is complex and its accuracy during the axial acceleration phase had to be checked against the predictions of a simple one-dimensional snow-plow model. The radial implosion phase could not be checked against a simple physical model because none existed which could give even a physically acceptable quasi-equilibrium radius. Recently, Zakaullah[33] has developed a two-dimensional model with scaling parameters suitable for device design.

Simple physical models have been constructed for the plasma focus based on the snow-plow equation. As is well known this model when applied to a radial compression gives a zero-radius column. Attempts have been made to overcome this by devising a retarding kinetic pressure term. Other attempts use criteria for the minimum radius such as the Larmor radius. However Lee[29] has shown that these methods are not energy-consistent and therefore should be replaced by an energy-balance model which provides the correct end-point for the implosion trajectory, thus giving the correct quasi-equilibrium radius. Combining the conventional snow-plow model with an energy-balance criterion enables a complete energy-consistent trajectory to be obtained[43].

The snow-plow model however is essentially a structureless model. Potter[34] has suggested a slug model which he has applied to the specific case of a constant current, constant length pinch to obtain a collapsing layer with structure. We extend this slug model to the radial compression phase of the plasma focus, allowing the length of the pinching column and the plasma current to vary self-consistently.

2.2 The Plasma Focus Dynamics:

We shall consider two distinct phases of the plasma focus dynamics (a) the axial phase and (b) the radial pinch phase.

Figure 4 illustrates the two phases of the focus dynamics.

In this model when the capacitor at voltage V_o is switched onto the focus tube breakdown first occurs across the back-wall insulator. A current sheath is formed axisymmetrically. It lifts off from the backwall and is then propelled by its own $J_r B_\theta$ force down the annular channel in the z-direction. When the current sheath comes to the position $z = z_o$ the radial phase starts. The radial pinch proceeds as shown in Fig. 4b.

For the axial phase, we shall consider a snow-plow model in which when the current sheath is at position z, all its accumulated mass is also at position z. This is an approximation which does not give rise to any fundamental problem in the axial phase.

In the radial phase, however, if this 'thin' snow-plow model is used it will give rise to a compression to zero radius unless the compression is correctly terminated by an energy balance principle. However, if a slug-model (with structure) is used, a shock front will separate out from the current sheath (magnetic piston) and a finite thickness plasma layer will result. This layer will be propelled radially inwards by the $J_z B_\theta$ force. As the plasma layer collapses inwards the whole column elongates (since the compression is open-ended at one end). In the slug-model when the shock hits the axis, the piston stops and a quasi-equilibrium is formed. However, a check with energy balance indicates that the piston will continue to move a little so that the final quasi-equilibrium radius should be determined by energy balance.

It is well known that the majority of neutrons are produced in the break-up phase following the radial quasi-equilibrium described above. However no theory yet exists to explain this break-up phase; and we shall hence confine ourselves to the relatively well-ordered description of the dynamics of the axial and radial pinch phase; in the hope that an understanding of these phases could eventually lead to greater understanding of the final break-up phase.

The Axial Phase - Snow-plow Model:

The Equation of Motion

In the axial phase, consider that the current sheath scoops up (snow-plows) all the mass it encounters. Thus at a position z, the mass entrained by the sheath is:

$$\rho_o\{\pi(b^2 - a^2)z\} ;$$

and the rate of change of momentum of the sheath is:

motion: $$\frac{d}{dt}\{\pi\rho_o(b^2 - a^2)z\frac{dz}{dt}\} = \frac{\mu I^2}{4\pi}\ell n\frac{b}{a} \qquad (1)$$

where the right hand side is the force exerted by the self-magnetic field ($B = \mu I/2\pi r$) of the current sheath integrated over the whole current sheath between r=b to r=a. In this equation z and I, the circuit current, are in general functions of time. To determine the current I, the circuit equation is needed.

The Circuit Equation

The equivalent circuit of the focus tube is presented schematically below.

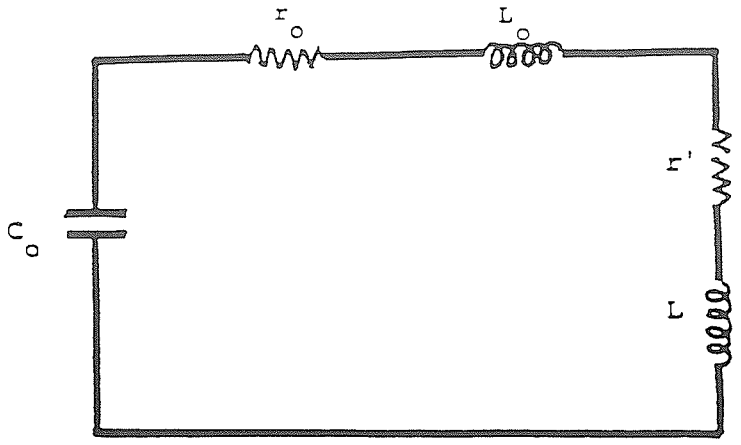

Equivalent circuit of plasma focus tube

Here C_o, L_o, r_o are the fixed capacitance, inductance and resistance of the external elements and r' and L are the plasma resistance and inductance respectively. Assume that r_o and r' are negligibly small, we may use Kirchhoff's second law to write the voltage equation for the

circuit. Thus:

$$\text{Circuit:} \qquad \frac{d}{dt}\{(L_o + L)I\} = V_o - \frac{\int_o^t I dt}{C_o} \tag{2}$$

where the plasma inductance may be written as a function of z:

$$L = \frac{\mu}{2\pi} \ln\frac{b}{a}\, z \tag{3}$$

Equation (3) thus may be written as:

$$\text{Circuit:} \qquad \frac{dI}{dt} = \frac{V_o - \frac{\int I dt}{C_o} - \frac{\mu}{2\pi} \ln\frac{b}{a} I\frac{dz}{dt}}{\{L_o + \frac{\mu}{2\pi} \ln\frac{b}{a}\, z\}} \tag{4}$$

Equations (1) and (4) are the two equations determining the behaviour of z and I.

Normalization

Equations (1) and (4) may be written in normalized form for the following purpose:

a) To simplify the system of equations so that its basic functional dependance may be seem more clearly,

b) To introduce scaling parameters which enable all ranges of operation of the shock tube to be covered simply by a variation of the scaling parameters. The identification of the correct scaling parameters is equivalent to identifying the ratios which govern the regimes of operation of the shock tube.

For the axial phase of the plasma focus there are two relevant ratios:

i) the ratio of the capacitor discharge time to the transit time of the sheath from z=0 to $z=z_o$.

ii) the ratio of L_o to the maximum tube axial inductance.

c) To obtain an expression for the characteristic transit time, which is derived naturally in the process of normalization.

The first step in normalization is to choose the correct reference quantities to normalize the variables. Here we take:

$$\zeta = \frac{z}{z_o}, \qquad \tau = \frac{t}{t_o}, \qquad i = \frac{I}{I_o}$$

where z_o = length of the axial phase,

$t_o = \sqrt{(L_o C_o)}$, the angular frequency of the L_o-C_o circuit (the short-circuited capacitor bank),

and $I_o = V_o/\sqrt{(L_o/C_o)}$, the peak current of the L_o-C_o circuit.

With this normalization, the equation of motion (1) becomes:

motion:
$$\frac{d^2\zeta}{d\tau^2} = \frac{\alpha^2 \iota^2 - (\frac{d\zeta}{d\tau})^2}{\zeta} \tag{5}$$

where the first scaling parameter is introduced as a ratio of the two characteristic times t_o and t_a:

$$\alpha = \frac{t_o}{t_a}$$

and t_a appears naturally as a characteristic axial transit time defined as:

$$t_a = \left\{ \frac{4\pi^2(b^2 - a^2)}{\mu \ell n \frac{b}{a}} \right\}^{\frac{1}{2}} \frac{z_o \rho_o^{\frac{1}{2}}}{I_o} \tag{6}$$

Similarly, the circuit equation becomes:

circuit:
$$\frac{d\iota}{d\tau} = \frac{1 - \int \iota d\tau - \beta \iota \frac{d\zeta}{d\tau}}{1 + \beta\zeta} \tag{7}$$

where the second scaling parameter is seen to be a ratio of two inductances:

$$\beta = \frac{\frac{\mu}{2\pi} \ell n \frac{b}{a} z_o}{L_o}$$

Equations (5) and (7) may be integrated to give the solution of ι and ζ.

Initialization

The initial conditions are:

$$\tau = 0, \quad \zeta = 0, \quad \frac{d\zeta}{d\tau} = 0, \quad \frac{d^2\zeta}{d\tau^2} = \sqrt{(\frac{\alpha^2}{3})}, \quad \iota = 0$$

$$\frac{d\iota}{d\tau} = 1 \quad \text{and} \quad \int \iota d\tau = 0$$

Integration

Equations (5) and (7) may now be integrated for any selected

values of α and β. Even a linear method such an Euler's give sufficient accuracy with time step of $\Delta\tau = 0.001$.

The integrations stops at $z = z_o$.

The Radial Compression Phase:

Radial Shock Motion

Figure 4b shows the geometry of the compressing column. At a given time t the magnetic piston has moved to the position r_p from 'a' driving a shock front ahead of it at position r_s. All the gas encountered by the shock front in its journey from 'a' to r_s is now contained between r_s and r_p. This forms a 'slug' of plasma. Because of the diverging streamlines through the region bounded by r_s and r_p conditions through the slug are in general functions of r and may not be considered to be uniform from one value of r to another at any given time t. However because the shock-front is assumed to be thin the planar shock-jump equations hold across the shock front.

In the radial phase the magnetic piston is knwon to be highly supersonic and therefore the sound speed in the slug is large compared to the particle speed. Under these conditions we may make the assumption that the one quantity that may be taken as uniform across the slug is the pressure P. Thus this pressure P may be related by the shock-jump equations to the shock speed $v_s = dr_s/dt$ as: (see Ch. VI Sec. 2.12 of this Volume)

$$P = \frac{2}{\gamma + 1} \rho_o v_s^2 \tag{8}$$

Further, at the magnetic piston we may equate the pressure P to the magnetic pressure P_B so that: (see Ch. VI Sec. 2.9 of this Volume)

$$P = P_B \tag{9}$$

where
$$P_B = \frac{\mu I^2}{8\pi^2 r_p^2} \tag{10}$$

Thus from Eqns. (8) to (10) we have:

radial shock motion
$$v_s = \frac{dr_s}{dt} = -\left\{ \frac{\mu(\gamma+1)}{\rho_o} \right\}^{\frac{1}{2}} \times \frac{I}{4\pi r_p} \tag{11}$$

where the negative sign indicates radial inward motion.

Axial Shock Motion

Since the compression is open at one end we expect an axial shock to be propagated in the z-direction. Further we may assume that the pressure driving the radial shock is the same as that driving the axial shock. Thus, the length of the radial compression z_f increases during the compression and this is one of the major factors responible for the high compressions in the plasma focus. We may write

Axial shock motion:
$$\frac{dz_f}{dt} = -\frac{dr_s}{dt} \tag{12}$$

The Circuit Equation

The circuit equation for the system in the pinch phase may be written in the same manner as in Eqn. (2); but we note that now:

$$L = \frac{\mu}{2\pi}\left(\ell n\frac{b}{a}\right)z_o + \frac{\mu}{2\pi}\left(\ell n\frac{b}{r_p}\right)z_f \tag{13}$$

where both z_f and r_p vary. Thus the circuit equation may be written as:

circuit equation
$$\left\{L_o + \frac{\mu}{2\pi}\left(\ell n\,\frac{b}{a}\right)z_o + \frac{\mu}{2\pi}\left(\ell n\,\frac{b}{r_p}\right)z_f\right\}\frac{dI}{dt}$$
$$+ I\frac{\mu}{2\pi}\left(\ell n\,\frac{b}{r_p}\right)\frac{dz_f}{dt} - I\frac{\mu}{2\pi}\frac{z_f}{r_p}\frac{dr_p}{dt} = V_o - \frac{\int I dt}{C_o} \tag{14}$$

Radial Piston Motion

Equations (11), (12) and (14) are insufficient to define the problem since there are four variables r_s, r_p, z_f and I to be determined as functions of time. The fourth equation may be obtained by applying the adiabatic expansion law to a fixed mass of gas in the slug at any given instant. For this we write:

$$PV^{\gamma} = \text{constant} \tag{15}$$

$$\text{or}\quad \frac{\gamma dV}{V} + \frac{dP}{P} = 0 \tag{16}$$

where γ is the effective specific heat ratio of the plasma and the volume of the slug is:

$$V = \pi(r_p^2 - r_s^2)z_f \tag{17}$$

To eliminate V from Eqn. (16) we need to differentiate Eqn. (17) to obtain dV as a function of dr_p, dr_s and dz_f. To do this we need to

consider very carefully so that the differential quantities dr_p, dr_s and dz_f are applied to a fixed mass of gas. For example when the piston moves by dr_p no new mass of gas is introduced into the corresponding new volume V + dV. However when the shock front moves from r_s to $r_s + dr_s$ it admits into the new volume V + dV a new mass of gas. This new mass of gas is compressed by a ratio $(\gamma+1)/(\gamma-1)$ and will occupy part of the increase in volume, so that the actual increase in volume available to the original mass of gas in volume V does not correspond to the increment dr_s but to an effective (reduced) increment $dr_s x2/(\gamma+1)$. This also applies to the increment dz_f.

Thus to apply the adiabatic law of Eqn. (16) to the slug we need to write the differential of Eqn. (17) in the following form:

$$dV = 2\pi(r_p dr_p - \frac{2}{\gamma+1} r_s dr_s) z_f + (r_p^2 - r_s^2)\frac{2\pi}{\gamma+1} dz_f \qquad (18)$$

giving us:

$$\frac{dV}{V} = \frac{2(r_p dr_p - \frac{2}{\gamma+1} r_s dr_s) z_f + (r_p^2 - r_s^2)\frac{2}{\gamma+1} dz_f}{z_f(r_p^2 - r_s^2)} \qquad (19)$$

We may also eliminate dP/P from Eqn. (16) by writing from Eqn. (8) and Eqn. (11):

$$\frac{dP}{P} = \frac{2dv_s}{v_s} = 2\left(\frac{dI}{I} - \frac{dr_p}{r_p}\right) \qquad (20)$$

Substituting Eqns. (19) and (20) into Eqn. (16) and rearranging we obtain the adiabatic law in the following form:

Radial piston motion

$$\frac{dr_p}{dt} = \frac{\frac{2}{\gamma+1}\frac{r_s}{r_p}\frac{dr_s}{dt} - \frac{r_p}{\gamma I}\left(1 - \frac{r_s^2}{r_p^2}\right)\frac{dI}{dt} - \frac{1}{\gamma+1}\frac{r_p}{z_f}\left(1 - \frac{r_s^2}{r_p^2}\right)\frac{dz_f}{dt}}{(\gamma-1)/\gamma + (1/\gamma)\, r_s^2/r_p^2} \qquad (21)$$

Normalization

The four equations (11), (12), (14) and (21) form a close set of equations which may be integrated for r_s, r_p, z_f and I. For this phase the following nomalization procedure is adopted:

$\tau = t/t_c$, $\iota = I/I_o$ as in the axial phase but with

$$\kappa_p = r_p/a, \quad \kappa_s = r_s/a \quad \text{and} \quad \zeta_f = z_f/a .$$

This gives us, after re-arrangement, the set of equations representing the generalized slug model in normalized form as follows:

Radial shock
$$\frac{d\kappa_s}{d\tau} = -\alpha\alpha_1 \iota/\kappa_p \tag{22}$$

Axial shock
$$\frac{d\zeta_f}{d\tau} = -\frac{d\kappa_s}{d\tau} \tag{23}$$

Radial piston
$$\frac{d\kappa_p}{d\tau} = \frac{\frac{2}{\gamma+1}\frac{\kappa_s}{\kappa_p}\frac{d\kappa_s}{d\tau} - \frac{\kappa_p}{\gamma\iota}\left(1 - \frac{\kappa_s^2}{\kappa_p^2}\right)\frac{d\iota}{d\tau} - \frac{1}{\gamma+1}\frac{\kappa_p}{\zeta_f}\left(1 - \frac{\kappa_s^2}{\kappa_p^2}\right)\frac{d\zeta_f}{d\tau}}{(\gamma-1)/\gamma + (1/\gamma)\,(\kappa_s^2/\kappa_p^2)} \tag{24}$$

Current
$$\frac{d\iota}{d\tau} = \frac{1 - \int \iota d\tau + \frac{\beta_1}{F}(\ell n \kappa_p/c)\iota\frac{d\zeta_f}{d\tau} + \frac{\iota\beta_1}{F}\frac{\zeta_f}{\kappa_p}\frac{d\kappa_p}{d\tau}}{\{1 + \beta - (\beta_1/F)(\ell n \kappa_p/c)\zeta_f\}} \tag{25}$$

where $c = b/a$ and $F = z_o/a$. The new scaling parameters introduced for the pinch phase are:

$$\alpha_1 = \{(\gamma+1)(c^2-1)\}^{\frac{1}{2}}\, F/(2\ell nc) \quad \text{and} \quad \beta_1 = \beta/\ell nc .$$

Thus whereas the scaling factors α and β enable the axial phase to be scaled for ratios of capacitor to axial run-down times and axial phase inductance to external inductance, the scaling factors $\alpha\alpha_1$ and β_1 allow the radial phase to be scaled for ratios of capacitor to radial pinch times and for characteristic pinch to external inductances.

The radial phase starts after the axial phase reaches $\tau = \tau_a$ at which time: $\zeta = 1$, $\iota = \iota_a$, $\kappa_s = 1$, $\kappa_p = 1$, and $\zeta_f = 0$.

The radial phase ends when $\kappa_s = 0$ at which time the shock front has reached the axis and the position of κ_p represents κ_m the radius of the quasi-equilibrium column for the pinch phase of the plasma focus.

2.3 Integration:

The integration of Eqns. (5) and (7) and subsequently Eqns. (22)

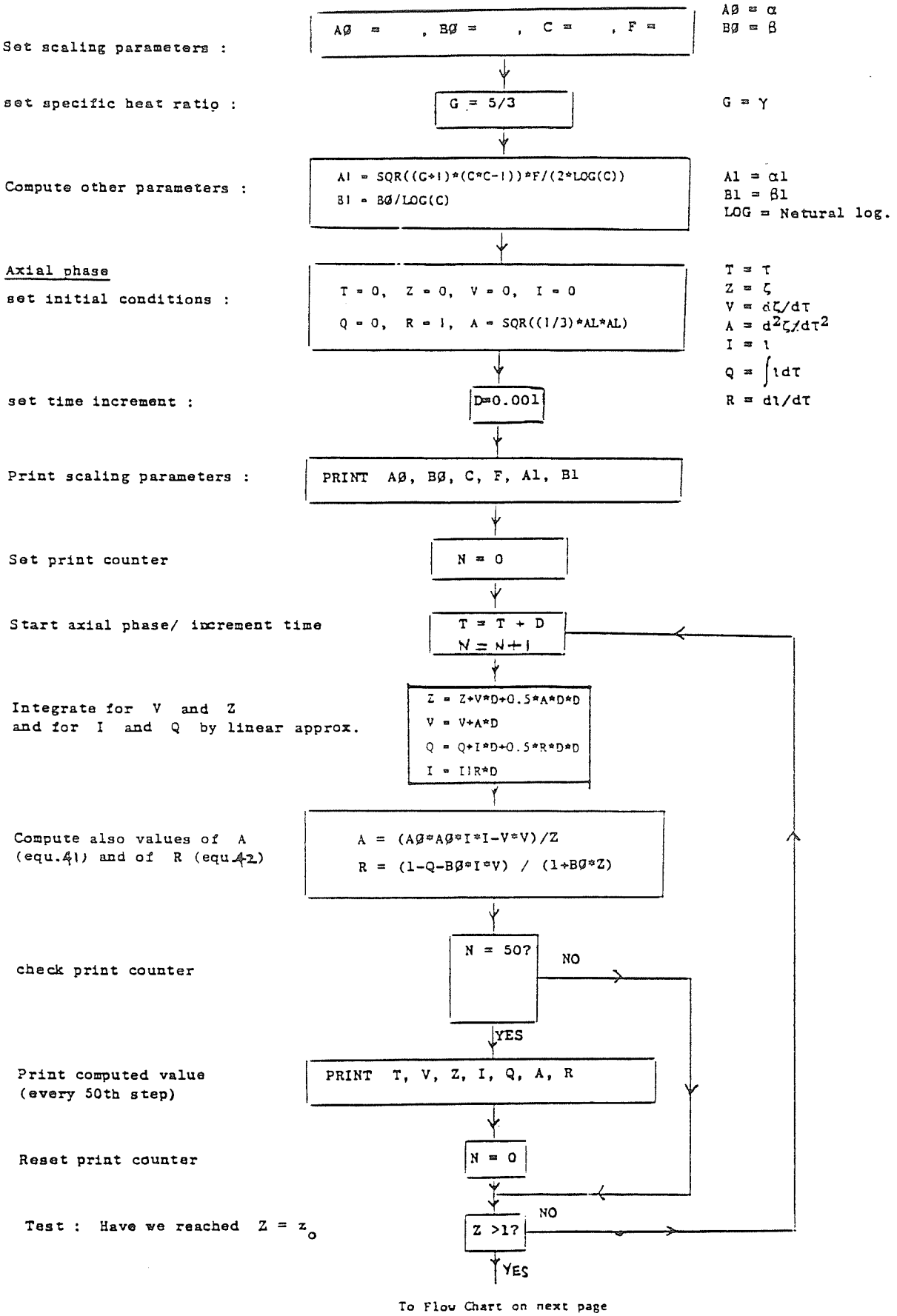

Fig. 13 Flow Chart of Plasma Dynamics Computation of Plasma Focus

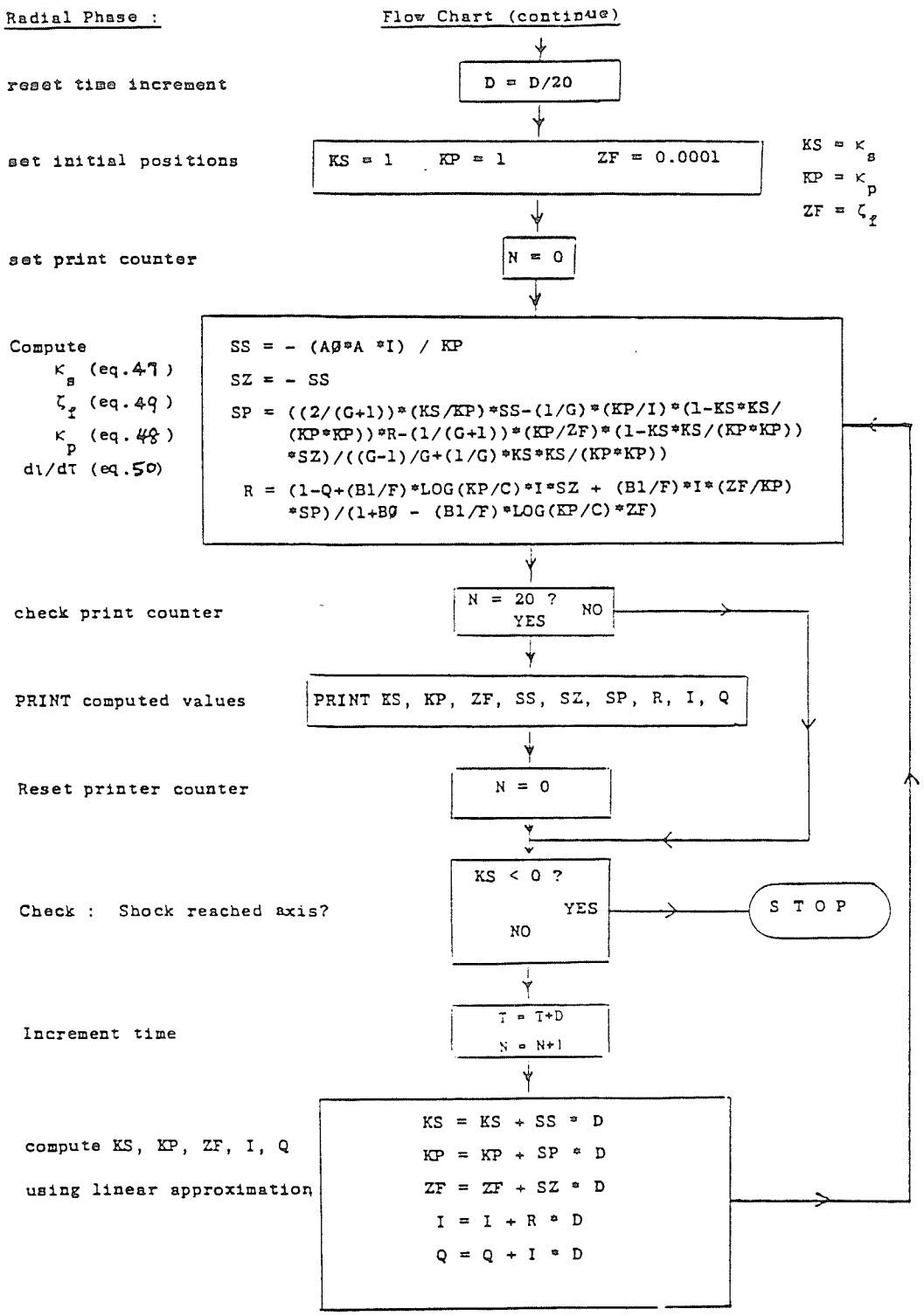

Fig. 13 (continued)

to (25) has been performed using a simple linear approximation method which was checked against a Runge-Kutta method and found to be of sufficient accuracy when 1000 time-steps were taken in each phase[56]. The program runs well in the BASIC language. The flow chart is shown in Fig. 13.

2.4 Results and Discussion:

A typical set of results is shown in Figs. 10a and 10b. Figure 10a shows the trajectory ζ versus τ in the axial phase and the current waveform ι versus τ for both phases. It is seen that already in the axial phase the current has flattened out and reaches a peak value of $0.6I_o$ at around $\tau=1.2$. The slight but clearly noticeable dip in the current just past $\tau = 1.6$ corresponds to the radial collapse phase. The trajectories of this phase κ_p and κ_s versus τ are shown in Fig. 10b on expanded time-scale. For the condition of: $a=1.5$, $b=1.0$, $F=6.4$, $\gamma=5/3$ and $c=3.4$ it was found that the quasi-equilibrium radius ratio of the plasma focus pinch is 0.16.

This model presents a relatively simple way for computing the plasma focus trajectory with a quasi-equilibrium radius ratio. The simplicity and low computing requirements of the model makes it very useful for design and optimization studies. The coupling mechanism between the plasma and the magnetic field has been assumed to be purely electromagnetic and this limits the accuracy of the model towards the end of the trajectory as the quasi-equilibrium column is being formed. This is because towards the end of the pinch phase the electron Hall parameter attains values greater than unity and the plasma may become anomalously resistive. This effect, not included in the present dynamic model probably plays a dominant role in the experimentally observed complex structure and dynamics of the actual plasma focus in its phases subsequent to the pinch phase we have discussed.

2.5 Energy Balance Theory for the Quasi-Equilibrium Radius Ratio:

Is the end point of the slug model consistent with energy balance?

For a fast radial compression with no losses it has been found[24,35,43] that the quasi-equilibrium radius is defined from a consideration of energy and pressure balance. These balance conditions give the following

$$\iota_m^2 = \frac{2(\gamma-1)}{f_{rs}\ell_m}\int_{\kappa_m}^{1}\frac{\iota^2\ell d\kappa}{\kappa} \qquad (26)$$

where f_{rs} = reflected shock overpressure,

ι_m = normalized current at the time quasi-equilibrium is reached,

ℓ_m = length of the compressed column at quasi-equilibrium,

and κ_m = radius ratio at quasi-equilibrium.

As an approximation to solve this integral we may assume that during the radial phase ι = constant and $\ell = a-r$ (as indicated by the slug model). Then for $\gamma = 5/3$ and $f_{rs} = \gamma$, the energy balance condition of Eqn. (21) gives

$$\kappa_m = 0.15 \ .$$

Thus the energy balance theory predicts that the radius of the focus pinch column is reduced further from 0.16 (pinch ratio when shock hits axis according to slug model) to a final value of 0.15 . The approximate values of the pinch focus ratios and the further compression (after the shock goes on-axis) have been observed in streak photographs for both deuterium and argon plasma focus[46], and in recent x-ray photographs[47].

Recent observations have shown that when the shock front hits the axis the piston continues to move as though "it were not aware that the shock front had hit the axis". This is of course as expected since the information that the shock front had hit the axis is only communicated to the piston at the local small disturbance speed. The local small disturbances created by the shock front hitting the axis propagates radially outwards in coalescence as the reflected shock wave so that the piston is only aware of these events when hit by the reflected shock front. This is, of course, in variance with the slug model; the breakdown of the model in this region being due to the importance of the fact that the small disturbance speed is not infinite. A simple and may be effective empirical method to complete the solution may be simply to decouple the piston, as suggested by the experimental observations, letting it move in freely until it hits the reflected shock. The trajectory of the reflected shock may be estimated from Guderley's paper[55].

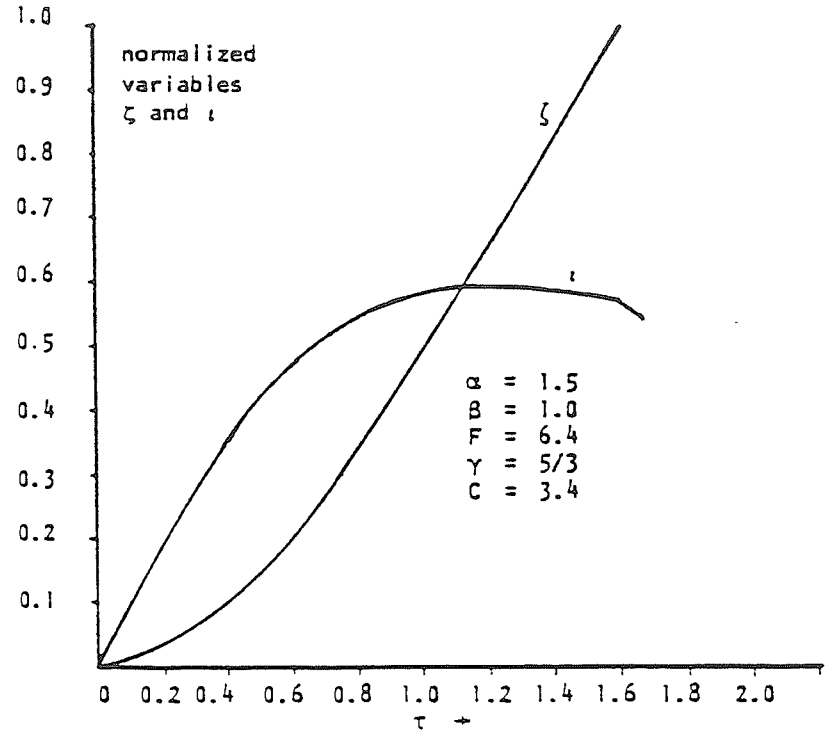

Fig. 14a Solutions of ζ and ι as functions of τ-axial phase

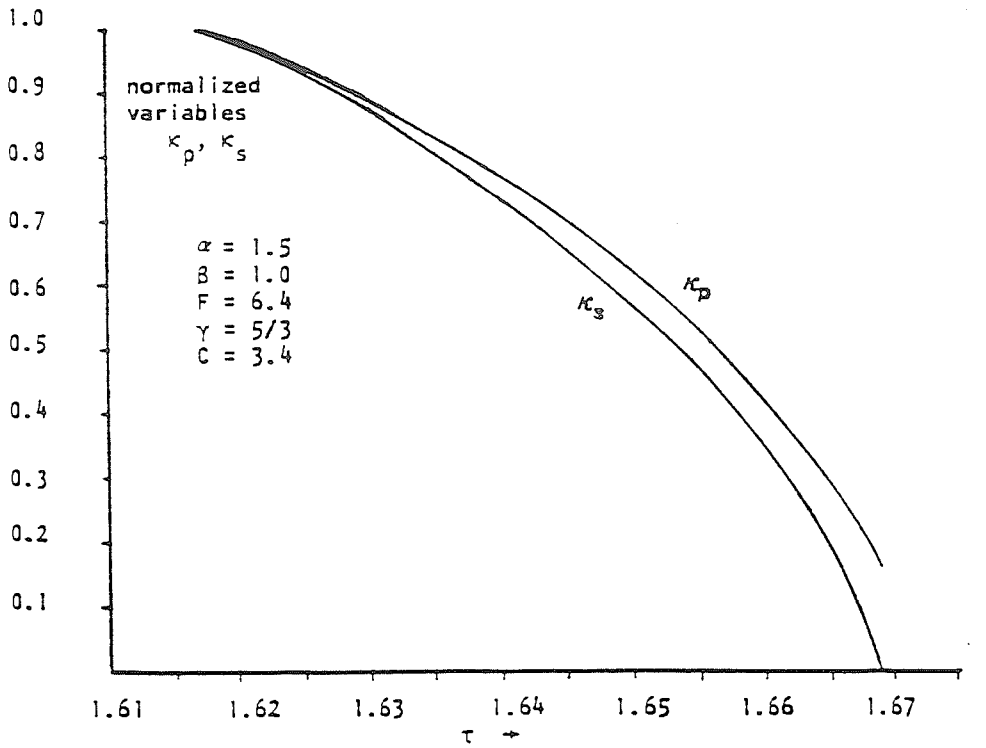

Fig. 14b Solutions of κ_p and κ_s as functions of τ - radial phase

DESIGN OF THE PLASMA FOCUS EXPERIMENT

3.1 Cost Effective Physics:

In order to implement a project whereby a developing country may produce a suitable package for sharing technology with other developing countries with the aim of initiating experimental plasma research it is necessary to consider the cost effectiveness of the device to be chosen. Does it produce a rich variety of plasma phenomena? Does it require an expensive vacuum system? Can its power supplies, control electronics and basic diagnostics be packaged at reasonable cost? What physical mechanisms operate to make the chosen device perform better at lower packaging cost than other devices? Can we understand and model the design and performance of the device so that we may effectively do research on it? What are the areas of research and potential applications of the device?

From the point of view of the production of a plasma with conditions of density and temperature sufficient for plasma fusion studies at an affordable cost there is little doubt that the class of fast magnetic compression devices known generally as the pinch, including the linear z-pinch, the superfast pinch, the gas-puff pinch and the plasma focus offers the best potential. We have considered this class of device and found that the plasma focus is most cost effective having the same power supply, control electronics and basic diagnostic requirements as the simple z-pinch and a much cheaper vacuum system with only rotary pump requirement, yet producing more intense plasma phenomena including copious x-rays, relativistic electron beam (REB) and fusion neutrons, all in one small easily packaged facility. What is the physics behind this cost effectiveness?

3.2 Cost Effectiveness of Various Types of Pinches:

We first recall that the neutron yield Y from a plasma fusion source is:

$$Y = \tfrac{1}{2}n^2 \langle\sigma v\rangle \quad \text{(volume)(time)} \tag{27}$$

We note that Y is proportional to the square of n, the number density of the fusion fuel. We also note that starting from temperatures below 1 keV as one struggles to heat a plasma up towards a few keV, the effective cross section $\langle\sigma v\rangle$ for a thermalised deuterium plasma rises very rapidly with fuel temperature T. For example between 1 to 2 keV, $\langle\sigma v\rangle$ for the D-D fusion reaction goes up by a factor of 25! - and between 2 to 5 keV, another factor

of 30!. Thus the neutron yield is very sensitive to temperature. It is also proportional to the square of density.

In the pinch a large electric current is discharged from a capacitor bank through a gas between two electrodes. The current rises rapidly and due to the skin effect and wall conditions, electric breakdown first occurs across the glass wall of the container, forming a sheath of current along the glass wall. The electromagnetic $\underline{J}\times\underline{B}$ force in such a geometry acts radially inwards at every point of the current sheath so that, if the current is large enough, the current sheath and the heated gas (plasma) it entrains implode supersonically to form a hot dense column around the axis of the device.

The condition of balance between the hydrostatic pressure of the hot plasma and the constricting magnetic pressure gives the equation for the plasma temperature as:

$$T = \frac{\mu_o I^2}{8\pi N} \tag{28}$$

where $N = \pi n r^2$ is the line density (particles m^{-1}) of the pinch. From this equation it would appear that since the temperature T depends on I^2 any temperature can be reached simply by increasing I to a sufficient value. However a pinch is essentially a dynamic device. The formation of the column has to occur in a time matched to the risetime of the current pulse, otherwise essentially the column is no longer there to obey the pressure balance equation when the current has risen to its peak value. Because of the dynamic nature of the problem the final temperature reached depends also on the implosion speed of the front of the plasma layer, which takes the form of a strong shock front. For deuterium the temperature dependence has the form:

$$T = 2.3 \times 10^{-5} \quad (\text{shock speed})^2 \tag{29}$$

Because of the dynamic nature of the problem it is essential for optimum use of the capacitor energy for the imploding shock wave to reach the axis at about the time of peak current. Now a typical well-designed capacitor bank for a pinch (say 20 kV, 60 μF, low inductance) has a current risetime of about 3 μs. In general it is difficult (and expensive) to design a capacitor bank of this conventional type for a much shorter risetime, and the bigger the bank capacity the longer tends to be the risetime.

So we consider a typical current risetime of 3 μs. A typical implosion speed cannot be much less than 10 cm/μs. At this speed the shock temperature in deuterium is 2×10^5 K, any slower and it is doubtful whether the magnetic 'piston' would be clearly formed. Even at this slow speed a radius of 30 cm for the pinch tube is required in order to match the current risetime. Now the imploding magnetic pressure is

$$P_m = \frac{\mu_o I^2}{8\pi^2 r^2} \qquad (30)$$

and with such a large pinch tube radius it is difficult to get enough magnetic pressure in the early stages of the implosion to start a clean compression unless the gas pressure is low. Thus a conventional pinch is limited by a (slow) current risetime of 3 μs, so that the pinch has to be operated with a large radius and hence low initial density. Moreover the speed (and hence temperature) becomes limited because of time-matching consideration.

What about the compressed density? Equation (26) gives us the following useful information:

(a) κ_m (and hence the compressed density ratio $\Gamma = \kappa_m^{-2}$) does not depend on the absolute magnitude of the current or the absolute length of the pinch.

(b) κ_m (hence Γ) depends on the time fuction of the current[5] and length.

(c) κ_m (hence Γ) depends on γ and f_{rs}. The smaller is γ, the smaller is κ_m and the larger is Γ[54]. As γ approaches the lower limiting value of 1, κ_m approaches zero and Γ tends to infinity. The larger is f_{rs}, the smaller is κ_m and the larger is Γ. The value of f_{rs} for a reflected shock on-axis, i.e. just after reflection is $f_{rs} \simeq 4$ for cylindrical geometry[58]. As the reflected shock travels out from the axis we may expect f_{rs} to decrease towards a limiting value of 1.

For example for a constant current pinch with constant length, with $\gamma = 5/3$ and $f_{rs} = 1.6$, Eqn. (26) gives $\kappa_m = 0.301$ and hence a density compression ratio of $\Gamma = 11$. The corresponding figures for the deuterium plasma focus are estimated to be $\kappa_m = 0.14$ and $\Gamma = 50$. These values are independent of the magnitude of the plasma current. This limitation of the ability to compress is a serious one and implies that the performance of the pinch as a radiation source depends on its initial density.

There are several concepts to overcome this limitation. The gas-embedded axis-initiated z-pinch uses a laser to start a pinch discharge on-axis thus obviating the problem of matching the electrical risetime to the pinch collapse time and allowing the formation of a very small radius pinch (sub mm radius) in a very dense plasma (initial density up to several atmospheres). The device is however plagued with problems of instability[38]. The hollow pinch uses a controlled gas jet to form a thin plasma sheath which is then pinched into a vacuum. Using argon, krypton or xenon, the sheath does not thicken very much during the implosion because these gases[54] are in the 'freely ionizing' regime with a γ value having a small value of the order of 1.1. Because of the short distance between the imploding shock front and the magnetic piston the reflected shock from the axis hits the piston after a much shorter distance than that compared with a conventional pinch. The value of f_{rs} is hence closer to 4 than in a conventional pinch with its thicker plasma sheath. Thus the hollow-pinch has a reduced κ_m and has been operated successfully in the heavier gases, particularly krypton and xenon, for the production of x-rays for x-ray lithography and microscopy. However from the technical point of view the hollow pinch requires the additional development of a rather precise gas valve system. It is also not known to operate well in deuterium, probably because the collapsing deuterium sheath thickens as its γ goes to 5/3 once the sheath reaches a speed of the order of 10 cm/μs.

Ultra high power pinches have also been operated with pulse forming lines to reduce current risetimes so that the pinch may be operated at smaller radius, hence higher density[38]. This high power approach adds more complex and expensive technology.

3.3 Cost Effective Feature of the Plasma Focus:

On the other hand the plasma focus uses a very simple principle to overcome the time mismatch. Essentially it allows a conventional (slow risetime of 3 us or more) capacitor bank to drive a very fast pinch (typically 1 cm radius in 50 ns) at a sufficiently high density and a large current during the time of pinch. Thus at low cost plasma conditions may be achieved which are more intense than that produced even in high-cost pinches.

The plasma focus uses a conventional capacitor bank to drive a device which has two sections:- the first section is a coaxial electromagnetic shock tube whose length is matched to the capacitor risetime. The rising capacitor current drives a shock wave axially down the shock tube at a suitable speed until the shock wave reaches the end of the tube at peak current. Then by the geometry of the device (see Fig. 4) the axial drive phase is simply converted to a radial compression or pinch phase.

The pinch phase is very intense (see Eqns. 28 and 30) because it starts at a very large current (typically 500 kA) and at a relatively small radius (typically 1 cm). Thus the operating pressure may be relatively high (10 torr in D_2 for a plasma focus against 0.1 torr or less for a pinch). The increased density and temperature more than compensates for the reduced volume in terms of the neutron yield Y as given in Eqn. (27).

Having seen from the basic physics mechanism that the plasma focus is capable of high levels of performance without special technological development the next step in the development of an educational package is to consider the modelling and design of a practical device.

3.4 Cost Effective Design of a Plasma Focus:

Design of the plasma focus may be based on the dynamic model, described in Chapter 2, which considers the focus dynamics in two separate phases - the axial run-down (shock tube) phase which crucially delays the radial focus, or pinch phase until the plasma current has reached its peak value (see Fig. 4). The first design point is therefore to have:

$$t_r = t_{a\ exp} \tag{31}$$

where

$$t_r = \frac{2\pi}{4} t_o \tag{32}$$

with

$$t_o = \sqrt{L_o C_o} \tag{33}$$

and

$$t_{a\ exp} \sim 2t_a \tag{34}$$

where

$$t_a = 2\pi \left[\frac{(c^2-1)}{\mu \ell n c}\right]^{\frac{1}{2}} \frac{z_o \rho_o^{\frac{1}{2}}}{(I_o/a)} \tag{35}$$

Equation (35) comes from the equation of motion of the axial phase and Eqn. (34) from an analysis of the trajectory.

Here t_r is the current risetime and $t_{a\ exp}$ is the transit time of the plasma layer for the axial phase. The quantities t_o and t_a are characteristic times of the axial phase according to the model. Here L_o is the inductance of the capacitor C_o together with all connections up to the plasma section of the focus tube, $c = b/a$, 'a' and 'b' are respectively the inner and outer radii of the focus tube, z_o its length, ρ_o the ambient gas density, μ the permeability of the plasma (same as the permeability of free space) and

$$I_o = V_o/(L_o/C_o)^{\frac{1}{2}} \tag{36}$$

where V_o is the initial voltage on the capacitor.

The second design point involves the characteristic 'pinching' time of the plasma focus phase. This may be shown from the equations of motion of the radial phase to be

$$t_p = \frac{4\pi}{\mu^{\frac{1}{2}}(\gamma+1)^{\frac{1}{2}}} a \frac{\rho_o^{\frac{1}{2}}}{(I_o/a)} \tag{37}$$

where γ is the specific heat ratio of the plasma. From this expression of t_p it is noted that the ratio of the characteristic axial transit time to characteristic focus time is

$$\frac{t_a}{t_p} = \frac{(\gamma+1)^{\frac{1}{2}}}{2} \frac{(c^2-1)^{\frac{1}{2}}}{(\ell nc)^{\frac{1}{2}}} F \tag{38}$$

where $F = z_o/a$.

A crucial factor in the operation of the Mathers plasma focus is that the axial phase occurs over a relatively long period $t_{a\ exp}$ enabling the build up of capacitor current. The pinch phase then occurs over a relatively short period t_p. During this time t_p approximately 10-20% of the initially stored energy is transferred to the pinch plasma in approximately 2% of the current risetime. This results in a power enhancement factor during the pinching phase which is crucial to the operation of the plasma focus. It is important then that the ratio t_a/t_p be of the order of 30 - 50 for the Mathers focus. Incidentally this results in a ratio of radial speed to axial speed of 2.5 for almost all plasma focus machines, large or small.

The third point to be considered in the design is that there are limits[56] of speed and pressure in the operation of the plasma focus. In deuterium for good focussing and consistent neutron yield, the axial speed just before focussing should be between the limits 6-10 cm/μs; the lower limit being the minimum speed required for a good snowplowing action in the axial phase and the higher limit being imposed by restriking of the discharge at the backwall or in the shock tube section. The limits of test gas pressure appears to be between 0.5 torr to 20 torr for deuterium; the lower limit apparently governed by re-striking; the upper limit by current filamentation.

The design of a plasma focus may take as a starting point the availability, or choice, of a capacitor bank. For the present exercise from the point of view of economy and cost-effectiveness a single Maxwell capacitor rated at C_o = 30 μF, V_o = 15 kV with an equivalent series inductance, ESL, of less than 40 nH was selected. A parallel-plate geometry was selected for the capacitor connections and the switch, with coaxial cables being used to connect the plasma focus input flanges. The value of L_o was estimated at 110 nH. Having fixed C_o and L_o Eqns. (33) and (32) give a value of t_r of 2.9 μs. Eqn. (36) yields I_o = 248 kA. The time matching condition of Eqn. (31) fixes $t_{a\ exp}$ at 2.9 μs. The value of z_o was then chosen at 16 cm to give an average axial speed of 5.5 cm/μs or a peak axial speed[10] of ∿9 cm/μs just before the focus phase. This axial speed is expected to be suitable for a good focussing action in deuterium.

The value of I_o is considerably smaller than most operational plasma focus machines which typically have I_o of the order of 500 kA or more. Observing from Eqn. (35) that the axial speed is $\sim I_o/(a(c^2-1)^{\frac{1}{2}}\rho_o^{\frac{1}{2}})$ and from Eqn. (37) that the radial speed is $\sim I_o/(a\cdot\rho_o^{\frac{1}{2}})$ it is noted that a reduction in I_o may be compensated in the first instance by a reduction in 'a' in order to maintain the axial speed within the speed limit indicated earlier. Thus we design for a = 9.5 mm and b = 32 mm which are smaller than typical values of most operational plasma focus devices. Moreover the value of $\frac{b}{a} \sim 3.4$, in this case, is near optimum. It is also noted that the value $t_a/t_p \simeq 40$ for this design.

Having fixed the values of I_o, z_o, b and a and t_r it remains to fix the value of ρ_o from Eqn. (35). This gives $\rho_o = 0.21 \times 10^{-3}$ kgm^{-3}. This is the density of deuterium at 0.9 torr, which is within the pressure limits for deuterium focus operation as mentioned earlier.

The above design parameters have been subjected to a computation using the dynamic model in which the axial trajectory is computed using a snowplow model and the radial dynamics is traced using a generalized slug-model which considers the pinching plasma of increasing length with the plasma layer lying between a shock front at position r_s and magnetic piston at position r_p (see Fig. 4). This model has the advantage of giving a realistic final pinch radius ratio. Using the design parameters for the present device, the scaling parameters for the generalized slug model are:

$$\alpha = \frac{t_o}{t_a} = 1.26, \qquad \text{and } \beta = \frac{L_a}{L_o} = 0.36 ,$$

where L_a = maximum inductance of axial phase = $z_o(\mu/2\pi)\ell nc$. Also

$$\alpha_1 = \frac{t_a}{t_p} = 40.0 , \quad \text{and } \beta_1 = \frac{\beta}{\ell nc} = 0.294 .$$

The other parameters used for the model are c = 3.37, F = 16.84 and γ = 5/3 (for fully ionized deuterium).

The computation indicates a strong focus with a large focussing voltage spike. The parameter α was varied between 0.7 to 1.5 (corresponding to pressure range of 0.5 torr to 2 torr) and the computation repeated at each α. Good focussing was indicated over this range of pressure. These computation results add confidence to the design of the plasma focus. However it has been found that machine effects such as current and mass shedding[56], reduced channel size due to boundary effects and current re-strike which are not included in the dynamic model may alter the actual performance of the plasma focus. It is therefore to be expected that in actual operation the focus may need to be tuned by a variation of the five parameters V_o, ρ_o, z_o, a and b. If the design is not too far from optimum, operation over a range of ρ_o may be sufficient to establish a regime of good focus.

3.5 Scaling of Neutron Yield:

Experimental data on neutron yield have indicated a scaling law for neutron yield per pulse Y as a function of capacitor energy E. This scaling law (for operation in deuterium) may be written approximately as:

$$Y = 10\ E^2 \qquad (39)$$

where E is in joules; and appears to be approximately followed over the whole range of energy over which data is available i.e. 1 kJ to 1 MJ.

This scaling law may only be used with care since this scaling must depend on how efficiently the energy is coupled into the focus region. In other words, 2 devices having the same storage energy could be expected to have quite different yields unless they have been optimised within similar ranges of parameters such as external inductance and capacitor voltage.

A similar scaling law with tube current has been deduced from experimental data as:

$$Y \sim I^{3.3} \qquad (40)$$

This rule has to be used even more carefully for several reasons. The first reason is that for the two scaling laws to be both true implies that those devices whose data contribute to the deduction of the laws must have been operated with a fixed relationshop between E and I. Secondly the neutron production should probably be scaled to the focus current rather than the tube current, as it is known that these two currents are not the same and it has not been proven that the focus current is always a fixed fraction of the tube current for all devices.

However this does not mean that the scaling laws have no use. Most capacitors used for focus work are in the voltage range of 20 - 40 kV and are connected so that the total bank (stray) inductance is in the region of 20 - 40 nH. The ratio b/a is in the range 2 - 3.5 and with a capacitance of 20 - 100 μF, most of these devices can be similarly optimised so that corresponding to an energy of 1 kJ one can expect reliable neutron production $N \sim 10^7$ per pulse. In the other extreme of 1 MJ neutron pulse $\sim 10^{13}$ can be expected. An $n\tau$ scaling has recently also been suggested[48].

SUB-SYSTEMS OF THE PLASMA FOCUS EXPERIMENT

The emphasis of this discussion will be on the design and construction of a simple, fully operational device. The first step in the planning of a focus experiment is probably in the assessment of the capacitor bank characteristics.

4.1 Capacitor Bank:

Firstly the operating voltage. There is a lower limit to the operating voltage given by the inductive voltage drop across the focus tube during the axial acceleration phase. This is estimated from (d/dt)(LI) where L, here, is the tube inductance. We take the approximation that

$$\frac{d}{dt}(LI) \sim I \frac{dL}{dt} \tag{41}$$

since for the part of the acceleration period when this voltage is greatest, the current would have risen to large values so that the term L dI/dt is small compared to I dL/dt.

With $L = \frac{\mu}{2\pi}(\ell n \frac{b}{a}) z$, we have

$$I \frac{dL}{dt} = I \frac{\mu}{2\pi}(\ell n \frac{b}{a}) \frac{dz}{dt} \tag{42}$$

Typically with $\ell n \frac{b}{a} \sim 1$ and $I \sim 2 \times 10^5$ A, this gives an inductance voltage of 0.4 kV per unit axial speed of 10^4 m/sec (1 cm/μs). The range of suitable axial speeds in a plasma focus tube has been found to be rather small. The lower limit is fixed by the requirement for the electromagnetic mechanism to operate with sufficient efficiency. This is generally taken to be in the region of 3 - 4 cm/μs in deuterium, corresponding to a shock temperature of 20,000°K - 30,000°K. One cannot hope to reduce the speed further to, say, 1 cm/μs since $T_2 \sim v_s^2$ and the full-ionization electrical conductivity $\sigma \sim v_s^3$ and at 1 cm/μs the temperature is a mere 2000°K with certainly insufficient ionization (consequently electrical conductivity) for the electromagnetic drive to be operative.

On the other hand experimental observations also show that it is difficult to obtain consistent focussing action when the axial speed approaches or exceeds 10 cm/μs because of current spoke formation. The range of acceptable axial speeds would appear to be between 8 - 10 cm/μs.

Thus from Eqn. (42) the inductive tube voltage is in the range of 3 - 4 kV for a small plasma focus. The capacitor bank driving this back emf should therefore have an initial voltage several times this. We have chosen for cost effectiveness a Maxwell fast discharge capacitor rated 15 kV 30 μF, hence with maximum energy storage of 3.3 kJ. The equivalent series inductance of this capacitor is rated at less than 40 nH.

Connections between elements of the bank must be of low inductance. These may be by means of wide parallel plates clamped close together with insulating films of mylar sandwiched by outer layers of polyethene.

For ease of connection between the parallel plate output of the capacitor bank to the coaxial input of the focus tube short coaxial cables may be used. By using a sufficiently large number of these cables in parallel, the inductance may be suitably reduced.

The life expectancy of this Maxwell capacitor operating at full voltage, 80% voltage reversal with 3 μs risetime is estimated, from Manufacturers derating curves, to be 50,000 discharges. For research usage this should give a life expectancy in excess of 10 years.

4.2 Spark-gap Switch and Triggering Electronics:

A simple parallel-plate spark gap with a swinging cascade configuration (see Fig. 15) was developed giving a low inductance at minimum cost. The ratio of the gap is 3:2 ($4\frac{1}{2}$-3 mm). The gap is triggered via an isolating capacitor from an 800-V SCR unit via a TV transformer that was found to have a step-up ratio of 50 times and a risetime of 1 μs. The isolating capacitor is a 1 m length if UR67 coaxial cable. The parallel-plate spark gap is made from $\frac{1}{2}$-in. thick copper plates and proved maintenance free for 200 discharges between 13-15 kV before it was cleaned. The triggering jitter was found to be within ± 50 ns. The circuit is shown in Fig. 15a. The SCR trigger circuit is shown in Fig. 15b.

The arrangement for the capacitor, the connecting plates, the spark gap and the output coaxial cables is shown in Fig. 16a. To keep the inductance low, the Earth plate of the capacitor (labeled no. 10) is extended nearly up to the anode and insulation is provided by a nylon cap (no. 5) around the anode stud. The cap dips into a pool of oil (no. 4) that is prevented from splashing out by means of an O-ring (no. 8). Mylar

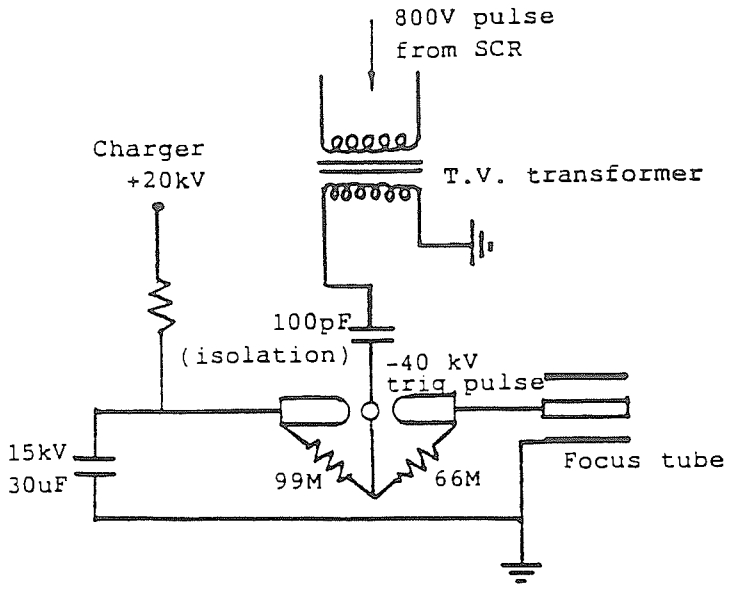

Fig. 15a Circuit for the swinging-cascade spark gap and focus tube.

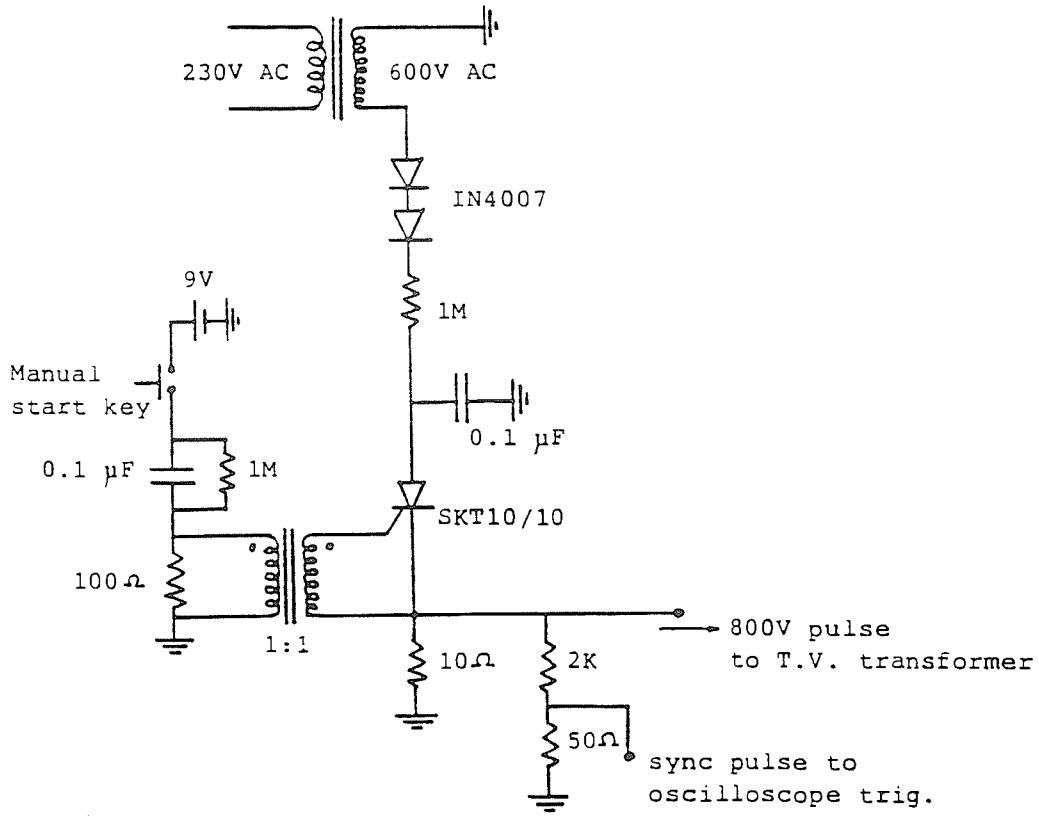

Fig. 15b Trigger and synchronizing electronics.

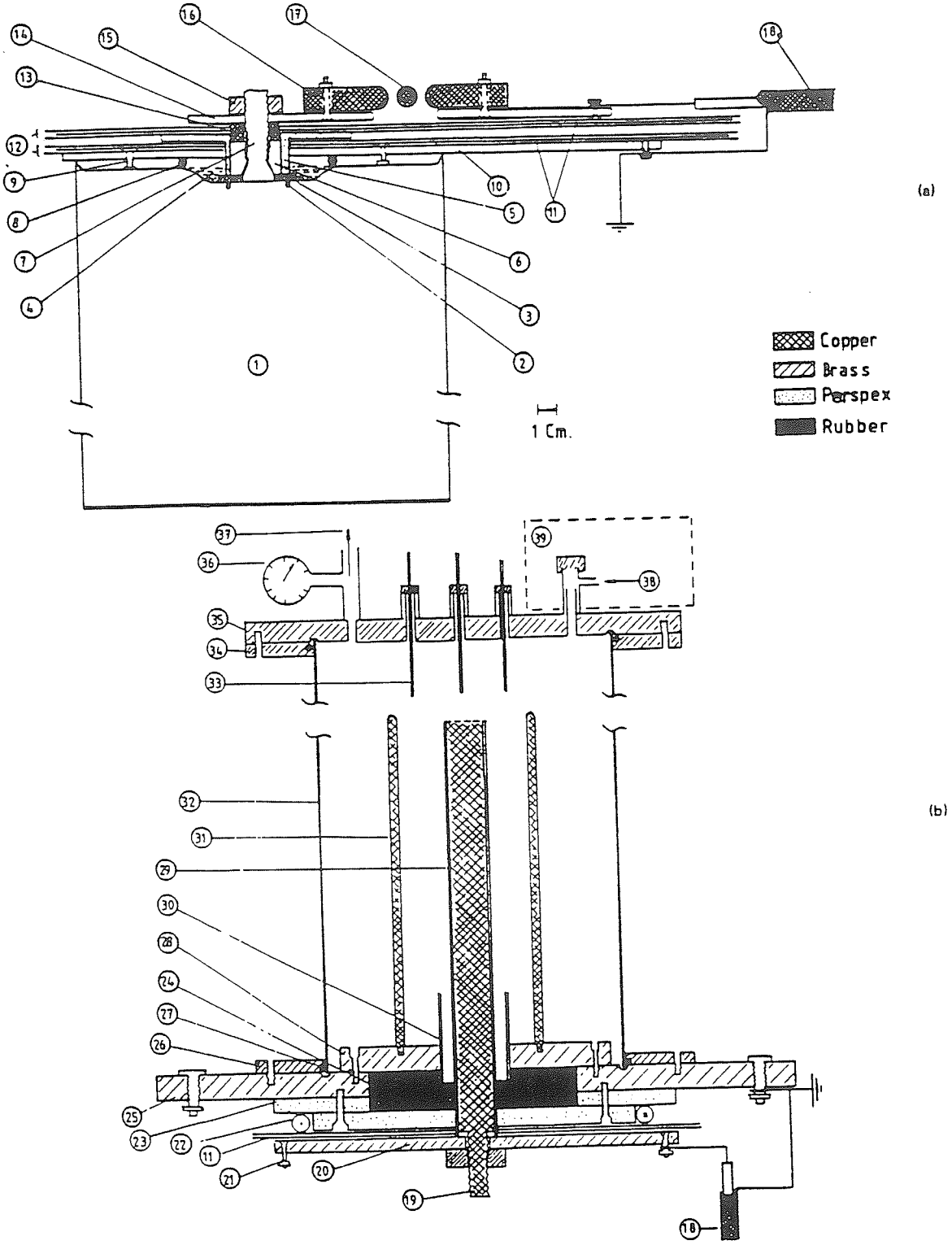

Fig. 16 The Plasma Focus Device.

(a) The capacitor connecting plates, the spark gap, and output coaxial cables. 1 = 15-kV, 30-μF capacitor; 2 = capacitor O-ring seal; 3 = washer; 4 = oil; 5 = nylon cap; 6 = steel nut; 7 = capacitor output seal; 8 = O-ring seal; 9 = Earth stud; 10 = Earth plate; 11 = 5-mil Mylar film; 12 = polyethelene film; 13 = copper ring HV connector; 14 = capacitor high-voltage (HV) output plates; 15 = lock nut for HV plate; 16 = HV electrode for swinging cascade spark gap; 17 = trigger electrode; and 18 = output coaxial cables (16 in parallel). (b) The plasma focus tube. 18 = input coaxial cables (16 in parallel); 19 = stud of anode; 20 = anode collector plate; 21 = connecting points for coaxial cable HV lead; 22 = Rogowski coil; 23 = perspex spacer; 24 = rubber holder; 25 = cathode collector plate; 26 = mild steel flange; 27 = O-ring seal; 28 = focus cathode support plates; 29 = focus anode; 30 = glass insulator; 31 = focus cathode (6 rods); 32 = mild steel focus chamber; 33 = movable magnetic probe in glass jacket; 34 = flange; 35 = back flange; 36 = diaphragm gauge; 37 = outlet to vacuum pump; 38 = inlet for test gas; 39 = wax container with indium foil and PM-scintillator activation counter.

sheets (no. 11), 2 in. wider all around than the conducting plates, sandwiched by polyethylene sheets (no. 12) complete the insulation between the HV plate (no. 14) and the Earth plate as shown in Fig. 16a. The Earth plate (no. 10) runs unbroken to the output position where the Earths of the coaxial cables connect. On top of the insulating sheets the HV plate is connected to the spark gap. Between the spark gap electrodes and all along it is placed a ½-in. diameter copper tubing (no. 17) that acts as the trigger electrode. The output plate of the spark gap is connected to the focus tube by means of 16 coaxial cables (no. 18) used in parallel.

4.3 The Plasma Focus Tube:

Essential to the structure of the focus tube is the backwall (see Fig. 16b) insulator. The glass insulator (no. 30) plays an important role in the symmetrical formation of the current sheet and has to be properly mounted to avoid being broken by vibrations. In the present design this glass insulator is mounted in a rubber holder (no. 24) which when compressed tightly and symmetrically by the brass flange (no. 28) grips the glass insulator. The rubber holder also acts as a vacuum and high-voltage seal. Figure 16b also shows the anode collector plate (no. 20) and the cathode collector plates (no. 25) onto which the coaxial cables connect.

The plasma chamber (no. 32) consists of a 30 cm length of 6½-in. diameter mild steel tubing that is chromed. Vacuum is provided by a single-stage rotary pump reaching an ultimate base pressure ~0.01 torr. The system was adjusted for a leakage rate of less than 2 μ/min and pressure is read with a mechanical diaphragm gauge. Operating at a test pressure of 1 torr and with a delay of less than 5 min between gas filling and focus operation, the air impurity in the system is about 2%. This level of vacuum proved to be sufficient for operating with good focus in various gases and good neutron yield when operated in deuterium.

4.4 Some Simple Diagnostics:

To measure the relative strength of the plasma focus action, a Rogowski coil (no. 22) with an integration time constant of 200 μs displayed on a 50 MHz CRO is used to measure the current flowing into the anode. A resistive voltage divider (not shown in figure) with 15 ns response time is strapped across the anode collector plate (no. 20) and the cathode collector plate (no. 25) to measure the voltage across the focus tube. In a plasma focus device, the axial drive phase is characterized by a smooth near-

sinusoidal rising current and a corresponding smooth waveform with a voltage value[56] that is proportional to the axial drive speed as the rate of change of current reduces to zero at peak current. As the focus occurs, the strong electromechanical action draws energy from the magnetic field pumping the energy into the compressing plasma. This mechanism is indicated in the distinctive current dip and voltage spike displayed by the current and voltage waveforms. In general, the stronger the focus, the more severely the plasma is compressed and the bigger the current and voltage spike.

To measure the magnetic field a 10-turn 1 mm coil jacketed in a 3 mm glass tubing (no. 33) is inserted into the focus tube and orientated to measure the azimuthal magnetic field. The passage of the current sheath driving the plasma layer may be measured as a sharp rise in magnetic field as the sheath sweeps past the probe. This measurement may be used to confirm the dynamics required to ensure a good focus.

An indium foil activation system is used to count fusion neutrons from the plasma. The system consists of an indium foil covering an NE 102 scintillator sittings on the photocathode of a 2-in. photomultiplier tube. The assembly is placed in a paraffin wax enclosure so as to thermalize the fusion meutrons. The detector is placed on the end flange of the plasma focus tube (no. 39). The PM tube is connected to a counter via a discriminator and a preamplifier and has a calibration constant of 5×10^4 neutrons per count, the counts being taken for a 30 seconds period immediately after the focus is fired.

4.5 Nitrogen Laser Shadowgraph System:

A very simple nitrogen laser system has been developed for pulsed plasma diagnostics using shadowgraphic, Schlieren or Mach Zehnder Optics[49].

The laser is excited by the conventional voltage swinging circuit schematically described in Fig. 17. The circuit theory of the parallel plate transmission line type of laser has been discussed in previous papers[60,61]. The two energy storage capacitors C_1 and C_2 of the circuit consist of a common earth plate, which is a 22 cm x 60 cm strip of kitchen aluminum kitchen foil laid on top of a flat aluminum plate (for electrical contact and mechanical support). Figure 18 shows the constructional details of the laser. On top of the foil are laid 3 sheets of 2 mil Mylar which extends at least 10 cm beyond the edges of the conductors all round. The high voltage plates of C_1 and C_2 are 22 cm x 40 cm and 22 cm x 17 cm strips

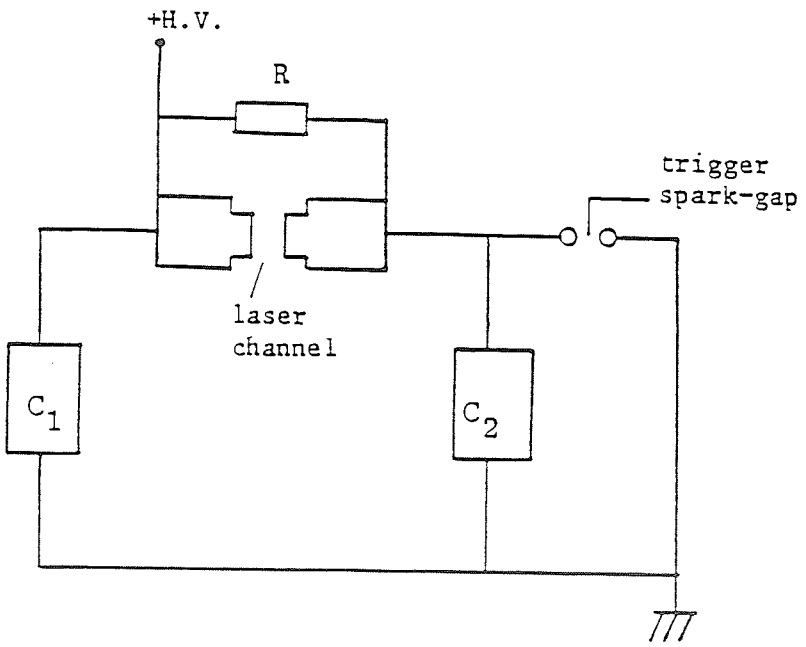

Fig. 17 Equivalent circuit of the nitrogen laser.

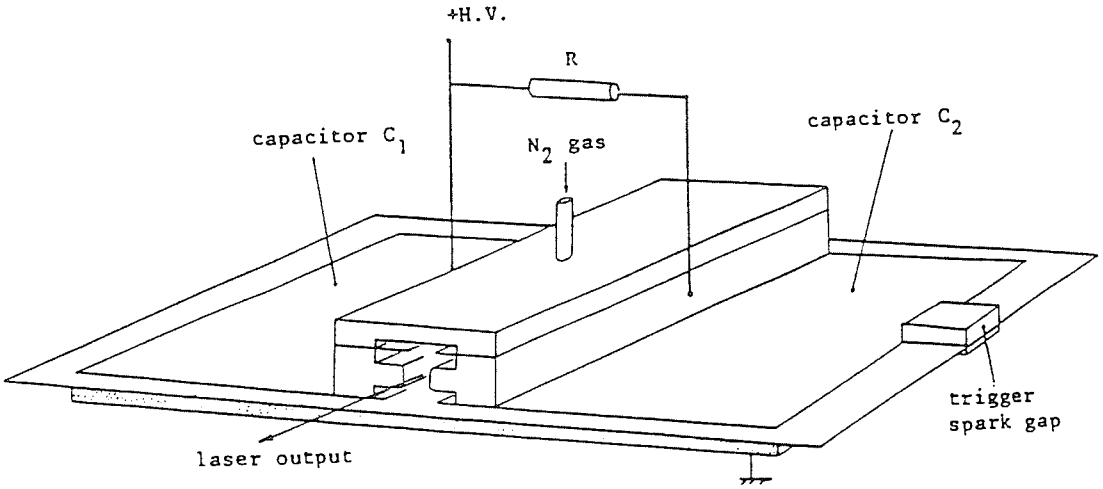

(a)

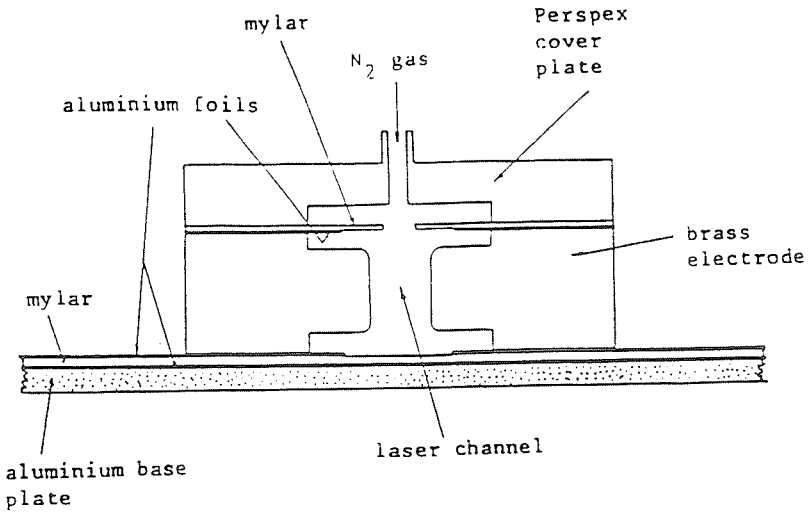

(b)

Fig. 18 (a) Sketch of a basic TEA nitrogen laser with Blumlein circuit.
(b) Cross-sectional view of the laser channel showing the preionizer system using aluminium foil-Mylar combination. The Mylar strips improve the preionization effect. (Ref. 49,50).

of aluminum foil laid on top of the mylar sheets. The measured values of C_1 and C_2 are 15 and 6 nF, respectively. On top of the foils are placed glass plates (6 mm thick) of approximate dimensions to prevent mechanical flexing of the foils during charging and discharging of the capacitors. The capacitor C_2 is mounted to a swinging cascade triggered spark gap. These high voltage capacitor plates are separated by a gap over which the laser channel is placed so that each side of the channel makes pressure contact with one of the capacitors. The electrodes of the laser channel are made of 20 cm long brass strips with cross-sectional dimensions of 0.5 in x 1 in and shaped as shown in Fig. 18b. The perspex plate is screwed onto the laser electrodes on the upper side over the top. Admission and evacuation of the nitrogen gas at atmospheric pressure is made through the middle and the ends of the channel, respectively.

In the arrangement shown, the edges of the high voltage capacitor plates (aluminum foils) are allowed to protrude beyond the edges of the laser electrodes into the laser cavity to act as corona blades for preionization. These form the set of blades on the lower side of the laser channel. A similar set of corona blades is placed on the upper side of the laser channel. The laser channel gap is set to 3 mm while the blades separation is typically set to about 40 percent greater than that of the main gap. The edges of the foils function as auxiliary corona electrodes which provide an initial distributed corona discharge to photoionize and prepare the laser channel for glow formation. The low-energy surface discharges acting as preionizing UV radiation sources are formed early during the rise of the voltage pulse across the laser gap and are distributed by corona charging of the Mylar surfaces that extend beyond the edges of the foils.

Optimum energy is obtained at a gap separation of 3 mm with a value of 300 μJ at 15 kV. The laser pulse duration is 1 ns with good beam quality.

The 1 ns pulse width of the nitrogen laser is sufficiently short to provide a freezing of motion of the order of 0.2 mm at a speed of 20 cm/μs.

The laser shadowgraphic set-up is as shown in Fig. 19. The laser pulse is correctly timed to catch the plasma focus at any time during the axial or radial phase by using variable delay units linking the plasma focus triggering pulse to the laser triggering pulse.

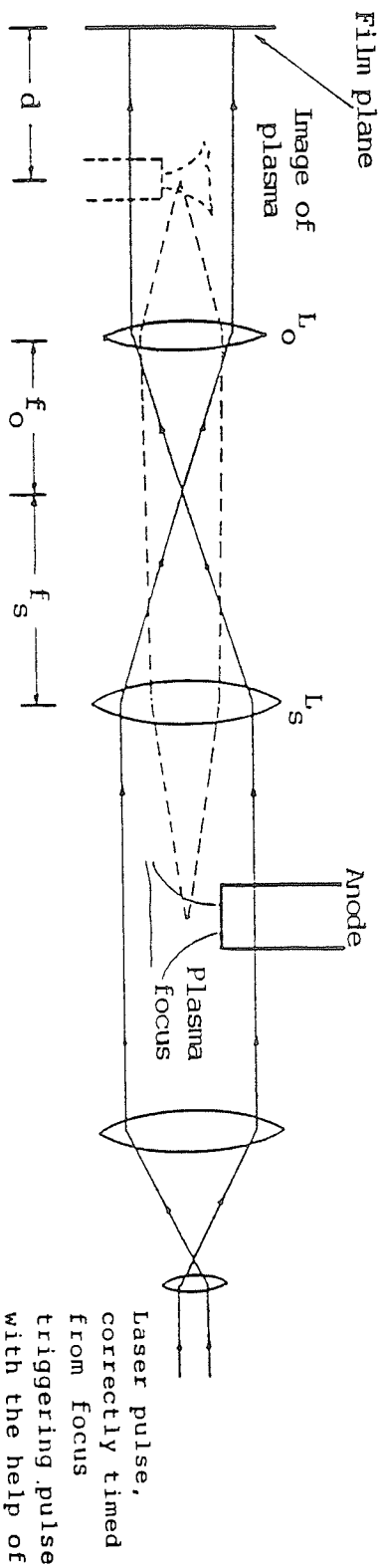

Fig. 19 Optical layout of the shadowgraph system. The plasma focus chamber, window and interference filter are not shown. (Ref. 50).

4.6 High Voltage Charger:

We may consider the question of power supplies for charging the capacitors. The alternative to buying costly power supplies is simply to build them. For example to charge a 15 kV 30 μF capacitor bank a power supply may be build up of the following components:

i) a transformer with an output rating of 15 kV RMS, 50 mA.

ii) 50 pieces of the commonly available 1N4007 diodes, each the size of a grain of rise, rated at 1 kV blocking voltage, 1 A current.

iii) Connect these diodes in series and insert into a plastic hose (garden hose variety will do) filled with transformer oil. Design connectors to fit the ends of the plastic hose so that the ends of the diode chain protrude out, one at each end, whilst keeping the oil in.

Connect one end of the transformer to the positive side of the capacitor via the diode chain (observe polarity) in series with a suitable current-limiting resistor. Connect the other end of the transformer to the earth side of the capacitor. The simple half-wave rectifier system will quite satisfactorily perform its duty fo charging up the capacitors, especially if some care is taken to avoid sharp points at the connections exposed to air.

The design of the charger must incorporate a feature to dump the capacitor bank to ground through a ballast resistor in the event of power failure. Also a word of warning must be heeded about the high voltage of such a charger and the capacitor bank. These two pieces of equipment are definitely lethal and sufficient care must be given to the safety procedure to be observed in the design and operation of such equipment.

A more efficient way to build a charger is to use switching methods so that the voltage transformation may be done at frequencies higher than the mains frequency. This would involve the use of more efficient, weight-effective, cost-effective ferrite cores. For example for the nitrogen laser charger the EHT power supply of a television set may be used. A simple adaptation from such a set results in a 2 kg palm-sized 25 kV (variable) power supply with 1 mA current which is ample for the nitrogen laser.

SOME RESULTS AND APPLICATIONS

5.1 Results:

The system was tested between 13 and 15 kV in various gases including air, argon, hydrogen and deuterium. The strength of the focusing action is gauged from the current dip and voltage spike. Figure 20a shows an oscillogram of the current and voltage waveforms of the plasma focus in 0.5 torr of air, with focusing action about 1 μs after peak current. Figure 20b shows a deuterium focus, at 13 kV, 2.5 torr with focusing action occurring at peak current. The deuterium focus shows signs of a secondary focus occurring some 0.4 μs after the first voltage spike. The occurrence of definite clean dynamics in the axial region preceding the focus region is confirmed by magnetic probe measurements. Figure 20c shows the output of a magnetic probe (lower trace) placed at z = 10.2 cm (i.e. in the axial drive region 10.2 cm from the backwall) in a discharge of 15 kV, 3.5 torr of deuterium. From this oscillogram and in comparison with the current oscillogram (upper trace) it is found that the current sheath arrives 0.6 μs before focusing occurs off the end of the anode at z = 16 cm giving a speed of 9.7 cm/μs (corresponding, from shock theory, to a temperature $\sim 2 \times 10^5$ K) over this section (z = 10.2 – 16 cm) of the axial drive region. From the risetime (10%-90%) of the magnetic signal and the speed this gives a current sheath thickness of 2 cm. The thickness and speed of this current sheath is typical of that in a good plasma focus system. The current dip during focusing is also seen as a dip in the magnetic probe output that shows two other current dips occurring at 0.2 and 0.6 μs after the dip. These confirm the occurrence of multiple focusing in deuterium in the device.

In air good focus was obtained at 13 and 15 kV in a narrow pressure range of 0.5-1.1 torr. In argon the pressure range for good focusing is greater at 0.3-3 torr. At 15 kV very strong focusing action was obtained at 0.8 torr. In helium the range of focusing is from 0.7 to 3.5 torr while in carbon dioxide focusing is observed below 1 torr. In hydrogen the pressure range for focusing is 1.1-6 torr. However, it is noticed that the focusing action, although definite, is not as intense, in terms of a focusing voltage spike, as in argon. The strongest focus

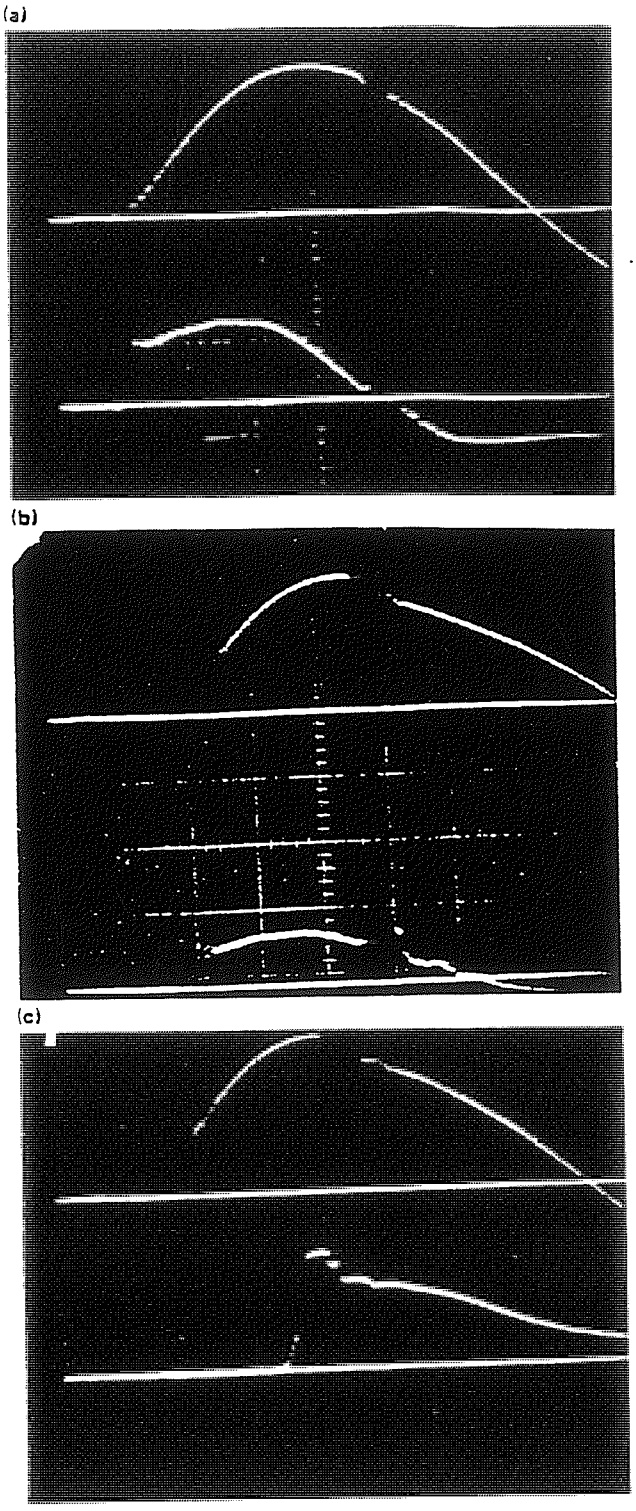

Fig. 20 (a) Current (upper trace) and voltage (lower trace) of plasma focus in air: 13 kV, 0.5 Torr; Top trace: 73 kA/cm; Bottom trace: 2 kV/cm; Time scale (horizontal): 1 μs/cm. (b) Current and voltage trace of plasma focus in deuterium: 13 kV, 2.5 Torr; Top trace: 75 kA/cm; Bottom trace: 4 kV/cm; Time scale (horizontal): 1 μs/cm. (c) Current and magnetic trace of plasma focus in deuterium: 15 kV, 3.5 Torr; Magnetic probe placed at $z = 10.2$ cm; Top trace: 73 kA/cm; Bottom trace: 0.6 T/cm.

in hydrogen occurs at 3.3-4.3 torr. In deuterium strong focus is observed at 1-5 torr with best focusing at 2.5-3 torr.

In deuterium when operated at 15 kV and optimum pressure conditions of 3 torr consistent counts of 1000-2000 are obtained using the PM-scintillator counter. This corresponds to 0.5×10^8 neutrons per shot.

The system shows remarkably consistent and reproducible operation. Six systems were assembled one after the other and tested over a period of 2 months. Each system was assembled and tested over a period of 1 week averaging between 100-200 shots in the various gases. Once a system has been established to be operating normally, that is, without undue leakage and after an initial period of out-gasing involving some three to five discharges, proper focusing is achieved for better than 95% of the discharges, apart from those discharges deliberately operated outside the established suitable pressure range for the gas used.

5.2 Temperatures and Densities:

It is of interest to estimate the range of temperatures and densities available in this device. This is best discussed separately for each of the two phases of operation, namely, the axial drive phase and the radial collapse phase. In deuterium in typical operating conditions in the axial drive phase between z = 8 and z = 16 cm a steady plasma temperature of 2×10^5 K may be estimated (Eqn. 29) in a 1-D slug length of 4 cm. For operating at an ambient density of 3 torr of deuterium, complete ionization is achieved at this temperature giving an ion density and an electron density each of about 10^{18} per cm^3 since a shock mass density ratio of 4 may be expected for a strong fully ionized deuterium shock. In the radial focus phase, soft x-ray techniques[5,40] have been used to estimate temperatures in a similar small plasma focus to be 0.7-3 keV while interferometric techniques[30] have been used to measure peak electron densities in the maximum compressed pinch column of $1-5 \times 10^{19}$ per cm^3. These experimental results agree with computations based on the dynamic theory already discussed.

When heavier gases such as argon are used as the test gas the dynamic theory predicts enhanced compression due to the specific heat ratio[22] being reduced below 5/3. In the case of argon, higher temperature (about 4 keV) and electron densities (10^{20} per cm^3), may then be predicted

by the dynamic theory applied to the pinch phase. There is also experimental evidence[23] to back up these predictions.

At such high temperatures, thermodynamic computations shows that even argon becomes almost fully ionized[54] and experimental work shows that worthwhile spectroscopic studies may be made of the focus using, e.g. argon as a test gas. Peacock[57] et al. have used a 2 m Rowland circle grating spectrograph and a de Broglie spectrometer to obtain spectrograms of argon and neon focus discharges. The results are sufficiently reproducible for identification of transitions in H-like and He-like Ne and Ar ions. If line profile scans are to be made then it is usual to obtain a profile over a number of discharges. The question of reproducibility then becomes important. In the present setup the reproducibility has been studied by using two simultaneous monitoring criteria. First, the neutron yield of each discharge is monitored and those that are beyond 10% of the average may be rejected. Second, the voltage spike is monitored for its time position and its shape (rate of rise, single spike, or multiple spikes). The time position of its peak (single peak spike) may be used as a reference point to fix the time position of the photomultiplier output. A discharge with a voltage spike shape that does not conform with the average shape may also be rejected. A close study of the data shows that when the system is properly set up and adjusted, at least 80% of the discharges are sufficiently reproducible for scanning applications.

5.3 Experiments and Applications:

It may also be of interest to inquire about the types of experiments that may be done on a plasma focus machine. First, as already mentioned in detail earlier, the axial drive phase may be used to study plasma dynamics and energetics[19]. The use of simple voltage, current and magnetic probes, together with a coupled circuit-dynamic analysis enables one to obtain the dynamics and energetics of the system and also shock plasma temperature and densities. These may be confirmed with spectroscopic and interferometric measurements to check the validity of the dynamic model used.

In the radial pinch phase, the pinching action is more severe than the Z or theta pinch for two reasons. The first is that the use of the axial drive phase delays the focus pinch so that it occurs at peak

current and enables a smaller radius pinch to occur at higher ambient density. Second, the smaller radius pinch is an elongating pinch that also contributes to an enhancement of pinch compression due to the smaller resulting pinch radius ratio[29]. Thus even a small plasma focus achieves sufficiently intense plasma conditions to produce consistent nuclear fusion and may be used as the lowest-cost device for demonstrating nuclear fusion from a plasma. Even a simple 3 kJ device such as the one presently discussed here may be used as a starting point for studying neutronics. For example, measurement of the half-life of ^{116}In has been carried out[58] using the UNU/ICTP PFF as the neutron source. It is known that the deuterium focus produces a deuteron beam[30] of several hundred keV. The effect of this beam on targets may also be studied for the enhancement of neutron yield. The corresponding electron beam, accelerated in the opposite direction into the anode, has relativistic speed and may be taken out of the system by using a hollow electrode. Thus the focus may also be used as a REB source. These two effects, i.e. consistent neutron and REB production, are not available in the Z pinch and theta pinch because of insufficient densities (10^{17} per cm^3) and temperatures (several hundred eV). This demonstrates the enhanced intensity of the plasma focus device.

The REB may also be used to sputter anode material downstream of the focus[30,59]. By using different materials as inserts in the anode face, different materials may be sputtered.

The question of neutron scaling is by no means closed. Lee[52] has shown that the observed neutron scaling of $Y \sim E^2$ and $Y \sim I^4$ is due to the speed limitation (10 cm/μs axial speed) and density limitation (about 20 torr) which has been observed for all plasma focus, small or large. If the focus could be operated with increased axial speed, say to 20 cm/μs, there are reasons to believe that the neutron yield would increase dramatically. Recent laser Schlieren photographs[49] (Fig. 21) have given some clues that the speed limitation may be due to current sheet - shock front decoupling at higher speeds associated with sheath inclination and a γ-effect. Further studies should be made to see if conditions may be adjusted to remove the speed limitation and hence improve the neutron scaling law.

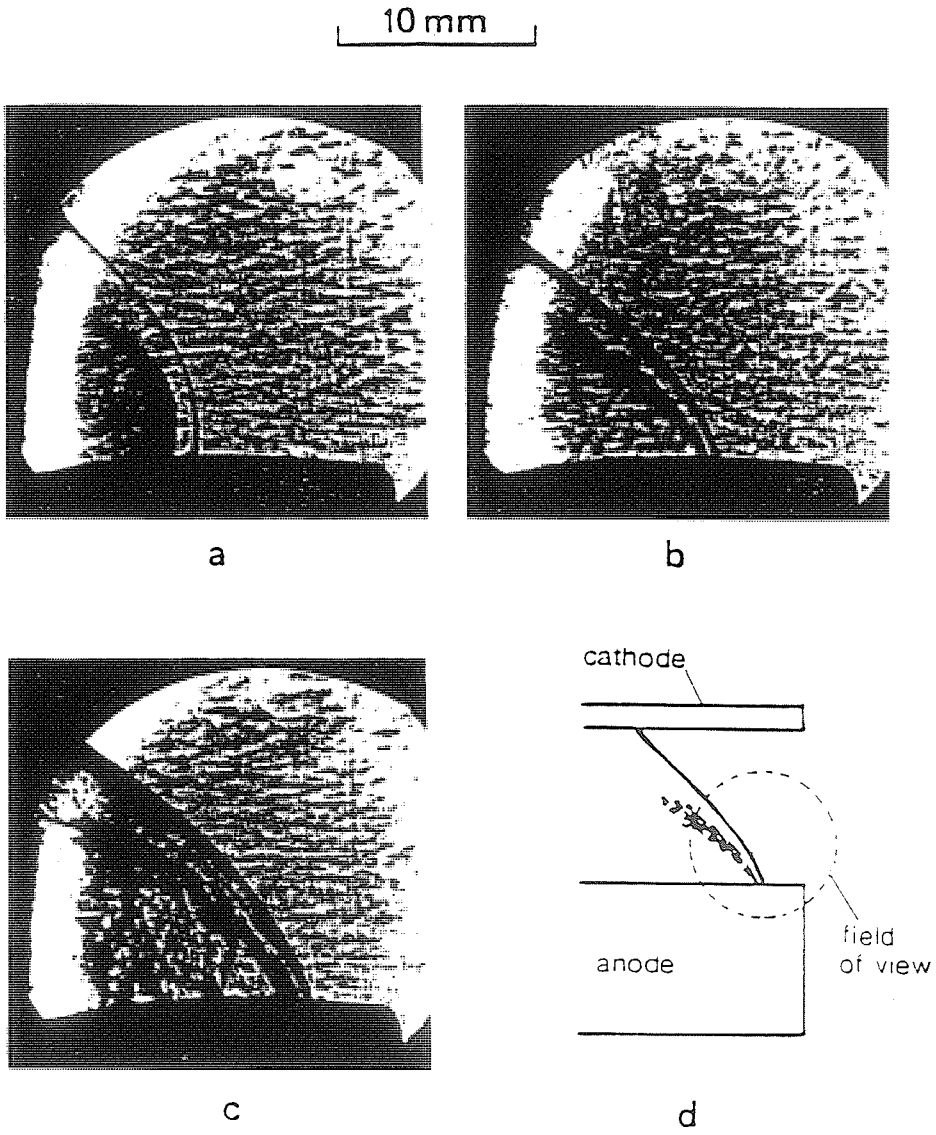

Fig. 21 Schlieren images of the plasma focus discharge in the axial rundown phase. The plasma focus device was operated at 14 kV and with deuterium gas at (a) 1 mbar, (b) 9 mbar, and (c) 14 mbar.

Other experiments and applications may be listed.

a) for studying a plasma under nuclear fusion conditions.

b) for developing diagnostics for fast pulsed plasmas.

c) as a neutron source for blanket studies for fusion reactors, pulsed neutron radiography, pulsed activation analysis, nuclear weapons simulation.

d) as an intense source for UV light, soft x-ray and electromagnetic radiation for spectroscopic applications, pump source for UV and soft x-ray laser, x-ray diagnostics and Electromangetic Pulse (EMP) studies.

e) for production of extreme magnetic fields and associated possibility of solid state compressions.

f) as a thermonuclear reactor; potential exists because of the observed $Y \sim E^2$ relationship.

In the experience of the UNU Training Programme the study of plasma dynamics particularly in the axial drive phase and the demonstration and study of plasma nuclear fusion are in themselves sufficiently interesting and of sufficient scope for a good beginning to be made in the field of experimental plasma physics.

REFERENCES

1. P.P. Petrov, N.V. Filippov, T.I. Filippova and V.A. Khrabrov in "Plasma Physics and the Problem of Controlled Thermonuclear Reactions" (Ed. M.A. Leontovich) Vol. IV pg. 198, Pergamon, New York (1960)
2. N.V. Filippov, T.I. Filippova and V.P. Vinogradov, Nucl. Fusion Supple. Pt. 2, 577 (1962)
3. N.V. Filippov and T.I. Filippova, Proc. of Second Conf. on Plasma Physics and Controlled Nucl. Fusion Research 1965, 2, IAEA (1966)
4. J.W. Mather, Phys. Fluids Supple., 7, 5 (1964)
5. J.W. Mather, Phys. Fluids, 8, 366 (1965)
6. J.W. Mather, Procs. of Second Conf. on Plasma Physics and Controlled Fusion Research 1965, 2, IAEA (1966)
7. E.H. Beckner, J. Appl. Phys., 37, 4944 (1966)
8. M.J. Bernstein, D.A. Meskan and H.L.L. van Paassen, Phys. Fluids, 12, 193 (1969)
9. C. Maissonnier, F. Cipolla, C. Gourlan, M. Haegi, J.G. Linhart, A. Robouch and M. Samuelli, Procs. 3rd Conf. on Plasma Phys. and Controlled Nucl. Fusion, Novosibirsk 1968, 2, IAEA Vienna (1969)
10. N.J. Peacock, Procs. 3rd Conf. on Plasma Phys. and Controlled Nucl. Fusion, Novosibirsk 1968, 2, IAEA Vienna (1969)
11. C. Patou, A. Simmonet, J.P. Watteau, Phys. Lett. A, 29, 1 (1969)
12. G. Decker, D.J. Mayhell, O.M. Friedrich, A.A. Dougal, Bull. Amer. Phys. Soc. (2), 13, 1543 (1968)
13. S. Lee, Y.H. Chen, S.P. Chow, B.C. Tan, H.H. Teh and S.P. Thong, Inter, J. Electronics, 33, 85 (1972)
14. S.P. Chow, S. Lee and B.C. Tan, J. Plasma Phys., 8, 21 (1972)
15. G.R. Hogg and J. Tendys, AAEC/E 280 (Australia) (1973)
16. M. Itoh, K. Hatori and K. Hirano, Jap. J. Appl. Phys., 13, 1033 (1974)
17. H. Conrads, D. Gollwitzer and H. Schmidt, Procs. 6th European Conf. on Controlled Fusion and Plasma Physics, Moscow, pg. 367 (1973)
18. L. Michel, K.H. Schoenbach and H. Fisher, Appl. Phys. Lett., 24, 57 (1974)
19. M. Gryzinski, A. Jerykiewicz and J. Nowikowski, Bull. de l'Academie Polonaise des Sciences techniques XXII, 2 (1974)
20. G. Decker, G. Pross, B. Rueckle, H. Schmidt and M. Shakhatre, Procs. 3rd Topical Conf. on pulsed high beta plasma, Culham (1975)
21. S. Lee and Y.H. Chen, Malaysian J. Science, 3B, 159 (1975)

22. J. Gratton, H. Kelly, M. Milanese, and J. Pouzo, Phys. Lett., A62, 422 (1977)

23. F. Gratton and J. Vargas, Procs. 7th European Conf. on Controlled Nucl. Fusion, Lausanne, I, 64 (1975)

24. S. Lee and T.H. Tan, Procs. 7th European Conf. on Controlled Nucl, Fusion, Lausanne, I, 65 (1975)

25. S. Sinman and A. Sinman, Fusion Energy - 1981 (ICTP, Trieste) IAEA-SMR-82, Vienna, pg. 327 (1982)

26. S. Lee, Fusion Energy - 1981 (ICTP, Trieste) IAEA-SMR-82, Vienna, pg. 289 (1982)

27. R. Gratton, C. Ferro Fontan, H. Kelly, J. Pouzo, M. Milanese, A. Sicardi Schifino, G. Lesin and M. Esper, Fusion Energy - 1981 (ICTP, Trieste), IAEA-SMR-82, Vienna, pg. 275 (1982)

28. S. Lee, Bul. Fiz. Mal., 3, 197 (1981)

29. S. Lee, Plasma Phys., 25, 571 (1983)

30 G. Decker and R. Wienecke, Procs. Twelfth Inter, Conf. on Phenomena in Ionized Gases, Eindhoven 1975, 2, 155 (1976)

31. Y.H. Chen "Parametric Study of Focus Optimization" Ph.D. Thesis, University of Malaya (1978)

32. S. Lee and Y.H. Chen, Procs. Twelfth Inter, Conf. on Phenomena in Ionized Gases, Eindhoven 1975, 1, 353 (1976)

33. S. Lee, Bul. Fiz. Mal., 2, 240 (1981)

34. D.E. Potter, Nucl. Fusion, 18, 813 (1978)

35. S. Lee, J. Appl. Phys., 54, 3603 (1983)

36. S. Lee and Y.H. Chin, Bul. Fiz. Mal., 2, 105 (1981)

37. S.P. Thong and S. Lee, Mal. J. Science, 2(B), 157 (1973)

38. M.G. Haines, Phil. Trans. Roy. Soc. Lond., A300, 649 (1981)

39. S. Lee, Y.H. Chen, S.P. Chow, B.C. Tan, H.H. Tah and S.P. Thong, Inter, J. Electronics, 33, 85 (1972)

40 S. Lee and Y.H. Chen, Fusion Energy - 1981 (ICTP, Trieste) IAEA-SMR-82 Vienna, pg. 297 (1982)

41. Y.H. Chen and S. Lee, Inter. J. Electronics, 35, 341 (1973)

42. C.S. Wong, S. Lee and S.P. Moo, Mal. J. Science, 6(B), 167 (1980)

43. S. Lee, J. Phys. D: Appl. Phys., 16, 2463 (1983)

44. D.E. Potter, Phys. Fluids, 14, 1911 (1971)

45. Reports of the IAEA Consultants' Meeting on IAEA Report (1978) Fusion Programme for Developing Countries.

46. T.Y. Tou and S. Lee, Bul. Fiz. Mal., 4, 189 (1983)

47. M. Sadowski, H. Herold, H. Schmidt and M. Shakhatre, Phys. Lett., 105A, 117 (1984)

48. H.J. Kaeppeler, A. Hayd, M. Maurer and P. Meinke, IPF-83-2. Institut für Plasmaforschung der Universitaet Stuttgart (1983)

49. K.H. Kwek, T.Y. Tou and S. Lee, J. Fiz. Mal., 9, 36 (1988); IEEE Trans. on Intrumentation and Measurement, IM-38, 103 (1989)

50. K.H. Kwek "Pinch Structure of a Plasma Focus", Ph.D. Thesis, University of Malaya (1989 - submitted)

51. S. Lee, T.Y. Tou, S.P. Moo, M.A. Eissa, A.V. Gholap, K.H. Kwek, S. Mulydrono, A.J. Smith, Suryadi, American J. Phys., 56, 62 (1988)

52. S. Lee "The sharing of fusion-related technology among developing countries" - invited paper read at the Energy Independence Conference, Rio de Janeiro, August 1987; Procs. "Fusion Energy and Plasma Physics" World Scientific, edited by P.H. Sakanaka, pg. 754 (1988)

53. Mohammad Zaka-ullah "A parametric study of the dense plasma focus" Ph.D. Thesis, Quaid-I-Azam University (1988)

54. S. Lee, Australian J. Phys., 36, 891 (1983)

55. G. von Guderley, Luftfahrtforschung, 19, 302 (1942)

56. "Laser and Plasma Technology", World Scientific, Ed. by S. Lee et al (1985)

57. N.J. Peacock et al., J. Phys. B 2, 798 (1969)

58. S.P. Moo and S. Lee, Singapore J. Phys., 4, 131 (1987)

59. S. Lee, Harith Ahmad, T.Y. Tou, K.H. Kwek and C.S. Wong, J. Fiz. Mal., 7, 1 (1986)

60. S. Lee, A.V. Gholap, A.J. Smith, K.H. Kwek, A.C. Chew, T.Y. Tou and S. Sapru, J. Fiz. Mal., 6, 165 (1985)

61. A.J. Smith, K.H. Kwek, T.Y. Tou, A.V. Gholap and S. Lee, IEEE J. Quan. Electronics QE-23, 283 (1987)

A CURRENT-STEPPING TECHNIQUE TO ENHANCE PINCH COMPRESSION - AN EXPERIMENTAL STUDY

S.H.Saw, S.Lee & C.S.Wong
Plasma Research Laboratory, University of Malaya
59100 Kuala Lumpur, Malaysia.

ABSTRACT

The current-stepping technique involves the shaping of the current-time profile during compression. This is done by discharging a second capacitor bank onto the pinch unit at a suitable time during the approach to quasi-equilibrium in the compression due to the first capacitor bank. It has been shown theoretically that this is able to reduce the quasi-equilibrium radius ratio k_p by approximately 2 times. This is possible because k_p depends on the time variation of the current and not on the absolute value of the current.

Another effect which affects k_p is the thermodynamic effects of the real gas. For an ideal gas with specific heat ratio γ of 1.67, k_p reached is approximately 0.3 for a constant current pinch. A smaller k_p will be reached for any gas compression with an average γ below 1.67. As γ approaches 1.67, k_p will approach 0.3.

A low technology capacitor-capacitor combination is first attempted to study the enhancement in compression by current-stepping. Unfortunately no significant reduction in k_p is observed. It turns out that the compression during the first stage is too slow such that upon current-stepping, the reduction in k_p is masked by an increased in k_p as γ approaches 1.67 from an average of 1.2. Numerical computation indicates that for the enhancement in compression to be observed, γ should averages at least 1.4 during the first compression. This requires a faster pinch unit with a corresponding increase in pinch impedance of the first capacitor bank to avoid the first capacitor bank from shorting out the pinch tube during the switching of the second capacitor bank. A Marx-Marx combination is proposed to drive a new current-stepped pinch which is expected to minimise the γ masking effect so that the reduction in k_p is observed.

INTRODUCTION

It has been shown by Lee[1,2] that one of the methods to enhance the plasma produced by gas compression is to implement the current-stepping technique which involves the shaping of the time profile of the driving current source. It is possible to obtain a maximum enhancement in compression resulting in a reduction of the

quasi-equilibrium radius ratio, k_p by aprroximately 2 times. This will lead to a 4-folds and a 16-folds increase in the plasma density and the plasma temperature respectively since the plasma density is directly proportional to the square of the final radius while the plasma temperature is directly proportional to the square of the compressing shock speed or the plasma density.[3]. It is suggested that as a prelude to radiation cooling, current-stepping can be introduced to achieve a denser and hotter plasma.

At quasi-equilibrium, the following expression can be obtained by assuming energy balance and pressure balance condition.

$$\int_{r_m}^{r_o} \frac{\mu_o I^2}{8\pi^2 r_p^2} (2\pi r_p l)\, dr_p = \frac{1}{(\gamma-1)} \frac{R_o T_m \varkappa}{M} (\rho_m \pi r_m^2 l) \qquad (1)$$

where ρ_m, T_m, $\varkappa$, γ are respectively the density, the temperature, the departure coefficient and the specific heat ratio of the plasma in the final state at r_m and R_o and M are respectively the universal gas constant and the molecular weight of the ambient gas. The integration is done from initial radius r_o to final radius r_m. It is assumed that the total work done by the gas compression goes into the internal energy of the compressed gas without any loss.

Simultaneously at quasi-equilibrium, the pressure balance is achieved when the kinetic pressure exerted by the plasma in the final stage exceeds the magnetic pressure by a factor, f_{rs} called the reflected shock pressure jump factor[4,5]. Thus:

$$\rho_m \frac{R_o T_m \varkappa}{M} = f_{rs} \frac{\mu_o I_m^2}{8\pi^2 r_m^2} \qquad (2)$$

where I_m is the current flowing at the time the pinch reaches quasi-equilibrium at r_m. f_{rs} is obtained numerically as 1.67.

From equation (1) an expression for the temperature of the plasma at quasi-equilibrium is obtained as shown below

$$T_m = \frac{M(\gamma-1)}{\rho_m R_o \varkappa} \frac{\mu_o}{4\pi^2 r_m^2} \int_{r_m}^{r_o} \frac{I^2}{r_p} dr_p \qquad (3)$$

Another expression for the plasma temperature at

quasi-equilibrium can also be obtained independently from equation (2) as

$$T_m = f_{rs} \frac{\mu_o I_m^2 M}{8\pi^2 r_m^2 \rho_m R_o \alpha} \tag{4}$$

From equation (3) and (4) the following condition governing the quasi-equilibrium radius ratio is obtained:

$$I_m^2 = \frac{2(\gamma-1)}{f_{rs}} \int_{r_m}^{r_o} \frac{I^2}{r_p} dr_p \tag{5}$$

It is obvious from equation (5) that the minimum radius r_m is determined by the integral of the curent and not by the absolute value of the current.

One of the way to tailor the time-profile of the driving current is by discharging 2 capacitor banks in parallel; with the second bank faster than the first bank; consecutively after a suitable time delay determined by the extend of approach to quasi-equilibrium. When equation (5) is divided by I^2 and the ratio represented by ψ, a value of 1 would indicate the quasi-equilibrium point while any values between 0 to 1 represent the extend of approach to quasi-equilibrium. A schematic diagram of the current sources for the current-stepping model is shown in Fig. 1.

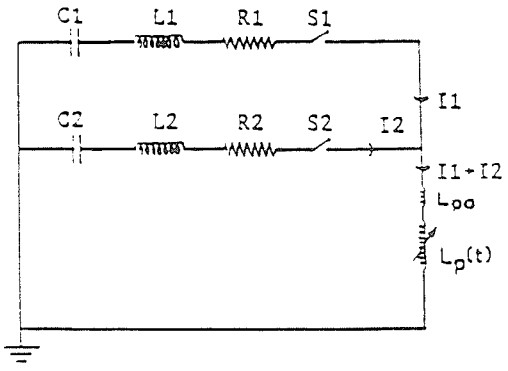

Fig. 1 A schematic diagram of the arrangement for a current-stepped pinch.

EXPERIMENTAL STUDY ON THE CURRENT-STEPPED PINCH : FIRST ATTEMPT

A first attempt is carried out utilising technology and facilities currently available in the laboratory to avoid high cost. A capacitor-capacitor combination unit, UMCSZP[6], is designed based on the slug model[7]. The first stage is powered by 3 units of 20 μF, 10 kV, 40 nH capacitors connected in parallel via parallel plates to give 60 μF, 10 kV maximum. When connected to the pinch unit, a 9 kV discharge produces a current which rises to 251 kA in 3.4 μs. The initial rate of current-rise is 1.2×10^{11} A/s. The second stage comprises of 22 μF, 60 kV, 26 nH

Julich bank[8] operating at 18 kV. Upon switching, it delivers a current of 463 kA in 1.3 μs to the pinch unit with an initial current rise of 5.5 x 10^{11} A/s. The parameters of the Z-pinch unit are as follows: radius 7.5 cm, length 15 cm, inductance 6.8 nH, operating pressure (0.4 - 2.0) mbar Hydrogen. A schematic of the UMCSZP main set-up is shown in Fig. 2.

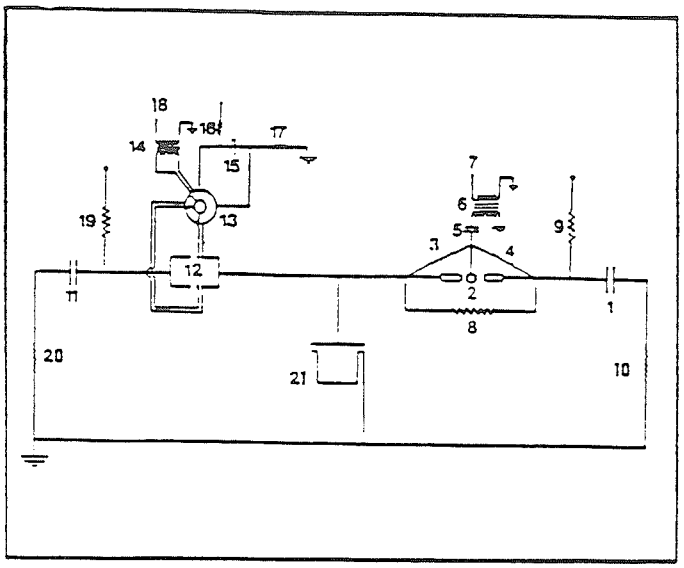

Fig.2 A schematic of the UMCSZP main current set-up. 1.C1=60μF,9kV, 2.air spark gap 3. 94MΩ, 4. 141MΩ, 5. isolating capacitor, 6.t.v. transformer,1:15, 7. -800V, 8. 9MΩ, 9. 200kΩ, 10. R_e, 11. C2 = 12 x 1.81μF, 18kV, 12. pressurized spark-gaps, 2 @ 1.81μF, 13. spark-gaps triggering pulses distributer ring, 14. isolation transformer,(1:-1), 15. 0.6 μF,-30kV, 16. 300kΩ,17. 6kΩ, 18 -16kV, 19. 6kΩ @ 1.81μF, 20. R_e, 21. Z-pinch chamber.

Electrical measurements of the current and voltage were obtained using Rogowski coil[9,10] and voltage probe[11]. Simultaneously streak photography of the space integrated, time resolved radial profile is recorded using the IMACON camera. The results obtained for single Z-pinch compression and for current-stepped Z-pinch compression are as shown in Fig. 3 and Fig. 4 respectively. Analysis of the results indicates that upon

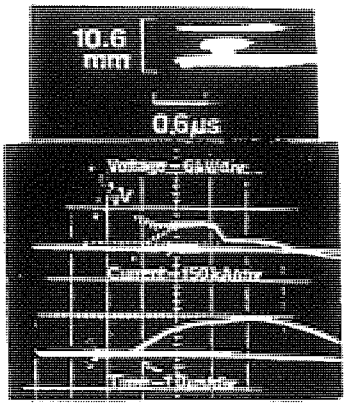

Fig. 3 Current and voltage signals and time-resolved radial profile of the single compressional Z-pinch.

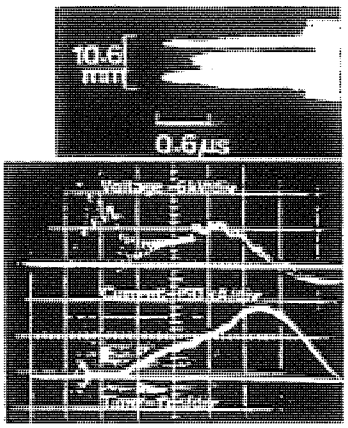

Fig. 4 Current and voltage signals and time resolved radial profile of the current-stepped Z-pinch.

current-stepping there is no obvious enhancement in the compression to lead to a smaller k_p predicted by theory. It is

found that the minimum radius ratio achieved with current-stepping at various time before equilibrium is approximately the same as that produced without current-stepping. This suggests the existence of other factors which have the effect of increasing the radius ratio of the compression upon current-stepping. One of the parameters which affects compression and is drastically increased upon current-stepping is the specific heat ratio, γ of the gas. For an increase in the average value of the γ from a value of ~ 1.2 during the first compression to 1.6 upon the switching of the second bank, the minimum radius ratio will be increased. As such the expected reduction in the radius ratio upon current stepping is masked by the increase due to γ. This is not predicted by our earlier computation based on the slug model since an ideal gas with γ equal to 1.67 is assumed. An improvement is made to the slug model to take into account the thermodynamic effects of the real gas. The relation of γ with shock speed is first determined by solving the three equations: namely the Saha Equation, the Thermal Equation and the Caloric Equation simultaneously[12]. It is then incorporated into the slug model to enable the transient value of γ corresponding to the shock speed to be used in the numerical simulation of the pinch dynamics. This new model now predicts no enhancement in the quasi-equilibrium radius ratio for the present set-up as observed in the experiment. However, this model also predicts a smaller minimum radius ratio than observed experimentally. This is probably due to the diffusion of the current sheath resulted from the slow first compression. Another experimental observation of current-stepping experiment is that the radius ratio obtained for discharge with current-stepping is generally slightly bigger compared to the radius ratio obtained without current-stepping. Measurements of the magnetic fields[13] taken at various distances show that the current profile broaden upon current-stepping before resuming to implode further as shown in Fig. 5. This may be interpreted as indicating that the resistivity of the current channel is still high due to inefficient pinching of the first pinch.

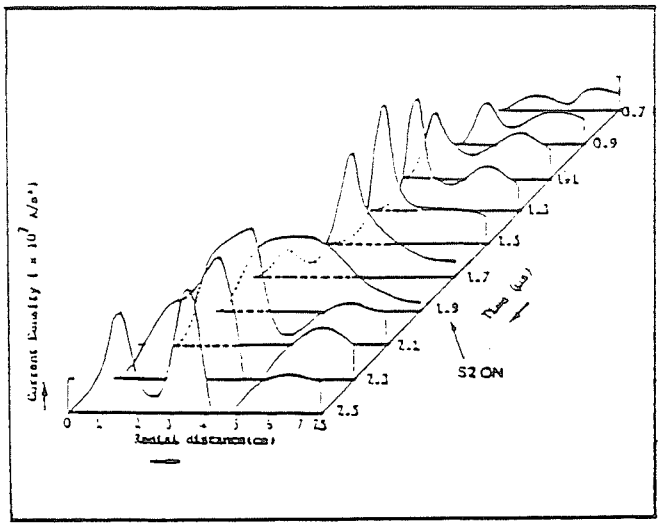

Fig. 5 History of the radial current density profile of a current-stepped Z-pinch.

DISCUSSION

A summary of the results obtained experimentally compared to the results predicted by the theory with γ constant and γ varying is shown in Table 1.

From the results obtained so far, it is obvious that the effect of pinch enhancement by the current-stepping technique cannot be observed using the present system of capacitor-capacitor combination. In order to be able to observe the effect of current-stepping the compensating effect of γ must be reduced if not eliminated. This is only possible by increasing the speed of the first compression such that the average γ is greater than 1.4. This would require the compressing shock speed to be increased to above 10 cm/μs. With this improvement, the plasma will also be heated to higher temperature and hence its resistivity will be reduced.

ψ	UMCSZP Theory γ-constant k_p	UMCSZP Experiment k_p	UMCSZP Theory γ-varying k_p	MLCSZP Theory γ-varying k_p
1.0	0.24	0.21	0.11	0.17
0.08	0.19	0.23	0.11	0.16
0.4	0.19	0.23	0.11	0.13
0.8	0.18	0.23	0.10	0.12

Table 1. Theoretical and experimental quasi-equilibrium radius ratio, k_p (r_m/r_o) for single stage Z-pinch and current-stepped Z-pinch. (ψ = 1.0 corresponds to single stage Z-pinch while ψ < 1.0 indicates the various times of switching of S2 based on the extend of approach to quasi-eqiulibrium).

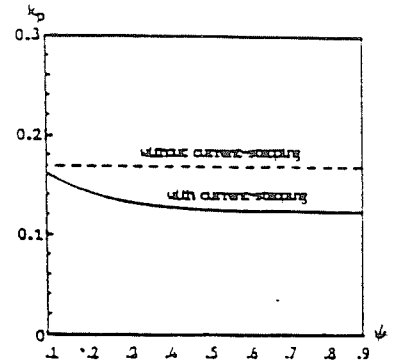

Fig. 6 Quasi-equilibrium radius ratio, k_p, for MLCSZP before switching of S2 and at various times of switching of S2.

A Marx-Line combination system, MLCSZP is designed based on the improved slug model to provide a first compression with average shock speed of 10 cm/μs. The first compression is powered by a 150 kV, 0.6 μF, 600 nH Marx constructed from 3 capacitors each rated at 1.8 μF charged to 50 kV. The second compression is driven by a 2Ω, 1.5 m water-line charged to 150 kV by another Marx of 150 KV, 0.1μF. The Z-pinch chamber is of length 5 cm and radius 6 cm. The operating pressure is 0.14 mbar Hydrogen. With this new design a reduction in the radius ratio by a factor of 1.4 upon current-stepping is predicted by the improved slug model. Fig.6 shows the value of k_p reached upon current

-stepping at various conditions of quasi-equilibrium compared to the value of k_p reached without current-stepping. It is also expected that with the increase in the shock speed the magnetic Reynolds number will also increase, thereby improving the fluid-field coupling thus leading to the confinement of the current in a thin sheath. The high impedances of the Marx-Line system would also ensure larger fraction of current flow into the plasma current channel upon current stepping.

ACKNOWLEDGEMENT

This work is supported by the research grant R & D 04-40 of the University of Malaya.

REFERENCES

1. S.Lee, J.Phys.D:Apopl.Phys 17, 733 (1984)
2. S.Lee, Plasma Physics, 25, 571 (1983)
3. A.G.Gaydon & J.R.Hurle, The Shock Tube in High Temperature Physics. London: Chapman & Hall Ltd., Chapter 2 (1963)
4. G.von Gudeeley, Luftfahrtforschung 19, 302 (1942)
5. S.Lee, Rep. IC/85/65 IAEA & UNESCO, ICTP Trieste,Italy (1985)
6. S.H.Saw etc., Procs. Sypm. on Small Scale Lab. Plasma Expt. Trieste,Italy, (1987)
7. Jalil Ali etc., J.Fiz.Mal.5, 135 (1984)
8. P.Cloth & H.Conrads, Nucl.Sci.Eng.62, 591 (1977)
9. Rogowski W. & Steinhaus W., Arch. Elektrotech.1, 141 (1912)
10. J.Cooper, Plasma Physics 5, 285 (1963)
11. R.Keller, Rev.Sci.Instrum. 35, 1057 (1964)
12. S.H.Saw etc.,J.Fiz.Mal 9,93 (1988)
13. R.H.Huddlestone & S.L.Leonard, Eds., Plasma Diagnostic Techniques. New York: Academic Press, Chapter 3 (1965)

Nonperturbing Plasma-Focus Measurements in the Run-Down Phase

T. Y. TOU, S. LEE, AND K. H. KWEK

Abstract—Simultaneous and nonperturbing measurements involve using a multislit streak camera, two high-voltage probes, and a Rogowski coil are carried out to enable an equivalent-circuit analysis to be made of a plasma-focus discharge in the run-down phase. A leak current is assumed to flow at the insulator. The calculations show that maximum constant values of diode voltage, V_p = 5.3 kV, and pinch current, I_p = 200 kA, are attained during the run-down phase; the product of these two parameters show an upper limit in the input power. From the multislit streak camera, a limiting run-down speed, v_s = 9.2 cm/μs, for the plasma sheath is observed which suggests a constant rate of change of inductance. These observations indicate a steady-state operation of the plasma focus for this duration.

I. Introduction

In the plasma-focus experiment, a uniform and homogeneous current sheath is essential for maximizing energy transfer and neutron output [1]. The formation of the current sheath depends on the initial discharge conditions at the glass insulator [1], [2], which for many years received considerably less attention in comparison with other phases of plasma dynamics, pinch formation, and emission characteristics. When large plasma-focus devices failed to achieve their scaled neutron yield, investigation of this initial phase became urgent because a leak current was found to flow behind the main current sheath. For example, the Frascati experiment [3] at full energy had a neutron yield [4] of only 1/9 of what it should be owing to a leak current at the insulator [5]. The presence of a leak current at the insulator has also been reported by several other groups [6]–[8].

The cause of a leak current largely could be linked to the residual plasma near the insulator and in the run-down region. Interferometric and spectroscopic measurements [4] showed some 30 percent of the initial filling density being left at these regions owing to inefficient snowplow action by the propagating current sheath. The residual plasma and the ablation of material from the insulator [9] could allow the current to crowbar the circuit under an increasing diode voltage generated in the annulus of the focus tube. A second breakdown at the insulator region has been observed [10], which prevented further increment in the pinch current.

Numerical calculations with a one-dimensional three-fluid code [11] for the Z-pinch geometry showed that the ionization process during ignition has a strong influence on the current-sheath formation. Recently, a two-dimensional three-fluid MHD code [12] for plasma-focus calculations took into account the effect of ionization phenomena. With this code, the sheath dynamics and the occurrence of residual plasma were studied in the Frascati Experiment [3], in the faster POSEIDON experiment [13], and the fast SPEED experiments [1]. The code demonstrated that fast-current buildup during the initial phase was favorable for preventing residual plasma and that owing to this, the POSEIDON device shows better performance than the slower Frascati one. In other case studies, a much lower level of residual plasma was shown to occur in the SPEED device which experimentally has shown very good performance when compared with the large, low-voltage devices.

On the other hand, a simple physical model has been presented by Eltgroth [14] for simulating the current histories in the Frascati [3] and Livermore [15] machines. In this model, the leak current and mass loss behind the current sheath are necessary in order to produce a reasonable match with the experimental observations. Apparently, more detailed experimental investigations on the initial and run-down phases are required for a better insight on their influences on the plasma-focus performance.

Magnetic probe measurements [16] in our Mather-type [17] plasma-focus device [18] (20 kV, 12 kJ) have shown evidence of leak current. These measurements were difficult in the high-voltage, high-current-density plasma and in the presence of strong shocks; these conditions placed stringent requirements on the probe design. In this paper, simple planar geometry for the current sheath is considered, which then allows the plasma-sheath motion (results from the multislit streak camera) to be incorporated into an equivalent-circuit analysis of the plasma-focus discharge. For this analysis, requisite measurements using two high-voltage probes, a Rogowski coil and a multislit streak camera, are carried out. These measurements are simultaneous and nonperturbing to the current sheath until it reaches the high-voltage probe at the end of the focus tube. Therefore, the analysis is meaningful only for the run-down phase for which the diode voltage V_p, pinch

Manuscript received July 5, 1988; revised November 21, 1988.

T. Y. Tou was with the Plasma Research Laboratory, Department of Physics, University of Malaya, 59100 Kuala Lumpur, Malaysia. He is now at the Plasma Research Laboratory, Research School of Physical Sciences, Australian National University, Canberra, Australia.

S. Lee and K. H. Kwek are with the Plasma Research Laboratory, Department of Physics, University of Malaya, 59100 Kuala Lumpur, Malaysia.

IEEE Log Number 8826063.

0093-3813/89/0400-0311$01.00 © 1989 IEEE

current I_p, leak current I_L, leak resistance R_L, and current-sheath R_p are calculated.

II. Experiment

For the simple situation of a current sheath whose thickness is much less than the length of the plasma-focus tube, an equivalent circuit is always convenient to describe its dynamic behavior [1], [17]. A schematic of our experimental setup is shown in Fig. 1(a), while its equivalent circuit for our plasma-focus device is shown in Fig. 1(b). A leak current, I_L, is assumed to flow at the insulator. During discharge, the plasma-focus tube is a load generator where impedance may be comparable to or greater than that of the conventional capacitor banks. This load impedance tends to limit the total discharge current, I, especially during the compression phase.

For the experiment presented here, the filling pressure is 10 mbar of D_2 and the capacitor voltage is 14 kV. The total discharge current, I, is measured with a Rogowski coil which is shunted by a small resistor ($\sim 0.1\ \Omega$) at its output leads so that the coil operates as a self-integrating current transformer. Two voltage signals, V and V_R, are monitored with resistive high-voltage probes. The first probe is connected between the positive and negative flanges (electrical feedthrough) behind the focus tube, which is represented electrically by an inductance, L_e, and resistance, R_e. The voltage due to $L_e = 25$ nH and $R_e = 1.5$ mΩ have been found to constitute a significant proportion in the measured voltage, V, given by

$$V = V_p + L_e \frac{dI}{dt} + IR_e. \tag{1}$$

The other probe is connected from the inner electrode to the outer electrode (to one of the cathode rods) at the end of the focus tube. Assuming that the magnetic field due to the pinch current, I_p, is negligible in front of the current sheath, this probe largely measures the resistance component, V_R, of the diode voltage, V_p. V_R (see Fig. 2) may be written as

$$V_R = I_p R_p \tag{2}$$

where R_p is the current-sheath resistance.

The diode voltage, V_p, has generally been [1], [17] given as

$$V_p = \frac{d}{dt}(L_p I_p) + I_p R_p = I_L R_L \tag{3}$$

at the insulator.

The inductance, L_p, may be defined as a function of the instantaneous position, z, of the current sheath if the volume behind it is linked with magnetic flux. In coaxial systems where the outer electrode or cathode is a cage of rods, one would expect the magnetic field to extend into the volume between and beyond the cathode-rod gaps. This increases the annulus inductance over that for two concentric cylindrical conductors. By assuming a flat current sheath, Eltgroth [14] has derived an expression for the annulus inductance and for the electrode geometry

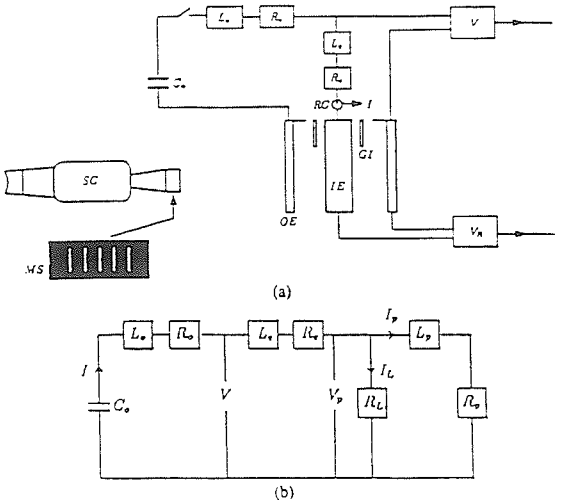

Fig. 1. (a) Schematic of the experimental setup. *IE*: inner electrode; *OE*: outer electrode; *GI*: glass insulator; *SC*: streak camera; *MS*: blackened microscope slide with an array of transparent slits; *RC*: Rogowski coil; C_0, L_0, and R_0 are, respectively, the capacitance, inductance, and the resistance of the capacitor bank; L_e and R_e are the inductance and the resistance of the high-voltage feedthrough behind the focus tube; V: voltage measured during the discharge; V_R: measured resistive current-sheath voltage; and I: total discharge current. (b) The equivalent circuit for a plasma-focus discharge.

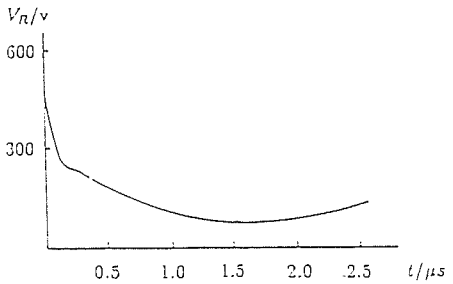

Fig. 2. Resistive voltage, V_R, of the current sheath, measured at the end of the focus tube.

with an even number of cathode-rods (6) in our device; this is given as

$$L_{pp} = 2.3\, z(\text{nH}) \tag{4}$$

where z is in cm.

A multislit streak camera [19] is set up to map out the plasma-sheath motion in the focus-tube annulus; we obtain the plasma-sheath position, z, as a function of time, t, during the run-down phase. Fig. 3 shows the results for that part of the plasma sheath adjacent to the inner electrode. In order to incorporate the information from this figure into the circuit analysis, it is necessary to assume a flat current sheath so that

$$L_p = L_{pp}. \tag{5}$$

We assume also the current-sheath position to be that of the luminous plasma sheath. Thus, values of L_p are estimated from Fig. 3.

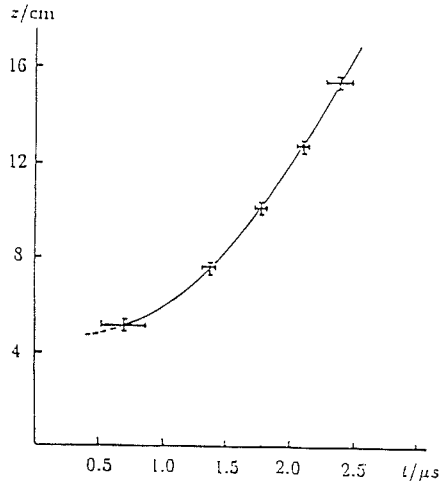

Fig. 3. Distance-time diagram of the luminous current sheath adjacent to the inner electrode (results from the multislit streak camera).

The circuit analysis begins with solving (1) for the diode voltage, V_p, and then (3) for the pinch current, I_p, leak current, I_L (difference between I and I_p), and the leak resistance, R_L. The current-sheath resistance, R_p, is calculated from (2). The following section will discuss the experimental observations and calculations.

III. Discussion of the Results

Results from this experiment are presented in two parts: Observations from the multislit camera, and calculated results.

A. Observations from the Multislit Camera

The initial phase is described [9] as the formation of current sheaths at the insulator and their lift-off in the radial direction, like an inverse pinch, to form a parabolic current sheath. In the conventional plasma focus, this phase takes a few-hundred nanoseconds before the parabolic current sheath lifts off the upper edge of the insulator and propagates downstream in the annular of the focus tube. We observed the axial lift-off at $t \sim 0.4$ μs, as shown in Fig. 3. The current sheath accelerates initially, but at $t \sim 1.7$ μs it begins to approach a maximum constant speed of about 9.2 cm/μs. This situation would mean that the rate of change of the inductance ($\dot{L}_p$) is constant and so macroscopic steady-state dynamics of the current sheath may be proposed. The observation of a maximum constant speed substantiates the results from numerical simulation [20] and the experimental observations in a coaxial shock tube by Keck [9], who attributed the cause of it to the ablation of material from the insulator. We will come to this problem again in subsection B. below.

B. Calculated Results

Fig. 4 presents the measured voltage, V, and the calculated diode voltage, V_p. When high-voltage breakdown occurs at the glass insulator, V is simply $(L_e/(L_e + L_0))V_0$, where V_0 is the charging voltage of the capacitor bank. The measured voltage, V, is observed to dip and rise within the next 200 ns. Detailed studies [21] reviewed that this is caused by a collective time-dependent resistance of ignitrons (eight pieces in parallel) and their switching jitters. These two effects prevent a prompt current buildup during the initial discharge, as shown in Fig. 5.

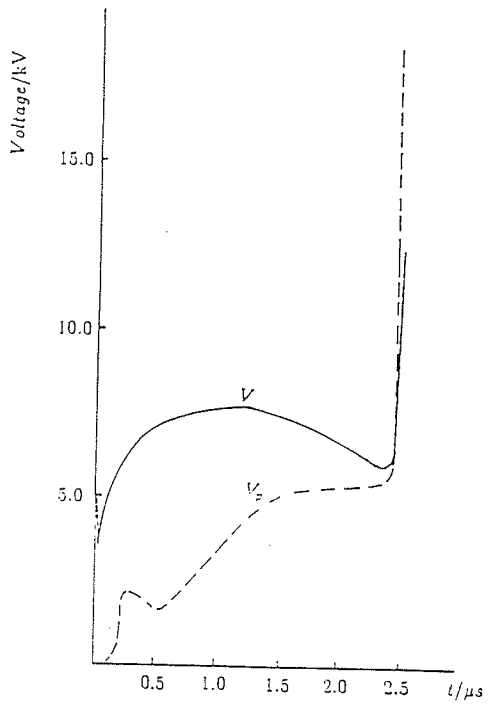

Fig. 4. V is the measured voltage during the plasma-focus discharge, while V_p is the calculated diode voltage generated by the propagating current sheath.

The diode voltage, V_p, is always found to be low for $t \leq 0.2$ μs, which may suggest that the current sheaths are confined to the glass insulator. Within the next 200 ns, however, V_p rises sharply, to about 1.2 kV, indicating possibly a fast inverse pinch of current sheaths. A small dip is observed at about 0.6 μs, which is the result of a slow initial run-down and a decreasing V_R. Thereafter, V_p increases steadily, mainly as a result of an increasing rate of change of inductance. At $t = 1.7$ μs, it approaches a maximum constant value of about 5.3 kV.

The pinch current, I_p, is presented in Fig. 5, showing a steady rise for the first part of the run-down phase; that is, for $t \leq 1.7$ μs. The maximum constant value of $I_p \simeq 200$ kA represents about 78 percent of the total discharge current. The remainder current, I_L, is taken to flow across the insulator surface (Fig. 1(b)).

A rather sudden saturation in the pinch current, I_p, could likely be explained by a second breakdown [10] at the insulator region in which a saturated I_p was measured by

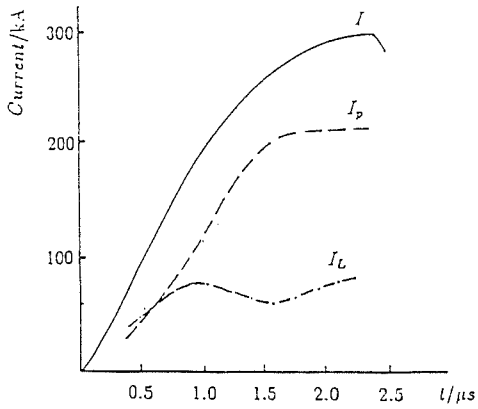

Fig. 5. I is the measured total discharge current, I_p is the calculated pinch current, and I_L is the leak current which is assumed to flow across the glass insulator.

a magnetic probe. A second breakdown is possible when the diode voltage, V_p, exceeds the holding voltage for the insulator region which results in more leak current I_L crowbarring the circuit. Similarly, the sharp voltage spike during the compression phase is known to cause restrikes [22], [23] at the insulator, and the leak current has been observed to surge rapidly [4], [6]. The presence of residual plasma would tend to promote the second breakdown and lower the holding voltage of the insulator.

A saturated I_p could be seen to limit the $\underline{J} \times \underline{B}$ driving force behind the current sheath, and this would then limit the run-down speed, v_z. These two effects stabilize the diode voltage, V_p, at a limiting value. However, it appears that I_p, V_p, and v_z adjust self-consistently, which results in macroscopic steady-state dynamics. This could only be possible when the input power ($I_p V_p$) is constant.

Fig. 6 shows the current-sheath resistance, R_p, which varies from about 10 mΩ at the axial lift-off to 0.4 mΩ at its minimum. We expect that the current sheath is rather resistive owing to the low level of ionization under these initial discharge conditions. It is thus likely that the current sheath is initially porous (due to inefficient snowplow action) and that residual plasma are left behind in this region, which furnish ground for leak current. This range of values for R_p agrees with that reported for MINI-FOKUS [24], which has similar electrical and geometrical parameters with our device. In the same figure, the leak resistance, R_L, is shown to vary between 25 and 100 mΩ.

IV. Conclusion

We have observed, from the points of view of gross dynamics and the input power, that a steady-state operation of the focus tube was established (~ 0.8 μs) towards the later part of the run-down phase. It should be noted that all the experimental measurements are simultaneous and nonperturbing to the current sheath. The calculated I_p was found to be lower than that from the magnetic-probe measurements [16], which show the same saturation profile under the same discharge conditions. The difference

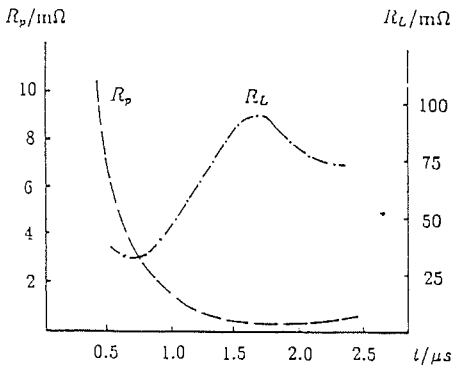

Fig. 6. R_p is the calculated current-sheath resistance and R_L is the leak resistance.

of 10 percent in the pinch current, I_p, is clearly owing to an over-estimate of the inductance, L_p, when a planar geometry is assumed for the current sheath. Nevertheless, the above plasma-focus calculations in the run-down phase show that a leak current and a possible second breakdown at the insulator have strong influence on the gross dynamics of the current sheath. These phenomena also establish an upper limit in the input power from the capacitor bank to the focus tube.

References

[1] G. Decker, R. Deutsch, and G. Pross, "The first and the final fifty nanoseconds of a fast focus device," *Phys. Fluids*, vol. 26, no. 2, p. 571, 1983.

[2] R. Deutsch and W. Kies, presented at the 4th Int. Workshop on Plasma Focus and Z-pinch Research, Warsaw, Poland, 1985.

[3] C. Gourlan *et al.*, "Recent progress in 1 MJ plasma focus and scaling for neutron production," in *Proc. 7th Int. Conf. on Plasma Phys. and Controlled Nucl. Fusion Res. 1978* (Innsbruck, Austria). Vienna: IAEA, 1979, vol. II, p. 123.

[4] C. Gourlan, H. Kroegler, Ch. Maisonnier, T. Oppenländer, and J. P. Rager, "Measurement of current density distribution in a 1 MJ plasma focus device," in *Proc. 8th Eur. Conf. on Plasma Phys. and Controlled Nucl. Fusion* (Prague, Czechoslavakia), 1977. Vienna: IAEA, 1978, vol. II, p. 247.

[5] T. Oppenländer, "Measurement of magnetic field and current density distribution in the Frascati 1 MJ plasma focus device," Associazione EURATOM-CNEN sulla Fusione, Centro di Frascati, Rome, Italy, Report, Mar. 1978.

[6] S. P. Chow, S. Lee, and B. C. Tan, "Current sheath studies in a coaxial plasma focus gun," *J. Plasma Phys.*, vol. 8, part 1, p. 21, 1972.

[7] P. G. Eltgroth, Lawrence Livermore Nat. Lab., Livermore, CA, Rep. no. UCIR-1249, 1978.

[8] T. Oppenländer, G. Pross, G. Decker, and M. Trunk, "The plasma focus current in the compression phase," *Plasma Phys.*, vol. 19, part 2, p. 1075, 1975.

[9] J. Keck, "Current speed in a magnetic annular shock tube," *Phys. Fluids Suppl.*, vol. S16, 1964.

[10] H. Krompholz, W. Neff, F. Rühl, K. Schönbach, and G. Herziger, "Formation of the plasma layer in a plasma focus device," *Phys. Lett.*, vol. 77A, no. 4, p. 246, 1980.

[11] S. V. Bazdenkov and V. V. Vikhrev, "Electrode regime of non-cylindrical Z pinch," *Sov. Phys. J.*, vol. 2, no. 3, p. 250, 1976.

[12] K. Behler and H. Bruhns, "Three-fluid magnetohydrodynamical simulation of plasma focus discharges," *Phys. Fluids*, vol. 30, no. 12, p. 3767, 1987.

[13] H. Herold *et al.*, "Investigation of the neutron production phases of large plasma focus discharges," in *Proc. 9th Int. Conf. on Plasma Phys. and Controlled Nucl. Fusion Res. 1982* (Baltimore, MD). Vienna: IAEA, 1983, vol. II, p. 405.

[14] P. G. Eltgroth, "Comparison of plasma focus calculations," *Phys. Fluids*, vol. 25, no. 12, p. 2408, 1982.
[15] T. Wainwright, Lawrence Livermore Nat. Lab., Livermore, CA, Rep. no. UCRL-19175, 1981.
[16] K. H. Kwek, unpublished paper, Universiti Malaya, Kuala Lumpur, Malaysia.
[17] J. W. Mather, in *Methods of Experimental Physics*, vol. 9, part B, p. 187.
[18] S. Lee and Y. H. Chen, "Geometrical optimization of the plasma focus," presented at the Symp. on Plasma Res., Theory and Experiment, ICTP, Trieste, Italy, 1981; published in *Fusion Energy—1981*, IAEA-SMR-82, p. 296.
[19] T. Y. Tou and S. Lee, "Multi-slit streak photography for plasma dynamics studies," *Rev. Sci. Instr.*, to be published.
[20] D. E. Potter, "Numerical studies of the plasma focus," *Phys. Fluids*, vol. 14, no. 9, p. 1911, 1971.
[21] T. Y. Tou, "Pinch radius ratio of the plasma focus," Ph.D. thesis, Universiti Malaya, Kuala Lumpur, Malaysia, 1986.
[22] A. Bernard, A. Coudeville, and J. P. Watteau, "Neutron yield of a focus device in various experiments," *Phys. Lett.*, vol. 33A, no. 8, p. 477, 1970.
[23] A. Bernard, A. Coudeville, A. Jolas, J. Launspach, and J. de Mascureau, "Experimental studies of the plasma focus and evidence for nonthermal process," *Phys. Fluids*, vol. 18, no. 2, p. 180, 1975.
[24] T. Oppenländer, "Messung der axialen stromichterteilung am plasmafokus," Master's thesis, Universitat Stuttgart, Stuttgart, West Germany, 1976.

*

T. Y. Tou received the B.Sc. and Ph.D. degrees in physics from the University of Malaya, Kuala Lumpur, Malaysia, in 1982 and 1987, respectively. He is currently a Postdoctoral Fellow at the Plasma Research Laboratory, Research School of Physical Sciences, Australian National University, Canberra.

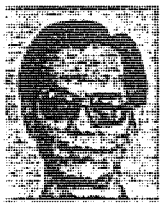

S. Lee received the B.Sc. and M.Sc. degrees in physics from the University of Malaya, Kuala Lumpur, Malaysia, in 1964 and 1966, respectively. He received the Ph.D. degree from the Australian National University, Canberra, in 1970.

Since 1970 he has lectured at the University of Malaya, where he is currently Professor of Applied Physics and Leader of the Research Groups on Plasma and Pulse Technology. He was a Alexander von Humboldt Research Fellow at Kernforschungsanlage, Julich, West Germany, in 1975–1976, a Commonwealth Academic Staff Fellow at the Imperial College, London, Eng., in 1981–1982, and a Visiting Professor and United Nations University Special Fellow at Flinders University of South Australia in 1986–1987. He is currently President of the newly formed Asian-African Association for Plasma Training (AAAPT). He is the author of more than 100 research papers, and is an ardent advocate and implementor of South-South technology creation and transfer, especially in plasma, fusion, laser and pulse technology.

Dr. Lee is a Chartered Physicist and Fellow of the Institute of Physics, U.K., and the Vice-President of the Malaysian Institute of Physics.

*

K. H. Kwek received the B.Sc. and M.Sc. degrees in physics from the University of Malaya, Kuala Lumpur, Malaysia, in 1980 and 1982, respectively.

Current Sheath Structures of the Plasma Focus in the Run-Down Phase

K. H. KWEK, T. Y. TOU, AND S. LEE

Abstract—**The current carrying plasma sheath in a 12-kJ plasma focus is studied in the axial run-down phase by means of the Schlieren technique. Subnanosecond ultraviolet light pulses from a preionized, transversely excited, atmospheric nitrogen laser provide sufficiently fine temporal and spatial resolutions for such investigation where the propagation speed of the current sheath is of the order of 10 cm/μs. It is observed that the current sheath grows thicker if it is driven at speeds beyond an optimum value of about 8 cm/μs (when the neutron yield is maximum). The thickening of the sheath is seen as an effect of the ratio of the specific heats. At the speed of 11 cm/μs the effect of the temperature gradient at the electrode surface broadens the sheath further. Slow driving speeds are observed to result in an inefficient and leaky piston.**

I. INTRODUCTION

THE NEUTRON yield is the parameter that is taken to be a measure of the quality of the plasma focus device. In all plasma focus experiments, the average number of neutrons Y_n produced by the *D–D* fusion reactions has the characteristic feature that significant values of Y_n are only detected within a well-defined range of values of the deuterium gas filling pressure. Outside this pressure range the neutron yield decreases in both high and low pressure limits, as shown in Fig. 1. It has been suggested that the neutron production is, in some way, related to the evolution of the current sheath structures already existing during the rundown phase [1], [2]. This hypothesis was arrived at through numerical considerations of electromechanical work performed on the sheath during the axial propagation. The failure of large devices (where the energies are of the order of several hundred kJ) to achieve their scaled neutron yield [3] due to the presence of leakage current flowing behind the main current sheath also points to the importance of the role of the sheath structure in neutron production. In such high current (several MA) devices, the sheath formation is very much affected by the high input power [4].

So far, little attention has been paid to the structure of the current sheath in the run-down phase, as compared to the emphasis given to the radial compression or the pinch phase of the plasma focus. The structure of the current sheath produced in the plasma focus has been studied theoretically and numerically through different approaches ranging from one-dimensional models to two-dimensional MHD codes [5]–[8]. None of these except the model developed in [8] included the process of ionization of the gas swept by the current sheath. The dependence of the structure of the current sheath on external parameters such as the filling pressures can also be drawn generally from this model. Experimentally, most of the work done during this phase has been centered around detection of light intensities emitted by the current sheath and magnetic and pressure probe measurements [9]–[13]. No work has been done so far to actually "visualize" the current sheath boundaries in the run-down phase with the exception of the Schlieren observations in [14]. However, the dependence of the structure of the current sheath on the filling pressure or propagation speed was not investigated.

The purpose of this paper is to draw attention to the importance of the structure of the current sheath which has definite bearing on the compression of the plasma pinch in the final collapse phase of the plasma focus, and

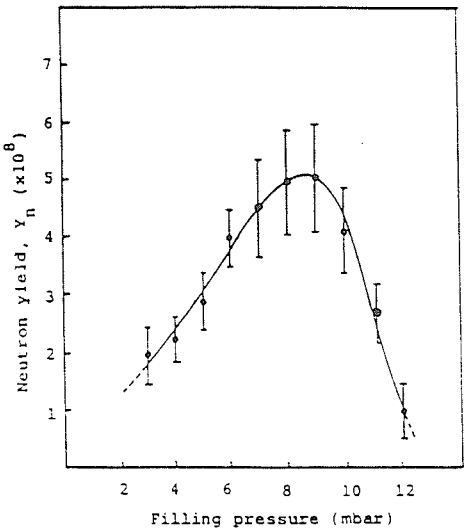

Fig. 1. Typical curve of neutron yield (measured using foil activation technique) as a function of deuterium gas filling pressure. The full circles are the mean values (averaged over 15 shots), and the error bars are the standard deviations of the means. The curve is obtained from the plasma focus device used in this work with the capacitor bank of 62 μF operated at 14 kV.

Manuscript received February 12, 1990; revised June 20, 1990. This work was partially supported by the Third World Academy of Sciences under Grant TWAS-RG-87-84 and by a University of Malaya Research Grant.

K. H. Kwek and S. Lee are with the Department of Physics, University of Malaya, 59100 Kuala Lumpur, Malaysia.

T. Y. Tou is with the Institute for Advanced Studies, University of Malaya, 59100 Kuala Lumpur, Malaysia.

IEEE Log Number 9038629.

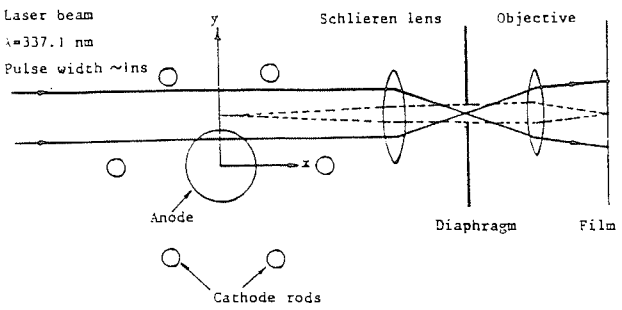

Fig. 2. Schematic of the Schlieren setup showing the relevant coordinates. The plasma focus electrodes are shown ends-on.

hence on the neutron yield. It definitely merits more detailed investigations to enhance our understanding of the plasma focus operation.

II. Experimental Arrangement

The experiments were performed on a 12-kJ (62 μF, 20 kV) Mather-type plasma focus device [15], [16]. Details of the parameters of the device can be found in [16]. Fig. 2 shows schematically the experimental setup of the Schlieren diagnostic technique. A transversely excited atmospheric nitrogen laser [17] was used to provide subnanosecond light pulses at a 337.1-nm wavelength. A system of corona blades was incorporated into the laser channel to provide preionization prior to the main laser discharge. This renders the output beam homogeneous and uniform in intensity to provide good Schlieren images. For sheath velocities of the order of 10 cm/μs during the run-down phase, the subnanosecond exposure time provides sufficiently fine spatial resolution to permit the observation of sheath structures in the submillimeter range. The expanded laser beam passes through the plasma focus chamber and is refocussed onto a diaphragm by the Schlieren lens, which together with the objective images the plasma onto the film plane, resulting in bright field pictures of the density gradients inside the plasma. The plasma radiation is suppressed by means of an interference filter. In the experiment a minimum deviation angle of 1 mrad was used.

III. Discussion of Results

Fig. 3(b) shows the current sheath during the run-down phase near the end of the center electrode. The field of view is equivalent to that shown schematically in Fig. 3(a). The filling deuterium gas pressure is at 9 mbar and the device is operated at 14 kV. Fig. 3(c) is a schematic representation of Fig. 3(b). In the coordinate system used, the end of the center electrode is at $z = 0$ mm and the surface is at $y = 12.5$ mm.

As expected, the current sheath across the electrodes is not planar, but canted backwards from the inner electrode (anode) to the outer electrode (cathode) owing to the radial dependence of the magnetic pressure gradient. The total accelerating force $\vec{j} \times \vec{B}_\theta$, where $\vec{j}$ is the current density and $\vec{B}_\theta$ is the induced magnetic field, acting perpendicular to the current boundary leads to radial and axial motions. The $(\vec{j} \times \vec{B}_\theta)_r$ radial component is outward and, in a sense, forces the sheath against the inner surface of the outer electrode. The axial component $(\vec{j} \times \vec{B}_\theta)_z$ varies with $1/r^2$ across the electrodes and leads to higher sheath velocities near the surface of the anode. Owing to the parabolic current boundary, plasma flows outward from the anode to cathode along the current boundary as the propagation of the sheath continues. The radial force and centrifugal flow will cause plasma pileup and stagnation at the outer electrode. It is well known that this problem, if not alleviated, will degrade the quality of the focussing action during the radial compression and hence the neutron production. For the plasma focus device used, the use of 6 rods as outer electrodes prevents the occurrence of such stagnation and buildup of the plasma.

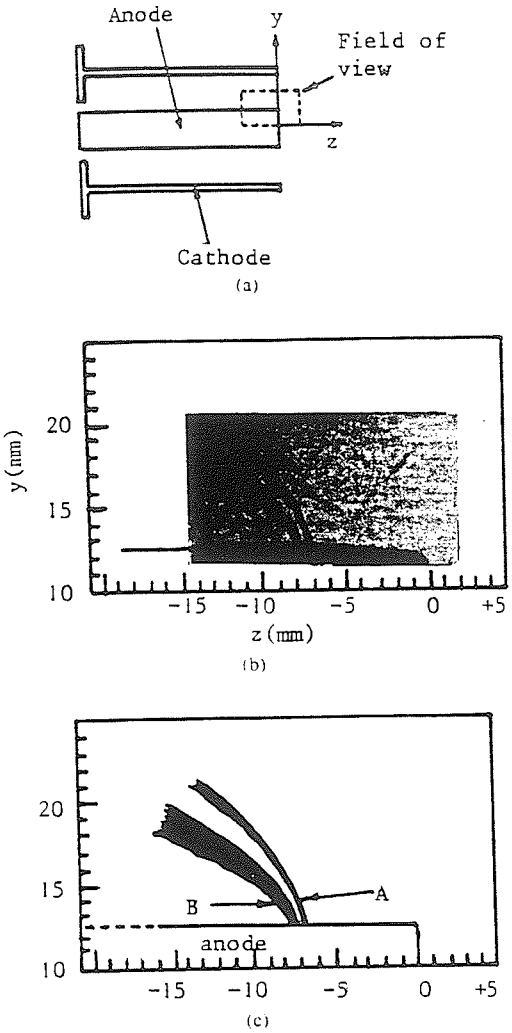

Fig. 3. (a) Field of view. (b) Schlieren image of the current sheath (deuterium focus at 9 mbar and 14 kV). (c) Sketch of the image in (b).

The current sheath produced in plasma focus devices can be thought of as a strong ionizing shock wave, driven by a magnetic piston, propagating into a rest gas and ionizing it. Between the moving shock and the piston there exists a finite volume of compressed plasma. Two gradient zones can be identified in the Schlieren image shown in Fig. 3(b). A frontal region identified as "A" corresponds to the gradient zone immediately after the plasma layer. Another region, "B," can be identified at the plasma–magnetic field interface. The dark line at region A is generally sharp, smooth, and well defined along the parabolic sheath, especially in the vicinity where the sheath intersects the anode ($z = -7$ mm and $12.5 < y < 15$ mm). In contrast, the line at region B is sharp and well defined only at the region, $z = -7$ mm, $12.5 < y < 15$ mm. Elsewhere, the dark line is rather broad and diffuse, especially in the regions towards the outer electrode ($y > 15$ mm). An interpretation of this behavior is that the magnetic piston is more efficient in the region just above the anode surface than in the region further away where the diffusion of the magnetic field into the plasma sheath occurs. Numerical studies [6], [7] and analytical steady-state fluid modeling [5] show that the temperatures fall with increasing radius (as the magnetic pressure falls). Due to finite and increasing resistivity, the diffusion of the magnetic field increases. The thickness of the layer also increases with increasing radius, as can be seen from the Schlieren image. This is in accord with the results of [18], wherein the broadening was attributed to the decreased plasma temperature at a larger radius.

From the above observations, it would seem that in the region adjacent to the anode surface the current sheath is properly formed due to efficient snowplowing by the magnetic piston, and between the moving shock and the piston there exists a compressed finite volume of hot plasma. The thickness of the plasma sheath in this region is about 1 mm and the shock is very nearly perpendicular to the surface. When the sheath diffracts at the truncated end of the anode, it is this small volume of compressed plasma that participates in the radial compression. It is thus important that the plasma sheath in this region is properly formed and compressed for good neutron production.

In a strong, equilibrium shock, where the Rankine–Hugoniot conditions are applied to the transition conditions across the shock, we have the well-known shock jump equation [19] for mass density:

$$\rho_s = \frac{\gamma + 1}{\gamma - 1} \rho_0 \qquad (1)$$

where ρ_0 is the filling density, ρ_s is the density immediately behind the shock, and γ is the ratio of the specific heats. $(\gamma + 1)/(\gamma - 1)$ is the shock compression and expresses the compressibility of the plasma. The compression of volume is $(\gamma - 1)/(\gamma + 1)$. In the strong shock limit, the compression of the plasma reaches a constant $(\gamma + 1)/(\gamma - 1)$, if γ is constant, and is independent of the piston pressure. If the driving force is increased, the density is unaffected and the temperature is simply increased. For simplicity, we consider a slab geometry of uniform plasma. After propagating a distance of 16-cm down the coaxial electrodes, the plasma layer would have a thickness of several centimeters if there were no mass loss. However, the Schlieren image indicates a much smaller value for the thickness (in the millimeter range). This apparent increase in compressibility of the plasma may be accounted for by noting that because of the canted nature of the sheath, some of the shocked gas is propelled towards the outer electrode. Since the outer electrode system is made out of rods rather than a solid cylinder, it is almost "transparent" to the mass flow. This mass loss allows the plasma sheath to be thinner than it would have been without the loss. It is also worthwhile to note that the above shock jump relation is for a free-running equilibrium shock, while it is only towards the end of the axial rundown phase that the current sheath reaches a macroscopic steady-state condition [13].

Fig. 4 shows Schlieren images of the current sheath towards the end of the run-down phase in different operating pressures. The peak speed is obtained by capturing images of the sheath at various positions along the anode and noting the respective times of arrival. The values of these speeds are confirmed through multislit streak photography [12]. The image shown in Fig. 4(d) is the same as that shown in Fig. 3(b) where the operating pressure yields the optimum number of neutrons.

It is quite apparent from the sheath appearances in Fig. 4(e) and (f) that the gradient zone at the plasma and magnetic field interface is no longer clearly defined. The turbulent-like nature of that region suggests that the magnetic piston is leaky and thus results in a progressively ineffective snowplowing as the operating pressure increases. The poor efficiency of the magnetic piston is the result of the slow driving speed of the piston, such that the temperatures in the sheath produced by the gas dynamic shock are not sufficiently high to produce complete ionization of the collected neutral gas. Thus the plasma becomes transparent to the magnetic field and leaks through. If the high ion temperature in the plasma focus is mainly due to randomization of the kinetic energy acquired by the ions during their radial acceleration [20], such a poor piston efficiency can strongly diminish the rate of fusion reactions. Thus, this establishes a high pressure limit.

As the operating pressure departs from the optimum value towards the lower pressure regime, several changes in the sheath structure can be observed. The thickness of the sheath in the region adjacent to the anode surface increases as the sheath velocity increases with reduced ambient pressure. This increase in thickness can be interpreted as the result of the effect of the specific heat ratio γ which determines the compressibility of the sheath. It is commonly assumed in most analysis and modeling [5]–[7] that γ takes the constant value of $5/3$. However, this is only true when the temperature is sufficiently high, as will be shown below in the calculation of the specific heat ratio for deuterium

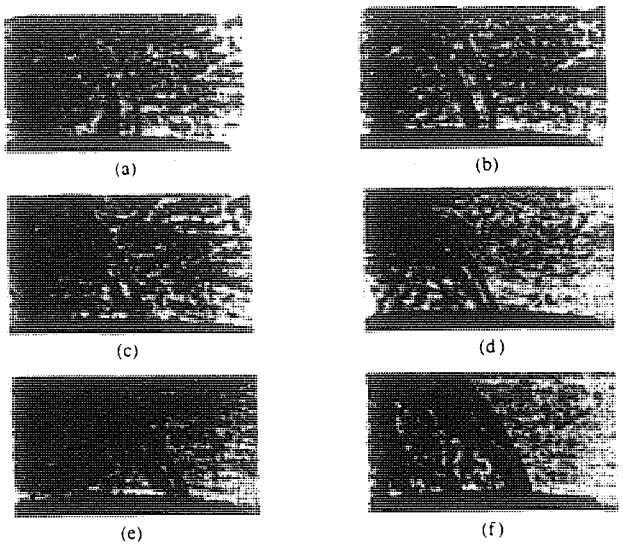

Fig. 4. Schlieren images of the current sheath in different operating pressures. Operating voltage is 14 kV. The field of view is the same as that shown in Fig. 3(a). (a) 1 mbar: 11 cm/μs. (b) 2 mbar: 10.2 cm/μs. (c) 4 mbar: 9.2 cm/μs. (d) 9 mbar: 8 cm/μs. (e) 11 mbar: 6 cm/μs. (f) 14 mbar: 5 cm/μs.

The value of γ may be defined in terms of the enthalpy per unit mass h as [21]

$$h = \frac{\gamma}{\gamma - 1}\frac{R_0}{M}TD \tag{2}$$

where

$$D = 1 + \sum_i i\alpha_i$$

the departure coefficient, R_0 = the universal gas constant, M = molecular (or atomic) weight, T = temperature, and α_i = fraction of ionization.

The enthalpy h may also be obtained by summing all the available modes of energy at a given temperature, giving the form:

$$h = \frac{5}{2}\frac{R_0TD}{M} + \frac{1}{m_a}\left[\sum_i \alpha_i E_i + \sum \alpha_i \bar{E}_i\right] \tag{3}$$

where m_a = mass of one atom of the gas, E_i = total ionization potential from the atom ground state to the ith ionization stage, and $\bar{E}_i$ = average excitation energy per ith ionized ion.

From (2) and (3) the expression for γ takes the form:

$$\frac{\gamma}{\gamma - 1} = \frac{5}{2} + \frac{m_a^{-1}\left(\sum_i \alpha_i E_i + \sum \alpha_i \bar{E}_i\right)}{(R_0TD)/M}. \tag{4}$$

The values of α may be computed for any given temperature by the use of Saha's equations. For deuterium, it is found that $\alpha_i \approx 1$ for T greater than 50 000 K. Thus,

$$\sum_i \alpha_i E_i + \sum \alpha_i \bar{E}_i \approx I_{\text{ion}}$$

where I_{ion} is the ionization potential of deterium.

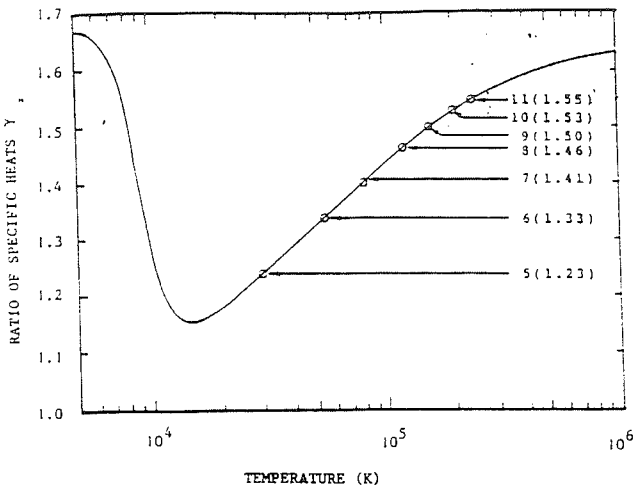

Fig. 5. Ratio of the specific heats γ as a function of temperature. The values shown just beside the pointers are speeds of propagation of the current sheath in cm/μs together with the values of γ in brackets. γ does not attain the value of 5/3 until the temperature exceeds 1 000 000 K.

The expression governing the relationship between the specific heat ratio γ, the temperature T, and the shock velocity v_s are obtained through strong shock-jump equations [19] and is given as:

$$T = 2.4 \times 10^{-4}\frac{M}{D}\frac{\gamma - 1}{(\gamma + 1)^2}v_s^2. \tag{5}$$

A plot of γ as a function of temperature is shown in Fig. 5. In the figure the values of γ and their corresponding shock speed are also indicated on the plot. From the plot it can be seen that the γ does not attain the value of 5/3 until the temperature exceeds 10^6 K.

The higher value of γ at $v_s = 11$ cm/μs when compared to the value of γ at $v_s = 8$ cm/μs indicates that the compression of the plasma is weaker at the lower pressure limit where the speed of propagation of the plasma sheath is high. Thus the sheath is thicker. An increase in compression in both an argon plasma focus [22] and in a linear Z-pinch operated in argon [23] when compared to that of deuterium or hydrogen plasmas has been observed. This effect has been explained solely on the basis of the difference in the effective value of γ of the argon plasma when compared with the γ of the deuterium or hydrogen plasma [24].

Fig. 4(a) also shows that the thickness of the sheath at the anode surface is broader than that above it. In all other images (except Fig. 4(e) and (f)), the minimum thickness of the sheath is at the anode surface. Numerical studies of the sheath development considering the influence of electron and ion heat conduction show that the temperature near and adjacent to the anode surface is reduced by heat losses to the electrode [6]. Decreasing temperatures towards the wall of the electrode give rise to an increasing shock thickness [18]. As a consequence, the sheath thickness increases towards the anode. Hence the sheath structure in the vicinity of the electrode in Fig. 4(a) may also

be interpreted as an effect of a temperature gradient coming into play.

IV. Conclusions

We have tried to show the significance of the current sheath structure in the run-down phase on the neutron production in the plasma focus. Operating the plasma focus device under different filling pressures leads to structural changes in the sheath as is revealed by the Schlieren images. The present results strongly indicate that ionization processes during the propagation of the sheath in the run-down phase plays an important role in determining the operating pressure regime. In most successful plasma focus devices the optimum operating pressures seem to be centered around 10 mbar regardless of the energy of the devices. Furthermore, the speeds of propagation of the sheath in the run-down phase are seldom greater than 10 cm/μs (see [25, table I]). More detailed investigations into the structure of the current sheath are definitely required before this peculiar behavior of the plasma focus can be understood properly.

References

[1] R. Gratton, H. Kelly, M. Milanese, and J. Pouzo, "On the upper limit for the efficient operation of a plasma focus device," *Phys. Lett.*, vol. 62A, no. 4, p. 422, 1980.

[2] M. Milanese and J. Pouzo, "Critical analysis of plasma focus design based on the implications of an upper pressure limit," *Nucl. Fusion*, vol. 25, no. 7, p. 840, 1985.

[3] C. Gourlan *et al.*, "Recent progress in 1 MJ plasma focus and scaling for neutron production," in *Proc. 7th. Int. Conf. Plasma Phys. and Controlled Nuci. Fusion Res.* (Innsbruck, Austria), 1978. Vienna: IAEA, 1979, vol. II, p. 123.

[4] W. Kies, "Power limits for dynamical pinches?" *Plasma Phys. Contr. Fusion*, vol. 28, no. 11, p. 1645, 1986.

[5] G. Herziger, H. Krompholz, W. Schneider, and K. Schönbach, "A steady-state fluid model of the coaxial plasma gun," *Phys. Lett.*, vol. 71A, no. 1, p. 54, 1979.

[6] D. E. Potter, "Numerical studies of the plasma focus," *Phys. Fluids*, vol. 14, no. 9, p. 1911, 1971.

[7] K. Behler and H. Bruhns, "Three-fluid magnetohydrodynamical simulation of plasma focus discharges," *Phys. Fluids*, vol. 30, no. 12, p. 3767, 1987.

[8] L. Bilbao, H. A. Bruzzone, and H. J. Kelly, "Structure of a plane and stationary ionizing current sheath," *Plasma Phys. Contr. Fusion*, vol. 26, no. 12B, p. 1535, 1984.

[9] S. P. Chow, S. Lee, and B. C. Tan, "Current sheath studies in a coaxial plasma focus gun," *J. Plasma Phys.*, vol. 8, part 1, p. 21, 1972.

[10] T. Oppenländer, "Measurement of magnetic field and current density distribution in the Frascati 1 MJ plasma focus device," Associazione EURATOM-CNEN sulla Fusione, Centro di Frascati, Rome, Italy, Rep. No. 78.6, Mar. 1978.

[11] L. Bilbao, H. A. Bruzzone, H. Kelly, and M. Esper, "Structure of a plasma-focus current sheath from magnetic and optical measurements," *IEEE Trans. Plasma Sci.*, vol. PS-13, p. 202, Aug. 1985.

[12] T. Y. Tou and S. Lee, "Multi-slit streak photography for plasma dynamics studies," *Rev. Sci. Instr.*, vol. 59, p. 2370, 1988.

[13] T. Y. Tou, S. Lee, and K. H. Kwek, "Nonperturbing plasma-focus measurements in the run-down phase," *IEEE Trans. Plasma Sci.*, vol. 17, p. 311, Apr. 1989.

[14] C. R. Haas, R. Noll, F. Rühl, and G. Herziger, "Schlieren diagnostic of the plasma focus," *Nucl. Fusion*, vol. 24, no. 9, p. 1216, 1984.

[15] J. W. Mather, in *Methods of Experimental Physics*, vol. 9. New York: Academic, 1971, part B, p. 187.

[16] S. Lee and Y. H. Chen, "Geometrical optimization of the plasma focus," presented at the Symp. on Plasma Res., Theory and Experiment, ICTP, Trieste, Italy, 1981 (published in *Fusion Energy—1981*, IAEA-SMR-82).

[17] K. H. Kwek, T. Y. Tou, and S. Lee, "A preionized nitrogen laser as a diagnostic light source for fast pulsed experiments," *IEEE Trans. Instrum. Meas.*, vol. 38, p. 103, 1989.

[18] R. A. Gross, "Thickness of a shock wave in hydrogen," *Phys. Fluids*, vol. 10, p. 1853, 1967.

[19] R. A. Gross, "Strong ionizing shock waves," *Rev. Mod. Phys.*, vol. 37, no. 4, p. 724, 1965.

[20] L. A. Artsimovich, *Controlled Thermonuclear Reactions*. London: Oliver and Boyd, 1964, p. 129.

[21] A. B. Cambel, *Plasma Physics and Magnetofluidmechanics*. New York: McGraw-Hill, 1963, p. 104.

[22] T. Y. Tou, "Pinch radius ratio of the plasma focus," Ph.D. thesis, Universiti Malaya, Kuala Lumpur, Malaysia, 1986.

[23] P. F. M. Baldock *et al.*, "High density high temperature plasma production in fast Z-pinch," presented at the 9th Ann. Conf. on Plasma Physics, Oxford, UK, 1982.

[24] S. Lee, "Radius ratios of argon pinches," *Aust. J. Phys.*, vol. 36, p. 891, 1983.

[25] H. Krompholz, F. Rühl, W. Schneider, K. Schönbach, and G. Herziger, "A scaling law for plasma focus devices," *Phys. Lett.*, vol. 82A, no. 2, p. 82, 1981.

*

K. H. Kwek received the B.Sc., M.Sc., and Ph.D. degrees in physics from the University of Malaya, Kuala Lumpur, Malaysia, in 1980, 1982, and 1989, respectively.

*

T. Y. Tou received the B.Sc. and Ph.D. degrees in physics from the University of Malaya, Kuala Lumpur, Malaysia, in 1982 and 1987, respectively.

He was a Postdoctoral Fellow at the Plasma Research Laboratory, Research School of Physical Sciences, Australian National University, Canberra, from 1987 to 1989. He is currently a Research Fellow at the Institute for Advanced Studies, University of Malaya.

*

S. Lee received the B.Sc. and M.Sc. degrees from the University of Malaya, Kuala Lumpur, Malaysia, in 1964 and 1966, respectively. He received the Ph.D. degree from the Australian National University, Canberra, in 1970.

Since 1970 he has lectured at the University of Malaya, where he is currently Head of the Physics Department and Professor of Applied Physics. He is also Leader of the Research Groups on Plasma and Pulse Technology. He was an Alexander von Humbolt Research Fellow at Kernforschungsanlage, Julich, West Germany, in 1975–1976, a Commonwealth Academic Staff Fellow at the Imperial College, London, England, in 1981–1982, and a Visiting Professor and United Nations University Special Fellow at the Flinders University of South Australia in 1986–1987. He is currently President of the newly formed Asian-African Association for Plasma Training (AAAPT). He is the author of more than 100 research papers and is an advocate and implementor of South-South technology creation and transfer, especially in plasma, fusion, laser, and pulse technology.

Dr. Lee is a Chartered Physicist and Fellow of the Institute of Physics (UK) and the Vice President of the Malaysian Institute of Physics.

HALF-LIFE MEASUREMENT OF ^{116}In USING PLASMA FOCUS NEUTRONS

S.P. MOO, C.K. CHAKRABARTY and S. LEE
Plasma Research Laboratory
Physics Department, University of Malaya
59100 Kuala Lumpur.

Received 2 May 1989

Abstract

The half-life of the ground state of ^{116}In has been measured many times. However, there is considerable scatter in the value reported. In an investigation on the usefulness of the plasma focus as a neutron source, the half-lives of several nuclides have been measured. This paper reports the measurement of the half-life of ^{116}In.

Introduction

The half-life of the ground state of ^{116}In has been measured many times.[1] However, there is considerable scatter in the value reported, from a low of 12.5 ± 2 s (Wilhemlmi et al.[2]) to a high of 15.6 ± 0.5 s (Brzosko et al.[3]). The value with the highest accuracy quoted is 14.10 ± 0.03 s (Beckurts et al.[4]).

In an investigation on the usefulness of the small plasma focus device[5,6] as a neutron source, the activation of indium in the reaction ^{115}In(n, γ) ^{116}In has been investigated and the half-life of ^{116}In measured. Even with the relatively cheap and simple plasma focus neutron source, we have been able to obtain a value comparable with the result of Beckurts et al.

Method

The present investigation involves two plasma focus devices, the UNU/ICTP PFF[5] and the UMDPFI[7]. With deuterium as the filling gas the former yields $\approx 10^8$ neutrons/burtst while the latter yields $\approx 50 - 100$ ns. The experimental arrangement used in this investigation is shown schematically in Fig. 1. The D – D neutrons are slowed down by 40 mm of paraffin before impinging on an indium foil of diameter 50 mm and thickness 0.2 mm. An NE-102 plastic scintillator optically coupled to a photomultiplier is used to detect the β particles emitted. The β activity of the indium foil before and after the neutron burst is recorded by means of a multichannel analyser operating on the multiscaling mode at 3 s dwell time.

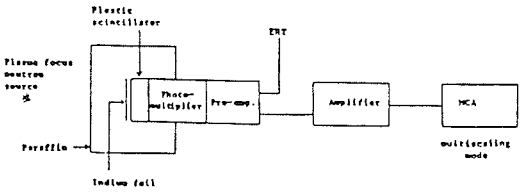

Fig. 1. Schematic diagram of equipment for half life measurements.

Results and discussion

Table 1 shows the possible isotopes formed[1] when natural indium is exposed to slow neutrons. From the combination of activation cross sections and abundances, it is clear that the contribution to the total β activity from ^{114}In is negligible (less than 0.2%). At early times the dominant contribution comes from the ground state of ^{116}In. Contribution from the isomeric state ^{116}In^{m1} is small, its initial activity being about 2% of the initial activity of the ground state. Furthermore, because of its relatively long half-life (54 min), its contribution to the detector counts can be considered as a component of the constant background in the first 90s of the decay.

Fifteen independent measurements of the indium activity are made with the UNU/ICTP PFF and another seven with the UMDPFI. The maximum counts in the first set of measurements ranged between 300/channel and 1100/channel while in the second set they ranged between 1000/channel and 2700/channel. The decay curve of one of the runs is shown in Fig. 2. It is consistent with a single decay component. For the determination of the half-life, the counts recorded in 30 channels (90 s) of the decay curve starting from the second channel after the neutron burst, are considered. After background substraction, a weighted least squares fit[8,9] is applied to each of the decay curves over the region where the net counts exceed three times the background counts. The weight applied is given by

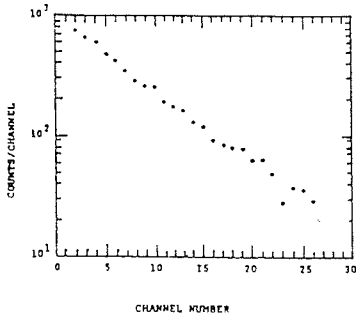

Fig. 2 Beta decay curve of ^{116}In.

Table 1. The possible isotopes formed when natural indium is exposed to slow neutrons.

Isotopes (abundance)	Activation Cross Section (b)	Products (half-life)	Radiation of interest
^{113}In (4.3%)	3	^{114}In (72 s)	β^- (1.99 MeV)
	8	^{114}In^{m1} (50d)	
^{115}In (95.7%)	42	^{116}In (14s)	β^- (3.3 MeV)
	161	^{116}In^{m1} (54 m)	β^- (1.0 MeV)
	91	^{116}In^{m2} (2.2 s)	γ (164 keV)

Table 2. The half-life of ^{116}In.

	Tish paper		Earlier results		
Run No.	Set 1 $t_{1/2}$ (s)	Set 2 $t_{1/2}$(s)	$t_{1/2}$(s)	References	Year
1	14.90 ±0.74	14.24 ± 0.23	15.6 ± 0.5	Brzosko et al.[3]	1965
2	13.94 ±0.92	14.17 ± 0.28	14.10 ± 0.03	Beckurts et al.[4]	1963
3	13.97 ±0.41	14.62 ± 0.28	14.05 ± 0.26	Ducat & Thomas[10]	1960
4	14.28 ±0.58	14.06 ± 0.35	13.4 ± 0.4	Domanic & Sailor[11]	1960
5	14.34 ±0.28	14.13 ± 0.21	14.5 ± 0.4	Capron et al.[12]	1959
6	14.25 ±0.39	14.21 ± 0.18	12.5 ± 2	Wilhemli et al.[2]	1953
7	14.04 ±0.46	14.40 ± 0.24	13 ±	Cork & Lawson[13]	1939
8	13.12 ±0.79				
9	13.11 ±0.73				
10	14.49 ±0.62				
11	14.30 ±0.55				
12	14.55 ±0.46				
13	14.60 ±0.27				
14	13.80 ±0.44				
15	13.78 ±0.30				
	14.20 ± 0.15	14.25 ± 0.13	(weighted mean value)		

$$w_i = (y_i - b)^2 / (\sqrt{y_i} + \Delta b)^2$$

where y_i is the count at channel i, b is the average background and Δb is the error of the background. Our results show that the fitting routine yields a consistent value of the half-life when the fitted interval exceeds about 2 $t_{1/2}$.

The half-life calculated from the 2 sets of measurements are listed in Table 2. For the first set of measurements, the calculated values of the half-life range from 13.11 s to 14.90 s while the statistical errors range from 0.27 s to 0.92 s. The scatter for the second set of measurements is smaller, the calculated values of the half-life range from 14.06 s to 14.62 s while the individual statistical errors range from 0.18 s to 0.35 s. The weighted mean is 14.20 ± 0.15 s for the first set and 14.25 ± 0.13 s for the second set. A possible systematic error of 0.1 s arising from uncertainties in the background subtraction and from dead time losses is included in the final errors quoted. Also listed in Table 2 are earlier measurements of the half-life of ^{116}In. Our values agree well with the measurement of Beckurts et al.[4] (14.10 ±0.03 s) and with Ducat and Thomas[10] (14.05 ± 0.26 s).

Acknowledgement

This work was supported by the University of Malaya and the Ministry of Science and Technology.

References

1. C.M. Lederer, V.S. Shirley, *Tables of Isotopes*, 7th Ed. (1978).
2. Z. Wilhelmi, R. Brunsz and C. Dabrowski, Bull. Akad. Polon. Sci. 1, 105 (1953) as reported by A. Ducat and R.H. Thomas, Nucl. Phys. 15, 525 (1960)
3. J. Brzosko, P. Decowski, K. Siwek-Diament and Z. Wilhelmi, Nucl. Phys. 74, 438 (1965).

4.K.H. Beckurts, M. Brose, M. Knoche, G. Kruger, W. Ponitz and H. Schmidt, Nucl. Sci. Eng. 17, 329 (1963).
5.S. Lee, T.Y. Tou, S.P. Moo, M.A. Eissa, A.V. Gholap, K.H. Kwek, S. Mulyodrono, A.J. Smith, Suryadi, W. Usada and M. Zakaullah, Am. J. Phys. 56, 62 (1988).
6.S.P. Moo and S. Lee, Sing. J. Phys. 4, 131 (1987).
7. S. Lee and Y.H. Chen, Fusion Energy – 1981 (ICTP, Trieste) IAEA – SMR 82, Vienna, p.297.
8.S.L. Meyer, *Data Analysis for Scientists and Engineers*, Wiley, New York (1975).
9.K.S. Krane and L. Schecter, Am. J. Phys. 50, 82 (1982).
10.A. Ducat and R.H. Thomas, Nucl. Phys. 15, 525 (1960).
11.F. Domanic and V.L. Sailor, Phys. Rev. 119, 208 (1960).
12.P.C. Capron and A. VanderStricht, Nucl. Sci. Abstr. 13, No. 358 (1959).
13.J.M. Cork and L.J. Lawson, Phys. Rev. 56, 291 (1939).

Sequenced nitrogen lasers

S. Lee and K. H. Kwek
Plasma Research Laboratory, University of Malaya, 59100 Kuala Lumpur, Malaysia

Jalil Ali,[a] M. V. H. V. Prabhakar,[b] Y. S. Shishodia,[c] and A. G. Warmate[d]
(United Nations University) International Centre for Theoretical Physics, Training Programme on Plasma and Laser Technology, Physics Department, University of Malaya, 59100 Kuala Lumpur, Malaysia

(Received 26 September 1988; accepted for publication 3 January 1989)

A pulsed nitrogen laser may consist of a laser channel sitting astride two parallel-plate capacitors, one of which is the voltage-swinging capacitor and the second is the laser discharge capacitor. A multichannel nitrogen laser system is proposed for which the laser discharge capacitor of the first laser channel also acts as the voltage-swinging capacitor of the second laser channel, the laser discharge capacitor of the second laser channel also acts as the voltage-swinging capacitor of the third laser channel, and so on. This enables several laser channels to be fired to obtain full power laser pulses in a precision sequence when operated in the "prompt sequencing" mode.

I. INTRODUCTION

The transversely excited pulsed nitrogen laser may use two capacitors, the voltage-swinging capacitor C_1 and the laser discharge capacitor C_2 such as shown in Fig. 1 (circuit e and circuit 1 only without circuits 2 and 3). When the external spark gap S is triggered I_e starts flowing in circuit e and the voltage across the first laser channel V_{g1} starts to rise towards $V_2 - (-V_1)$ as C_1 discharges. The laser channel is typically set to break down at 1.3–1.7 of V_1. When V_{g1} exceeds this set value I_1 starts to flow. Discharge uniformity requiring a dV_g/dt of 0.5 kV/ns or greater[1,2] may generally be improved by the use of preionizers.[3–5] A time resolution of 1 ns is needed for optical imaging of fast phenomena such as the plasma focus.[6]

For the study of fast dynamics it is often advantageous to obtain pictures in a real-time movielike sequence with frame separation of several nanoseconds. This has been achieved using one nitrogen laser pulse by beam division and optical delay[7] or by mode locking a nitrogen laser-pumped dye laser.[8] These methods have the drawback of reduced power. A multiframing system using several nitrogen lasers controlled by delay lines has been reported.[9] The sequencing precision is, however, not good, being limited by the inherent jitters of the individual spark gaps of the lasers.

In our present development we connect several nitrogen lasers as an electrical network so that the lasers are fired in sequence. The system has the potential of multiframing at precise intervals of a few nanoseconds and with each frame having the full power of a single nitrogen laser pulse.

II. THEORY

We consider three laser channels to be fired in sequence as shown in Fig. 1. The voltage difference across the three channels are denoted respectively by V_{g1}, V_{g2}, and V_{g3}. In general, the capacitors C_1, C_2, C_3, C_4 are charged to voltage V_1, V_2, V_3, and V_4, respectively. As discussed earlier, the first laser channel breaks down when the voltage-swinging C_1 discharges, enabling C_2 to discharge I_1 through the first laser channel. The discharge of C_2 pulls the right-hand side of the second laser channel downwards from V_2 towards $-V_2$ so that C_2 whilst powering the first laser channel, also acts as the voltage swinging capacitor for the second laser channel. If the voltage swing is sufficient to break down the second laser channel, then C_3 discharges I_2, powering the second laser channel whilst simultaneously acting as the voltage-swinging capacitor for the third laser channel until C_4 is able to discharge I_3 through the third laser channel.

III. EQUATIONS

We take the laser channel inductance and resistance to be L_g and r_g for each laser gap. The stray inductance leading up to the laser gap on each side is taken to be $L_{s1} \simeq L_{s2} = L_s$.

The relevant equations may be written as follows.

A. Circuit *e*

$$(L_e + L_1)\frac{dI_e}{dt} - L_1\frac{dI_1}{dt} + r_e I_e = V_1 - \int_0^t \frac{(I_e - I_1)}{C_1}\,dt. \tag{1}$$

Circuit e is switched on at $t = 0$.

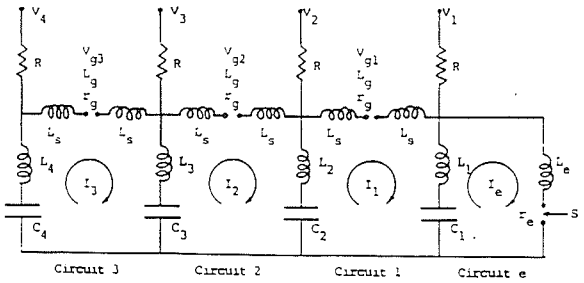

FIG. 1. Circuit diagram of the three-channel sequenced nitrogen laser.

[a] Permanent address: Physics Department, Technology University of Malaysia, Kuala Lumpur, Malaysia.
[b] Permanent address: Department of Physics and Astrophysics, University of Delhi, Delhi, India.
[c] Permanent address: University Science Instrumentation Centre, University of Rajasthan, Jaipur, India.
[d] Permanent address: Physics Department, Rivers State University of Science and Technology, Port Harcourt, Nigeria.

 0021-8979/89/114133-05$02.40

The voltage difference across the first laser channel is

$$V_{g1} = (V_2 - V_1) + \frac{\int (I_e - I_1)dt}{C_1} - \frac{\int (I_1 - I_2)dt}{C_2} + L_1 \frac{dI_e}{dt} + L_2 \frac{dI_2}{dt} - (2L_s + L_1 + L_2) \frac{dI_1}{dt}. \quad (2)$$

Circuit 1 is switched on when V_{g1} reaches a preset value, e.g., $1.6V_1$.

B. Circuit 1

$$(2L_s + L_g + L_1 + L_2) \frac{dI_1}{dt} - L_2 \frac{dI_2}{dt} - L_1 \frac{dI_e}{dt} + r_g I_1 = (V_2 - V_1) + \frac{\int I_2 - I_1}{C_2} dt + \frac{\int I_e - I_1}{C_2} dt. \quad (3)$$

The voltage difference across the second laser channel is

$$V_{g2} = (V_3 - V_2) + \frac{\int (I_1 - I_2)dt}{C_2} - \frac{\int (I_2 - I_3)dt}{C_3} + L_2 \frac{dI_1}{dt} + L_3 \frac{dI_3}{dt} - (2L_s + L_2 + L_3) \frac{dI_2}{dt}. \quad (4)$$

Circuit 2 is switched on when V_{g2} reaches a preset value.

C. Circuit 2

$$(2L_s + L_g + L_2 + L_3) \frac{dI_2}{dt} - L_3 \frac{dI_3}{dt} - L_2 \frac{dI_1}{dt} + r_g I_2 = (V_3 - V_2) + \frac{\int I_3 - I_2}{C_3} dt + \frac{\int I_1 - I_2}{C_2} dt. \quad (5)$$

The voltage difference across the third laser channel is

$$V_{g3} = (V_4 - V_3) + \frac{\int I_2 - I_3}{C_3} dt - \frac{\int I_3}{C_4} dt + L_3 \frac{dI_2}{dt} - (2L_s + L_3 + L_4) \frac{dI_3}{dt}. \quad (6)$$

Circuit 3 is switched on when V_{g3} reaches a preset value.

D. Circuit 3

$$(2L_s + L_g + L_3 + L_4) \frac{dI_3}{dt} - L_3 \frac{dI_2}{dt} + r_g I_3 = (V_4 - V_3) - \frac{\int I_3}{C_4} dt + \frac{\int (I_2 - I_3)}{C_3} dt. \quad (7)$$

Equations (1), (3), (5), and (7) are the equations governing the discharge of the four circuits while Eqs. (2), (4), and (6) are the equations determining the times of switching on, respectively, circuit 1, circuit 2, and circuit 3 relative to time $t = 0$.

E. Normalization

The variables are normalized in the following manner:

$\tau = t/t_0$,

where the unit time is $t_0 = \sqrt{(L_1 C_1)}$,

$\iota_e = I_e/I_0$

with a unit current of $I_0 = V_1/\sqrt{(L_1/C_1)}$. Also

$\iota_1 = I_1/I_0$, $\iota_2 = I_2/I_0$, $\iota_3 = I_3/I_0$,

and

$\nu_{g1} = V_{g1}/V_1$, $\nu_{g2} = V_{g2}/V_1$,

and

$\nu_{g3} = V_{g3}/V_1$. We thus obtain the following normalized equations.

1. Circuit e

$$\frac{d\iota_e}{d\tau} = \left(1 - \int (\iota_e - \iota_1)d\tau + \frac{d\iota_1}{d\tau} - \alpha_e \iota_e\right) \Big/ (1 + \beta_e), \quad (8)$$

$$\nu_{g1} = (\nu_2 - 1) + \int (\iota_e - \iota_1)d\tau - \left(\int (\iota_1 - \iota_2)d\tau \Big/ \delta_2\right) + \frac{d\iota_e}{d\tau} + \beta_2 \frac{d\iota_2}{d\tau} - (1 + 2\beta_s + \beta_2) \frac{d\iota_1}{d\tau}. \quad (9)$$

Circuit 1 is switched on only when ν_{g1} reaches the preset value of F_1.

2. Circuit 1

$$\frac{d\iota_1}{d\tau} = \left[(\nu_2 - 1) + \left(\int (\iota_2 - \iota_1)d\tau \Big/ \delta_2\right) + \int (\iota_e - \iota_1)d\tau + \beta_2 \frac{d\iota_2}{d\tau} + \frac{d\iota_e}{d\tau} - \alpha_g \iota_1\right] \Big/ (1 + \beta_2 + \beta_g + 2\beta_s), \quad (10)$$

$$\nu_{g2} = (\nu_3 - \nu_2) + \left(\int (\iota_1 - \iota_2)d\tau \Big/ \delta_2\right) - \left(\int (\iota_2 - \iota_3)d\tau \Big/ \delta_3\right) + \beta_2 \frac{d\iota_1}{d\tau} + \beta_3 \frac{d\iota_3}{d\tau} - (2\beta_s + \beta_2 + \beta_3) \frac{d\iota_2}{d\tau}. \quad (11)$$

Circuit 2 is switched on only when ν_{g2} reaches the preset value of F_2.

3. Circuit 2

$$\frac{d\iota_2}{d\tau} = \left[(\nu_3 - \nu_2) + \left(\int (\iota_3 - \iota_2)d\tau \Big/ \delta_3\right) + \left(\int (\iota_1 - \iota_2)d\tau \Big/ \delta_2\right) + \beta_3 \frac{d\iota_3}{d\tau} + \beta_2 \frac{d\iota_1}{d\tau} - \alpha_g \iota_2\right] \Big/ (\beta_2 + \beta_3 + \beta_g + 2\beta_s), \quad (12)$$

$$\nu_{g3} = (\nu_4 - \nu_3) + \left(\int (\iota_2 - \iota_3)d\tau \Big/ \delta_3\right) - \left(\int \iota_3 d\tau \Big/ \delta_4\right) + \beta_3 \frac{d\iota_2}{d\tau} - (2\beta_s + \beta_3 + \beta_4) \frac{d\iota_3}{d\tau}. \quad (13)$$

Circuit 3 is switched on only when ν_{g3} reached the preset value of F_3.

4. Circuit 3

$$\frac{d\iota_3}{d\tau} = \left[(\nu_4 - \nu_3) - \left(\int \iota_3 d\tau \Big/ \delta_4\right) + \left(\int (\iota_2 - \iota_3) d\tau \Big/ \delta_3\right) + \beta_3 \frac{d\iota_2}{d\tau} - \alpha_g \iota_3\right] \Big/ (\beta_3 + \beta_4 + \beta_g + 2\beta_s). \tag{14}$$

Equations (8), (10), (12), and (14) are used to compute for ι_e, ι_1, ι_2, and ι_3. Equations (9), (11), and (13) are used to determine the times of switching on, respectively, circuit 1, circuit 2, and circuit 3.

The scaling parameters are

$$\beta_e = L_e/L_1, \quad \beta_2 = L_2/L_1, \quad \beta_3 = L_3/L_1,$$
$$\beta_4 = L_4/L_1, \quad \beta_s = L_s/L_1, \quad \beta_g = L_g/L_1,$$
$$\delta_2 = C_2/C_1, \quad \delta_3 = C_3/C_1, \quad \delta_4 = C_4/C_1,$$
$$\nu_2 = V_2/V_1, \quad \nu_3 = V_3/V_1, \quad \nu_4 = V_4/V_1,$$

and

$$\alpha_e = r_e/\sqrt{(L_1/C_1)}, \quad \alpha_g = r_g/\sqrt{(L_1/C_1)},$$

where r_e and r_g are, respectively, the spark gap and laser channel resistance, and the preset breadown voltages of the laser channels are written, normalized to V_1, as F_1, F_2, and F_3.

IV. INTEGRATION PROCEDURE

The scaling parameters are first specified. At $\tau = 0$, Eq. (8) is integrated for ι_e numerically by linear approximation with the initial conditions of $\int \iota_e d\tau = 0$, $\iota_e = 0$, and $d\iota_e/d\tau = 1/(1+\beta_e)$. The quantities ι_1 and $d\iota_1/d\tau$ are kept at 0 until the value of ν_{g1} computed from Eq. (9) at each step reaches the preset value. At this time, Eq. (10) is brought into operation, switching circuit 1 on to compute the value of ι_1 simultaneous with ι_e from Eq. (8). During the simultaneous integration of Eqs. (8) and (10), $\int \iota_2\, d\tau$, ι_2, and $d\iota_2/d\tau$ are kept at zero and ν_{g2} is computed at each step from Eq. (11) to determine when circuit 2 is switched on by bringing Eq. (12) into the integration scheme. Equations (8), (10), and (12) are then simultaneously integrated for ι_e, ι_1, and ι_2. During this integration, $\int \iota_3\, d\tau$, ι_3, and $d\iota_3/d\tau$ are kept at zero whilst ν_{g3} is computed at each step from Eq. (13) to determine when circuit 3 is switched on after which time all from Eqs. (8), (10), (12), and (14) are simultaneously integrated for ι_e, ι_1, ι_2, and ι_3.

V. RESULTS OF COMPUTATION

A. Case 1: Uniform capacitances and charging voltages—prolonged sequencing mode

We first consider a system with identical laser heads and with all capacitors identical and charged to the same voltage. Typically such a system may have

$$L_e = 12 \text{ nH}, \quad L_1 = L_2 = L_3 = L_4 = 0.15 \text{ nH},$$
$$L_g = 0.1 \text{ nH}, \quad L_s = 0.1 \text{ nH},$$
$$C_1 = C_2 = C_3 = C_4 = 10 \text{ nF}, \quad r_g = 0.08\ \Omega,$$
$$r_e = 0.12\ \Omega, \quad V_1 = V_2 = V_3 = V_4 = 16 \text{ kV},$$

with laser channel breakdown set at 21 kV giving scaling parameters of

$$\beta_e = 80, \quad \beta_2 = \beta_3 = \beta_4 = 1, \quad \beta_g = 0.7, \quad \beta_s = 0.7,$$
$$\delta_2 = \delta_3 = \delta_4 = 1, \quad \alpha_g = 0.7, \quad \alpha_e = 1,$$
$$\nu_2 = \nu_3 = \nu_4 = 1, \quad \text{and} \quad F_1 = F_2 = F_3 = 1.3.$$

The system of equations (8), (10), (12), and (14) is integrated with time incremental steps of 0.002 of $t_0 = \sqrt{(L_1 C_1)} = 1.2$ ns. The unit of current is $I_0 = 130$ kA. The results are shown in Fig. 2.

On switching circuit e it is observed that current ι_e begins to flow and the laser channel voltage difference ν_{g1} begins to rise as the voltage on C_1 begins to drop. At $\tau = 17.8$, ν_{g1} has risen to the preset value of $F_1 = 1.3$. The first laser channel breaks down. Current ι_1 begins to flow. The voltage across the second laser channel ν_{g2} now swings up with a short time constant of

$$\sqrt{[(1+\beta_g+\beta_2+2\beta_s)\delta_2/(1+\delta_2)]} \simeq 1.5 t_0,$$

superimposed on a longer time constant of $\sqrt{[\beta_e(1+\delta_2)]} \simeq 13 t_0$, the latter being due to the slower discharge of C_1 and C_2 together into the branch circuit of the large inductance L_e.

From the point of view of sequencing precision, particularly in consideration of dV_g/dt, we would prefer the second laser channel to reach the preset F_2 in the first fast swing, a mode which we shall term "prompt sequencing." However, it is found that when operated with uniform capacitances and voltages such as our present case, ν_{g2} only reaches F_2 in

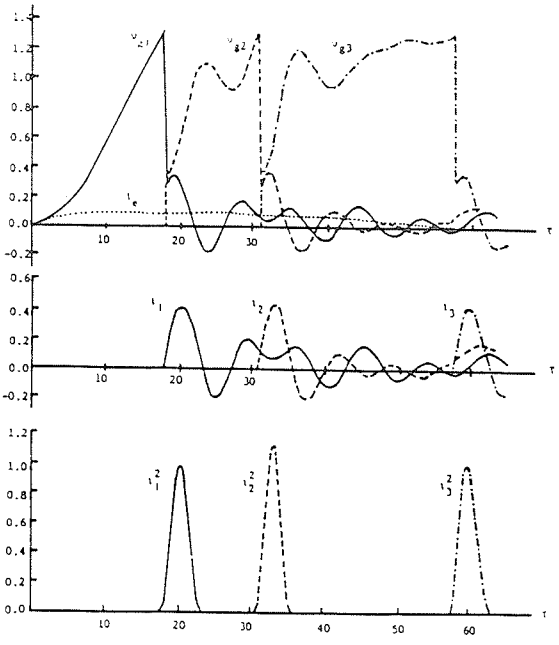

FIG. 2. Computed voltages across the laser channel, laser currents, and laser currents squared as functions of time; all variables are normalized. Parameters used are those for a "prolonged sequencing" mode.

the second fast swing, a mode we shall term "prolonged sequencing" whenever the breakdown occurs later than the first fast swing. That this second upswing is related to the oscillation of the ι_1 trace superimposed on the oscillation of ι_e is confirmed by examining the ι_1 and ι_e traces.

When the laser channel 2 has broken down, ι_2 begins to flow and v_{g3} begins its swing upwards again with a short time constant swing superimposed on a longer time constant. For our present parameters v_{g3} does not reach the preset value of $F_3 = 1.3$ until its fourth swing, as confirmed by examining the corresponding trace of ι_2. After the third laser channel has broken down the current ι_3 flows. The laser current pulses have the following characteristics:

First pulse: amplitude $= 0.42\, I_0$,

$$\text{FWHM of power curve} = 2.0 t_0;$$

second pulse: amplitude $= 0.44\, I_0$,

$$\text{FWHM of power curve} = 1.5 t_0;$$

third pulse: amplitude $= 0.42\, I_0$,

$$\text{FWHM of power curve} = 1.1 t_0.$$

These are the pulses responsible for producing the nitrogen laser pulses. It is noticed that with the scheme of uniform capacitances and voltages we have a "prolonged sequencing" mode with the three laser producing pulses separated, respectively, by $13t_0$ and $26t_0$.

The prolonged sequencing mode has the additional disadvantage of a slow dV_g/dt particularly for the breakdown of the third laser channel. It is doubtful from the ramp obtained in Fig. 3 of less than 0.1 kV/ns for dV_{g3}/dt whether that laser channel could lase consistently even with preionizers.

B. Case 2: The prompt sequencing mode

Prompt sequencing may be obtained by using progressively reduced capacitances in the sequence of capacitors. This may be aided by progressively increasing the voltages in the sequence of capacitors thus enabling also pulse power compensation. Both arrangements have been computed.

Figure 3 shows the result of an arrangement with reducing capacitances but with the same voltage on all capacitors. The changed parameters are

$$C_1 = 24\ \text{nF}, \quad C_2 = 12\ \text{nF}, \quad C_3 = C_4 = 6\ \text{nF},$$
$$r_g = 0.06\ \Omega, \quad r_e = 0.08\ \Omega,$$

and

$$V_1 = V_2 = V_3 = V_4 = 14\ \text{kV},$$

giving scaling parameters of

$$\beta_e = 80, \quad \beta_2 = \beta_3 = \beta_4 = 1, \quad \beta_g = 0.7, \quad \beta_s = 0.7,$$
$$\delta_2 = 0.5, \quad \delta_3 = \delta_4 = 0.25, \quad \alpha_g = 0.75, \quad \alpha_e = 1,$$
$$\nu_2 = \nu_3 = \nu_4 = 1, \text{ and } F_1 = F_2 = F_3 = 1.6.$$

Here $t_0 = \sqrt{(L_1 C_1)} = 1.9\ \text{ns}, I_0 = 175\ \text{kA}$, and the computation shows in Fig. 3 that prompt sequencing is achieved with the following pulses:

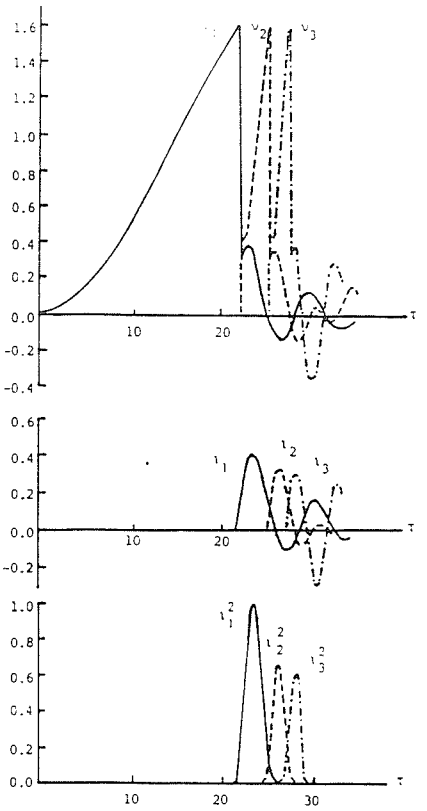

FIG. 3. Computed voltages across the laser channel, laser currents, and laser currents squared as functions of time; all variables are normalized. Parameters used are those for a "prompt sequencing" mode.

First pulse: amplitude $= 0.4\, I_0$,

$$\text{FWHM of power curve} = 2.0\ t_0;$$

second pulse: amplitude $= 0.34\, I_0$,

$$\text{FWHM of power curve} = 1.5 t_0;$$

third pulse: amplitude $= 0.32\, I_0$,

$$\text{FWHM of power} = 1.1 t_0,$$

with precise pulse separations of $2.5t_0$ and $2t_0$, respectively.

VI. SOME EXPERIMENTAL RESULTS: PROLONGED SEQUENCING MODE

An experiment has been carried out with an existing arrangement (see Fig. 4) using capacitors fabricated from aluminum foils insulated by three layers of 2-mil mylar

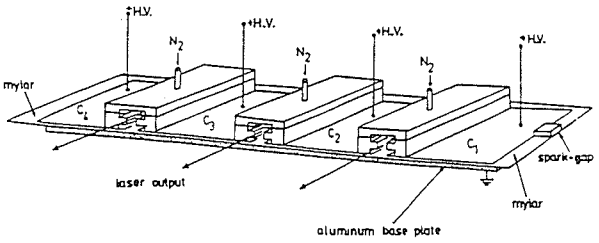

FIG. 4. Schematic of a three-channel sequenced nitrogen laser. The high-voltage plates of the capacitors C_1, C_2, C_3, and C_4 are made of aluminum foils

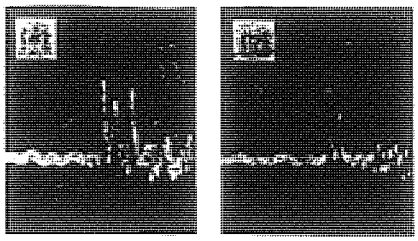

FIG. 5. Oscillograms of photodiode signal monitoring the three-channel sequenced nitrogen laser operated in the prolonged sequencing mode; time scale: 100 ns/div. (a) Shot with three laser pulses in "prolonged sequence." (b) Shot with the third laser pulse missing.

sheets to give capacitances of $C_1 \simeq C_2 \simeq C_3 \simeq C_4 \simeq 10$ nF. Three identical 20-cm-long laser channels are used each with 6-mm-thick electrodes separated by 3 mm and operated with a flow of nitrogen slightly above atmospheric pressure. Preionizing corona blades are used to promote uniform breakdown.[3] The three laser pulses are each suitably attenuated and imaged to fall onto a *p-i-n* photodiode which has its photocurrent recorded on a 100-MHz storage oscilloscope with the rise time of the system estimated to be 7 ns.

Figure 5(a) shows the three laser pulses separated by intervals, respectively, of 25 and 40 ns. This compares favorably with the predicted intervals of $13t_0$ and $26t_0$, if we take t_0 as 1.6 ns.

Figure 5(b) shows a shot where the third laser pulse is missing, which happens quite frequently. When the third laser pulse is missing, two things are observed: (a) The first two laser pulses are still present with consistent intensities and (b) the third laser tube flashes but with very poor spatial uniformity. The observations are entirely consistent with the results of Fig. 3 which have been discussed in Sec. V A.

VII. CONCLUSIONS

An electrical network for firing several nitrogen lasers in sequence is suggested. The circuit theory is developed and computation shows operation in two possible modes—the "prompt sequence" mode and the "prolonged sequence" mode. The prolonged sequence mode with relatively widely spaced laser pulses is predicted to be irreproducible in laser action of the late firing lasers due to a small rate of rise of voltages across the relevant laser channels. The prompt sequence mode with closely spaced laser pulses is predicted to have high sequencing precision since the sequential switching action does not depend on separate spark gaps but only depends on inherent voltage swings across the laser channels typically having the order of 5 kV/ns.

The theory has been tested experimentally with an existing arrangement of three nitrogen lasers having identical capacitances and charged to the same voltage. This gives rise to three laser pulses in a prolonged sequence as predicted by the theory. The pulse separation of 25 and 40 ns, respectively, compares favorably with that predicted by theory. When equipment becomes available, a prompt sequence arrangement will be tested.

ACKNOWLEDGMENTS

The authors acknowledge the aid of the International Centre for Theoretical Physics, the Third World Academy of Sciences (Research Grant) and the Malaysian National Science Advancement and Research Council. Three of us (M.V.H.V.P., Y.S.S., and A.G.W.) also acknowledge fellowships from the International Centre for Theoretical Physics without which this work would not have been possible.

[1] S. Lee, A. V. Gholap, A. J. Smith, K. H. Kwek, A. C. Chew, T. Y. Tou, and S. Sapru, J. Fiz. Malays. **6**, 165 (1985).
[2] A. J. Smith, K. H. Kwek, T. Y. Tou, A. V. Gholap, and A. Lee, IEEE J. Quantum Electron. **QE-23**, 283 (1987).
[3] K. H. Kwek, T. Y. Tou, and S. Lee, IEEE Trans. Instrum. Meas. (in press).
[4] G. Herziger, R. Woltermann-Windgasse, and K. H. Banse, Appl. Phys. **24** 267 (1981).
[5] V. Hassan and H. M. von Bergmann, J. Phys. E **13**, 632 (1980).
[6] S. Lee, T. Y. Tou, S. P. Moo, M. A. Eissa, A. V. Gholap, K. H. Kwek, S. Mulyodrono, A. J. Smith, Suryadi, W. Usada, and M. Zakaullah, Am. J. Phys. **56**, 62 (1988).
[7] J. P. Rager, L. E. Bilbao, H. A. Bruzzone, C. Gourlan, U. Guidoni, H. Koregler, S. Podda, B. R. Robouch, and K. Steinmetz, in *Proceedings of the VIIIth International Conference on Plasma Physics and Controlled Nuclear Fusion Research*, Brussels, 1980 (International Atomic Energy Authority, Vienna, 1981), Vol. II, p. 209.
[8] C. R. Hass, R. Noll, F. Ruehl, and G. Herziger, Nucl. Fusion **24**, 1216 (1984).
[9] K. Hirano, K. Shimoda, and S. Emori, Rev. Sci. Instrum. **50**, 1236 (1979).

INTERNATIONAL ATOMIC ENERGY AGENCY
UNITED NATIONS EDUCATIONAL, SCIENTIFIC AND CULTURAL ORGANIZATION
INTERNATIONAL CENTRE FOR THEORETICAL PHYSICS
I.C.T.P., P.O. BOX 586, 34100 TRIESTE, ITALY, CABLE: CENTRATOM TRIESTE

H4-SMR 393/55

SPRING COLLEGE ON PLASMA PHYSICS

15 May - 9 June 1989

Symposium on Third World Fusion Programmes
and South-North Collaboration

FUSION PROGRAMMES IN MALAYSIA

S. Lee

Department of Physics
University of Malaya
59100 Kuala Lumpur
Malaysia

UMKL-89-07
August 1989

FUSION PROGRAMMES IN MALAYSIA

S.Lee

Fusion Programmes in Malaysia

S. Lee
Physics Department, University of Malaya
59100 Kuala Lumpur, Malaysia.

Abstract:

Fusion Programmes in Malaysia are briefly reviewed with some attention to historical perspective and to the academic continuity from undergraduate through to doctoral programmes. The research in the areas of glow-discharge, small tokamak, pinch, current-stepped pinch, vacuum spark pinch and the plasma focus is then reviewed. The central research theme threading all this research is identified as a study of the limits and enhancement of compressions. Our work shows that in general density compressions are limited and independent of the absolute magnitude of the compressive force. Enhancement of compression may be achieved through time variation of the force field, e.g. specifically using a force-stepping technique, through a reduction in specific heat ratio and in the case of the pinch through an elongation of pinch length during the compression. These ideas are applicable to magnetic field compressions as well as to radiation-driven compressions and should prove useful to aid in understanding e.g. the plasma focus scaling laws.

This review also reports the experience of the research group in its attempt to share fusion related technology on a South-South basis by the development of specific training packages. One such package the UNU/ICTP Plasma Fusion Facility has already been developed and 8 sets have been sent back to the home institutes of the UNU/ICTP Fellow trainees. A compact torus FRC based on the Rotamak concept is also being developed.

Paper prepared for the Symposium on Third World Fusion Programmes and South-North Collaboration, 8-9th June 1989 Trieste, Italy.

1

Introduction

Fusion Research in Malaysia is centered in the Plasma Research Laboratory, University of Malaya. This laboratory was started in the early 1960's by S.P. Thong who at that time was associated in glow discharge work in collaboration with K.G. Emeleus of Queens University, Belfast. Aware of the work already on-going at that time in Britain on controlled fusion research Thong had the foresight to acqire from the British Government through the Colombo Plan 100 pieces of 40kV 0.6 μF fast discharge capacitors. Preliminary work with these and other capacitors resulted in the first Physics M.Sc thesis in Malaysia being produced on the topic of electric and electromagnetic shock waves under the supervision of H.H. Teh[1-3] in 1966.

In 1970 the technical problems of installing these capacitors were solved with a design dividing the 100 capacitors into 4 modules each switched by 2 ignitrons with the help of a voltage division technique proposed earlier by C.P. Lim. In 1972 1.9MA was measured in a full test[4]. This capacitor bank is still operational and will soon be converted to be switched by parallel plate swinging-cascade spark gaps. A plasma focus was designed and in October 1973 D-D nuclear fusion neutrons were measured from the focus by time-of-flight method giving an energy of 2.2 ± 0.1 MeV in a 'backward' direction.[5]

During this period of development and since then we have planned our research mainly on academic basis resulting in the production of 5 Ph.D [6-10] and 15 M.Sc theses[11-24] in plasma and fusion physics. Continuity between undergraduate and postgraduate work is maintained by undergraduate courses in plasma and fusion physics augmented by undergraduate experiments in glow discharge, electromagnetic shock tube and pulse electronics experiments.[25]

Experimental plasma research in Malaysia is currently carried out on the following devices : glow discharge, small tokamak, current-stepped Z pinch, vacuum spark x-ray source and the plasma focus. Various lasers are being developed for diagnostic work. A transistorised Rotamak which is a compact torus FRC with current drive is being developed at our associated Pulse Technology Laboratory and an elongating Z-pinch is being designed at the Technology University.

Programme areas

Over the years the research has developed a pattern propelled primarily by the academic needs and perceptions of individuals within a framework of limited infrastructure and financing typical of the university environment of a developing country. Yet a pattern has loosely developed and three broad areas may be identified:

I. Long-lived plasmas, production and diagnostic techniques.
II. Pulsed plasmas, production and properties and techniques for compression enhancement.
III. Development of fusion-related technology for research initiation in developing countries.

I. Long-Lived Plasmas

Work on these plasmas include the Glow Discharge, a Small Tokamak and recently we have started constructing a transistorised compact torus FRC device with current-drive from either a rotating magnetic field or from a transverse oscillating magnetic field. This device called the Rotamak was first developed at Flinders University of South Australia and was transistorised as a specific project to bring the technology of a compact torus FRC within the reach of a developing country.

Glow Discharge

Measurements on glow discharge[26] have been continued. Recent developments include pulsed Langmuir double probe studies[27] in various gases and a computer based data acquisition system[28].

Small Tokamak.

A small Tokamak was planned[29] and plasma obtained in June 1983 with the following parameters :

major radius R	0.25m
major radius a	0.05m
R/a	5
toroidal field B	0.5T
plasma current	10 kA
safety factor q	2.5
lifetime (optioally observed)	200 μs
operational pressure	10^{-3} torr
T_e	10 eV

Stabilization bank

Capacitance	60 μF
Charging voltage	26 kV
Coil inductance	63 μF
No. of turns	100
Coil current	25 kA
risetime	100 μs

Heating bank

Capacitance	100 μF
Charging voltage	4 kV
Coil inductance	360 μH
No. of turns	20
Coil current	2 kA
risetime	300 μs

The toroidal stabilization field, planned at 2T is severely reduced by induced current effects in the stainless steel wall of the plasma chamber.

Rotamak

In the Rotamak[30] a plasma current is driven around an axial bias field in such a direction that the axial field of the plasma current opposes the axial bias field. When the driven plasma current becomes large enough it reverses the original axial field in the central region. These reversed field lines in the central region join up with the field lines having the original direction in the outer regions to form a compact-torus field-reversed-configuratation with closed field lines. The Rotamak traditionally uses a magnetic field, rotating at a frequency between ω_e (plasma electron frequency) and ω_i (plasma ion frequency), to pull along the electrons, thus producing the current drive in the plasma.

In conventional Rotamak devices the RF generators for the rotating magnetic field require expensive triode valves. In a specific attempt to develop low-cost Rotamak technology suitable for the Third World transistorised RF generators using MOSFETS were developed at Flinders University. Moreover during that exercise it was found that an oscillating magnetic field transverse to the axial bias field was sufficient to produce the Rotamak configuration. This provided a further simplification.[31]

The Rotamak we are building uses a glow-discharge for preionisation and a MOSFET RF generator of 2 kW to power the oscillating transverse magnetic field at 500 kHz. We expect to drive a plasma current of 200 A in a chamber of diameter 25 cm holding an FRC plasma at a temperature of 7eV and an electron density of 10^{12}/c.c with a lifetime of several 10's of ms.

II. Pulsed Plasmas - Studies of Compression Limits and Enhancement

Much of our plasma and fusion-related programmes deal with pulsed plasmas and may be connected by the research theme of compression limits and compression enhancement. From energy and pressure consideration applied to fast compressions it may be shown that generally for a spherical compression driven by piston-like force field with force F, the final compressed radius r_m is related to the initial radius r_o by the compression limit expression.

$$F_m = \frac{f(\gamma)}{f_{rs}} \int_{r_m}^{r_o} F \frac{dr}{r}$$

where $f(\gamma)$ is a function of the specific heat ratio γ and f_{rs} is related to the reflected shock over-pressure as the reflected shock hits the incoming piston force field.

This simple relationship has the following important features, determining compression limits and indicating methods of enhancement. These features are:

1. It determines the radius ratio r_m / r_o and shows that the radius ratio is determined by energy and pressure considerations.

2. The radius ratio (hence density compression) is independent of the absolute peak magnitude of the force F.

3. The density compression depends on the space - or time - variation of the force field.

4. It depends on the specific heat ratio.

5. It depends on the reflected shock over-pressure factor factor f_{rs}.

For a radiation-driven compression in a spherical geometry[33] the corresponding energy balance equation is :

$$R_m = \frac{3\,(\gamma - 1)}{f_{rs}\, r_m} \int_{r_m}^{r_o} R\,dr$$

where R is the radiation power.

This expression may be used[33] to show that a square power pulse radiation piston will produce a density compression of only 27 for a $\gamma = 5/3$ fully ionised plasma whereas a sequenced double pulse each with linearly rising power may increase the compression limit to 1750 greatly increasing the fusion energy gain factor for a given absorbed energy in a spherical D - T target.

For a pinch the compression limit expression takes the form:

$$l_m^2 = \frac{2(\gamma - 1)}{f_{rs}\, \ell_m} \int_{\kappa_m}^{1} l^2\, \ell\, \frac{d\kappa}{\kappa}$$

where ι, κ and ℓ are the normalised current, radius and length respectively and m indicates the quantity at time of maximum compression. From this expression several methods of compression enhancement are proposed :

1. Pinch elongation, as in the elongating pinch or plasma focus.[34]
2. Reduction[35] of γ, e.g. as $\gamma \to 1$ $\kappa_m = \frac{r_m}{r_o} \to 0$,

   This applies particularly to high - Z plasmas which remains freely ionizing even at high temperatures e.g. argon or xenon in pinches, hollow pinches or plasma focus or high-Z plasmas in vacuum-spark pinches.[36, 37]

3. Current-stepped compressions.[38]

Effects of radiation cooling[20] have also been considered.

Vacuum Spark Pinch

In this experiment a cloud of high-Z material is injected into a vacuum gap by irradiating a pointed stainless-steel cathode with a 60MW ruby laser pulse. This high Z-material is then compressed using the current from a fast 22μF capacitor charged to 20kV. From x-ray emission experiments hot spots, possibly radiation collapsed, with electron temperatures up to 10 keV have been measured.[37]

Recently a miniature vacuum spark device using nF capacitors is being developed as an x-ray source.

Current-Stepped Pinch

In preliminary work a low performance linear Z-pinch with $\alpha = 15$, where α = electrical characteristic time/ pinch characteristic time, has been built for laser scattering diagnostics in a joint project with the Laser Group[8]. This pinch produces a plasma with $T_e \sim 30{,}000$ K estimated from observed converging shock waves.

Modelling of pinch has been carried out using circuit-coupled snow-plow model with energy balance limit[39-40]. A generalised slug model was also developed for general pinch computation including radiation cooling effects [20, 41].

Another pinch with $\alpha = 0.8$, $\beta = 0.9$ has been designed to give a hotter plasma with the aim of connecting to two sequenced capacitor banks for testing the current-stepped pinch compression enhancement effect.[42]

In preliminary work the design was constrained by existing conventional capacitor banks. It was decided to operate the 15cm diameter pinch at average collapse speed of 2.5 cm/μs increasing to 6cm/μs before the current step. However no increase in compression was observed since at this speed range the expected increase in compression may be cancelled by an increase in γ at 6cm/μs and beyond.

To remove this γ -compensation effect the current-stepped pinch needs to be run at a higher speed so that the γ remains at constant high value and does not change substantially during the current-step. The design considerations require a 150kV 0.6μF Marx generator to

provide a 70kA pulse to be current-stepped by means of a 150kV water-line pulsed-charged by a 0.1 μF, 150kV Marx. These are at present being constructed.

Plasma Focus

A Mather's type plasma focus, the UMDPF1[43], has been operated in the laboratory for a number of years. The following are the typical operating conditions:

inner electrode radius	1.3cm (hollow copper tube)
outer electrode radius	4.3cm (six copper rods)
length	16 cm
Capacitance	60μF (ignitron switched)
current	550kA at 20 kV
Current risetime	3½μs
pressure (D_2)	8 torr
neutron yield	10^9 per discharge

The device has also been operated in argon.

Measurements made on this device include device characterisation[43-45] soft X-ray pinhole photography and temperature measurement[46], shadowgraphs[47,48], holographic interferometry[19], neutron time of flight[5], neutron counting[16,49], neutron half-life measurements[50] and dynamic modelling[25,51]. We have also started work on charged particle measurements using emulsions and mass spectrometers.

The objectives of the plasma focus research are shifting more and more to the following :

development of diagnostics[53] and modelling of dynamics[57]
development of applications e.g.as neutron[50] or soft x-ray sources
development of fusion neutron scaling laws
development as a cost-effective training package for international cooperation[49, 52,58].

The latest development include a target technique[23] for determination of fusion neutron source structure in the plasma focus and more efficient nitrogen lasers [54,55] for focus diagnostics with shadowgraphy, Schlieren system and M-Z interferometry [56].

On the question of neutron scaling the plasma focus seems to be unduly restricted to a fusion neutron yield $\sim (\text{current})^4$ law due to an observed restriction of axial speed to 10cm per microsecond. We are studying the possibility of increasing this speed. Preliminary studies[58] seem to indicate that increasing the axial speed leads to a decoupling of the magnetic piston and shock front during the end of the axial phase - a natural consequence of the rise of γ towards 5/3. If this problem can be solved, by geometry, by seeding with small amounts of high-Z material, by gas puffing or current-stepping; this might lead to a yield- $\sim (\text{current})^7$ scaling with great consequence to the plasma focus as a fusion device.

Elongating Pinch

An elongating pinch[59] is being designed at the Plasma Research Laboratory of the University of Technology. This is a linear Z-pinch with a hole (radius $\sim 0.5r_o$) in the centre of each of the cathode and anode. To each hole is attached a straight side arm . When the plasma column pinches to the size of the hole any further

compression by the pinch current causes the plasma pinch to elongate into the side arms. This elongation will enhance compression and stability.

III. Development of Fusion-related Technology for research initiation in Developing Countries

In view of our relatively extensive experience in experimental plasma physics the Plasma research group has pioneered the concept [49,52] of sharing of fusion-related technology in developing countries. We have developed the concept of packaging cost-effectively an integrated facility consisting of well defined sub-systems which together make up a complete facility for research and training.

For example we have identified that the following sub-systems are necessary to start experimental research in a developing country on the plasma focus :

- simple vacuum system
- focus electrode system with vacuum feed-through and proper insulation
- small capacitor bank (3kJ) and high current switch
- control and triggering electronics
- power supplies
- simple diagnostics for current, voltage, magnetic field, x-ray, neutron and laser shadowgraphy
- plasma dynamic model with structure and chemistry suitable for use on a microcomputer.

These ideas expounded at the ICTP in Trieste[52] have been further developed with the help of the First[25], Second and Third Tropical Colleges[64] and has received full tests in the 6-months UNU Training Programme in Plasma and Laser Technology (1985/86) and a subsequent (UNU) ICTP Training Programme (1988). For these Training Programmes twelve UNU/ICTP Fellows (from Indonesia, India, Pakistan, Egypt, Nigeria, Sierra Leone and Thailand) have worked together with us to develop research packages for the plasma focus, glow discharge and nitrogen laser. The work has produced a number of research reports and papers[49,50,60-64]

During this Training Programme was developed a complete Fusion Facility[49] now designated as the UNU/ICTP PFF (Plasma Fusion Facility).

In the First Training Programme five complete sets of the device were tested over a period of two months, and each was found to work reliably producing well-defined dynamics and reproducible fusion neutron bursts. On 20th January 1986 ICTP Director Professor Abdus Salam honoured us with a visit to the training programme when he witnessed a fusion discharge.

As a result of the training programmes plasma focus fusion facilities are in various stages of development in Pakistan, Nigeria, Indonesia, Thailand, India, Sierra Leone and at Al Azhar University of Cairo. The first experimental plasma physics Ph.D has been produced in Pakistan and several M.Sc's in Nigeria.

The momentum generated by these results has led to the formation of the Asian African Association for Plasma Training (AAAPT) with the aim of extending the concept of effective hands-on training at progressively higher levels by making available resources in plasma physics of countries like China, Egypt and India. It is felt that our training resources in experimental plasma/fusion physics will become more comprehensive when we have developed a simple cost-effective package in a Tokamak-type plasma or a compact torus FRC plasma.

Conclusion

It may be seen that after some 28 years of plasma/fusion research in Malaysia our programmes are still physics-based aimed primarily at academic production and the development of practical methods for the sharing of plasma/fusion technology among the smaller Third World Countries. We feel that the time is not ripe for us in Malaysia to have a large programme, or a programme involving a 'large' or 'national-sized' machine. We see ourselves playing a useful role in fusion-related technology in the community of smaller Third World Countries. We hope to continue fulfilling this useful role, with the help of ICTP and TWAS, using small but high quality machines in the area of long-lived and pulsed plasmas.

Acknowledgement

The fusion research programmes in Malaysia are sponsored mainly by the Ministry of Science, Technology and the Environment under the Intensification of Research Priority Areas (IRPA) mechanisms through grants number 04-07-04-40, 02-07-04-33 and by the University of Malaya. The South-South fusion technology transfer programme is sponsored by the ICTP in Trieste, Italy under its OEA and ICAC programmes. We also acknowledge the help of the Third World Academy of Science, the United Nations University, the Alexander von Humboldt Foundation and the British Government Colombo Plan.

Reference

1. S.Lee, Some shock wave phenomena in a ring-electrode system, (M.Sc. Thesis UM 1966)
2. H.H.Teh and S.Lee Int. J. Electron. 22, 193 (1967)
3. H.H.Teh and C.K.Pang Int. J. Electron. 23, (1968)
4. S.P. Thong and S.Lee, Malaysian J. of Science 2(B) 157 (1973)
5. S.Lee and Y.H.Chen, Malsyaian J. of Science 3(B), 159 (1975)
6. Y.H.Chen, Parametric study of focus optimization (Ph.D Thesis UM 1978)
7. C.S.Wong, Experimental and numerical studies of a Laser-initiated vacuum spark, (Ph.D Thesis UM 1983)
8. S.M.Low, An investigation of a linear hydrogen plasma pinch using a low power dye laser, (Ph.D Thesis UM 1986)
9. T.Y. Tou, Pinch radius ratio of the plasma focus (Ph.D Thesis UM 1987)
10. K.H.Kwek; Pinch Structure in a Plasma Focus (Ph.D Thesis UM 1989)
11. C.K. Pang, Shock wave studies in a ring-electrode shock tube, (M.Sc Thesis UM 1969)
12. Y.H.Chen, Study of Coaxial plasma gun in mode 1 operation, (M.Sc Thesis UM 1972)
13. S.P.Chow, Current sheath studies in a coaxial plasma focus gun, (M.Sc Thesis UM 1972)
14. K.W.Lee, Current oscillations in glow discharge, (M.Sc Thesis UM 1972)
15. A.C.Chew, Plasma focus in an axial magnetic field, (M.Sc Thesis UM 1974)
16. C.S. Wong, Some neutron measurements of the plasma focus, (M.Sc Thesis UM 1978)

17. Y.C.Yong, Multiple ionization in an argon plasma focus, (M.Sc Thesis UM 1978)

18. Y.H.Chin, shadowgraphic studies of a plasma focus, (M.Sc Thesis UM 1981)

19. K.H.Kwek, Holographic interferometric measurements of electron densities in a dense plasma focus (M.Sc Thesis UM 1982)

20. Jalil B. Ali, The enhancement of pinch compression - A numerical study, (M.Sc Thesis UM 1986).

21. C.X.Ong, Exprimental Studies of a Toroidal Plasma (M.Sc Thesis UM 1987)

22. O.H.Chin, Construction and Characterisation of a Helium Glow Discharge (M.Sc Thesis UM 1988)

23. C.K.Chakrabarty, Plasma Focus neutrons - some measurements and applications (M.Sc Thesis UM 1989)

24. H.W.Lee, Construction and Operation of a ruby laser amplifier (M.Sc Thesis, UM 1989)

25. Laser and Plasma Technology Ed. S.Lee et al. (World Scientific Co. 1985)

26. H.H.Teh, Int.J.Electronics 22 (1967)

27. C.S.Wong, J. Fiz.Mal.5, 121 (1984)

28. C.S.Wong. S.H.Saw and O.H.Chin, J.Fiz.Mal.6, 115 (1985)

29. S.Lee, Fusion Energy -1981 IAEA-SMR-82, p.289-295, Procs. Symposium on plasma research, theory and experiment, ICTP, Trieste, Italy, June 1981.

30. I.R. Jones, Comments Plasma Phys and Controlled Fusion 10, 115 (1986)

31. S.Lee, S.Xu, I.R.Jones, to be published

32. I.R. Jones , Fusion Research in 'Small' Countries, Paper presented at plenary session 3rd Asia Pacific Physics Conference June 1988 Hong Kong, Procs. Vol. 1 pg. 162. World Scientific Ed. Y.W. Chan et al (1988).

33. S.Lee, Laser and Particle Beams 6, 597 (1988)
34. S.Lee, J. Appl. Phys. 54, 3603 (1983)
35. S.Lee, Australian J. Physics 36, 891 (1983)
36. S.Lee and H. Conrads, Phys. Lett. 57A, 233 (1976)
37. C.S. Wong and S.Lee, Rev. Sci. Instru. 55(7), 1125 (1984)
38. S. Lee, J. Phys. D: Applied Physics 17, 733 (1984)
39. S. Lee, Plasma Physics 25, 571 (1983)
40. S. Lee, J. Phys. D: Applied Physics 16, 2463 (1983)
41. Jalil B. Ali, S. Lee, T.Y.Tou and Y.C. Yong, J. Fiz. Mal. 5, 153 (1984)
42. S.H. Saw, C.S. Wong, S.Lee in "Small Plasma Physics Experiments" Ed. S. Lee and P.H. Sakanaka pg. 116 World Scientific (1988)
43. S. Lee, and Y.H.Chen, Fusion Energy - 1981, IAEA-SMR-82, p.296 - 303, Proc. Symposium on plasma research, theory and experiment, ICTP, Trieste, Italy, June 1981.
44. S.P. Chow, S. Lee and B.C. Tan, J. of Plasma Physics 8, 21 (1972)
45. S. Lee, Y.H.Chen, S.P. Chow, B.C. Tan, H.H.Teh and S.P.Thong, Int. J. Electronics 33, 85 (1972)
46. Y.H.Chen and S. Lee, Int. J. Electronics 35, 341 (1973)
47. S. Lee and Y.H.Chin, Bull. Phys. M'sia 2, 105 (1981)
48. S.Lee, Harith Ahmad, T.Y. Tou, K.H.Kwek and C.S. Wong, J. Fiz. Mal. 6, 23 (1985)
49. S. Lee, T.Y.Tou, S.P. Moo, M.A.Eissa , A.V.Gholap, K.H.Kwek, S. Mulyodrono, A.J.Smith, Suryadi, W.Usada, and M. Zakaullah, A simple facility for the teaching of plasma dynamics and plasma nuclear fusion, American J. Physics 56, 62 (1988)
50. S.P. Moo and S.Lee, Singapore J. Phys. 4,131 (1987)
51. S.Lee, A plasma focus model yielding trajectory and structure, Spring College on radiation in plasma, Trieste, May 1983; Published in "Radiation in Plasmas, p. 978-987, World Scientific Pub. Co. (1984)
52. S.Lee, Regional Centres for research transfer within South-east Asia Countries - Invited paper presented at the International Conf.on Physics & Development 1984, ICTP, Trieste, Italy.

53. T.Y.Tou and S.Lee Rev. Sci.Instru. 59, 2370 (1988)
54. K.H.Kwek, T.Y.Tou and S.Lee, IEEE Transactions IM-38, 103 (1989)
55. S.Lee, K.H.Kwek et al "Sequenced Nitrogen Lasers" Accepted. J. Appl. Phys. for May 1989
56. K.H.Kwek, T.Y.Tou and S. Lee J. Fiz. Mal. 9, 36 (1988)
57. T.Y.Tou, S.Lee and K.H.Kwek, Accepted IEEE Trans. Plasma Science.
58. S.Lee "The sharing of fusion related technology among developing countries" in "Fusion Energy and Plasma Physics" Ed. P.H. Sakanaka, pg. 754, World Scientific (1988)
59. Jalil Ali et al "Dynamics of an elongating pinch", Third Tropical College May/June 1988, to appear in Procs.
60. A.J. Smith, K.H.Kwek, T.Y.Tou, A.V. Gholap and S.Lee, IEEE J. Quantum Electronics QE-23, 283 (1987)
61. K.H.Kwek, A.J. Smith, T.Y.Tou, A.V.Gholap and S.Lee, J. Fiz. Mal. 7, 125 (1986)
62. S.Lee, A.V.Gholap. A.J. Smith, K.H.Kwek, A.C.Chew, T.Y.Tou and S.Sapru, J. Fiz. Mal. 6, 165 (1985)
63. C.S. Wong, O.H.Chin, M.A. Eissa, A.V. Gholap, S. Mulyodrono, C.X. Ong, S. Sapru, S.H.Saw, A.J. Smith, Suryadi and W. Usada, J.Fiz. Mal. 7, 45 (1986)
64. Laser and Plasma Technology Ed. S. Lee et al (World Scientific Co. 1988)

J. Fiz. Mal. 10, 61 (1989)

OBSERVATIONS OF COMPACT TORUS FRC IN SINGLE-PHASE OPERATION OF A TRANSISTORISED ROTAMAK

S. LEE*, S. Y. XU, G. COTTRELL and I. R. JONES

School of Physical Sciences,
Flinders University of South Australia,
Bedford Park SA 5042,
Australia

Received 24 April 1989

Abstract

A low-cost Rotamak was developed driven by transistorised RF generators producing 1.7 kW per phase at 170 V with a pulse duration of 40 ms. Compact torus field-reversed configurations (FRC) were observed with single-phase operation as well as with conventional two-phase Rotamak operation. These compact torus plasmas were stable for the duration of the RF drive. Operational regimes were mapped out delineating no-breakdown region, plasma current cut-off regions and FRC regions where the driven plasma currents were sufficient to produce the stable compact torus FRC. Radial and axial scans measuring poloidal field B_z demonstrated the magnetic configuration which was established. In either mode of operation the current drive efficiency was found to be 0.1A/W.

Introduction

There has been some interest recently to design low-cost plasma experiments which may be used for teaching and research initiation in developing countries. The requirements for suitable experiments are rather stringent. For whilst the experiments must be cost-effective and affordable it must also at the same time demonstrate some important aspects of plasma physics or plasma technology. Thus a plasma focus device known as the UNU/ICTP PFF has been designed[1] specifically for the purpose of research initiation in developing countries in experimental plasma physics. That device is low-cost and yet is suitable for teaching plasma dynamics and plasma nuclear fusion and may also be used as a source of plasma x-rays, relativistic electron beam and neutrons. The plasma focus represents a class of devices with short-lived (microsecond) plasmas and extreme conditions of densities and temperatures. On the other hand, much of fusion physics and technology is based on longer-lived plasma. Of growing importance is a class of device (the compact torus) known to be more efficient in usage of magnetic energy than the Tokamak which is the leading contender in the present international effort to harness fusion for energy purposes. It has been felt that the programme for low-cost plasma experiments should also include a device of the compact torus type.

We have considered the Rotamak from this point of view. The Rotamak[2] employs a current-drive technique which uses a rotating magnetic field to drive a continuous electron current in a plasma ring. This method of current drive has already resulted[2, 3] in reproducible and macroscopically stable plasmas in the longest lived compact torus configuration in the world. Plans are being made at Flinders University to scale up the Rotamak experiments to demonstrate performance at higher powers. For the present paper however we consider a scaled-down version in an effort to develop a teaching and research facility at a low-cost level.

In the Rotamak the rotating magnetic field is conventionally produced by RF (typically of frequency $\omega \sim 1$ MHz to fulfil the Rotamak condition that the ion Larmor frequency $\omega_i < \omega < \omega_e$ the electron Larmor frequency) applied to two pairs of Helmholtz coils with the axis of 1 pair perpendicular to the axis of the other pair. The RF applied to one pair is 90° out of phase with that applied to the other pair so

*Visiting Professor on leave from Physics Department, University of Malaya.

that the magnetic field due to the RF rotates with the frequency ω. This method is termed the conventional two-phase Rotamak drive. An additional externally generated magnetic field (the poloidal field) is oriented orthogonally to the two pairs of Helmholtz coils to provide a compensating force to the 'hoop force' of the driven plasma current in order to have equilibrium.

In the consideration of the Rotamak as a low-cost device the item that represents the highest cost in existing Rotamaks was identified as the RF generator. In past Rotamak devices[2-6] the RF generator, one for each pair of Helmholtz coils, uses an expensive triode valve or capacitor line generators. Technically then the key to the present problem lay with the development of a suitable low-cost RF generator.

In the process of this development was assembled a Rotamak driven by transistorised RF generators using MOSFETS. Moreover it was found that compact torus FRC was produced even when only one pair of Helmholtz coils was energised with the driving RF. This we term single-phase operation.

The device supplied 1.7 kW of RF power to each drive phase at 170V. Stable compact torus FRC was observed for the duration of the RF drive of 40 ms in both modes of drive namely the single-phase operation and the conventional two-phase Rotamak operation. Current-drive efficiency of 0.1 A/W was observed for both modes of drive, this efficiency being sufficient in either mode to produce the field reversed configuration (FRC) characteristic of the compact torus geometry.

Experimental

The experiments were carried out in the device shown schematically in Fig. 1. The glass spherical chamber had a radius of 14 cm and two side arms form part of a vacuum system with a base pressure of less than 10^{-6} torr. The poloidal ('vertical') field coil had 12 turns on each side and produced a B_z field of 0.107 G/A when measured at the centre of the vessel. The mirror ratio of the poloidal B_z field was measured as 1.7. The power supply to the coil could produce up to 250 A in a square pulse lasting 100 ms. It

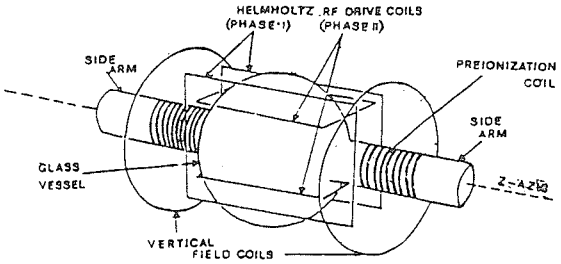

Fig. 1 Schematic diagram showing the rotamak configuration.

could also produce a linearly rising current for a ramped B_z field.

The rotating field Helmholtz coils were wound from insulated wire with each coil having 6 turns. The vertically located pair of coils had a measured inductance of 22 μH whilst the horizontally located pair of coils had 20μH. A composite capacitor made up of high voltage RF capacitors with an equivalent value of 1120 pf was inserted in series with each pair of driving Helmholtz coils for tuning purposes. Preionization coils of seven turns each fitted to the side arms of the vessel were connected to a 300W continuous RF supply operated at 8.7 MHz for most of these experiments.

In operation the system pressure was adjusted to the working pressure (typically several hundred micron) by the combination of a needle valve controlling the argon inlet and a butterfly valve controlling the pumping outlet. The preionization RF was then switched on producing an RF glow discharge in the glass vessel. The bias field was then triggered and after a variable delay follows the 1 MHz RF pulse of 40 ms duration.

Diagnostics include a Hall probe to measure B_z. This probe, with filters and amplifiers had a sensitivity of 5.8 mV/G and was movable along the z-axis to enable B_z to be measured as a function of the z-position. Another similar Hall probe was positioned to measure the value of B_z at $z = 0$ as a function of the radius r. A 5000-turn Rogowski coil was inserted around a half section of the plasma along glass tubing guides (see Fig. 2) so as to measure the driven azimuthal plasma current I_θ. Used with a RF choke, a 5 kHz low-pass filter, a 50-time amplifier and an active integrator terminated in a second 5 kHz filter the coil had a sensitivity of 0.44 mV/A.

Results

Experiments were carried out to determine the range of driven currents for both single as well as two-phase drive. The input RF voltage was fixed at 170 V. The applied B_z field and the test pressure in argon were treated as parameters. Results for single-phase operation are presented in this paper in Fig. 3–8.

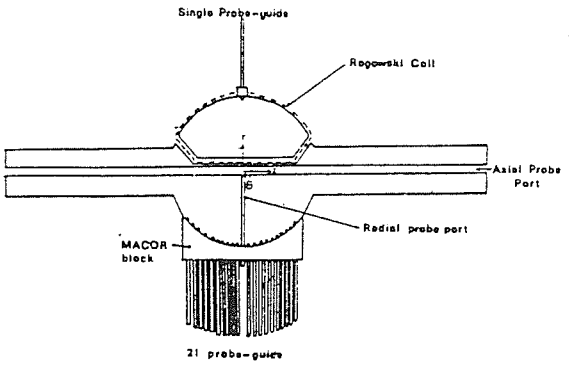

Fig. 2 Schematic diagram of the rotamak apparatus (top view) showing location of magnetic probe guides and Rogowski coil. The centre of the (r, θ, z) coordinates system used in the text is taken at the centre of the spherical discharge vessel.

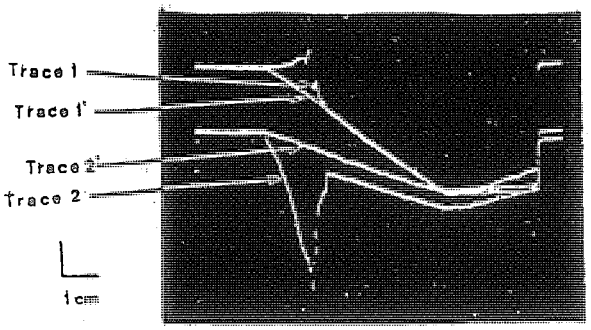

Fig. 3 Field-ramped experiment, single phase operation. Hall probe measurements, trace 1 and 1' for B_z at $r = 0$, $z = 0$ for the two cases with preionization (discharge) and without preionization (no discharge) respectively; ramped vacuum B_z field (Trace 1') of 0.65 G/ms. Time scale (horizontal) is 10 ms/cm; B_z amplitude is 6.8 G/cm. Rogowski coil measurement, traces 2 and 2' for I_θ with preionization and without preionization respectively. I_θ is 30 Acm^{-1}. (Pressure was 0.4 mtorr in argon; the RF pulse of 40 ms duration was applied at the start of the B_z ramp.)

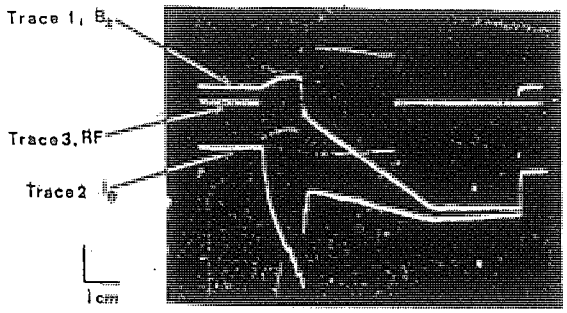

Fig. 4 Field ramped experiment (single phase operation).
Trace 1: Hall proble measurement (B_z); 6.8G per cm; horizontal scale; 10ms per cm. (Vacuum field ramped at 0.65G per ms)
Trace 2: Rogowski coil measurement (I_θ): 30A per cm.
Trace 3: RF envelope; 20 A per cm (pressure was 0.2 mtorr in argon; The RF pulse has a duration of 40 ms and starts at the same time as the vacuum field ramp.)

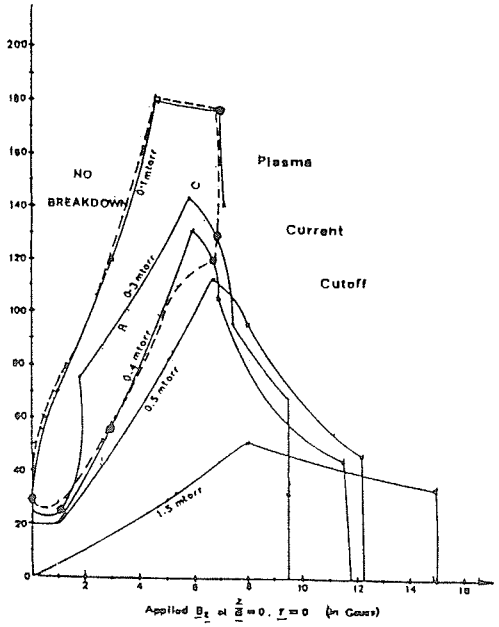

Fig. 5 Single-phase operational regime in argon with RF of 1MHz at 1.7 kW and preionization using 8.7 MHz RF. Each curve was obtained eith a vaccum B_z field ramp of 0.41G per ms at fixed pressure. The range of FRC operation for each fixed pressure is denoted by two large dark dots up to 0.4 mtorr, above which pressure no FRC operation was observed with the present single phase input power of 1.7kW.
The region encircled by the dashed line represents the FRC operational regime for single phase input at this power level of 1.7kW.

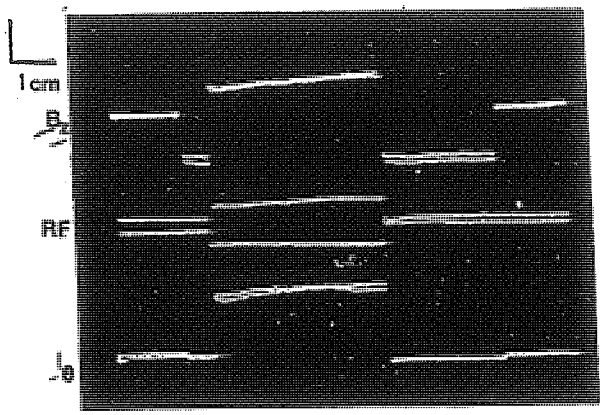

Fig. 6 Discharge with field reversal and stable for 40ms. Overlay of oscillograms for two identical discharges to show reproducibility at 0.2mtorr, vacuum B_z = 4.5G and RF of 1.7kW.
Top trace: B_z at $z = 0$, r =.0; 4.5Gper cm
Middle trace: Envelope of RF current; 40Aper cm (RF pulsed turned on 20ms after start of CRO traces, or 8ms after start of B_z field).
Bottom trace: Driven plasma current I_θ ; 110 Apercm Time scale (horizontal): 10ms per cm.

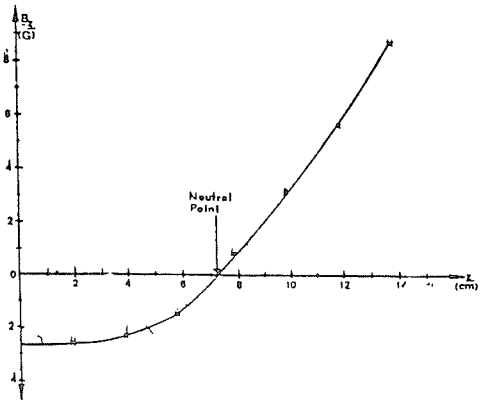

Fig. 7 B_z as a function of z along $r = 0$ at t = 31.5 ms referenced from start of RF pulse. Applied vacuum field of B_z = 5.5G at 0.3 mtorr argon, single phase RF drive of 1.7kW.

Field ramping experiments were carried out which enable a range of applied (vacuum) B_z fields to be covered in one discharge at a fixed pressure. An example is shown in Fig. 3 with a discharge carried out in 0.4 mtorr of argon. In this experiment the RF pulse is applied at the start of the B_z ramp and lasts 40 ms. In this oscillogram there are 2 sets of traces labelled 1 and 2 and 1′ and 2′. Traces 1 and 1′ are Hall probe measurements of B_z at $z = 0$ and $r = 0$

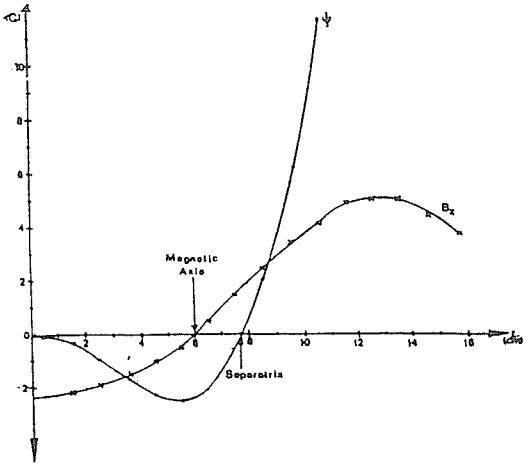

Fig. 8 B_z as a function of r along the line $z = 0$ at t = 31.5ms and conditions identical with those of Fig. 7.
Magnetic flux ψ as a function of r, derived from B_z,

for the cases respectively with and without preionization. Without preionization the plasma did not break down and hence trace 1′ represents the applied (vacuum) magnetic field B_z, ramping up at a rate of 0.65 G/ms. The horizontal line representing B_z = 0 at the start and at the end is of special importance in this oscillogram as the applied field B_z (see trace 1′) is always below this line and a Hall signal measured above this line indicates the occurence of field reversal and the establishment of a compact torus FRC. Thus trace 1 indicates measurable field reversal in the time period 3–8 ms after the start of the B_z ramp when the value of applied B_z was between 2–5 G. Cut-off of driven current, indicated by the B_z trace reverting to the trace 1′ occured at 14 ms when the value of the applied B_z field was 9 G. Traces 2 and 2′ show the output of the Rogowski system respectively with and without preionization. Trace 2′ (together with further careful observations) shows that the Rogowski system was directly affected by the applied B_z and registered a linearly ramping signal corresponding to the B_z ramp even when no plasma discharge took place. Thus subtraction of trace 2′ from trace 2 (with further subtraction of the obvious off-set between the two traces) enable a measure of the driven current at each value of

B_z. It is clear that current cut-off occured at t = 14 ms after the start of the B_z ramp.

Fig. 4 is another set of oscillogram taken at 0.2 mtorr with trace 1 measuring B_z indicating a clear regime of field reversal and trace 2 measuring the corresponding driven plasma current I_θ. Trace 3 shows the envelope of the driving RF current. At the start of the B_z ramp the RF current had a value of 24 A dropping to 18 A as the driven plasma current reached peak value and then rose to 35 A abruptly at current cut-off, and remaining at around that value for the rest of the 40 ms pulse duration of the RF pulse. The approximate halving of the RF current from the condition of no-load (i.e. plasma current cutoff) to the condition of maximum plasma loading (i.e. maximum plasma driven current) could indicate that the maximum driven current was limited by the power transfer from the RF source to the plasma.

From a series of such B_z-ramped experiments at different pressures a diagram of operational regime was mapped out giving driven current I_θ against applied B_z at various pressures. Indicated on the diagram are the current cut-off regions and the regions where breakdown could not occur despite the use of preionization RF. In the diagram (Fig. 5) the field reversed region is indicated by the letters FRC. This compact torus FRC region includes the low-pressure region of 0.1 mtorr–0.4 mtorr from small values of applied B_z to nearly cut-off values of B_z. For higher pressures the driven current was insufficient to reverse the applied B_z field.

From the diagram of operational regime a good operational point for FRC could be selected. For example, near-optimum current drive with field reversal is indicated for 0.2 mtorr with applied B_z of 4.5G. The measurements of two discharges were superimposed (to indicate degree of reproducibility) and shown in Fig. 6. The top trace shows the measurement of B_z at vessel centre z = 0, r = 0. The trace starts with B_z = 0. B_z was switched to a constant value of 4.5 G and when the RF was turned on at the time as indicated by the RF trace (middle trace) the field was immediately reversed as shown in the top trace. The cause of the field reversal, plasma driven current, is recorded in the bottom trace. The driven current rose from 140 A in a gradual manner to 170 A over a period of 40 ms and then abruptly dropped to zero when the RF pulse terminated. The B_z field indicates the establishment of a steady FRC with the value of field change ΔB_z rising from 6.5 G to 8 G.

To obtain some information about the magnetic field configuration a series of discharges were made at an applied field B_z (z = 0, r = 0) of 5.5 G at 0.3 mtorr with a driven current at the level of 125 A. During each discharge the value of B_z was measured at a probe position z and the value of z was scanned in 2-cm steps along the line r = 0. A second scan was made with another probe along the line z = 0, with r varied in 1-cm steps. Two discharges were recorded at each position and the oscillograms superimposed. The Rogowski coil output was also measured at each discharge. From these observations the discharges proved very reproducible. A graph of B_z against z was plotted for the time t = 31.5 ms from which a neutral point was determined at the position of z = 7.3 cm, r = 0 (see Fig. 7). A graph of B_z vs r was also plotted for the time t = 31.5 ms (see Fig. 8) from which the position of the magnetic axis was determined at r = 6 cm, z = 0. From the probe data of B_z vs r the values of flux

$\psi(r,z) = 2\pi \int_0^r rB_z(r,z)dr$ was computed with the approximation

$\psi(r,z) = 2\pi \Sigma\, rB_z(r,z)\,\Delta r$

These approximate values of ψ along the line z = 0 were plotted in the same Fig. 8, yielding the approximate position of the separatrix at r = 7.5 cm. Comparing the B_z and ψ graphs it may be seen that the large step-size of the integration for ψ has caused a left-ward shift of the ψ curve by about ½ cm; so that a more correct position of the separatrix along the line z = 0 should actually be closer to r = 8 cm. From these results a schematic extrapolation had been made of the expected magnetic configuration of the device at 0.3 mtorr, 31.5 ms into the RF drive. This is shown in Fig. 9.

The above results were obtained for single phase RF drive, PI say. Connecting the RF only to the other pair of coils, PII operation say, similar results were obtained. Finally both phases were connected and the discharge driven in the conventional Rotamak mode i.e. with the two phases simultaneously on but with a phase difference of 90° between the two drive pulse. The results obtained were similar with those of single-phase operation, except that the driven current I_θ and field swing ΔB_z were larger. These results are summarised in Fig. 10.

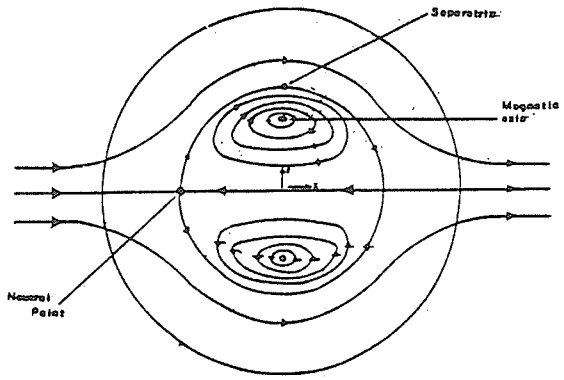

Fig. 9 Schematic interpretation of expected B_z field configuration at $t = 31.5$ ms for 1.7kW single phase RF drive at 0.3 mtorr argon. This interpretation is made from the measurement of the three points, neutral point, magnetic axis and separatrix from Fig. 7 & 8.

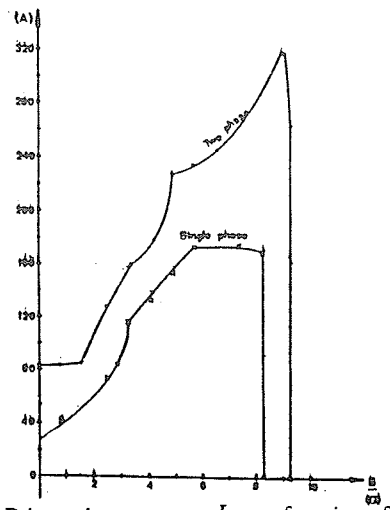

Fig. 10-Driven plasma current I_θ as a function of applied (vacuum) field B_E; with B_z measured at $r = 0$, $z = 0$. Operating pressure was 0.1 mtorr argon. The input power for single-phase operation was 1.7 kW and that for two-phase operation was 7 X 1.7 kW.

Conclusion

These experiments have demonstrated that a low-cost transistorised Rotamak can be built to produce stable long-lived compact torus field reversed configurations, so that these important concepts of plasma current drive and the FRC may be easily introduced in experiments. This is of special interest to some developing countries. The use of transistor technology has increased the flexibility of the device so that it may be easily characterised. For example the experimental turn-around time is very much reduced in the transistorised version. The RF frequency may also be rather easily changed.

In the present experiments with an input power of 1.7 kW per phase stable FRC configurations have been achieved lasting for the duration, 40 ms, of the RF drive pulse for conventional two-phase Rotamak drive as well as in operation with single-phase drive. The driven current has an efficiency of just under 0.1 A/W for conventional two-phase Rotamak operation at 9 G and just over 0.1 A/W for the single-phase mode at 6-7 G.

Acknowledgements

One of the authors (S.L.) acknowledges the assistance of a Flinders University Research Fellowship and a United Nations University Special Fellowship without which this work would not have been possible.

References

1. S. Lee et al – Amer. J. Phys. 56, 62 (1988).
2. I.R. Jones, Comments Plasma Phys and Controlled Fusion, **10**, 115 (1986).
3. I.R. Jones and H. Kirolous "Long Duration Rotamak Experiments", Twelfth European Conf. in Controlled Fusion and Plasma Phys, Budapest, Hungary 2-6 Sept 1985.
4. G. Durance and I.R. Jones, Phys. Fluids **29**, 1196 (1986).
5. W.N. Hugrass, I.R. Jones and M.G.R. Phillips, J. Plasma Phys. **26**, 465 (1981).
6. H. Tuczek, Procs. 3rd Int. Conf. Heating in Toroidal Plasmas Grenoble, G17 (1982).

Pulse Technology, Laser Development and Technology Resource Network

S. Lee
Jabatan Fizik
Universiti Malaya

In this paper I shall stress the importance of pulse technology in laser development and in developing the concept of a Laser and Plasma Technology Resource Network to help initiate experimental research in Third World Countries.

I. Pulse Technology

Pulse technology is the production, measurement and application of pulses. It encompasses all types of pulses whether mechanical, electrical, electromagnetic, optical, chemical or nuclear.

Pulses are characterised by pulse type, pulse shape (rise time , FWHM, fall time), pulse amplitude, pulse energy and PRF.

The advantage of considering pulse technology is that there are general principles applicable to all types of pulses , e.g. to obtain the most intense effects with a given energy, this energy should be delivered in a pulse ; the shorter the pulse time the greater the power. This is just as useful a concept in e.g. plasma as well as in laser technology ; and the electronic and electrical technology developed for plasma applications very often works just as well for lasers.

II. Pulsed laser applications

Pulse technology applied to laser development and applications may be divided into techniques involving electronics (including electrical) and those involving optics. Certain electronic and optical techniques are intimately coupled – hence optoelectronics.

Knowledge of pulse technology is very beneficial to pulsed laser applications, for example we may consider the development of the transversely excited pulsed nitrogen laser. This laser is based on the energy level scheme as depicted in Fig. 1, and uses an electrical discharge as a pump for pulse applications.

To be presented at :

1. Seminar Kebangsaan Teknologi Laser Pertama,15hb Okt 1989, Universiti Teknologi Malaysia, Skudai, Johor.

2. Second Regional Symposium on Optoelectronics , Nov. 27-28 , 1989, University Of Indonesia, Jakarta

A laser channel, transversely exited, is shown in Fig. 2. Technically for an efficient operation we may note two requirements :

(i) fast capacitor discharge to power the system

(ii) a uniform discharge, for maximum effective lasing volume and good laser beam quality.

Both the requirements may be assessed from an approach based on pulse technology.

Requirement of uniform volume discharge

Large current (tens of kilo amps) discharge tend to form arcs, localising the discharge along one or two narrow paths so that conditions in the laser channel are very non-uniform. What is the primary pulse requirement for uniform breakdown over the whole volume?

Consider the laser channel of Fig. 2 where the discharge voltage is applied transversely. The channel is made as uniform as possible but despite this there are bound to be non-uniformities in local gap spacing, electrode texture and surface 'whiskers' so that for a gap setting of 16kV breakdown a typical breakdown voltage distribution for the gap across the points A, B, C may be A (16.0kV), B (16.1kV) and C (15.9kV).

Consider a simple low inductance capacitor being used to power a laser channel as shown in Fig.3. The channel is set at 16.0kV. The capacitor is charged up. When the voltage reaches 15.9kV, the gap at point C breaks down and the voltage across the gap at C drops to say 10kV. A voltage lowering pulse travels out from point C at the speed of e.m. waves towards points B and A ahead of any gasdynamic disturbances propagating in the channel. Hence at points B and A there is no electrical breakdown and the capacitor discharges quickly across the channel only at point C in non-uniformity!.

Remedy?. Raise voltage across the gap quickly. How quickly?. Fast enough so that in the time it takes for the voltage reducing wave to reach point B, point B has risen to 16.1kV i.e. a rise of 0.2kV in the time it takes to travel from C to B at speed of 20cm/ns. If CB is of the order of 1 cm , 4kV/ns is required.

Thus the primary requirement for uniform breakdown (i.e. discharge across all points or a large number of points of the channel) is a large dVg/dt, rate of rise of voltage across the gap.[1] In this example 4kV/ns or 4×10^{9} V/s is

required - impossible to achieve using schematic 1 as shown in Fig. 3.

A voltage doubling swinger is used as shown in Fig. 4 to obtain dVg/dt of the order of kV/ns. In this schematic C_1 and C_2 are both charged to V_o. When the external spark gap is triggered, C_1 discharges through circuit e which should be lightly damped so that V_{G1} swings down from V_o through 0 towards $-fV_o$ where $f < 1$, say $f \sim 0.8$. V_{G2} remains at V_o supported by C_2. Thus the voltage across the laser channel $V_g = V_{G1} - V_{G2}$ swings from 0 towards $(1+f)\,V_o$ as shown in Fig. 5 in a time $\sim 3\sqrt{C_1 L_e}$.

Typically $C_1 = 5nF$, $L_e = 20nH$ (spark gap inductance dominates) and circuit e time constant $\sim\sqrt{(C_1 L_e)} \approx 10ns$ so that $3\sqrt{C_1 L_e} \approx 30ns$. If $V_o = 15kV$, $dVg/dt \approx 16(1+0.8)/30 \approx 1kV/ns$.

It is found that for atmospheric N laser this is insufficient to produce good uniformity and some corona spraying[4] technique along the entire channel is necessary together with the voltage doubling swinger to give a large number of arcs reasonably evenly distributed approximating a uniform discharge. Thus by this qualitative analysis we see that C_1 in the circuit e plays the role of a voltage swinging capacitor. C_2 is the laser power capacitor discharging rapidly through the laser channel into the capacitor C_1 to provide the fast laser pump.

Pulse analysis

A detailed circuit analysis could of course be carried out in order to obtain quantitative information on the pulse characteristics. Fig. 6 is the equivalent circuit for the nitrogen laser.

In general the governing equations of the two circuits e and circuit 1 are :

$$(L_e+L_1)\frac{dI_e}{dt} - L_1\frac{dI_1}{dt} + r_e I_e = V_o - \frac{1}{C_1}\int (I_e - I_1)\,dt \qquad (1)$$

and

$$(2L_s+L_g+L_1+L_2)\frac{dI_1}{dt} - L_1\frac{dI_e}{dt} + r_g I_1 = \frac{1}{C_1}\int(I_e-I_1)dt - \frac{1}{C_2}\int I_1 dt \qquad (2)$$

The voltage difference across the laser channel is:

$$V_g = \frac{1}{C_1}\int(I_e-I_1)dt - \frac{1}{C_2}\int I_1 dt + L_1\frac{dI_e}{dt} - (2L_s+L_1+L_2)\frac{dI_1}{dt} \qquad (3)$$

To solve this problem, the circuit parameters are first specified. At $t = 0$ Eq.(1) is integrated for I_e numerically by linear approximation with proper initial conditions. I_1 and dI_1/dt are kept at 0 until the value of V_g computed from Eq.(3) at each step reaches a preset value. At this time Eq.(2) is brought into operation, switching circuit 1 on to compute the value of I_1, simultaneously with I_e from Eq.(1). It is normal in these procedures to deal with normalised equations and scaling parameters[1].

The normalised variables are :

$$\tau = t/t_o \quad , \iota_e = I_e/I_o \quad , \iota_1 = I_1/I_o$$

where $t_o = \sqrt{(L_1 C_1)}$, $I_o = V_o / \sqrt{(L_1/C_1)}$

and the scaling parameters are

$$\beta_1 = L_2/L_1 \quad , \quad \delta = C_1/C_2 \quad , \quad \alpha_1 = r_g/r_e \text{ and } \beta_g = L_g/L_2$$

$$\beta_e = L_e/L_1 \quad , \quad \alpha_e = r_e/\sqrt{(L_2/C_2)}$$

and $\alpha_{eff-e} = \alpha_e \sqrt{\{1/(1+\beta_e)\}}$, circuit e damping factor

and $\alpha_{eff-1} = \alpha_e \alpha_1 \sqrt{\{1/((1+\beta_1+\beta_g)(1+\delta))\}}$, circuit 1 damping factor

Results

Using typical parameters :

$L_1 = 0.18\text{nH}$, $L_2 = 0.4$ nH , $L_s = 0.75\text{nH}$

$L_g = 3\text{nH}$, $C_1 = 10\text{nF}$, $C_2 = 20\text{nF}$, $L_e = 32\text{nH}$

and a slightly damped circuit e with $\alpha_{eff-e} = 0.1$ and a slightly damped circuit 1 with $\alpha_{eff-1} = 0.3$ we have pulse results as shown in Fig. 7 where the laser gap has been set to breakdown at 1.7 V_o or $v_g = 1.7$. The laser current is shown in the Fig. as ι_1 and the laser gap power as Π_o. The voltage on C_1 drops from 1.0 to -0.7 at $\tau = 34.0$, then rises sharply on laser gap breakdown and continues with an oscillation of periodic time $\sim 18t_o$ superimposed on the slower periodic time of $\sim 90t_o$ of the external circuit. This behaviour is also reflected in the ι_e curve.

The laser gap current i_1 rises to a peak value of 0.33 in a time of $4t_o$ and oscillates in a damped mode with a periodic time of $\sim 18t_o$ with modulation. The corresponding power developed across the laser gap resistence has a peak value of 0.42 and a FWHM value of $5.5t_o$. The voltage v_M that may be measured across the laser electrode (i.e. outside the laser channel) is also shown in Fig. 3.

From the above results the value of $\frac{dV_g}{dt}$ for a typical nitrogen laser may be estimated. We note that a typical value of $t_o = \sqrt{(L_o C_o)}$ is 1.3ns. Operating at a voltage of 15 kV , the average dV_g/dt is (1.7 x 15kV)/(34 x 1.3)ns. $\sim$0.5kV/ns.Such a value is experimentally known to be able to initiate the uniformity of discharge for a low pressure laser and is the primary pulse requirement for proper operation of the nitrogen laser.

The FWHM value for the power peak is $5t_o$ (6.7ns) for the critically damped laser channel and $5.5t_o$ (7.4ns) for the more typical case of the laser channel with effective damping factor of 0.3. It may be expected then that such a typical nitrogen laser will have a full width pulse of less than 7.4 ns after consideration of threshold effect. For example for the case of $\alpha_{eff-L} = 0.3$, if the lasing threshold is at a power level of 0.3 then the full width of the laser pulse would be $3.5t_o$ or 4.7ns. This is a typically observed value for a low pressure nitrogen laser.

Sequenced nitrogen lasers

Using the pulse technology concepts discussed above we may develop exciting laser systems such as sequenced nitrogen lasers to obtain real-time sequenced full power laser flashes with separations of several nanosecond. This is useful for imaging of fast events[2].An example of imaging using shadowgraph is shown in Fig. 8.

We consider 3 laser channels depicted in Fig.9. The equivalent circuit is as shown in Fig. 10.

The voltage difference across the three channels are denoted respectively by V_{g1}, V_{g2} and V_{g3}. In general , the capacitors C_1, C_2, C_3, C_4 are charged to voltage V_1, V_2, V_3 and V_4 respectively. As discussed earlier, the first laser channel breaks down when the voltage-swinging C_1 discharges,enabling C_2 to discharge I_1 through the first laser channel.

The discharge of C_2 pulls the right-hand side of the second laser channel downwards from V_2 towards $-V_2$ so that C_2 whilst powering the first laser channel, also acts as the voltage swinging capacitor for the second laser channel. If the voltage swing is sufficient to break down the second laser channel, then C_3 discharges I_2, powering the second laser channel whilst simultaneously acting as the voltage-swinging capacitor for the third laser channel until C_4 is able to discharge I_3 through the third laser channel.

Pulse circuit equations

We take the laser channel inductance and resistance to be L_g and r_g for each laser gap. The stray inductance leading up to the laser gap on each side is taken to be $L_{s1} = L_{s2} = L_s$.

The relevant equations may be written as follows.

A. Circuit e

$$(L_e + L_1)\frac{dI_e}{dt} - L_1\frac{dI_1}{dt} + r_e I_e = V_1 - \frac{\int_o^\tau (I_e - I_1)}{C_1} dt \qquad (4)$$

Circuit e is switched on at t = 0.

The voltage difference across the first laser channel is

$$V_{g1} = (V_2 - V_1) + \frac{\int (I_e - I_1)dt}{C_1} - \frac{\int (I_1 - I_2)dt}{C_2} + L_1\frac{dI_e}{dt} + L_2\frac{dI_2}{dt} - (2L_s + L_1 + L_2)\frac{dI_1}{dt} \qquad (5)$$

Circuit 1 is switched on when V_{g1} reaches a preset value, e.g. $1.6V_1$.

B. Circuit 1

$$(2L_s + L_g + L_1 + L_2)\frac{dI_1}{dt} - L_2\frac{dI_2}{dt} - L_1\frac{dI_e}{dt} + r_g I_1$$

$$= (V_2 - V_1) + \frac{\int(I_2-I_1)}{C_2}dt + \frac{\int(I_e-I_1)}{C_1}dt \qquad (6)$$

The voltage difference across the second laser channel is

$$V_{g2} = (V_3 - V_2) + \frac{\int(I_1 - I_2)dt}{C_2} - \frac{\int(I_2 - I_3)dt}{C_3}$$

$$+ L_2\frac{dI_1}{dt} + L_3\frac{dI_3}{dt} - (2L_s + L_2 + L_3)\frac{dI_2}{dt} \qquad (7)$$

Circuit 2 is switched on when V_{g2} reaches a preset value.

C. Circuit 2

$$(2L_s + L_g + L_2 + L_3)\frac{dI_2}{dt} - L_3\frac{dI_3}{dt} - L_2\frac{dI_1}{dt} + r_g I_2$$

$$= (V_3 - V_2) + \frac{\int(I_3-I_2)}{C_3}dt + \frac{\int(I_1-I_2)}{C_2}dt \qquad (8)$$

The voltage difference across the third laser channel is

$$V_{g3} = (V_4 - V_3) + \frac{\int(I_2-I_3)}{C_3}dt - \frac{\int I_3}{C_4}dt$$

$$+ L_3\frac{dI_2}{dt} - (2L_s + L_3 + L_4)\frac{dI_3}{dt} \qquad (9)$$

Circuit 3 is switched on when V_{g3} reaches a preset value.

D. Circuit 3

$$(2L_s + L_g + L_3 + L_4)\frac{dI_3}{dt} - L_3\frac{dI_2}{dt} + r_g I_3$$

$$= (V_4 - V_3) - \frac{\int I_3}{C_4}dt + \frac{\int (I_2 - I_3)}{C_3}dt \qquad (10)$$

Equations (4), (6), (8) and (10) are the equations governing the discharge of the four circuits while Eqs. (5), (7) and (9) are the equations determining the times of switching on, respectively, circuit 1, circuit 2 and circuit 3 relative to time t = 0.

E. Normalization

The variables are normalized in the following manner:

$\tau = t/t_o$,

where the unit time is $t_o = \sqrt{(L_1 C_1)}$,

$i_e = I_e/I_o$

with a unit current of $I_o = V_1/\sqrt{(L_1/C_1)}$. Also

$i_1 = I_1/I_o$, $i_2 = I_2/I_o$, $i_3 = I_3/I_o$,

and

$v_{g1} = V_{g1}/V_1$, $v_{g2} = V_{g2}/V_1$

and

$v_{g3} = V_{g3}/V_1$

The scaling parameters are

$\beta_e = L_e/L_1$, $\beta_2 = L_2/L_1$, $\beta_3 = L_3/L_1$,

$\beta_4 = L_4/L_1$, $\beta_s = L_s/L_1$, $\beta_g = L_g/L_1$,

$\delta_2 = C_2/C_1$, $\delta_3 = C_3/C_1$, $\delta_4 = C_4/C_1$,

$v_2 = V_2/V_1$, $v_3 = V_3/V_1$, $v_4 = V_4/V_1$,

and

$\alpha_e = r_e/\sqrt{(L_1/C_1)}$, $\alpha_g = r_g/\sqrt{(L_1/C_1)}$,

where r_e and r_g are respectively, the spark gap and laser channel resistance, and the preset breakdown voltages of the laser channels are written, normalized to V_1, as F_1, F_2, and F_3.

Integration Procedure

The scaling parameters are first specified. At $\tau = 0$, Eq(4) is integrated for ι_e, numerically by linear approximation with the initial conditions of $\int \iota_e d\tau = 0$, $\iota_e = 0$, and $d\tau_e/d\tau = 1/(1 + \beta_e)$. The quantities ι_I and $d\iota_1/d\tau$ are kept at 0 until the value of v_{g1} computed from Eq.(5) at each step reaches the preset value. At this time, Eq.(6) is brought into operation, switching circuit 1 on to compute the value of ι_1 simultaneous with ι_e from Eq.(4). During the simultaneous integration of Eqs. (4) and (6), $\int \iota_2 d\tau$, ι_2, and $d\iota_2/d\tau$ are kept at zero and v_{g2} is computed at each step from Eq.(7) to determine when circuit 2 is switched on by bringing Eq. (8) into the integration scheme. Equation (4) (6), and (8) are then simultaneously integrated for ι_e, ι_1, and ι_2. During this integration, $\int \iota_3 d\tau$, ι_3, and $d\iota_3/d\tau$ are kept at zero whilst v_{g3} is computed at each step from Eq.(9) to determine when circuit 3 is switched on after which time Eqs. (4), (6), (8) and (10) are simultaneously integrated for ι_e, ι_1, ι_2 and ι_3.

Results of Computation

Computation shows there are two modes, one designated as the prolonged sequencing mode giving rise to rather imprecise sequencing compared to the second designated as prompt sequencing mode.

Prompt sequencing may be obtained by using progressively reduced capacitances in the sequence of capacitors. This may be aided by progressively increasing the voltages in the sequence of capacitors thus enabling also pulse power compensation. Both arrangements have been computed.

Figure II shows the result of an arrangement with reducing capacitances but with the same voltage on all capacitors.
The Parameters are

$$C_1 = 24 \text{ nF}, \; C_2 = 12 \text{ nF}, \; C_3 = C_4 = 6 \text{ nF},$$

$$r_g = 0.06\,\Omega, \; r_e = 0.08\,\Omega$$

and

$$V_1 = V_2 = V_3 = V_4 = 14 \text{ kV}$$

giving scaling parameters of

$$\beta_e = 80, \; \beta_2 = \beta_3 = \beta_4 = 1, \; \beta_g = 0.7, \; \beta_s = 0.7$$

$$\delta_2 = 0.5, \; \delta_3 = \delta_4 = 0.25, \; \alpha_g = 0.75, \; \alpha_e = 1$$

$$v_2 = v_3 = v_4 = 1, \text{ and } F_1 = F_2 = F_3 = 1.6$$

Here $t_o = \sqrt{(L_1C_1)} = 1.9$ ns , $I_o = 175$ kA, and the computation shows in Fig. 11 that prompt sequencing is achieved with the following pulses :

First pulse : amplitude = $0.4\ I_0$,
FWHM of power curve = $2.0\ t_o$;
Second pulse amplitude = $0.34\ I_0$,
FWHM of power curve = $1.5\ t_o$;
Third pulse : amplitude = $0.32\ I_o$,
FWHM of power = $1.1\ t_o$,
with precise pulse separation of $2.5\ t_o$ and $2t_o$ respectively.

Preliminary experimental results have been obtained in agreement with some of these computed results , e.g. see Fig. 12.
The experimental results of Fig.12 were obtained with parameters which the theory predicts to produce a mode designated as prolonged sequencing as shown in Fig.12A using identical capacitors each 10nF. From the computed results it is seen that the dV_g/dt associated with the third laser pulse is very low typically less than 0.1kV/ns so that it is predicted that with this prolonged mode of operation the third laser pulse will be erratic because of poor channel uniformity. This is as observed often as in Fig 12(b).

In conjunction with multiple frame nitrogen laser systems a system using a ruby laser with fibre optic delay lines to sequentially switch a series of a nitrogen laser as shown in Fig.13 may prove more flexible and useful. Or a fast pulse low jitter system with delay cables may be used.

III. Technology Resource Network

The above discussion shows that through such theoretical analysis based on pulse technology we can develop useful systems if we are at the same time supported by the hardware of pulse technology.

Example of hardware

Laser head with preionisers;
fast low inductance capacitors ;
spark gap (low inductance , triggered) ;
triggering electronics , triggering system ;
power supplies ;
delay units (for synchronizingwith other events) ;

There now exist centres where basic technology, basic pulse technology and hard-ware have been developed for the past many years to a sufficient level to ensure self-sufficiency in several aspects to the extent of being able to practise South-South Technology transfer in important areas of pulse technology such as in optoelectronics laser and plasmas. However , a centre may be strong in some aspects e.g. HV electronic pulse techniques but not in another important area e.g. optics whilst another centre may be strong in optics but weak in the pulse electronics aspects.

There is a proposal for a Laser and Plasma Technology Resource Network with a display and documentation centre at the ICTP (International Centre for Theoretical Physics) , LAMP Laboratory . This was proposed by the AAAPT (Asian African Association for Plasma Technology) and is in the process of being set-up. The structure may be as depicted in Fig.[14]

Concept of a package

The technology transfer and exchange is based on the concept of packages . Each package is made up of carefully designed sub-systems. Each subsystem is made up of components. An example of a nitrogen laser package is shown in Fig. 15 which also shows an add-on package for shadowgraphy . The two packages together form a nanosecond shadowgraphy system.

Another example of a package is the UNU/ICTP PFF (United Nations University/International Centre for Theoretical Physics Plasma Fusion Facility)[3] shown in Fig. 16.

Documentation of packages

These packages should beside comprehensive hardware also have complete documentation as follows :

- . package outline ,
- . manuals on maintenance and experiments ,
- . manuals on sub-systems of the packages ,
- . the components of each sub-system.

Transfer levels

Exchange and transfer may be carried out at different levels as follows :

1. Package with training
   e.g. UNU/ICTP PFF package and nitrogen laser package and shadowgraphy package together with one or two 6-month training programmes.
2. Package without training
   e.g. nitrogen laser package
3. Sub-systems
   e.g. triggering electronics for nitrogen lasers or neutron yield counter.
4. Components
   e.g. a triggering transformer

The Kuala Lumpur Experience

1. UNU/ICTP Training Programme 1985/86
2. (UNU) ICTP Training Programme 1988
3. ICTP-UM Training Programme 1989/90

Equipment transferred (Packages and Sub-systems)

Institution	UNU/ICTP PFF	N_2 Laser	Shadow-graphy	Sub-system
Pakistan, QIA	√**			
Siera Leone, Njala UC	√	√*		
Nigeria, Rivstech	√*	√*	√	
India, Delhi U	√	√		
India, Rajashtan U	√	√		
India, SP College		√		
Thailand, PSU	√	√		
Egypt, Al Azhar U	√	√	√	X-ray camera
Indonesia, LAPAN	Flow simulator/			
Indonesia, PPNY	√			Glow discharge subsystems
Bangladesh, AEC				Glow discharge tube

** Resulted in Ph.D Thesis

* Resulted in M.Sc Thesis

Funding/Intrastructure

1. ICTP/UM : Laser and Plasma Technology Resource Network of the AAAPT project of ICAC-UM.
   Membership:
   Network of the AAAPT plus several other interested institutions.
2. TWAS/ICTP : Fellowships
3. TWAS South-South Fellowship with ICAC support
4. TWAS research grants
5. many other possibilities.

Conclusion

With the advent of the ICTP OEA (Office Of External Activities) South-South Science Technology and Research transfer is now a firmly established fact.

A Technology Resource Network will help to extend the transfer process and help build up our own indigeneous scientific capability in various fields including laser development, optoelectronics and pulse technology.

References

1. S.Lee, A.V. Gholap, A.J. Smith, K.H. Kwek, A.C. Chew, T.Y. Tou and S. Sapru, J. Fiz. Mal. , 6 , 165 (1985)

2. S.Lee, K.H. Kwek, Jalil Ali, M.V.H.V. Prabhakar, Y.S. Shishodia and A.G. Warmate, J. Appl. Phys. 65 , 4133 (1989)

3. S.Lee, T.Y. Tou, S.P. Moo, M.A. Eissa, A.V. Gholap, K.H. Kwek, S. Mulyodono, A.J. Smith , Suryadi, American J. Phys. , 56 , 62 (1988)

4. K.H. Kwek , T.Y. Tou and S. Lee, IEEE Trans. on Instrumentation and Measurements IM-38, 103 (1989.

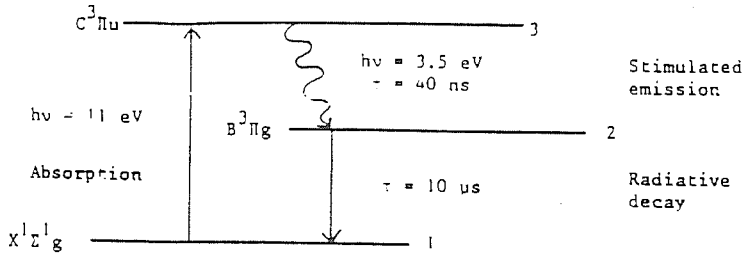

Fig. 1 Three level pumping scheme of Nitrogen Laser.

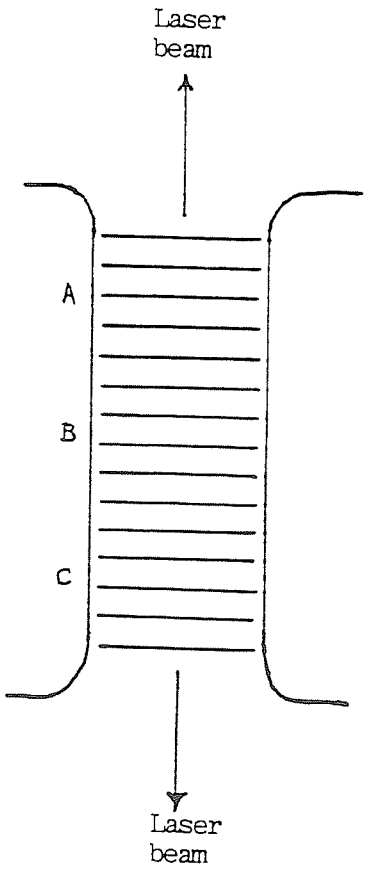

Fig. 2 Transversely excited nitrogen laser channel. Discharge between the two electrodes should be uniform occuring at A, B and C, i.e. over the whole channel.

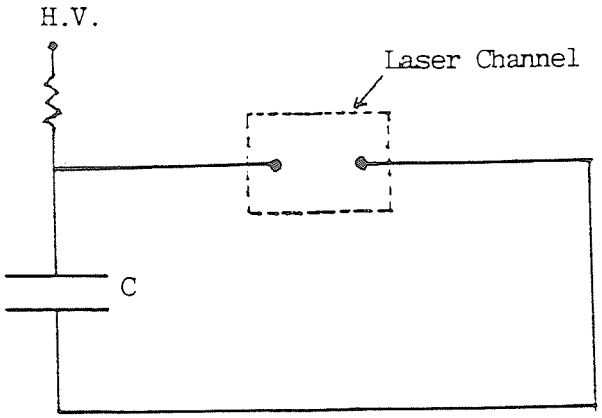

Fig. 3 Schematic for a simple capacitor discharge nitrogen laser system.
Why will this not work?

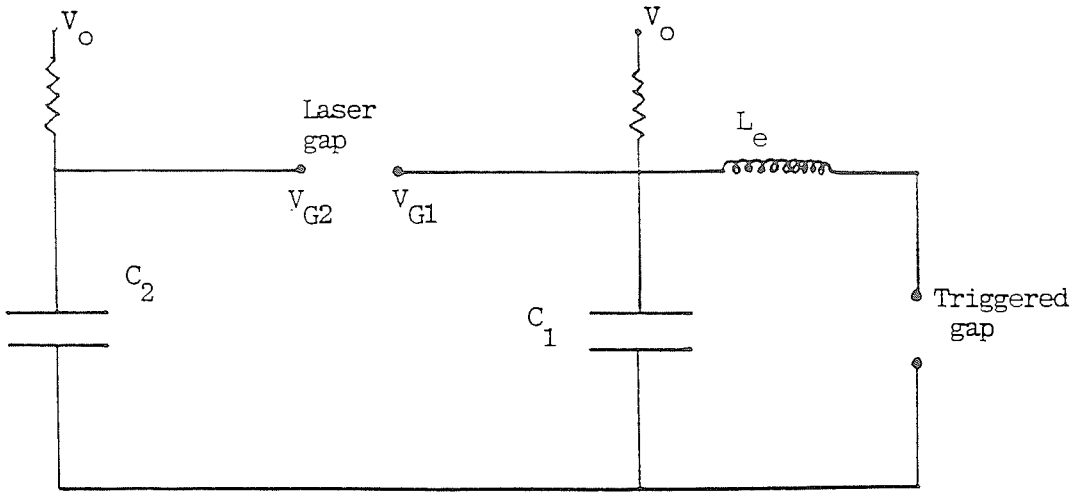

Fig. 4 Schematic 2 with voltage doubling swinger to achieve large dVg/dt

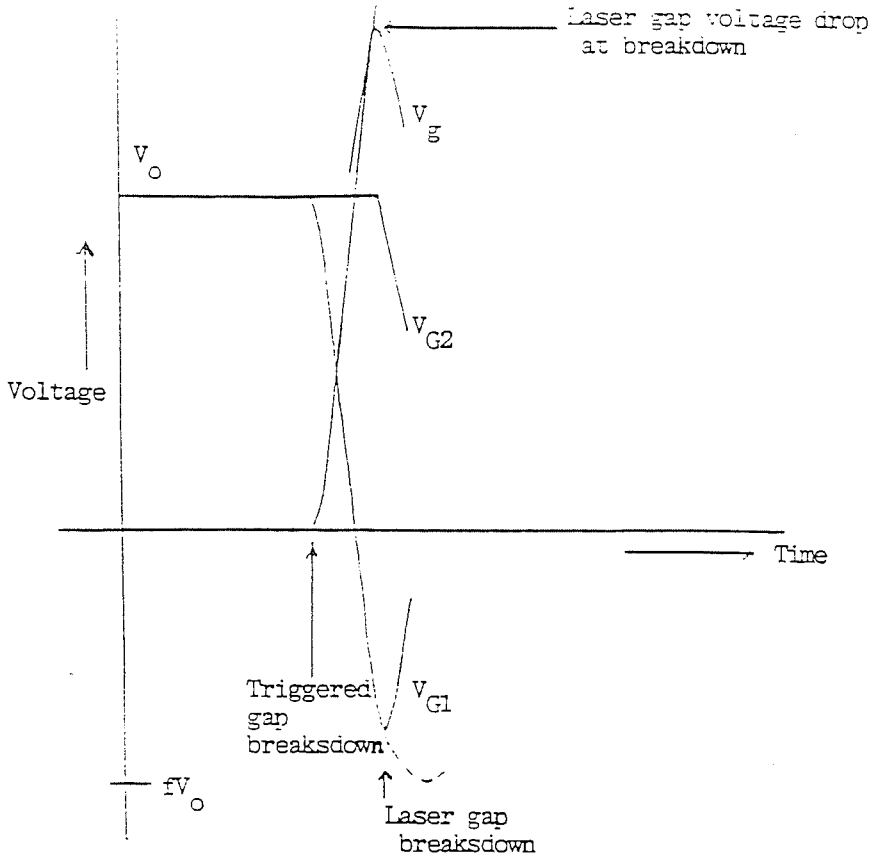

Fig. 5 Illustrating voltage doubling swinger mechanism to provide $\frac{dVg}{dt}$ of order 1kV/ns

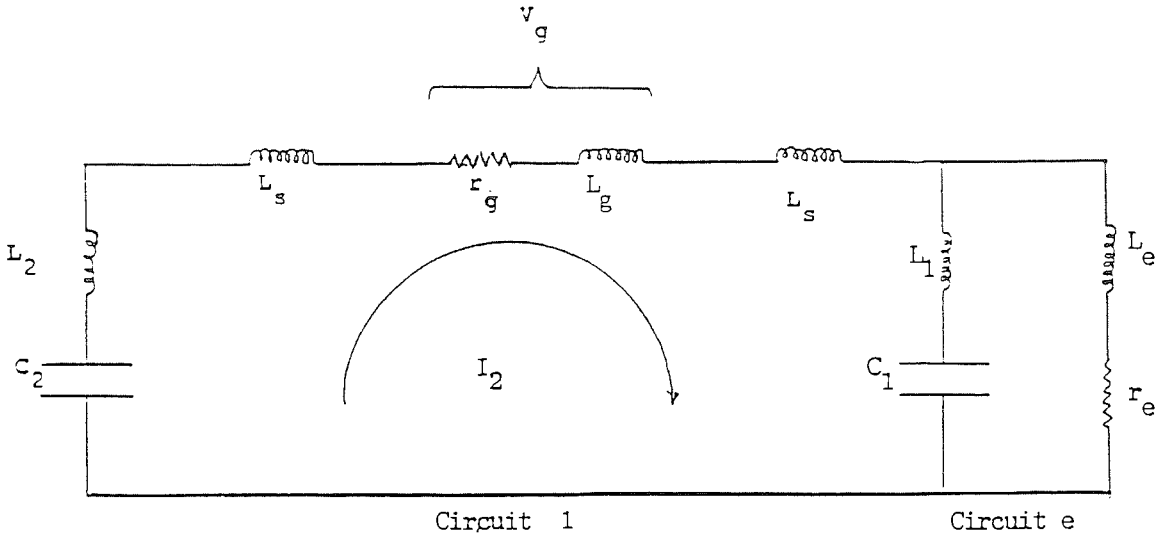

Fig. 6 Equivalent circuit of the nitrogen laser

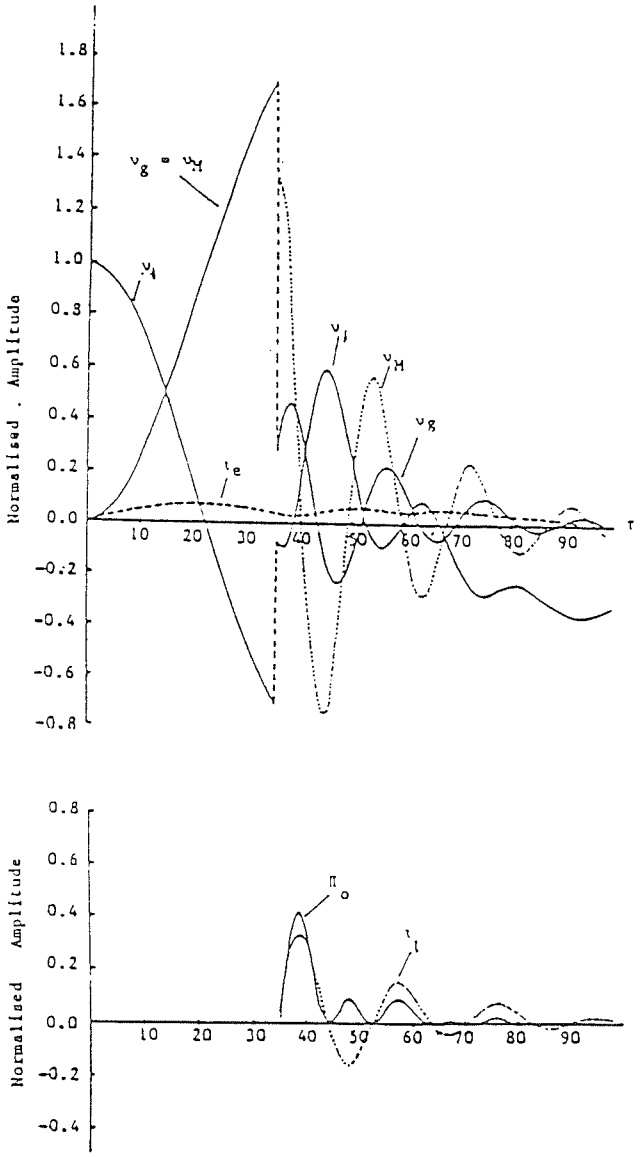

Fig. 7 Solution of currents, voltages and laser gap power for $\alpha_{eff\text{-}e}$ = 0.1 and $\alpha_{eff\text{-}L}$ = 0.3 (laser gap lightly damped).

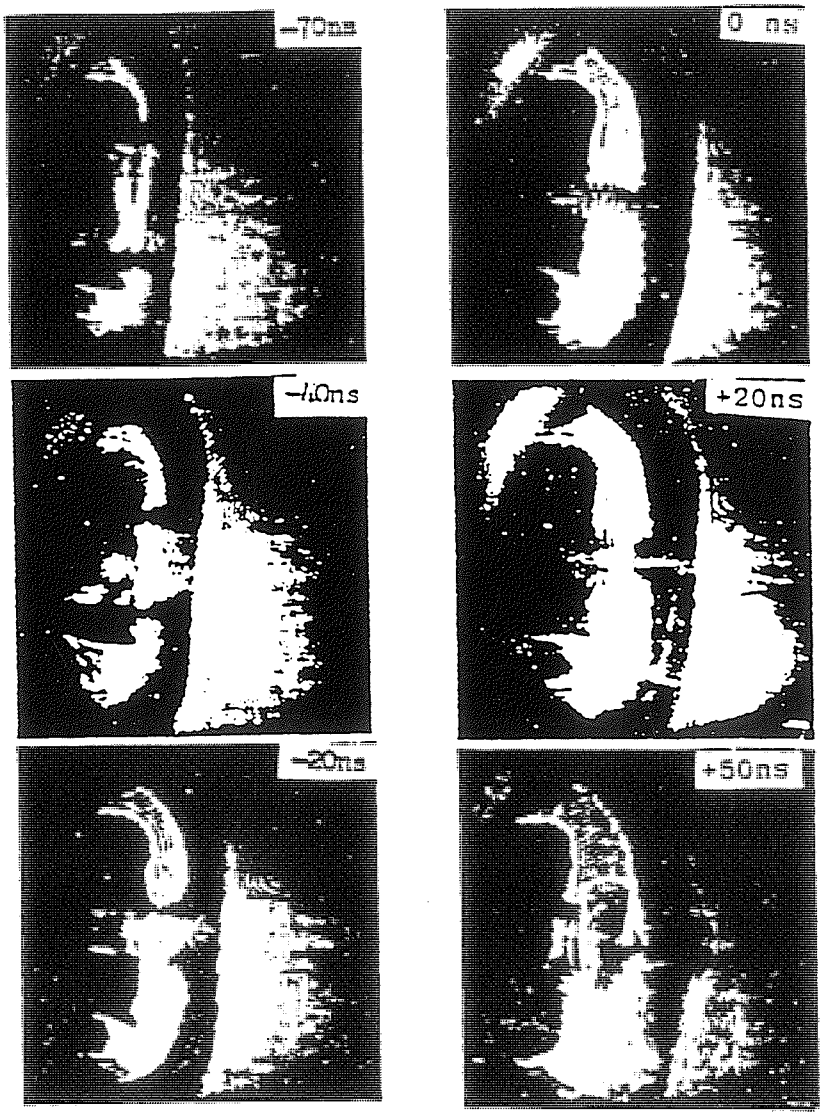

Fig. 8 Side on laser shadowgraph of a 20-kV 60 μF, 4-Torr deuterium plasma focus, showing a pinch ratio $r_p/r_0 \sim 0.13$.

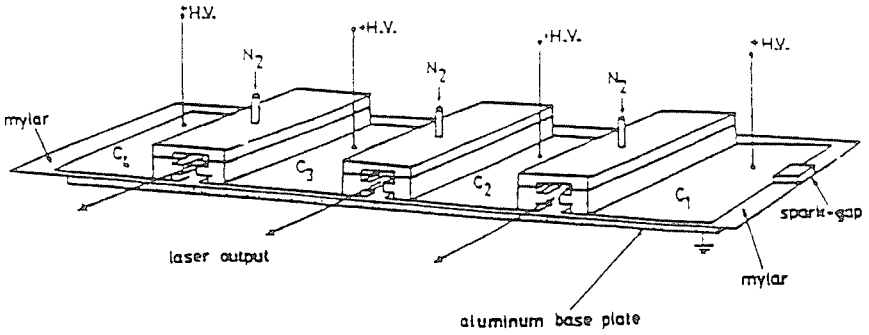

Fig. 9 Schematic of a three-channel sequenced nitrogen laser. The high-voltage plates of the capacitors C_1, C_2, C_3, and C_4 are made of aluminum foils.

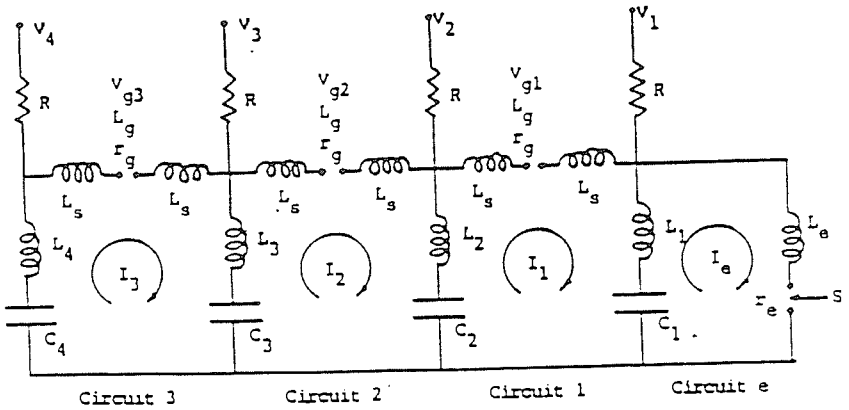

Fig. 10 Circuit diagram of the three-channel sequenced nitrogen laser.

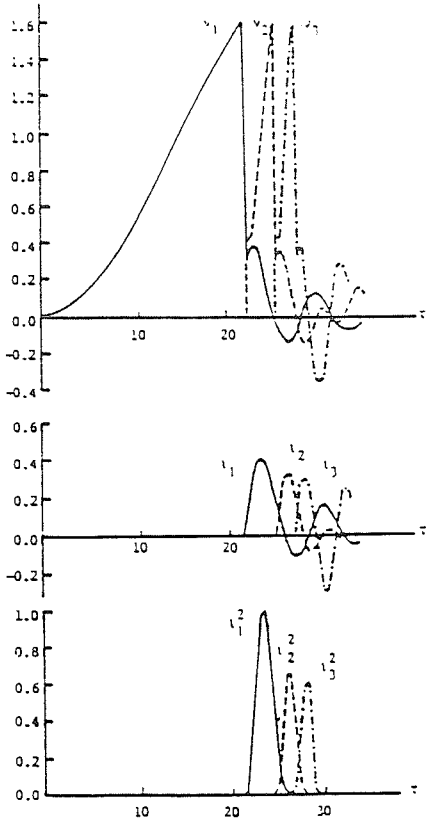

Fig. 11 Computed voltages across the laser channel, laser currents, and laser currents squared as functions of time; all variables are normalized. Parameters used are those for a "prompt sequencing" mode.

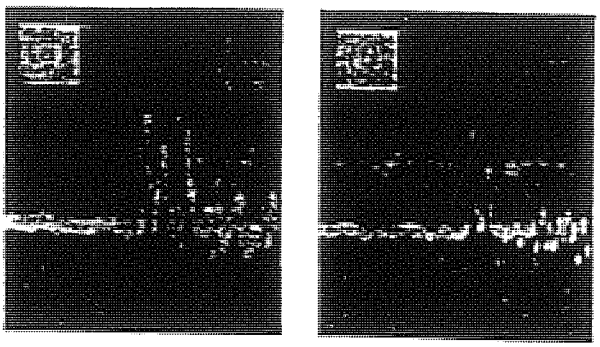

Time scale: 100ns/division.

Fig 12 Oscillograms of photodiode signal monitoring the three-channel sequenced nitrogen laser operated in the prolonged sequencing mode; time scale: 100 ns/div. (a) Shot with three laser pulses in "prolonged sequence." (b) Shot with the third laser pulse missing.

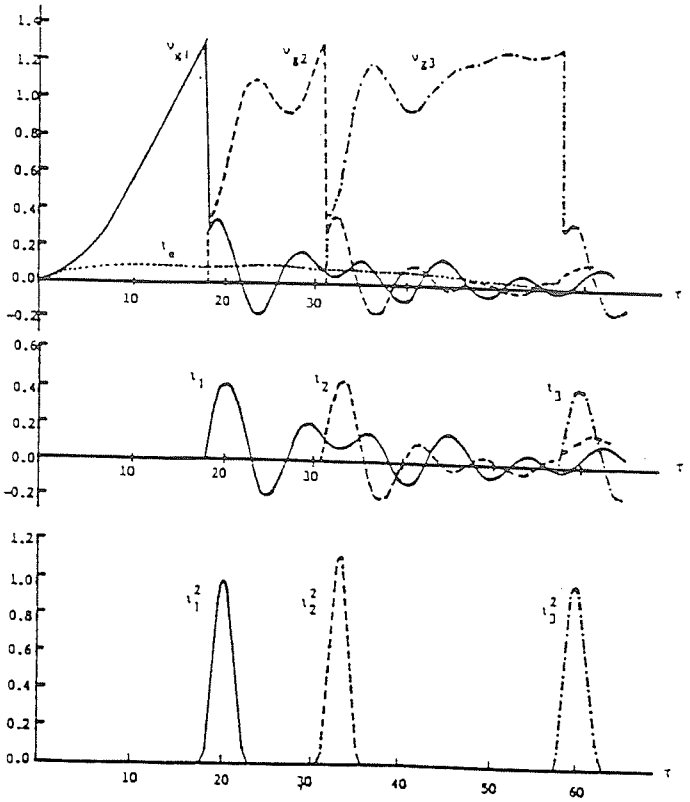

Fig 12A Computed voltages across the laser channel, laser currents, and laser currents squared as functions of time; all variables are normalized. Parameters used are those for a "prolonged sequencing" mode.

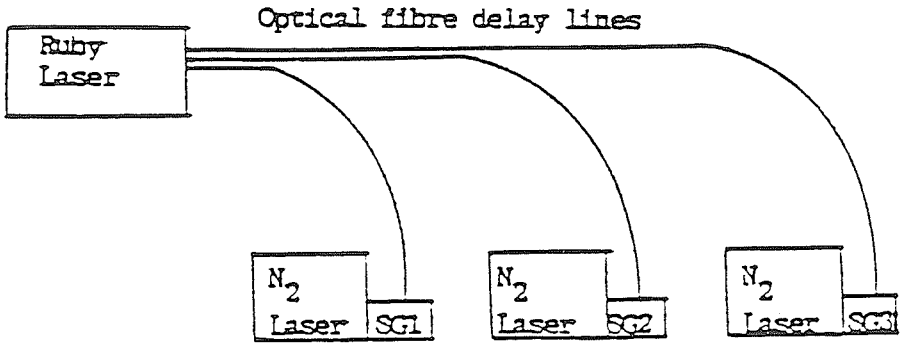

Fig. 13 Ruby Laser triggered multiframe nitrogen laser system. The fibre optical cables may be varied in length to provide suitable delays between frames.

Instead of the ruby laser and optical fibre delay system a fast pulser system e.g.30kV rising in 50ns coupled with coaxial cable delay lines of desired delays may be used.

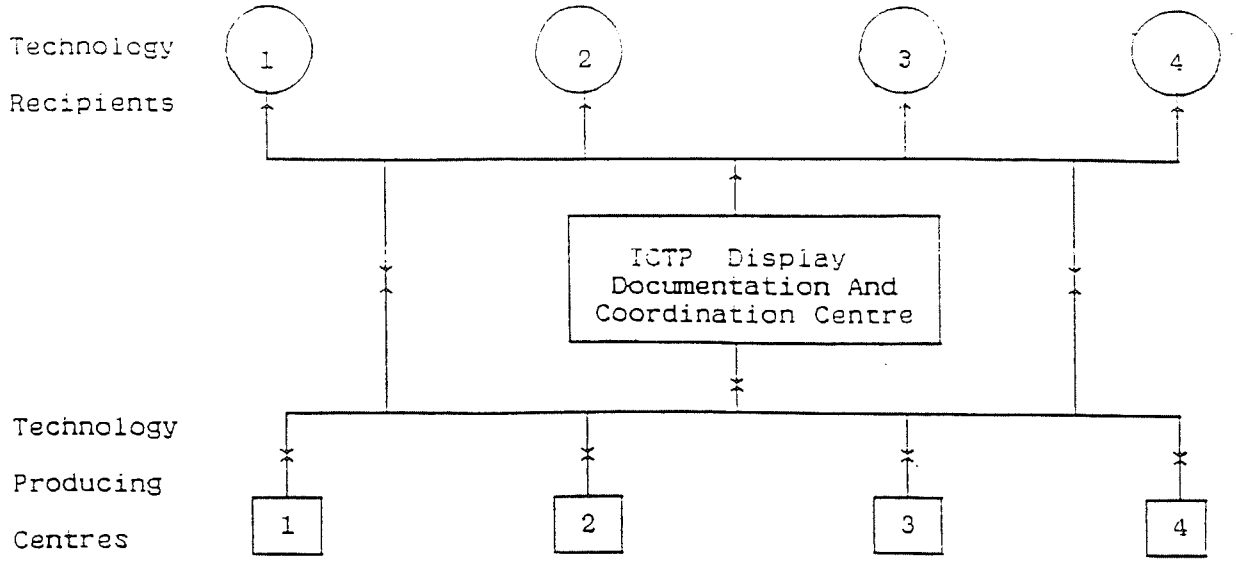

Fig. 14 Structure of Technology Resource Network

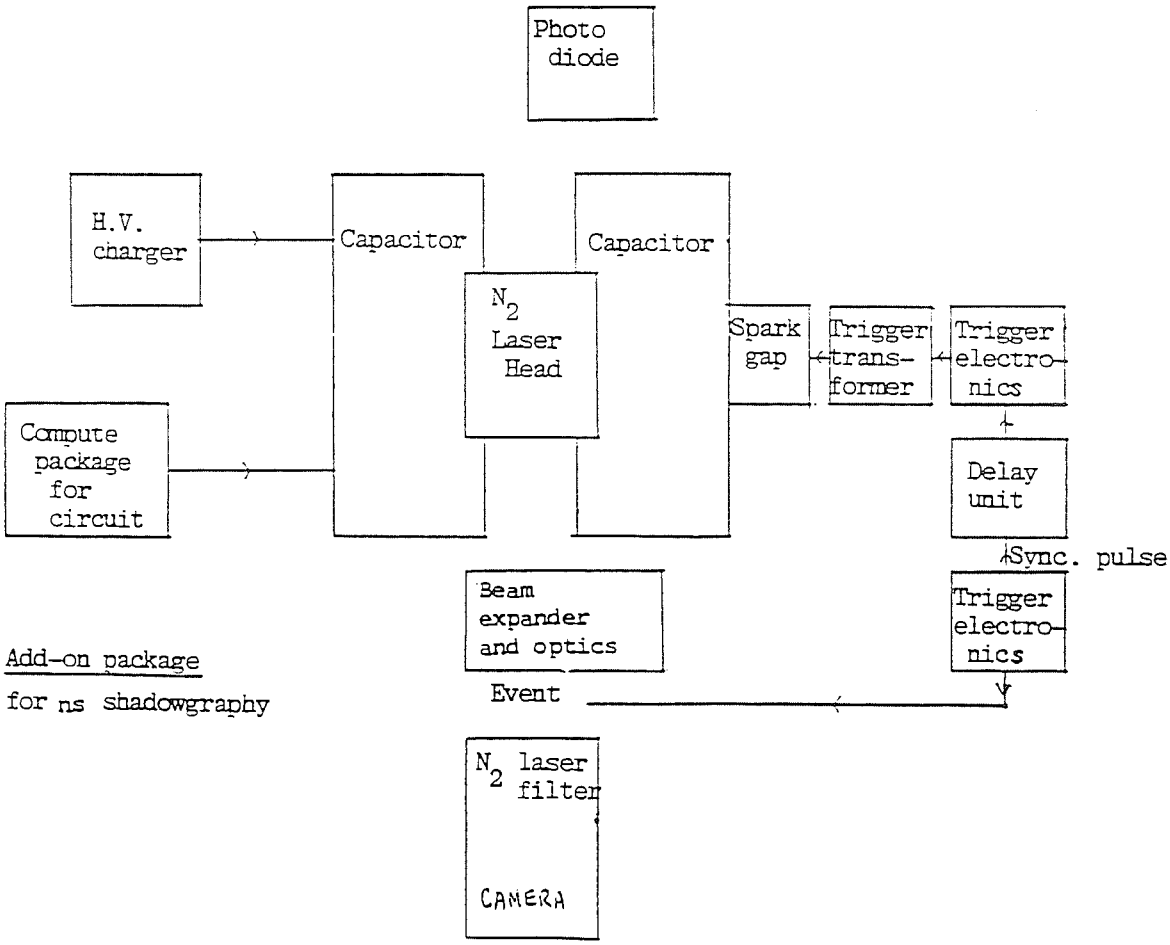

Fig 15 Nitrogen laser package and add-on Shadowgraphy package

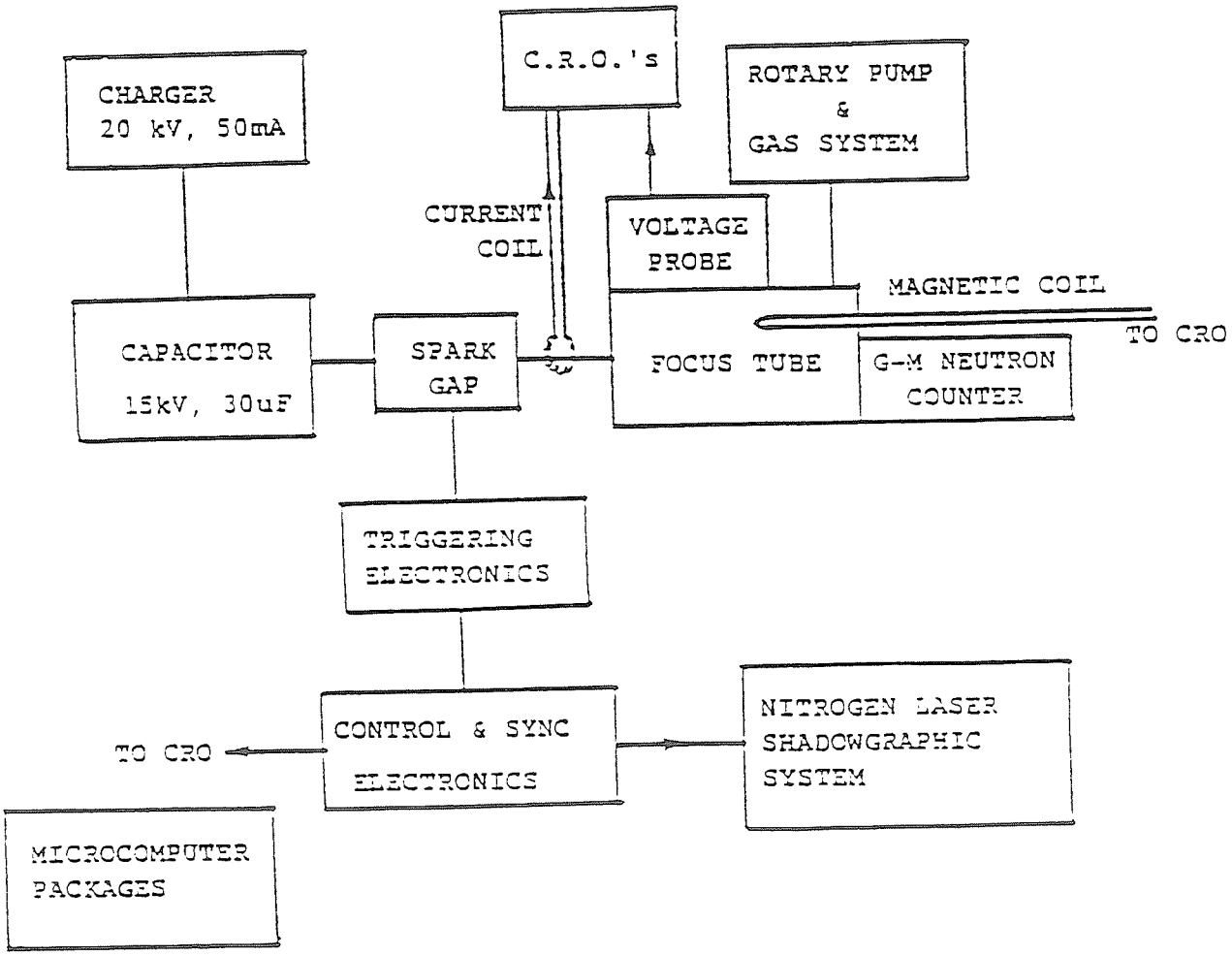

Fig. 16 Sub-systems for the UNU/ICTP PLASMA FUSION FACILITY

Diagnostics of the Plasma Focus

S. Lee
Physics Department
University of Malaya
59100 Kuala Lumpur, Malaysia.

Objectives

We shall describe here some diagnostics suitable for measurements in a plasma focus machine such as the UNU/ICTP PFF (Plasma Fusion Facility). The objectives of such diagnostics may be two-fold:

(a) Diagnostics for device description - to obtain increasingly accurate description of the dynamics and structure of the plasma.

(b) diagnostics for device development - to establish scaling laws and to seek ways to enhance the scaling laws from a better understanding of the focussing mechanisms brought about by better diagnostics. For the plasma focus the most important scaling laws are those for neutron yield. Complementing these there should also be scaling laws for yields of plasma x-ray, ion beams and REB. At the plasma dynamic level there are velocity scaling laws which may be central in the design of plasma focus devices.

The plasma focus device

A typical device is as shown in Fig. 1 which gives some details[1] of the UNU/ICTP PFF, conveniently divided into two sections: the capacitor bank and the plasma focus tube. Several diagnostics are shown in this diagram namely: the rogowsky current coil (no. 22), the movable magnetic probe (no. 33) and the neutron yield counter (no. 39).

The Sub-systems

The UNU/ICTP PFF may be conveniently considered as made up of sub-systems as shown in fig. 2.

The Scaling Laws

In the deuterium plasma focus systematic measurements have shown that the neutron yield scales[2] as stored electrical energy E (in Joules) in the following manner:

$$Y = 10E^2$$

or in terms of electric current flowing through the plasma focus I_f (in Amperes):

$$Y = 5 \times 10^{-13} I^4.$$

It is suggested[3] that these scaling laws are valid for the present generation of plasma focus machines because these machines, large (MJ) and small (kJ) all operate within a small range of densities (1-20 torr) and with almost uniform temperature (1keV).

---

*Paper prepared as invited lecture for the Beijing College on Plasma Physics October-November 1989, Beijing, Peoples Republic Of China.

Procs. Beijing College on Plasma Physics - Diagnostics
Nov 1989, Beijing - Ed. S.T. Tsai & Y.A. Li

The uniform temperature is related to a uniform axial drive speed of 8-10 cm/us resulting in a radial on-axis collapse speed of 20-25 cm/us. The speed (u) scaling law is:

$$u = K_s(I_p/a)/\rho^{\frac{1}{2}}$$

for both axial and radial speeds, where I_p/a is the plasma electrical current per unit anode radius and ρ is the mass density of the ambient gas.

Careful measurements have been used to establish these scaling laws. Similar laws should also be established for x-ray and beam yields. Further major improvement to the plasma focus may require the development of plasma focus devices with enhanced neutron scaling laws, by means of concerted, systematic diagnostic studies.

Control and synchronising electronics

All time-resolved diagnostics such as current, voltage, magnetic field, x-ray diode signals, time-resolved neutron signals, high speed framing or streak photography, pulsed nitrogen laser optical studies need to be synchronised with each other and with the plasma focus so that the time histories of the various quantities are known and related precisely to one another. The timing schematic that needs to be used may be as shown in Fig. 3. It is essential that all electronic pulses have short rise times and low jitters. Ideally the jitter of each chain of events as shown in the schematic should be reduced to the order of ns so that time relationships are known to that order of accuracy.

The CRO's shown in the schematic may be used to display current, voltage, magnetic field,x-ray diode signal, neutron signals as well as to display monitoring signals of the streak camera and nitrogen laser.

Current Measurement

The electric current flowing through the plasma focus is basically a damped sinusoid distorted by the time-varying impedance due to the plasma dynamics.Because of the rapid change in impedance as deduced from optical observation the frequency response should have an upper limit exceeding 10^9 (angular frequency) corresponding to a rise time less than 1 ns and a lower limit of 10^5 for changes in 10μs (a dynamic range in frequency response of 10,000). For the large currents flowing in the plasma focus, current measurements are most conveniently done by means of pick-up coils, or loops responding to the changing magnetic fields. The simplicity of the basic method sometimes gives rise to a wrong conception in the analysis of frequency response. It is worthwhile to stress that the limit of frequency response of a measuring system is imposed by all its components so that the worst component has the biggest effect. In the case of a rogowski coil (see Fig. 4) made self-integrating by means of a small terminating resistance r_t so that it is used in a high-frequency mode very often it is the self-inductance L_t of the terminating resistor that limits the nigh-frequency response of the system; rather than the coil itself. As an example the coil shown in Fig. 4 has the following characteristics :

1. Low frequency limit set by mode condition $\omega > \frac{r_t + r_c}{L_c}$

   (r_c and L_c are the coil resistance and coil self-inductance).

2. high frequency limit set by wire length ℓ $\omega > \frac{\text{speed of light}}{0.5\ell}$

3. high frequency limit set by self inductive effect of terminating resistor $\omega < r_t/L_t$

4. voltage amplitude V for current I threading major cross section of coil with n turns. $V = \frac{I}{n} r_t$

The conflicting requirements of wanting $(r_t + r_c)/L_c$ small enough, r_t/L_t large enough, $(I\ r_t/n)$ small enough and ℓ short enough usually results in a compromised upper limit of frequency response of 10^8 (rise time of 10 ns).

One way to improve the high frequency response is to use a small pick-up coil of a few turns (see below) hence low L_c, and place it in a fixed position shielded from the magnetic field of currents other than the one being measured. This coil in principle is then used in a low-frequency mode i.e. with a high frequency mode-limit. But because of the low value of L_c, the high frequency mode-limit may be extended to 10^9 even if the terminating resistor is limited to 50Ω by the coaxial cable used. Practically the upper frequency limit of such a system may then be set by the integrating system.

As far as the pick-up system is concerned, the best frequency response may be obtained by arranging for an annular channel in one of the conductors (preferably the earth return). Then instead of picking-up the magnetic flux in the channel with a coil, the whole channel is used as the coil i.e. with one single turn and the voltage picked up using a 50-Ω system. This is depicted in Fig. 5. The pick-up loop will have a high-frequency limit above 10^9 (limited only by transit time around the channel) but again the system response will be limited by the integrator circuit.

Calibration of the current monitor may be obtained[4] by using the current monitor to monitor a lightly damped discharge from a capacitance C charge to V_o for which the peak current $\hat{I}$ may be computed rom the measured reversal ratio f and the periodic time T as follows:

$$\hat{I} = \frac{\pi C V_o (1 + f)}{T}$$

Voltage Measurement

A simple voltage shunt such as shown in Fig.6 carefully assembled with short leads and low inductance 1 Watt resistors may be used to measure the voltage appearing across the plasma focus input flange which may spike to >50kV during focussing. This probe attenuates 100 times. The risetime of the probe is however limited to 20ns so that often the sharepest part of the voltage spike is probably not measured. An alternative is to use a capacitative voltage monitor[4] as shown in Fig.7 which has an output voltage V_{out} reduced from the input voltage V_{in} by:

$$V_{out} = \frac{C_1}{C_1 + C_2} \frac{Z}{Z + R} V_{in}$$

where Z is the impedance of the signal cable, usually 50Ω . This equation is valid if the longest time of interest τ_o is

$$\tau_o << \min (C_1 R_1 ; \tau^*)$$

where $\tau^* = C_1 Z \left(1 + 2 \frac{R + Z}{R_1} + \frac{R+Z}{R_2}\right)^{-1}$

Magnetic field measurement

This may be made by a small pick-up coil of a few (n) turns placed in a closed glass tubing for protection against the electric field and electric current (see Fig.1) and orientated so that the axis of the coil is in line with the expected direction of the magnetic field B. The output may be integrated by an integrating circuit of constant RC yielding an output college

$$V_{out} = \frac{n AB}{RC}$$

where A is the cross sectional area of the pick-up coil. The risetime of the coil is

$$t_r = \frac{L_c}{r_t}$$

where L_c is the coil self-inductance and r_t is the terminating resistance of the coil which is usually taken to be equal to 50 Ω which is the matching impedance of the transmission cable. For precision measurement it is also necessary to consider that the presence of the probe gives rise to a bow-shock which causes deflection of the plasma streamline and hence also the magnetic field lines. The magnetic probe may be calibrated using a known current and geometry in situ or separately using a Helmbolz arrangement.

Speed Measurement

A typical set of voltage, current and magnetic probe signals is shown in Fig.8. From the current signal the axial transit time taken by the plasma sheath starting from the backwall at I = 0 to the end of the axial region when focus occurs (at current discontinuity) may be measured. From this may be measured the average speed. This information may also be deduced from the voltage measurement. From the average speed using any simple model, the peak speed may be deduced. The energy input up to any time during the axial, and even radial phase, may be obtained by multiplying the current and voltage curve and measuring the area under the resultant power curve. The detailed trajectory of the plasma sheath may be obtained, in principle, from the voltage and current curve using a simple inductive model.

For a more accurate measurement of peak speed consider the magnetic probe placed at Z = 10.2cm i.e. 5.8 cm from the end of the centre electrode (at Z = 16cm). From this magnetic signal (Fig. 8c) both the arrival time at Z = 10.2cm (sharp rise of magnetic signal) and at Z = 16 cm (sharp dip of signal) are obtained from which the transit speed between Z = 10.2 cm and Z = 16 cm is obtained as 9.7 cm/μs.

From the speed measurement u_s) an estimate of temperature[2] may be obtained from shock theory.

For fully ionised shocks in hydrogen: $T = 1.13 \times 10^{-5} u_s^2$

For deuterium: $T = 2.26 \times 10^{-5} u_s^2$

For a gas in general: $T = 2.4 \times 10^{-4} M \frac{\gamma - 1}{(\gamma + 1)^2 D} u_s^2$

where M is the molecular weight, γ the specific heat ratio, D the departure coefficient. Both D and γ are thermodynamic functions of the temperature T and for any gas may be computed as functions of temperature[2].

For the example just given, the deuterium plasma sheath at the end of the axial transit region has a temperature of 2.1×10^5 K. Scaling law considerations give for a typical plasma focus a peak radial speed factor of 2.5 so that from the peak axial speed of 9.7 cm/μs we may deduce a peak radial speed of 24 cm/μs with an on-axis shock temperature of 1.33×10^6K and an on-axis reflected shock temperature of 3.3×10^6K. The final compression may be expected to raise the temperature further.

The magnetic probe may be used to obtain much more information. For example by positioning the probe at various Z positions and various radial positions between the inner and outer electrodes, the magnetic field structure[6] in the focus tube may be obtained at any given time. This is a very powerful method to obtain further information (besides speed) of sheath inclination, sheath thickness, multiple sheaths, sheath magnetic energy, current shedding, current loops plus magnetic instabilities.

Such information may be compared with streak photographs using either conventional streak photography or a multi-slit streak techniques[7] which gives a corresponding luminosity structure picture with one single streak photograph.

Neutron Yield Measurement

Neutron yield measurements may be made using a foil activation method[8] as shown in Fig.9. Typically, the counter is started a few ms after the focus discharge and the count of the β -radiation of the neutron-activated Indium foil is continued for 30 seconds with a sensitivity of 3×10^5 neutrons per count with the foil at 13 cm from neutron source, assumed isotropic. The photomultiplier may be replaced by a geiger-muller tube with reduced, but still adequate sensitivity.

The structure of the plasma focus neutron source may be investigated[9] with the above activation counter and with deuterided and non-deuterided control targets, placed at different distances from the plasma focus.

Neutron Time-of-Flight Measurement and Spectroscopy

Time-resolved neutron pulses may be observed using the arrangement[10] shown in Fig. 10. Two such detectors one placed near the focus and the other 10 - 100m away may be used to obtain the flight time and also the energy spread of the neutron pulse.

Soft x-ray pin-hole photography

A pinhole camera may be adapted for imaging soft x-ray by covering the pinhole with thin foil such as beryllium. Fig. 11 shows a 4-exposure pinhole camera[11].

Time-resolved soft x-ray measurements and temperature measurements

Silicon p-i-n diodes (QUANTRAD 100PIN250) may be used to provide time-resolved x-ray signals from the plasma focus. The arrangement may be as shown in Fig. 12. This arrangement may be used to measure electron temperature by the filter ratio method.

Refractive methods using a Nitrogen Laser light source

Recent development of the nitrogen laser[12] enables a very simple ns light source to be built for time-resolved imaging of fast plasma events. Such techniques combined with the plasma focus provide a really advanced research facility which may be most cost-effectively acquired by a developing country. At the nitrogen laser wavelength of λ = 337.1 nm the plasma refractivity, predominantly electron controlled, may be written as

$$\mu = 1 - 5.1 \times 10^{-23} n_e$$

with n_e written in cm^{-3}. This equation governs the refractive methods using the nitrogen laser in the shadowgraphic, Schlieren or interferometric mode. This laser offers such a powerful repertoire of diagnostic methods that it is worthwhile to describe it here in detail.

The laser is excited by the conventional voltage swinging circuit schematically described in Fig. 13. The circuit theory of the parallel plate transmission line type of laser has been discussed in previous papers[13]. The two energy storage capacitors C_1 and C_2 of the circuit consist[12] or a common earth plate, which is a 22 cm x 60 cm strip of aluminium kitchen foil laid on top of a flat aluminium plate (for electronic contact and mechanical support). Figure 14 shows the constructional details of the laser. On top of the foil are laid 3 sheets of 2 mil Mylar which extends at least 10 cm beyond the edges of the conductors all round. The high voltage plates of C_1 and C_2 are 22 cm x 40 cm and 22 cm x 17 cm strips of aluminium foil laid on top of the mylar sheets. The measured values of C_1 and C_2 are 15 and 6 nF, respectively. On top of the foils are placed glass plates (6 mm thick) of approximate dimensions to prevent mechanical flexing of the foils during charging and discharging of the capacitors. The capacitor C_2 is mounted to a swinging cascade triggered spark gap. These high voltage capacitor plates are separated by a gap over which the laser channel is placed so that each side of the channel makes pressure contact with one of the capacitors. The electrodes of the laser channel are made of 20 cm long brass strips with cross-sectional dimensions of 0.5 in x 1 in and shaped as shown in Fig. 14b. The perspex plate is screwed onto the laser electrodes on the upper side over the top. Admission and evacuation of the nitrogen gas at atmospheric pressure is made through the middle and the ends of the channel, respectively.

In the arrangement shown, the edges of the high voltage capacitor plates (aluminium foils) are allowed to protrude beyond the edges of the laser electrodes into the laser cavity to act as corona blades for preionization. These form the set of blades on the lower side of the laser channel. A similar set of corona blades is placed on the upper side of the lase channel. The laser channel gap is set to 3 mm

while the blades separation is typically set to about 40 percent greater than that of the main gap. The edges of the foils function as auxiliary corona electrodes which provide an initital distributed corona discharge to photoionize and prepare the laser channel for glow formation. The low-energy surface discharges acting as preionizing UV radiation sources are formed early during the rise of the voltage pulse across the laser gap and are distributed by corona charging of the Mylar surfaces that extend beyond the edges of the foils.

Optimum energy is obtained at a gap separation of 3 mm with a value of 300 μJ at 15 kV. The laser pulse duration is 1 ns with good beam quality.

The 1 ns pulse width of the nitrogen laser is sufficiently short to provide a freezing of motion of the order of 0.2mm at a speed of 20cm/μs.

The laser shadowgraphic, Schlieren & interferometric set-ups are as shown in Fig. 15. The laser pulse is correctly timed to catch the plasma focus at any time during the axial or radial phase by using variable delay units linking the plasma focus triggering pulse to the laser triggering pulse.

Results

A sequence of 1 ns exposure Schlieren photographs[11,12] for a 6 kJ plasma focus (in neutron optimised operation) is shown in Fig. 16. This sequence shows the collapse structure of the plasma focus including the symmetrical collapse on axis from t = 50 ns to t = 5 ns and the explosive plasma expansion from t = + 10 ns to t = + 50 ns. These photographs have been synchronised to neutron, x-ray and plasma focus voltage[11] as shown in Fig. 17. Two interferograms are shown in Fig.18 and the corresponding electron density distributions are shown in Fig. 19.

Diagnostics for focus development

What would we like to develop the focus for?

Some possibilities are listed below.

a) for studying a plasma under nuclear fusion conditions.

b) for developing diagnostics for fast pulsed plasmas.

c) as a neutron source for blanket studies for fusion reactors, pulsed neutron radiography, pulsed activation analysis, nuclear weapons simulation.

d) as an intense source for UV light, soft x-ray and electromagnetic radiation for spectroscopic applications, pump source for UV and soft x-ray laser, x-ray diagnostics and Electromagnetic Pulse (EMP) studies.

e) for production of extreme magnetic fields and associated possibility of solid state compressions.

f) as a thermonuclear reactor; potential exists because of the observed $Y \sim E^2$ relationship for neutron scaling.

The question of neutron scaling is by no means closed. Lee[3] has shown that the observed neutron scaling of $Y \sim E^2$ and $Y \sim I^4$ is due to the speed limitation (10cm/μs axial speed) and density limitation (about 20 torr) which has been observed for all

plasma focus, small or large. If the focus could be operated with increased axial speed, say to 20 cm/μs, there are reasons to believe that the neutron yield would increase dramatically. Recent laser Schlieren photographs (Fig. 20) have given some clues that the speed limitation may be due to current sheet - shock front decoupling at higher speeds associated with sheath inclination with consequent radial mass flow and γ-effect. Further detailed studies should be made to see if conditions may adjusted to remove the speed limitation and hence improve the neutron scaling law.

Multi-framing system:

In order to obtain comprehensive sequence of the plasma focus axial or radial transit, a multi-frame imaging system is essential. This may use a sequenced nitrogen laser technique[14] such as shown in Fig. 21a. Such a system in wich the laser discharge capacitor C_2 of the first laser acts as the voltage swinging capacitor of the second laser, and so on may be used to produce 3 closely spaced pulses, each full power, to give a 3-frame sequences, Fig. 21b.

An alternative method, with more flexible delays may be arranged using individual nirogen lasers whose spark gaps are triggered by a split ruby laser beam, each split beam triggering a nitrogen laser spark-gap by means of suitable optical fibres of variable length, such as shown schematically in Fig. 22, with each m of optical fibre giving a delay of 4ns.

Such multi-framing techniques used for Schlieren or shadowgraphy or interferometry or with Faraday rotation techniques for non-invasive magnetic field structure[15] determination will enable data to be collected in sufficient quantity comprehensively for development studies to be made.

REFERENCES

1. S.Lee, T.Y.Tou, S.P. Moo, M.A. Eissa, A.V. Gholap, K.H.Kwek, S. Mulydrono, A.J. Smith, Suryadi, American J. Phys., 56, 62 (1988).
2. Laser and Plasma Technology Ed. S.Lee, B.C.Tan, C.S.Wong and A.C.Chew (World Scientific Singapore 1985).
3. S.Lee " The sharing of fusion-related technology among developing countries" - invited paper read at the Energy Independence Conference, Rio de Janeiro, August 1987; Procs. "Fusion Energy and Plasma Physics" World Scientific, edited by P.H. Sakanaka, pg. 754 (1988).
4. M. Favre, "Pulse Technology2 - lecture delivered at Spring College on Plasma Physics ICTP Trieste June 1989 - to appear in Procs.
5. S.P. THong and S.Lee, Mal. J. Science, 2(B), 157 (1973).
6. S.Lee et al, Singapore J. Physics 3, 75 (1986).
7. T.Y. Tou, & S.Lee Rev. Sci. Instru. 59, 2370 (1988).
8. S.P. Moo and S.Lee, Singapore J. Phys.,4, 131 (1987).
9. C.K. Chakrabarty "Plasma focus Neutrons" M.Sc Thesis (U.M)(1988).
10. S.Lee and Y.H.Chen, Malaysian J. Science, 3B , 159 (1975).
11. K.H. Kwek "Pinch Structure of a Plasma focus", Ph.D Thesis, University of Malaya (1989)
12. K.H. Kwek, T.Y.Tou and S.Lee, J.Fiz.Mal., 9, 36 (1988);IEEE Trans.on Instrumentation and Measurement, IM-38, 103 (1989).
13. S.Lee, A.V. Gholap, A.J. Smith,K.H.Kwek,A.C.Chew, T.Y.Tou and S.Sapru, J.Fiz.Mal.,6 165 (1985).
14. S.Lee, K.H.Kwek et al J. App. Phys. 65, 4133 (1989).
15. A. Kasperczuk, R. Miklaszewski, M.Paduch, K. Tomaszewski, Z. Wereszczynski to appear in J. Fiz.Mal. (1989); R. Miklaszewski, Lecture at Spring College Plasma Physics Trieste (1989) - to appear in Procs.

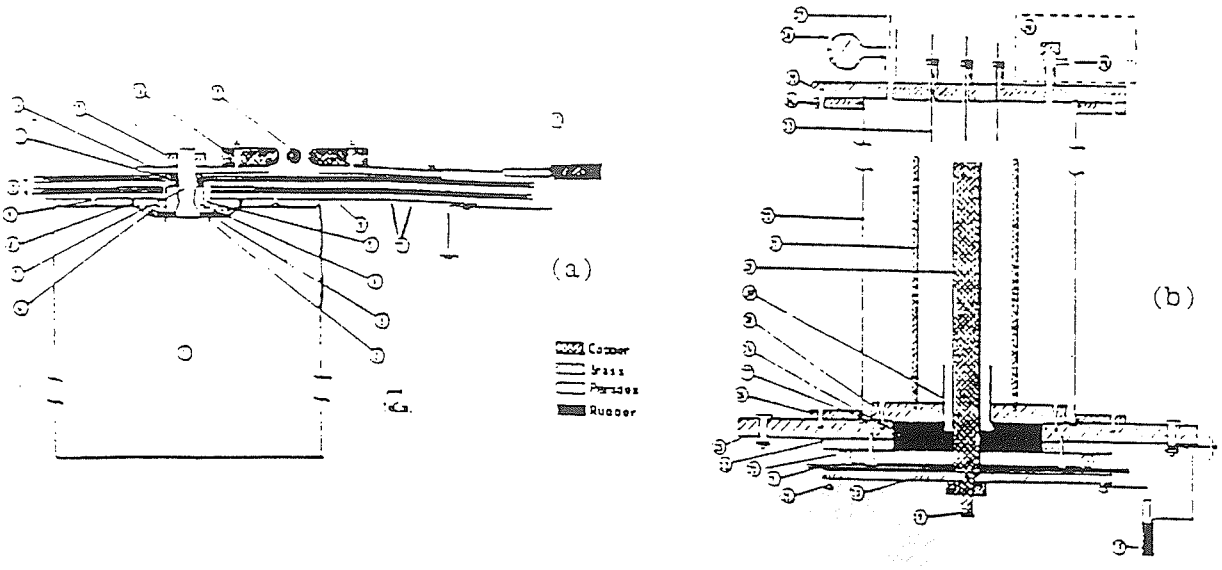

Fig. 1 (a) The capacitor connecting plates, the spark gap, and output coaxial cables. 1 = 15-kV, 30-uF capacitor; 2 = capacitor O-ring seal; 3 = washer; 4 = oil; 5 = nylon cap; 6 = steel nut; 7 = capacitor output seal; 8 = O-ring seal; 9 = Earth stud; 10 = Earth plate; 11 = 5-mil Mylar film; 12 = polyethylene film; 13 = copper ring HV connector; 14 = capacitor high-voltage (HV) output plate; 15 = lock nut for HV plate; 16 = HV electrode for swinging cascade spark gap; 17 = trigger electrode; and 18 = output coaxial cables (16 in parallel). (b) The plasma focus tube. 18 = input coaxial cables (16 in parallel); 19 = stud of anode; 20 = anode collector plate; 21 = connecting points for coaxial cable HV lead; 22 = Rogowski coil; 23 = perspex spacer; 24 = rubber holder; 25 = cathode collector plate; 26 = mild steel flange; 27 = O-ring seal; 28 = focus cathode support plate; 29 = focus anode; 30 = glass insulator; 31 = focus cathode (6 rods); 32 = mild steel focus enamoer; 33 = movable magnetic probe in glass jacket; 34 = flange; 35 = back flange; 36 = diaphragm gauge; ϕ7 = outlet to vacuum pump; 38 = inlet for test gas; 39 = wax container with indium foil and PM-scintillator activation counter.

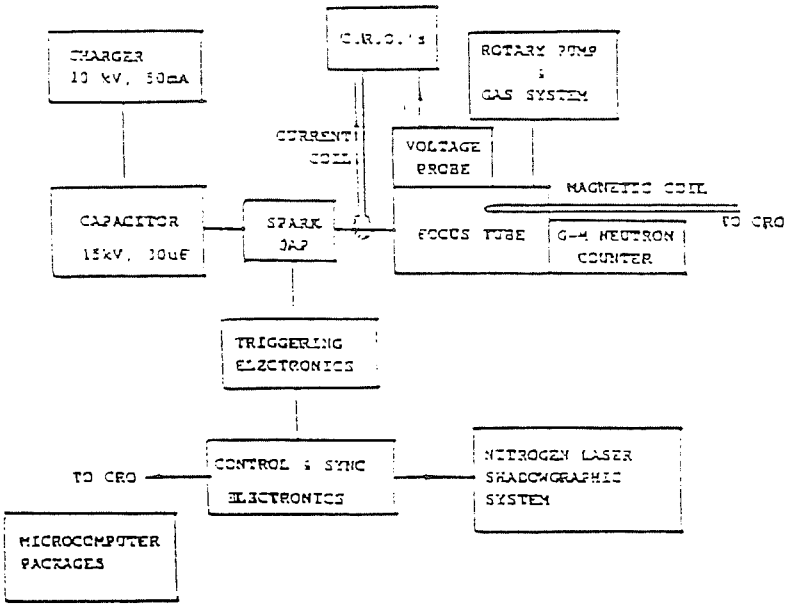

Fig. 2 Sub-systems for the UNU/ICTP PLASMA FUSION FACILITY

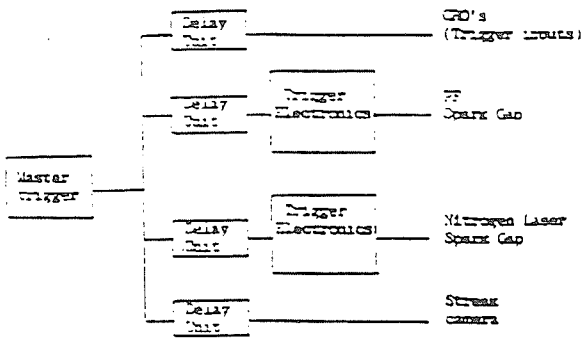

Fig. 3 Schematic of electronic control and synchronisation

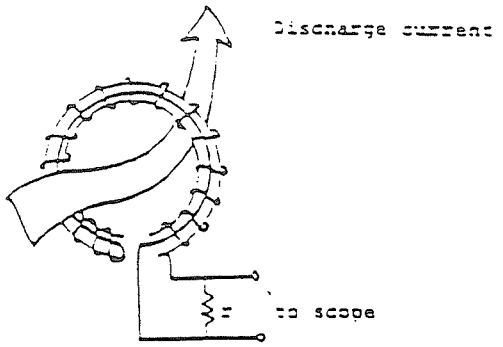

Fig. 4. Rogowski coil as a current transformer.

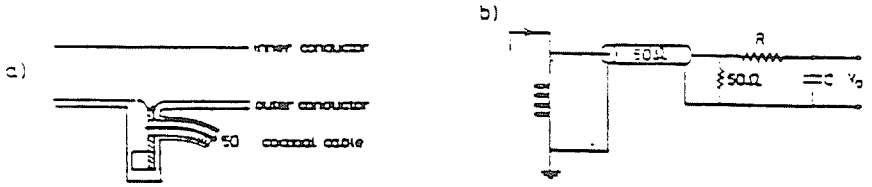

Figure 5 a) Cross section of a transmission line current monitor. The variation in magnetic flux inside an annular channel is picked-up and integrated to provide a current signal. b) Electric circuit for the current monitor shown in a).

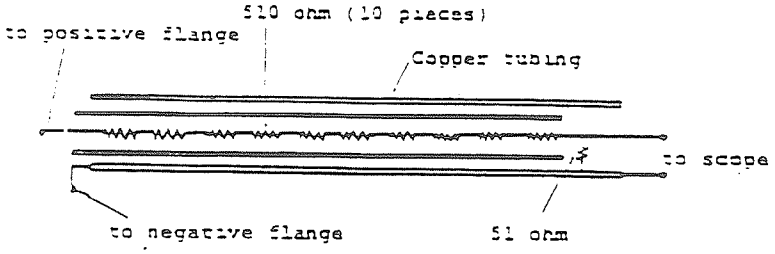

Fig. 6 High-voltage probe (100X attenuation)

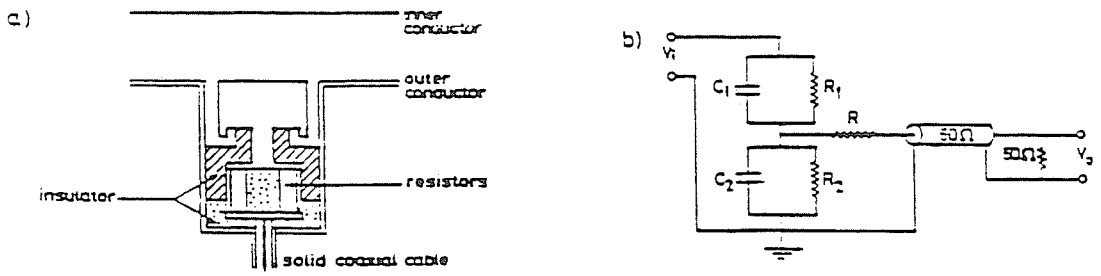

Figure 7 a) Cross section of a capacitive voltage monitor. The monitor acts as a capacitive divider between the inner and outer conductor of the line. A series resistance is added to increase the dividing ratio. b) Equivalent electric circuit of capacitive monitor shown in a).

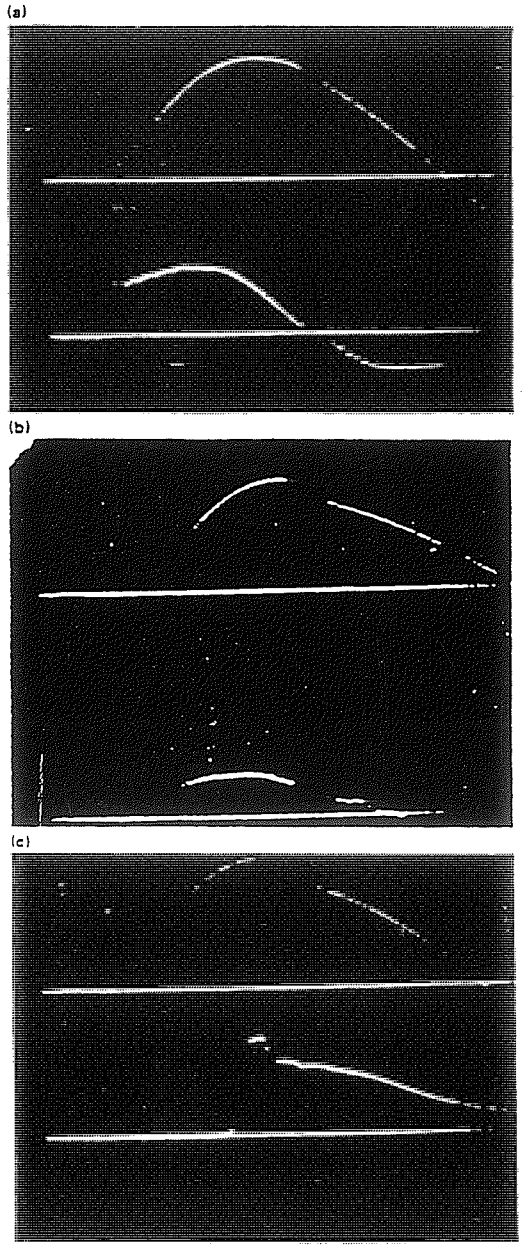

Fig. 8 (a) Current (upper trace) and voltage (lower trace) of plasma focus in air: 13 kV, 0.5 Torr: Top trace: 73 kA/cm: Bottom trace: 2 kV/cm: Time scale (horizontal): 1 μs/cm. (b) Current and voltage trace of plasma focus in deuterium: 13 kV, 2.5 Torr: Top trace: 75 kA/cm: Bottom trace: 4 kV/cm: Time scale (horizontal): 1 μs/cm. (c) Current and magnetic trace of plasma focus in deuterium: 15 kV, 3.5 Torr: Magnetic probe placed at z = 10.2 cm: Top trace: 73 kA/cm: Bottom trace: 0.6 T/cm.

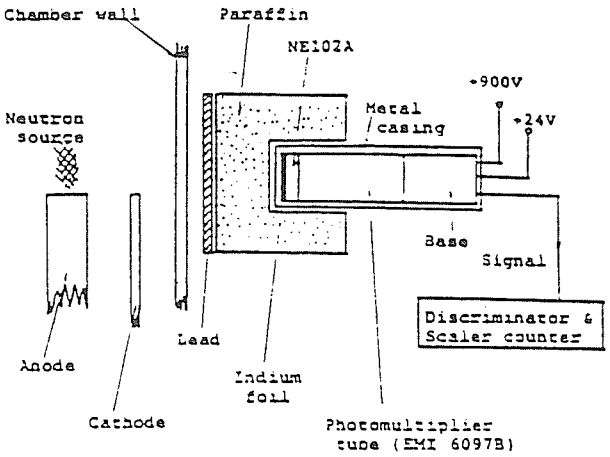

Fig. 9 Set-up for neutron flux measurement using foil activation counter.

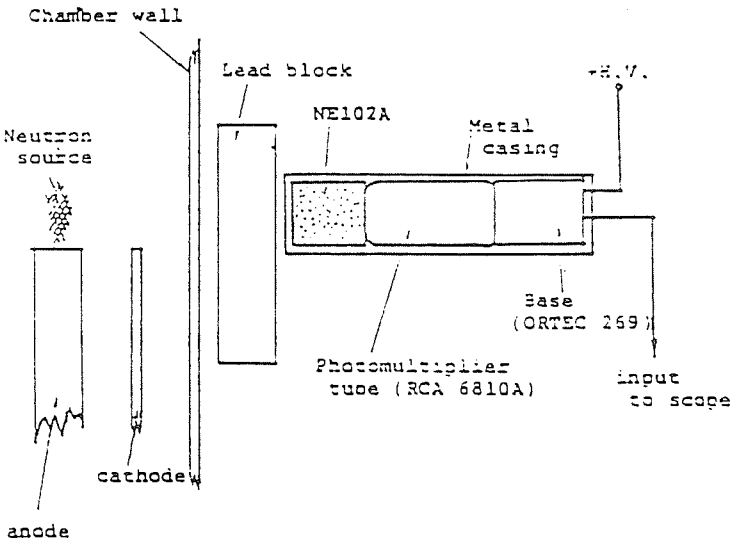

Fig. 10 Schematic of the scintillator-photomultiplier arrangement for time-resolved neutron observations.

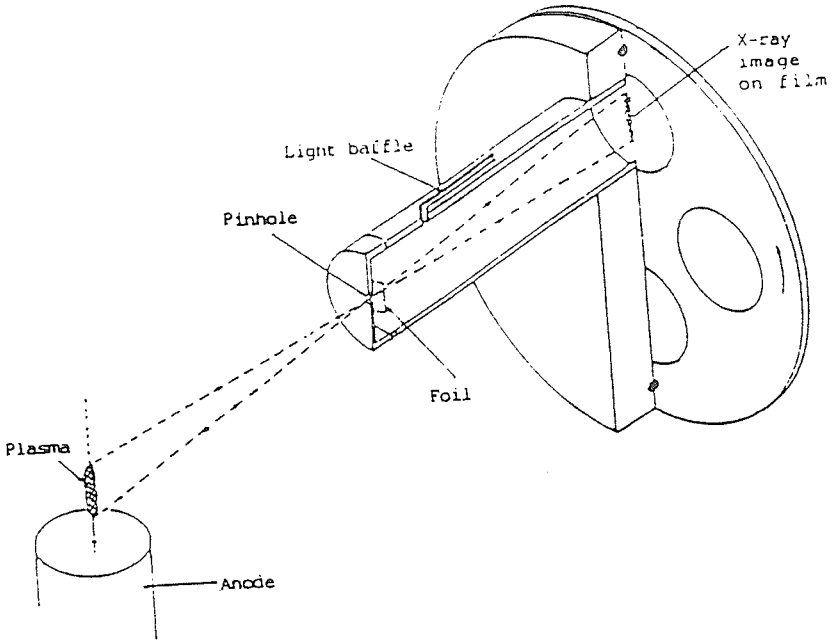

Fig. 11 X-ray pinhole camera.

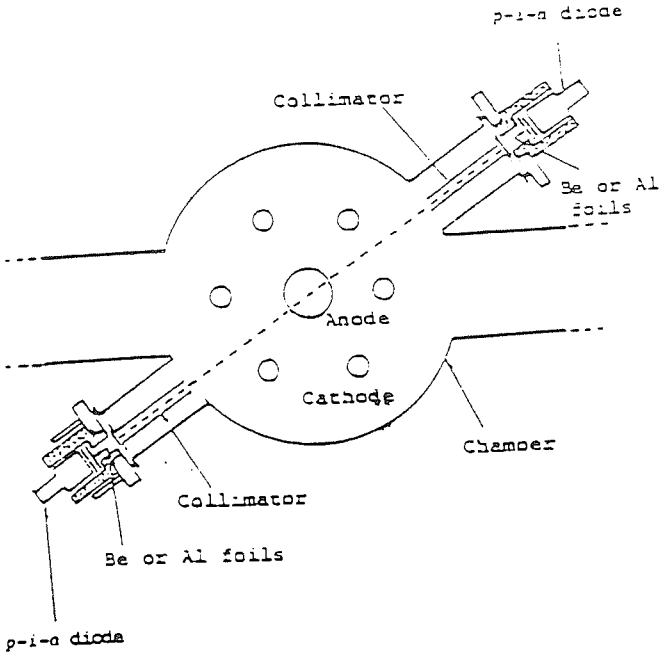

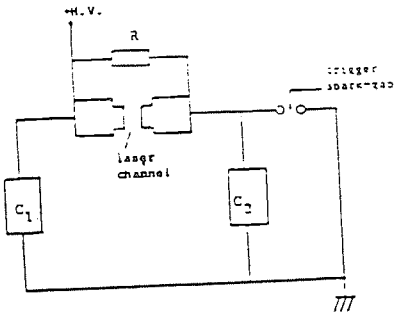

Fig. 13 Equivalent circuit of the nitrogen laser.

Fig. 12 Schematic of the experimental set-up for time-resolved X-ray observations and temperature measurement using X-ray *p-i-n* diode.

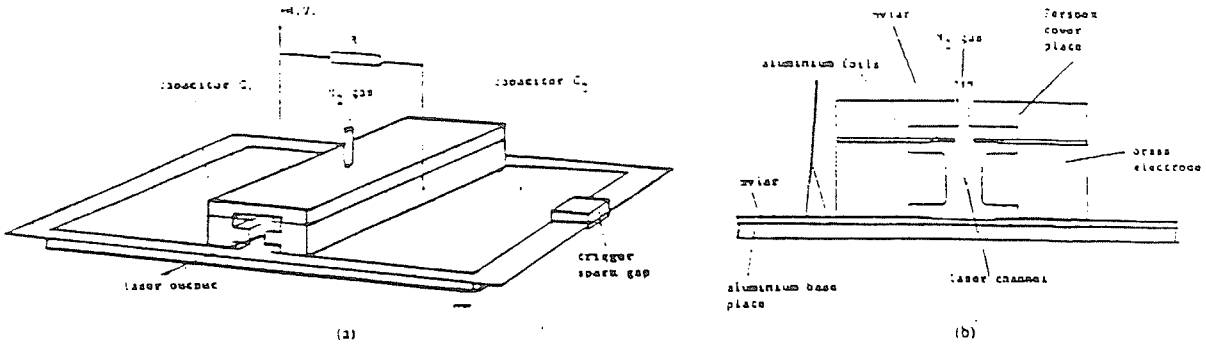

Fig. 14 (a) Sketch of a basic TEA nitrogen laser with Blumlein circuit. (b) Cross-sectional view of the laser channel showing the inclusion of the preionizer system using aluminium foil-Mylar combination. The mylar strips improve the preionization effect.

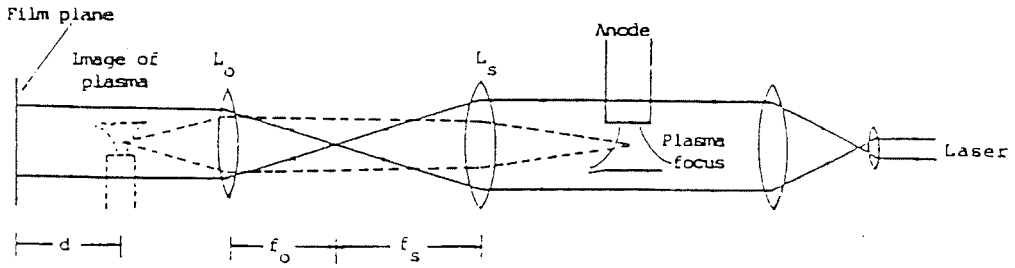

Fig. 15(a) Optical layout of the shadowgraph system. The plasma focus chamber, window and interference filter are not shown.

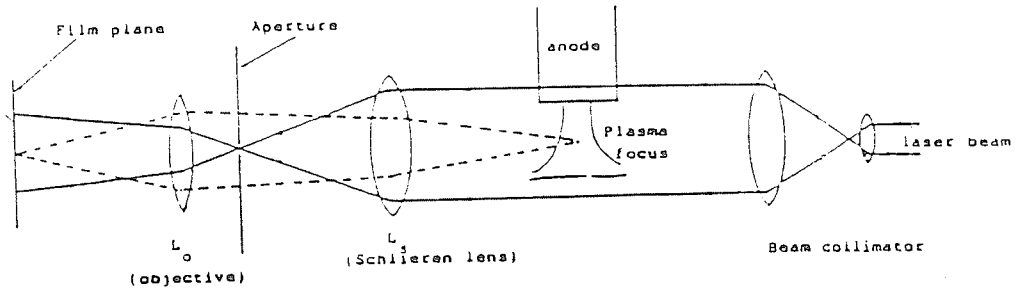

Fig. 15(b) Optical arrangement of the Schlieren system. The plasma focus chamber windows and interference filter are not shown.

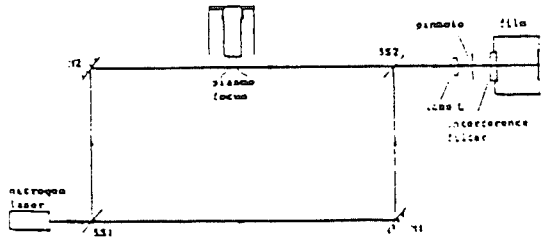

Fig. 15(c) Schematic set up of the Mach-Zehnder interferometry. Schlieren and shadowgraphic setup can be obtained by covering the reference beam and setting up the appropriate focusing optics.

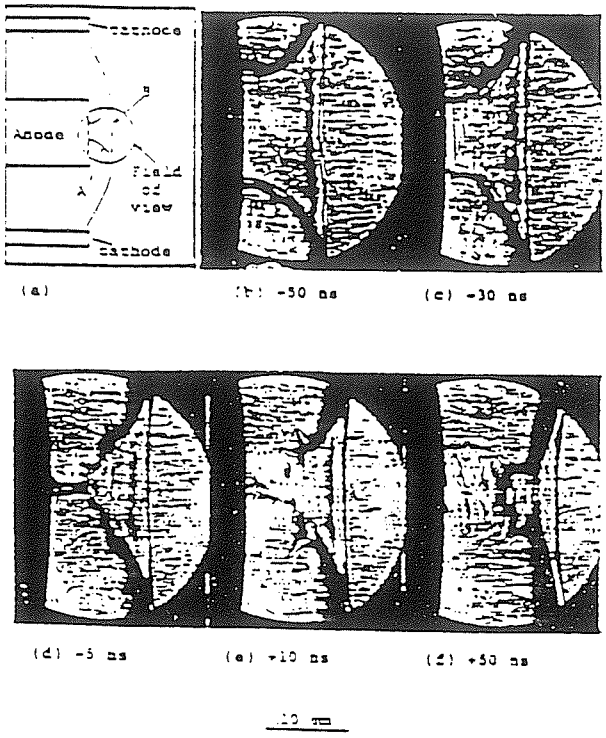

Fig. 16 A sequence of Schlieren images showing the plasma structures and dynamics. Experimental conditions: 9 mbar deuterium at 14 kV.

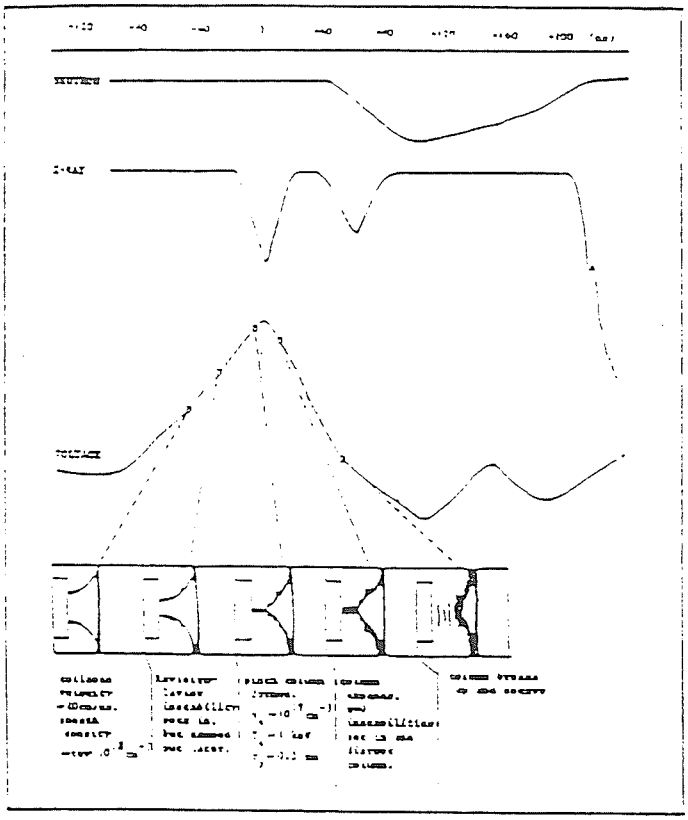

Fig. 17 Summary of the temporal development of the radial implosion process

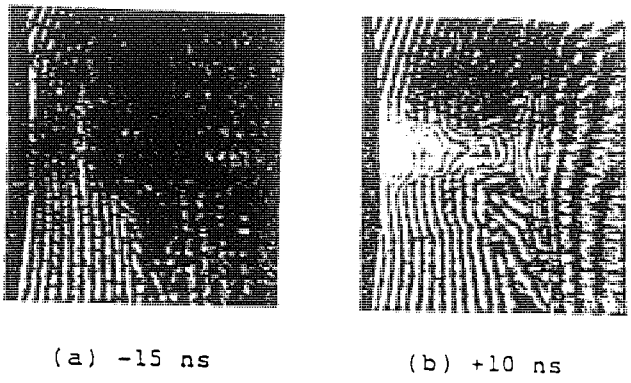

Fig 18 Interferograms corresponding to the formation and expansion of the pinch column.

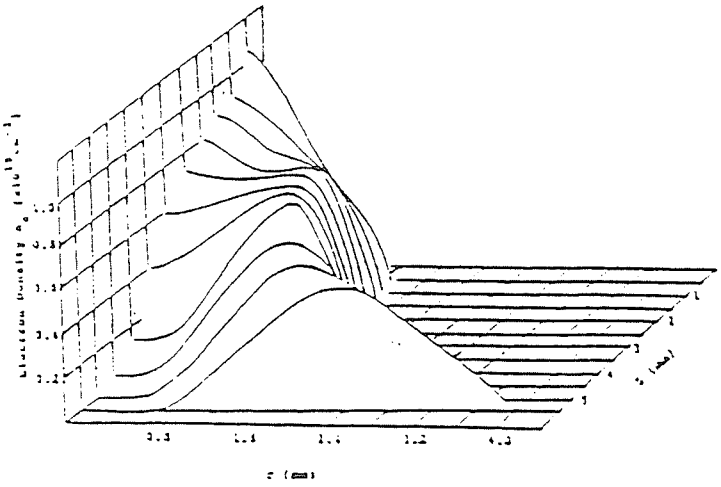

Fig. 19 (a) Electron density distribution during the formation of the pinch column at time t=-15ns.

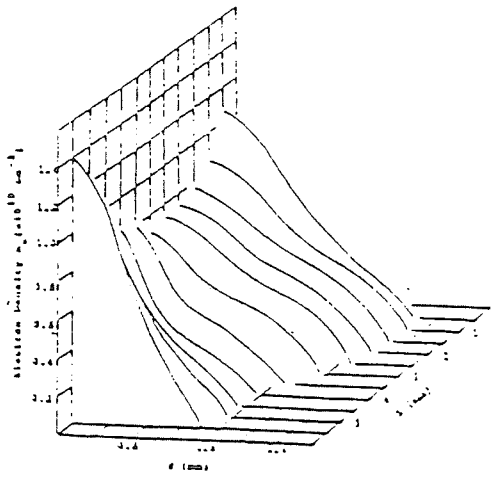

Fig. 19 (b) Electron density distribution during the expansion of the pinch column at time t=+10ns.

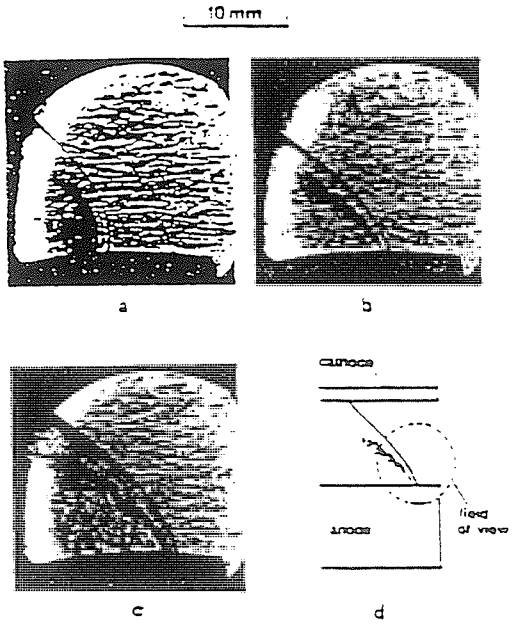

Fig. 20 Schlieren images of the plasma focus discharge in the axial rundown phase. The plasma focus device was operated at 14 kV and with deuterium gas at (a) 1 mbar, (b) 9 mbar, and (c) 14 mbar

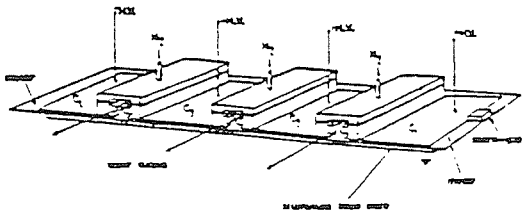

Fig. 21 (a) Schematic of a three-channel sequenced nitrogen laser. The high-voltage plates of the capacitors C_1, C_2, C_3, and C_4 are made of aluminimum foils.

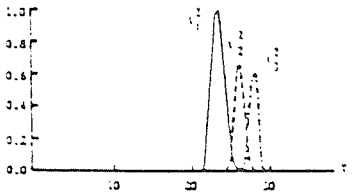

Fig. 21 (b) Computed voltages across the laser channel, laser currents and laser currents squared as function of time; all variables are normalized Parameters used are those for a "prompt sequencing" mode.

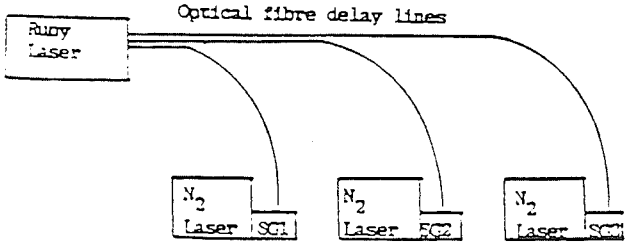

Fig. 22 Ruby Laser triggered multiframe nitrogen laser system. The fibre optical cables may be varied in length to provide suitable delays between frames.

JAPANESE JOURNAL OF APPLIED PHYSICS
VOL. 28, NO. 7, JULY, 1989, pp. 1264-1267

A Compact Low Voltage Flash X-Ray Tube

C. S. WONG, S. LEE, C. X. ONG† and O. H. CHIN†

Pulse Technology and Instrumentation Laboratory
Institute for Advanced Studies, University of Malaya, 59100 Kuala Lumpur, Malaysia
†Plasma Research Laboratory, Physics Department, University of Malaya, 59100 Kuala Lumpur, Malaysia

(Received February 13, 1989; accepted for publication March 25, 1989)

In this paper we describe the construction of a compact, low voltage flash X-ray tube. The device is powered by a small 25 kV, 3300 pF capacitor. Its design is of the vacuum spark configuration with a hollow cathode. The discharge is triggered by a low energy spark behind the hollow cathode; and the triggering spark is also powered by the main capacitor discharge. A 12 kΩ ballast resistor is connected to this auxiliary spark circuit to limit its current. The flash X-ray tube has been operated in air at pressures ranging from 10^{-1} to 10^{-4} mbar. At a charging voltage of 25 kV, the flash X-ray tube is able to produce X-ray pulses of several kilowatts in power.

KEYWORDS: pulsed X-ray source, vacuum spark configuration, hollow cathode, X-ray emission energy; electron beam

§1. Introduction

In recent years there has been much interest in the development of pulsed X-ray sources for various applications. Some of the high-power devices being considered include the plasma focus,[1] the gas-puff Z-pinch[2] and the laser produced plasma.[3] These devices are being developed as suitable soft X-ray sources for large-scale microlithography.

Besides the high-power devices mentioned above, several types of table-top miniature flash X-ray tubes with input energy in the range of several hundreds of millijoules to several joules have also been developed.[4-6] These devices may find applications in non-destructive testing of materials by the flash X-ray radiography technique; in X-ray induced nuclear fluorescence;[6] in flash X-ray diffraction studies,[7] and in flash radiography of biological substances.

Basically, a flash X-ray tube is operated by pulsing a pair of closely spaced electrodes with a high voltage pulse discharge. The main mechanism of X-ray emission is that of electron-target and electron-plasma interaction. Several methods of initiating the necessary electron beam production have been employed. One of the most common methods is by field emission at the cathode surface, which requires a high voltage pulse of several hundreds of kilovolts to be applied across the electrodes. Alternatively, a moderate power pulsed Nd-YAG laser may also be used to initiate the flash X-ray operation[4] by focussing the laser beam onto the cathode surface to release electrons from it. A third method makes use of an auxiliary electrode to produce a sliding spark with the cathode to initiate the discharge. The last method is the case of a vacuum spark discharge.[8]

In this paper we describe a compact flash X-ray tube of novel design based on the vacuum spark configuration. The device is triggered by a spark behind the cathode. The cathode is of the hollow cathode configuration whose electric field line pattern acts as an electrostatic lens to accelerate and focus the electrons produced by the triggering spark onto the tip of the anode. With the use of a self-firing air spark gap for switching and the simultaneously fired triggering spark arrangement, the operation of the flash X-ray tube has been greatly simplified.

§2. Design and Construction of the Flash X-Ray Tube

The design and construction of the flash X-ray tube is shown in Fig. 1. The flat-tip anode is made of stainless steel which is screwed onto a brass rod connected directly to the spark gap. The cathode is a brass plate which also

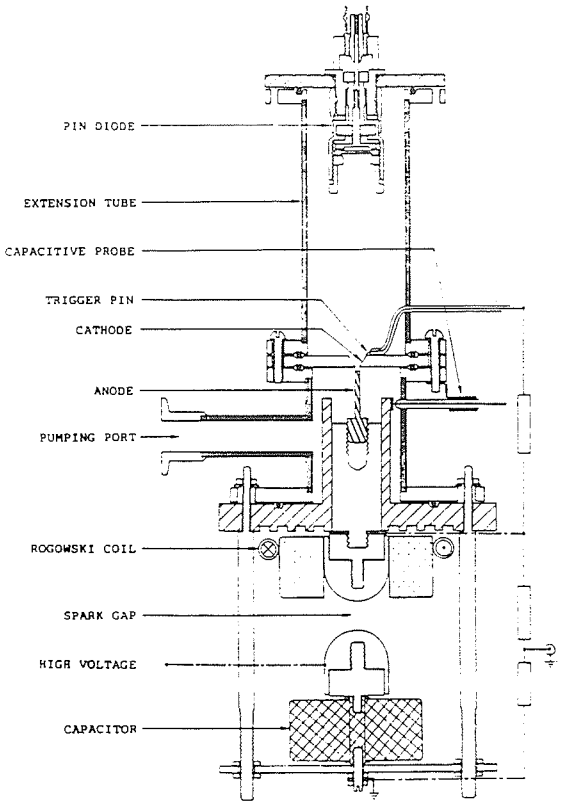

Fig. 1. The construction of the flash X-ray tube.

forms the top cover of the cylindrical chamber. It has a tapered hole at its centre facing the anode. Both the anode tip and the cathode hole are 2 mm in diameter. The inter-electrode spacing can be adjusted. The cylindrical perspex sleeving surrounding the anode holder prevents arcing between the anode holder and the wall of the chamber. The return path from the cathode plate to the capacitor earth is via the chamber wall and six brass rods. A 10 cm long copper extension tube is connected onto the cathode plate to act as diagnostic as well as application port. The chamber and the copper extension tube is evacuated together by a small rotary-diffusion pump system to a pressure of $<10^{-4}$ mbar.

The flash X-ray tube is powered by a single disc capacitor rated at 20 kV, 3300 pF. Despite its 20 kV rating by the manufacturer, the capacitor has been operated at 25 kV with no apparent problem. It is connected to the flash tube via a self-firing atmospheric air spark gap. A 1 MΩ resistor in series with a 50 Ω resistor is used as ballast resistor across the electrodes. A voltage pulse of about 1 V amplitude and 20 ns risetime can be tapped across the 50 Ω resistor during the spark gap firing. The rising edge of this voltage pulse is used for the purpose of scope triggering. A trigger pin is introduced behind the cathode plate beside the rim of the hole inside the copper extension tube, and it is connected to the anode side of the spark gap via a limiting resistor of $R_L=12$ kΩ. (Fig. 1) This novel arrangement allows a low energy spark between the trigger pin and the cathode to occur when the spark gap fires, thus initiating the breakdown of the inter-electrode gap. It was found that breakdown of the gap cannot occur at pressure $<10^{-1}$ mbar without the trigger spark. The schematic circuitry of the flash X-ray tube discharge system is shown in Fig. 2.

The performance of the flash X-ray tube is monitored by using various diagnostic techniques including the Rogowski coil for measuring the discharge current; capacitive voltage divider for measuring the transient voltage across the electrodes; Si PIN diode (Quantrad 100-PIN-250) for time-resolved X-ray measurements; and pinhole camera for time-integrated X-ray imaging. The capacitive voltage probe design is similar to that described elsewhere.[9] The PIN diode is mounted at the end of the diagnostic/application port indicated in Fig. 1. For X-ray detection, the diode is covered by aluminized mylar of 24 μm thickness and iron foil of 8 μm to give a pass band around the Fe-Kα line of 1.9 Å. This combination of absorption foil is used since it is expected that the X-ray emission in this case is predominantly due to electron beam bombardment of the stainless steel anode and a plasma formed by the vaporisation and heating of the anode material.

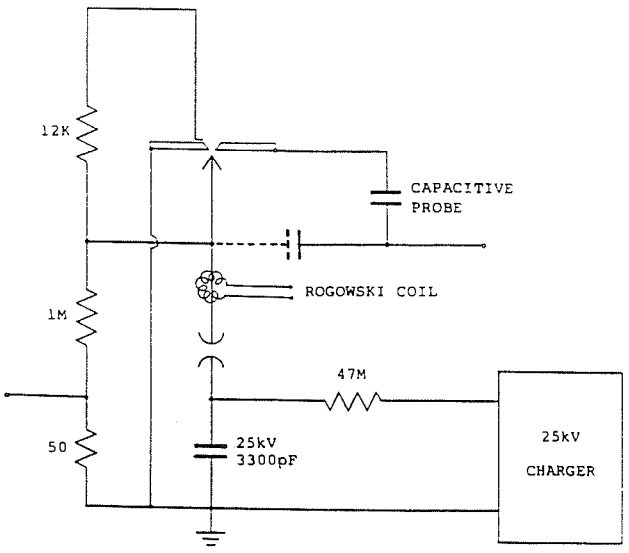

Fig. 2. Schematics of the flash X-ray tube discharge circuitry.

§3. Characteristics of the Flash X-ray Tube

The flash X-ray tube has been operated at an anode-cathode separation of 2 mm, a discharge voltage of 25 kV and over a pressure range of 10^{-1} to 10^{-4} mbar. Consistent X-ray output has been observed from a series of discharges. Three typical X-ray output waveforms ob-

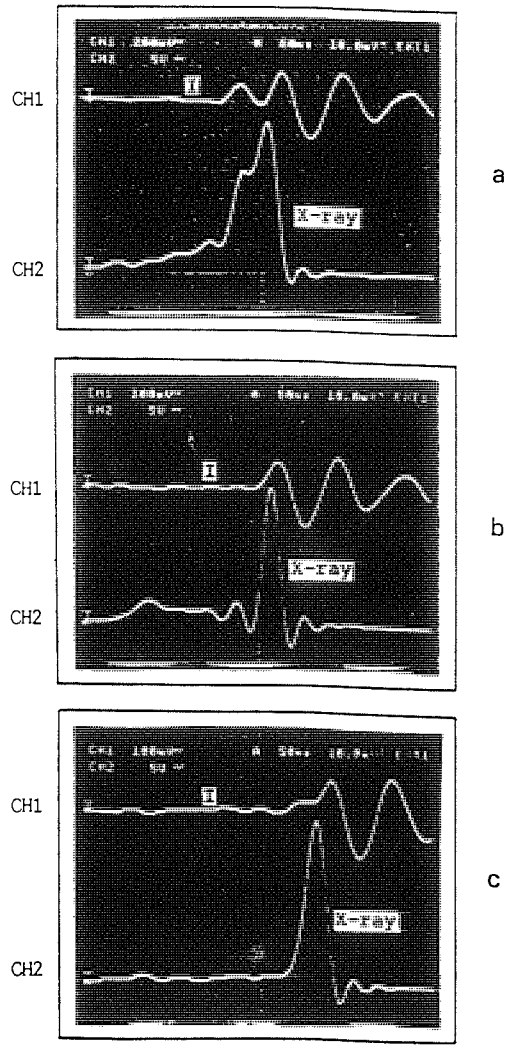

Fig. 3. X-ray and current waveforms of flash X-ray discharges at three pressures: (a) 9×10^{-3} mbar, (b) 1×10^{-3} mbar and (c) $<10^{-4}$ mbar.

tained at operating pressures of 9×10^{-3} mbar, 1×10^{-3} mbar and $< 10^{-4}$ mbar are displayed in Fig. 3 together with their corresponding discharge current waveforms. Generally, the X-ray waveform consists of 2 distinct phases. The first phase of X-ray emission starts well before the breakdown of the inter-electrode gap occurs. It lasts for some 150 ns at higher pressures to 250 ns at lower pressures of $< 10^{-4}$ mbar. At the instant of breakdown, as indicated by the start of the discharge current, the X-ray emission intensity rises sharply, marking the start of the second phase. This phase of X-ray emission is observed to extend into the first half cycle of the capacitor discharge. The obvious distortion of the discharge current waveform indicates the presence of severe electromechanical processes during this phase. A possible mechanism that may lead to such a strong interaction is the joule heating of the vaporised anode materials between the electrodes. The second phase of X-ray emission gives rise to a pulse of about 30 to 40 ns FWHM (typical). Comparison of the PIN diode signals using 2 sets of filters, one with 24 μm aluminized mylar only and the other with an additional layer of 8 μm Fe foil, indicates that the X-ray emitted consists of predominantly the Fe-Kα line radiation. Multiple X-ray pulses may be observed, mostly from discharges at the high pressure regime of operation. For the present set-up, the optimum pressure for high X-ray production is found to be at around 10^{-2} mbar. For low pressure discharges the second phase X-ray pulse may attain high peak value but narrow pulse width, thus the X-ray yield in terms of total energy emitted is low. On the other hand, the X-ray intensity is consistently low for high pressure discharges.

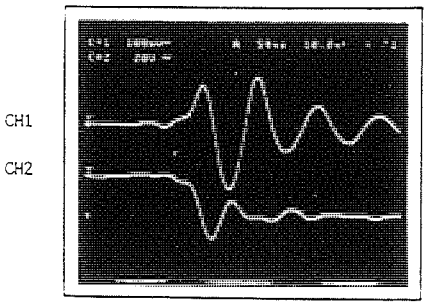

Fig. 4. Waveforms of the discharge current and the voltage across the electrodes recorded simultaneously for a typical flash X-ray discharge at 1×10^{-3} mbar.

A qualitative picture of the plasma dynamics can be deduced from the simultaneously recorded current and voltage waveforms of a typical discharge at 1×10^{-3} mbar as shown in Fig. 4. Corresponding to the flattening of the current waveform during the first half cycle of the discharge, the voltage across the electrodes is observed to hold at high level after a slight drop at breakdown. This is interpreted to be due to the plasma being resistive at the start of the discharge. It seems that there is efficient joule heating of the vaporised anode materials in the inter-electrode space during this time to produce a hot dense plasma emitting X-rays. This may contribute to the sharp rising X-ray signal corresponding to the flattening of the current waveform. Subsequently the plasma becomes a fully conducting channel across the electrodes. Pinching of the column[10] may occur, but it will not be effective due to the relatively low discharge current. Another possible explanation of the sharp X-ray pulse is that due to electron avalanche at breakdown, the intensity of X-ray from the anode tip caused by electron bombardment increases rapidly. This electron beam may also interact with the vaporised anode materials to produce X-ray.

The X-ray emitted from the present flash X-ray tube at

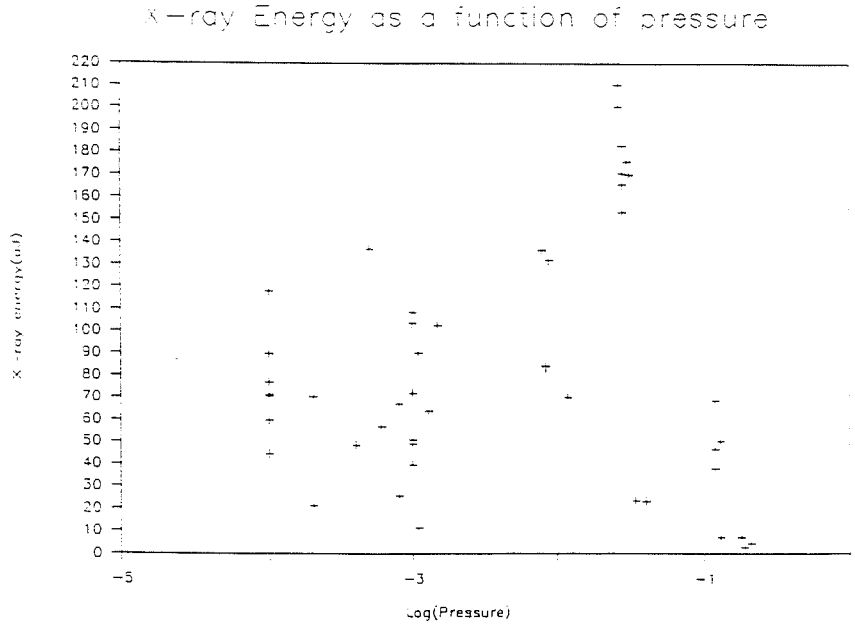

Fig. 5. A plot of X-ray output energy at various operating pressures.

operating pressure of around 10^{-2} mbar has been found to be sufficiently intense to produce single-shot pinhole image on Kodak Direct-Exposure-Film (DEF). Assuming the X-ray emitted consists of predominantly the Fe-Kα line radiation, the total X-ray energy emitted into 4π by the tube can be estimated from the PIN diode signals. The variation of the X-ray energy with operating pressure is shown in Fig. 5 for a series of discharges. It can be seen that the maximum X-ray energy produced by the X-ray tube in its present configuration is obtained at an operating pressure of 2.6×10^{-2} mbar and has a value of the order of 210 μJ. corresponding to an X-ray emission power of kilowatts in amplitude.

§4. Conclusion

We have described the construction and the characteristics of a flash X-ray tube of simple design, low cost and yet with reasonably intense X-ray emission. A severe distortion of the discharge current waveform suggests that the X-ray emitted originates not only from the electron beam bombardment of the anode as in the case of a self-initiating low pressure spark discharge reported earlier,[11] but also from an intensely heated plasma of the anode material. In many cases, the electromechanical interaction is so severe that the discharge current is observed to be almost completely flattened during the first half cycle of the discharge. Intense X-rays are produced from these discharges. Our study here indicates that the efficiency of the flash X-ray tube is strongly dependent on the operating pressure. It is believed that other system parameters such as the electrode configuration,[5] the input energy and the energy of the triggering spark are also important parameters affecting the efficiency of X-ray conversion in this type of flash X-ray tube. These are currently being investigated in this and other laboratories.

References

1) Y. Kato and S. H. Be: Appl. Phys. Lett. **48** (1986) 686.
2) I. N. Weinberg and A. Fisher: Nucl. Instrum. & Methods A**242** (1986) 535.
3) D. J. Nagel: Microelectron. Eng. **3** (1985) 557.
4) S. Roth and I. Freund: Rev. Sci. Instrum. **49** (1978) 104.
5) M. Skowronek, P. Romeas and P. Choi: *XIIth Int. Symp. on Discharges and Electrical Insulation in Vacuum, Paris* (1988).
6) F. Davanloo, T. S. Bowen and C. B. Collins: Rev. Sci. Instrum. **58** (1987) 2103.
7) Q. Johnson, A. C. Mitchell and Ian D. Smith: Rev. Sci. Instrum. **51** (1980) 741.
8) S. Lee and H. Conrads: Phys. Lett. 57A (1976) 233.
9) C. S. Wong: Rev. Sci. Instrum. **56** (1985) 767.
10) S. K. Handel: Ark. f. Fysik **28** (1964) 303.
11) C. S. Wong, C. X. Ong and P. Choi: to be published in *Proc. 3rd Tropical College on Appl. Phys., Kuala Lumpur, Malaysia* (1988).

J. Fiz. Mal. 11, 24 (1990)

SHADOWGRAPHY OF LASER INDUCED SPARKS

S. KUMAR, HARITH B AHMAD, S. LEE and C.Y. JING
Physics Department,
University of Malaya,
59100 Kuala Lumpur.

Abstract

This paper deals with the usage of shadowgraphy in the study of laser induced spark in air at atmospheric pressure. The spark plasma is produced using a Q-switched ruby laser (≅ 50 MW, FWHM or full width at half maximum ≅ 25 ns). A nitrogen laser, with an output energy of 120 μJ in a 3 ns pulse, is used as a source for shadowgraphy. Shock front velocities up to 5 cm/μs have been observed.

Introduction

The laser induced breakdown in gases has received wide spread attention from many research workers[1-10] especially in the 60's and early 70's. A great deal of work done in those times dealt with the study of the initial breakdown, formation and the subsequent motion of the spark plasma. The first reported shadow photographs of laser induced plasmas in gases were obtained by Malayshev[1] (1966). This initiated further work by Evtushenko[2], Korobkin[3], Askarayan[4], Buchl[5], and Holha[5] to quantitatively study the spark formation using laser shadowgraphy. In our lab, a 50 MW Q-switched ruby laser with FWHM of 25 ns was used to initiate the breakdown in air at atmospheric pressure. Shadowgrams were obtained using a nitrogen laser 120 μJ and ≅ 3 ns, pulse width, as a source for illumination. Experimental methods and results are discussed in the following sections. These studies follow earlier shadowgraphy work conducted in the plasma laboratory.[14,16]

Experimental Setup

The experimental setup is shown in fig. 1. The system comprises primarily of a JK 2000 Q-switched ruby laser operated at 50 MW with a pulse width of 25 ns. The laser beam is focused in air at atmospheric pressure under laboratory conditions by a glass lens (research quality) with

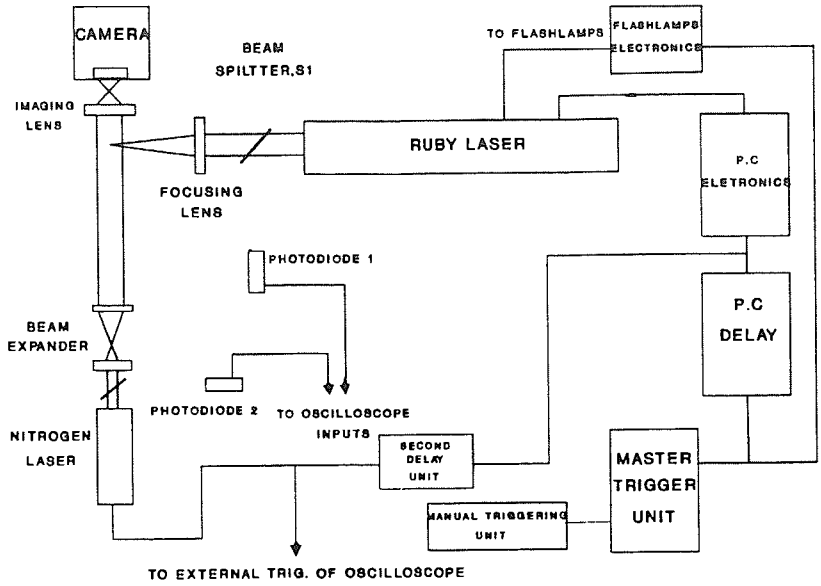

Fig. 1: Schematic Diagram Of Laser Spark Shadowgraphy Setup.

a focal length of 5 cm and a diameter of 2.54 cm to produce a spark. The other major component in this system is the laser shadowgraphy set-up which comprises of a nitrogen laser, a beam expander, an imaging lens and a photographic plate. The nitrogen laser beam is collimated to the required size using a pair of quartz lenses separated by the sum of their focal lengths in a telescope configuration. The JK 2000 trigger unit was used as the master trigger unit to generate and correlate the time sequence of the various events. In this experiment, when the whole system is triggered it is found that the nitrogen laser fires about 1 μs before the formation of the spark. The firing of the nitrogen laser was then delayed using the second delay unit so that the shadowgraphic flash could be made to coincide with various phases of the spark.

When the manual trigger unit is operated, it sends a pulse to the master trigger unit. This master trigger pulse triggers the flashlamp electronics as well as the pockel cell delay unit. The delay time between the onset of the flashlamp trigger pulse to the Pockel cell pulse is optimized at 1.28 ms so as to generate the sharp giant Q-switched pulse of 50 MW. The pulse used to trigger the Pockel cell electronics is also used to drive a second delay unit whose output triggers to the oscilloscope as well as the nitrogen laser. The air spark, nitrogen laser and ruby laser pulses are monitored using FND-100 photodiodes. The timing jitter between the production of the air spark and the nitrogen laser pulse is $\cong$ 90 ns which is largely due to the nitrogen laser. We used a 4 channel digital storage oscilloscope to time the ruby laser pulse, air spark and nitrogen laser pulse simultaneously. The shadowgraph image is recorded using a camera which houses a filter at the beam entrance. This filter is a band-pass filter with a center wavelength of 340 nm and bandwidth at FWHM of 12 nm.

Results

Fig. 2 shows an oscillogram of the ruby laser pulse and air spark. The spark luminosity starts before the ruby laser light reaches peak intensity. A sample of the shadowgraph obtained at t = 5 μs is shown in fig 3. These shadwographs are similar to those obtained by Malyshev[1]. In

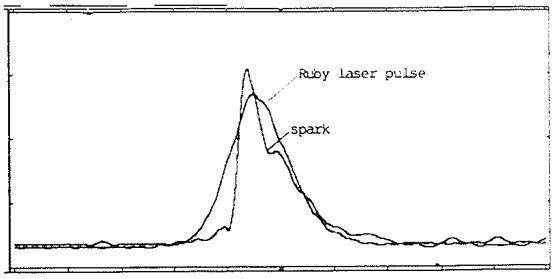

Fig. 2: Oscilloscope trace showing the photodiode signals of the ruby laser pulse and the air spark plasma.
The ruby laser trace is the peak which starts much earlier. (1 division in the x axis represents 20 ns).

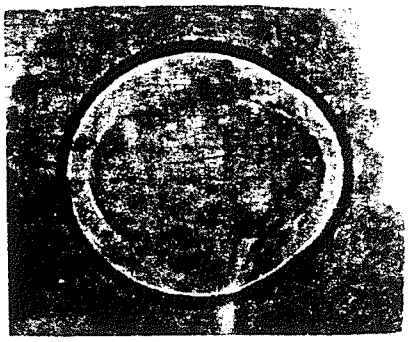

Fig. 3: A typical shadowgram of the air spark plasma taken at t $\cong$ 5 μs. (The direction of the beam is from left to right. Magnification: 1.08x).

this picture, we can see that there is a sharply defined front, which is actually the shock front moving outward axially as well as radially (axial means from left to right and radial means from down to up). From the shadowgraphs the radial and axial displacements were taken and a displacement versus time plot was made (see fig. 4). These displacements were calculated by measuring the diameter and dividing the value by half to obtain the increments in one particular direction. The gradient at particular points were taken from this plot and a plot of velocity versus time was made (see fig. 5). The right hand side of the scale in fig. 5 shows the velocity in terms of the Mach number.

From the plot of velocity versus time, we can see in the initial stages the axial velocity is almost twice than that of the radial value. From the oscillogram, we can see that the air spark is formed before the ruby laser light reaches peak intensity. It is to be expected that the region of breakdown will extend away from the focus, to-

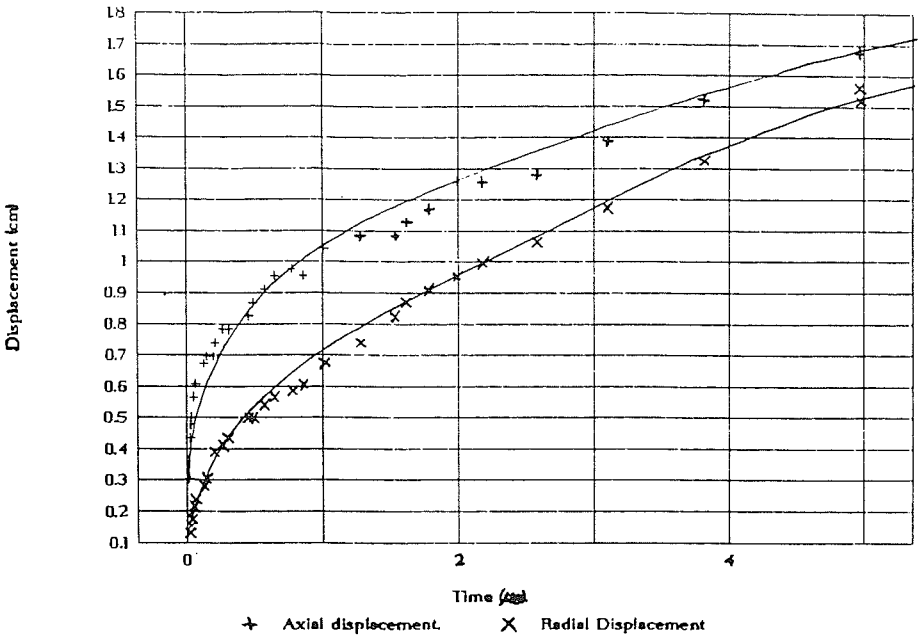

Fig. 4: Graph Of Displacement vs. Time.

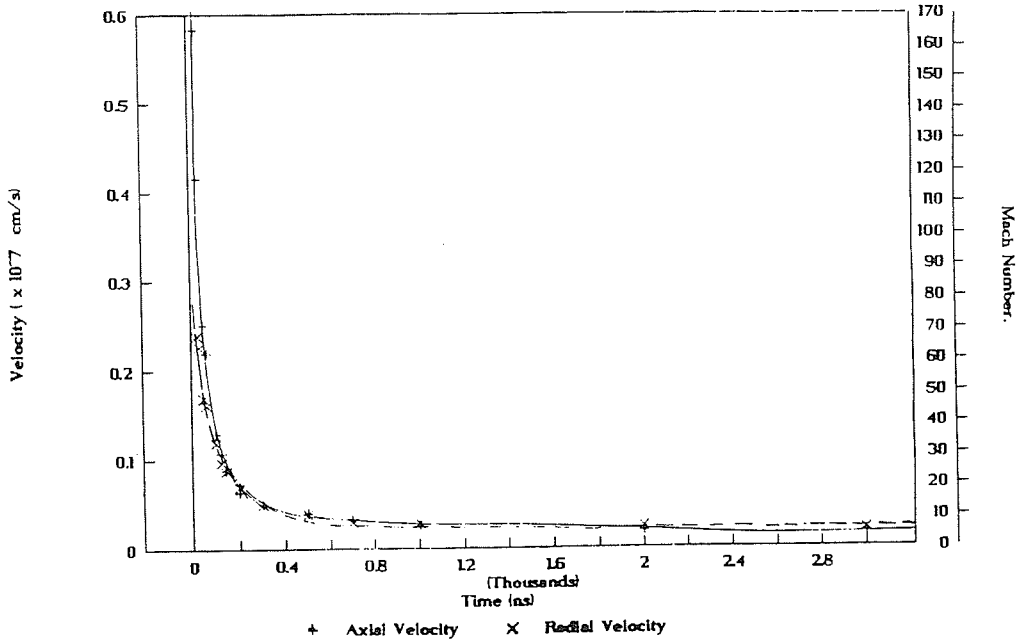

Fig. 5: Graph Of Velocity (cm/μs) vs. Time.

wards the focusing lens, until the peak laser pulse has passed. This is simply the fulfilment of the breakdown condition extended over a larger volume. This effect is often described as a "breakdown wave"[11,16]. It also could be due to multi-focusing as a result of spherical aberration of the lens used[13].

After the duration of the pulse, both the axial and radial velocities slowly decrease until their values become almost equal. The shadowgraphs taken were only up to 5 μs after the formation of the air spark. Further shadowgraphs taken after this time would reveal that these values would converge to one particular value.

Two phases can be distinguished in the expansion of the spark, corresponding to the time before and after the duration of the laser pulse. From the log-log plot of displacement versus time[10], we can observe that from the time of breakdown till the end of the laser pulse, the plasma front moves approximately as the 0.6^{th} power of time, decaying later towards a value of approximately 0.4. This dependence was derived by Ramsden and Savic[10] by interpreting the initial phase of the formation of the spark as a radiation-supported shock wave and analyzing it in terms of the Chapman-Jouguet detonation theory in reacting gases, replacing the reaction energy by the energy per unit of mass absorbed behind the shock front from the laser beam. It is assumed that if the radiant energy absorbed is much larger than the ambient enthalpy of air the three conservation equations and the Chapman-Jouguet condition lead to a very simple result. The later phase, i.e. at the end of the laser pulse, the expansion of the heated gas is analysed as a blast wave. From the log-log plot of displacement versus time (see fig. 6), this dependence is only true for the radial phase and not for the axial phase. The reason for this is lies in

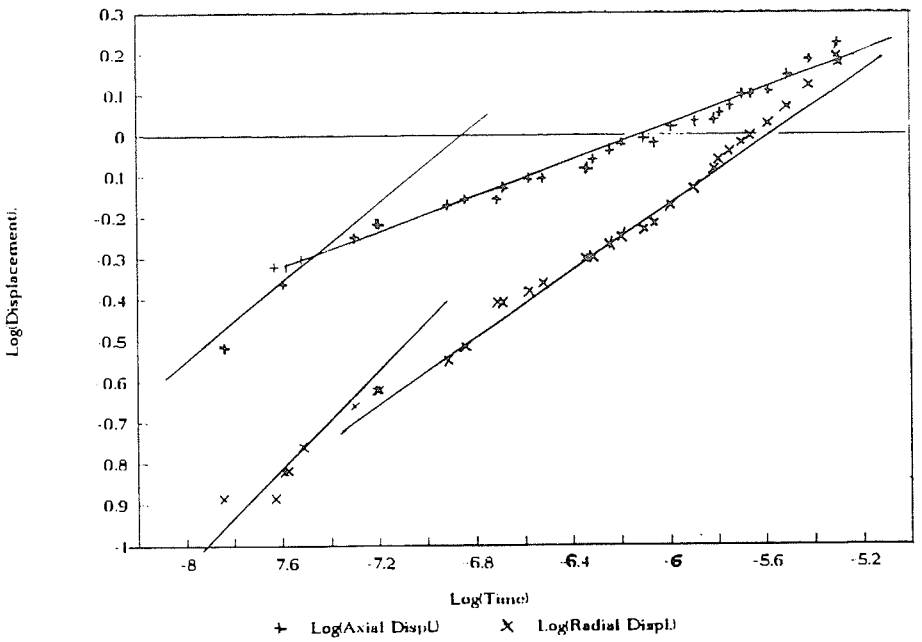

Fig. 6: Graph Of log (Displacement) vs. log (Time).

the difference between the energy received per unit mass of the gas for a laser driven 'detonation' and chemical explosive detonation used by Ramsden and Savic[10]. Detonation in a chemical explosive is a combustion process initiated by a shock[16]. The shock raises the density, temperature, pressure and entropy of the medium and sets off the chemical reaction in a thin layer immediately behind the shock front. The reaction energy then causes a fall in pressure and density to the Chapman-Jouget point together with a further rise in temperature and entropy. In the case of a laser driven 'detonation' no chemical reaction is involved. The initial shock front changes the transparent cold gas into a dense, cool, absorbing plasma. Incident laser energy is therefore deposited immediately behind the shock front. The resulting fall in pressure and density to the Chapman-Jouget point, together with the rise in temperature produces a hot plasma behind the detonation which is only weakly absorbing. The Hugoniot curve must be modified to allow for velocity dependence of the energy per unit of mass absorbed hind the shock front from the laser beam[11].

A pin hole picture of the air spark plasma was also taken. From this pin hole picture we can see that the shape of the air spark plasma is elongated in the axial direction. This results agrees with the shadowgrams we have already obtained and also with the work done by Askarayan[9].

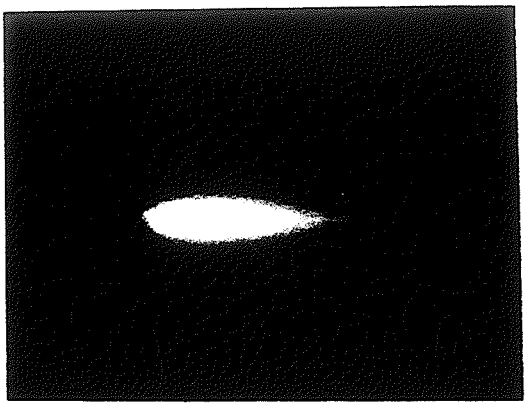

Fig. 7: A pin hole photograph of the air spark plasma. The direction of the beam is from left to right. (Magnification 7x).

References

1. G.M. Malyshev, G.V. Ostrovskaya & T. Ya. Chelidze, *Opt. iSpektrosk.* **20**, 374-5 (1966). (Transl: Opt & Spectrosc., **20**, 207-8 (1966)).
2. T.P. Evtushenko., G.M. Malyshev, G. V. Ostrovskaya, V.V. Semenov & T. Ya. Chelidze, *Zh. Tekh. Fiz.* **36**, 1115-7 (1966) (Transl: *Sov. Phys. Tech. Phys.* 11, 818-20 (1966)).
3. V. V. Korobkin, S.L. Mandel'shtam, P.P. Pashinin, A.V. Prokhindeev, A.M. Prokhorov, N.K. Sukhodrev & M. Ya. Shchelev, III, **Zh. Eksp. iTeor. Fiz. 53, 116-23 (1967). (Transl: Sov. Phys. JETP.**

3. V. V. Korobkin, S.L. Mandel'shtam, P.P. Pashinin, A.V. Prokhindeev, A.M. Prokhorov, N.K. Sukhodrev & M. Ya. Shchelev, III, *Zh. Eksp. iTeor. Fiz.* **53**, 116-23 (1967). (Transl: Sov. Phys. JETP. **26**, 79-85 (1968)).
4. G.A. Askar'yan, M.M. Savchenko & V.K. Stepanov, *Zh. Eksp. iTeor. Fiz. Pisma.* **10**, 161-5 (1969). (Transl: JETP. Lett. **10**, 101-3 (1969)).
5. K. Buchl. K. Hohla, R. Wienecke & S. Witkowski, Phys. Lett. **26A**, 248-9 (1968).
6. A.J. Alcock, E. Panarella & S.A. Ramsden, VII *International Conference on phenomena in ionized gases, Belgrade* (1965), Vol 3 pp. 224-7, Belgrade, Gradevinska Knjiga (1966).
7. A.J. Alcock, E. Panarella & S.A. Ramsden, Phys. Rev. Lett. **17**, 528-30 (1966).
8. K. Hamal, C. De Michelis & A.J. Alcock, **Opt. Acta. 16**, 463-9 (1969).
9. G.A. Askar'yan et. al. *Zh-Eksp. iTeor.Fiz. Pis'ma.* **5**, 150-4 (1967) (Transl: JETP. Lett. 5, 121-4 (1967)).
10. S.A. Ramsden & R. Savic, Nature. **203**, 1217-19 (1964).
11. Yu. P. Raizer, *Zh. Eksp. iTeor. Fiz.* **48**, 1508-19 (1965). (Transl: Sov. Phys. JETP. 21, 1009-17, (1965)).
12. B. Ya. Zel'dovich & Yu. P. Raizer, Physics of shock waves and high temperature hydrodynamic phenomena, New York Academic (1966).
13. C.G. Morgan, Rep. Prog. Phys. **38**, 621-665 (1975).
14. S. Lee & Y.H. Chin, Bull. Mal. Inst. Phys. **2**, 50 (1981).
15. T.Y. Tou, E.H. Yee, B.C. Tan and S. Lee, Proc. Asian Physics Symposium, Kuala Lumpur (Oct. 1987).
16. T.P. Hughes, *Plasmas and Laser Light*, Adam Higler Ltd (1975).

J. Fiz. Mal. 11, 1 (1990)

A SIMPLE SHADOWGRAPHIC SYSTEM AND SOME RESULTS

S. LEE, M.A. ALABRABA,[a] A. V. GHOLAP,[b] S. KUMAR, K.H. KWEK, M. NISAR,[c] R.S. RAWAT,[d] and J. SINGH
ICTP-UM Training Programme on Plasma and Pulse Technology
Physics Department, University of Malaya
59100 Kuala Lumpur, Malaysia

Received: 30 March 1990

Abstract

Design equations of a simple shadowgraphic system are given and a specific system is designed. Using this system some interesting results of a plasma focus discharge are presented including a) focusing dynamics in the presence of a target, b) sequential focus, c) focusing onto a thin wire target and d) structure of a negative polarity focus. These results could open up new lines of research for the plasma focus.

Introduction

The shadowgraph has been used extensively in the visualization of shock waves and turbulence in aerodynamic studies. In more recent years with the advent of laser light sources, time resolution has been improved with the nanosecond regime being readily accessible. Particularly with the easy availability of the nitrogen laser[1] and with the present effort to propagate research machines such as the plasma focus[2] to developing countries the diagnostics method of nanosecond shadowgraphy[3] opens up a method of assessing dynamics of new experimental set-ups, providing very quickly a comprehensive picture such as would be difficult to obtain by other methods including streak photography and magnetic mapping.

To demonstrate the ease and power of the method and to remove some of the remaining mysteries we first write down the design equations, produce a specific design and proceed to present a range of results of the focus in new and important set-ups.

Design of Shadowgraph System

The shadowgraph system is made up of subsystems as indicated by the block diagram of Fig. 1.

Fig. 1: Sub-system of the shadowgraphic set up.
1 = Nitrogen Laser.
2 = Beam expander using quarts lenses.
3 - Imaging system.
4 = Camera with Hilters.

The Laser

The nitrogen laser is now fairly readily available and can even be home-made,[1] with the high voltage power supply readily adapted from the high voltage supply of a television set. With some care fairly good beam quality and a pulse width of just under 1 ns (resolution of 0.2 mm) may be attained with a laser gap operated at atmospheric pressure. Details on the construction of such a laser has already been described.[1]

The Beam Expander

For the beam expander a design such as shown in Fig. 2 may be used, The design criteria may be listed here as:

(a) input lens diameter $D_1 \geqslant d$, the beam diameter so that the full beam may be used.
(b) distance between lenses is adjusted to equal $f_1 + f_2$, where f_1 = focal length of input lens

a) Present address: Physics Department, River State University of Science and Technology, Port Harcourt, Nigeria.
b) Present address: Physics Department, University of Zimbabwe, Harare, Zimbabwe.
c) Present address: Physics Department, Quaid-I-Azam University, Islamabad, Pakistan.
d) Present address: Department of Physics and Astrophysics, University of Delhi, India.

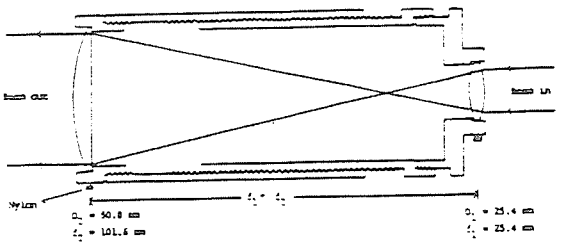

Fig. 2: Design of Beam expander.

and f_2 = focal length of output lens.

(c) in order to make use of the full diameter of output lens, for maximum system aperture put

$$\frac{D_2}{d} = \frac{f_2}{f_1} \qquad (1)$$

For our present system we use quartz lenses with $D_1 = 25.4$ mm, $D_2 = 50.8$ mm and $f_2 = 101.6$ mm. The laser input beam is about 1 cm, so that D_2 is almost fully used.

The Imaging System

For the imaging system we use an imaging lens, a plasma light reduction stop and a nitrogen laser filter centred at 337 nm (3 nm bandpass) and several neutral density filters of the thin-film Inconel-deposited glass type. The set-up is shown schematically in Fig. 3.

The imaging lens (focal length f_2) is placed at x cm from the event to be shadowgraphed. The parallel laser beam from the beam expander focuses at distance f_3 on the other side of the lens. A stop (diameter S ~ 1 mm) is placed at the focal point. Distance of imaging lens to the film in the camera is y cm.

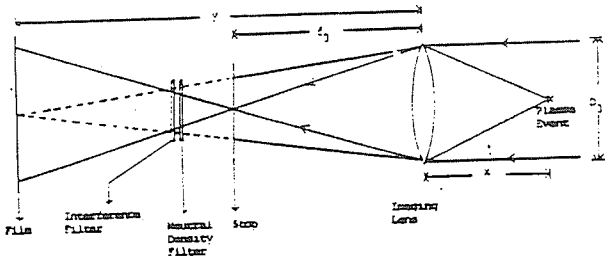

Fig. 3: Schematic of Imaging System.

To focus the event on the film, set

$$y = \frac{xf_3}{x - f_3} \qquad (2)$$

For our present system, we use an objective lens with $D_3 = 51$ mm and $f_3 = 30$ cm, and put $x = 40$ cm (note x should be greater than f_3). The stop is put at 30 cm from the lens and the film is placed at a distance from the lens of $y = 120$ cm in accordance with equation (2).

We note that the magnification M is

$$M = \frac{y}{x} = \frac{f_3}{x - f_3} \qquad (3)$$

giving us a value of 3 with our present set-up.

Also the total image size (size of the laser beam) on the film is $D_3 \times M$.

For the case of a highly luminous event, such as a plasma focus, in which the light from the event, even after filtering through the narrow bandpass filter, is still sufficiently strong to be of the same order as the laser light, the stop serves a very important function. It reduces the plasma light falling on the film whilst not stopping down the laser light if the stop size is bigger than the focused laser beam diameter at the stop.

If the plasma event produces light of intensity I, then light collected by lens D_3 is $I(D_3^2/4x^2)$. This light is focused by D_3 on to the film. At the place of the stop, this light beam has diameter R given by $R/D_3 = (y - f_3)/y$ which after substituting for y from equation (2) and simplifying gives

$$R = D_3 \frac{f_3}{x} \qquad (4)$$

Hence of the total light intensity I, the light intensity getting through the stop of diameter S is

$$\left(\frac{S}{R}\right)^2 \times I\frac{D_3^2}{4x^2} \qquad (5)$$

which after substituting for R from equation (4) and simplifying gives $(1/4)(S/f_3)^2$.

Thus the stop reduces the light collected at the film from $(I/4)\,(D_3/x)^2$ without stop, to the stopped value $(I/4)(S/f_3)^2$

The stop reduction ratio SR is therefore given by

$$\frac{I}{4}\left(\frac{S}{f_3}\right)^2 / \frac{I}{4}\left(\frac{D_3}{x}\right)^2$$

$$\text{or} \quad SR = \left(\frac{S}{D_3}\right)^2 \times \left(\frac{x}{f_3}\right)^2 \qquad (6)$$

In our present arrangement S = 1 mm, D_3 = 51 mm, x = 40cm, f_3 30 cm hence SR = 7 X 10^{-4}

Experimental Set-Up

The experimental set-up is shown in Fig. 4.

We use the plasma focus designated as the United Nations University/International Centre for Theoretical Physics Plasma Fusion Facility (UNU/ICTP PFF) which is a 3 kJ plasma focus device operated at the neutron optimized point of 3 torr deuterium at 15 kV and 176 KA peak current.[2]

Its inner hollow copper electrode has a diameter of 2 cm and a length of 16 cm. The outer electrode consists of 6 copper rods forming a diameter of 6 cm.

The shadowgraph system has already been described in some detail. Polaroid film is used for recording. For these experiments a bandpass filter centred at 340 nm having a passband of 12 nm and several neutral density filters are used to obtain the correct nitrogen laser intensity recorded on the film. The set-up is as shown in Fig. 4.

The electronic timing sequence is as shown in Fig. 5. The instant of plasma focus is defined as the time of voltage spike using a voltage divider placed across the focus anode and cathode. From earlier work[2] it is known that the voltage spike time corresponds to the time of maximum plasma compression.

To synchronize the plasma focus and the laser flash it was necessary to determine the focus time t_f and the laser flash time t_L and then to match these by use of a delay unit. The plasma focus time $t_f - t_o$, defined here as the time of voltage spike, was found to be 5.86 ± 0.09 μs. The jitter is due to the parallel plate swinging-cascade spark-gap jitter and the focus run-down time jitter.

The instant of laser flash measured with a photodiode BPX65, with the delay unit by-passed, was found to be $t_L - t_o$ = 1.50 ± 0.05 hs. This jitter was mainly due to the laset spark-gap.

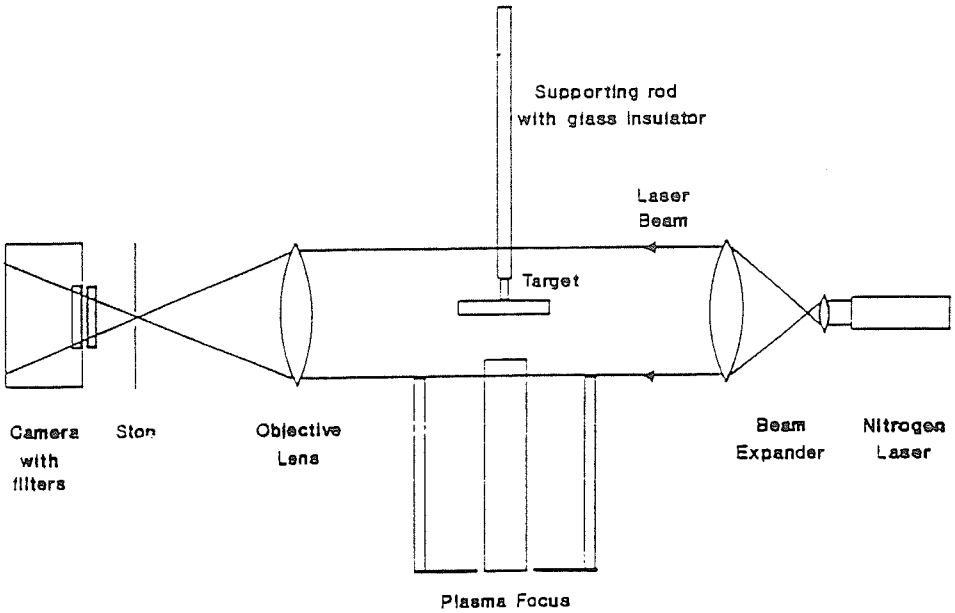

Fig. 4: Schematic of Shadowgraphic Set-up.

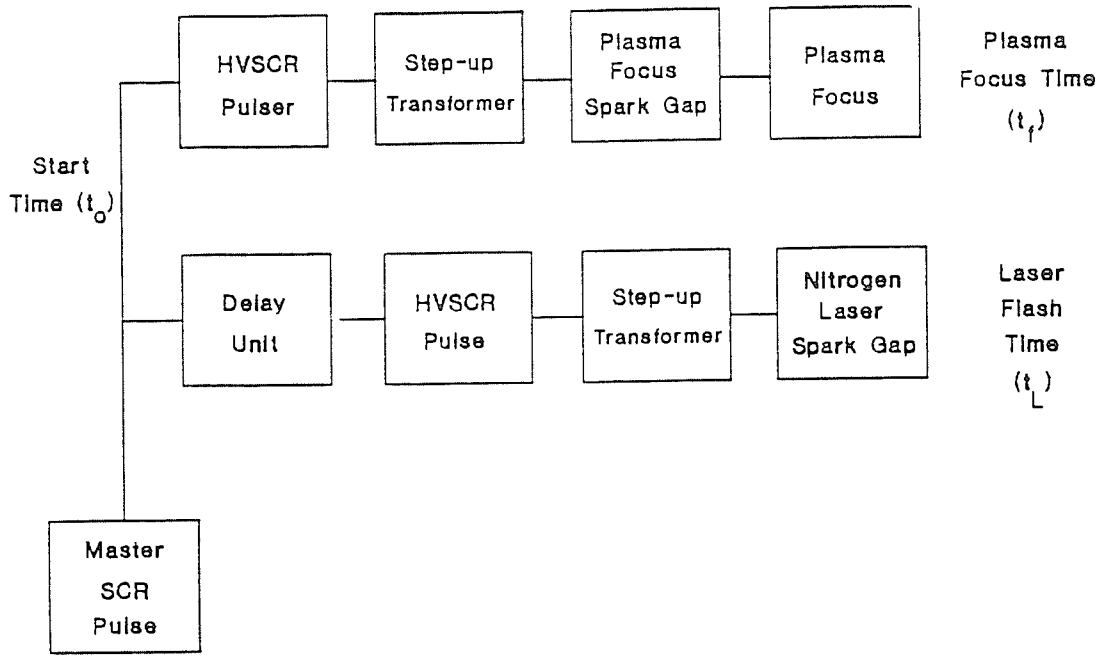

Fig. 5: Block Diagram of Electronic Time Sequence in Experimental Set-ip.
(SCR: Silicon Controlled Rectifier; HVSCR: High Voltage SCR).

Therefore the required delay is $t_f - t_L \cong 4.36$ μs. With the times set thus, the synchronization has a jitter range typically of about 0.1 μs. Since the focusing (pinch) time takes about 0.1 μs and the laser pulse time is 3 ns (in these experiments), the jitter will allow, over a large number of shots, shadowgraphs to be taken of different instants during the focus collapse. We denote the time of voltage spike as t = 0. Hence, e.g., – 10 ns means 10 ns before the voltage spike.

The target (see Fig. 4) consists of a brass disc, 5 mm thick having a diameter of 25 mm hanging from a brass support rod of 3 mm diameter. The target is kept at floating potential as the support rod is insulated from the earthed chamber by a glass tubing of diamter 6 mm.

Results

Fig. 6 shows a composite shadowgraph sequence with the target at 1.5 cm from the focus anode. Fig. 6c of this sequence shows that there is no interaction between the radially collapsing current sheet and the target up to the time 6 ns before maximum compression as indicated by the corresponding timing oscillogram, Fig. 7, showing the voltage spike (which identifies the instant of maximum compression) and the laser pulse. At the measured speed of 20 cm/μs there is only a further radial compression of 1.2 mm. The rate of elongation of the plasma focus is known to be of the some order as the rate of radial compression[4] hence we can extrapolate a further elongation of 1.2 mm at maximum compression. In fact from Fig. 6c, we can safely state that there is no interference of the current sheet by a target placed at further than 1 cm which is the anode radius. Fig. 6d shows a shadowgraph 31 ns after peak compression with the curved return current path clearly seen but with no sign of the pinch column.

The situation depicted by Fig. 6d is known to be the time during which the pinch column has expanded and is in a quiescent condition[9] corresponding to the time just after peak neutron emission. The shadowgraph shows clearly that the current sheet at this time still has not reached the target.

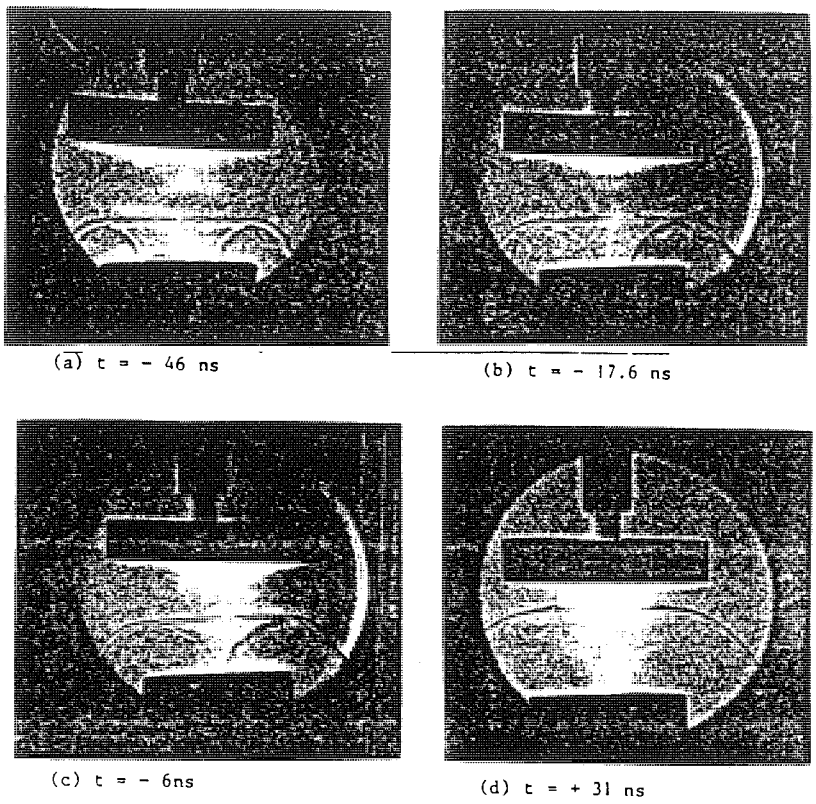

Fig. 6: Shadowgraphs of current sheet configuration before and after peak compression with a flat target at a distance of 1.5 cm from anode face.

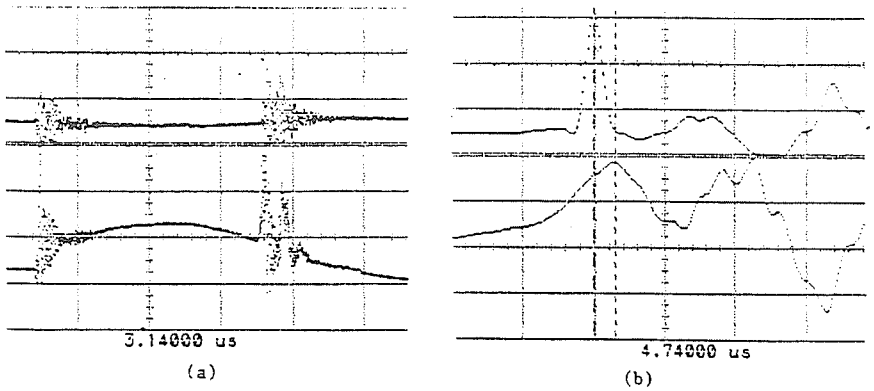

Fig. 7: Timing Oscillograms for Fig. 6c.
(a) Top trace: photodiode signal of laser pulse
Bottom trace: voltage signal of focus 1 μs/div.
(b) Same as (a), but with expanded time scale 20 ns/div.
From this Oscillogram the time of the laser pulse is determined to be t = – 6 ns; i.e. 6 ns before maximum plasma compression or voltage pulse maximum.

Examination of several sequences of shadowgraphs with the target at increasingly closer distances from the anode shows that for this focus machine targets may be used with distances as close as 10 mm without interference of the focusing current sheet of the focus proper. This is of importance to the study of beam-target neutron production experiments.[5,6]

On the other hand when the target is at e.g. 7 mm (see Fig. 8) the current sheet reaches the target before maximum compression (Fig. 8b) and is deemed to interfere with the focus dynamics.

Examination of the sequence of shadowgraphs also revealed an interesting phenomenon. For example in the sequence with the target at 7 mm as shown in Fig. 8 the current sheet has reached the target about the time of focus maximum compression (see Fig. 8b). Following that the current sheet climbs over the target, so to speak, as seen in Fig. 8c. Fig. 8c shows this current sheet advancing at an axial speed of 5 cm/

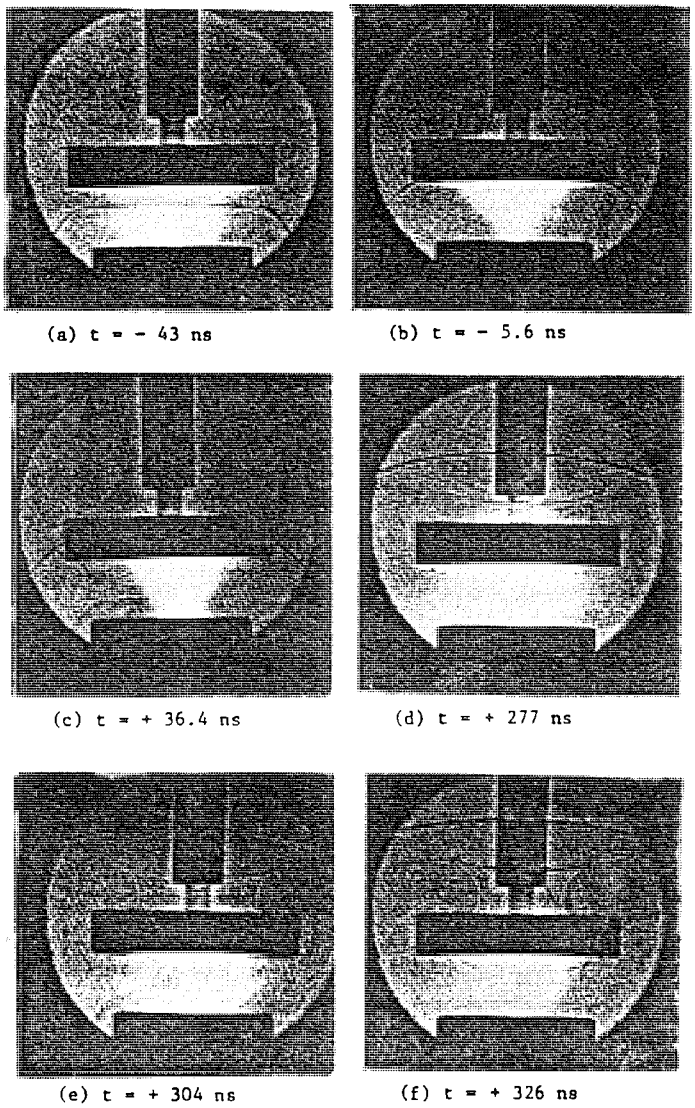

Fig. 8: Shadowgraphic sequence (composite) of current sheet configurations with the flat target at a distance of 7 mm from the anode face.

μ over the disc which we may now interpret as a new "anode". This axially advancing axisymmetric current sheet then collapses onto the glass tube surrounding the brass support rod as seen in Fig. 8 d-f. This raises the interesting question whether, if the brass support rod with its insulating tubing were removed, a new focus could be formed beyond the target. If so a metal disc placed say 1 cm beyond the anode face would after the usual focus and after a small interval of say 300 ns, present in effect a new anode face producing a fresh focus event. In this manner by a series of separated discs, a series of plasma focus may be produced sequentially in one discharge, each disc sequentially becoming a fresh anode face. It is necessary of course to adjust the discharge parameters to provide a sufficiently long sustaining electric current I to adequately power each focus up to the last one in the sequence keeping in mind the speed scaling factor of $[(I/a)/\sqrt{\rho}]$, where a is the anode radius and ρ the ambient density. Further work on this will be started.

Results for an axial wire target experiment were also obtained. These are shown in Fig. 9. These shadowgraphs with the corresponding voltage waveform, show the formation of a strong focus onto the centrally located wire target. The copper wire target used here has a diameter of 1 mm which is smaller than the usual focus diameter of 2 mm and the results indicate a focus on target with similar, though a little weaker voltage spike characteristic and similar shadowgraph characteristic as a free focus. Since the focusing voltage spike has an amplitude that is proportional to $\dot{r}/r$ (radial velocity divided by radius), it is clear that the use of a thinner wire target, say of 100 μm diameter, would restore the focus voltage spike as well as its overall intensity. This indicates that even with our small focus, having only 3 KJ energy it should be possible to carry out plasma implosion experiments on thin fibres, deuterated or otherwise for neutron yield enhancement experiments or for plasma target interaction experiments.[7,8] Incidentally Fig. 9c shows the 'bubble' formation that occurs after a

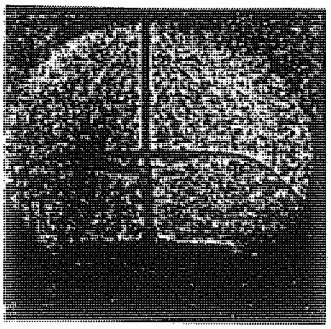

(a) = 0 ns

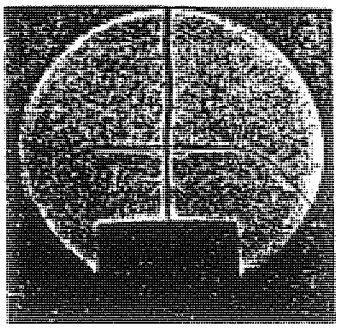

(b) t = + 46 ns

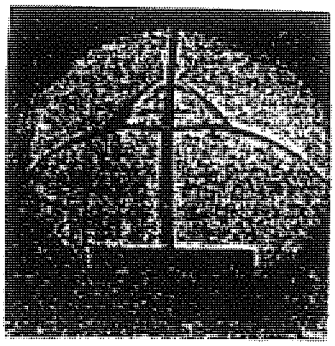

(c) = + 80 ns

Fig. 9: Shadowgraphs of plasma focus collapse onto a 1 mm axially located wire.

strong focusing event. The observation of such a bubble also is an indication of strong focusing.

Finally we show some shadowgraphs taken of a negative-polarity plasma focus that is a plasma focus run with the centre electrode negative. We keep all parameters the same as the UNU/ICTP PFF except the polarity. We also vary the pressure from 3 torr upwards to 10 torr. Such a reversed polarity focus is important as its studies could help in the understanding of good focus mechanism.[9] So far very little is known of the negative polarity focus except that its neutron yield is considerably lower than that of the ordinary, i.e. inner-electrode positive, focus. Shadowgraphs could at least answer the following question: Is it the axial run-down phase that is responsible for the poor neutron yield? or the radial phase?

We compare the axial run-down phase of the normal positive polarity focus, Fig. $10a_1$, and the negative polarity focus Fig. $10b_1$. No difference is descernable, neither in inclination nor thickness of layer. However Fig. $10a_2$ and $10b_2$ comparing the start of focus (or radial phase) for the two polarities may hold the key to the difference in focusing effect on polarity. Fig. $10a_2$ for

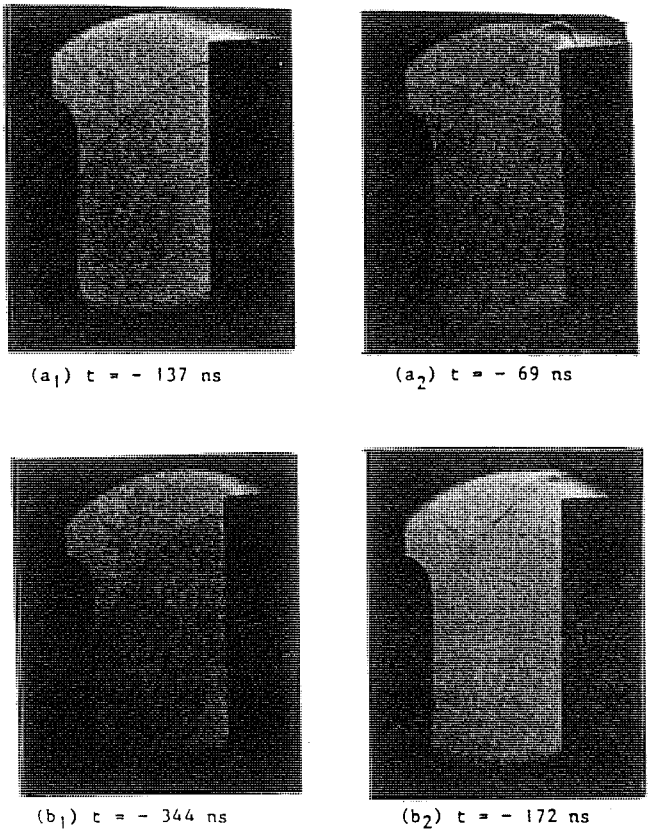

Fig. 10: Comparison of axial phase and start of radial phase for the normal positive polarity focus versus the negative polarity focus
(a_1) Positive polarity, end of axial phase
(a_2) Positive polarity, start of radial phase
(b_1) Negative polarity, end of axial phase
(b_2) Negative polarity, start of radial phase.
In each shadowgraph, the anode is on the right pointing upwards and the cathode is on the left. Axial motion is upwards.

normal positive polarity shows an uninterrupted progression from axial phase to clear radial collapse. Fig. $10b_2$ for the negative polarity case shows that even after the current sheet has gone some distance beyond the end of the anode the radial collapse still has not started, with the current sheet still faintly and diffusely 'attached' to the 'corner' of the anode.

In Fig. 11 we examine the pinching in the radial phase for the case of negative polarity. The negative polarity radial phase produce shadowgraphs that look distinctly different from the normal polarity collapse of e.g. Fig. 6. The column in Fig. 11 is faint and diffuse in appearance and it is clear that further studies on this phenomenon should concentrate on the radial phase rather than the axial phase. Fig. 12 shows the voltage signal of the negative polarity focus corresponding to Fig. 11.

Fig. 13 shows the negative polarity focus at 6 torr. At this higher pressure the column appears more distinct but the focus is still weak as apparent from voltage signal.

Conclusion

This work has demonstrated that the shadowgraph may be built as a very simple system. Yet belying its simplicity it may immediately be applied to produce very quick yet authoritative results as demonstrated with three situations in these experiments namely (a) interaction of flat targets with plasma focus dynamics, leading to a concept of a sequential focus, (b) feasibility study of focusing onto an axial wire target and (c) negative polarity focus – deciding which phase is responsible for poor focusing.

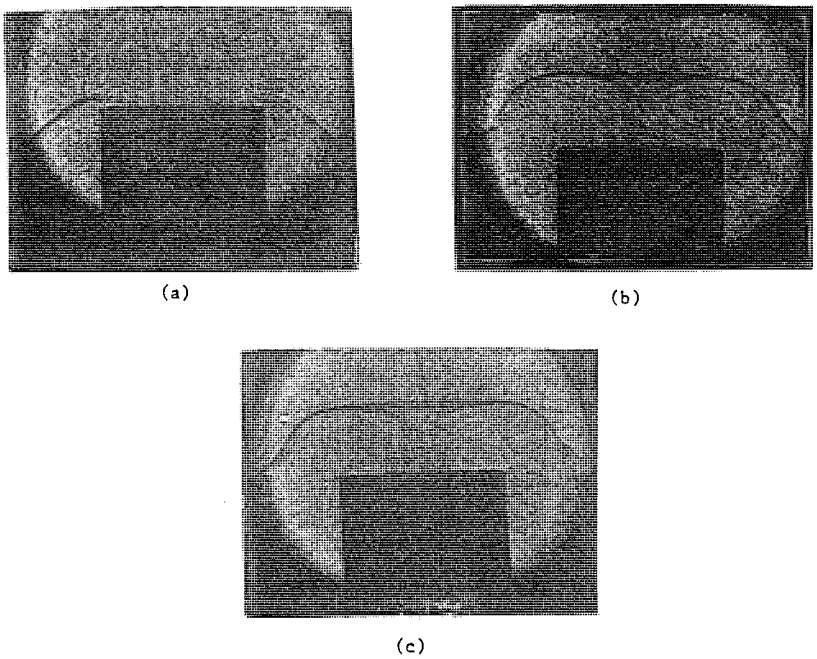

Fig. 11: Radial phase of negative polarity Plasma focus at 15 kV 3 torr deuterium. These shadowgraphs may be compared with those of Fig. 6 which are for the normal positive polarity focus.

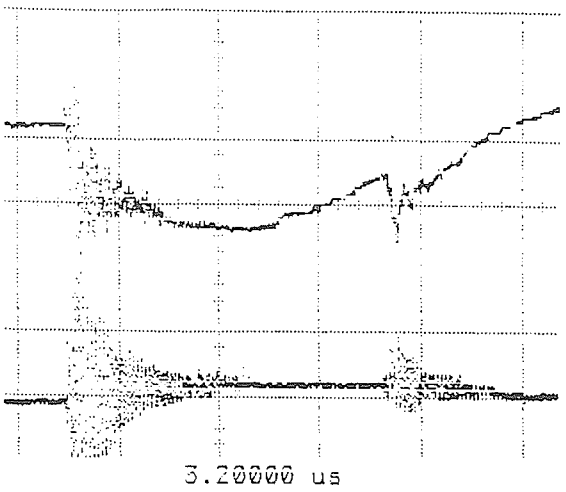

Fig. 12: Timing oscillograms for Fig. 11. Top trace: Voltage signal of negative polarity Plasma Focus.
Bottom trace: Photodiode signal of laser pulse 1 hs/div. From an expanded version of this oscillogram the time of the laser pulse is determined to be t = – 56 ns, i.e. 56 ns before maximum .

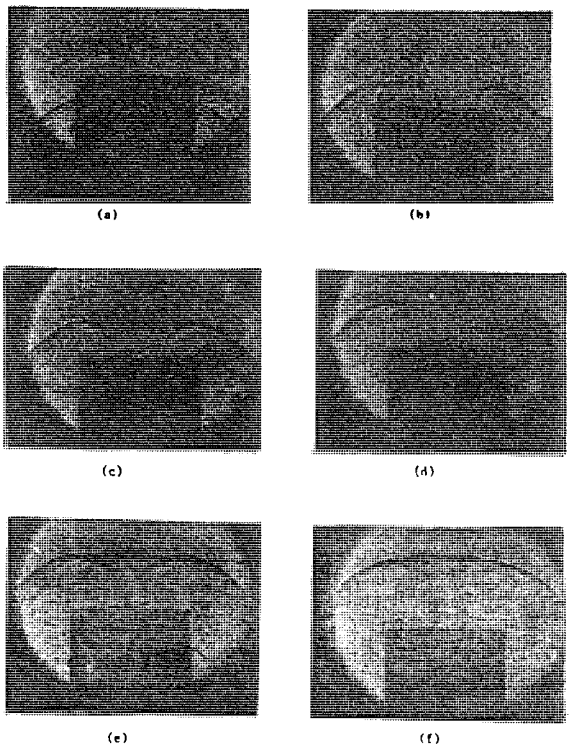

Fig. 13: Radial phase of negative polarity plasma focus at 15 kv, 6 torr of Deuterium. The focus although less diffuse in structure is actually weaker when judged from the corresponding voltage spike. The shadowgraphs a-f are in time sequence with (a) as the earliest, before the focus and (f) as the latest shadowgraph, after the focus.

PLASMA FOCUS DYNAMICS - ITS ROLE IN AN AAAPT TRAINING PROGRAMME

S. Lee
ICAC-UM
Physics Department
University of Malaya
59100 Kuala Lumpur
Malaysia

Abstract

A brief description of the Asian African Association for Plasma Training is given with a listing of its 8 activities carried out in the past 2 years. Its present effort to establish the Plasma and Laser Technology Resource Network is also described. The experience of the AAAPT points to the effectiveness of training packages and equipment packages in helping developing countries initiate/strengthen research in experimental physics. One such package is the UNU/ICTP Plasma Fusion Facility which has successfully been installed in 9 institutions in 7 countries. The sub-system concept and the sub-systems in this package, or facility, has been extensively described. However very often overlooked is that such a package must be at the same time supported by a comprehensive theoretical model, so that the experimental work benefits from the complementary understanding of modelling and computation. The plasma focus dynamics model supporting the UNU/ICTP PFF package is discussed and shown to agree with the experimental features of current dip, voltage spike and axial and radial trajectory. Moreover the basic model is extended to predict the behaviour of a cascading focus, an invention of the recent AAAPT-associated ICTP-UM Training Programme. The model and results are discussed in detail.

Invited review paper prepared for the Third Summer School on Plasma Physics, Tsingdao City, People's Republic of China, 15-22 August 1990.

Procs. Third Summer School on Plasma Physics, Aug. 1990
Tsingdou, P.R. China, Ed. Tsai Shih-Tung & LI Yin An.

Introduction

The Asian-African Association for Plasma Training (AAAPT) was formed[1] to carry out the following activities:

- o to conduct Plasma Physics training programmes for Asian and African countries
- o to develop research packages for transfer and research initiation
- o to exchange scientists
- o to publish a newsletter

The AAAPT now has 23 member institutions in 16 countries. Starting from its formation the following have been its activities:

- o Formation on 7 June, 1988 (during the Third Tropical College on Applied Physics) in Kuala Lumpur, Malaysia
- o Second (UNU)ICTP Training Programme, Kuala Lumpur, Malaysia, June-October 1988
- o Beijing College on Plasma Diagnostics[2], Beijing, P.R. China, October-November 1988
- o Third ICTP-UM Training Programme, Kuala Lumpur, Malaysia, December 1989 - May 1990
- o Regional College on Plasma Applications, Songkla, Thailand, January 1990
- o Fourth Tropical College on Applied Physics, Kuala Lumpur, Malaysia, May-June 1990
- o Third Summer School on Plasma Physics, Tsingdao, P.R. China, August 1990
- o Basic Course on Plasma Physics - Theory, Islamabad, Pakistan, September-November 1990.

The AAAPT is currently also spearheading the establishment of the Plasma and Laser Technology Resource Network (PLTRN) with the following description[3]:

Aim: To assist development of equipment packages.
To assist distribution of equipment packages.

Concept:

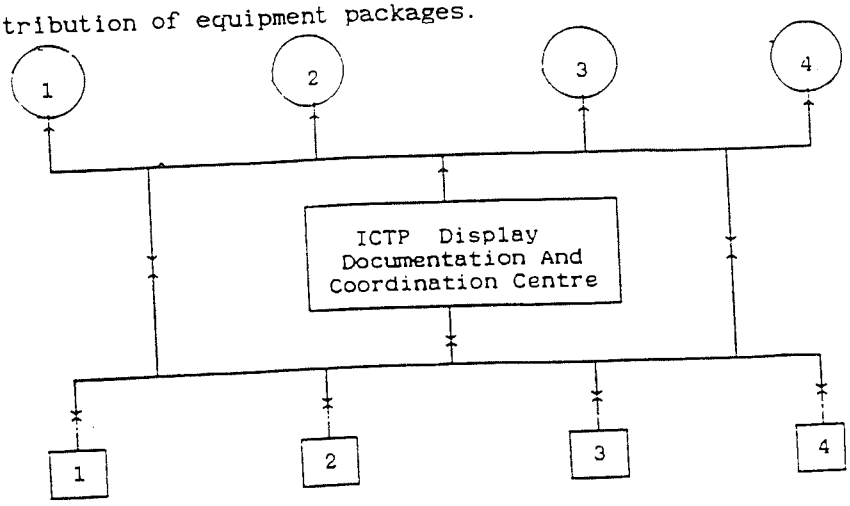

Proposal:

PLTRN be established at ICTP to benefit as many Third World scientists as possible.

Funding and contributions: ICAC's, AAAPT, ICTP, TWAS, etc.

Actions taken:

Nitrogen Laser Education and Application package already installed at ICTP (contributed by ICAC-UM).

Optical Fibre Monochromator (OFMS) package already completed and sent to ICTP (contributed by AAAPT, project of Plasma Physics Division, Chinese Academy of Science, Beijing).

Multi-purpose plasma devices, pinch and glow discharge device completed, to be donated to University of Cairo (contributed by AAAPT, project of Egypt Atomic Energy Authority, Plasma and Nuclear Division).

Other packages being planned include:

- o Laser Shadowgraphy System
- o Plasma Fusion Facility
- o Theta Pinch
- o Transistorised Rotamak FRC System
- o YAG Laser package
- o Hologram System

Summary: Training Programmes of the AAAPT

- o Training programmes for research transfer have been set up with proper S-S-N interaction criteria.
- o Basis of transfer: research facility package with comprehensive hands-on training programme and equipment follow-up.
- o Results: transfer of significant research activities to 10 institutions in 7 South countries.
- o Results: Research papers[4-7] and postgraduate theses up to Ph.D. level.
- o Out of these programmes has grown the AAAPT bringing expertise of more advanced South countries contributing 8 activities in 2 years.
- o AAAPT attempts to open up the technology resources of the more developed South countries to other South countries through the PLTRN.

Training packages

Among all the activities of the AAAPT, experience has shown that one very effective way of establishing the transfer of technology for the initiation of research is the use of training packages[4].

A training package is usually evolved around an experimental facility which is carefully planned so that it may be transferred at low cost to

various developing countries so as to enable experimental research (associated with that particular facility) to be started or strengthened in the recipient country. For pedagogical reasons the package is divided into sub-systems, so that each sub-system may be taught separately. When eventually put together all the sub-systems form the complete facility to be transferred. A typical package is the UNU/ICTP PFF which is shown schematically in Fig. 1. This package has been used for three training programmes each lasting between 4-6 months. The result of these training programmes has been the establishment of operational plasma focus research activities in 9 institutions in 7 countries (see accompanying Table).

A very important sub-system of the package is the computation of plasma focus dynamics using microcomputer packages (see Fig. 1). This sub-system has usually been overlooked in the description of the package. It is however vitally important to the design and understanding of the plasma focus and has recently led to a new and rather exciting concept developed during the course of a training programme.

Plasma focus dynamics

The proper operation of the plasma focus depends on the correct adjustments to the driving current density, electrode geometry and operational pressure. The design[8] of these parameters should ensure the correct speed of about 10 cm/μs in the axial run-down phase and 25 cm/μs on-axis speed in the radial implosion phase at a filling pressure of several torr for a small focus operated in deuterium. It is a well-known and unfortunate factor that higher speeds seem not to be conducive to a consistent good neutron yield. The axial and radial phase dynamics is illustrated in Fig. 2. The geometry of the compressed plasma column in its densest phase before break-up is shown in Fig. 3 where the length of the column is shown to be a little smaller than the anode radius, and the radius of the deuterium plasma column is about 0.15 of the anode radius. These dimensions are experimentally observed and conform to the results of computations. The column remains compressed for 30-50 ns for a small focus but this lifetime increases according to the anode size which follows a scaling according to available driving current or stored energy. At about the time of the maximum compression the plasma emits copious X-rays, REB, deuteron beams and fusion neutrons.

In the axial phase[8] a snow-plow model is often found adequate to compute the gross dynamics. This may be written as follows (refer Fig. 2a):

$$\frac{d}{dt}\left\{\pi\rho_0\left(c^2-1\right)a^2 z\frac{dz}{dt}\right\} = \frac{\mu I^2}{4\pi}\ell nc \qquad (1)$$

where $c = b/a$.

With a coupled circuit equation:

$$\frac{d}{dt}\left\{\left[L_0+L\right]I\right\} = V_0 - \frac{\int_0^t Idt}{C_0} \qquad (2)$$

where V_0 is the initial voltage on C_0 and the tube inductance $L = \mu'(\ell nC)z$ where $\mu' = \mu/2\pi$.

These two equations may be written in the non-dimensionalised form:

Phase: axial phase (AI):

$$\text{Motion:} \quad \frac{d^2\zeta}{d\tau^2} = \frac{\alpha^2\iota^2 - \left[\frac{d\zeta}{d\tau}\right]^2}{\zeta} \qquad (3)$$

$$\text{Circuit:} \quad \frac{d\iota}{d\tau} = \frac{1 - \int \iota d\tau - \beta\iota\frac{d\zeta}{d\tau}}{1 + \beta\zeta} \qquad (4)$$

where $\tau = t/t_0$, $\zeta = z/z_0$, $\iota = I/I_0$ [with $t_0 = \sqrt{(L_0C_0)}$, $I_0 = V_0/\sqrt{(L_0/C_0)}$] are the normalised time, distance and current. The normalisation reveals that besides the electrical circuit characteristic time of t_0, the characteristic tube length of z_0 and the characteristic electrical amplitude of I_0 there is another characteristic time, defined as the axial transit time of t_a given in the scaling parameter α where

$$\alpha = t_0/t_a \quad \text{and} \quad t_a = 2\pi\left[\frac{(c^2-1)}{\mu\ell nc}\right]^{1/2}\left[\frac{z_0\rho_0}{(I_0/a)}\right]^{1/2}$$

The scaling parameter β is

$$\beta = \frac{L_a}{L_0}$$

where L_a is the maximum tube inductance in the axial phase with $L_a = \mu'(\ell nc)z_0$.

We note that the scaling parameter α may be used in a consideration of the matching of the electrical time t_0 with the axial transit time t_a and β may be used in a consideration of matching the tube maximum inductance (axial phase) with the external inductance.

The axial phase tube voltage may also be written in normalised form:

$$v = \beta\left[\zeta\frac{d\iota}{d\tau} + \iota\frac{d\zeta}{d\tau}\right] \qquad (5)$$

For the radial implosion phase an elongating pinch (length z_f) may be modeled with a plasma slug layer[8] bounded by a radially inward moving shock front (position r_s) and an inward moving magnetic piston (position r_p)

pushing the layer radially onto the axis (refer Fig. 2b). The equations developed for this phase may be written in this form:

Radial phase:

radial shock motion: $$\frac{dr_s}{dt} = -\left[\frac{\mu_0(\gamma+1)}{\rho_0}\right]^{\frac{1}{2}} \frac{I}{4\pi r_p} \tag{6}$$

axial shock elongation motion: $$\frac{dz_f}{dt} = -\left[\frac{2}{\gamma+1}\right]\frac{dr_s}{dt} \tag{7}$$

radial piston motion:

$$\frac{dr_p}{dt} = \frac{\frac{2}{\gamma+1}\frac{r_s}{r_p}\frac{dr_s}{dt} - \frac{r_p}{\gamma I}\left[1-\frac{r_s^2}{r_p^2}\right]\frac{dI}{dt} - \frac{1}{\gamma+1}\frac{r_p}{z_f}\left[1-\frac{r_s^2}{r_p^2}\right]\frac{dz_f}{dt}}{\left\{\left[\frac{\gamma-1}{\gamma}\right] + \frac{1}{\gamma}\left[\frac{r_s}{r_p}\right]^2\right\}} \tag{8}$$

circuit equation:

$$\left\{L_0+\mu'\left[\ell nc\right]z_0 + \mu'\left[\ell n\frac{b}{r_p}\right]z_f\right\}\frac{dI}{dt} + I\mu'\ell n\frac{b}{r_p}\frac{dz_f}{dt}$$

$$- I\mu'\frac{z_f}{r_p}\frac{dr_p}{dt} = V_0 - \frac{\int I dt}{C_0} \tag{9}$$

These equations may be normalised into the following form; where lengths in this phase are normalised to a for example:

$$\kappa_s = r_s/a, \qquad \kappa_p = r_p/a, \qquad \zeta_f = z_f/a$$

Phase 2: Radial phase (RI)

Radial shock: $$\frac{d\kappa_s}{d\tau} = -\frac{\alpha\alpha_1\iota}{\kappa_p} \tag{10}$$

Axial shock: $$\frac{d\zeta_f}{d\tau} = -\left[\frac{2}{\gamma+1}\right]\frac{d\kappa_s}{d\tau} \tag{11}$$

Radial piston:

$$\frac{d\kappa_p}{d\tau} = \frac{\left(\frac{2}{\gamma+1}\right)\frac{\kappa_s}{\kappa_p}\frac{d\kappa_s}{d\tau} - \frac{1}{\gamma}\frac{\kappa_p}{\iota}\left[1-\frac{\kappa_s^2}{\kappa_p^2}\right]\frac{d\iota}{d\tau} - \left(\frac{1}{\gamma+1}\right)\frac{\kappa_p}{\zeta_f}\left[1-\frac{\kappa_s^2}{\kappa_p^2}\right]\frac{d\zeta_f}{d\tau}}{\left(\frac{\gamma-1}{\gamma}\right) + \left(\frac{1}{\gamma}\right)\left(\frac{\kappa_s^2}{\kappa_p^2}\right)} \tag{12}$$

Circuit: $$\frac{d\iota}{d\tau} = \frac{1 - \int \iota d\tau + \beta_f \frac{\iota\zeta_f}{\kappa_p}\frac{d\kappa_p}{d\tau} + \beta_f\left(\ell n\frac{\kappa_p}{c}\right)\iota\frac{d\zeta_f}{d\tau}}{1 + \beta - \beta_f\left(\ell n\frac{\kappa_p}{c}\right)\zeta_f} \tag{13}$$

where $\beta_f = \beta/(F\ell nc)$ and $F = z_0/a$ and

$$\alpha_1 = \left[(\gamma+1)(c^2-1)\right]^{1/2} F/[2\ell nc] .$$

The scaling parameter α_1 is also identified as $\alpha_1 = t_a/t_p$ where t_p is the characteristic radial collapse or pinch time of:

$$t_p = \frac{4\pi}{[\mu_0(\gamma+1)]^{1/2}} \frac{a\rho_0^{1/2}}{(I_0/a)}$$

Tube voltage may be written in non-dimensional form as

$$v = \left[\beta-\beta_f\left(\ell n\frac{\kappa_p}{c}\right)\zeta_f\right]\frac{d\iota}{d\tau} - \beta_f\iota\left[\frac{\zeta_f}{\kappa_p}\frac{d\kappa_p}{d\tau} + \left(\ell n\frac{\kappa_p}{c}\right)\frac{d\zeta_f}{d\tau}\right] \tag{14}$$

where the tube voltage consists of 2 terms, the first being the product of tube inductance with rate of change of current and the second is the product of current with rate of change of position. Approaching the densest phase both the radial and axial speed are of the order of 20 cm/μs and in particular the radial speed term i.e. the term with the factor $d\kappa_p/d\tau$ in equation (14) tends to dominate the voltage because of the small value of κ_p in the denominator. This term in dimensional form is $\mu' I z_f [dr_p/dt]/r_p$ and for values typical of a small plasma focus with $I = 1.5\times10^5$, $z_f = 10^{-2}$, $r_p = 10^{-3}$, $dr_p/dt = 2.5\times10^5$, this contribution to the tube voltage is typically 75 kV so that the inductance voltage due to the radial collapse of the current sheet may be used to explain the observed voltage spike during focus.

In order to model the observed subsequent drop in the voltage spike it is necessary to go on to a third phase, the elongating large plasma column

phase. Following the maximum compression, experimental observations show that the plasma column breaks up into a large volume plasma. It is a characteristic of shadowgraphs taken at this time that no plasma column is visible indicating that for the purpose of modeling one may take as a first approximation the current path to be large and uniformly spread out with the current path linking the anode to the moving current sheet flowing uniformly in a column of radius a. This is distinct from the case of phase 1 or phase 2 where all current paths are thin and indicated by a single arrow. In this model we also assume that phase 2 moves instantaneously into phase 3. Although this must be considered a deficiency of this model it is not too far (from the viewpoint of gross dynamics), from experimental observations in which the transition from phase 2 to phase 3 is astonishingly rapid particularly for small machines.

For this phase the two governing equations in non-dimensional form are:

Phase 3: Elongating large column phase (RAI):

$$\text{Elongating Motion:}\quad \frac{d^2\zeta}{d\tau^2} = \frac{\alpha^2\iota^2 L_1 - h\left[\frac{d\zeta}{d\tau}\right]^2}{1 + h(\zeta-1)} \tag{15}$$

where $h = c^2/(c^2-1)$, $L_1 = \left(\ell nc + \frac{1}{4}\right)/\ell nc$

$$\text{Circuit:}\quad \frac{d\iota}{d\tau} = \frac{1 - \int \iota d\tau - \beta\iota\frac{d\zeta}{d\tau}L_2}{1 + \beta + \beta(\zeta-1)L_2} \tag{16}$$

where $L_2 = \left(\ell nc+\frac{1}{4}\right)/\ell nc$.

In this phase the lengths are normalised to z_0, e.g. $\zeta = z/z_0$, and the voltage recovery, i.e. voltage drop back to small values typically several kV may be obtained from the inductive voltage expression:

$$v = \beta\left[1 + \left(1+\frac{1}{4\ell nc}\right)\left(\zeta-1\right)\right]\frac{d\iota}{d\tau} + \beta\left(1+\frac{1}{4\ell nc}\right)\iota\frac{d\zeta}{d\tau} \tag{17}$$

Solution

The two governing equations of phase 1, i.e. equations (3) and (4) are solved by numerical integration for the two variables ι and ζ, using linear approximation amongst the three quantities $\int\iota d\tau$, ι and $d\iota/d\tau$ and amongst the three quantities ζ, $d\zeta/d\tau$ and $d^2\zeta/d\tau^2$.

To start the integration we may use the following starting point:

$$(\tau)_0 = 0, \quad \left(\int d\tau\right)_0 = 0, \quad (\iota)_0 = 0, \quad \left(\frac{d\iota}{d\tau}\right)_0 = 1$$

$$(\zeta)_0 = 0, \quad \left(\frac{d\zeta}{d\tau}\right)_0 = 0, \quad \left(\frac{d^2\zeta}{d\tau^2}\right)_0 = \alpha\sqrt{2/3}$$

We increment time, by a small amount ($\Delta\tau$) typically 0.001, and we may use linear approximation to generate $(\int \iota d\tau)_{n+1}$ and $(\iota)_{n+1}$ from $\left(\frac{d\iota}{d\tau}\right)_n$, and $(\zeta)_{n+1}$ and $\left(\frac{d\zeta}{d\tau}\right)_{n+1}$ from $(d^2\zeta/d\tau^2)_n$, thus:

$$\left(\int \iota d\tau\right)_{n+1} = \left(\int \iota d\tau\right)_n + (\iota)_n(\Delta\tau) + \frac{1}{2}\left(\frac{d\iota}{d\tau}\right)_n (\Delta\tau)^2$$

$$(\iota)_{n+1} = (\iota)_n + \left(\frac{d\iota}{d\tau}\right)_n \Delta\tau$$

Similarly

$$(\zeta)_{n+1} = (\zeta)_n + \left(\frac{d\zeta}{d\tau}\right)_n (\Delta\tau) + \frac{1}{2}\left(\frac{d^2\zeta}{d\tau^2}\right)_n (\Delta\tau)^2$$

$$\left(\frac{d\zeta}{d\tau}\right)_{n+1} = \left(\frac{d\zeta}{d\tau}\right)_n + \left(\frac{d^2\zeta}{d\tau^2}\right)_n (\Delta\tau)$$

and then use the governing equations (3) and (4) and the newly evaluated $(\int \iota d\tau)_{n+1}$, $\iota_{n+18}, \zeta_{n+1}$ and $(d\zeta/d\tau)_{n+1}$ to generate the next values of the second order changes namely $(d^2\zeta/d\tau^2)_{n+1}$ and $\left(\frac{d\iota}{d\tau}\right)_{n+1}$. At every step equation (5) is also used to evaluate the voltage ν. This phase is integrated until $\zeta = 1$.

For phase 2, the four governing equations i.e. (10), (11), (12) and (13) are used to obtain the 4 variables κ_s, κ_p, ζ_p and ι.

To start the integration of this radial phase, we use as starting values the following final values of phase 1: τ, $\int \iota d\tau$, ι and $\frac{d\iota}{d\tau}$. Other initializing values are, $\kappa_s = 1$, $\kappa_p = 1$, $\zeta_f = 0$, taking care that for the first point, the last term in the numerator of equation (12) is put to 0, as otherwise a computation would not proceed since $\zeta_f = 0$ at the first point. The time increment $\Delta\tau$ for this and other radial phases is taken as 0.00002.

The integration proceeds, using linear approximation described earlier, until $\kappa_s = 0$ at which point the minimum κ_p is achieved. At each step the voltage ν is also evaluated using equation (14).

For phase 3, the two governing equations, i.e. equations (15) and (16) are used to solve for ζ and ι.

To start the integration of this phase we use as starting values the following final values of phase 2; τ, $\int \iota d\tau$, ι and $\zeta = 1 + (\zeta_f/F)$

(renormalising the value of ζ_f to z_0). We also use as starting value the final value of $d\zeta/d\tau$ of axial phase AI.

The integration proceeds using linear approximation until $\zeta = 1.3$, say, z_1/z_0. Voltage ν is computed from equation (17).

As an example computations are carried out for the UNU/ICTP PFF which has been designed with the following parameters:

$C_0 = 30\times10^{-6}$ F, $L_0 = 110\times10^{-9}$ H, $v_0 = 15\times10^{3}$ V
$a = 0.95\times10^{-2}$ m, $b = 3.2\times10^{-2}$ m, $z_0 = 0.16$ m
$\rho_0 = 0.21\times10^{-3}$ kg^{-3} (1 torr D_2) giving
$I_0 = 2.5\times10^{5}$ A, $c = 3.37$, $F = 16.8$
$t_0 = 1.8\times10^{-6}$ s, $t_a = 1.45\times10^{-6}$ s $t_p = 35.8\times10^{-9}$ s

The scaling parameters are
$\alpha = t_0/t_a = 1.26$ $\beta = L_a/L_0 = 0.36$
$\alpha_1 = t_a/t_p = 40.04$, $\beta_F = 0.017$.

The results are shown in Fig. 4; showing the axial trajectory ζ, the current ι with its characteristic current dip and very sharp voltage spike during the radial collapse phase. Fig. 5 shows the radial trajectories and speeds.

Thus the dynamics computation package of the UNU/ICTP PFF is able to very simply model the major current, voltage and trajectory characteristics of the plasma focus. This package may be used to design effective focus machines from any chosen point of view e.g. kinetic energy during collapse, thermal energy of dense phase, or from the point of view of magnetic energy storage or voltage spike.

To illustrate the usefulness of this simple model a development during the recent December 1989 - May 1990 training programme will be briefly described.

Dynamics of the cascading plasma focus - an invention of a Training Programme

In this recent study shadowgraph[7] were taken of a flat disc target placed near and downstream of the anode of a plasma focus in order to assess whether the target disturbed the focusing dynamics. It was found that, when the target was at a distance from the anode greater than the anode radius, there was no disturbance on the dynamics of the focus proper (see Fig. 6). However it was further observed (see Fig. 7) that after the focus proper the current sheet moved axially until it reached the disc target whereupon the current sheet propagated around the disc target and pinched or focused again beyond it. It was as though the disc target had become a new "anode". The

question then arose naturally whether a series of separated discs placed downstream of the main anode could each become sequentially a new anode to the advancing plasma current sheet resulting in a series of sequential plasma focus. Such a device may be called a cascade or a cascading plasma focus.

A model is set up for the case of two discs to produce three cascading focus events. As described earlier each focus event is divided into three parts: an axial run-down phase (denoted by A), a radial collapse phase (denoted by R) and a large column elongation phase or radial extension phase (denoted by RA). There are altogether nine phases (AI, RI, RAI, AII, RII, RAII, AIII, RIII, RAIII) in this model with two auxiliary disc anodes as depicted in Fig. 8.

The equations for the first focus event are exactly as already described for the 3 phases of the plasma focus AI, RI and RAI. The only difference is in the termination of phase 3, where for the case of the cascading focus we integrate until $\zeta = \zeta_1$ where $\zeta_1 = z_1/z_0$ is the starting position of the first auxiliary disc anode (see Fig. 8). We continue with the modeling of the remaining phases.

Phase 4 - AII:

The two governing equations of this axial phase are:

$$\text{Motion:} \quad \frac{d^2\zeta}{d\tau^2} = \frac{\alpha^2\iota^2 L_3 - h_1\left(\frac{d\zeta}{d\tau}\right)^2}{1 + h_1(\zeta-1)} \tag{18}$$

$$\text{where } L_3 = \frac{\ell nc_1}{\ell nc}, \quad \text{and } h_1 = \frac{c^2-d_1^2}{c^2-1};\ d_1 = a_1/a \text{ and } c_1 = c/d_1.$$

$$\text{Circuit:} \quad \frac{d\iota}{d\tau} = \frac{1 - \int \iota d\tau - \beta\iota\frac{d\zeta_i}{d\tau}L_4}{1 + \beta + \beta L_3(\zeta-1) + \frac{\beta}{4\ell nc}(\zeta_i-1)} \tag{19}$$

To start the integration of this phase we use as starting values the following final values of phase 3: τ, $\int \iota d\tau$, ζ, $d\zeta/d\tau$.

The integration proceeds until $\zeta = \zeta_2 = z_2/z_0$.

Phase 5 - RII:

The 4 governing equations of this radial phase are:

$$\text{Radial shock:} \quad \frac{d\kappa_s}{d\tau} = -\frac{\alpha\alpha_1\iota}{\kappa_p} \tag{20}$$

Axial elongation: $$\frac{d\zeta_f}{d\tau} = -\left(\frac{2}{\gamma+1}\right)\frac{d\kappa_s}{d\tau} \tag{21}$$

Radial piston:

$$\frac{d\kappa_p}{d\tau} = \frac{\left(\frac{2}{\gamma+1}\right)\frac{\kappa_s}{\kappa_p}\frac{d\kappa_s}{d\tau} - \frac{1}{\gamma}\frac{\kappa_p}{\iota}\left(1-\frac{\kappa_s^2}{\kappa_p^2}\right)\frac{d\iota}{d\tau} - \left(\frac{1}{\gamma+1}\right)\frac{\kappa_p}{\zeta_f}\left(1-\frac{\kappa_s^2}{\kappa_p^2}\right)\frac{d\zeta_f}{d\tau}}{\left(\frac{\gamma-1}{\gamma}\right) + \left(\frac{1}{\gamma}\right)\left(\frac{\kappa_s^2}{\kappa_p^2}\right)} \tag{22}$$

Circuit: $$\frac{d\iota}{d\tau} = \frac{1 - \int\iota d\tau + \beta_f\frac{\iota\zeta_f}{\kappa_p}\frac{d\kappa_p}{d\tau} + \beta_f\left(\ell n\frac{\kappa_p}{c}\right)\iota\frac{d\zeta_f}{d\tau}}{1 + \beta - \beta_f\left(\ell n\frac{\kappa_p}{c}\right)\zeta_f + \beta L_3(\zeta_2-1) + \frac{\beta}{4\ell nc}(\zeta_1-1)} \tag{23}$$

To start the integration of this radial phase we use as starting values the following final values of phase 4: τ, $\int\iota d\tau$, ι and $d\iota/d\tau$. Other initialization values are: $\kappa_s = d_1$, $\kappa_p = d_1$, $\zeta_f = 0$.

The integration proceeds until $\kappa_s = 0$ at which point the minimum κ_p is achieved.

Phase 6 - RAII:

The 2 governing equations of this axial phase are:

Motion: $$\frac{d^2\zeta}{d\tau^2} = \frac{\alpha^2\iota^2 L_5 - h\left(\frac{d\zeta}{d\tau}\right)^2}{1 + h_1(\zeta_2-1) + h(\zeta-\zeta_2)} \tag{24}$$

Circuit: $$\frac{d\iota}{d\tau} = \frac{1 - \int\iota d\tau - \beta\iota\frac{d\zeta}{d\tau}L_4}{1 + \beta + \beta L_3(\zeta-1) + \left(\frac{\beta}{4\ell nc}\right)(\zeta-\zeta_2+\zeta_1-1)} \tag{25}$$

where $L_4 = (\ell nc_1+\frac{1}{4})/(\ell nc)$.

To start the integration of this phase we use as starting values the following final values of phase 5: τ, $\int\iota d\tau$, ι and $\zeta = \zeta_2 + \zeta_f/F$. We also use as starting value the final value of $d\zeta/d\tau$ of axial phase AII.

The integration proceeds until $\zeta = \zeta_3 = z_3/z_0$.

Phase 7 - AIII:

The two governing equations of this axial phase are:

$$\text{Motion:}\quad \frac{d^2\zeta}{d\tau^2} = \frac{\alpha^2\iota^2 L_6 - h_2\left[\frac{d\zeta}{d\tau}\right]^2}{1 + h_1^2(\zeta-1) + h_2(\zeta-\zeta_2)} \tag{26}$$

$$\text{Circuit:}\quad \frac{d\iota}{d\tau} = \frac{1 - \int\iota d\tau - \beta\iota\frac{d\zeta}{d\tau}L_6}{1+\beta+\beta L_3(\zeta_2-1)+\left(\frac{\beta}{4\ell nc}\right)(\zeta_1-1+\zeta_3-\zeta_2)+\beta L_6(\zeta-\zeta_2)} \tag{27}$$

where $L_6 = \ell nc_2/\ell nc$, $h_2 = \dfrac{c^2-d_2^2}{c^2-1}$ and $d_2 = \dfrac{a_2}{a}$.

To start the integration of this phase we use as starting values the following final values of phase 6: τ, $\int\iota d\tau$, ι, ζ and $d\zeta/d\tau$.

The integration proceeds until $\zeta = \zeta_4 = z_4/z_0$.

Phase 8 - RIII:

The four governing equations of this radial phase are:

$$\text{Radial shock:}\quad \frac{d\kappa_s}{d\tau} = -\frac{\alpha\alpha_1\iota}{\kappa_p} \tag{28}$$

$$\text{Axial elongation:}\quad \frac{d\zeta_f}{d\tau} = -\left(\frac{2}{\gamma+1}\right)\frac{d\kappa_s}{d\tau} \tag{29}$$

Radial piston:

$$\frac{d\kappa_p}{d\tau} = \frac{\left(\frac{2}{\gamma+1}\right)\frac{\kappa_s}{\kappa_p}\frac{d\kappa_s}{d\tau} - \frac{1}{\gamma}\frac{\kappa_p}{\iota}\left(1-\frac{\kappa_s^2}{\kappa_p^2}\right)\frac{d\iota}{d\tau} - \left(\frac{1}{\gamma+1}\right)\frac{\kappa_p}{\zeta_f}\left(1-\frac{\kappa_s^2}{\kappa_p^2}\right)\frac{d\zeta_f}{d\tau}}{\left(\frac{\gamma-1}{\gamma}\right) + \left(\frac{1}{\gamma}\right)\left(\frac{\kappa_s^2}{\kappa_p^2}\right)} \tag{30}$$

$$\text{Circuit:}\quad \frac{d\iota}{d\tau} = \frac{1 - \int\iota d\tau + \beta_f\frac{\iota\zeta_f}{\kappa_p}\frac{d\kappa_p}{d\tau} + \beta_f\left(\ell n\frac{\kappa_p}{c}\right)\iota\frac{d\zeta_f}{d\tau}}{1+\beta-\beta_f\left(\ell n\frac{\kappa_p}{c}\right)\zeta_f+\beta L_3(\zeta_2-1)+\beta L_6(\zeta_4-\zeta_2)+\frac{\beta}{4\ell nc}(\zeta_3-\zeta_2+\zeta_1-1)} \tag{31}$$

To start the integration of this radial phase we use as starting values the following final values of phase 7: τ, $\int\iota d\tau$, ι and $d\iota/d\tau$. Other initialization values are: $\kappa_s = d_2$, $\kappa_p = d_2$ and $\zeta_f = 0$.

The integration proceeds until $\kappa_s = 0$ at which point the minimum κ_p is achieved.

Phase 9 - RAIII:

The two governing equations of this axial phase are:

$$\text{Motion:} \quad \frac{d^2\zeta}{d\tau^2} = \frac{\alpha^2 \iota^2 L_7 - h\left(\frac{d\zeta}{d\tau}\right)^2}{1 + h_1(\zeta_2 - 1) + h_2(\zeta_4 - \zeta_2) + h(\zeta - \zeta_4)} \tag{32}$$

Circuit:

$$\frac{d\iota}{d\tau} = \frac{1 - \int \iota d\tau - \beta \iota L_8 \frac{d\zeta}{d\tau}}{1+\beta+\beta L_3(\zeta_2 - 1)+\beta L_6(\zeta - \zeta_2)+\left(\frac{\beta}{4\ell nc}\right)(\zeta - \zeta_4 + \zeta_3 - \zeta_2 + \zeta_1 - 1)} \tag{33}$$

where $L_7 = \dfrac{\left(\ell nc_2 + \frac{1}{4}\right)}{\ell nc}$

To start the integration of this phase we use as starting values the following final values of phase 8: τ, $\int \iota d\tau$, ι and $\zeta = \zeta_4 + \zeta_f/F$. We also use as starting value the final value of $d\zeta/d\tau$ of axial phase AIII.

The integration proceeds until $\zeta = \zeta_5 = z_5/z_0$ where z_5 may be taken as $z_5 = z_4 + z_4 - z_3$.

Voltage equations

Besides the measurement of current, another common and informative measurement that may readily be made of the plasma focus is the voltage V_p across the input of the focus. This may be computed noting that:

$$V_p = \frac{d}{dt}\left[L_p I\right] . \tag{34}$$

where we have assumed a purely inductive model.

These are written, for each of the nine phases, in normalized form with $\nu = V_p/V_0$, where V_0 = initial voltage on capacitor, as follows:

$$\text{Phase 1:} \quad \nu = \beta\left[\zeta \frac{d\iota}{d\tau} + \iota \frac{d\zeta}{d\tau}\right] \tag{35}$$

It is seen that the tube voltage contains two terms, the first being the product of displacement and rate of change of current and the second the product of current and speed. As the current peaks and stays near constant, the second, which we call, speed term dominates.

$$\text{Phase 2:}\quad \nu = \left[\beta-\beta_f\left(\ell n\frac{\kappa_p}{c}\right)\zeta_f\right]\frac{d\iota}{d\tau} - \beta_f\iota\left[\frac{\zeta_f}{\kappa_p}\frac{d\kappa_p}{d\tau}+\left(\ell n\frac{\kappa_p}{c}\right)\frac{d\zeta_f}{d\tau}\right] \tag{36}$$

In the radial phase, the form of the voltage equation contains the two terms with the same dependence as in the axial phase. But in the radial phase the speed term has a much greater magnitude especially the term involving the piston speed $d\kappa_p/d\tau$ since this term has κ_p in the denominator and this has a larger effect as κ_p goes to smaller values.

$$\text{Phase 3:}\quad \nu = \beta\left[1 + \left(1+\frac{1}{4\ell nc}\right)\left(\zeta-1\right)\right]\frac{d\iota}{d\tau} + \beta\left(1+\frac{1}{4\ell nc}\right)\iota\frac{d\zeta}{d\tau} \tag{37}$$

$$\text{Phase 4:}\quad \nu = \beta\left\{\left[1 + L_3\left(\zeta-1\right) + \left(\frac{1}{4\ell nc}\right)\left(\zeta_1-1\right)\right]\frac{d\iota}{d\tau} + L_3\iota\frac{d\zeta}{d\tau}\right\} \tag{38}$$

$$\text{Phase 5:}\quad \nu = \left\{\beta\left[1 + L_3\left(\zeta_2-1\right) + \left(\frac{1}{4\ell nc}\right)\left(\zeta_1-1\right)\right] - \beta_f\left(\ell n\frac{\kappa_p}{c}\right)\zeta_f\right\}\frac{d\iota}{d\tau}$$
$$- \beta_f\iota\left[\left(\ell n\frac{\kappa_p}{c}\right)\frac{d\zeta_f}{d\tau} + \frac{\zeta_F}{\kappa_p}\frac{d\kappa_p}{d\tau}\right] \tag{39}$$

$$\text{Phase 6:}\quad \nu = \beta\left[1 + L_3\left(\zeta-1\right) + \frac{1}{4\ell nc}\left(\zeta-\zeta_2+\zeta_1-1\right)\right]\frac{d\iota}{d\tau} + \beta\iota\left(L_3 + \frac{1}{4\ell nc}\right)\frac{d\zeta}{d\tau} \tag{40}$$

$$\text{Phase 7:}\quad \nu = \beta\left[1 + L_3\left(\zeta_2-1\right) + \left(\frac{1}{4\ell nc}\right)\left(\zeta_1-1+\zeta_3-\zeta_2\right) + L_6\left(\zeta-\zeta_2\right)\right]\frac{d\iota}{d\tau}$$
$$+ L_6\beta\iota\frac{d\zeta}{d\tau} \tag{41}$$

$$\text{Phase 8:}\quad \nu = \left\{\beta\left[1 + L_3\left(\zeta_2-1\right) + L_6\left(\zeta_4-\zeta_2\right) + \left(\frac{1}{4\ell nc}\right)\left(\zeta_1-1+\zeta_3-\zeta_2\right)\right]\right.$$
$$\left. - \beta_f\left(\ell n\frac{\kappa_p}{c}\right)\zeta_f\right\}\frac{d\iota}{d\tau} - \beta_f\iota\left[\left(\ell n\frac{\kappa_p}{c}\right)\frac{d\zeta_f}{d\tau} + \frac{\zeta_f}{\kappa_p}\frac{d\kappa_p}{d\tau}\right] \tag{42}$$

$$\text{Phase 9:}\quad \nu = \beta\left[1 + L_3\left(\zeta_2-1\right) + L_6\left(\zeta-\zeta_2\right) + \frac{1}{4\ell nc}\left(\zeta-\zeta_4+\zeta_3-\zeta_2+\zeta_1-1\right)\right]\frac{d\iota}{d\tau}$$
$$+ \beta\iota\left(L_6 + \frac{1}{4\ell nc}\right)\frac{d\zeta}{d\tau} \tag{43}$$

Results

Computations were carried out using this model with a view of designing a cascading focus system based on the 3kJ plasma focus designated as the UNU/ICTP PFF.[4] The scaling parameters are α, β, γ, c, F, ζ_1, ζ_2, ζ_3, ζ_4, d_1 and d_2. In order to reduce the large number of possible combinations to arrive at a combination that will provide good focusing characteristic (large

voltage spike, significant current dip), for all 3 cascading focus events we note that the speed scaling[4] in both axial and radial phase is dependent on the factor $(I/a)/\sqrt{\rho_0}$, so that it is necessary to maintain the value of (I/a) during each of the cascade focusing events. Thus basically we adjust the scaling parameters from the values of the UNU/ICTP PFF so that the first focus of the cascade focus occurs earlier than the focus of the UNU/ICTP PFF. Also to maintain the value of (I/a), the auxiliary anodes are designed with radii a_1 and a_2 a little less than a.

Thus whereas the UNU/ICTP PFF was numerically optimized with the parameters $\alpha = 1.26$, $\beta = 0.36$, $F = 16.8$, $c = 3.37$ and $\gamma = 5/3$; the cascading plasma focus is redesigned with $\alpha = 1.7$, $\beta = 0.27$, $F = 12$, $c = 3.37$, $\gamma = 5/3$ and with $\zeta_1 = 1.083$, $\zeta_2 = 1.167$, $\zeta_3 = 1.25$, $\zeta_4 = 1.333$, $d_1 = 0.85$ and $d_2 = 0.7$.

These parameters correspond to the cascading plasma focus operating with the following conditions: $V_0 = 15$ kV, $C_0 = 30$ μF, $L_0 = 110$ nH, $a = 1$ cm, $z_0 = 12$ cm, $z_1 = 13$ cm, $z_2 = 14$ cm, $z_3 = 15$ cm, $z_4 = 16$ cm, $a_2 = 0.85$ cm, $a_3 = 0.7$ cm and pressure = 1 torr in deuterium. (Due to current and mass shedding[4], not included in the present modeling, the actual operational pressure would be closer to 3 torr).

The 9-phase model was computed with the above scaling parameters, using equations (3)-(4) for phase 1, equations (10)-(13) for phase 2, equations (15)-(16) for phase 3, equations (18)-(19) for phase 4, equations (20)-(23) for phase 5, equations (24)-(25) for phase 6, equations (26)-(27) for phase 7, equations (28)-(31) for phase 8 and equations (32)-(33) for phase 9. The voltage across the focus tube was also computed for each phase using equations (35)-(43).

The results are presented in Figs. 9-11. In Fig. 9 are presented the current ι and voltage ν waveforms. The current reaches a peak value of 0.787 at $\tau = 1.335$ at the end of phase 1 just before the start of phase 2 (see Fig. 10). During this phase 2, it drops to 0.765 or by 2.8% of the peak value, with the steepest part of the drop occurring at $\tau = 1.3515$. This steep drop of current corresponds to the peak voltage which spikes up to a value of $\nu = 8.28$ corresponding to a piston speed of 5.9 (see Fig. 11a) scaled to characteristic speed of z_0/t_0. These three effects, namely the current dip, the voltage spike (contributed mainly by the term $(d\kappa_p/d\tau)/\kappa_p$ [see voltage equation (36)] and the fast radial piston speed are the "classic" characteristics of a plasma focus. During this radial phase a further, though smaller, contribution to the voltage spike [see equation (36)] is the high axial elongation speed of up to 12.6.

After the radial phase RI, our model allows for a radial extension phase

RAI during which the current remains practically constant at I = 0.7648 (see Fig. 9) dropping gradually to 0.757. The tube voltage drops to a value of 0.347, slightly above the AI final value of 0.27. This higher value is due to the extra inductance term of $\frac{1}{4}\mu' z_f$ during the RA phase. The axial speed stays practically constant, see Fig. 10, at 1.23 only slightly higher than the final axial speed of phase 1. Phase RAI moves on to phase AII characterized by almost constant current, slightly lower tube voltage and slightly higher axial speed.

At the end of phase AII, the second focus event occurs with the current dipping noticeable by another 2.5% from 0.757 to 0.738 in a short time interval of 0.012 (see Fig. 9). The voltage spikes up to 9.14 at τ = 1.45 contributed mainly by the high piston speed. This radial collapse again has all three classic indication of a plasma focus. The phases RAII and AIII have similar characteristics as the earlier axial phases, almost constant current, tube voltage and axial speed.

At the end of phase AIII, the third focus event occurs during phase RIII this time with a current dip of 2.5% from 0.729 to 0.711 and a voltage spike of peak value 10.5 corresponding to a peak piston speed of 10.1 at τ = 1.55. This focus event also has all three characteristics of a strong plasma focus. Indeed the parameters having been adjusted so that this third focus in the cascading series occurs at τ = 1.55 and moreover with the relevant anode having a radius of 0.7 of the main anode, this assures that there is ample near-peak current so that the value of I/a_2 ensures the highest radial speed and largest voltage spike during RIII of all the three focus events.

Following this radial phase RIII, we follow the plasma dynamics through one more axial phase RAIII to bring the voltage down to the small values that characterizes an axial phase. The current further drops gradually during this phase.

Fig. 11a, 11b and 11c show the results of the computation on the radial phases RI, RII and RIII. These three graphs fill in the three gaps in Fig. 10. On an expanded time scale each of the three graphs of Fig. 11a, 11b and 11c shows the shock trajectory κ_s and the piston trajectory κ_p and the corresponding speed graphs $d\kappa_s/d\tau$ and $d\kappa_p/d\tau$ vs τ. Also displayed is the elongation speed $d\zeta_f/d\tau$.

In Fig. 11a showing results for the first of the radial phases, the plasma starts pinching at $\kappa_s = \kappa_p = 1$ at the time τ = 1.335. Up to τ = 1.347 the speeds $d\kappa_s/d\tau$, $d\kappa_p/d\tau$ and $d\zeta_f/d\tau$ have risen to values around 4 from initial values of about 1 (in a time interval of 0.012). But in the next smaller time interval of 0.003 from 1.347 to 1.350 the values of $d\kappa_s/d\tau$ and $d\zeta_f/d\tau$ have risen to over 16 and 12 respectively, whilst the value of $d\kappa_p/d\tau$

has risen to 9 and then drops sharply to zero in the very last instant as the radially imploding shock front goes on axis.

The very large voltage spike of RI of Fig. 9 is due to the large value attained by $d\kappa_p/d\tau$ in the small interval of 0.003 from 1.345 to 1.350, coupled to the decreasing value of κ_p during this short interval of time.

The feature of κ_p. κ_s and the speeds $d\kappa_s/d\tau$, $d\kappa_p/d\tau$ and $d\zeta_f/d\tau$ follow the same pattern for the other 2 radial phases RII and RIII.

It may be commented that the radial collapse speed and the voltage spike, say of RI, coming out of these computations are too large when compared with voltage measurements on a plasma focus. It would be correct to say that because the slug model assumes instantaneous signal communication between the shock front and piston this leads to the computed exceedingly large values. If we consider the communication delay due to finite small disturbance speed between the piston and shock front (of the order of 0.3 mm/μs or in the non-dimensionless units of these calculation 0.1 units of distance in 0.002 units of time) then, because in the slug model the piston pressure drives the shock front and the motion of the shock front creates volume for the piston to move into, a communication delay of 0.002 or 0.003 in time between the piston and shock front would mean that the shock front would at any instant feel the considerably smaller pressure of the piston at an earlier time and likewise the piston would feel the effect of the shock front at an earlier position. This delay effect if incorporated into the model would considerably slow down both the shock front and piston as they near the axis, and hence also reduce the voltage spike. Another mechanism which needs to be considered in this context is the different mass shedding factor in the axial and radial phases.

Operating the cascading focus in deuterium a neutron pulse may be expected with each focus. It may be necessary to use hollow auxiliary anodes i.e. with a hole in the centre in order not to disturb the deuteron beam-gas target mechanism responsible for a proportion of the fusion reaction in a plasma focus.

Conclusion

This paper has reviewed briefly the activities of the AAAPT in the past two years. The importance of training packages and their sub-systems is emphasized and it is pointed out that an experimental package should be supported with a theoretical/computational sub-packages. The example of the UNU/ICTP Plasma Fusion Facility is cited and a description of the plasma focus dynamics model is given demonstrating how such a model may be used to design the plasma focus and predict all the major dynamics and electro-dynamic behaviour of the focus. It is further demonstrated that this model

	UNU/ICTP PFF	EMST Flow Simulator	Nitrogen Laser System	Laser Shadowgraph System	Glow Discharge
Cairo, AL Azhar U.	X		X	X	
Jaipur, Rajathan U.	X•		X•		
Delhi, Delhi U.	X•		X•	X•	
Srinaga, SP Coll.			X		
Jakarta, LAPAN (Space research)		X•			
Yogyakarta, PPNY (nuclear research)	X				X
Islamabad, QIAU	X•+		X•	X•	
Port Harcourt, US&T	X•+		X•+	X•	
Njala, S. Leone, NUC	X•				
Songkla, PSU	X		X		

• Also used for M.Sc. and Ph.D. theses programme.

+ Have produced Ph.D./M.Sc. theses from these facilities.

Table 1. Facilities transferred as training packages

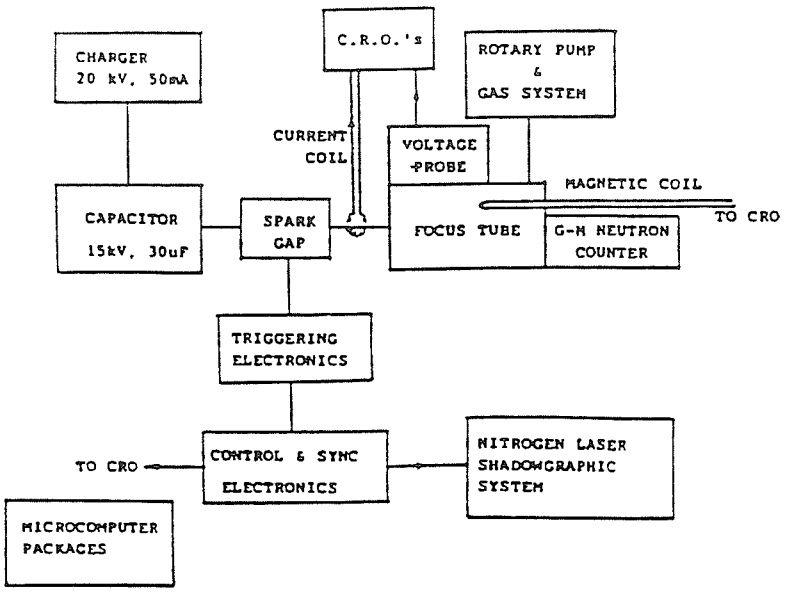

Fig.1 Sub-systems for the UNU/ICTP PLASMA FOCUS FACILITY

has helped in the invention of a new device called the cascading plasma focus resulting from a recent training programme. This is an indication that the AAAPT training programmes are not only cost effective but also have excellent research potential, particularly when the experiments are backed by effective computational models.

References

1. S. Lee and M.H.A. Hassan "Third World nuclear fusion programmes and South-South collaboration in plasma technology" in "Laser and Plasma Technology". Ed. C.S. Wong, S. Lee, B.C. Tan, A.C. Chew, K.S. Low and S.P. Moo, World Scientific, pg. 145-193 (1990).

2. "Beijing College on Plasma Physics: Diagnostics". Ed. by Shih-Tung Tsau and Yin-an Li, Procs, (1989)

3. S. Lee, "Training programmes for reseach transfer - experience and results", Review Lecture at 4th Tropical College on Applied Physics, Kuala Lumpur, Malaysia, May-June 1990.

4. S. Lee et. al., "A simple facility for the teaching of plasma dynamics and plasma nuclear fusion", American J. Phys. 56, 62 (1988).
S. Lee, "A plasma focus model yielding trajectory and structure" in "Radiation in Plasmas". Ed. B. McNamara, World Scientific Pub. Co., p. 967-977 (1984); also "Technology of the plasma focus" in "Laser and Plasma Technology", S. Lee et. al., World Scientific Pub. Co., p. 387-420 (1985).

5. A.J. Smith et. al., IEEE J. Quan. Elec. QE-23, 283 (1987).

6. S. Lee et. al., J. Fiz. Mal. 6, 165 (1985).

7. S. Lee et. al., J. Applied Phys. 65, 4133 (1989).

8. S. Lee, "Technology of a small plasma focus incorporating some experience with the UNU/ICTP PFF", Invited Lecture at Spring College on Plasma Physics; Procs. entitled "Small Plasma Physics Experiments". Ed. S. Lee and P.H. Sakanaka, World Scientific Oub. Co., (1990).

9. S. Lee, M.A. Alabraba, A.V. Gholap, S. Kumar, K.H. Kwek, M. Nisar, R.S. Rawat and J. Singh "Effect of targets on plasma focus dynamics". Accepted for publication by IEEE Trans. Plasma Science (1990).

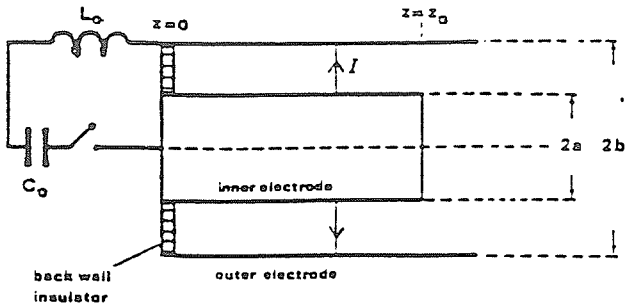

Fig. 2a Phase 1: axial acceleration phase

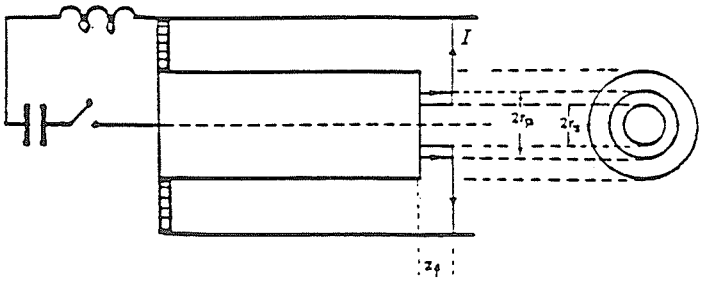

Fig. 2b Phase 2: radial compression phase

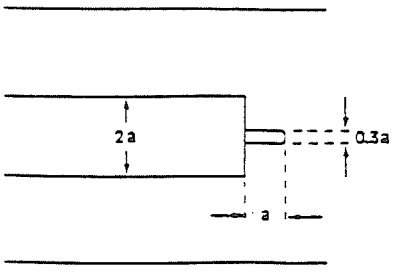

Fig. 3 Compressed column of the plasma focus

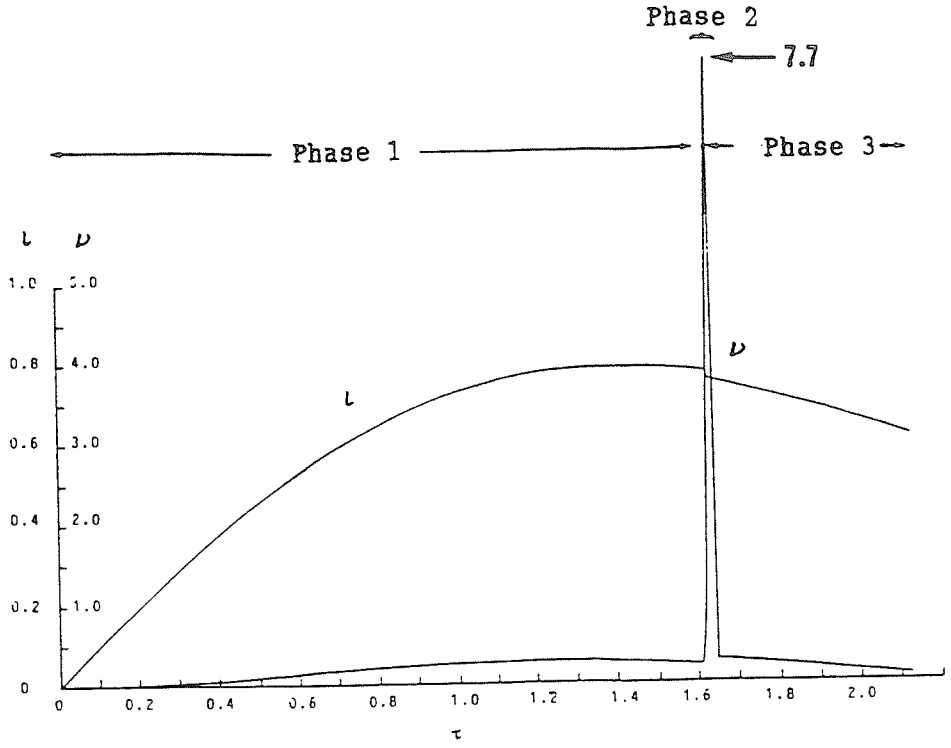

Fig. 4 Current ι and voltage ν for UNU/ICTP PFF with α = 1.26, β = 0.36, F = 16.8, c = 3.37, γ = 5/3.

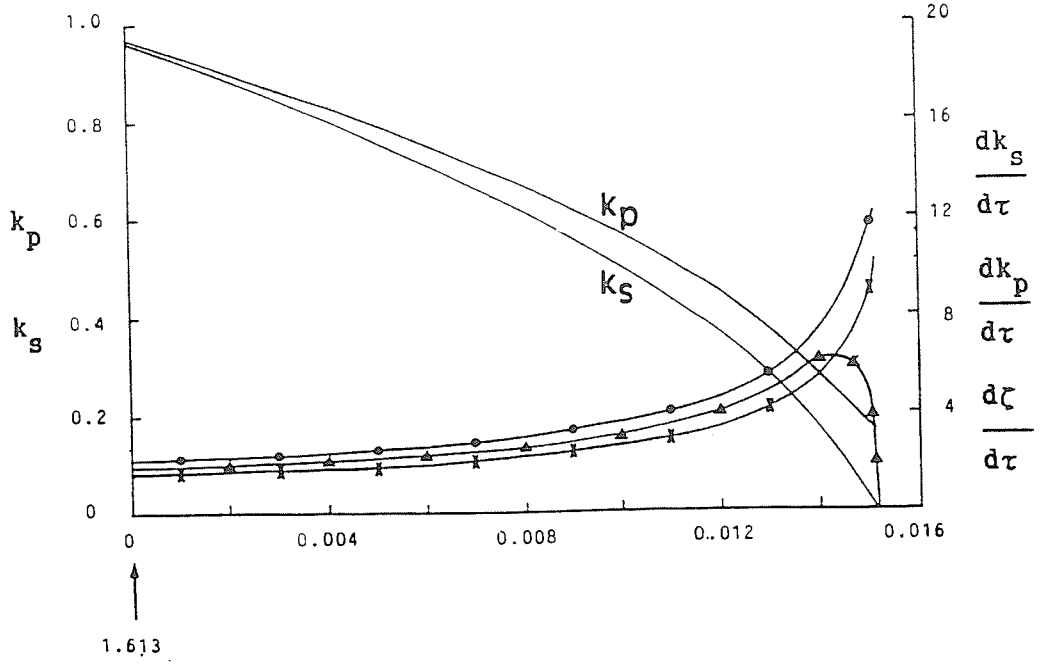

Fig. 5 Radial phase: Trajectories of phase 2 radial shock (k_s) and radial piston (k_p) for UNU/ICTP PFF. Also given are radial shock speed $dk_s/d\tau$ (●), radial piston speed $dk_p/d\tau$ (▲) and focus column elongation rate $d\zeta/d\tau$ (X).

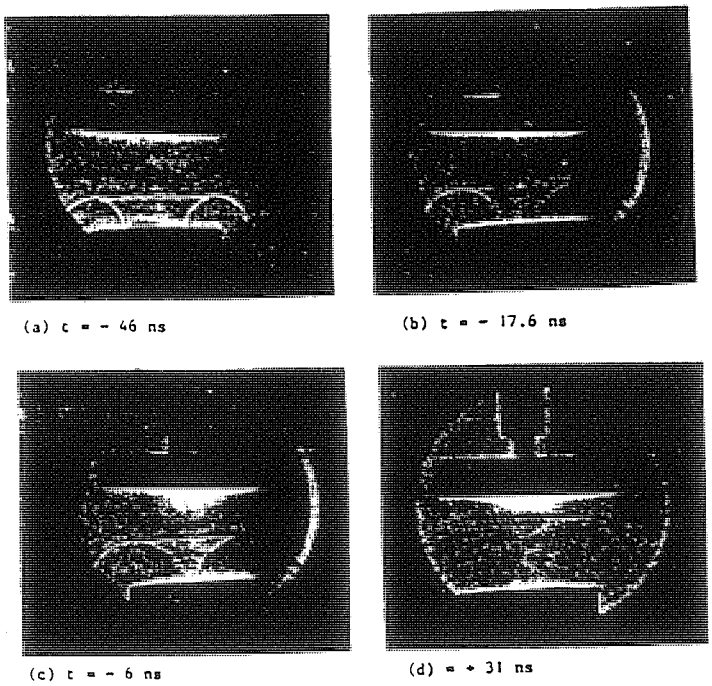

Fig. 6 Shadowgraphs of current sheet configuration before and after peak compression with a flat-target at a distance of 1.5 cm from anode face.

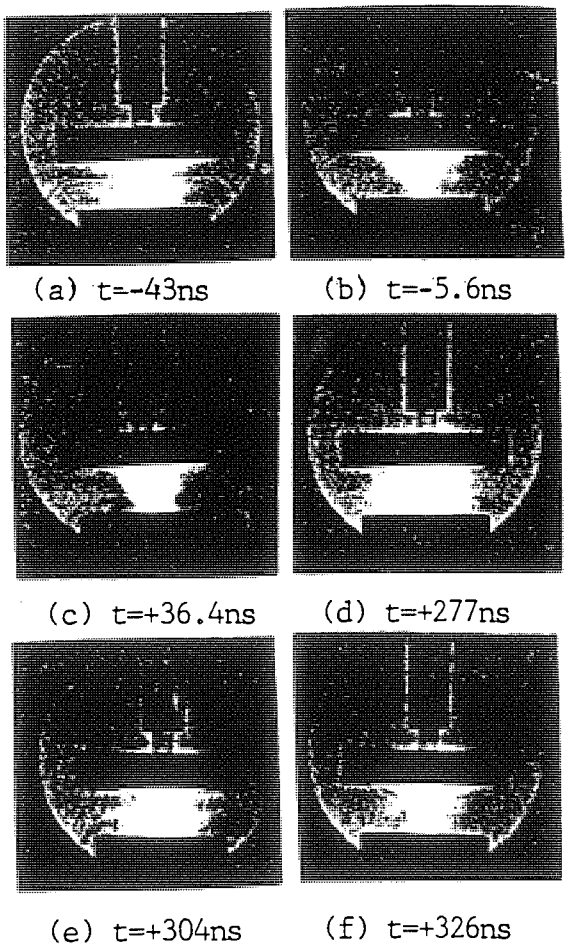

Fig. 7 Shadowgraphic sequence (composite) of current sheet configurations with the flat-target at a distance of 7 mm from the anode face.

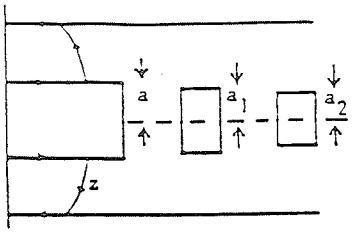

Phase 1: AI

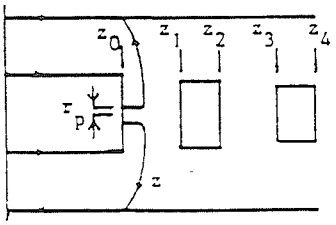

Phase 2: RI

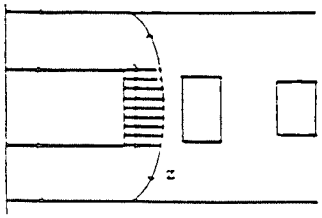

Phase 3: RAI

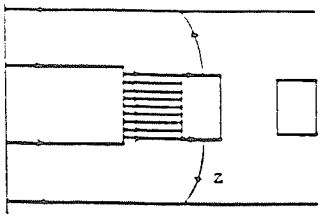

Phase 4: AII

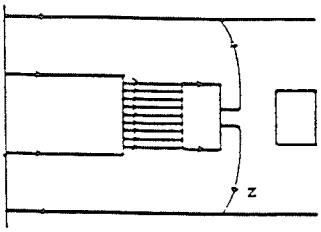

Phase 5: RII

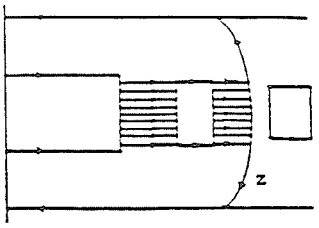

Phase 6: RAII

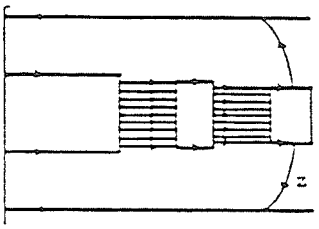

Phase 7: AIII

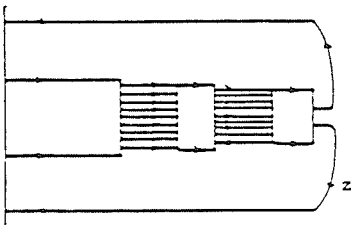

Phase 8: RIII

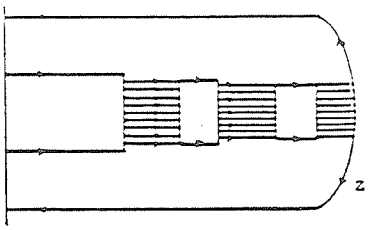

Phase 9: RAIII

Fig. 8: The 9 phases of the cascading plasma focus model.

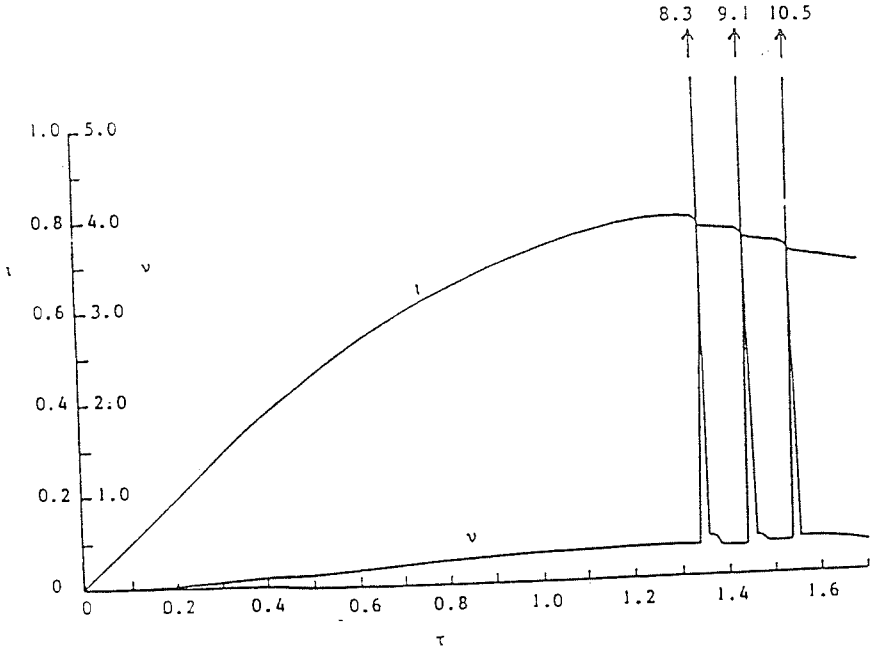

Fig. 9 : Current ι and voltage ν for cascade focus with $\alpha = 1.7$, $\beta = 0.27$, $F = 12$, $c = 3.37$, $\gamma = 5/3$, $\zeta_1 = 1.083$, $\zeta_2 = 1.167$, $\zeta_3 = 1.25$, $\zeta_4 = 1.333$, $d_1 = 0.85$ and $d_2 = 0.7$. (To help identify the 9 phases their time intervals are given here:

Phase 1 AI	:	$\tau = 0 - 1.335$
Phase 2 RI	:	$\tau = 1.335 - 1.352$ (first voltage spike)
Phase 3 RAI	:	$\tau = 1.352 - 1.369$
Phase 4 AII	:	$\tau = 1.369 - 1.437$
Phase 5 RII	:	$\tau = 1.437 - 1.449$ (second voltage spike)
Phase 6 RAII	:	$\tau = 1.449 - 1.473$
Phase 7 AIII	:	$\tau = 1.473 - 1.539$
Phase 8 RIII	:	$\tau = 1.539 - 1.548$ (third voltage spike)
Phase 9 RAIII	:	$\tau > 1.548$).

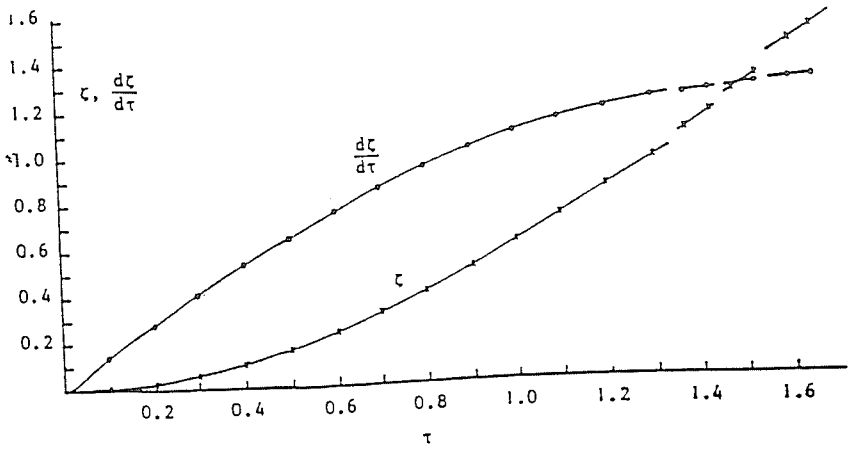

Fig. 10: Axial position ζ and axial speed during the phases AI, AII, AIII and RAI, RAII and RAIII for cascading focus with parameters given in Caption of Fig. 3. The three gaps represent the three phases RI, RII and RIII, results of which are given separately in Figs. 5a, 5b and 5c.

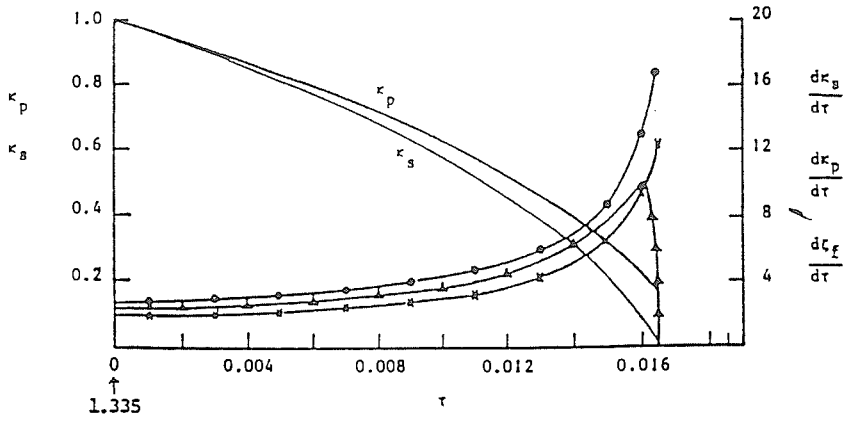

Fig. 11a: Radial phase RI: Trajectories of radial shock (κ_s) and radial piston (κ_p) for cascade focus with parameters same as Fig. 3. Also given are the radial shock speed $d\kappa_s/d\tau$ (•), radial piston speed $d\kappa_p/d\tau$ (▲) and focus column elongation rate $d\zeta_f/d\tau$ (×).

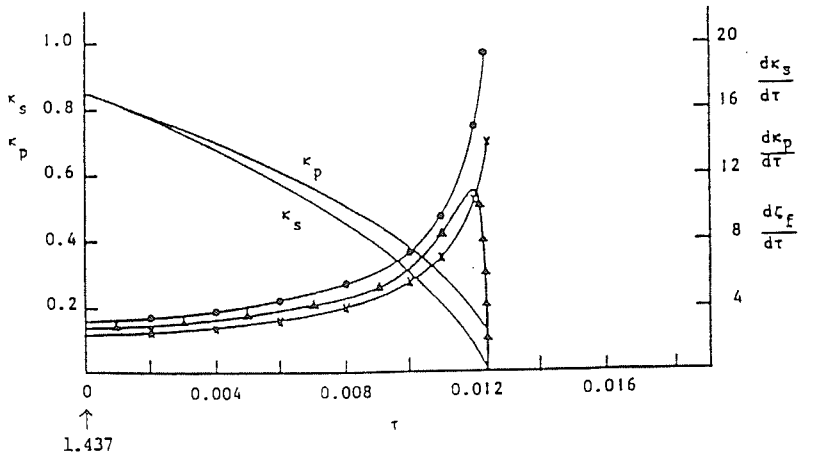

Fig. 11b: Radial Phase RII: Trajectories of radial shock (κ_s) and radial piston (κ_p) for cascade focus with parameters same as Fig. 3. Also given are the radial shock speed $d\kappa_s/d\tau$ (•), radial piston speed $d\kappa_p/d\tau$ (▲) and focus column elongation rate $d\zeta_f/d\tau$ (×).

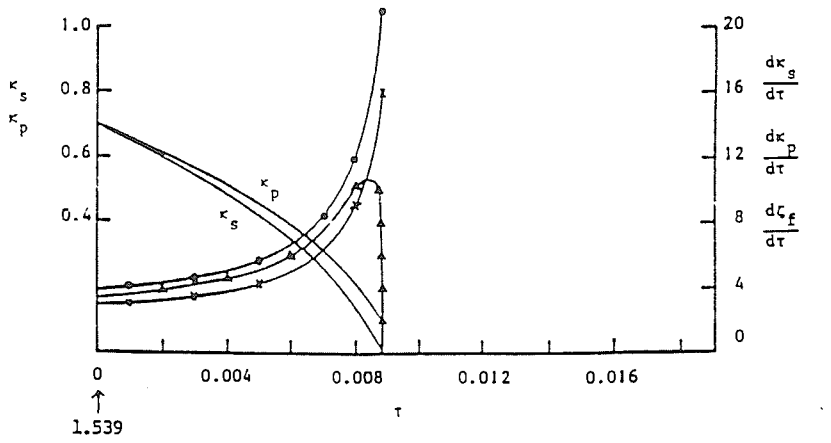

Fig. 11c: Radial Phase RIII: Trajectories of radial shock (κ_s) and radial piston (κ_p) for cascade focus with parameters same as Fig. 3. Also given are the radial shock speed $d\kappa_s/d\tau$ (•), radial piston speed $d\kappa_p/d\tau$ (▲) and focus column elongation rate $d\zeta_f/d\tau$ (×).

TRAINING PROGRAMMES FOR RESEARCH TRANSFER EXPERIENCE AND RESULTS

S. Lee
ICAC - UM
Physics Department
Universiti Malaya
59100 Kuala Lumpur
Malaysia

Abstract

Invited Paper - International Conf. on Physics & Physicists for Development - Univ. Twente, Netherlands, Sept 1990 (to appear in Procs)
Invited Paper - 4th Tropical College on Applied Physics - Kuala Lumpur June 1990 (to appear in Procs).

I. Need for Training Programmes

In the 1980's there have been greatly increased opportunities for South-South as well as South-North scientific interactions. Consider just one example: the activities sponsored by the ICTP and its Office of External Activities:

Year 1989:

387 Federated Agreements, each providing 3 visits to ICTP, Trieste, Italy;

500 Associates;

40 Scientific Colleges and Conferences at Trieste;

139 External activities, Workshops, Colleges, Conferences, Training Programmes, Physics and Mathematics Teaching Programmes;

The creation of 9 Affiliated Centres (ICAC's) and 4 Networks.

These ICTP activities alone sponsored an estimated 5000 South-South and South-North visits for Third World Physicists in 1989.

With all thesw exchange activities, it it timely to put emphasis on activities which optimise results to achieve lasting effects. Beyond the conference halls, beyond the laboratory visits, at the end of an activity one question is often heard from the Third World physicist "What can I do back home? How can I do it?". One way to answer this question is through Training Programmes for South-South transfer of experimental research and research facilities.

II. Training Programme for South-South Research Transfer

(1) Aim: To initiate/Strengthen experimental research in a specific field in several developing countries.

Method: By transfer of an integrated package of expertise, components and equipment.

Concept:

SOUTH	SOUTH
Centre for Training Programme for Research Transfer of specific technology/facility	Recipient Group building up specific technology/facility
Contribution	Contribution
1. Manpower and infrastructure. 2. Planning and organisation. 3. Design of specific facility. 4. Detailed course content. 5. Teaching - Open Box approach. 6. Construction of facility. 7. Follow-up equipment and expertise.	1. Man-power and commitment. 2. Basic mechanical and electronic workshop facilities. 3. Basic laboratory equipment and space.

NORTH

International Organisations
Contribution
1. Living & travel expenses for recipient participants. 2. Cost of parts and labour and freight for follow-up equipment. 3. Cost of follow-up visits and scientific exchange. 4. Coordination and technical expertise.

(ii) Identification of a Centre for Research Transfer

The Centre shall have:-

1. specific and specialised research activity in the area of physics it is offering.
2. sufficient experience and productivity in that area of physics including: development of undergraduate courses, production of post-graduate theses (preferably to doctoral level) and research papers.
3. a self-contained technical infrastructure for the research.
4. evolved the technical infrastructure at the centre itself so that the technical infrastructure may be adapted to another developing country without excessive cost in equipment and funding.
5. a willingness (enthusiasm) to take the initiative to prepare a comprehensive program to teach, in one package, all the technology required to carry out research in the designated subject area.

(iii) Role of the Centre

The Centre should on its own initiative:-

1. Identify a facility (modelled on its own experience) that may be built and on which research may be carried out fruitfully.
2. Plan a breakdown of the facility into its basic technical sub-systems.
3. Define the major technical requirements (related to the working principle) of each component so that its design and building may be adapted to suit local technical capabilities and individual needs.
4. Plan the basic theory and model needed to optimise the parameters of the facility, and on which the behaviour of the facility may be studied fruitfully and with possibility of extension.
5. Plan for computation and numerical modelling to be done with modest computing facilities like microcomputers.
6. Plan the building of the power and control systems and basic diagnostics so that these may be built in simple (preferably modular) form in the local environment.

7. Plan a comprehensive series of experiments and lectures to demonstrate all the above in modular as well as in assembled working form.
8. Identify the basic equipment that may not profitably be home-built in the framework of the particular program, such as, for example, vacuum pumps, oscilloscopes, electronics and power components.
9. Select the participants (bearing in mind the suitability also of the environment of the home institutions).
10. Conduct a course (from 3-6 months as necessary) based on the above for a group of 2-8 participants.
11. Provide facilities for construction of the facility to be transferred.
12. Oversee the design, construction and testing of the facilities by the participants.
13. Arrange air freighting of facility.
14. Provide follow-up.

III. ICTP-UM Training Programmes in Plasma, Laser and Pulse Technology at ICAC-UM, Kuala Lumpur.

(i) Programmes

These were 4-6 month training programmes held as follows:

1985/86	UNU/ICTP Training Programme	- 8 UNU Fellows
1988	ICTP(UNU) Training Programme	- 4 ICTP Fellows - 2 TWAS Fellows
1989/90	ICTP-UM Training Programme	- 3 ICTP (ICAC-UM) Fellows - 4 TWAS (ICAC-UM) Fellows

(ii) Facilities for transfer

These were carefully packaged. Each package is made up of carefully designed sub-systems. Two of the packages are shown in Fig. 1 and Fig. 2.

IV. Results of ICTP-UM Training Programmes

(i) Facilities transferred

Experimental plasma/fusion/laser research has been initiated in 5 Third World countries. Facilities transferred include the following:

	UNU/ICTP PFF	EMST Flow Simulator	Nitrogen Laser System	Laser Shadowgraph System	Glow Discharge
Cairo, Al Azhar U.	X		X	X	
Jaipur, Rajasthan U.	X*		X*		
Delhi, Delhi U.	X*		X*	X*	
Sringaga, SP Coll.			X		
Jakarta, LAPAN (Space research)		X*			
Yogyakarta, PPNY (Nuclear research)	X				X
Islamabad, QIAU	X*+		X*	X*	
Port Harcourt, US&T	X*+		X*+	X*	
Sierra Leone, NUC	X*				
Songkla, PSU	X		X		

*- Also used for M.Sc. and Ph.D. theses programme.

+- Have produced Ph.D./M.Sc. theses from these facilities.

(ii) Results - research publications

Each of the training programmes has produced research publications in which the team of trainees also participate. Among these publications are the following:

Device development

- Fusion package for research transfer.

"A Simple Facility for the Teaching of Plasma Dynamics and Plasma Nuclear Fusion"
Amer. J. Phys. 56, 62 (1988)
S. Lee, T.Y. Tou, S.P. Moo, M.A. Eissa, A.V. Gholap
K.H. Kwek, S. Mulyodrono, A.J. Smith and M. Zakaullah.

- Nitrogen Laser Development.

IEEE J. Quan. Elec. QE-23, 283 (1987)
A.J. Smith, K.H. Kwek, T.Y. Tou, A.V. Gholap and S. Lee

J. Fiz. Mal. 6, 165 (1985)
S Lee et. al.

New Devices

"Sequenced Nitrogen Lasers"

J. Appl. Phys. 65, 4133 (1989)
S Lee, K.H. Kwek, Jalil Ali, M.V.H.V. Prabhakar,
Y.S. Shishodia and A.G. Warmate.

"Effect of Targets on Plasma Focus"

IEEE J. Plasma Science (accepted for Dec 1990 issue)
S. Lee, M.A. Alabraba, A.V. Gholap, S. Kumar. K.H. Kwek,
M. Nisar, R.S. Rawat and J. Singh.

"Cascading Plasma Focus"

Submitted to J. Applied Physics
S. Lee

Some of the published results are shown in Figs. 3-10.

V. Consequent Development of Organisations

(i) ICAC-UM

As a result of our involvement in the implementation of the concept of Training Programmes for Research Initiation the Physics Department, University of Malaya has been invited to be an Affiliated Centre of the International Centre for Theoretical Physics. We aim to continue and expand activities as a training centre for research transfer.

(ii) Asian African Association for Plasma Training (AAAPT)

In order to widen the scope for technology and research transfer among Third World countries the AAAPT was formed in 1988 with the following objectives:

- Plasma Physics training programmes in Asia and Africa.
- Development of research packages for transfer.
- Exchange of scientists.
- Newsletter.

Activites (and associated activities):

- Formation on 7.6.1988 (during Third Tropical College on Applied Physics), Kuala Lumpur, Malaysia.
- 2nd (UNU)ICTP Training Programme, Kuala Lumpur, Malaysia, June-Oct 1988.
- Beijing College on Plasma Diagnostics, Beijing, P.R. China, Oct-Nov 1989.
- 3rd ICTP-UM Training Programme, Kuala Lumpur, Malaysia, Dec 89 - May 1990.
- Regional College on Plasma Applications, Songkla, Thailand, January 1990.
- 4th Tropical College on Applied Physics, Kuala Lumpur, Malaysia, May-June 1990.
- Third Summer School on Plasma Physics, Tsingdao, P.R. China, 15-22 August, 1990.
- Basic Course on Plasma Physics - Theory, Islamabad, Pakistan, September-December 1990.

The ICAC-UM and the AAAPT have also taken the initiative to propose the formation of a Plasma and Laser Technology Resource Network.

(iii) Plasma and Laser Technology Resource Network

Aim: To assist development of equipment packages.
To assist distribution of equipment packages.

Concept:

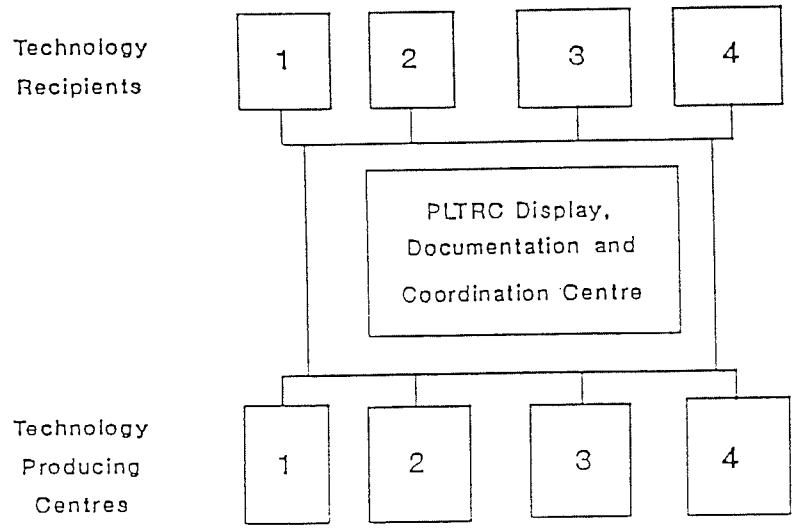

Structure of Technology Resource Network.

Proposal:

PLTRC be established at ICTP to benefit as many Third World scientists as possible.
Funding and contributions: ICAC's, AAAPT, ICTP, TWAS, etc.

Actions taken:

Nitrogen Laser Education and Application package already installed at ICTP (contributed by ICAC-UM).
Optical Fibre Monochromator (OFMS) package already completed and sent to ICTP (contributed by AAAPT, Project of Chinese Academy of Science, Beijing).
Multi-purpose plasma devices, pinch and glow discharge device completed, to be donated to University of Cairo (contributed by AAAPT, project of Egypt Atomic Energy Authority, Plasma and Nuclear Fusion Division).

Other packages being planned include:

Laser Shadowgraphy System

Plasma Fusion Facility

Multi-channel X-ray Spectrometer

(These will be transferred to the ICTP by the end of 1990).

Theta pinch

Transistorised Rotamak FRC System

YAG Laser package

Hologram System

VI. Conclusion

- Training programmes for research transfer have been set up with proper S-S-N interaction criteria.

- Basis of transfer: research facility package with comprehensive hands-on training programme and equipment follow-up.

- Results: transfer of significant research activities to 10 institutions in 7 South countries.

- Results: Research papers and postgraduate theses up to Ph.D. level.

- Out of these programmes has grown the AAAPT bringing expertise of more advanced South countries contributing 8 activities in 2 years.

- AAAPT attempts to open up the technology resource of the more developed South countries to other South countries through the PLTRN.

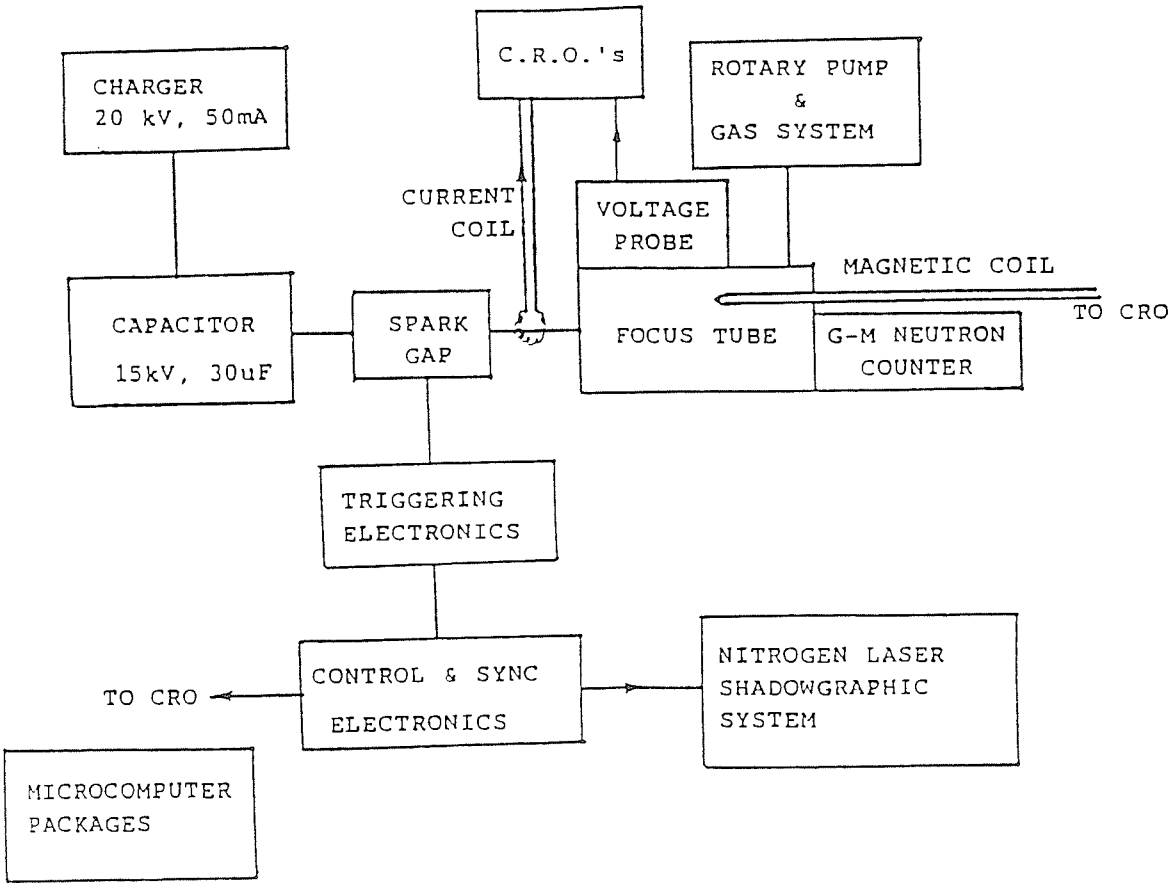

Fig. 1. Sub-systems for the UNU/ICTP PLASMA FUSION FACILITY

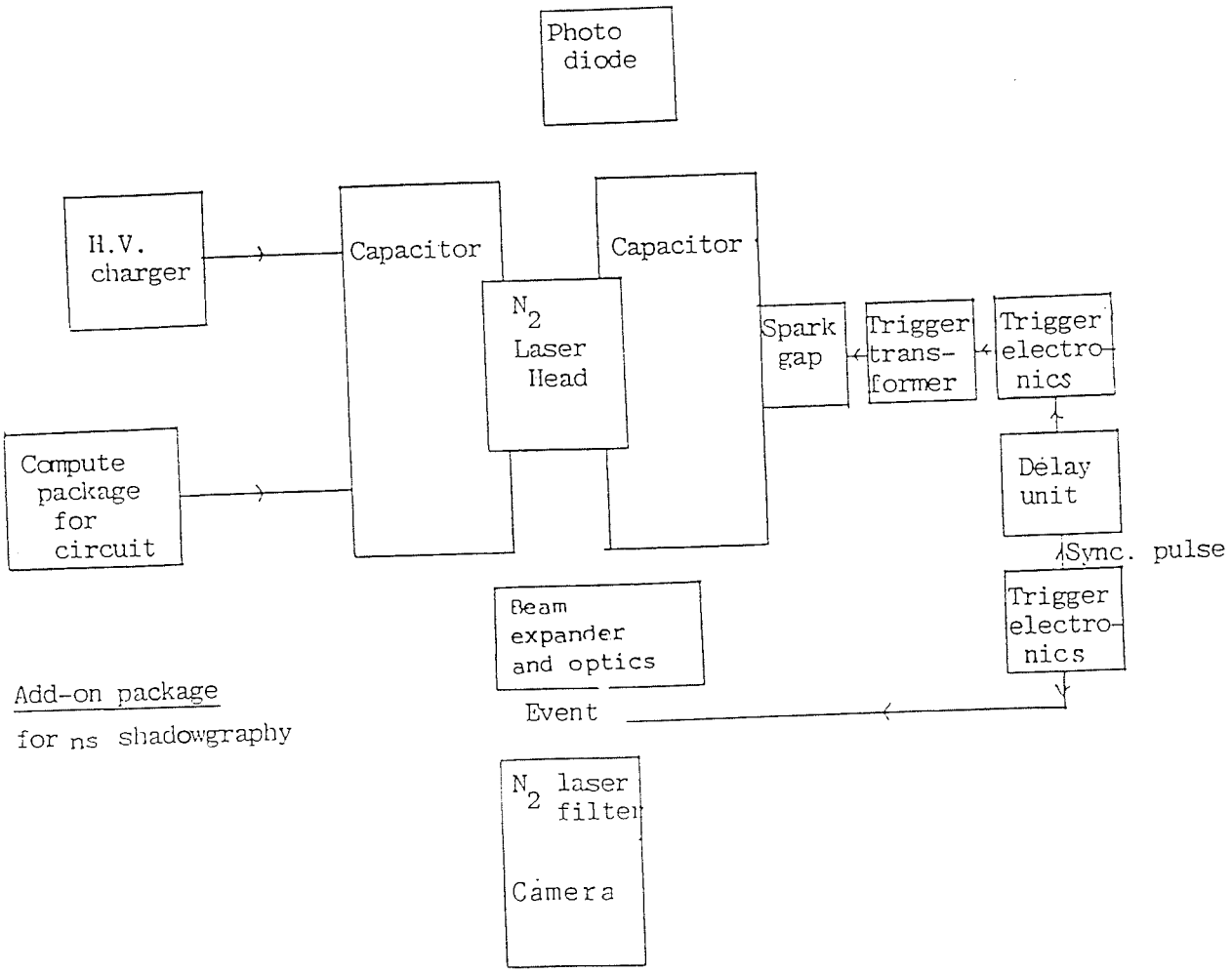

Fig.2 Nitrogen laser package and add-on Shadowgraphy package

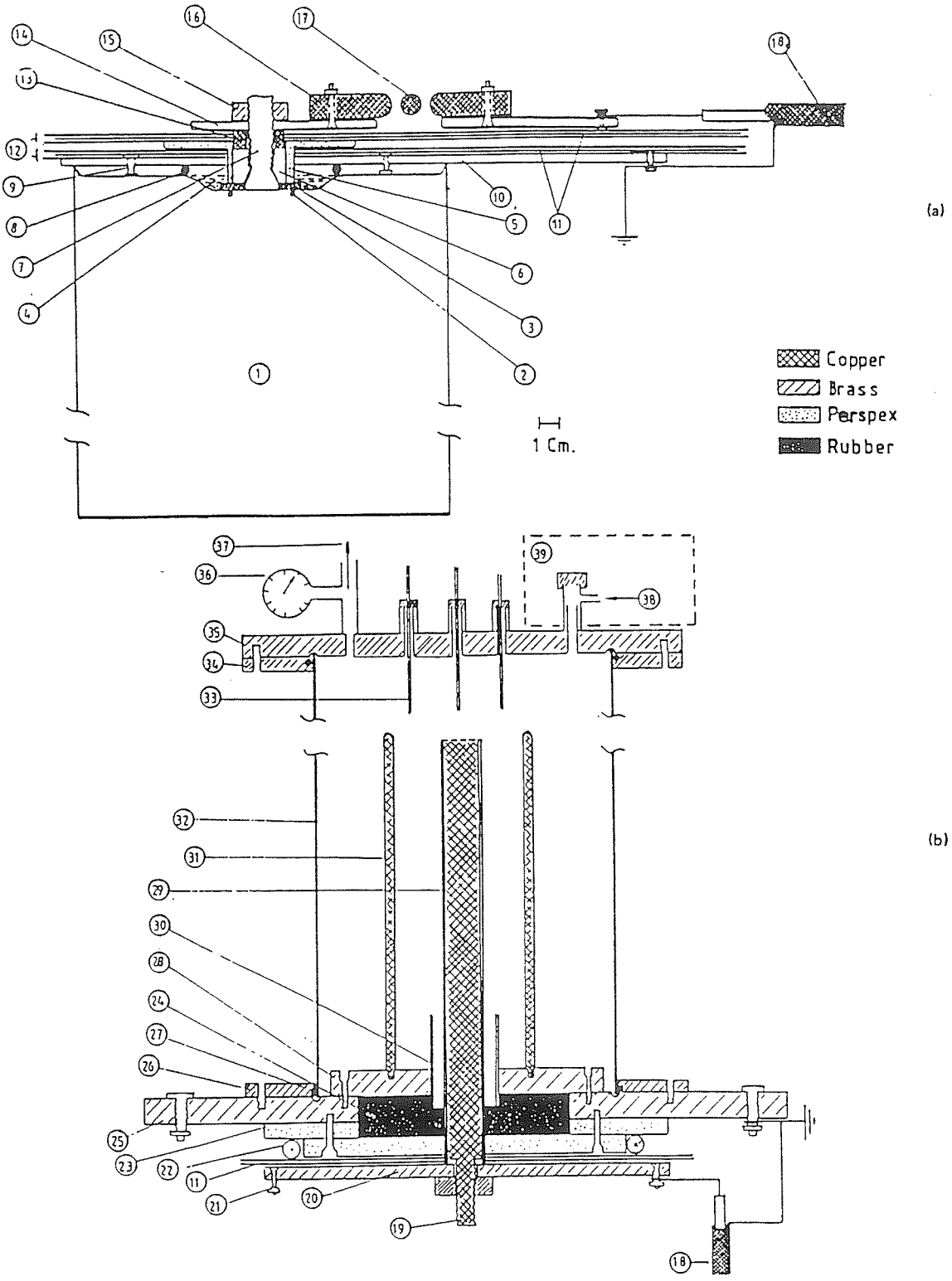

Fig. 3. (a) The capacitor connecting plates, the spark gap, and output coaxial cables. 1 = 15 kV, 30 μF capacitor; 2 = capacitor O-ring seal; 3 = washer; 4 = oil; 5 = nylon cap; 6 = steel nut; 7 = capacitor output seal; 8 = O-ring seal; 9 = Earth stud; 10 = Earth plate; 11 = 5-mil Mylar film; 12 = polyethelene film; 13 = copper ring HV connector; 14 = capacitor high-voltage (HV) output plates; 15 = lock nut for HV plate; 16 = HV electrode for swinging cascade spark gap; 17 = trigger electrode; and 18 = output coaxial cables (16 in parallel). (b) The plasma focus tube. 18 = input coaxial cables (16 in parallel); 19 = stud of anode; 20 = anode collector plate; 21 = connecting points for coaxial cable HV lead; 22 = Rogowski coil; 23 = perspex spacer; 24 = rubber holder; 25 = cathode collector plate; 26 = mild steel flange; 27 = O-ring seal; 28 = focus cathode support plates; 29 = focus anode; 30 = glass insulator; 31 = focus cathode (6 rods); 32 = mild steel focus chamber; 33 = movable magnetic probe in glass jacket; 34 = flange; 35 = back flange; 36 = diaphragm gauge; 37 = outlet to vacuum pump; 38 = inlet for test gas; 39 = wax container with indium foil and PM-scintillator activation counter.

Fig 3. Research results-development of the UNU/ICTP Plasma Fusion Facility

plasma layer may be measured as a sharp rise in magnetic field as the sheath sweeps past the probe. This measurement may be used to confirm the dynamics required to ensure a good focus.

An indium foil activation system is used to count fusion neutrons from the plasma. This system consists of an indium foil covering an NE 102 scintillator sitting on the photocathode of a 2-in. photomultiplier tube. The assembly is placed in a paraffin wax enclosure so as to thermalize the fusion neutrons. The detector is placed on the end flange of the plasma focus tube (no. 39). The PM tube is connected to a counter via a discriminator and a preamplifier and has a calibration constant of 5×10^4 neutrons per count, the counts being taken for a 30-s period immediately after the focus is fired.

IV. RESULTS

The system was tested between 13 and 15 kV in various gases including air, argon, hydrogen, and deuterium. The strength of the focusing action is gauged from the current dip and voltage spike. Figure 4(a) shows an oscillogram of the current and voltage waveforms of the plasma focus in 0.5 Torr of air, with focusing action about 1 μs after peak current. Figure 4(b) shows a deuterium focus, at 13 kV, 2.5 Torr with focusing action occurring at peak current. The deuterium focus shows signs of a secondary focus occurring some 0.4 μs after the first voltage spike. The occurrence of definite clean dynamics in the axial region preceding the focus region is confirmed by magnetic probe measurements. Figure 4(c) shows the output of a magnetic probe (lower trace) placed at $z = 10.2$ cm (i.e., in the axial drive region 10.2 cm from the backwall) in a discharge of 15 kV, 3.5 Torr of deuterium. From this oscillogram and in comparison with the current oscillogram (upper trace) it is found that the current sheath arrives 0.6 μs before focusing occurs off the end of the anode at $z = 16$ cm giving a speed of 9.7 cm/μs (corresponding, from shock theory, to a temperature $\sim2\times10^5$ K) over this section ($z = 10.2$–16 cm) of the axial drive region. From the rise time (10%–90%) of the magnetic signal and the speed this gives a current sheath thickness of 2 cm. The thickness and speed of this current sheath is typical of that in a good plasma focus system. The current dip during focusing is also seen as a dip in the magnetic probe output that shows two other current dips occurring at 0.2 and 0.6 μs after the first dip. These confirm the occurrence of multiple focusing in deuterium in the device.

In air good focus was obtained at 13 and 15 kV in a narrow pressure range of 0.5–1.1 Torr. In argon the pressure range for good focusing is greater at 0.3–3 Torr. At 15 kV very strong focusing action was obtained at 0.8 Torr. In helium the range of focusing is from 0.7 to 3.5 Torr while in carbon dioxide focusing is observed below 1 Torr. In hydrogen the pressure range for focusing is 1.1–6 Torr. However, it is noticed that the focusing action, although definite, is not as intense, in terms of a focusing voltage spike, as in argon. The strongest focus in hydrogen occurs at 3.3–4.3 Torr. In deuterium strong focus is observed at 1–5 Torr with best focusing at 2.5–3 Torr.

In deuterium when operated at 15 kV and optimum pressure conditions of 3 Torr consistent counts of 1000–2000 are obtained using the PM-scintillator counter. This corresponds to $0.5–1\times10^8$ neutrons per shot.

The system shows remarkably consistent and reproducible operation. Six systems were assembled one after the other and tested over a period of 2 months. Each system was assembled and tested over a period of 1 week averaging between 100–200 shots in the various gases. Once a system

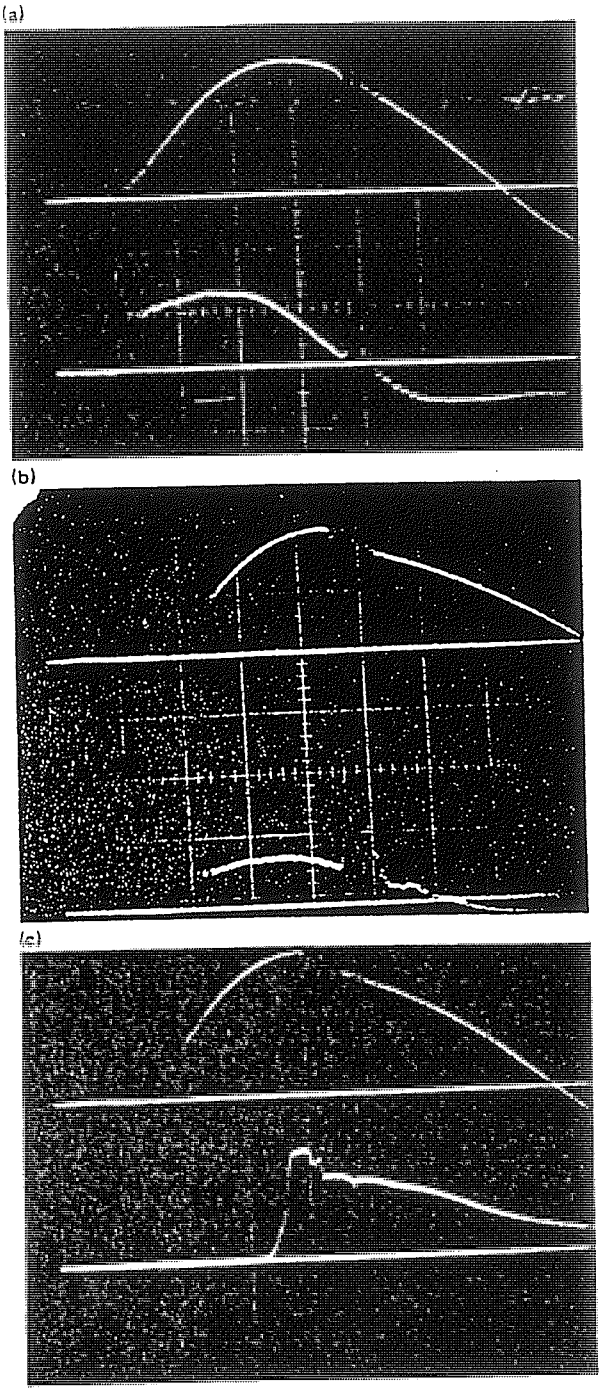

Fig. 4. (a) Current (upper trace) and voltage (lower trace) of plasma focus in air: 13 kV, 0.5 Torr; Top trace: 73 kA/cm; Bottom trace: 2 kV/cm; Time scale (horizontal): 1 μs/cm. (b) Current and voltage trace of plasma focus in deuterium: 13 kV, 2.5 Torr; Top trace: 75 kA/cm; Bottom trace: 4 kV/cm; Time scale (horizontal): 1 μs/cm. (c) Current and magnetic trace of plasma focus in deuterium: 15 kV, 3.5 Torr; Magnetic probe placed at $z = 10.2$ cm; Top trace: 73 kA/cm; Bottom trace: 0.6 T/cm.

Fig 4. Research results- some measurements of the UNU/ICTP PFF

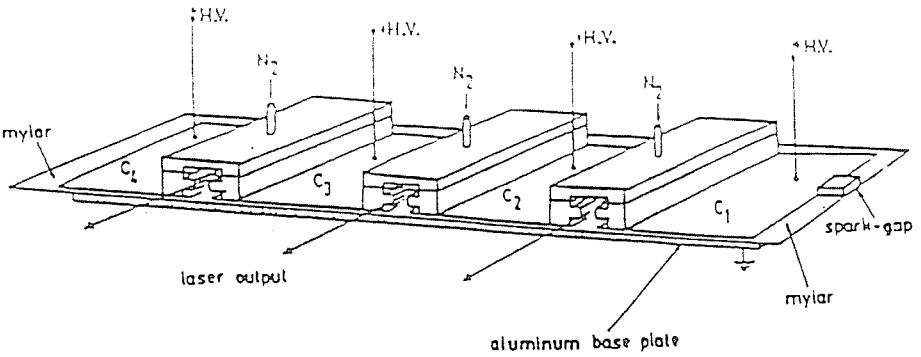

Fig. Schematic of a three-channel sequenced nitrogen laser. The high-voltage plates of the capacitors C_1, C_2, C_3, and C_4 are made of aluminum foils.

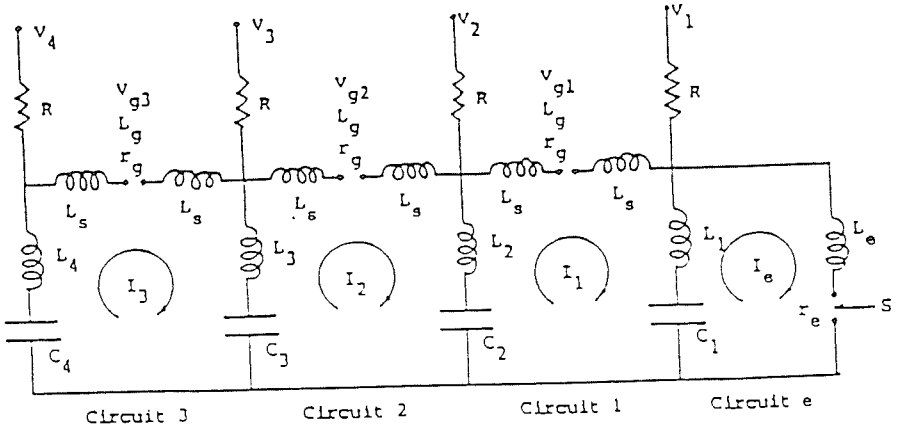

Fig Circuit diagram of the three-channel sequenced nitrogen laser.

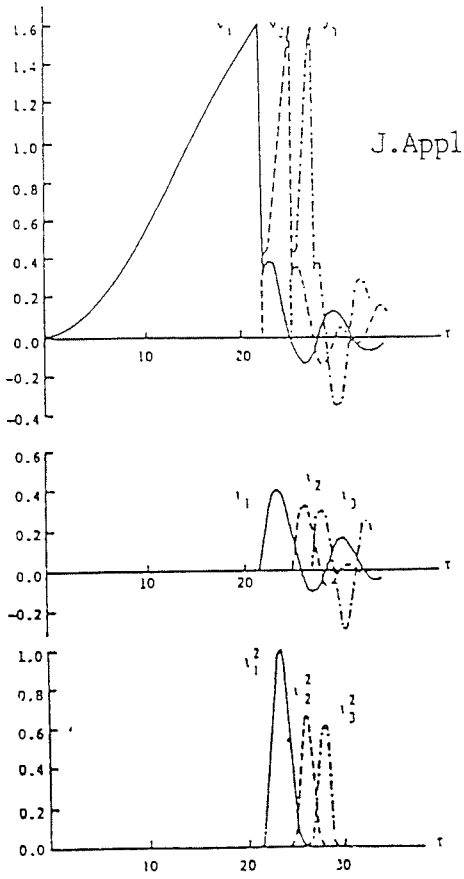

J.Appl.Phys 65 4133 (1989)

Fig Computed voltages across the laser channel, laser currents, and laser currents squared as functions of time; all variables are normalized. Parameters used are those for a "prompt sequencing" mode.

Fig 5 Research results- Development and results of Sequenced Nitrogen Laser

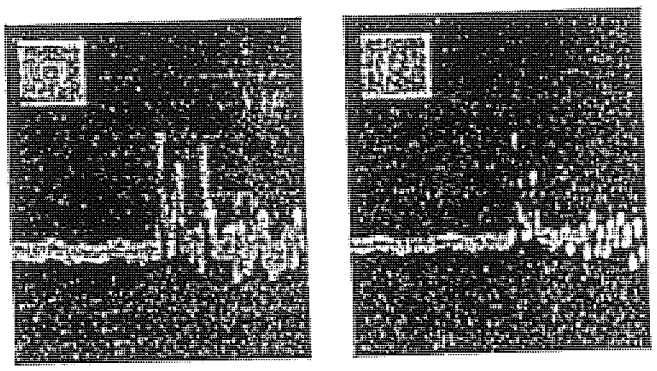

Time scale: 100ns/division.

Fig Oscillograms of photodiode signal monitoring the three-channel sequenced nitrogen laser operated in the prolonged sequencing mode; time scale: 100 ns/div. (a) Shot with three laser pulses in "prolonged sequence." (b) Shot with the third laser pulse missing.

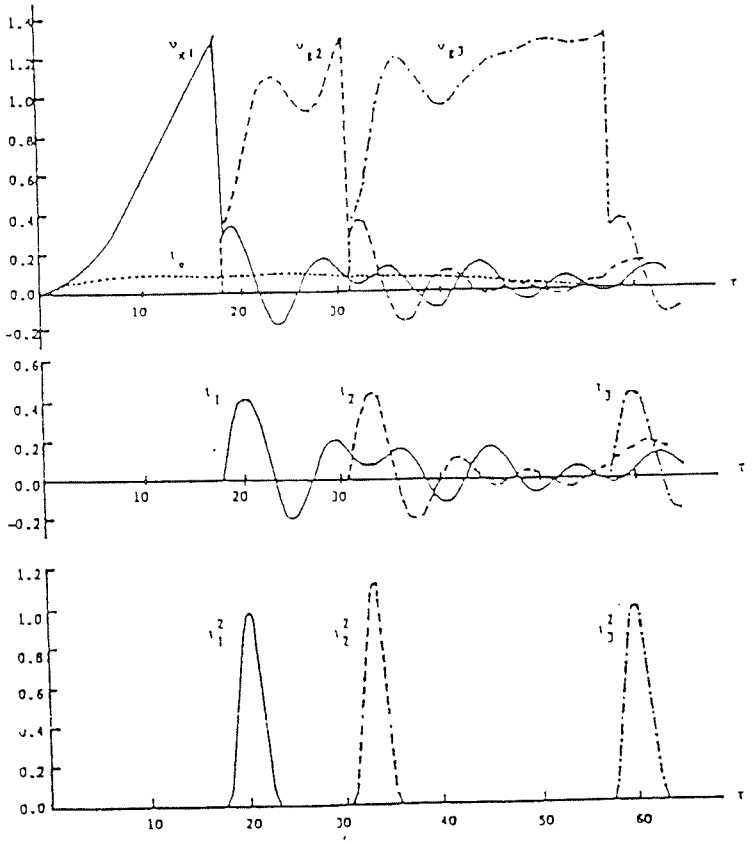

Fig Computed voltages across the laser channel, laser currents, and laser currents squared as functions of time; all variables are normalized. Parameters used are those for a "prolonged sequencing" mode.

Fig 6 Research results- Sequenced Nitrogen Lasers- J.Appl.Phys.65 4133, (1989)

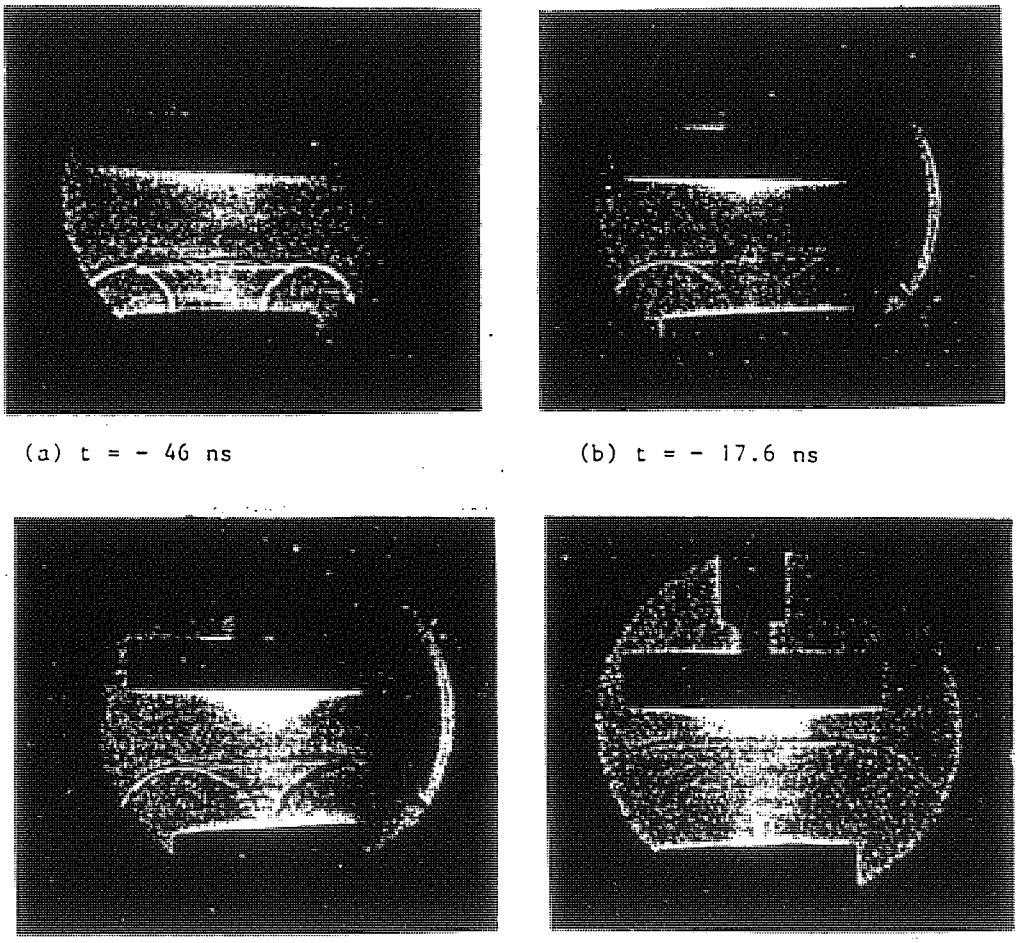

(a) t = - 46 ns

(b) t = - 17.6 ns

(c) t = - 6 ns

(d) = + 31 ns

Fig Shadowgraphs of current sheet configuration before and after peak compression with a flat target at a distance of 1.5 cm from the anode face

Fig.7.Research results- 1-nanosecond laser shadowgraphs of the UNU/ICTP PFF- IEEE Trans Plasma Science (Dec 1990)

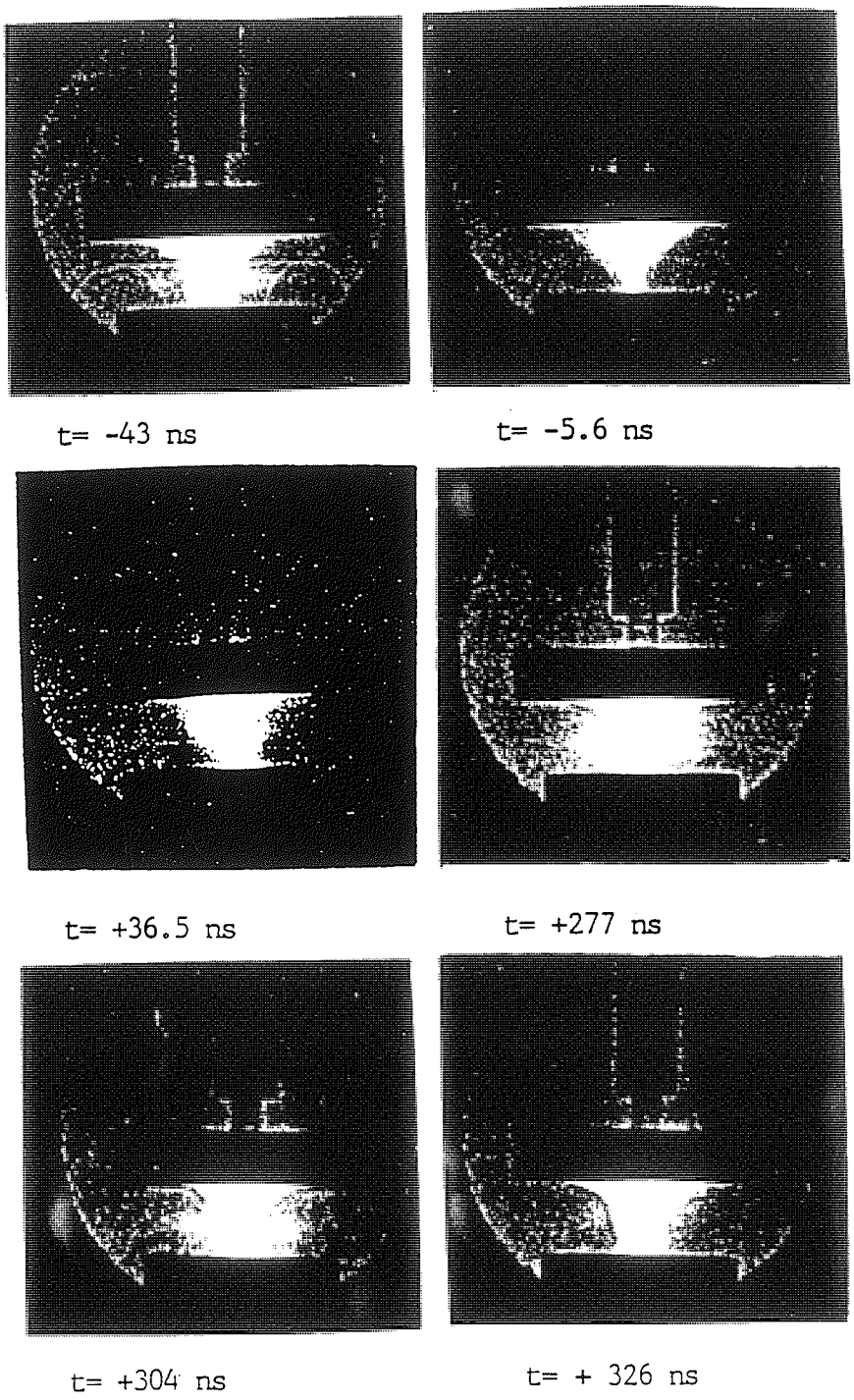

Fig Shadowgraphic sequence (composite) of current sheet configurations with the flat target at a distance of 7 mm from the anode face

Fig 8 Research results- developing the concept of the Cascading Plasma Focus

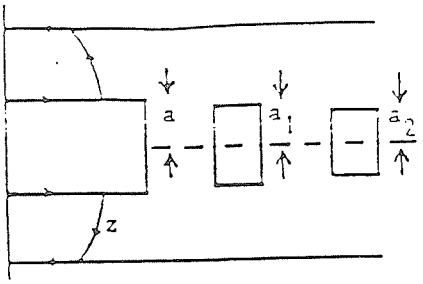

Phase 1: AI

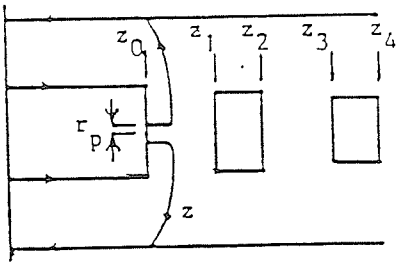

Phase 2: RI

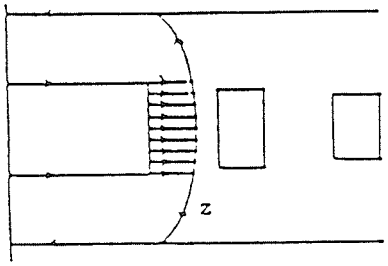

Phase 3: RAI

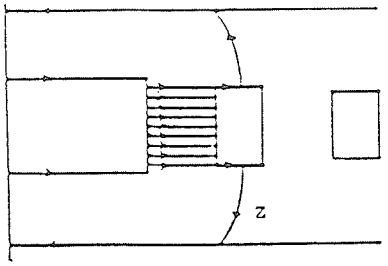

Phase 4: AII

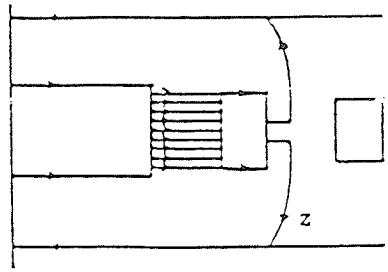

Phase 5: RII

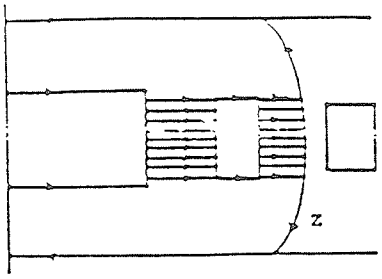

Phase 6: RAII

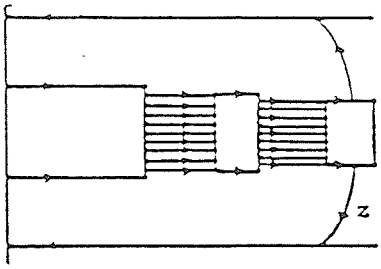

Phase 7: AIII

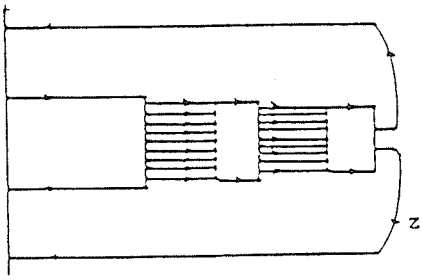

Phase 8: RIII

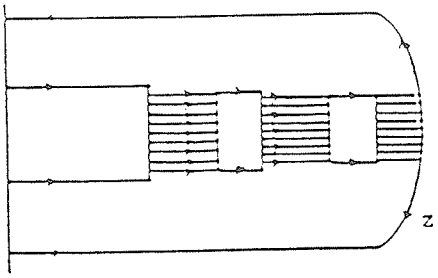

Phase 9: RAIII

Fig. The 9 phases of the cascading plasma focus model.

Fig 9 Research results- Developing the concept of the Cascading Plasma Focus

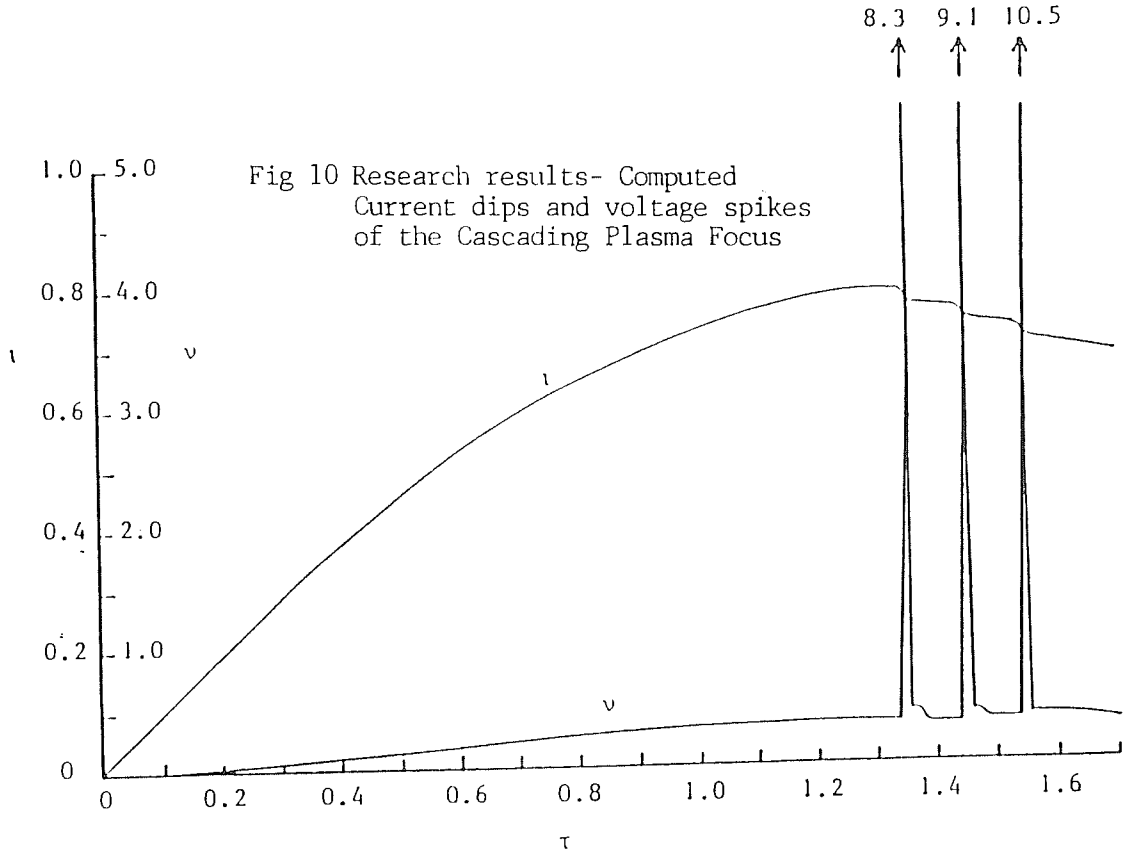

Fig 10 Research results- Computed Current dips and voltage spikes of the Cascading Plasma Focus

Fig. Current ι and voltage ν for cascade focus with $\alpha = 1.7$, $\beta = 0.27$, $F = 12$, $c = 3.37$, $\gamma = 5/3$, $\zeta_1 = 1.083$, $\zeta_2 = 1.167$, $\zeta_3 = 1.25$, $\zeta_4 = 1.333$, $d_1 = 0.85$ and $d_2 = 0.7$.
(To help identify the 9 phases their time intervals are given here:

Phase 1 AI	:	$\tau = 0 - 1.335$
Phase 2 RI	:	$\tau = 1.335 - 1.352$ (first voltage spike)
Phase 3 RAI	:	$\tau = 1.352 - 1.369$
Phase 4 AII	:	$\tau = 1.369 - 1.437$
Phase 5 RII	:	$\tau = 1.437 - 1.449$ (second voltage spike)
Phase 6 RAII	:	$\tau = 1.449 - 1.473$
Phase 7 AIII	:	$\tau = 1.473 - 1.539$
Phase 8 RIII	:	$\tau = 1.539 - 1.548$ (third voltage spike)
Phase 9 RAIII	:	$\tau > 1.548$).

Effect of Targets on Plasma Focus Dynamics

S. LEE, M. A. ALABRABA, ASHOK VASUDEO GHOLAP, S. KUMAR, K. H. KWEK, MOHAMMAD NISAR, R. S. RAWAT, AND JASBIR SINGH

Abstract—**Shadowgraphs were taken of a 3-kJ plasma focus in the presence of a flat disc target placed downstream of the anode and a 1-mm wire target inserted along the axis at the anode. Three observations were made: (i) The flat disc target does not affect the dynamics of the focus proper when it is placed downstream at a distance greater than the anode radius; (ii) the current sheet moves over the disc and forms a pinch beyond it as though the disc has become a new anode; and (iii) the plasma focuses strongly onto a 1-mm wire on axis.**

These observations may be used to design beam-target experiments in a plasma focus machine. They indicate the possibility of focus-fibre experiments, and also raise the possibility of and indicate the guidelines for designing a sequential focus device.

I. Introduction

THE PLASMA focus is recognized as a device which is very suitable for the study of plasma dynamics [1] as well as being a simple source for neutrons, X rays, and particle beams. In some studies, targets are used as a diagnostic tool for the observation of deuteron beams. For example Cloth and Conrads [2] and Bernard *et al.* [3] have used a target technique to show the importance of the beam-gas target mechanisms for the neutron production in the plasma focus, and to demonstrate the presence of a high energy component in the deuteron beam and to study the duration of the beam.

More recently, Moo *et al.* [4] have used a metal target and deuterated target placed at various axial distances from the end of the anode in a plasma focus device (3-kJ device designated as the UNU/ICTP PFF [1]). The neutron yields are measured with each of these flat targets and are compared to the yield without them. Results are obtained that are consistent with the interpretation that a beam-target mechanism plays a primary role (85%) in the neutron production in this device.

In those experiments, Moo *et al.* [4] were careful to keep the target distance no less than 2 cm from the anode of radius 1 cm, as it was believed from current and voltage measurements that the target beyond 2 cm did not disturb the focusing dynamics.

To demonstrate the validity of this viewpoint, we have carried-out experiments in the plasma focus UNU/ICTP PFF to obtain shadowgraphs in the presence of a flat target at varying distances from the anode. We also examined the focusing dynamics in the presence of an axial thin-wire target protruding into the hollow anode. The rationale of this second experiment with a thin-wire target was to check whether strong focusing action still occurred in the presence of an axial thin-wire target. The answer to this question and the dynamics of this situation are important in considering focus experiments of the deuterated-fibre-type such as arise naturally as a sequel to the fibre pinch experiments of Sethian *et al.* [5] or inertial compression experiments using targets bathed in the plasma of a focus as suggested by Gratton *et al.* [6].

In the course of these experiments with a flat-target, observations made of the post-focusing dynamics suggest the possibility of sequential focusing as a result of the flat target. These observations are also reported.

II. Experimental Setup

We use the plasma focus designated as the United Nations University/International Center for Theoretical Physics Plasma Fusion Facility (UNU/ICTP PPF), which is a 3-kJ plasma focus device. This device is operated at the neutron optimized point of 3-torr deuterium at 15-kV and 176-kA peak current [1].

Its inner hollow copper electrode has a diameter of 2 cm and length of 16 cm. The outer electrode consists of 6 copper rods forming a diameter of 6 cm.

The shadowgraph system uses as a light source a TEA nitrogen laser [7] of wavelength 337 nm, a quartz beam expander, and a quartz objective lens used together with a plasma light reduction stop. Polaroid film is used for recording. A bandpass filter centered at 340 nm, having a passband of 12 nm and several neutral density filters, are used to obtain the correct nitrogen laser intensity recorded on the film. The setup is shown in Fig. 1.

The electronic timing sequence is shown in Fig. 2. The instant of plasma focus is defined as the time of voltage spike using a voltage divider placed across the focus anode and cathode. From earlier work [1] it is known that the voltage spike time corresponds to the time of maximum plasma compression.

Manuscript received March 30, 1990; revised July 24, 1990.

S. Lee, S. Kumar, K. H. Kwek, and J. Singh are with the Plasma Research Laboratory, Department of Physics, University of Malaya, 59100 Kuala Lumpur, Malaysia.

M. A. Alabraba is with the ICTP Training Program on Plasma and Pulse Technology, University of Malaya, 59100 Kula Lumpur, Malaysia, and the Department of Physics, River State University of Science and Technology, Port Harcourt, Nigeria.

A. V. Gholap is with the ICTP Training Program on Plasma and Pulse Technology, University of Malaya, 59100 Kuala Lumpur, Malaysia, and the Department of Physics, University of Zimbabwe, Harare, Zimbabwe.

M. Nisar is with the ICTP Training Program on Plasma and Pulse Technology, University of Malaya, 59100 Kuala Lumpur, Malaysia, and the Department of Physics, Quaid-I-Azam University, Islamabad, Pakistan.

R. S. Rawat is with the ICTP Training Program on Plasma and Pulse Technology, University of Malaya, 59100 Kuala Lumpur, Malaysia, and the Department of Physics and Astrophysics, University of Delhi, India.

IEEE Log Number 9040083.

0093-3813/90/1200-1028$01.00 © 1990 IEEE

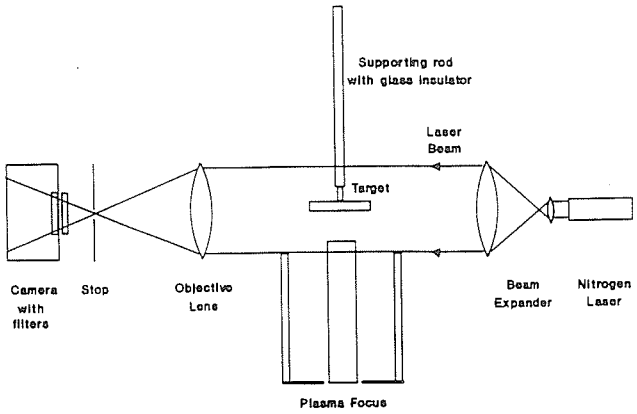

Fig. 1. Schematic of shadowgraph setup.

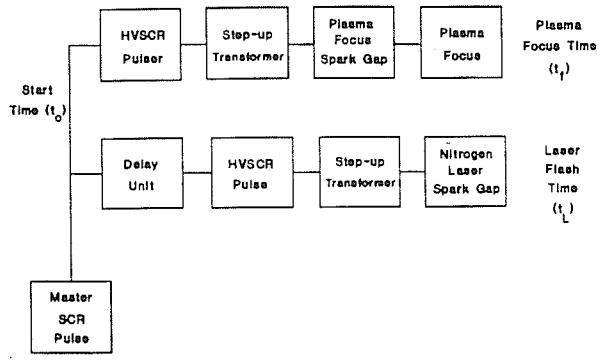

Fig. 2. Block diagram of electronic time sequence in experimental setup. SCR = silicon controlled rectifier. HVSCR = high voltage SCR.

To synchronize the plasma focus and laser flash, it was necessary to determine the focus time t_f and laser flash time t_L and then to match these by use of a delay unit. The plasma focus time $t_f - t_0$, defined here as the time of voltage spike, was found to be 5.86 ± 0.09 μs. The jitter is due to the parallel plate swinging-cascade spark-gap jitter and the focus run-down time jitter.

The instant of laser flash measured with a photodiode BPX65, with the delay unit by-passed, was found to be $t_L - t_0 = 1.50 \pm 0.05$ μs. This jitter was due mainly to the laser spark-gap.

Therefore the required delay is $t_f - t_L \simeq 4.36$ μs. With the times set thus, the synchronization has a jitter range typically of about 0.1 μs. Since the focusing (pinch) time takes about 0.1 μs and the laser pulse time is 3 ns (in these experiments), the jitter will allow, over a large number of shots, shadowgraphs to be taken of different instants during the focus collapse. We denote the time of voltage spike as $t = 0$. Hence, for example, -10 ns means 10 ns before the voltage spike.

The target (see Fig. 1) consists of a brass disc, 5-mm thick having a diameter of 25 mm hanging from a brass support rod of 3-mm diameter. The target is kept at floating potential as the support rod is insulated from the earthed chamber by a glass tubing of a 6-mm diameter. When the wire target is used, the disc target shown in Fig. 1 is replaced with a 1-mm axially located copper wire that is held at the supporting rod and extends along the axis into the hollow anode.

III. Results

Fig. 3 shows a composite shadowgraph sequence with the target at 1.5 cm from the focus anode. For this sequence the neutron yield per shot is estimated as being typically [4] 0.1×10^8. This compares with a yield of 1.2×10^8 when no target is used. The reduction is postulated [4] to be due to interference of the target with a deuteron beam accelerated downstream out of the focus region. Further details of neutron yield variation with target position is the subject of another paper [4]. Fig. 3(c) of this sequence shows that there is no interaction between the radially collapsing current sheet and the target up to the time 6 ns before maximum compression, as indicated by the corresponding timing oscillogram (Fig. 4) showing the voltage spike (which identifies the instant of maximum compression) and laser pulse. At the measured speed of 20 cm/μs there is only a further radial compression of 1.2 mm. The rate of elongation of the plasma focus is known to be of the some order as the rate of radial compression [1]; hence we can extrapolate a further elongation of 1.2 mm at maximum compression. In fact, from Fig. 3(c), we can safely state that there is no interference of the current sheet by a target placed at further than 1 cm, which is the anode radius. Fig. 3(d) shows a shadowgraph 31 ns after peak compression, with the curved return current path clearly seen but with no sign of the pinch column.

The situation depicted by Fig. 3(d) is known to be the time during which the pinch column has expanded and is in a quiescent condition [9] corresponding to the time just after peak neutron emission. The shadowgraph shows clearly that the current sheet at this time still has not reached the target.

Examination of several sequences of shadowgraphs with the target at increasingly closer distances from the anode shows that for this focus machine, targets may be used with distances as close as 10 mm without interference of the focusing current sheet of the focus paper.

On the other hand, when the target is at, for example, 7 mm (see Fig. 5), the current sheet reaches the target before maximum compression (as indicated by the voltage maximum in Fig. 5(b)) and is deemed to interfere with the focus dynamics. This interference is consistent with a further reduced neutron yield per shot of below 10^6.

Examination of the sequence of shadowgraphs also revealed an interesting phenomenon. For example, in the sequence with the target at 7 mm as shown in Fig. 5, the current sheet has reached the target about the time of focus maximum compression (see Fig. 5(b)). Following that, the current sheet climbs over the target, so it seems, as seen in Fig. 5(c). Fig. 5(c) shows this current sheet advancing at an axial speed of 5 cm/μs over the disc, which we may now interpret as a new "anode." This axially advancing axisymmetric current sheet then collapses

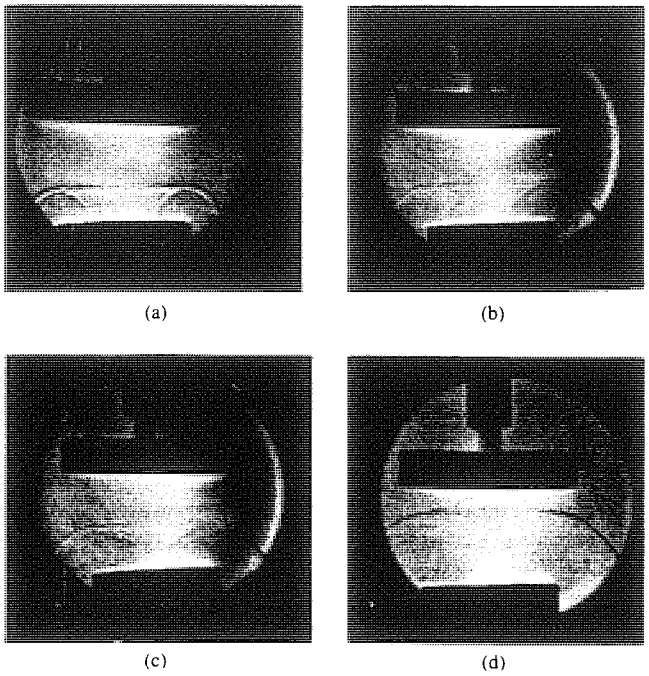

Fig. 3. Shadowgraphs of the current sheet configuration before and after peak compression with a flat target at a distance of 1.5 cm from the anode face. (a) $t = -46$ ns. (b) $t = -17.6$ ns. (c) $t = -6$ ns. (d) $t = +31$ ns.

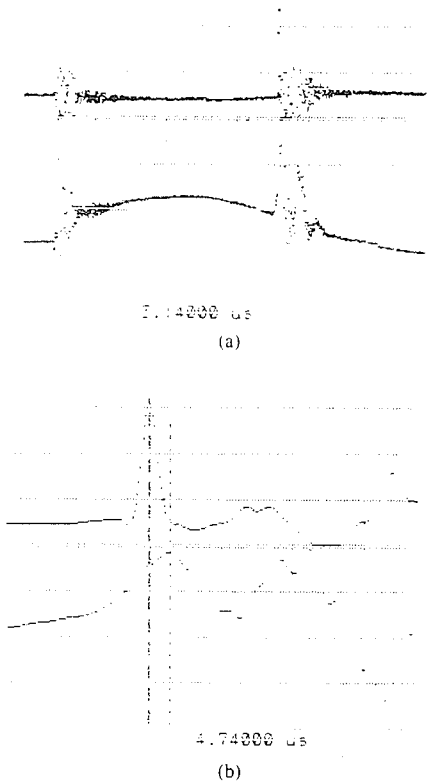

Fig. 4. Timing oscillograms for Fig. 3(c). (a) Top trace: Photodiode signal of laser pulse. Bottom trace: Voltage signal of focus 1 μs/div. (b) Same as (a), but with an expanded time scale of 20 ns/div. From this oscillogram the time of the laser pulse is determined to be $t = -6$ ns; i.e., 6 ns before maximum plasma compression or voltage pulse maximum.

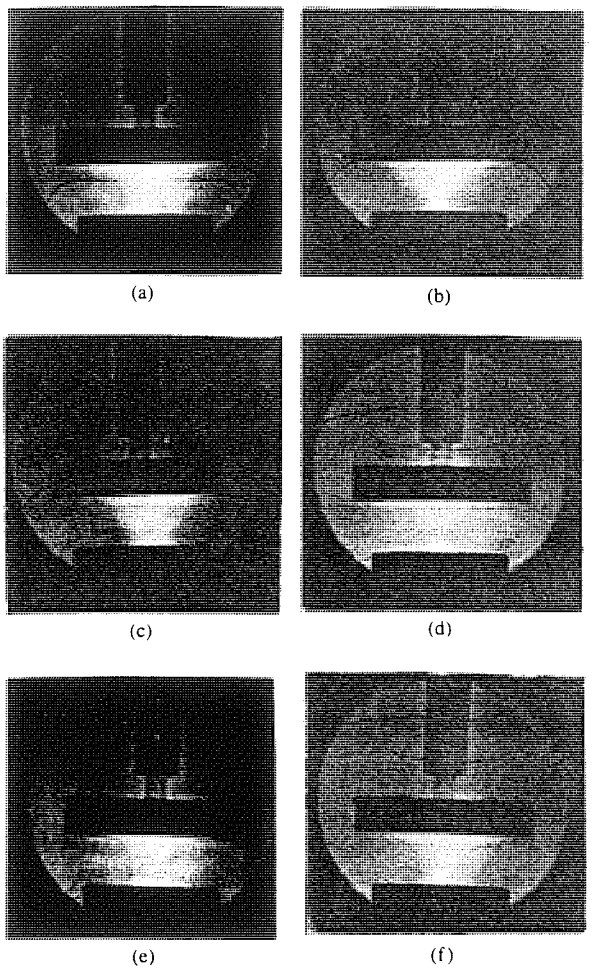

Fig. 5. Shadowgraphic sequence (composite) of current sheet configurations with the flat target at a distance of 7 mm from the anode face. (a) $t = -43$ ns. (b) $t = -5.6$ ns. (c) $t = +36.4$ ns. (d) $t = +277$ ns. (e) $t = +304$ ns. (f) $t = +326$ ns.

onto the glass tube surrounding the brass support rod, as seen in Fig. 5(d)–(f). This raises the interesting question whether, if the brass support rod with its insulating tubing were removed, a new focus could be formed beyond the target. If so, a metal disc placed, say, 1 cm beyond the anode face would, after the usual focus and after a small interval of, say, 300 ns, present in effect a new anode face producing a fresh focus event. In this context, the new "anode" refers to the effect of the disc as a continuation of the dynamic system, with a current sheath linking the disc to the cathode and with consequent axial drive. In this manner, by a series of separated discs, a series of plasma focus may be produced sequentially in one discharge, each disc sequentially becoming a fresh anode face. It is necessary, of course, to adjust the discharge parameters to provide a sufficiently long-sustaining electric current I to adequately power each focus up to the last one in the sequence, keeping in mind the speed-scaling factor of $[(I/a)/\sqrt{\rho}]$, where a is the anode radius and ρ is the ambient density. Further work on this is planned.

Results for the axial wire target experiment were also obtained. These are shown in Fig. 6. These shadowgraphs

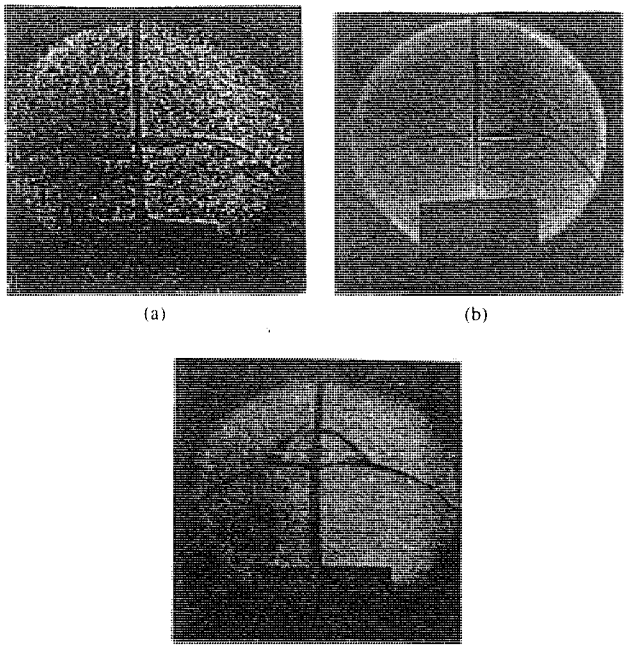

Fig. 6. Shadowgraphs of plasma focus collapse onto a 1-mm axially located wire. (a) $t = 0$ ns. (b) $t = +46$ ns. (c) $t = +80$ ns.

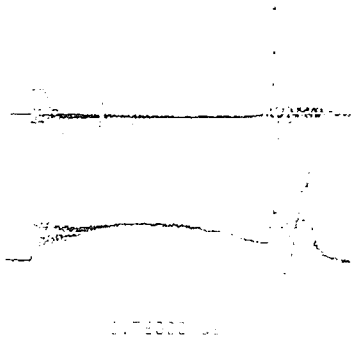

Fig. 7. Voltage waveform, bottom trace, showing strong focusing action onto axially located wire corresponding to Fig. 6. The top trace is of the nitrogen laser pulse corresponding to Fig. 6(a). The time scale is 1 μs/div.

with the corresponding voltage waveform (Fig. 7) show the formation of a strong focus onto the centrally located wire target. The copper wire target used here has a diameter of 1 mm that is smaller than the usual focus diameter of 2 mm, and the results indicate a focus on target with similar, though a little weaker, voltage spike characteristic and a similar shadowgraph characteristic as a free focus. Since the focusing voltage spike has an amplitude that is proportional to $\dot{r}/r$ (radial velocity divided by radius), it is clear that the use of a thinner wire target, of, say, 100-μm diameter, would restore the focus voltage spike as well as its overall intensity. This indicates that even with our small focus, having only 3-kJ energy, it should be possible to carry-out plasma implosion experiments on thin fibers, deuterated or otherwise for neutron yield enhancement experiments or for plasma-target interaction experiments. Incidentally, Fig. 6(c) shows the "bubble" formation which occurs typically after a strong plasma focusing event. It would be interesting to carry-out neutron yield and soft X-ray measurements in these axial target experiments.

IV. Conclusion and Discussions

The shadowgraphs show that for the UNU/ICTP PFF, a flat target placed at a distance further than 10 mm does not affect the dynamics of the focusing event. Interaction may occur tens of nanoseconds later as the current sheet moves forward to hit the target. But such postfocus interaction does not affect the focus proper, and the attendant effects like neutron, soft X-ray, or beam production which all occur for this device within 50 ns of focus maximum. The presence of the target, however, could block the deuteron beam and reduce its beam–gas interaction as indicated by the reduced neutron yield. The soft X-ray yield in the presence and absence of targets should similarly be studied.

However, it must be borne in mind that this distance of 10 mm need not necessarily apply to all machines. From the shadowgraphs and even from a simple model of the plasma focus [8] which treats the focus as an elongating pinch, pressure considerations dictate that the rate of elongation is about equal to the rate of radial collapse. In that model, the radially collapsing shock front has a velocity driven by the constricting magnetic pressure. Since the axially moving shock front associated with the plasma elongation is driven by the same constriction pressure, the collapse speed is the same as the elongation speed. This means that the pinch length at maximum focus is about the radius of the anode. The rule of thumb is then this: A target should be placed at a distance from the anode greater than the radius of the anode in order to avoid target interference of the dynamics of the focus proper. This agrees with both focus theory as well as the present shadowgraph observations.

The flat-target experiments also indicate the possibility of using spaced flat discs as auxiliary anodes to produce sequential focus events. It should be interesting to further examine this effect to produce sequenced neutron and soft X-ray pulses with possible applications for neutron radiographic and soft X-ray cinematography.

Finally, the shadowgraphs taken with the thin axial wire target experiments show that the focus will form with reduced voltage spike on even a relatively thick (1 mm) wire. Preliminary calculations show that a thinner wire target (say a fiber of radius 0.1 mm) will restore the voltage spike to the value of the free focus. This is because the focusing voltage spike has an amplitude inversely proportional to the radius of the magnetic piston. In this connection we assume, and this assumption is consistent with the shadowgraphs of the focusing process (for example, Fig. 3(a)–(c)), that the fiber is not dynamically affected by the focus until the plasma sheath hits it. On impact, the focus plasma will then vaporize and heat the thin target to form a pinch of the original fiber material, although obviously a higher energy focus should be used. Such experiments open up several interesting possibilities.

A word about reproducibility. Each shadowgraph in this paper is 90% reproducible; i.e., it may be repeated in nine discharges out of ten when the system is properly adjusted. Such reproducibility [1] is typical of this small 3.3-kJ plasma focus that has been designated as the UNU/ICTP PFF.

Acknowledgment

The authors acknowledge the contributions of the International Center for Theoretical Physics to the ICTP-UM Training Program for Plasma Pulse Technology, without which this work would not have been possible. The authors also acknowledge the TWAS Travel grants to AVG and MAA which also contributed to this work, and the assistance of M. Favre, T. S. Toh, C. J. Wong, L. H. Soo, and L. C. Ching.

References

[1] S. Lee *et al.*, *Amer. J. Phys.*, vol. 56, p. 62, 1988.
[2] P. Cloth and H. Conrads, *Nucl. Sci. Eng.*, vol. 62, p. 591, 1977.
[3] A. Bernard *et al.*, *Nucl. Instrum. Methods*, vol. 145, p. 191, 1977.
[4] S. P. Moo, C. K. Chakrabarty, and S. Lee, *IEEE Trans. Plasma Sci.*, to be published.
[5] J. D. Sethian, A. E. Robson, K. A. Gerber, and A. W. DeSilva, *Phys. Rev. Lett.*, vol. 59, p. 892, 1987.
[6] R. Gratton, A. R. Piriz, and J. O. Pouzo, *Nucl. Fusion*, vol. 26, p. 483, 1986.
[7] K. H. Kwek, T. Y. Tou, and S. Lee, *IEEE Trans. Instrum. Meas.*, vol. 38, p. 103, 1989.
[8] S. Lee, "Technology of the plasma focus," in *Laser and Plasma Technology*, S. Lee *et al.*, Eds. Singapore: World Scientific, 1985, p. 387.
S. Lee, "Technology of a small plasma focus," in *Small Plasma Experiments II*, S. Lee and P. H. Sakanaka, Eds. Singapore: World Scientific, 1980, p. 113.
[9] G. Decker and R. Wienecke, in *Proc. 12th Int. Conf. Phenomena in Ionized Gases* (Eindhoven), 1975, J. G. A. Hölscher and D. C. Shram, Eds. Amsterdam: North-Holland, 1976, vol. 2, p. 155.

*

S. Lee received the B.Sc. and M.Sc. degrees in physics from the University of Malaya, Kuala Lumpur, Malaysia, in 1964 and 1966, respectively. He received the Ph.D. degree from the Australian National University, Canberra, in 1970.

Since 1970 he has lectured at the University of Malaya, where he is currently Professor of Applied Physics and Leader of the Research Groups on Plasma and Pulse Technology. He was a Alexander von Humbolt Research Fellow at Kerntorschungsanlage, Julich, West Germany, in 1975-1976, a Commonwealth Academic Staff Fellow at the Imperial College, London, Eng., in 1981-1982, and a Visiting Professor and United Nations University Special Fellow at Flinders University of South Australia in 1986-1987. He is currently President of the newly formed Asian-African Association for Plasma Training (AAAPT). He is the author of more than 100 research papers, and is an ardent advocate and implementor of South-South technology creation and transfer, especially in plasma, fusion, laser and pulse technology.

Dr. Lee is a Chartered Physicist and Fellow of the Institute of Physics, UK, and the Vice-President of the Malaysian Institute of Physics.

*

M. A. Alabraba received the M.Phil. degree in physics from the Rivers State University of Science and Technology, Port-Harcourt, Nigeria, in 1989. He is in the Ph.D. degree program of the same University and currently is a Research Fellow at the Plasma Research Laboratory, University of Malaya, Kuala Lumpur, Malaysia.

Ashok Vasudeo Gholap obtained the B.Sc. and M.Sc. degrees from Holkar Science College, Indore, India, and the Ph.D. degree from Shri G.S. Institute of Technology and Science, Indore, in 1971.

He was a Senior Lecturer and Head of the Physics Department at Rivers State University of Science and Technology, Port Harcourt, Nigeria, and has carried out research at the University of Malaya as a United Nations University Fellow and Third World Academy of Science Research Fellow. He is currently attached to the University of Zimbabwe, Harare.

*

S. Kumar received the B.Sc.(Hons.) degree in physics from the University Malaya, Kuala Lumpur, Malaysia, in 1989, where he is currently pursuing the M.Sc. degree.

*

K. H. Kwek received the B.Sc., M.Sc., and Ph.D. degrees in physics from the University of Malaya, Kuala Lumpur, Malaysia, in 1980, 1982, and 1989, respectively.

*

Mohammad Nisar received the M.Sc. degree in physics from Quaid-i-Azam University, Islamabad, Pakistan, in 1987. He is in the Ph.D. degree program of the same University and is currently a Research Fellow at the Plasma Research Laboratory, University of Malaya, Kuala Lumpur, Malaysia.

*

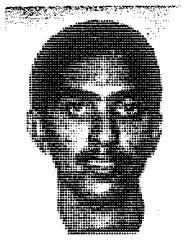

R. S. Rawat received the B.Sc. and M.Sc. degrees in physics from the University of Delhi (India) in 1985 and 1987, respectively. He is involved in the Ph.D. program at the same University and is currently a Research Trainee participating in the I.C.T.P. Training Program on Plasma and Pulse Technology (1989-1990) at the University of Malaya, Kuala Lumpur, Malaysia.

*

Jasbir Singh obtained the Diploma in electrical engineering (communications) from Universiti Teknologi, Malaysia, in 1978.

He is presently attached as a Technical Assistant with the Plasma Research Laboratory at the University of Malaya, Kuala Lumpur, Malaysia.

Laser Induced Plasmas and Fusion

S. Lee

Physics Department
Universiti Malaya
59100 Kuala Lumpur
Malaysia.

1. Laser produced plasmas

When a powerful laser beam is focussed to a small point in air, there is a breakdown of the air resulting in the appearance of an air spark, producing plasma using only light. This was first reported in 1963.[2]

Fundamental to this laser-plasma interaction are the following equations relating the electric field E(V/m) of the electromagnetic field to the lignt intensity I($Js^{-1}m^{-2}$), the photon flux $\Phi(m^{-2})$, P the radiation power (Js^{-1}) and $P_R(Nm^{-2})$ the radiation pressure for area illumination with focussing circle of radius r(m)

$$E = 19.4\ I^{\frac{1}{2}} = 11\frac{P^{\frac{1}{2}}}{r} \qquad \ldots\ 1$$

$$\Phi = 6 \times 10^{18}(I/h\nu) \qquad \ldots\ 2$$

$h\nu$, energy of photon in eV.

$$I = \frac{P}{\pi r^2} \qquad \ldots\ 3$$

$$P_R = 3.3 \times 10^{-9}\ I \qquad \ldots\ 4$$

---

* Invited paper to be presented at Second South East Asian Laser School, Yogyakarta, Indonesia. Jan 1991.

Electric fields associated with Q-switched laser pulses attain very large values. For example a 1 MW pulse focussed to a radius of 0.1 mm gives rise to an electric field of $\frac{11 \times 10^3}{10^{-4}} \sim 10^8$ V/m or 1 MV/cm. However this electric field, very large in comparison with breakdown threshold of electric sparks (30 kV/cm in atmospheric air) is not sufficient for air breakdown by laser pulses which requires[1] about 5 MV/cm. Typically electron densities of $5 \times 10^{19} cm^{-3}$ and temperatures of 5×10^5 °K are attained in air sparks created by Q-swithed laser pulses.

The main difference between laser produced sparks, and electric sparks is that the laser produced sparks require a multi-photon absorption mechanism before electron cascade.

As an example we have taken laser shadowgraphs[5] to show the development of air sparks. These shadowgraphs, together with the parameters of the set up are shown in the accompanying Figure 1.

When a powerful laser pulse is focussed onto the surface of a solid, plasma is produced from the heating at the focus site and material is ablated from the surface. The threshold intensity is of the order of several GW/cm^2. As material is ablated, the reaction, the rocket effect, presses on the ablated surface.

An example of this effect is shown in the following Figure 2, showing shadowgraphs of the shock wave produced

from plasma ablated from a focussed ruby laser pulse onto a surface.[5]

II. Laser fusion

Heat a small pellet from all sides (Fig. 3). Material is ablated from surface of pellet. Resultant rocket effect, if ablation pressure is sufficient, compresses the pellet. If sufficiently high temperature and density are created, fusion reactions will take place.

Fusion reactions that are considered

$$D^2_1 + T^3_1 \rightarrow n^1_0 + He^4_2 + 17.6 \text{ MeV} \quad \ldots\ldots \quad 5$$

(Ideal ignition temperature: 4keV)

$$D^2_1 + {}_1D^2 \rightarrow n^1_0 + He^3_2 + 3.2 \text{ MeV} \quad \ldots\ldots \quad 6$$

(IIT : 40 keV)

$$D^2_1 + D^2_1 \rightarrow T^3_1 + P^1_1 + 4.0 \text{ MeV} \quad \ldots\ldots \quad 7$$

(IIT : 40 keV)

Temperature equivalence: 1 keV = 1.14×10^7 °K

The potential of nuclear fusion may be seen by the following example. The deuterium in 1 litre of sea water undergoing fusion produces the energy equivalent to 300 litre of gasoline.

Reaction cross section[3] is expressed by $\langle \sigma V \rangle$ as shown in the following Figure 4.

III. Conditions for laser fusion

1. Input energy required for breakeven

To heat the pellet to fusion conditions requires the input of laser energy. The gain factor G is defined as the ratio (fusion energy produced)/(thermal energy input).

The energy required to heat a pellet of radius R to temperature T is: (where n is electron density and also ion density).

$$E_{thermal} = 3nkT \cdot \frac{4}{3}\pi R^3 = 4\pi(nR)^3 \frac{kT}{n^2} \quad \ldots\ldots \quad 8$$

The fusion energy is

$$E_{fusion} = \left(\frac{n}{2}\right)^2 \langle\sigma V\rangle Q \left(\frac{4}{3}\pi R^3\right)\tau \quad \ldots\ldots \quad 9$$

where $\langle\sigma V\rangle$ is the fusion cross-section corresponding to temperature T and Q is the fusion energy per reaction. The time interval during which fusion takes place, τ, may be taken to be the pellet disassembly time. This has a value of R/V_s where V_s is the velocity of small disturbances. Considering that more mass lies in the outer half of the radius than the inner half a more correct disassembly time[4] is found to be

$$\tau = \frac{R}{4V_s} \quad \ldots\ldots \quad 10$$

Therefore, gain factor

$$G = \frac{E_{fusion}}{E_{thermal}} = \frac{\frac{1}{4} n^2 \langle\sigma V\rangle Q \frac{R}{4V_s}}{3nkT} \quad \ldots\ldots \quad 11$$

At breakeven,

$$G = 1 \text{ and } nR = \frac{48\ V_s\ kT}{\langle \sigma V \rangle Q} \qquad \ldots\ldots \quad 12$$

Substituting this expression of nR in eqn. (8)

$\therefore$ At breakeven:

Input energy required to heat plasma,

$$E_{thermal} = 4\pi \left[\frac{48 V_s kT}{\langle \sigma V \rangle Q}\right]^3 \frac{kT}{n^2} \qquad \ldots\ldots \quad 13$$

$$\text{Thus } E_{thermal} \sim \frac{1}{n^2} \qquad \ldots\ldots \quad 14$$

For a temperature of 10 keV required energy in laser pulse is :

$$E_{Laser} = 1.6 \left(\frac{n_s}{n}\right)^2 \text{ MJoule} \qquad \ldots\ldots \quad 15$$

where solid density, $n_s = 5 \times 10^{22}\ cm^{-3}$

Thus energy input required to heat pellet up to breakeven condition is inversely proportional to density squared. That is, compression reduces energy requirement. In the context of laser inertial confinement fusion, this compression typically starts from solid density and goes considerably above solid density.

At solid density i.e. with no compression 1.6 MJ is required to fulfil G=1. However this is not a sufficient condition since for energy applications G has to be much larger than 1.

2. Gain factor G as function of compression

The gain G may be rewritten as[6]

$$G = \left(\frac{E}{E_{BE}}\right)^{1/3} \Gamma^{2/3} \qquad \ldots\ldots \quad 16$$

for a 50:50 D-T mixture at 10.3 keV

Here Γ = ratio of compressed density to initial liquid D-T density and E_{BE} = 1.6 MJ absorbed by the pellet. This formula may also be written as:

$$G = \left(\frac{E}{E_{BE}}\right)^{1/3} \kappa_m^{-2} \qquad \ldots\ldots \quad 17$$

where κ_m is the radius ratio, (final radius)/(initial radius) of the compression.

3. Radius R and range of α particles

A commonly accepted scheme is based on the implosion of a pellet (a shell containing the D-T fuel) with consequent self-heating through nuclear reactions in a central ignition region of high temperature with radius R. The compressed density may be hundreds of times solid density and α-particles (ionised He) are generated from the D-T fusion reaction each carrying 3.5 MeV of energy (see Eq. 5). To assist the process of heating and burning it is necessary to absorb these α-particles so that a fusion burn wave would propagate radially outwards from the central ignited (fusion) region. This will lower the laser energy requirement. The range of α-particles R_α

under these conditions may be written as:

$$R_\alpha = \left(\frac{n_s}{n}\right)\left(\frac{T}{T_{10}}\right) cm \qquad \text{where } T_{10} = 10 \text{ keV} \qquad \ldots. 18$$

Thus for $n = 10^3 n_s$ at fuel temperature $T = 10$ keV

$$R_\alpha \sim 10^{-3} \text{ cm}$$

Thus if the pellet size is of the order of mm, the α-particles will assist in the heating. The neutrons have a much greater range and will not assist in this self-burn process.

4. Confinement criterion ($n\tau$)

To heat the pellet to a high temperature a fixed amount of energy has to be invested. To recover this energy from the pulsed compression, the nuclear fusion burn must last for a sufficient time τ which may be taken as the confinement time of the system. This is expressed in the Lawson's criterion for pulsed fusion system with a conversion efficiency of 1/3.

The confinement criterion for breakeven is

$$n\tau = 10^{14} \text{ s-cm}^{-3} \qquad \text{D-T} \qquad \ldots. 19$$

$$n\tau = 10^{16} \text{ s-cm}^{-3} \qquad \text{D-D} \qquad \ldots. 20$$

A figure of $n\tau = 2 \times 10^{15}$ s-cm^{-3} is aimed for in a fusion reactor.

Confinement criterion (ρR)

$$\text{Since } \tau = \frac{R}{4V_s}$$

$$n = \frac{\rho}{m_i}$$

$$n\tau = \frac{\rho R}{4 m_i V_s} \quad \ldots\ldots \quad 21$$

Thus for $n\tau = 2\times10^{15}$ s-cm^{-3}, $m_i = 2\times1.6\times10^{-27}$ kg, $V_s = 10^6$ m/s

we have $\rho R = 3$ gm/cm^2

Since liquid density of D-T is 0.2 gm/cm^3

for $\rho R = 3$ gm/cm^2 we may draw up the following table:

R	ρ required	density compression ratio	$\kappa = \frac{\text{final radius}}{\text{initial radius}}$
15cm	0.2gm/cm^3	1	1
5cm	0.6gm/cm^3	3	0.7
1cm	3gm/cm^3	15	0.4
1mm	30gm/cm^3	150	0.19
0.1mm	300gm/cm^3	1500	0.09

R = 15cm corresponds to 3kg of D-T fuel which, if undergoes fusion completely produces an energy equivalent of about 300 kiloton TNT.

R = 1mm corresponds to 1 mg of D-T fuel has a fusion energy equivalent of 100 kg TNT (340 MJ).

Thus whilst bomb-sized 'pellets' do not require compression to fulfil the Lawson's criterion, reactor sized pellets may need large compression of 100-1000 times with corresponding radius reduction to $\frac{1}{10}$ original size.

Can this order of compression be achieved?

5. Gain factor, coupling efficiency, and burn fraction

The Gain factor G also depends on the coupling efficiency η and the burn fraction ϕ.

We may write

$$E_{fusion} = m E_b \phi \qquad \text{.... 22}$$

m = mass of fuel
E_b = fusion output per unit mass
ϕ = fraction of burn

Laser Energy to heat to required condition:

$$E_L = \frac{m E_h}{\eta} \qquad \text{.... 23}$$

E_h = energy per unit mass required to heat and compress
η = coupling efficiency

$$\therefore \quad G = \frac{E_{fusion}}{E_{Laser}} = \eta\phi \frac{E_b}{E_h} \qquad \text{.... 24}$$

For example,

at 5keV, estimated $E_b = 3.4 \times 10^{11}$ J/gm

$E_h = 5.8 \times 10^{8}$ J/gm

If $\phi = 50\%$

$\eta = 10\%$

$\therefore \quad G = 30$

Such a gain is insufficient for a practical reactor.

6. Central zone heating and Gain ennancement

We may divide the energy expended in a compression into two separate parts

Energy expended = energy of compression without heating, E_F or (Fermi Energy)

+ energy of heating, E_h

The Fermi energy is much less than the energy of heating and hence gain G may be enhanced by heating only the central zone of a pellet.

Then the enhanced $$G = \frac{n\phi E_b}{E_c + (\frac{m_h}{m}) E_h} \quad \ldots\ldots 25$$

$\frac{m_h}{m}$ is fraction of fuel that is heated.

7. Burn fraction ϕ

The burn fraction f_b may be estimated in the following way:

Reaction rate: $$\frac{dn}{dt} = -\tfrac{1}{2} n^2 \langle \sigma V_i \rangle \quad \ldots\ldots 26$$

giving, on integration:

$$\frac{1}{n} - \frac{1}{n_o} = \frac{1}{2} \langle \sigma V_i \rangle \tau \quad \ldots\ldots 27$$

where n_o = initial number density,

n = number density of particles that have not undergone fusion.

$$\phi = \frac{n - n_o}{n_o}$$

Noting $\tau = \frac{R}{4V_s}$ and $n_o R = \frac{\rho R}{m}$

$$\therefore \quad \phi = \frac{\rho R}{\beta + \rho R} \qquad \ldots\ldots 28$$

where $\beta = \frac{8 m_i V_s}{\langle \sigma V_i \rangle} \sim 6.3$ at 20 keV D-T.

$$\therefore \quad \phi = \frac{\rho R}{6.3 + \rho R} \qquad \ldots\ldots 29$$

For $\rho R = 3$ gm/cm^2 (required for confinement)

$f_b = 0.3$ i.e. 30% fuel burn-up before disassembly.

8. Critical design requirements

In consideration of the above, the following have been put up as requirements to achieve target gain of 100 considered necessary for reactor purposes[3]

a. coupling efficiency η from absorbed energy to heated fuel must be higher than 5% $\eta > 5\%$

b. preheating of the core must be less than 10eV at liquid density

c. radius of compressed core must be less than $\frac{1}{30}$ initial radius $\kappa_m < \frac{1}{30}$

d. density of compressed fuel must exceed 200 g/cm^3

$\rho_m > 1000\, \rho_o \quad \rho_o = 0.2$g/cm^3

e. temperature of ignition plasma 10 keV

f. radius of compressed fuel must be larger than range of α-particles $R_m > R_\alpha$

9. Limits to compression?

Can we compress as much as we like or are there limits to compression? It is known but not widely discussed that to achieve high compressions, laser pulse profiling is required. The profiling is usually accomplished in relation to computer programmes which are designed interactively with experiments to help improve compressions.

It is however possible to set limits of compression[6] through simple physical mechanisms as we know that the physics determining the compression is governed by the laws of conservation of energy, momentum and the thermodynamic equations of state; so that in principle the limits of compression may be defined by an examination of these equations.

A simplified basic model may be set up as follows. Consider a spherical pellet irradiated uniformly by intense radiation as illustrated in Figure 5. The radiation power $P(Js^{-1})$ has associated with it radiation intensity $I=P/(4\pi r^2)$ $(Js^{-1}m^{-2})$ in this spherical geometry.

Assume the radiation pressure is fully coupled on the surface of the pellet and continues for the period of the pulse. Assume that the radiation pressure is sufficient to cause the radiation piston to implode supersonically. Then a shock front will propagate ahead of the piston, the shock front being the transition region between ambient pellet condition and piston compressed condition. The situation is shown in Figure 6a where both the imploding radiation

piston and the converging (radially inwards) shock front are moving inwards. When the shock front has converged onto the pellet centre a reflected shock moving radially outwards is propagated. This is shown in Figure 6b and also in Figure 7. In Fig.7 the region A represents ambient condition, B shocked condition and C reflected shock condition. The point M represents the time and radius of maximum compression just before pellet disassembly.

Energy equation

The work per unit mass done by the converging piston up to point M is

$$W_m = \frac{1}{(\frac{4}{3}\pi\rho_m r_m^3)} \int_{r_m}^{r_o} \frac{3.3\times10^{-9}}{(4\pi r^2)} P.4\pi r^2 \, dr \quad .... 30$$

where the subscript m denotes the quantity at point of time M. The plasma internal energy U per unit mass is:

$$U_m = CD \frac{T_m}{\gamma-1} \quad .... 31$$

where C is the Universal Gas Constant divided by the molecular weight, D the departure coefficient, γ the specific heat ratio.

At time M, assume that the plasma particles have no directed kinetic energy. Assume also no energy gain and no energy loss. Hence we may equate W_m and U_m to obtain the temperature:

$$T_m = \frac{3.3\times10^{-9}(\gamma-1)}{\frac{4}{3}\pi\rho_m r_m^3 \, CD} \int_{r_m}^{r_o} P dr \quad ....32$$

Pressure equation

Next consider the pressure relationship at time M. The plasma kinetic pressure $P_m = CD\rho_m T_m$ exceeds the radiation pressure P_{Rm} by the reflected shock pressure jump factor f_{rs}. This gives us

$$T_m = \frac{3.3\times10^{-9}\ P_m f_{rs}}{4\pi r_m^2\ \rho_m\ CD} \qquad \ldots\ldots\ 33$$

Energy and Pressure balance point

From the values of T_m obtained through energy balance and through pressure balance[6] we obtain :

$$P_m = \frac{3(\gamma-1)}{f_{rs}\ r_m} \int_{r_m}^{r_o} P dr. \qquad \ldots\ldots\ 34$$

This equation specifies the radius r_m at which both the energy and pressure conditions of equations 32 and 33 are simultaneously met. This equation shows

- The radius ratio $\kappa_m = r_m/r_o$ is independent of the absolute magnitude of the radiation power which may be P_m or any fraction of it.
- The radius ratio is a function of:

  γ

  f_{rs}

  and the pulse shape (as a function of r or t)

Example 1. Square pulse radiation power R=constant

Taking P=constant, $\gamma = \frac{5}{3}$, $f_{rs} = 4$

Eqn. 34 integrates to give

$$\kappa_m = 0.33 \quad \text{or} \quad \Gamma_m = 27$$

Example 2 Stepped square pulse - enhanced compression

The effect of pulse shape may be seen from Figure 8 which follows the LHS F_L and RHS function F_R of Equation 34 where $F_L = P_m$ and $F_R = [3(\gamma-1)/f_{rs} r_m] \int_{r_m}^{r_o} P dr$. From this Fig. it is seen that as the compression progresses with decreasing κ as the F_L function approaches the F_R function if the radiation power is suddenly increased from P_m to nP_m, say, F_L goes up vertically, but F_R, being an integral rises less abruptly than the rise in F_L. Thus the meeting point of F_R and F_L is moved to a smaller value of κ.

Thus Eqn. 34 is able to predict the compression enhancement effect of pulse shaping.

Effect of pulse shaping

The effect of pulse shaping has been computed for various cases using $P_m = 10^{16}$W, $r_o = 100\mu$m of 50:50 DT at 10.3 keV, through the use of equations 34, 15, 16, and 32 together with a snowplow equation which gives the characteristic time of compression for $r_o = 100\mu$m and $\rho_o = 0.2$ g/cm^3

$$\text{as } t_p = \left(\frac{4\pi \times 10^8 \rho_o r_o^4}{P_o}\right)^{1/2} = 5\times10^{-3} P_o^{-\frac{1}{2}} \quad \ldots\ldots 35$$

For this case of $P_m = 10^{16}$W, $r_o = 100\mu$m D-T pellet we have 50ps for the characteristic compression time at a speed of 2×10^6 ms^{-1}. The computations yield[6]

	Case 1 square pulse	Case 2 Linearly rising pulse	Case 3 stepped square pulse	Case 4 stepped linearly rising pulse
T_m(keV)	26	16	14	7
E (MJ)	0.5	0.4	0.45	0.38
$K_m(r_m/r_o)$	0.33	0.2	0.17	0.083
$\Gamma_m(\frac{\rho_m}{\rho_o})$	28	125	203	1750
G	6	16	23	90

G for $r_o = 100\mu m$, $P_m = 10^{16}W$

IV. Physics and Technology of Laser Fusion

To understand actual experiments there is a whole body of physics that needs to be studied in detail. These include: Absorption of laser light in plasmas - classical absorption, collective effects, resonance absorption; filamentation and self-focussing; energy transport, flow of heat and material; implosion symmetry and stability; target hydrodynamics, uniformity and efficiency of ablation pressure. This may be summarised[4] in Figure 9 showing the interaction processes surrounding a pellet driven by intense laser pulse. Figure 10 and Figure 11 show the time history[3,4] of a laser compression and the relationship of the trajectory with a typical driven pulse. There is also the technology of targets - for direct laser drive, and

with high gain targets; indirect drive using the Osaka cannon-ball concept in which a space around the target is filled either with plasma - plasma drive; or with x-ray - radiation drive. Above all there is the technology of high power lasers, glass lasers, UV excimer lasers. These include the 12 beam glass laser Gekko XII of Osaka University with 20 kJ, 1ns [2×10^{13}W] in 12 beams, the 24 beams of LANL ANTARCS with 40kJ in 1ns or 4×10^{13}W.

A glimpse of target fabrication technology may be seen in Figure 12 which shows the assembly of the Osaka "cannon-ball", with the experimental parameters of Figure 13. A view of the NOVA glass laser facility of LLNL, 10 beams with 120 kJ output is shown in Figure 14. Figure 15 shows a ICF reactor design.

References

In the preparation of the above paper the following papers have been used as general and specific references:

1. C.De Michelis, IEEE J. Q. Electronics QE-5, (1969).
2. C. Grey Morgan, "Laser-Plasma Interactions" Review Paper delivered at First Tropical College on Applied Physics (1984); Procs. "Laser and Plasma Technology" pg. 624, Ed. S. Lee, B.C.Tan et.al, World Scientific (1985).
3. C. Yamanaka,"Review of Laser Fusion" Invited Paper presented at Energy Independence Conference, Aug. 1987, Rio de Janeiro; Procs. "Fusion Energy and Plasma Physics" pg. 567, Ed. P.H.Sakanaka, World Scientific (1988).

4. H.C. Pant, "Inertial Confinement Fusion Using Lasers" Review paper presented at the Third Tropical College on Applied Physics (1988); Procs. "Laser and Plasma Technology", pg. 210, Ed. by C.S.Wong, S.Lee, B.C.Tan et.al., World Scientific (1990).

5. Suresh Kumar, S.Lee, Harith Ahmad, J. Fizik Malaysia 11, 24 (1990) also Suresh Kumar, M.Sc. Thesis (UM)-in preparation (1991).

6. S. Lee, Laser and Particle Beams 6, 597 (1988).

1(a)

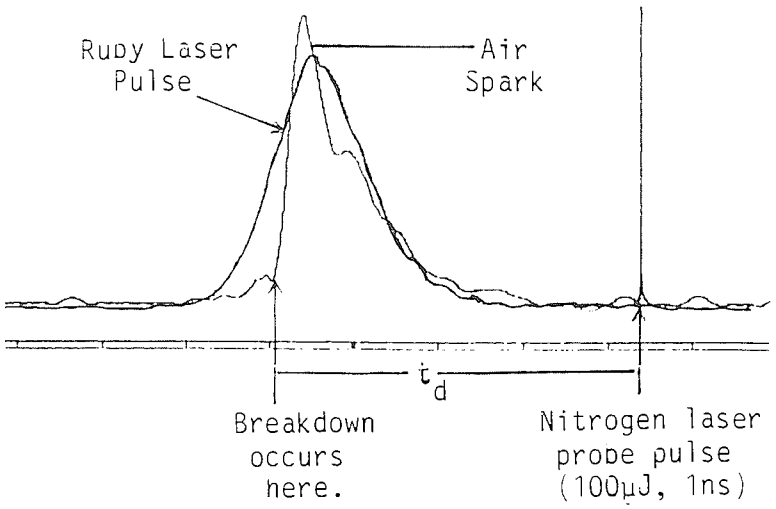

Ruby laser pulse characteristics.

Energy:- 1.18 J

Pulse width :- 60ns

Average Power:- 20 MW

Peak Power:- 50 MW

Focal spot size:- 0.15 mm

Peak Power density :- 7×10^{10} W/cm

Air at atmospheric pressure.

1(b) Shadowgrapns at different t_d.

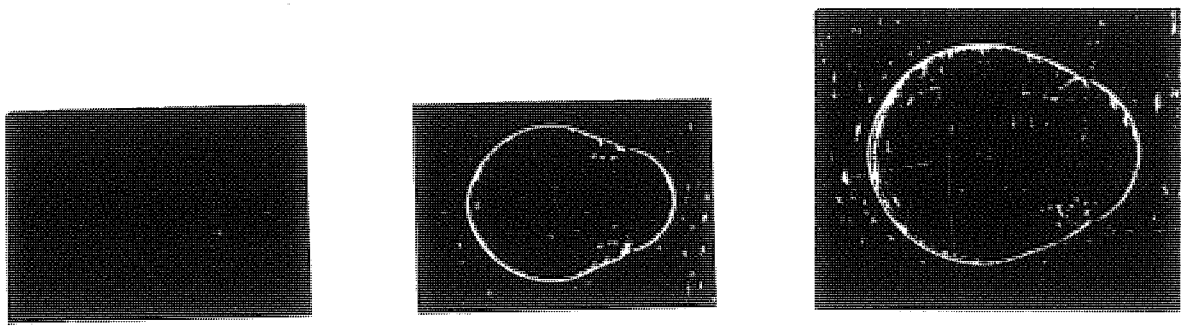

t_d = 60 ns t_d = 2.0 μs t_d = 8.0 μs

1(c)

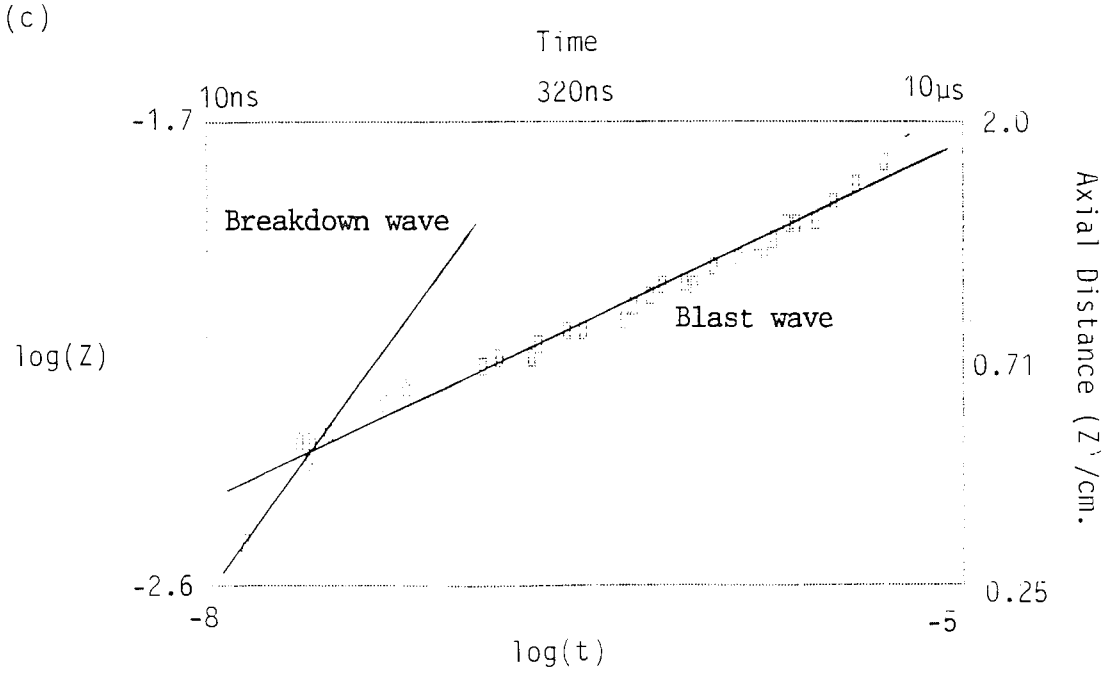

Fig.1 Shadowgrapns of Laser Induced Breakdown in Air.

2(a)

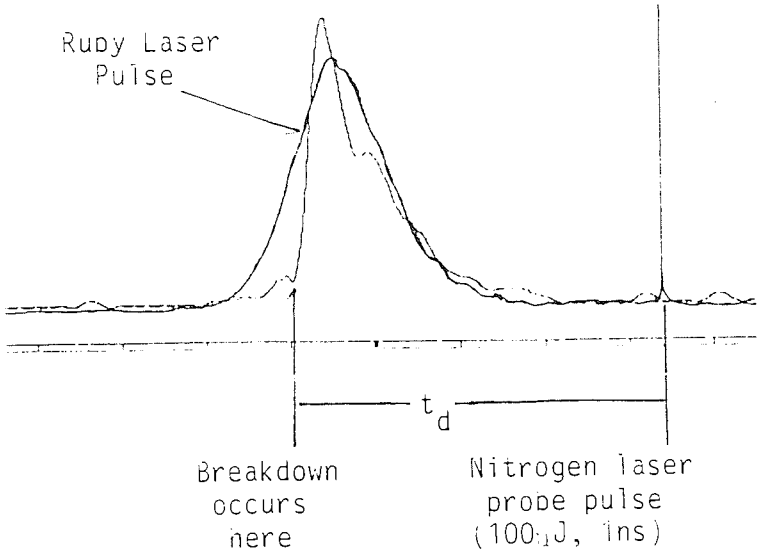

Ruby laser pulse characteristics.

Energy:- 0.6 J

Pulse width:- 80 ns

Average Power:- 7.5 MW

Focal spot size:- 0.09 mm

Power density:- 3×10^{10} W/cm^2

Graphite Target.

2(b) Shadowgraphs at different t_d.

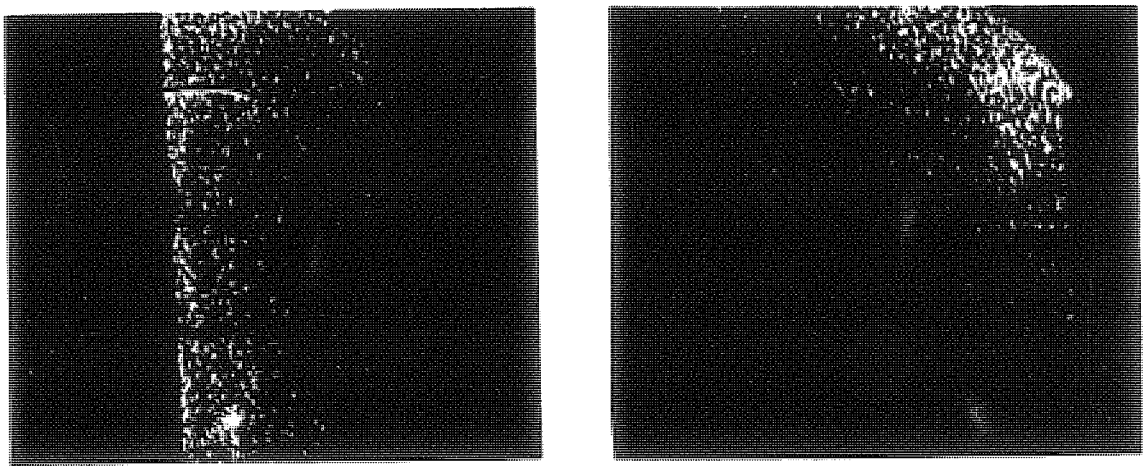

t_d = 9.0 μs

t_d = 152 μs

Fig.2 Shock Waves and Abalation Produced by a Focused Ruby Laser Beam on a Graphite Block.

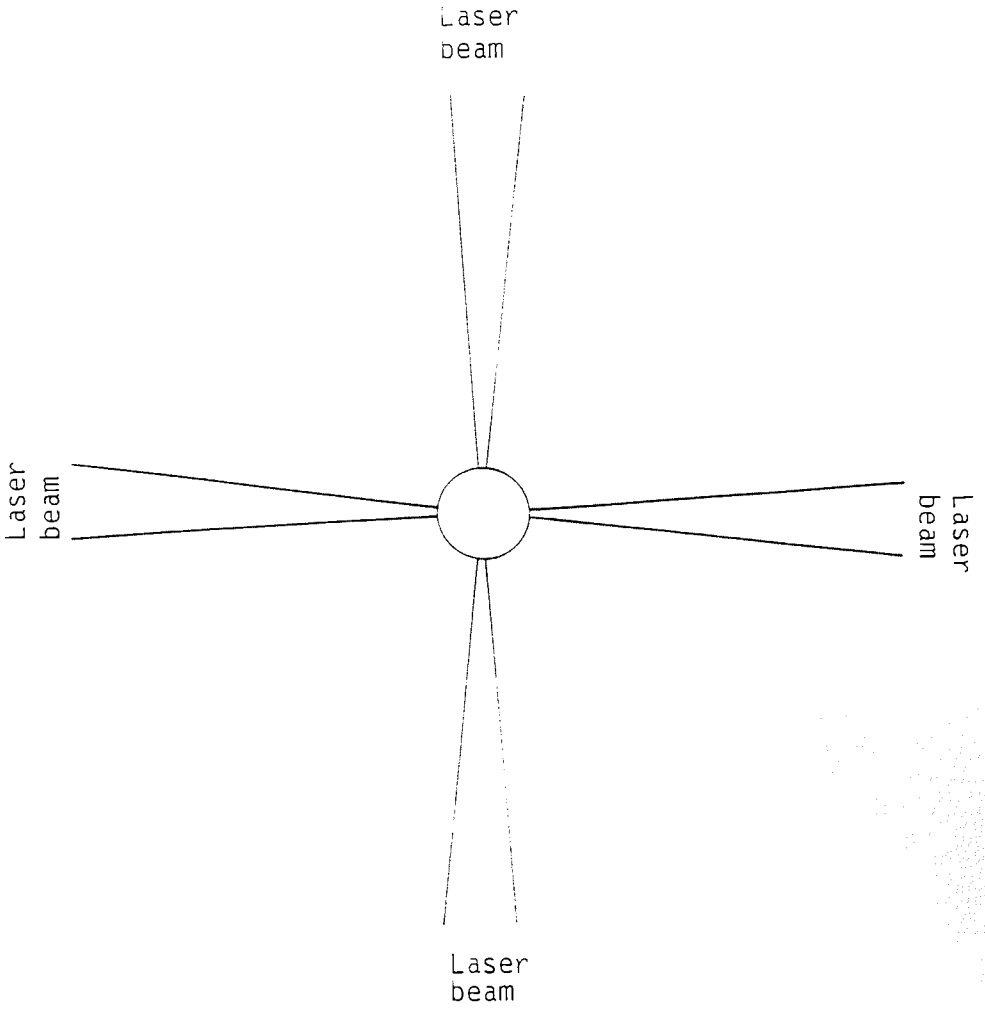

Fig. 3. Heating of pellet

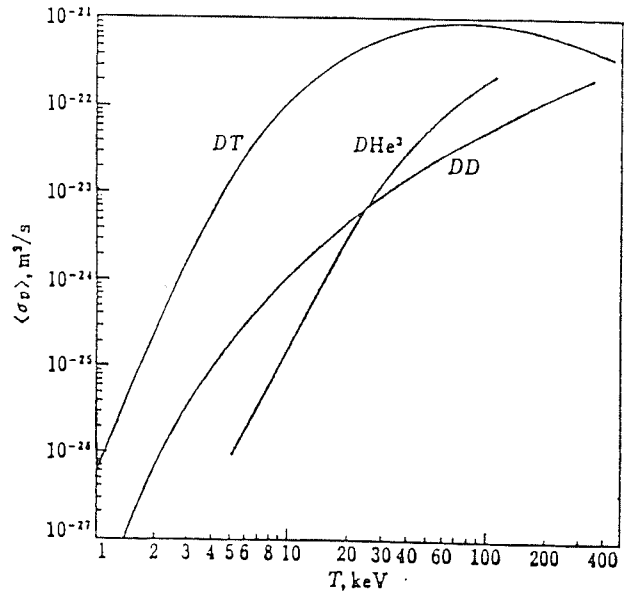

Fig. 4. Values of <σV > of typical fusion reactions.

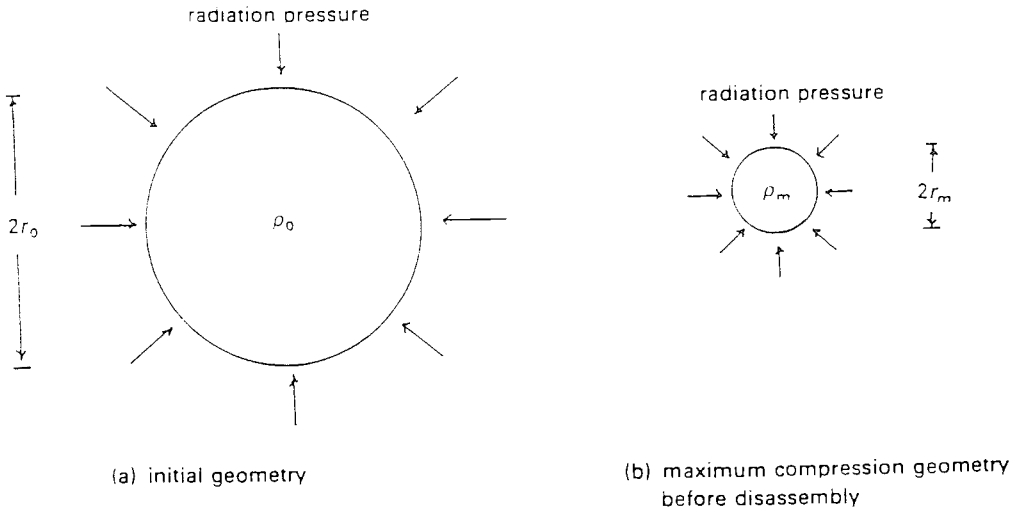

Fig. 5. Idealized representation of spherical compression of pellet by radiation piston.

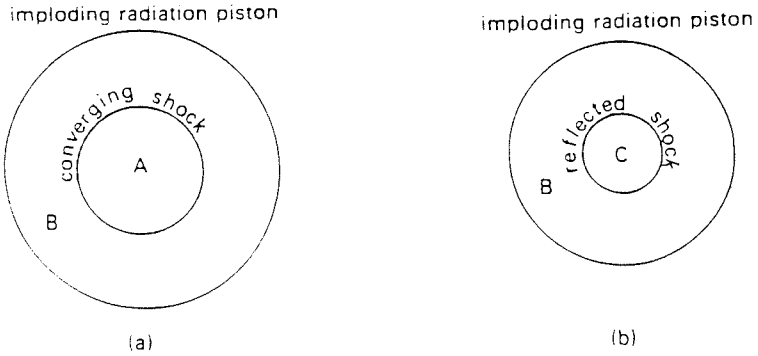

Fig. 6. (a) Imploding radiation piston driving a converging (forward) shock, before the forward shock has hit the centre. Region A=ambient pellet condition, region B= piston compressed (singly shocked) condition. (b) Imploding radiation piston driving a diverging (reflected) shock, after the forward shock has hit the centre. Region B=singly shocked region, region C=doubly shocked region.

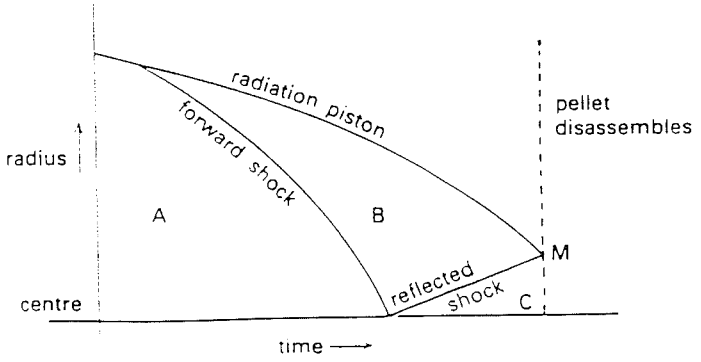

Fig. 7. Trajectory of pellet compression showing regions, A, B and C of figure 2.

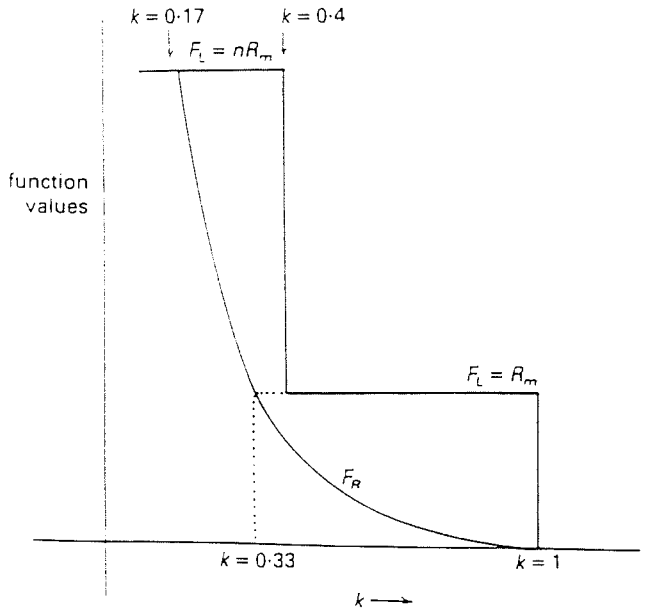

Fig. 8. Illustrating the effect of a stepped square pulse in shifting the convergence point of functions F_L and F_R to a smaller radius.

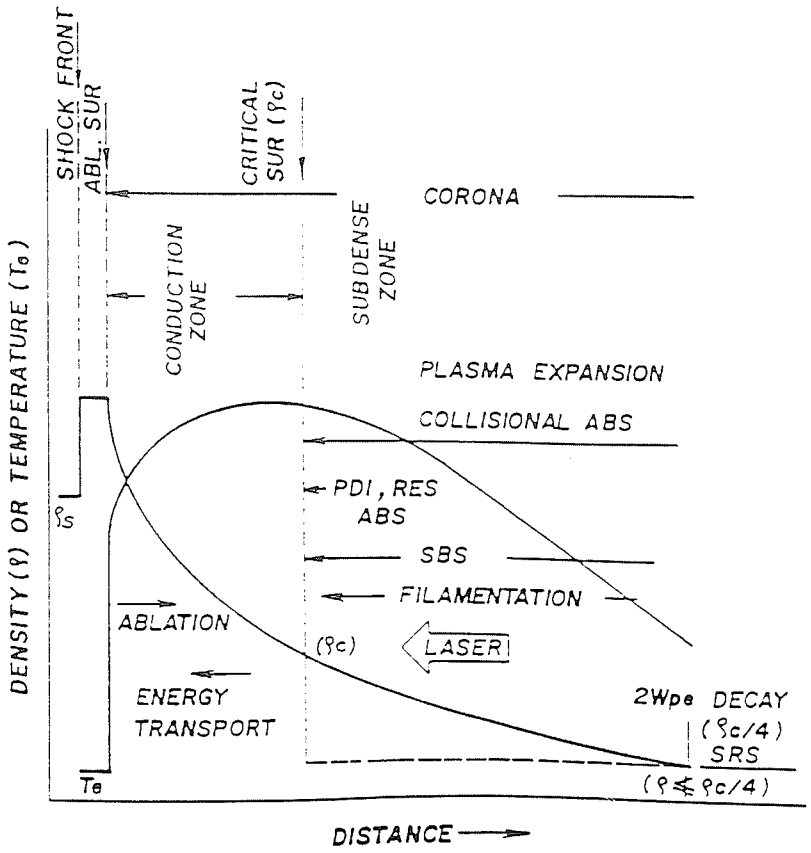

Fig.9. Plasma density and temperature profiles in a solid target-laser interaction. Figure shows various interaction processes considered with their region of occurence.

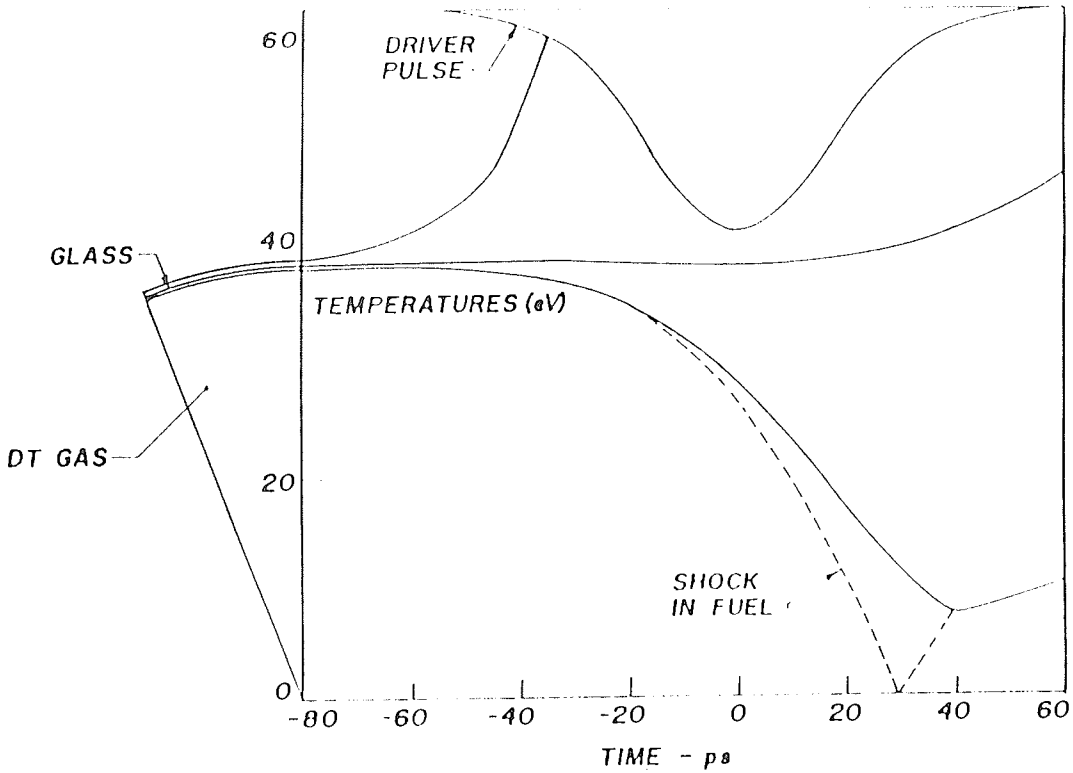

Fig. 10. The typical exploding-pusher target is characterized by a thin glass pusher irradiated with a short, high intensity laser pulse. High super-thermal-electron preheat and a strong ion shock wave in the fuel lead thermonuclear temperatures and low final density.

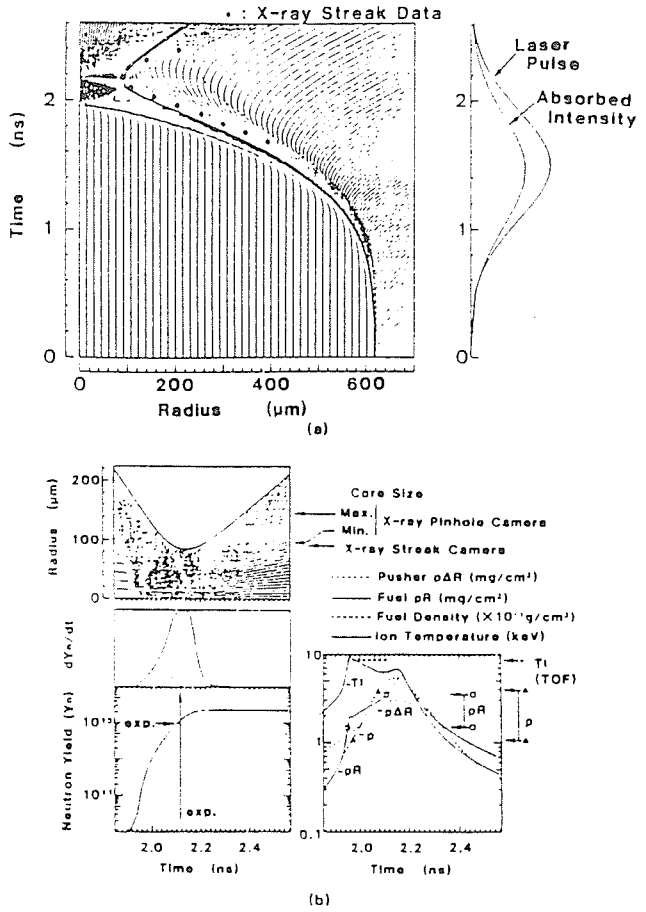

Fig. 11. Flow diagram and temporal evolutions of neutron yield, ion temperature, fuel density and areal mass density for GMB of 1235μm diam. and 1.31μm thickness with 6.2atm DT.
(a) flow diagram and the positions of the pusher-fuel contact surface which are measured by X-ray streak camera.
(b) neutron yield, ion temperature, fuel density and areal mass density of a simulation. Arrows indicate the experimental results.

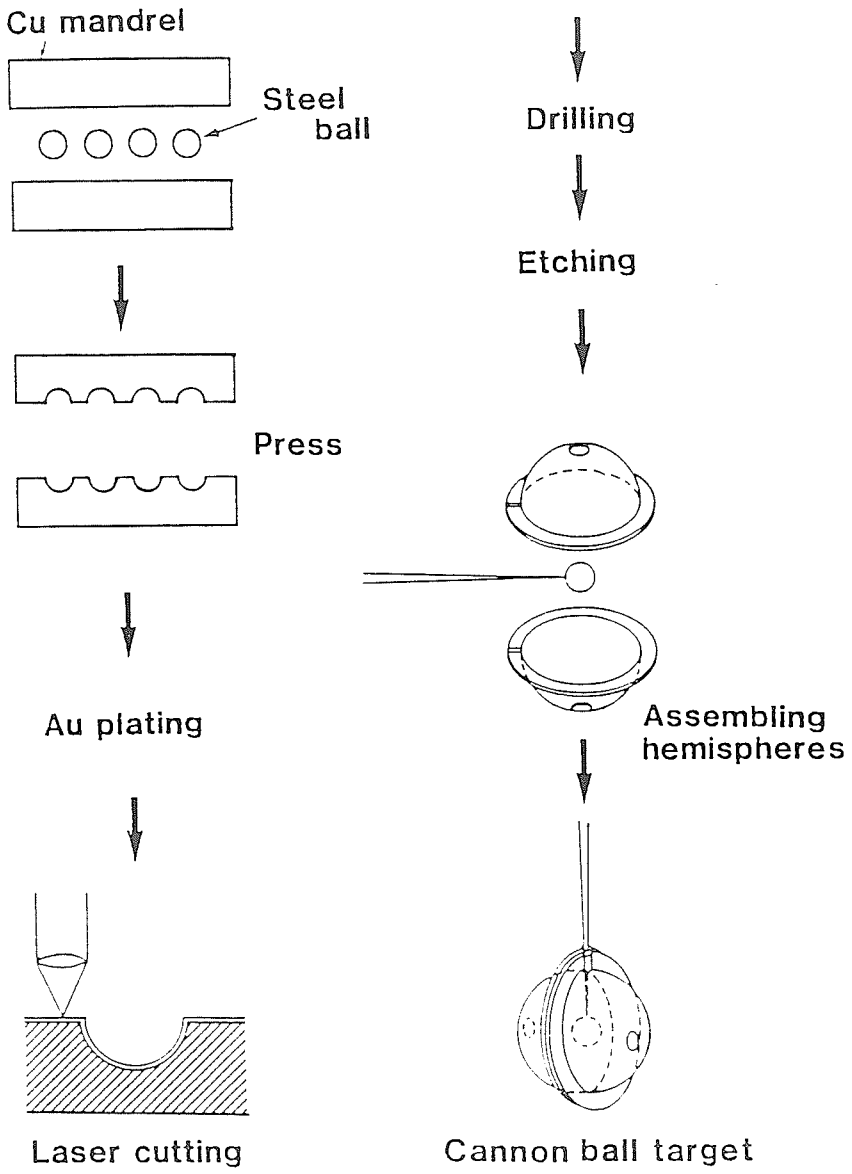

Fig. 12. Fabrication process of a cannon ball target.

Target and laser parameters	
Outer shell radius (R_{out})	1 mm～1.25mm
Outer shell thickness (Au)	>15 μm
Inner shell radius (R_{in})	400μm ～800 μm
Inner shell thickness	10 μm ～15μm
Laser pulse width	1nsec
Laser energy	10kJ

Figure 13. Target for radiation drive cannon ball implosion.

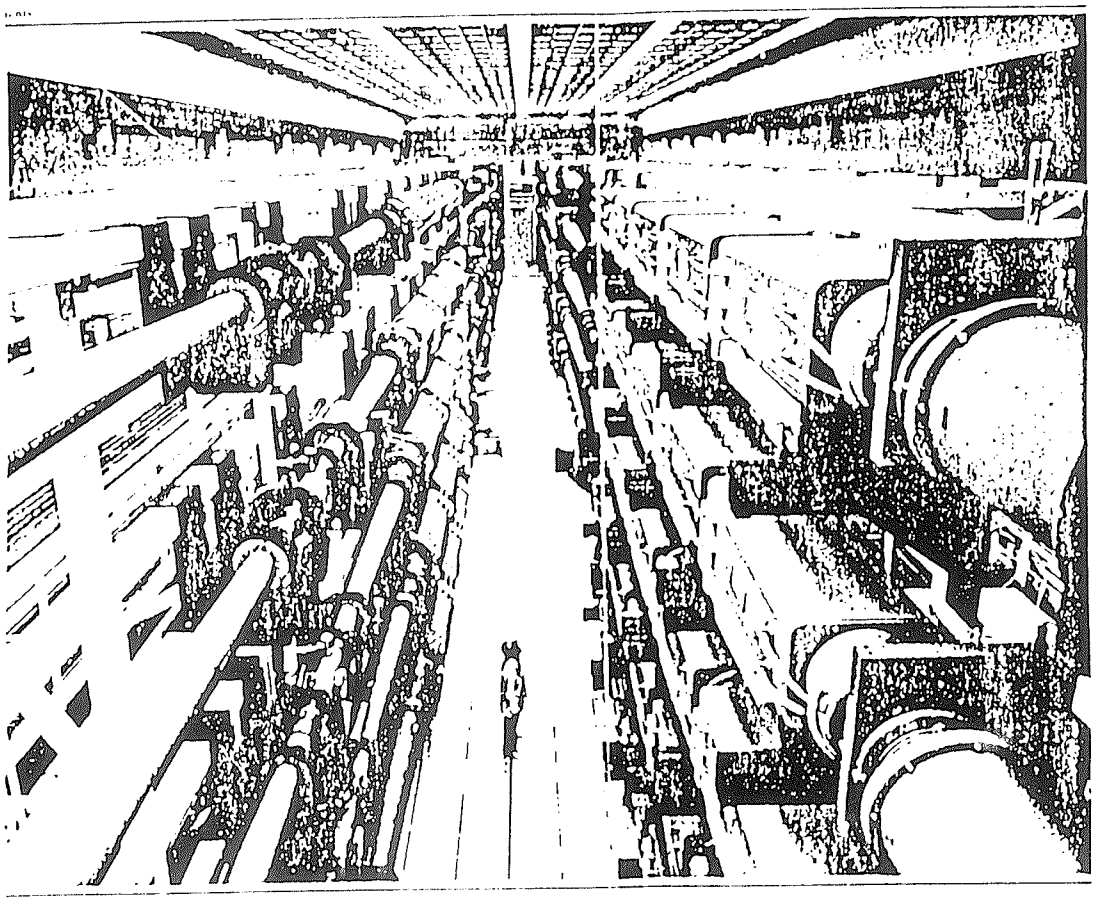

Fig. 14. NOVA laser system in Lawrence Livermore National Laboratory.

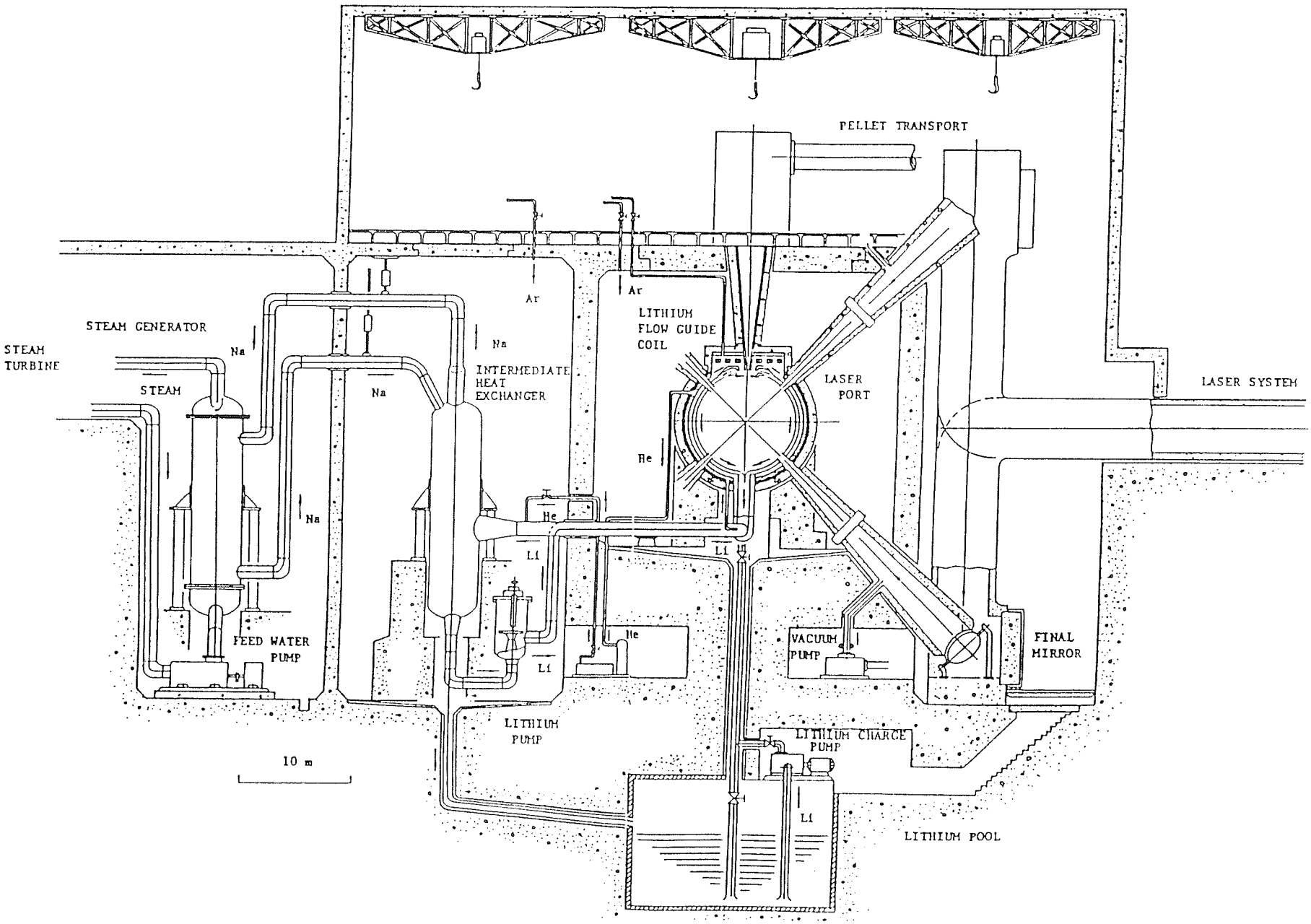

Fig. 15. Cross-sectional view of the reactor room of SENRI-I

An Investigation of the Ion Beam of a Plasma Focus using a metal obstacle and a deuterated target

S.P. Moo, C.K. Chakrabarty and S. Lee

Plasma Research Laboratory, Physics Department, University of Malaya 59100 Kuala Lumpur, Malaysia

Abstract

This paper reports the results of an experiment using a metal (copper) obstacle and a deuterated target to study the ion beam properties of a 3.3 kJ, 15 kV plasma focus. The plasma focus is operated at 3 torr deuterium and neutron yield measurements are made with the obstacle or the target placed at various axial positions from the end of the anode. It is found that in the normal operation of the focus without an obstacle or a target, less than 15 % of the neutrons are produced within the pinch column, and that more than 85 % of the neutrons arise from the deuterium ion beam bombardment of the deuterium gas in the region 20 mm - 60 mm from the end of the anode. The neutron production is highest between 30 mm - 40 mm from the anode.

IEEE Trans. on Plasma Science (accepted)

Introduction

Recent experiments [1-12] on the plasma focus have yielded a lot of data on the ion beam generated in the plasma discharge. A variety of techniques have been employed. These include the use of Thomson parabola spectrometers, ion pinhole cameras, track detectors, time-of-flight Faraday cups, time-of-flight neutron spectrometers, nuclear activation and nuclear emulsions. A simple technique which involves the bombardment of a solid target with the ion beam has also yielded useful data. In fact, using such a technique, Cloth and Conrads [13], and Bernard et al. [14] have confirmed the importance of the beam - gas target mechanism for the neutron production in the plasma focus. They further showed the presence of a high energy component ($E > 600$ keV) in the deuterium ion beam. Bernard et al. have also suggested the use of a deuterated target for studying the duration of the deuterium beam.

In this paper we report the results of an experiment using a metal (copper) obstacle and a deuterated target placed, in turn, at various axial distances from the end of the anode in a plasma focus device. The neutron yields with and without a solid target are measured and compared.

Based on documented experimental results [1,2,9,13,14] it is reasonable to interpret our neutron yield measurements from the perspective of a deuteron beam - target mechanism whilst not excluding the possiblities of non-beam mechanisms such as thermonuclear fusion. Our results of neutron yields using a copper obstacle and a deuterated target are consistent with a beam-target mechanism playing a primary role (more than 85 %) with a non-beam mechanism being responsible for the rest of the yields.

Experiment

The plasma focus device used in this work is the 3.3 kJ UNU/ICTP PFF [15]. It is operated at 3 torr deuterium at 15 kV and 180 kA peak current. Neutron yield measurement is by means of an indium foil - NE102 plastic scintillator activation detector [16] placed 170 mm from the end of the anode.

The deuterated target (obtained from Amersham Int. Ltd) has an effective diameter of 25.4 mm and contains about 10^{20} deuterium atoms absorbed in a thin layer of titanium deposited on copper. By means of a target holder, kept at floating potential, the deuterated target or a copper obstacle of similar size can be placed at various axial positions (z) from the end of the anode or be withdrawn to the rear chamber wall (z = 130 mm). The outer diameter of the target holder is 40 mm. The relative sizes of the target and electrodes of the focus device is shown schematically in Fig. 1. From voltage and current signals it is observed that the focusing dynamics of the plasma focus is not affected by the presence of a solid obstacle placed more than 10 mm from the end of the anode. This is in agreement with the observations of Bernard et al. and Cloth and Conrads. Further evidence for this has been obtained from shadowgraphs [17] taken with a TEA nitrogen laser during the focusing phase of the plasma focus. Thus to avoid disturbing the focusing action, the obstacle or target is placed no nearer than 20 mm from the end of the anode.

With the copper obstacle, 10 shots are fired at each position, starting from z = 20 mm. The gas filling is renewed after every 5 shots and each time the obstacle position is changed. For each shot the neutron count is recorded. The interval between shots is several

minutes. The above procedure is repeated with a deuterated target. In this case, however, the target is moved in steps toward the anode. This is to avoid any premature deterioration of the deuterated target. The total number of shots is 120, covering 6 positions. Of these, 6 shots (5 %) are "bad" ones with low neutron yields. They are excluded from the data analysis. Another 13 shots (about 10 %) have relatively higher neutron yields (generally larger than about 3 times the sample standard deviations). These "exceptional" shots are analysed separately from the "normal" shots.

Results and discussion

In the interpretation of the experimental results it may be necessary to consider the consequences to the deuterium plasma when the high discharge current impacts and heats the obstacle or target with the release of contaminants. This is best considered from two aspects:

Firstly, consider the effect within a shot. From the time history of the neutron pulse, it is known that the bulk of the neutrons in this device is produced within $\approx$ 80 ns after maximum compression. Thus for the obstacle/target contaminants to have a significant influence on the neutron production, the current sheet must arrive at the obstacle/target well within $\approx$ 80 ns after maximum compression. From shadowgraphic observation [17], it is estimated that the current sheet would reach the closest obstacle/target position (z = 20 mm) about 100 ns after peak compression. Hence,the release of contaminants from the obstacle or target by the discharge current occurs too late to influence the neutron yield within a shot.

Secondly, consider the effect of the contaminants on the next shot.

Since the shots are separated by several minutes, and each shot lasts only a few microseconds, the question can be resolved by looking at the sequence of shots to examine if there is a consistent increase or reduction in neutron yields as the series progresses. An examination of the repeated neutron measurements with the deuterated target at each position shows no definite trend which suggests (i) significant loss of gas from the target as a result of the ion beam bombardment or discharge current heating, and (ii) significant enhancement of the working gas density due to the deuterium gas released from the target in the preceding shot. Similarly, an examination of the repeated measurements with the copper obstacle shows no trend which suggests significant deterioration of the performance of the plasma focus in a sequence of 5 shots due to the contamination of the working gas by the copper released from the obstacle and the holder in the preceding shot. It is to be noted that in the routine operation of the plasma focus, copper is always released from the anode as a result of discharge current heating and bombardment by energetic electrons.

As the plasma focus device emits radiation in the uv region, and this emission begins in the axial run-down phase [18], uv radiation ablation [19] of the target/obstacle could cause the release of contaminants before the pinching occurs. Extrapolating from the results of Sincerny et al. [19], and assuming that 3 % of the stored electrical energy in the focus is converted into uv radiation, it is estimated that the contaminants released will have travelled no further than 2 mm from the target/obstacle in the period upto 100 ns after peak compression. In the present investigation where the target/obstacle is placed further than 10 mm from the end of the pinch column, it is unlikely that this source of contaminants will influence

the neutron yield.

For the "normal" shots, the average neutron counts y_c and y_d as a function of position (z) of the copper obstacle and the deuterated target respectively, are shown in Fig. 2. The error bars shown correspond to one sample standard deviation. The neutron counts at position z = 130 mm are statistically the same for y_c and y_d and they are in agreement with the case without an obstacle or a target. The average neutron yield in normal operation is about 1×10^8 neutrons per discharge.

For the copper obstacle, it is seen that the neutron counts are affected when the obstacle is less than 50 mm from the anode. As z decreases, y_c decreases fairly sharply. At z = 20 mm the neutron count is about 16 % of the value without an obstacle. Thus over 85 % of the neutrons produced in the plasma focus arises from the deuterium ion beam - deuterium gas interaction within the first 60 mm downstream of the anode. The contribution from the thermonuclear source which is expected to take place in the pinch column is therefore less that 15 %. This result is in general agreement with reported measurements, for instance, Bernard et al. [14].

For the deuterated target, the neutron counts increase as the target approaches the anode and reach a maximum at z = 50 mm - 40 mm. This trend has been noted by Cloth and Conrads with a lithium hydride target. In their case they observed a maximum when the target was at about 40 mm from the anode. At closer positions y_d decreases fairly sharply and reaches to about the same value as the case of the copper obstacle at z = 20 mm. Thus, there appears to be no enhancement of neutron production with the deuterated target at this position. This observation differs from the observation of Bernard et al. who

reported a five-fold increase in neutron production when a metal target was replaced by a CD_2 target at 13 mm from the end of the anode in a 27 kJ, 40 kV plasma focus operating at 1.5 torr deuterium. In the case of Bernard et al., however, the effect of discharge current heating of the target was likely as it was much closer to the anode, probably within the pinch column.

Both the y_c and y_d curves show large sample variation of the neutron yields. This is due to the large shot-to-shot fluctuation common in the plasma focus device. A comparison of y_c and y_d shows that they are significantly different for 20 mm < z < 60 mm. At a given target position, the difference $(y_d - y_c)$ gives the neutron counts y_{bt} arising from the bombardment of the deuterated target alone. This is plotted in Fig. 3. The curve shows that the deuteron beam at 20 mm < z < 60 mm is sufficiently energetic to yield neutrons with the deuterated target. For the deuterated target alone a maximum in the neutron yield occurs at z = 30 mm - 40 mm. Fig. 3 also shows the neutron counts y_{bg} arising from the bombardment of the deuterium gas in the chamber per centimeter of the gas. This is obtained from the y_c curve of Fig. 2. Although the dispersion of data is large, the trend is certain and agrees with the y_{bt} curve; a maximum also occurs at z = 30 mm - 40 mm. The observation that both y_{bt} and y_{bg} are not higher at the nearest position used is difficult to understand as it implies that either the deuterium ion beam is most energetic or most intense at z = 30 mm - 40 mm. Another possibility is that the presence of the a solid target at z = 20 mm has disturbed the ion beam generation mechanism even though it may not have disturbed the focusing action.

The observation that y_{bt} and y_{bg} are not highest at the nearest

position used is also rather unexpected. There is , however, some evidence for this in the work of Krompholz et al. [20]. Using an entirely different approach, a shadow bar technique, to investigate the location of the neutron production in a 1 kJ, 20 kV plasma focus operating at 4 torr deuterium, Krompholz et al. reported that the neutron production within the ≈ 10 mm long focus amounted to probably less than 10 %, while neutron production outside 30 mm and 70 mm from the anode amounted to ≈ 80 % and ≈ 50 % respectively. Thus, ≈ 20 % of the neutrons were produced in the first 30 mm from the anode with ≈ 10 % of the neutrons being produced within 10 mm - 30 mm. In the region 30 mm - 70 mm about 30 % of the neutrons were produced. This would imply that, outside the pinch column, the neutron production did not peak immediately, but at a position beyond 30 mm from the anode.

It is rather fortuitous that every target position is represented in the 13 shots with relatively higher neutron yields. As a result, it is possible to analyse these 13 "exceptional" shots separately. Fig. 4 shows the variation of the neutron counts (single shot) Y_c and Y_d as a function of the position of the copper obstacle and the deuterated target respectively. The error bars in this case are the usual one standard deviation counting errors. Shown in Fig. 5 are the corresponding neutron counts Y_{bt} (= Y_d - Y_c) arising from beam - deuterated solid target interaction, and Y_{bg} arising from beam - deuterium gas target interaction. The similarities between Fig. 2 and Fig. 4 ,and between Fig. 3 and Fig. 5 are very obvious, indicating that the same mechanism may be responsible for the neutron production in "normal" shots and in "exceptional" ones.

It is to be noted that the present investigation is based on a small focus, and the conclusion that can be drawn from it is not true

for large foci, such as the Poseidon [21], which are known to exhibit different plasma dynamical characteristics.

Acknowledgement

This work was supported by a grant from the Ministry of Science, Technology and the Environment under the IRPA Program.

References

[1] V. Nardi, A. Bortolotti, J.S. Brzosko, M Esper, C.M. Luo, F. Pedrielli, C. Powell, and D. Zeng, "Stimulated acceleration and confinement of deuterons in focused discharges - Part I," IEEE Trans. Plasma Sci., vol.16, p 368, 1988.

[2] M. Sadowski, J. Zebrowski, E. Rydygier, and J. Kucinski, "Ion emission from plasma-focus facilities," Plasma Physics and Controlled Fusion, vol.30, p 763, 1988.

[3] U. Jager and H. Herold, "Fast ion kinetics and fusion reaction mechanism in the plasma focus," Nuclear Fusion, vol.27, p 407, 1987.

[4] D.J. Weidman and M.J. Rhee, "Measurement of the time-resolved energy spectrum and the ion acceleration mechanism," in Proc. 1987 Workshop on Plasma Focus and Z-pinch (Toledo, Spain), edited by A. Folkierski (Imperial College), p 20.

[5] Toshikazu Yamamoto, Katsuji Shimoda, and Katsumi Hirano, "Neutrons, X-rays and charged particle beams emission in a 65 kV plasma focus," Jpn. J.Appl. Phys. vol.24, p 324, 1985.

[6] U. Jager, L. Bertalot, and H. Herold, "Energy spectra and space resolved measurements of fusion reaction protons from plasma focus devices," Rev. Sci. Instrum., vol. 56, p 77, 1985.

[7] M.J. Rhee, C.M. Luo, R.F. Schneider, and J.R. Smith, "Charge state resolved energy spectra of He, N, Ar, and Ne ions," in Proc. 3rd Int. Workshop on Plasma Focus Research, edited by H. Herold and H.J. Kaeppeler, (Stuttgart), IPF-83-6, p 47, 1983.

[8] N.V. Filippov, "Plasma-focus experiments at the Kurchatov Institute, Moscow (review)," Sov. J. Plasma Phys., vol. 9, p 14, 1983.

[9] W. Stygar, G. Gerdin, F. Venneri, and J. Mandrekas, "Particle beams generated by a 6 - 12.5 kJ dense plasma focus," Nuclear Fusion, vol.22, p 1161, 1982.

[10] G. Gerdin, W. Stygar, and F. Venneri, "Faraday cup analysis of ion beams produced by a dense plasma focus," J. Appl. Phys., vol. 52, p 3269, 1981.

[11] H. Herold, A. Mozer, M. Sadowski, and H. Schmidt, "Design and calibration of a Thomson ion analyzer for plasma focus studies," Rev, Sci. Instrum., vol. 52, p 24, 1981.

[12] R.L. Gullickson and H.L. Sahlin, "Measurements of high energy deuterons in the plasma-focus device," J. Appl. Phys. vol. 49, p 1099, 1978.

[13] P. Cloth and H. Conrads, "Neutronics of a dense-plasma focus - An investigation of a fusion plasma," Nucl. Sci. Eng. vol.62, p 591, 1977.

[14] A. Bernard, A. Coudeville, J.P. Garconnet, A. Jolas, J. De Mascureau, and C. Nazet, "Structure of current sheath and fast-particle beams in the focus experiment," in Proc. Berchtesgaden Conf. Plasma Physics and Controlled Nuclear Fusion Research, (IAEA, Vienna, 1976), IAEA-CN-35/E18-4, p 471.

[15] S. Lee, T.Y. Tou, S.P. Moo, M.A. Eissa, A.V. Gholap, K.H. Kwek, S. Mulyodrono, A.J. Smith, Suryadi, W. Usada, and M. Zakaullah, "A simple facility for the teaching of plasma dynamics and plasma nuclear fusion," Am. J. Phys. vol.56, p 62, 1988.

[16] C.S. Wong, S. Lee, and S.P. Moo, "Neutrons measurements of a 12 kJ plasma focus," Malaysian J. Sci., vol. 6(B), p 167, 1980.

[17] S. Lee, M.A. Alabraba, A.V. Gholap, S.Kumar, K.H. Kwek, M. Nisar, R.S. Rawat, and J. Singh, "Effect of targets on plasma

focus dynamics," (accepted for publication in IEEE Trans.Plasma Sci.)

[18] J.J. Fanning, and K. Kim, "Mather-type dense plasma focus as a new optical pump for short-wavelength high-power lasers", J. Appl. Phys., vol. 55, p 2795, 1984.

[19] P. Sincerny, R. Stringfield, and C. Gilman, "Plasma blow-off from electrode surfaces in the presence of vacuum-ultraviolet radiation", IEEE Trans. Plasma Sci., vol. PS-11, p 196, 1983.

[20] H. Krompholz, L. Michel, K.H. Schonbach, and Heinz Fischer, "Neutron-, ion-, and electron-energy spectra in a 1 kJ plasma focus," Appl. Phys. vol.13, p 29, 1977.

[21] H. Herold, L. Bertalot, K. Hirano, U. Jager, H.J. Kaeppeler, M. Sadowski, H. Schmidt, R. Schmidt, M. Shakhatre, A. Shyam, G. Bockle, K. Matl, N. Wenzel, R. Wolf, R. Batzner, H. Hinsch, and K. Hubner, "Two phases of neutron production in the Poseidon plasma focus", Plasma Phys. and Contr. Fusion Res. 1984 (Proc. 10th Int. Conf. London, 1984), paper IAEA-CN-44/D-III-6-3.

Figure Captions

Fig. 1. Schematic diagram of the plasma focus showing the relative sizes of the electrodes and target. 1 = chromed mild steel focus chamber; 2 = copper target holder; 3 = target; 4 = cathode (6 copper rods); 5 = hollow copper anode.

Fig. 2. Variation of the average neutron counts y_c and y_d as a function of position (z) of the copper obstacle and the deuterated target respectively. The point at z = 130 mm is the average of 17 shots with the obstacle/target withdrawn to the end wall of the chamber. It corresponds to about $1X10^8$ neutrons per shot.

Fig. 3. Variation with position (z) of the average neutron counts due to the deuterated target alone (y_{bt}), and due to per centimeter of the deuterium gas in the chamber (y_{bg}).

Fig. 4. Variation of single shot neutron counts Y_c and Y_d as a function of position of the copper obstacle and the deuterated target respectively.

Fig. 5. Variation with position of the neutron counts (single shot) due to the deuterated target alone (Y_{bt}) and due to per centimeter of the deuterium gas in the chamber (Y_{bg}).

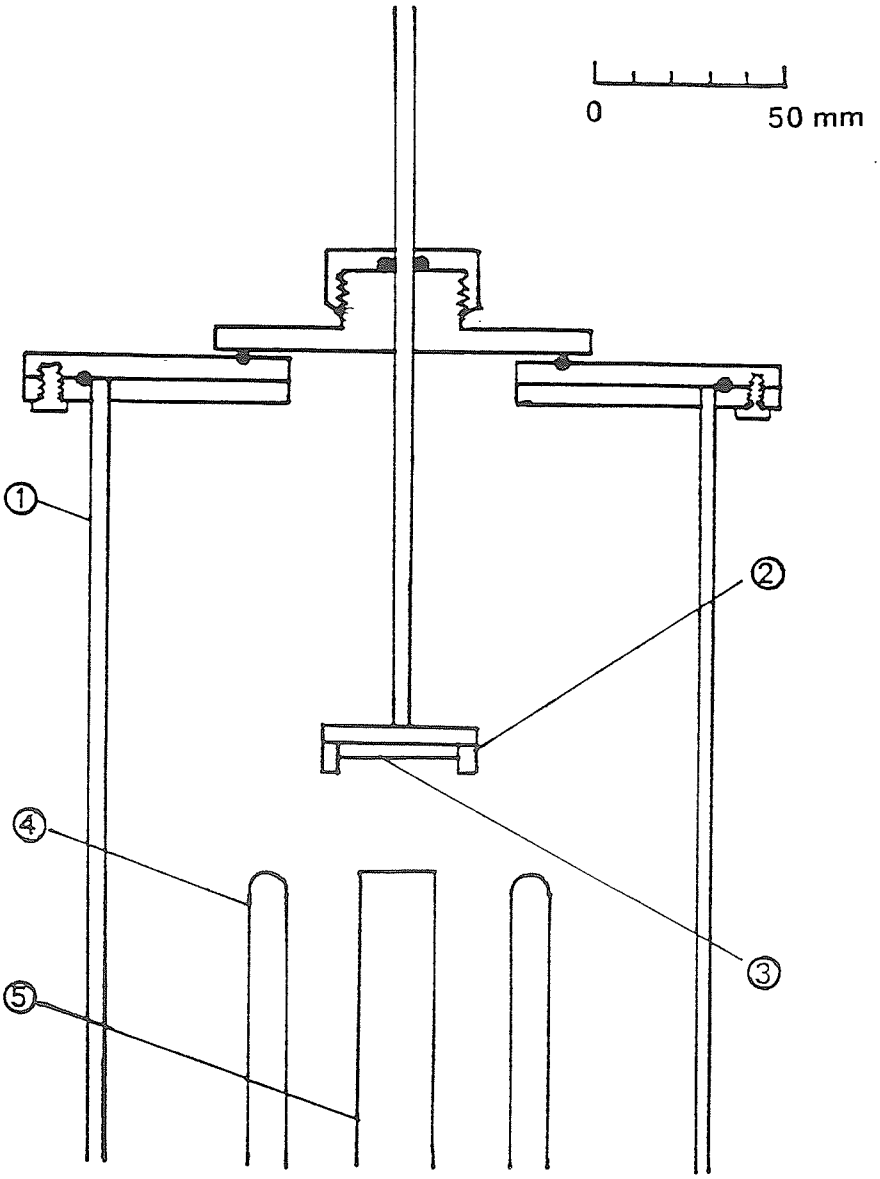

Fig. 1. Schematic diagram of the plasma focus showing the relative sizes of the electrodes and target. 1 = chromed mild steel focus chamber; 2 = copper target holder; 3 = target; 4 = cathode (6 copper rods); 5 = hollow copper anode.

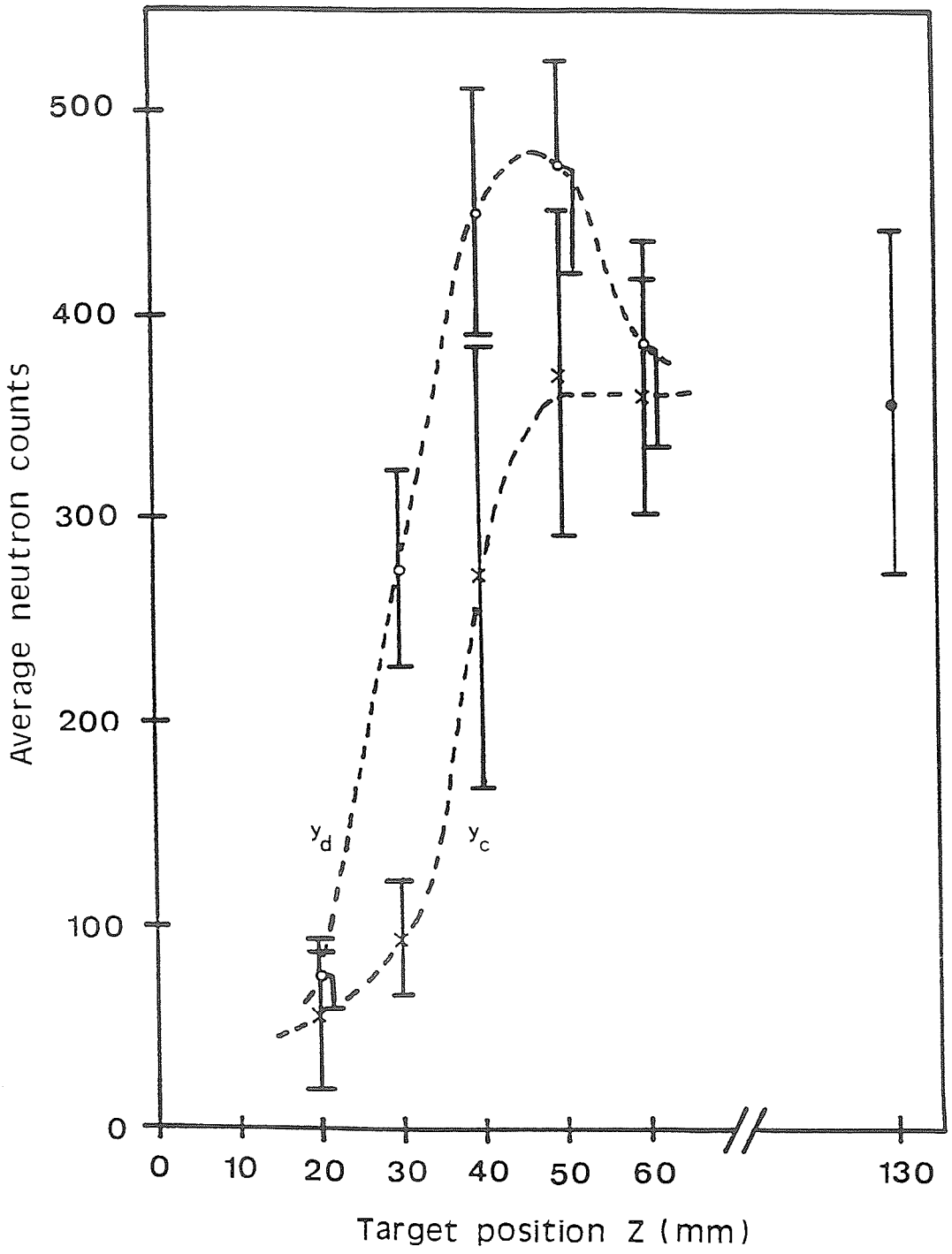

Fig. 2. Variation of the average neutron counts y_c and y_d as a function of position (z) of the copper obstacle and the deuterated target respectively. The point at z = 130 mm is the average of 17 shots with the obstacle/target withdrawn to the end wall of the chamber. It corresponds to about $1X10^8$ neutrons per shot.

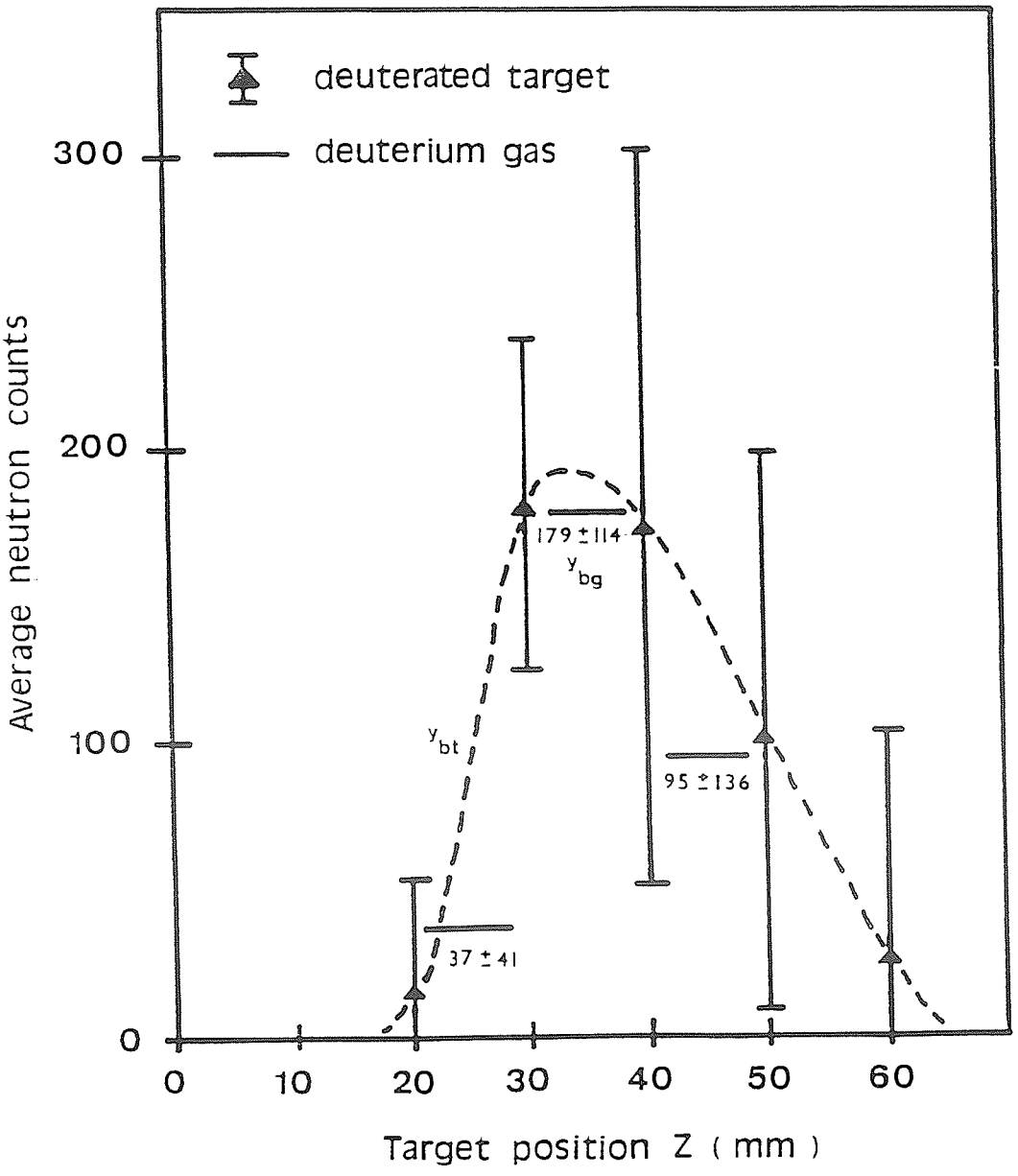

Fig. 3. Variation with position (z) of the average neutron counts due to the deuterated target alone (y_{bt}), and due to per centimeter of the deuterium gas in the chamber (y_{bg}).

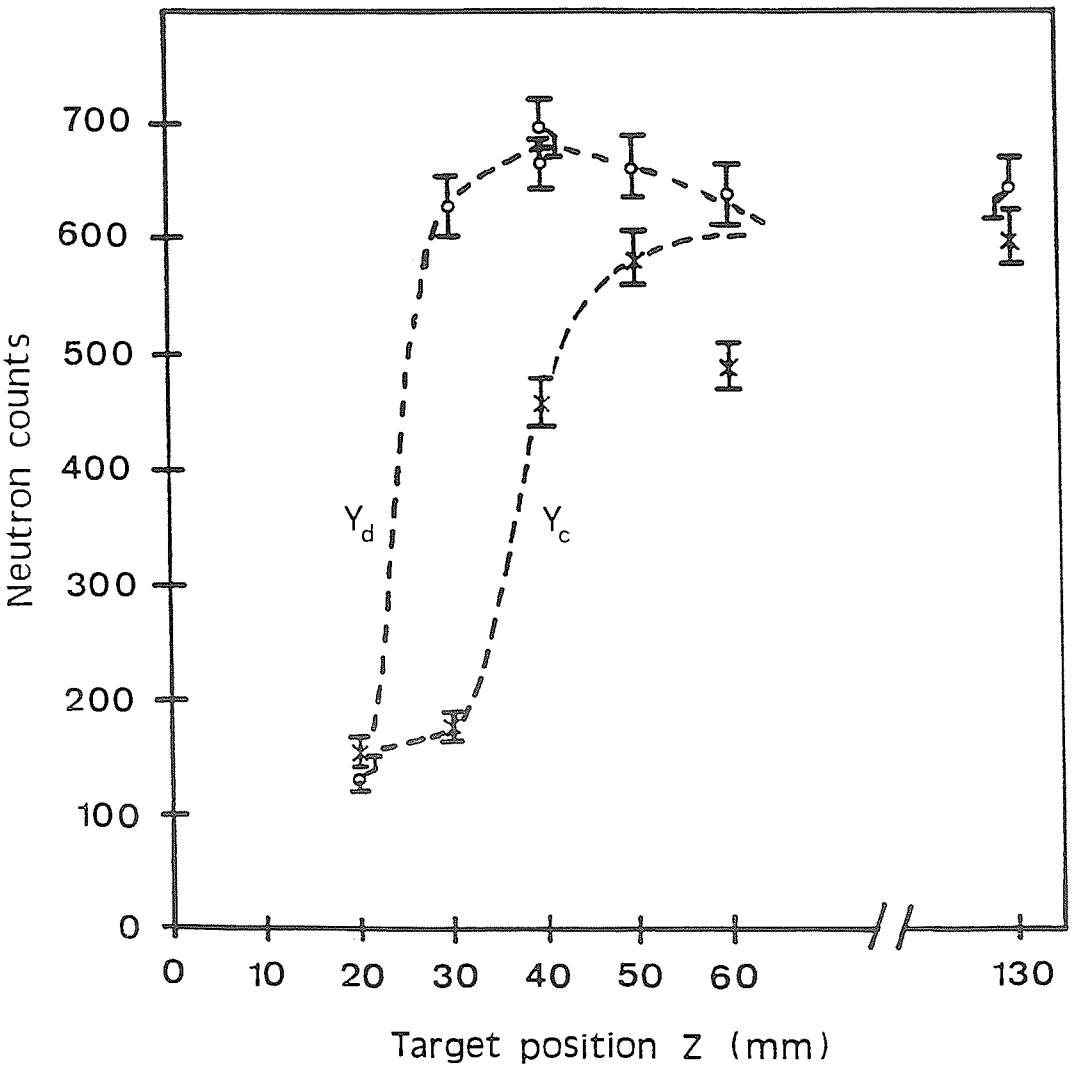

Fig. 4. Variation of single shot neutron counts Y_c and Y_d as a function of position of the copper obstacle and the deuterated target respectively.

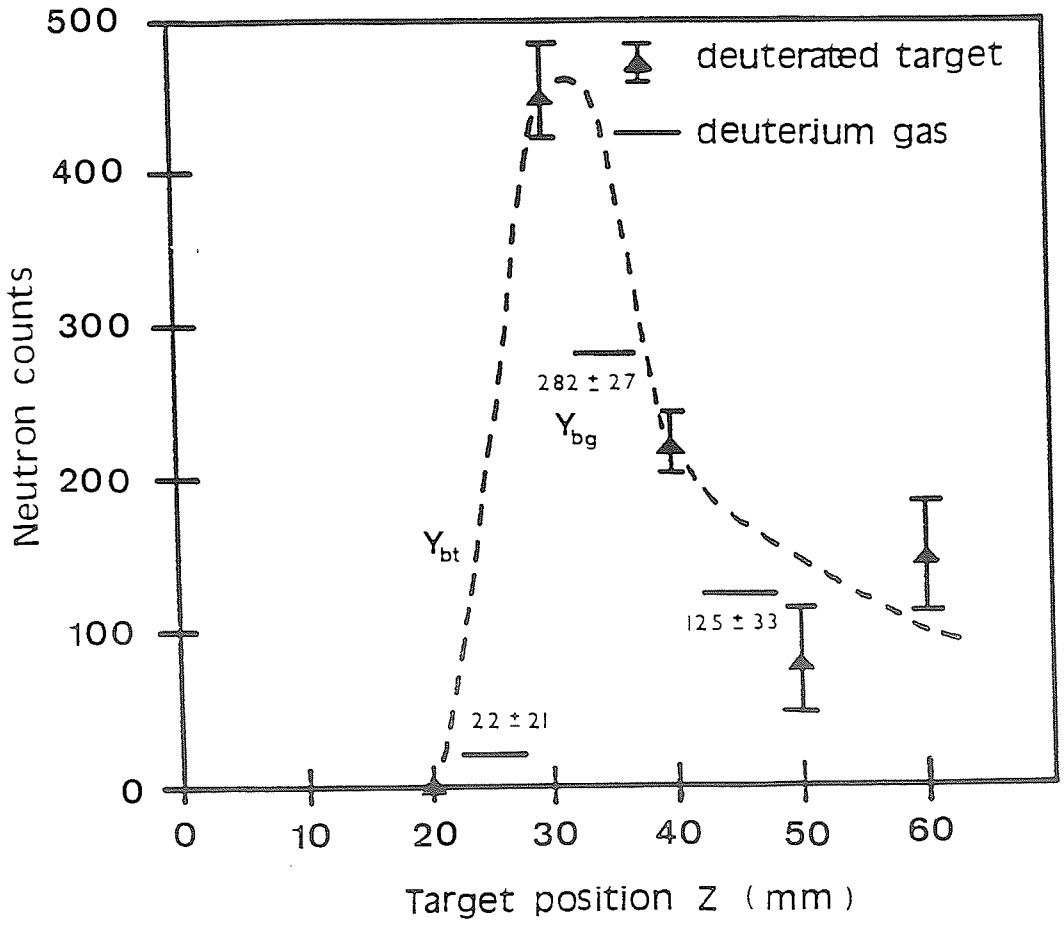

Fig. 5. Variation with position of the neutron counts (single shot) due to the deuterated target alone (Y_{bt}) and due to per centimeter of the deuterium gas in the chamber (Y_{bg}).